frontiers | Research Topics

Magnetoencephalography: Methodological innovation paves the way for scientific discoveries and new clinical applications

Edited by
Rafeed Alkawadri, Rei Enatsu, Matti Hämäläinen and Anto Bagic

Published in
Frontiers in Neurology

ISSN 1664-8714
ISBN 978-2-83250-997-5
DOI 10.3389/978-2-83250-997-5

About Frontiers

Frontiers is more than just an open access publisher of scholarly articles: it is a pioneering approach to the world of academia, radically improving the way scholarly research is managed. The grand vision of Frontiers is a world where all people have an equal opportunity to seek, share and generate knowledge. Frontiers provides immediate and permanent online open access to all its publications, but this alone is not enough to realize our grand goals.

Frontiers journal series

The Frontiers journal series is a multi-tier and interdisciplinary set of open-access, online journals, promising a paradigm shift from the current review, selection and dissemination processes in academic publishing. All Frontiers journals are driven by researchers for researchers; therefore, they constitute a service to the scholarly community. At the same time, the *Frontiers journal series* operates on a revolutionary invention, the tiered publishing system, initially addressing specific communities of scholars, and gradually climbing up to broader public understanding, thus serving the interests of the lay society, too.

Dedication to quality

Each Frontiers article is a landmark of the highest quality, thanks to genuinely collaborative interactions between authors and review editors, who include some of the world's best academicians. Research must be certified by peers before entering a stream of knowledge that may eventually reach the public - and shape society; therefore, Frontiers only applies the most rigorous and unbiased reviews. Frontiers revolutionizes research publishing by freely delivering the most outstanding research, evaluated with no bias from both the academic and social point of view. By applying the most advanced information technologies, Frontiers is catapulting scholarly publishing into a new generation.

What are Frontiers Research Topics?

Frontiers Research Topics are very popular trademarks of the *Frontiers journals series*: they are collections of at least ten articles, all centered on a particular subject. With their unique mix of varied contributions from Original Research to Review Articles, Frontiers Research Topics unify the most influential researchers, the latest key findings and historical advances in a hot research area.

Find out more on how to host your own Frontiers Research Topic or contribute to one as an author by contacting the Frontiers editorial office: frontiersin.org/about/contact

Magnetoencephalography: Methodological innovation paves the way for scientific discoveries and new clinical applications

Topic editors

Rafeed Alkawadri — University of Pittsburgh Medical Center, United States
Rei Enatsu — Sapporo Medical University, Japan
Matti Hämäläinen — Massachusetts General Hospital, Harvard Medical School, United States
Anto Bagic — University of Pittsburgh, United States

Citation

Alkawadri, R., Enatsu, R., Hämäläinen, M., Bagic, A., eds. (2022). *Magnetoencephalography: Methodological innovation paves the way for scientific discoveries and new clinical applications*. Lausanne: Frontiers Media SA.
doi: 10.3389/978-2-83250-997-5

Table of contents

frontiers | Frontiers in Neurology

TYPE Editorial
PUBLISHED 24 November 2022
DOI 10.3389/fneur.2022.1056301

OPEN ACCESS

EDITED AND REVIEWED BY
Jan Kassubek,
University of Ulm, Germany

*CORRESPONDENCE
Rafeed Alkawadri
rafeed.alkawadri@pitt.edu;
https://www.humanbrainmapping.net/contactus

SPECIALTY SECTION
This article was submitted to Applied Neuroimaging, a section of the journal Frontiers in Neurology

RECEIVED 28 September 2022
ACCEPTED 13 October 2022
PUBLISHED 24 November 2022

CITATION
Alkawadri R, Enatsu R, Hämäläinen M and Bagić A (2022) Editorial: Magnetoencephalography: Methodological innovation paves the way for scientific discoveries and new clinical applications.
Front. Neurol. 13:1056301.
doi: 10.3389/fneur.2022.1056301

Editorial: Magnetoencephalography: Methodological innovation paves the way for scientific discoveries and new clinical applications

Rafeed Alkawadri[1]*, Rei Enatsu[2], Matti Hämäläinen[3,4] and Anto Bagić[1]

[1]University of Pittsburgh Comprehensive Epilepsy Center (UPCEC), Department of Neurology, University of Pittsburgh Medical Center (UPMC), Pittsburgh, PA, United States, [2]Department of Neurosurgery, Sapporo Medical University, Sapporo, Japan, [3]Department of Radiology, Harvard Medical School, Boston, MA, United States, [4]Department of Neuroscience and Biomedical Engineering, School of Science, Aalto University, Espoo, Finland

KEYWORDS

magnetoencephalography, epilepsy, source localization, epilepsy surgery, source estimate, functional mapping, electromagnetism

Editorial on the Research Topic
Magnetoencephalography: Methodological innovation paves the way for scientific discoveries and new clinical applications

In 1971, less than five decades after the inception of electroencephalography (EEG), the first real-time magnetoencephalogram was obtained at MIT using a SQUID magnetometer, propelling magnetoencephalography (MEG) as a feasible approach for studying the human brain (1, 2). Then, in 1992, a multidisciplinary research group at the Low-Temperature Laboratory (LTL) of the Helsinki University of Technology (now part of Aalto University) produced the first whole-head MEG system with more than 100 channels (3). The key to this success was the fruitful interactions between the neuroscientists, physicists, mathematicians, engineers, and clinicians who worked together on the instrumentation, analysis methods, and actual neuroscience and clinical applications. Their success reverberated into several research laboratories worldwide, paving the way for MEG to become a recognized method for studying the brain.

During the 21st century, both basic neuroscience and clinical MEG studies have benefited from the use of high-quality open-source academic software packages, which have enhanced the rigor and reproducibility of scientific investigations using MEG. In addition, Optically Pumped Magnetometers (OPMs), novel room-temperature magnetic field sensors, hold promise for significantly improving the spatial resolution and sensitivity of MEG (4). These new devices will also enable the adaptation of the MEG array to the size of the head so that a high signal-to-noise ratio can be achieved, even in

studies of early brain development (5). To fully capitalize on these advances, one needs improvements to forward and inverse modeling techniques, as well as to the biophysical models of assemblies of neurons. The latter make it possible to suggest mechanisms underlying the observed macroscopic neural currents, lead to new testable hypotheses, and provide links between recordings in animal models and human MEG (6). Portable and real-time brain-computer MEG-based interfaces will likely become more integrated in the future (2, 7, 8).

The only established clinical applications of MEG, however, are the localization and characterization of epileptic activity (9) and presurgical mapping of the eloquent cortex (10). New studies give hope that MEG, used in combination with EEG and other non-invasive brain imaging methods, will in the future be harnessed for better diagnosis and for monitoring treatment efficacy in several neurological and psychiatric diseases (11, 12).

To that end, MEG has already changed clinical approaches and improved surgical outcomes in epilepsy (13–19), but, paradoxically, it has not yet secured its place in clinical practice (20–23). Furthermore, among the over 20 million patients with drug-resistant epilepsy (DRE) worldwide (2, 24), millions of potential surgical candidates continue to suffer unnecessarily because of the vast underutilization of surgery for epilepsy (2, 15, 25, 26). It appears that the epilepsy community does not have an efficient solution for this cardinal challenge (15, 25–27). Perhaps the blatant lack of synergies between MEG practitioners and the epilepsy community represents an opportunity to change this unfavorable clinical reality; i.e., these two groups could come together to promote non-pharmacologic DRE treatment options and thereby considerably increase the number of comprehensively evaluated patients, including many who could unquestionably benefit from an MEG (9, 23, 28). Yet it seems that previously initiated (i.e., currently stagnant and challenging) efforts to harmonize clinical MEG practice must materialize before we can expect MEG to take its proper place and be used at proper volume in clinical practice (29, 30). Considering that epilepsy surgery is an underutilized tool at large, this possibly applies even more to the underuse of MEG in the context of non-invasive presurgical mapping of the eloquent cortices as part of preparation for surgical interventions (9, 10, 23), where variability in clinical practice may be even greater and the concerted efforts of clinical magnetoencephalographers and neurosurgeons are necessary. In addition to the promise of possible new uses, such as ictal MEG (31, 32), real-world advances have been complicated by logistical concerns, e.g., the duration of recording; monetary, regulatory, or simply practice styles (e.g., handling referrals in less well-established indications such as non-surgical EEG-negative epilepsies); or attitudes toward research (33). However, this has opened doors that allow a more thoughtful approach to applying forward and inverse solutions between old, well-known, and practical ones, like single-point (i.e., single equivalent current dipole) solutions, and perhaps theoretically better and more realistic ones that are already gaining momentum after a slight lag taking advantage of computational and hardware exponential advances. Another ongoing challenge is the lack of a good platform for worldwide data repositories, as well as of consortia that would allow real-time collaboration in an area still practiced in the form of medical art and expert consensus. This is not just a problem with MEG, but with epilepsy surgery in general.

In this collection, we aimed to provide a comprehensive update on the most recent advances in MEG utilization in clinical pre-surgical evaluation, functional mapping, cognitive neuroscience, source localization techniques, and the most recent technological advances. We also highlight network analysis as a newly emerged technique that has approached the pathophysiology of epilepsy from different perspectives. In no particular order: Laohathai et al. discussed fundamental proficiency in the practice of MEG in clinical epilepsy care. Cao et al. presented a perspective on using quantitative network analysis methods for assessing the epileptogenic zone. Sun et al. used magnetoencephalography and graph theory analysis to reveal the dynamics of functional connectivity networks during seizure termination in patients with childhood absence epilepsy. Aung et al. discussed how MEG's excellent temporal and spatial resolutions contribute to the understanding of a subject with both clinical and surgical importance: i.e., what constitutes the boundary between focal, frontal, and generalized epilepsies. Khan et al. reported on different frequency-specific hubs accounting for age-specific maturation. Matsubara et al. discovered that specific functional connectivity was bolstered in patients with benign adult familial myoclonus epilepsy, implying that ipsilateral sensorimotor responses may be a pathologically enhanced motor response homologous to the giant component. Jousmäki offered a unique set of skills and tools that enhance or complement existing commercial solutions with practical mapping applications both in clinical research and in practice. Similarly, Anastasopoulou et al. presented an innovative system that derived kinematic profiles of oro-facial movements during speech, with multiple potential cross-disciplinary applications. Clarke et al. presented a practical approach to addressing noise in data *via* pre-processing and demonstrated it with infant MEG data. Lastly, Mylonas et al. presented a multimodal, non-invasive neurophysiological approach for sleep spindle source localization and discussed its potential clinical applications.

Since its early clinical studies, MEG has provided a non-invasive tool with almost unparalleled temporal and spatial resolutions for various clinical and investigative situations. It has not yet settled in the clinical mainstream, mainly due to the lack of awareness about its indications and potential among practicing physicians, along with its suboptimal representation in the clinical training curricula. This is in addition to the known practical challenges in clinical settings, with their complex and expensive technical prerequisites and environments that are hardly ideal for investigating the true breadth of potential clinical applications. Furthermore, practical implementation of theoretical advances in the software and hardware solutions

could potentially replace current, more invasive clinical approaches—for instance, by accurately assessing deep sources and subcortical structures. We believe this journal issue provides a stepping-stone in the right direction to future scientific discoveries and new clinical applications.

Author contributions

RA, RE, MH, and AB: draft of the manuscript, conceptualization, and revision of the manuscript. All authors contributed to the article and approved the submitted version.

Acknowledgments

The guest editors acknowledge all authors and reviewers of the included manuscripts.

Conflict of interest

The authors declare that the research was conducted in the absence of any commercial or financial relationships that could be construed as a potential conflict of interest.

Publisher's note

All claims expressed in this article are solely those of the authors and do not necessarily represent those of their affiliated organizations, or those of the publisher, the editors and the reviewers. Any product that may be evaluated in this article, or claim that may be made by its manufacturer, is not guaranteed or endorsed by the publisher.

References

1. Cohen D. Magnetoencephalography: detection of the brain's electrical activity with a superconducting magnetometer. *Science.* (1972) 175:664–6. doi: 10.1126/science.175.4022.664

2. Alkawadri R. Brain-computer interface (BCI) applications in mapping of epileptic brain networks based on intracranial-EEG: An update. *Front Neurosci.* (2019) 13:191. doi: 10.3389/fnins.2019.00191

3. Hämäläinen MS. Magnetoencephalography: a tool for functional brain imaging. *Brain Topogr.* (1992) 5:95–102. doi: 10.1007/BF01129036

4. Boto E, Meyer SS, Shah V, Alem O, Knappe S, Kruger P, et al. A new generation of magnetoencephalography: room temperature measurements using optically-pumped magnetometers. *Neuroimage.* (2017) 149:404–14. doi: 10.1016/j.neuroimage.2017.01.034

5. Jas M, Jones SR, Hämäläinen MS. Whole-head OPM-MEG enables noninvasive assessment of functional connectivity. *Trends Neurosci.* (2021) 44:510–2. doi: 10.1016/j.tins.2021.04.006

6. Hämäläinen M, Lundqvist D. MEG as an enabling tool in neuroscience: transcending boundaries with new analysis methods and devices. *Magnetoencephalogr Signals Dyn Cortical Networks.* (2019) 2019:3–39. doi: 10.1007/978-3-030-00087-5_81

7. Mcclay WA, Yadav N, Ozbek Y, Haas A, Attias HT, Nagarajan SS. A real-time magnetoencephalography brain-computer interface using interactive 3D visualization and the Hadoop ecosystem. *Brain Sci.* (2015) 5:419–40. doi: 10.3390/brainsci5040419

8. Paek AY, Kilicarslan A, Korenko B, Gerginov V, Knappe S, Contreras-Vidal JL. Towards a portable magnetoencephalography based brain computer interface with optically-pumped magnetometers. In: *2020 42nd Annual International Conference of the IEEE Engineering in Medicine & Biology Society (EMBC): IEEE.* (2020). p. 3420–3.

9. Bagic A, Funke ME, Ebersole J, Committee APS. ACMEGS Position Statement Committee: American Clinical MEG Society (ACMEGS) position statement: the value of magnetoencephalography (MEG)/magnetic source imaging (MSI) in noninvasive presurgical evaluation of patients with medically intractable localization-related epilepsy. *J Clin Neurophysiol.* (2009) 26:290–3. doi: 10.1097/WNP.0b013e3181b49d50

10. Bagić A, Bowyer S, Kirsch H, Funke M, Burgess R. ACMEGS Position Statement Committee American Clinical MEG Society (ACMEGS) Position Statement# 2: the value of magnetoencephalography (MEG)/magnetic source imaging (MSI) in noninvasive presurgical mapping of eloquent cortices of patients preparing for surgical interventions. *J Clin Neurophysiol.* (2017) 34:189–95. doi: 10.1097/WNP.0000000000000366

11. O'reilly C, Lewis JD, Elsabbagh M. Is functional brain connectivity atypical in autism? A systematic review of EEG and MEG studies. *PLoS ONE.* (2017) 12:e0175870. doi: 10.1371/journal.pone.0175870

12. Roberts TP, Kuschner ES, Edgar JC. Biomarkers for autism spectrum disorder: opportunities for magnetoencephalography (MEG). *J Neurodev Disord.* (2021) 13:1–9. doi: 10.1186/s11689-021-09385-y

13. Sutherling WW, Mamelak AN, Thyerlei D, Maleeva T, Minazad Y, Philpott L, et al. Influence of magnetic source imaging for planning intracranial EEG in epilepsy. *Neurology.* (2008) 71:990–6. doi: 10.1212/01.wnl.0000326591.29858.1a

14. Knowlton RC, Razdan SN, Limdi N, Elgavish RA, Killen J, Blount J, et al. Effect of epilepsy magnetic source imaging on intracranial electrode placement. *Ann Neurol.* (2009) 65:716–23. doi: 10.1002/ana.21660

15. Englot DJ, Nagarajan SS, Imber BS, Raygor KP, Honma SM, Mizuiri D, et al. Epileptogenic zone localization using magnetoencephalography predicts seizure freedom in epilepsy surgery. *Epilepsia.* (2015) 56:949–58. doi: 10.1111/epi.13002

16. Murakami H, Wang ZI, Marashly A, Krishnan B, Prayson RA, Kakisaka Y, et al. Correlating magnetoencephalography to stereo-electroencephalography in patients undergoing epilepsy surgery. *Brain.* (2016) 139:2935–47. doi: 10.1093/brain/aww215

17. Rampp S, Stefan H, Wu X, Kaltenhauser M, Maess B, Schmitt FC, et al. Magnetoencephalography for epileptic focus localization in a series of 1000 cases. *Brain.* (2019) 142:3059–71. doi: 10.1093/brain/awz231

18. Burgess RC. MEG for greater sensitivity and more precise localization in epilepsy. *Neuroimaging Clin N Am.* (2020). 30:145–58. doi: 10.1016/j.nic.2020.02.004

19. Burgess RC, Alkawadri R. Electromagnetic source imaging for stereo EEG planning. In: *A Practical Approach to Stereo EEG. demosMedical.* (2020). p. 35–48.

20. Bagic AI. Disparities in clinical magnetoencephalography practice in the United States: a survey-based appraisal. *J Clin Neurophysiol.* (2011) 28:341–7. doi: 10.1097/WNO.0b013e3181ce162a

21. Shiraishi H, Ozaki I, Iguchi Y, Ishii R, Kamada K, Kameyama S, et al. Questionnaire survey of current status and problems in clinical applications of magnetoencephalography (MEG) in Japan. *Jpn J Clin Neurophysiol.* (2012) 40:119–30. doi: 10.11422/jscn.40.119

22. Bagić A. An ignored lighthouse: is there underappreciation and underutilization of electro-magnetic source imaging? *Clin Neurophysiol.* (2014) 125:2322–3. doi: 10.1016/j.clinph.2014.04.017

23. Bagic AI, Burgess RC. Utilization of MEG among the US epilepsy centers: a survey-based appraisal. *J Clin*

Neurophysiol. (2020) 37:599–605. doi: 10.1097/WNP.0000000000000716

24. Begley C, Wagner RG, Abraham A, Beghi E, Newton C, Kwon CS, et al. The global cost of epilepsy: a systematic review and extrapolation. *Epilepsia.* (2022) 63:892–903. doi: 10.1111/epi.17165

25. Wiebe S. Still an elusive target: guiding practice for epilepsy surgery. *Neurology.* (2010) 75:678–9. doi: 10.1212/WNL.0b013e3181eee510

26. Engel J Jr, Wiebe S. Who is a surgical candidate? *Handb Clin Neurol.* (2012) 108:821–8. doi: 10.1016/B978-0-444-52899-5.00030-7

27. Haneef Z, Stern J, Dewar S, Engel J Jr. Referral pattern for epilepsy surgery after evidence-based recommendations: a retrospective study. *Neurology.* (2010) 75:699–704. doi: 10.1212/WNL.0b013e3181eee457

28. Bagic AI, Burgess RC. Clinical magnetoencephalography practice in the United States ten years later: a survey-based reappraisal. *J Clin Neurophysiol.* (2020) 37:592–8. doi: 10.1097/WNP.0000000000000693

29. Bagic AI, Barkley GL, Chung CK, De Tiege X, Ebersole JS, Funke ME, et al. Clinical practice guidelines or clinical research guidelines? *Clin Neurophysiol.* (2018) 129:2054–5. doi: 10.1016/j.clinph.2018.06.015

30. Bagić AI, Rampp S. It is time to harmonize clinical MEG practice internationally. *Clin Neurophysiol.* (2020) 131:1769–71. doi: 10.1016/j.clinph.2020.04.020

31. Alkawadri R, Krishnan B, Kakisaka Y, Nair D, Mosher JC, Burgess RC, et al. Localization of the ictal onset zone with MEG using minimum norm estimate of a narrow band at seizure onset versus standard single current dipole modeling. *Clin Neurophysiol.* (2013) 124:1915–8. doi: 10.1016/j.clinph.2013.03.016

32. Alkawadri R, Burgess RC, Kakisaka Y, Mosher JC, Alexopoulos AV. Assessment of the utility of ictal magnetoencephalography in the localization of the epileptic seizure onset zone. *JAMA Neurol.* (2018) 75:1264–72. doi: 10.1001/jamaneurol.2018.1430

33. Alkawadri R, Burgess R, Isitan C, Wang IZ, Kakisaka Y, Alexopoulos AV. Yield of repeat routine MEG recordings in clinical practice. *Epilepsy Behav.* (2013) 27:416–9. doi: 10.1016/j.yebeh.2013.02.028

frontiers in Neurology

REVIEW
published: 14 October 2021
doi: 10.3389/fneur.2021.722986

Practical Fundamentals of Clinical MEG Interpretation in Epilepsy

*Christopher Laohathai[1,2], John S. Ebersole[3], John C. Mosher[4], Anto I. Bagić[5], Ai Sumida[4], Gretchen Von Allmen[1] and Michael E. Funke[1]**

[1] Division of Child Neurology, Department of Pediatrics, McGovern Medical School at UTHealth, Houston, TX, United States, [2] Department of Neurology, Saint Louis University, Saint Louis, MO, United States, [3] Northeast Regional Epilepsy Group, Atlantic Health Neuroscience Institute, Summit, NJ, United States, [4] Department of Neurology, McGovern Medical School at UTHealth, Houston, TX, United States, [5] University of Pittsburgh Comprehensive Epilepsy Center (UPCEC), Department of Neurology, University of Pittsburgh Medical Center, Pittsburg, PA, United States

Magnetoencephalography (MEG) is a neurophysiologic test that offers a functional localization of epileptic sources in patients considered for epilepsy surgery. The understanding of clinical MEG concepts, and the interpretation of these clinical studies, are very involving processes that demand both clinical and procedural expertise. One of the major obstacles in acquiring necessary proficiency is the scarcity of fundamental clinical literature. To fill this knowledge gap, this review aims to explain the basic practical concepts of clinical MEG relevant to epilepsy with an emphasis on single equivalent dipole (sECD), which is one the most clinically validated and ubiquitously used source localization method, and illustrate and explain the regional topology and source dynamics relevant for clinical interpretation of MEG-EEG.

Keywords: magnetoencephalography, magnetic source imaging, equivalent current dipole, epilepsy, epilepsy surgery

OPEN ACCESS

Edited by:
Peter Sörös,
University of Oldenburg, Germany

Reviewed by:
Hermann Stefan,
University Hospital Erlangen, Germany
Dang Khoa Nguyen,
Université de Montréal, Canada

***Correspondence:**
Michael E. Funke
michael.e.funke@uth.tmc.edu

Specialty section:
This article was submitted to Applied Neuroimaging, a section of the journal Frontiers in Neurology

Received: *09 June 2021*
Accepted: *06 September 2021*
Published: *14 October 2021*

Citation:
Laohathai C, Ebersole JS, Mosher JC, Bagić AI, Sumida A, Von Allmen G and Funke ME (2021) Practical Fundamentals of Clinical MEG Interpretation in Epilepsy. Front. Neurol. 12:722986. doi: 10.3389/fneur.2021.722986

INTRODUCTION

Epilepsy surgery continues to not only be a necessity, but the most effective option for many patients with drug resistant epilepsy (DRE) (1). The availability of these procedures has grown, as reflected by the expansion of National Association of Epilepsy Centers (NAEC) accredited epilepsy centers from 133 centers in 2011 (2) to 261 centers in 2021 (NAEC Webinar, April 6th, 2021). The cohort of patients who presented for presurgical evaluation has also changed, with increased representation of extratemporal epilepsy surgery (3). Extratemporal epilepsy, in comparison with temporal lobe epilepsy, has been associated with worse outcomes (1) and requires additional specific investigations. Magnetoencephalography (MEG) is one of these neurophysiologic assessments (4, 5).

MEG is a non-invasive recording of cerebral activity as reflected outside of the skull in the form of magnetic fields generated by neuronal electrical currents (6). In comparison to electroencephalography (EEG), MEG is more sensitive to tangential sources from sulci and cortical planes. As the cortical surface consists of many gyrations and fissures, simulated computation analysis suggests that MEG can record 95% of cortical activity, significantly more than EEG which is more attuned to radial sources (7). Source localization by MEG is followed by co-registration with brain MRI, which provides anatomical correlation (magnetic source imaging; MSI) (8). MEG data has been proven to show correlation with electrocorticography in specific cases (9). In a study of 69 patients with suspected neocortical epilepsy, MEG provided non-redundant information in 33% of the patients and benefited 21% of patients who received surgery (10). Post-operative seizure

freedom at 12-month has been associated with both complete intracranial sampling (62 vs. 25% seizure freedom) and complete resection (88 vs. 52% seizure freedom; complete defined by ≥ 70% dipole removal) of MEG clusters (11).

However, despite the considerable growth of surgical epilepsy centers and increased representation of extratemporal epilepsy, the availability of MEG remains relatively scarce. There are only 22 American Clinical Magnetoencephalography Society (ACMEGS) affiliated centers in the United States, representing less than 17% of the total NAEC accredited epilepsy centers (12). This is likely an outcome of multiple institutional (e.g., practice setting, economic priorities, strength of epilepsy program, patient profile, available personnel) and systemic (e.g., regulatory issues, insurers landscape) factors that are incompletely understood but are strongly influenced by the deeply habituated patterns of clinical practice (12). Given limited availability, the experience in MEG analysis and interpretation has been relatively constrained to the selected institutions with pre-existing technology and experienced personnel. The initial steps toward learning clinical magnetoencephalography can prove difficult even for clinical neurophysiologists and epileptologists outside of clinically productive MEG centers. This barrier is, in part, due to the lack of appropriate basic clinical literature. We view that an accessible review on practical fundamentals of clinical MEG localization and interpretation in epilepsy is much needed to narrow this knowledge gap.

This narrative review aims to explain the basic practical concepts of clinical MEG relevant to epilepsy with an emphasis on single equivalent dipole (sECD), which is one the most clinically validated and ubiquitously used source localization method, and illustrate the regional topology and source dynamics relevant for clinical interpretation of MEG-EEG (13). The information presented is gathered through an extensive review of available literature, supplemented by clinical examples provided by the authors, and supported by clinical experience from authors with long-term experience in the clinical MEG field. The article strives to make MEG localization and interpretation in epilepsy more understandable so that readers can recognize its utilities and limitations, facilitate the learning of clinical MEG, and raise awareness of clinical MEG's relevance to epilepsy surgery.

BASIC CONCEPTS OF CLINICAL MEG

Basic Concepts of Source Localization and Methodologies

Neuronal activity consists of an intracellular "primary current," whose circuit is completed by an induced extracellular "volume current." The extracellular volume current creates scalp potentials that can be recorded by electroencephalography (EEG). The primary current and volume current simultaneously produce a magnetic field that can be recorded by MEG. For a given primary current, the calculation of corresponding scalp potential and the external magnetic field is termed a "forward problem." In contrast, the "inverse problem" is the modeling of the implied primary current and its source location from the recorded MEG or EEG. The goal of clinical MEG in epilepsy is predominantly aimed toward solving this inverse problem.

MEG is recorded by relatively large coils in a variety of configurations (magnetometers, axial gradiometers, or planar gradiometers) in sensor space that are coupled with superconducting quantum interference devices (SQUIDs) to detect the magnetic field. Most MEG software will automatically and implicitly handle the integration of magnetic fields passing through these coils. The primary requirement for the sensor model is the accurate registration of the patient's scalp to the MEG helmet (14).

Solving the forward problem adequately requires adequate knowledge of the patient's head geometry. In epilepsy, a patient's recent MRI acquired with an epilepsy protocol that includes a sequence showing detailed cerebral anatomy (e.g., SPGR, BRAVO, MPRAGE, MULTI-ECHO) with 1 mm thickness or less, skin to skin, is used as the basis for the head model. Assumptions about the head model is where MEG and EEG have their greatest differences. Since external magnetic fields are less affected by tissue conductivity, a MEG head model represented as a single compartment sphere fitted to the inner skull surface, or as a tessellation of just the inner skull surface is generally adequate (15). A more sophisticated head model would first tessellate the inner skull, outer skull, and scalp as mesh of interconnected triangles, which has a much more realistic appearance than simple spheres. Solving, however, the electromagnetic fields on these triangles requires a more complicated mathematical approach and software, known as the Boundary Element Method (BEM). A study of MEG in epilepsy found no differences between three spherical shells and BEM models for single focal source localization (16). EEG, in contrast, is critically sensitive to the parameters of a multi-centric sphere or to the tessellation of the skull and scalp boundaries, requiring an accurate specification of skull and scalp thickness, and the conductivity values of the brain, skull, and scalp (17, 18).

This paper will primarily address source modeling of MEG data, while considering scalp EEG data and its temporal dynamics when it assists in the interpretation of MEG results. An example of the basics of data acquisition and minimum practice standards can be found in the ACMEGS's clinical practice guideline (5). Having described the head and sensor models that are registered to the patient, we next discuss the generation and interpretation of the primary neuronal current.

Conceptual and Practical Aspects of Equivalent Current Dipole (ECD) Modeling

MEG is a non-invasive measure of neural activity, and it is widely-assumed that this activity arises from the columnar organization of cortical gray matter. Because of the inherent distance from outside the scalp to the cortex, these models are of a macro scale, such that the term "primary current" summarizes all of the fine micro-scale features of intracellular sources, sinks, induced currents, and transmembrane currents into a single conceptual primary current that traverses up and down the cortical column (19).

Basic cortical modeling assumptions of an evoked response suggest that MEG data represent the summed post-synaptic potentials (PSP) of approximately one million pyramidal neurons (6). For an evoked response, this resultant PSP current represents approximately 10 μA flowing along an effective cortical depth of 2 mm. Accordingly, the primary current is modeled as a "current dipole" of 20 μA/mm, which is equivalently and more generally expressed as 20 nano-ampere-meters (nAm). In contrast, an epileptic spike is 5–25 times stronger, about 100 to 500 nAm, which would require a larger number of pyramidal cells. The constant value of maximum dipole moment density across mammalian species ranges from 1 to 2 nAm/mm^2 (referred to here as Okada's Constant of 1 nAm/mm^2) (20); therefore, we can reasonably infer that MEG measures the activity of a relatively large "patch" of cortex.

Using this physiologic interpretation of the primary current, we can propose that the equivalent current dipole (ECD) is a simple, but plausible model for it. The ECD model represents both a source location and orientation, the latter expressing the direction of current flow (**Figure 1A**). In particular, the single equivalent current dipole (sECD) models the data as if it is arising from a single spot on the cortex. Six parameters define the sECD: 1) x, y, z of location, 2) azimuth and elevation orientation, and 3) dipolar strength. ACMEGS clinical practice guideline (CPG) advised that clinically relevant dipoles should have current strength between 50 and 500 nAm (21). Additional general approach to determine whether this model is indeed appropriate for measured data will be discussed later in this review.

Selection of Discharges and Model Worthiness

The selection of MEG discharges for modeling is a multi-faceted approach, involving three fundamental components: 1) waveform morphology, 2) corresponding magnetic field, and 3) anatomical localization. One approach is to first determine that a waveform is epileptiform, i.e., spike like, followed by confirming that its field is appropriately dipolar, and finally ensuring that the dipole solution is localized near an appropriately oriented cortex (**Figure 2**). However, these three concepts have many finer points, which will be covered in this section. The criteria for general acceptance of individual dipoles, commonly termed "fitting," will be discussed in a separate segment.

By standard consensus, typical waveform morphologies that favor ECD modeling are those that fit the definition of traditional spikes and sharp waves (21). It has been found that MEG spikes have a tendency to have a shorter duration and sharper morphology than simultaneously recorded EEG waveforms (22). MEG spikes had a duration in range of 27–120 ms when correlated with simultaneous intracranial recording (23). However, in the same way that focal slowing in EEG may reflect underlying epileptic activity (24), MEG signals are subjected to noise which can decrease visibility of epileptic waveform and its magnetic isofield contour map. For waveforms that are potentially epileptiform but not suitable for individual modeling due to small peak magnitude, signal averaging is a method that increases the signal to noise ratio (SNR) resulting in increased visibility (21, 25) (**Figure 3**). Although methods can differ across laboratories, the authors average only waveforms with similar magnetic isofield locations and morphology, and similar electromagnetic field patterns. This prevents dipole mislocalization if multiple sources are present, and avoids signal cancellation that can occur especially with intra-sulcal sources. The disadvantage of averaging is that it can be complex, and require experience.

An important practice to follow in averaging is consistency of waveform selection. In order to increase the SNR of a spike type accurately, selection of the averaging trigger point must be constant, such as the waveform's peak or a given point on its rising phase. The number of waveforms required for optimal averaging is patient dependent. A study in one patient, which included analysis of MEG averaging, showed that signal-to-noise of epileptic activity does not increase in the same way as an evoked response, but still exhibited a significant increase with averaging, and noise bias was resolved after averaging of 10 spikes (26).

After a waveform is selected, its field pattern must be evaluated prior to modeling. Important points to consider are the number of polarities, distance between extremas, and the spatio-temporal progression. A single focal source best suited for sECD modeling should produce one distinct dipolar field (**Figure 1B**). If a source shows multiple polarities, one can attempt to identify an early or dominant magnetic field that is consistently present, or consider other methods such as multiple ECDs or extended source modeling methods. It must be noted that basal sources close to the edge of sensor array can be less conspicuous. Extremas in close proximity would also suggest that the source is close to the sensors.

Spatio-temporal progression of a magnetic field during a waveform's rise to peak must also be evaluated (21). A stable source would exhibit a near-constant field pattern throughout its time course from rise to peak, typically with increasing field strength. The modeling of these sources at the peak is comparatively reliable, and signal peaks are often selected by some practitioners for ease of averaging. However, there are some signals that exhibit rotation and progression from rise to peak, which suggests a propagating pattern (**Figure 4**).

Finally, localization is one of the critical elements of a dipole's "model worthiness" (21). Recent observations have concluded that dipoles localized to peri-Sylvian, supramarginal, and peri-Rolandic regions frequently represent benign MEG variants (27). Epileptic semiology, imaging data, corresponding EEG findings, and overall MEG localization need to be considered for the interpretation of dipoles localized to these regions. Clinical interpretation though integration of multiple data can be complex, and is further detailed in the latter part of this review.

General Approach to Acceptance and Interpretation of Individual Dipoles

MEG software programs can always "fit" dipoles to the data at any particular time; however, the fit will generally be poor or unacceptable by statistical standards. The universal three questions asked of any fitting routine for a given source model are: 1) is the model in error, 2) are the parameters significant,

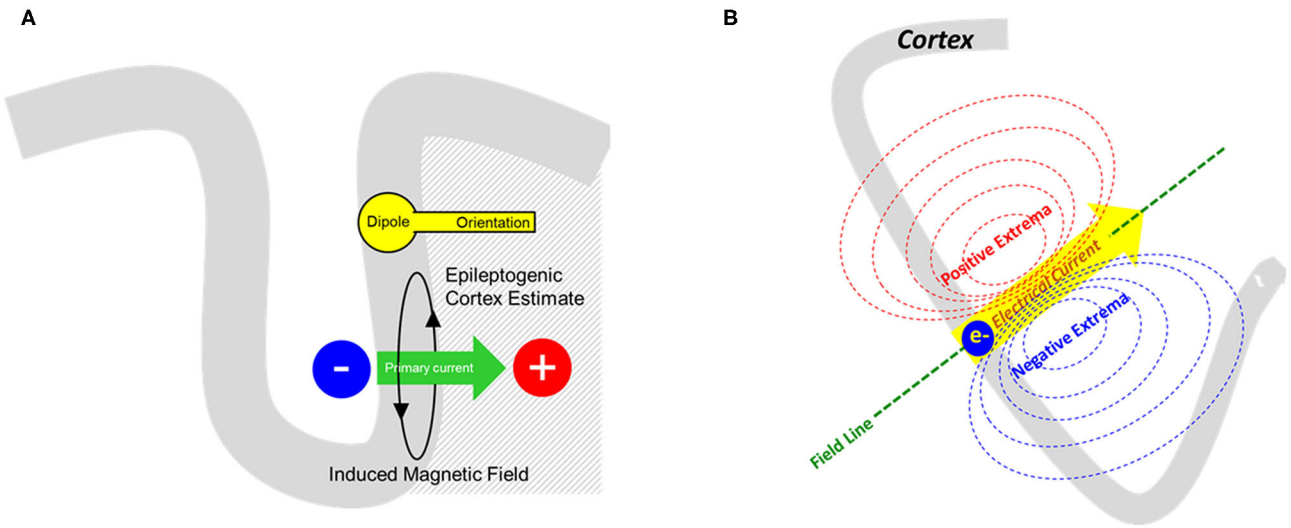

FIGURE 1 | (A) From the measured magnetic field, an equivalent current dipole model can solve the inverse problem and provide a representation of primary current as shown here. The cortical source is represented by rounded dipole (a.k.a. "head") whereas the direction of primary current flow (green arrow) is represented by the dipole orientation (a.k.a. "vector" or "tail"). **(B)** Schematic representation of a dipolar magnetic field pattern produced from a single electrical current source. The distance between the extremas would also signify the depth of the source in respect to the sensor.

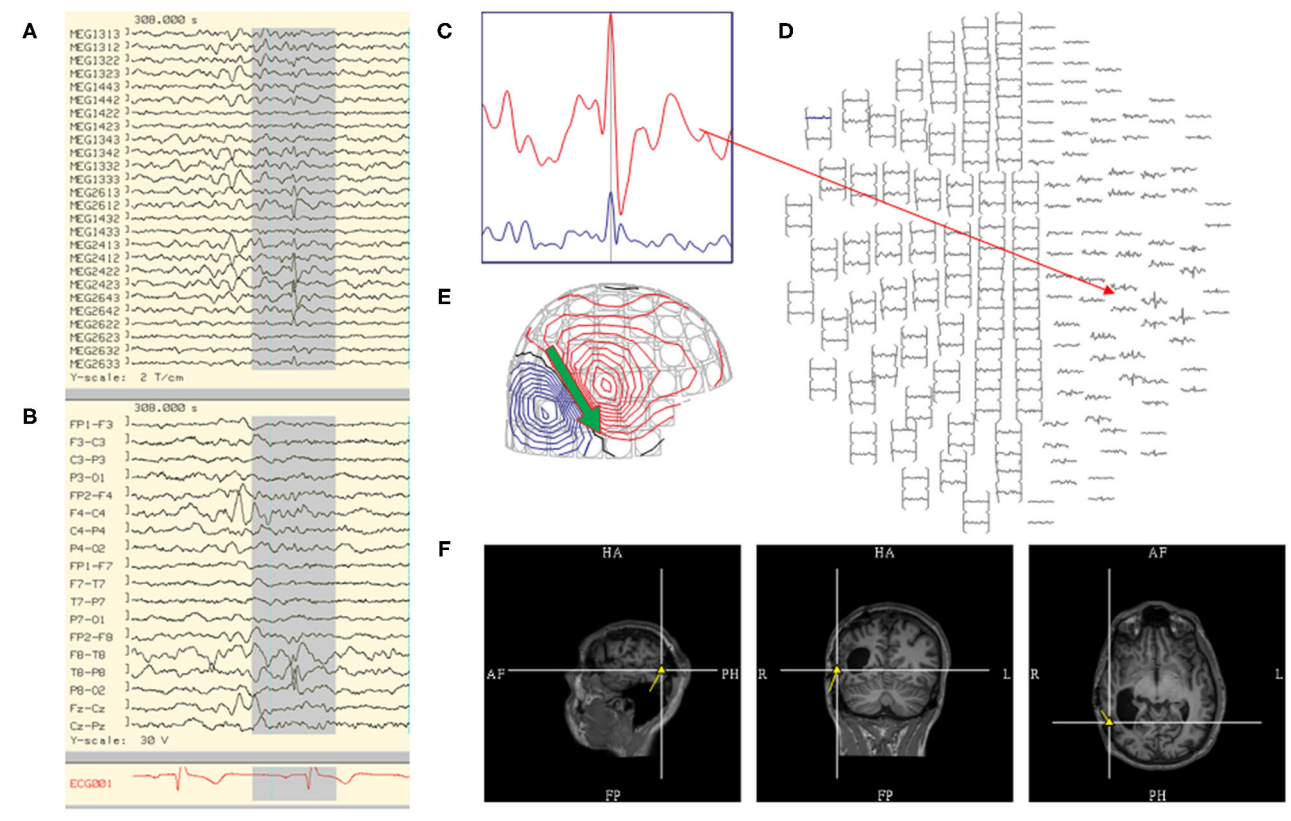

FIGURE 2 | Steps in the analysis of an MEG spike include reviewing: **(A)** MEG tracing, **(B)** EEG tracing, **(C)** MEG signal selection from **(D)** magnetic isofield map, **(E)** dipolar electro-magnetic field pattern where the primary current is represented by an arrow (green), and **(F)** localization through sECD method yielding a dipole model (yellow) that is coregistered to MRI.

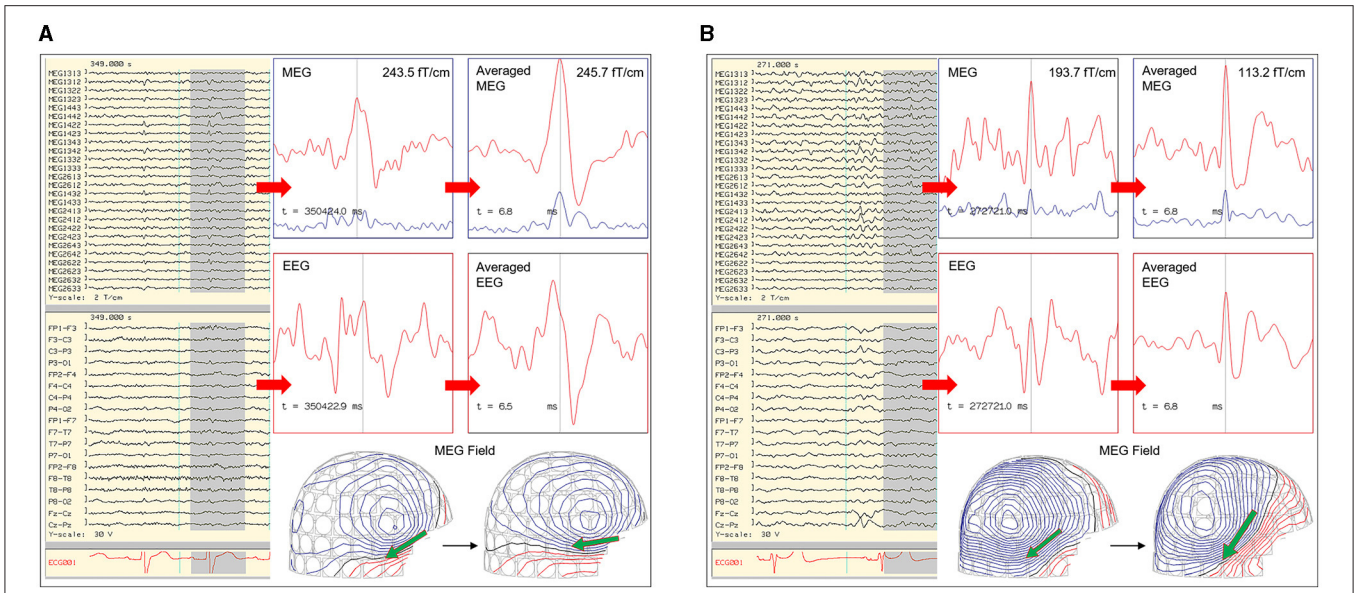

FIGURE 3 | Utilization of averaging to increase signal to noise for signal detection and modeling. **(A)** MEG-EEG recording that showed MEG signals (channel MEG1442, MEG2612) with a right temporal isofield that lacked an epileptiform morphology and EEG correlate. The averaged MEG signals showed a better epileptiform morphology and EEG correlate. **(B)** MEG-EEG recording that showed a small right hemispheric EEG signal with a comparatively less visible MEG correlate, having a right temporal isofield. Averaged EEG and MEG signals show an improved epileptiform morphology.

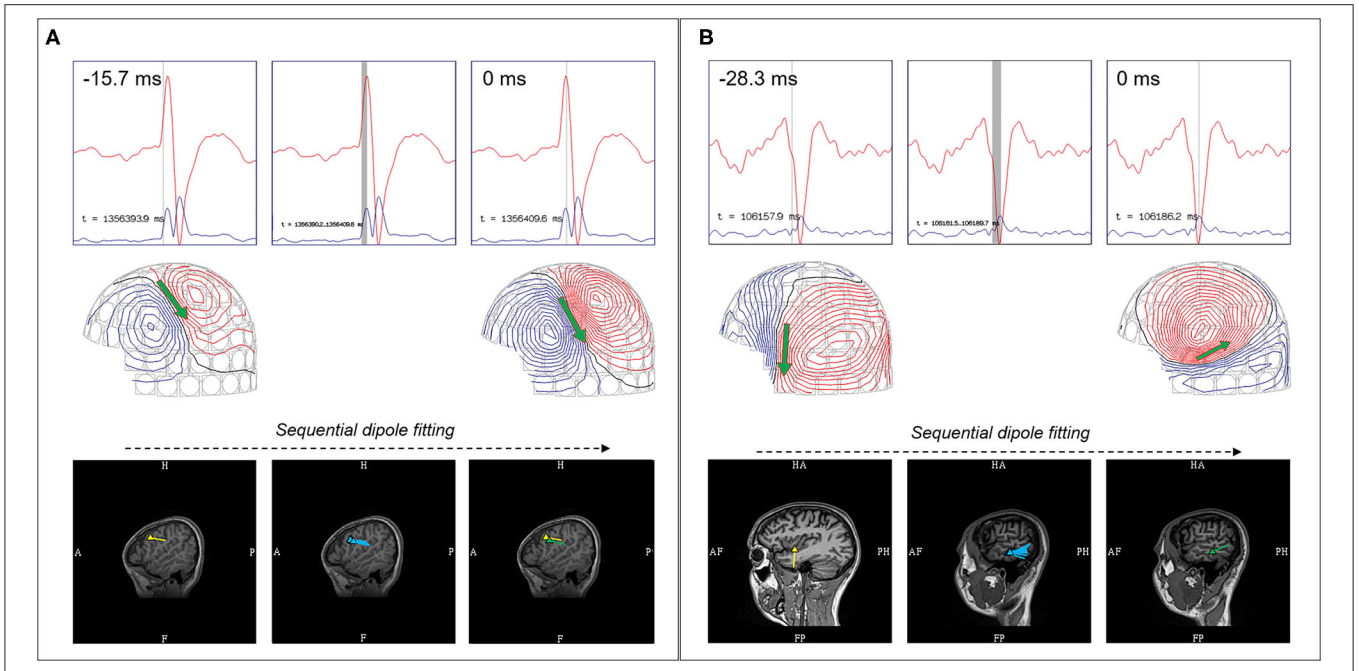

FIGURE 4 | Comparison between stable and propagating sources. **(A)** Stable source with earliest localizing dipole (yellow), sequential dipoles (blue), and dipole at MEG peak (green), showed similar sublobar localization. **(B)** Propagating sources showed earliest localizing dipole (yellow) over the left mid-superior temporal gyrus, but sequential dipoles (blue) and dipole at MEG peak (green) showed propagation to the posterior middle temporal gyrus.

and 3) are the parameters interpretable. The sECD model meets the third criterion readily, since the sECD represents a relatively focal patch of cortical activity, which makes it a workhorse for source modeling in clinical evaluations for epilepsy surgery. In contrast, models that comprise many overlapping ECDs or more distributed source models are comparatively lacking in this

third point, as they can create many alternate interpretations or possibilities for the clinician. Accordingly, the sECD model is the most commonly used and comprehensively validated technique, and gained acceptance as the standard method for clinical MEG performed for presurgical evaluation of epilepsy by the ACMEGS (21).

The test for error of a sECD model answers the first critical question. Crucial to this test is to establish the normal "noise" or "baseline" of the data. The methods of baseline noise measurement can differ across laboratories. In our laboratories, the noise calculation is achieved using the variance and cross-covariance of each channel of data during a baseline period before the spike. The residual is then normalized by this baseline to calculate "goodness of fit" (GOF), which is a test for error that is accomplished through several means and often reported as "normalized variance not explained." The goodness of fit of greater than 70% is a frequently used parameter of acceptance (5). An alternative, and probably better measure of error, is the "chi-square" test which sums the normalized squared error into a single chi-square statistic (28). If the resultant statistic is too large relative to the number of channels, also known as the degrees of freedom, the model is considered in error and rejected.

If the model is not rejected due to error, the second question is whether or not it is "significant." Our institutional preference is to confirm the confidence volume (CV), or volume of error, of the dipole localization (29). The CV is the region that encompasses the uncertainty of dipole location due to noise that was established at baseline. If the SNR is low, either because the source is weak or deeply located, the noise would dominate the location estimate resulting in a large CV, which would reject the model as "not significant." There can also be unacceptable CV's at higher SNR, if the selected region of interest from the sensor array is too small, or if the sECD model is too close to the edge of the sensor array. Therefore, a small CV indicates that 1) the SNR of the ECD is adequate, 2) enough sensors were used for source modeling, and 3) the model was not too close to the edge of the recording array.

It must again be emphasized that a source model must pass both the initial test for error (chi-square; GOF), and subsequent one for significance (CV; SNR). Once accomplished, a sECD can be interpreted as a model of abnormal epileptic activity. The sECD models shown in this paper were accepted based upon the following fit parameters: "reduced chi-square" less than 2 (i.e., the chi-square statistic is not greater than twice the number of channels), GOF $\geq$ 80% (defined as 100% minus the normalized variance not explained), CV less than 1,000 mm^3, and dipole strength between 100 and 500 nAm.

Clinical Integration of Dipoles (MSI) and Conventional EEG

It is accepted that MEG and EEG are complementary, each providing a different perspective. More importantly, in MEG performed for epilepsy surgery evaluation, simultaneous MEG and EEG recordings are recommended as a clinical standard (21, 30, 31). We would further endorse this to the extent that simultaneous MEG and EEG recordings are, in fact, required for MEG performed for epilepsy surgery. The importance of EEG recording in MSI are to 1) exclude known benign-epileptiform EEG variants that can present in MEG, 2) evaluate significance of dipoles localized to regions associated with benign MEG-unique variants, 3) increase detection of MEG waveforms with low SNR, 4) determine source localization credibility, and 5) distinguish EEG unique spike types.

It has been shown that benign epileptiform EEG variants such as sleep transients can be presented in MEG, and simultaneous EEG recording can prevent these waveforms from being modeled and erroneous reported as pathologic. Benign MEG-unique variants were also briefly alluded to during the discussion of model worthiness and will continued to be discussed in relation to illustrated anatomical contexts. In summary, this is a term describing MEG sharps or spikes without epileptiform EEG correlate that are localized to specific cortical regions, and are unlikely to have pathologic significance in most patients (27, 30). However, if these MEG spikes were shown to have epileptiform EEG correlate, these spikes would be considered pathologic and their models would be reported. Without concurrent EEG recording, the interpretation of these MEG dipoles would be limited. From these standpoints, EEG recording is necessary for accurate dipole interpretation for epilepsy surgery.

EEG recording also aids the detection of less visible MEG signals. MEG is attuned to sources localized to deep sulci, fissures, and cortical planes with tangential fields, but has less detection capability in sources that are radially oriented. However, predominant radial sources can still have some smaller tangential component, and EEG can be utilized as a detection tool. In this context, the MEG signals from these sources can be detected through averaging using the EEG as the trigger (**Figure 3B**).

The EEG is also used to support an MSI result. There are two important points to consider for comparative MEG and EEG analysis, which are 1) MEG-EEG peak latency differences, and 2) congruent source orientation. The latencies between MEG and EEG peaks are useful in determining whether MSI is likely to represent the source or propagation pattern. A MEG peak that is significantly delayed compared to the EEG peak may suggest that the MEG peak is potentially a propagated activity. An MEG-EEG peak latency difference of greater than 10 ms is considered significant in our laboratories. However, it should also be noted that a study of frontotemporal lobe spikes demonstrated that the observed propagation of peak activity can be more rapid in EEG, whereas propagation of the MEG peak had a velocity similar to the intracranial EEG recording (32). The congruence of source orientation has to also be considered, and this can be preliminarily determined from the EEG field map (**Figure 5**).

MEG and EEG unique discharges can occur across studies (33, 34). Such EEG waveforms should always be averaged to assess underlying MEG signals. If no MEG correlate is found, the presence of these EEG-unique discharges must be noted, as they can represent different sources. Furthermore, it is clinically useful and important to confirm that typical epileptiform EEG discharges of concern were captured during the MEG study.

Comprehensive MEG interpretation must take into consideration the EEG correlate, particularly if the MEG

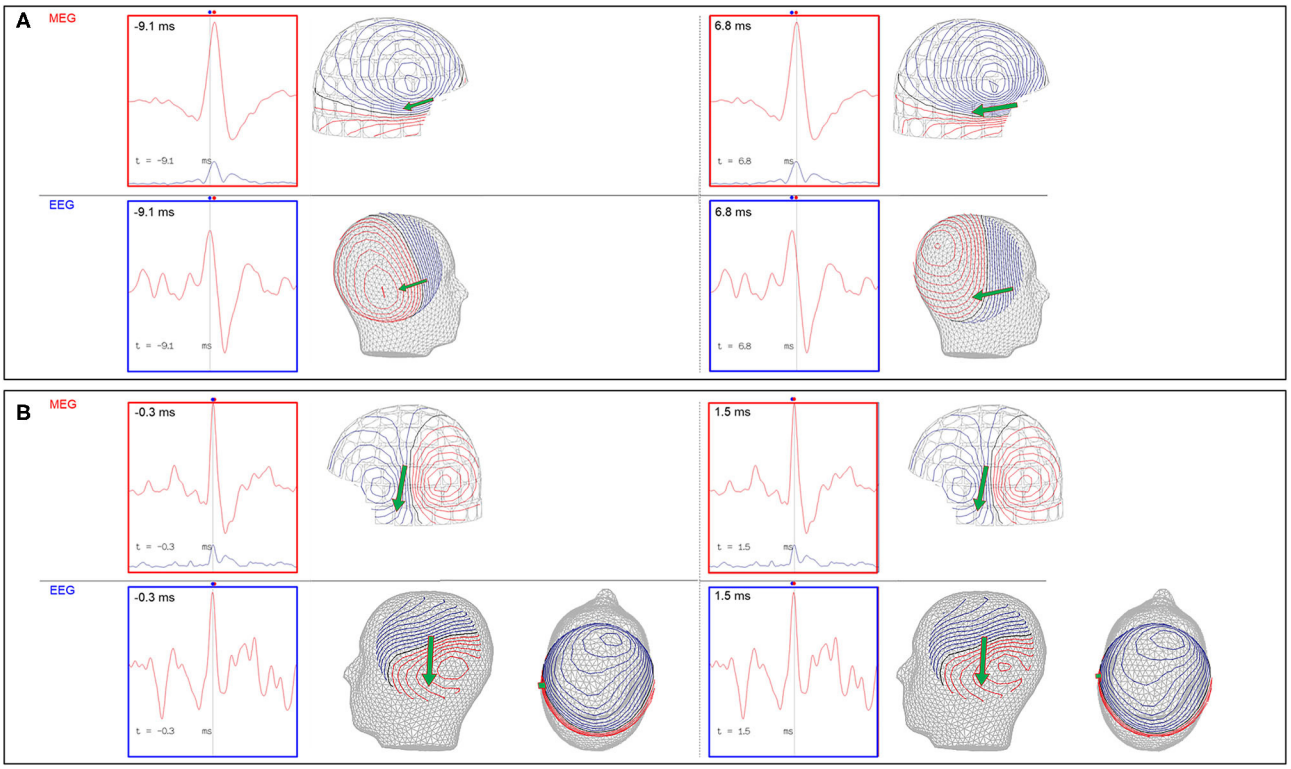

FIGURE 5 | Importance of MEG-EEG integrative analysis (red dots: time of MEG peaks; blue dots: time of EEG peaks; green arrow: MEG source localization). **(A)** Right temporal MEG spike peak lags that of the EEG (15.9 ms). Although the dipoles are congruent, the earlier EEG spike with an anterior field pattern raises the possibility of a preceding anterior source. **(B)** Left temporal MEG spike without a significant MEG-EEG peak latency difference. Although this patient's 22-channel scalp EEG tracing showed bifrontal maximal negativity, this EEG field pattern can be explained by both the MEG and EEG dipole sources.

peaks are significantly delayed compared to EEG, if the MEG and EEG field patterns are discordant, and when there are EEG-unique sources without an MEG correlate even after averaging. Under these conditions, the source representation through MSI would be incomplete, and EEG source imaging (ESI) would be beneficial (30). Although the current version of the ACEMGS clinical practice guideline (21) does not indicate an inclusion of ESI with MSI as a standard procedure, this may change in the next iteration (35).

Reflection on Integrated Use of MSI and ESI

ESI is a source localization technique using the EEG signal, which adds an additional dimension to results obtained from MSI. Specifically, it provides confirmation of MEG source configuration, adds the source's radial component, assists in evaluation of sources where the EEG significantly precedes MEG and where MEG may represent a propagated activity, and localizes EEG-unique radial sources. Some physiologic limiting factors exist with ESI, since an EEG spike require a larger cortical activation area (36), and the localization results are typically deeper than MEG (30). ESI also requires an increased number of electrodes than that typically used to increase source localization accuracy, such as at least 32 channels (37). From forward modeling using a human skull phantom and comparing 122 channel MEG to 64 channel EEG recording, the averaged localization error from EEG (BEM: 7.63 mm; spherical 8 mm) is greater than MEG (BEM 3.4 mm; spherical 4.14 mm) (38).

Despite some localizing limitations, there is utility to ESI given that it complements MSI, and EEG data is readily available. However, implementation of ESI is limited by the complexity of its volume conductor model (36, 39). In contrast to a magnetic field, electrical activity traversing from the cortex to the skull passes through spaces with different conductivity values. Because of this, a conductor model for ESI is more complicated, and typically includes at least 3 layers comprising of brain, skull, and skin. There are models with even a greater number of compartments, and localization depends on conductivity values and ratios (17, 18).

The strengths and weaknesses of ESI in clinical practice has been reviewed (36, 39). Aside from certain conditions that were described here, the authors have noted the ability of ESI to assist localization of temporal and basal sources, whereas it has limitations in frontal lobe epilepsy. These two reviews supplement the original article on the combination of MEG and EEG source modeling (30). It must be emphasized that the added benefit of ESI should always be considered in patients possessing EEG spikes that precede MEG spikes and EEG-unique spike types. However, as there is no current national or international

practice guideline for ESI (35), its usage remains complementary to MSI (5) and conventional EEG analysis.

Dipole Clusters: Definition, Types, Clinical Interpretation, and Significance

A "cluster" is a frequently used term in sECD modeling to describe a pattern of distribution or grouping of individual spike dipoles that are localized closely together within a volume. Although this is a commonly used term in clinical MEG, it currently does not have a standard definition. There are two variables that would define a cluster, first is the number of dipoles, and second is the volume which it occupies. Different author groups have proposed and used varying numbers, but the number of at least five dipoles used in some publications (11, 40) is probably conservative and falls in line with the ACMEGS recommendation that a minimum number of 5 model worthy MEG epileptiform discharges should be present in a study to be clinically sufficient for interpretation (5). The volume of involvement also differs in the literature, as different criteria reflecting either anatomical regions (11) or mathematical measurements (41) have been used. Since there is no standard definition, epileptologists typically refer to dipoles that are localized closely together as "a cluster," and those that are more loosely dispersed as "a scatter" or simply scattered. It is likely that this definition gap will be closed in the future as the work on harmonizing clinical MEG practice internationally is advancing (35) (**Figure 6**).

Dipole clusters can provide insight into the nature of underlying pathology, and guide subsequent surgical planning. Three factors that should be considered when approaching dipole clusters are 1) the number of clusters and their distribution, 2) density of dipoles within a given cluster and their orientation uniformity, and 3) presence of a radiologic correlation. Patients with a single dipole cluster (42–45) and those whose dipoles are confined to the same lobe (46) have been found to have more favorable post-operative outcomes. This is additionally supported by the finding that a monofocal cluster is more likely to overlap with the ictal onset zone, while multifocal clusters may reflect a widespread epileptic network (42). Lower dipole density may suggest a regional hypothesis, as evidenced by the finding that the cluster in Type 1 focal cortical dysplasia, commonly associated with lobar atrophy (47, 48), are looser or scattered in comparison to Type 2 and 3 (40), and those with dense clusters have better post-operative seizure freedom outcome (49). Dysplastic tissues are associated with less spike-variance (50), and inconsistent dipole orientations can signify underlying widespread epileptic network (51). These understandings are further substantiated by the recent study which associated monofocal clusters and dense dipole clusters with uniform orientation with a better operative outcome (11). A very recent study in MRI-negative pediatric patients, using inter-dipole distance of 15 mm to define "clusterness," also showed that dipoles that clustered were closer to seizure onset zone (16.2 mm) than those that were scattered (30.4 mm) (52).

Radiologic correlation is also an important factor in the integration of dipole clusters. The presence of a contributory lesion close to a MEG cluster would supports its epileptogenicity (53). The role of MEG also extends to the identification of a probable contributory lesion in MRIs with multiple lesions, or in lesions of indeterminate significance (54). In MRI-negative epilepsy, the presence of an MEG cluster should prompt a radiologic review, especially since MRI abnormalities may not be readily appreciated from initial interpretations (55–57). It should be noted that an MEG can identify epileptogenic lesions that remained unidentified under conventional three Tesla MRI (57, 58). The size of the dipole cluster compared to the size of the imaged lesion is also variable. In a study of focal cortical dysplasia with 1.5T MRI that used a correlation coefficient of greater than 98% and a CV limit of 5 cm^3 as an acceptance parameter, more than half of the dipole clusters were larger than the lesion ($n = 11/21$); 33% were similar to the lesion ($n = 7/21$); and 14% were smaller than the lesion ($n = 3/21$) (41). A non-Type 2 cortical dysplasia was also more likely to have a cluster larger than the MRI lesion as compared to Type 2 (70 vs. 36%) (41).

Aside from the fact that underlying pathology affects the size of a dipole cluster, evidence also exists that modeling parameters can also affect dipole density. SNR has an inverse relationship with CV (59), and it has been shown that a cluster would become more dispersed with incremental noise introduction (60). As such, localization of dipoles with large CV or modeling sources with low SNR can result in loose clusters or scattered dipoles. Clinical MEG practitioners must be aware of these issues and their potentially misleading effect on the incorporation of the MEG results in an implantation scheme and resection plan.

The finding of a monofocal and dense MEG dipole cluster with uniform orientation and a corresponding MRI lesion would nicely satisfy a restricted focal hypothesis. In practice, supplemental electrocorticography may still be required to establish the full extent of the irritative zone (61). The presence of scattered dipoles, multifocal clusters, or loose clusters with variable dipole orientation and the absence of a corresponding lesion, are all factors that support a regional or network hypothesis. This is especially when these loose clusters or scattered dipoles are observed under fit parameters that utilized small CV limits or higher SNR values. However, even in these cases MEG remains useful as it can provide an approximate anatomical location of the involved regions from which epileptologists can formulate an epileptic network prior to invasive recording.

ECD Modeling of Ictal Onset

Ictal events can occur during MEG studies, and a recent review reported seizures during MEG in 7–24% of patients (62). Ictal MEG provides useful source information at the time of seizure onset, in addition to that of interictal spikes. However, in addition to the modeling challenges and necessary cautions, limitations on ictal data interpretation can occur if the signal is of low amplitude or there is excessive myogenic artifact.

Currently, there is no consensus on how to model the MEG of ictal onset. We have identified 14 articles on ictal MEG to

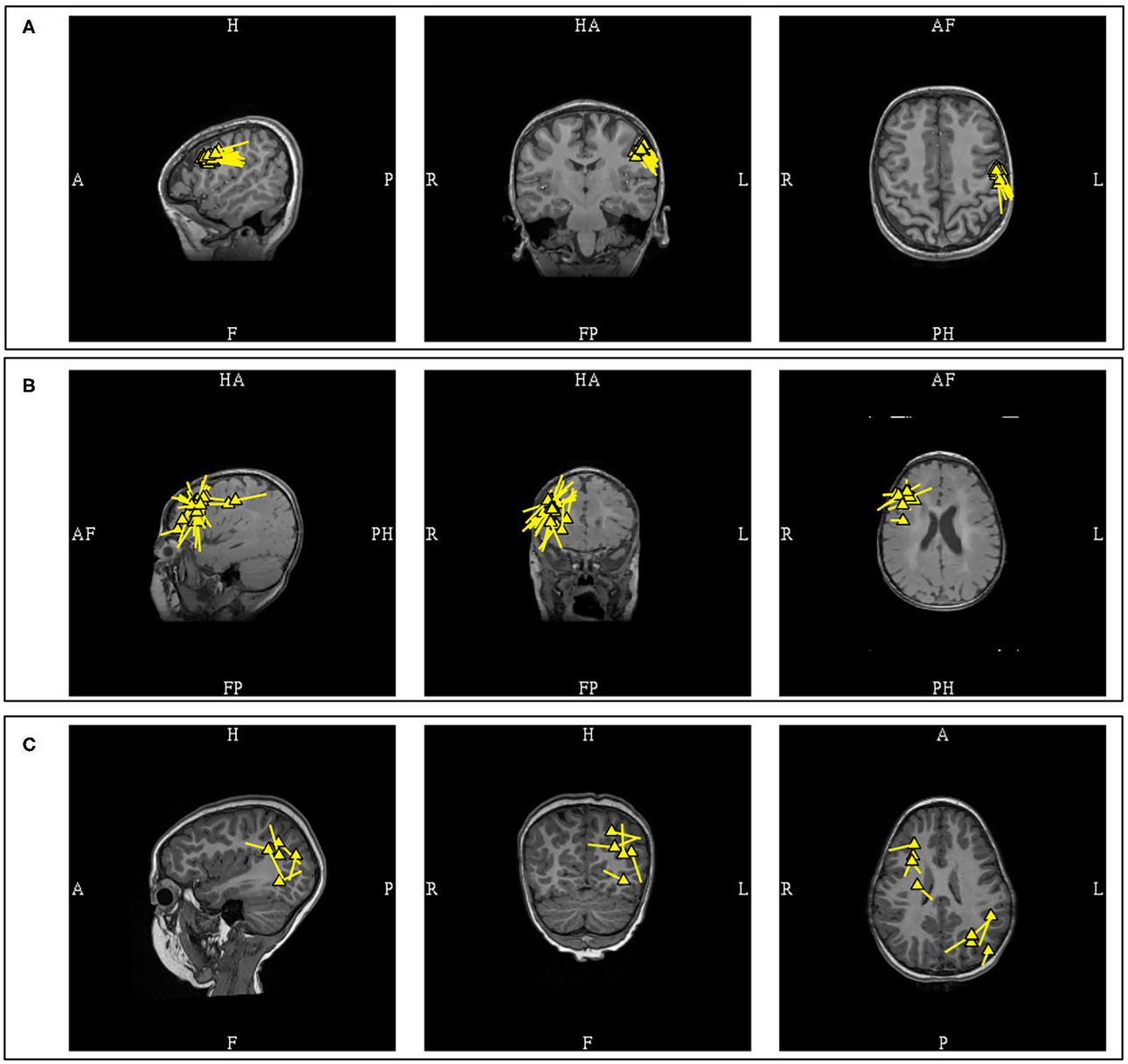

FIGURE 6 | MEG-MRI coregistration summary demonstrating varied cluster patterns. **(A)** Monofocal tight cluster with uniform vector orientation localized to the left pre-central region, with dipoles posteriorly oriented. **(B)** Monofocal loose cluster with variable vector orientation localized to the right dorsolateral frontal region, with additional posterior scattered dipoles. **(C)** Multifocal and scattered dipoles over the right fontal and left parieto-occipital regions.

compare their approaches, including modeling methods and localization findings. ECD modeling was used utilized in 8 publications (63–70), distributed source modeling in 4 articles (68–72), beamformers analysis in 3 studies (69, 72, 73), multiple signal classification (MUSIC) in 1 report (69), and maximum entropy of mean (MEM) in 1 study (74). Some authors used more than one modeling method (68, 69, 72). In one report the source localization method could not be determined (75). From these data, we found that ECD modeling is still a widely used method for MEG ictal onset localization.

Despite this, we have also found that ECD modeling methodologies also differ among the groups. There appear to be two basic approaches: 1) modeling individual early ictal waveforms (5 groups) (63–67), and 2) modeling averaged early discharges (2 groups) (68, 70). Modeling methods also varied between single dipole fit, sequential dipole fit, or multiple dipoles fitting. One study that utilized ECD modeling did not detail its procedure (69). Although ECD modeling techniques showed differences across the publications, the resultant outcome of all appears to be favorable. One older study advocated that an

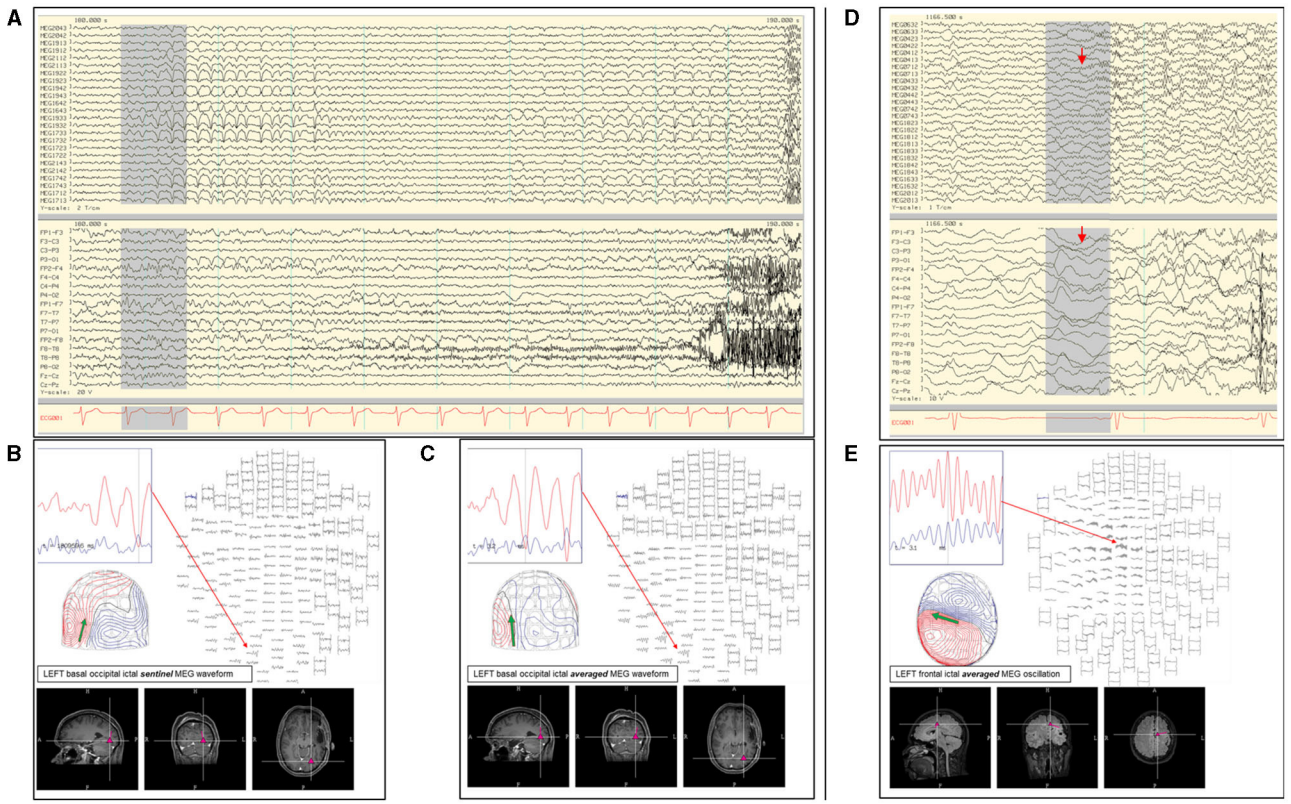

FIGURE 7 | (A) Ictal MEG-EEG recording of a patient showing MEG onset at the left occipital channels (MEG1922; MEG1942; MEG1933; MEG1733) with corresponding left parieto-occipital EEG changes. Single ECD analysis of **(B)** sentinel MEG sharp wave and **(C)** averaged MEG rhythmic activity showed consistent localization at the left inferior occipital lobe. **(D)** Ictal MEG of a patient with broad left hemispheric encephalomalacia who lacked interictal MEG and EEG discharges, with ictal EEG onset showed oscillating activity over the left mid-parasagittal region and MEG channels showing a corresponding sustained faster frequency (MEG0712). **(E)** Early oscillating signals during the initial 120 ms were averaged showing a dipolar field suitable for modeling, which was localized to the left frontal region and used to guide electrocorticography.

ictal MEG as at least equivalent to invasive EEG in 5 out of 6 patients (64).

In our practice, we have adopted both the modeling of individual and averaged early ictal waveforms (**Figures 7A–C**). The isofield of the sentinel waveform is analyzed to determine its stability prior to modeling. In cases with multiple repetitive spiking, the source of each would be analyzed individually and chronologically. However, the modeling of sentinel spikes does have limitations, since ictal onset pattern may be low signal-to-noise fast activity, while later more visible ictal spikes are in fact propagated activities (21). Despite its high spatial resolution, sECD localization of the ictal origin depends on modeling of the earliest recognizable ictal MEG activity and not subsequent propagated activity (76). This is a factor to consider always when modeling ictal discharges, especially those from sources in the interhemispheric fissures that are prone to fast contralateral propagation. These propagated signals may be more visible which can result in false lateralization. Averaging of early ictal waveforms or oscillations can be a useful method for modeling of seizure onset, as it increases SNR and reduces dipole variance (**Figures 7D,E**). Bandpass filtering of 3–15 Hz for temporal seizures and 3–25 Hz for extratemporal seizures can be used to improve MEG and EEG ictal data with excessive noise or artifacts that significantly impair signal selection and source analysis.

Sometimes seizures cannot be analyzed by an ECD. In a study of 44 patients with ictal MEG, sECD modeling was successful in at least one seizure in 66% of the patients, but there were other seizures that could not be modeled in this way and required extended source models (63). This group suggested that a resection area guided by MNE has a stronger correlation with seizure freedom, and they advocated using extended-source localization as a primary method of ictal MEG analysis. In contrast, another study that implemented multiple methods [sECD, sLORETA, MUSIC, and SAM(g2)] reported no difference between localizations using sECD and extended source models (69). We view that magnetoencephalographers should also learn to use extended source modeling techniques, especially since ECD modeling of ictal onset may be unsuccessful or the result questionable. When in doubt, a magnetoencephalogrpher should compare the ECD model of ictal onset with the result obtained from another modeling method.

CLINICAL INTERPRETATION OF DIPOLES BASED ON ANATOMICAL LOCATION

Temporal Lobe Dipoles

The temporal lobe is a complex anatomical structure, with many surfaces and varied propagation patterns. Classification of temporal dipoles into those of anterior and posterior regions have been suggested (77). These can be further sub-classified into three groups: anterior temporal horizontal (ATH), anterior temporal vertical (ATV), and posterior temporal vertical (PTV), that correlate with temporal tip, anterior superior, and posterior superior temporal planes sources, respectively (77). The orientation of these dipoles are in reference to the cortical anatomy. The ATH and ATV dipoles are associated with anterior temporal sources (mesial, entorhinal, temporal tip), and some ATV can represent a later ATH propagation activity. The PTV dipoles are more commonly associated with lateral neocortical surface, superior temporal plane, temporal base, and structural lesions, but invasive recordings have shown that seizure onsets associated with PTV dipoles can also be unlocalized or mesial in origin. This anterior and posterior classification was later reaffirmed (78).

It was hypothesized that the source origins of ATH and ATV dipoles should lie within the resection boundary of standard temporal lobectomy (77). Surgical outcomes through this approach was later investigated in patients diagnosed with temporal lobe epilepsy (79). Using the central sulcus as the landmark, the patients were classified as anterior temporal group if there were greater than 70% of dipoles localized to the temporal lobe anterior to the central sulcus. In the absence of neocortical lesion, standard anterior temporal lobectomy in anterior temporal MEG group was associated with good outcome (100% Engel 1; $n = 5/5$). In contrast, the outcome in non-anterior MEG group were variable (67% Engel 1; $n = 4/6$), and presence of extratemporal dipoles were noted in some of these patients who continued to have seizures.

A study in patients with established mesial temporal lobe epilepsy found that the patient's MEG dipoles were localized to the anterior temporal region, without posterior or extra-temporal localization (80). Another study in mesial temporal lobe epilepsy also reported that the dipoles were localized to the anterior temporal lobe, with the majority of the dipoles being horizontal or mixed (81). This study also noted that non-concordant localizations were found with predominantly vertical dipoles suggesting propagated activity, but the presence of posterior temporal dipoles was not mentioned. Presence of temporoparietal MEG propagation in mesial temporal epilepsy has also been associated with continued seizures after epilepsy surgery (82). The initial separation of the temporal MEG dipoles into anterior and posterior divisions is a practical approach with surgical relevance, and the presence of predominantly anterior temporal dipoles is more convincingly suggestive of anterior or mesial temporal sources (**Figure 8**).

Posterior temporal dipoles are comparatively more variable and can be divided into three categories: 1) benign MEG-unique variant, 2) pathologic and lesional, and 3) pathologic but non-lesional. Benign MEG-unique variants can be observed in the posterior temporal region over the peri-Sylvian area, and dipoles localized here are typically benign especially if they are bilateral or have 180 degree opposing orientations (27). Suggestive features of epileptogenicity, aside from EEG correlation, may include unilaterality, uniform orientation, and clinical suspicion. For pathologic PTV dipoles, the presence of a corresponding lateral temporal lesion would suggests that these dipoles are likely from a lateral temporal source (78). However, additional possibilities need to be considered in non-lesional patients as PTV dipoles have also been observed in patients with seizures of mesial temporal (77) and operculo-insular onset (83). Similarly, we have also observed PTV dipoles that are unlikely to originate from lateral temporal lobe in our practice (**Figure 9**). Subdural EEG recordings in some patients with temporal epilepsy and PTV dipoles also reported widespread seizure onset involving both medial and lateral temporal contacts (78). Clinical context and experience is therefore needed to interpret dipoles localized to the posterior temporal region.

Frontal Lobe Dipoles

The frontal lobe is the most frequent location for MEG spikes in extratemporal epilepsies (84, 85), and for this lobe MEG has shown a better yield as a localizing test than EEG (86). Using easily identifiable anatomical fissure boundaries (Sylvian, interhemispheric, and Rolandic fissures), the frontal lobe can be separated into four anatomical surfaces: orbitofrontal (inferior), lateral, medial interhemispheric, and posterior peri-Rolandic (posterior) surfaces. The interhemispheric and peri-Rolandic sources of frontal origins will discussed in the later segment, but dipoles from these sources would typically exhibit orientation toward the frontal lobe (87, 88) (**Figures 10**, **11A**).

Orbitofrontal epilepsy can have variable electrographic and clinical findings, and the literature has demonstrated cases where MEG is a useful localizing tool (86, 89) even when other ancillary studies were negative (90). The data on MEG dipoles from this source is limited, but it is observed that MEG dipoles from this region are typically of basal frontal origin with upward tail orientation. Lateral orbitofrontal dipoles are oriented more medially and medial orbitofrontal dipoles more laterally. However, dipoles localized to the lateral orbitofrontal region should also raise the possibility of anterior mesial temporal sources, given its close proximity and common situations where mesial temporal discharges to propagate to the orbitofrontal cortex (91).

The lateral frontal surface comprises of the majority of the frontal cortical area, and MEG dipoles localizations to this region are variable. The interpretation of MEG dipoles in this location relies on cluster topology. A single, dense, and uniform cluster is exceedingly helpful in defining a focal area of interest in such a large anatomical region (11).

MEG has been shown to improve surgical outcome in frontal lobe epilepsies (44). Case series has shown that 90% of MEG dipoles in frontal lobe epilepsy are localized to within 3 cm of the lesion, but data also suggest that underlying pathology may play

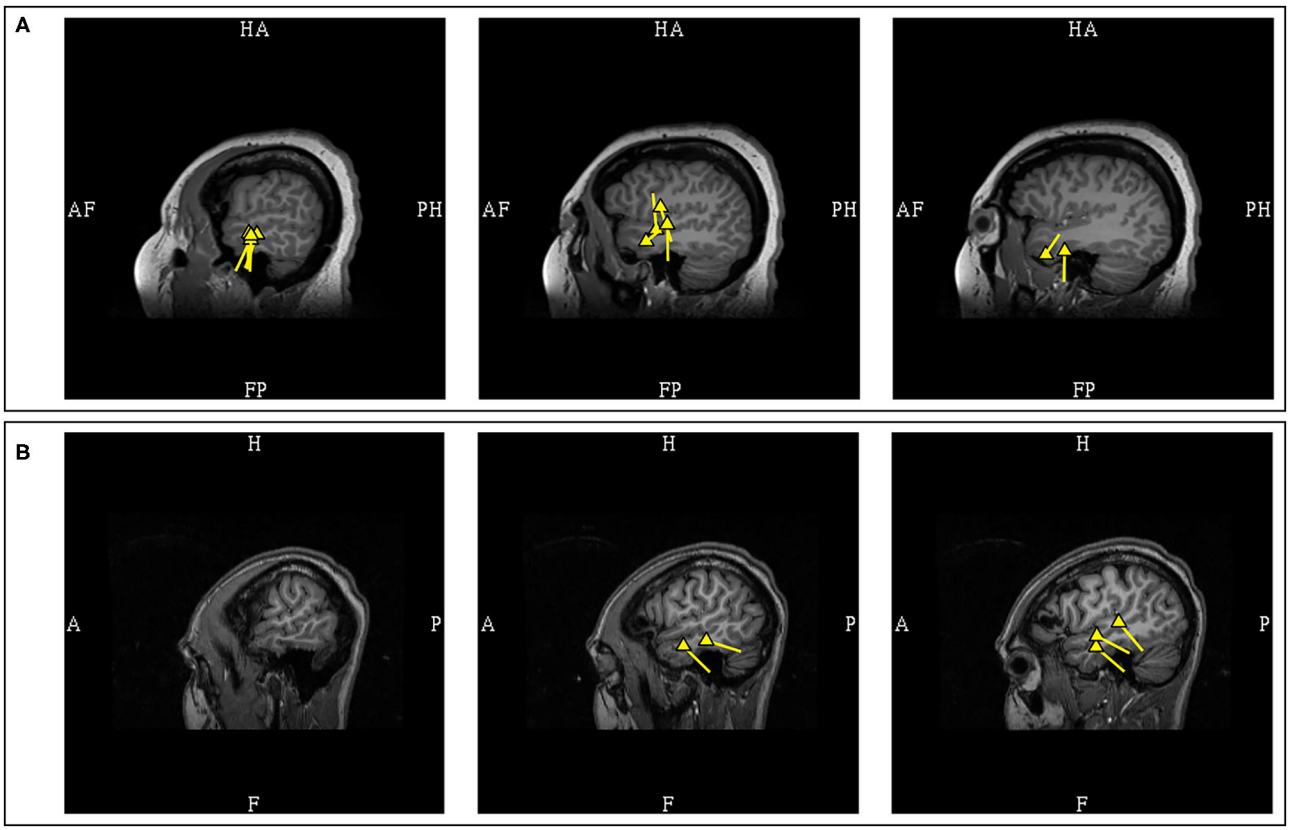

FIGURE 8 | MEG-MRI coregistration summary in two patients with temporal dipoles. **(A)** Frequent anterior temporal dipoles were suggestive of anterior temporal source. Imaging review revealed temporal tip encephalocele. **(B)** Temporal dipoles broadly distributed over anterior and posterior temporal region provides comparatively limited suggestion of seizure onset in the absence of a lateral temporal lesion.

a role in the proximity of dipole to lesion (43). However, it must be emphasized that frontal MEG findings can be influenced by the depth of the interhemispheric sources (92), rapid propagation time (93), and the mesial temporal-orbitofrontal connection (91). Consideration of potential propagated activity should be always be factored in the interpretation of MEG results in non-lesional patients.

Posterior Cortex (Parietal and Occipital Lobes) Dipoles

MEG is also useful in the localization of posterior cortex epilepsies (4, 94), including those patients with electro-radiographic discordance (95) or false-lateralizing EEG findings (96). Posterior cortex sources are less common, and represent only approximately five percent of MEG findings in patients with refractory epilepsies in a large study (85), which limits the available literature. A case series of MEG in posterior cortex epilepsies, using linearly constrained minimum variance (LCMV) and MUSIC algorithms, showed accurate detection of irritative and epileptogenic zones with MEG (97). Negative results tended to be from medial and basal sources, which is similar to a study that reported less MEG sensitivity in other anterior basal regions (98). Localization of these basal sources were still feasible in some patients.

Careful consideration is required in the analysis of posterior cortex discharges, given that somatosensory, posterior peri-Sylvian, supramarginal (27) and medial occipital (30, 99) cortices are sites of common benign MEG variants. Interpretation of MEG-unique dipoles localized to these regions would require additional ancillary features to determine their significance, and an EEG correlate spike is an important distinguishing feature. Similar to posterior temporal dipoles, bilateral localization, 180 degree opposing orientations, and absence of an EEG correlate are features that would suggest that these discharges are probably benign (27). Clinical context will be required to determine their significance (**Figure 12**).

Posterior cortex epilepsies have increased representation in pediatric population in the form of benign occipital epilepsy. Although typically self-limited, there are case reports of patients who continued to have intractable epilepsy (100). Given that MEG is typically performed as a part of pre-surgical evaluation, recognizing MEG features of benign focal epileptic syndrome in contrast to a potentially resective etiology is important in pediatric patients. Benign occipital epilepsy of childhood (101), like benign Rolandic epilepsy (87), has sulcal localizations. The dipoles are frequently observed in the parietooccipital

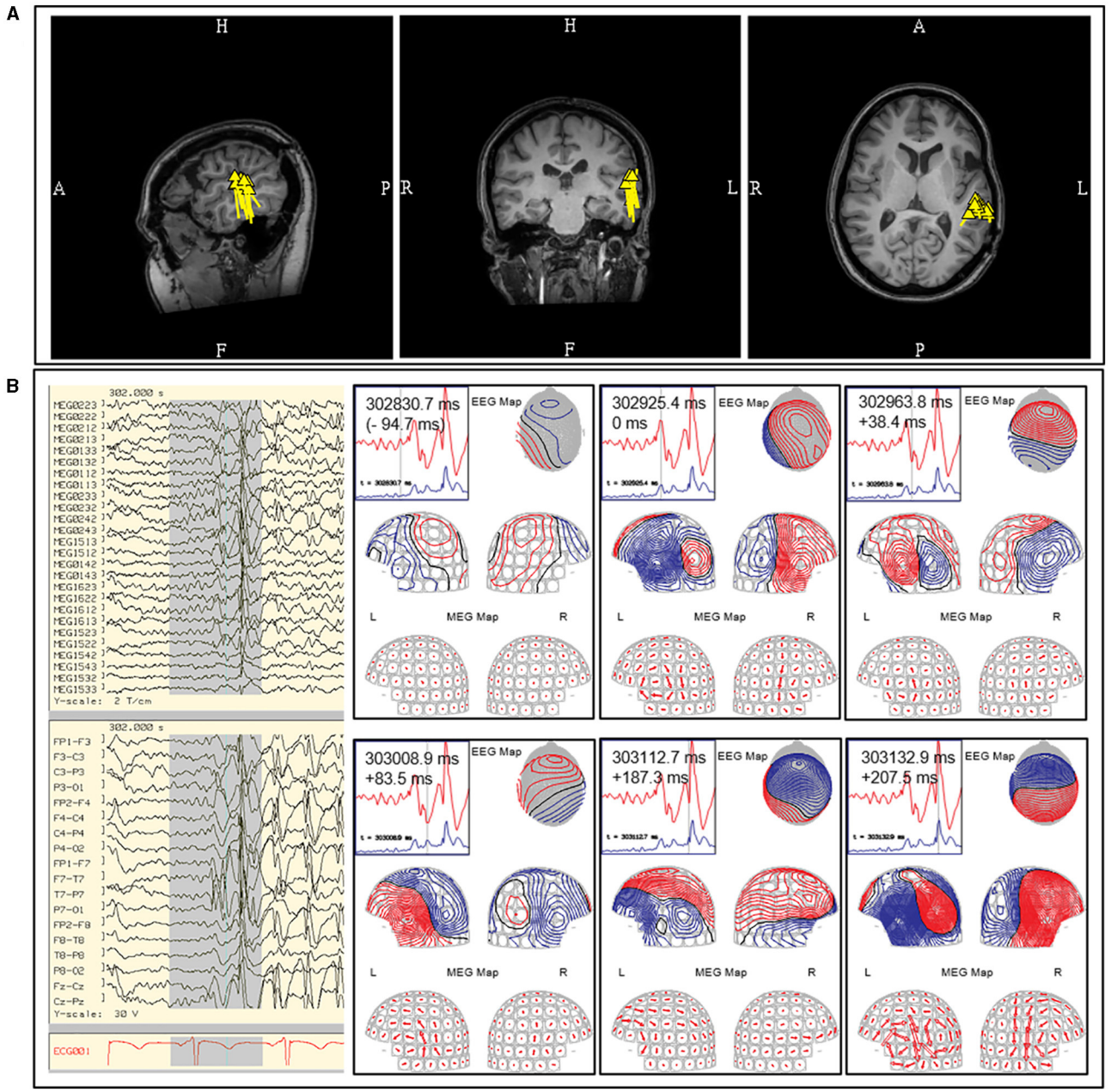

FIGURE 9 | Example of posterior temporal vertical dipoles that represent propagated activity. This MEG was performed in a patient with prior subdural recording which indicated a left frontal onset, but continued to have seizure after resection. The MEG study contained both **(A)** independent focal left posterior temporal discharges that formed a tight and uniform cluster and **(B)** bilateral posterior temporal discharges that were rapidly synchronous (upper middle diagram at 302925.4 ms; initial peak defined as 0 ms; left-right peak difference $<$ 10 ms). Data from prior subdural recording and the presence of bilateral synchronous discharges suggest alternate source of origin for this MEG cluster. The MEG current (arrow plot) suggested an underlying left frontotemporal current that cannot be modeled. These findings were described to the referring epileptologist.

and calcarine sulcus, and occasionally in the central sulcus. The variable sulcal locations of MEG dipoles, especially the involvement of the central sulcus, can be an important distinguishing feature of benign epileptic syndromes. However, the study also demonstrated that the dipoles in benign occipital epilepsy can show significant clustering with uniform vectors (a.k.a. dipole orientation), and can be unilateral in some patients (101). This conceivably would lead to its possible presentation as a monofocal sulcal cluster, similar to those commonly associated with lesional, bottom of the sulcus, focal cortical dysplasia (41). This finding should prompt an imaging review, and possibly usage of higher resolution MRI, as such dysplasia can be missed

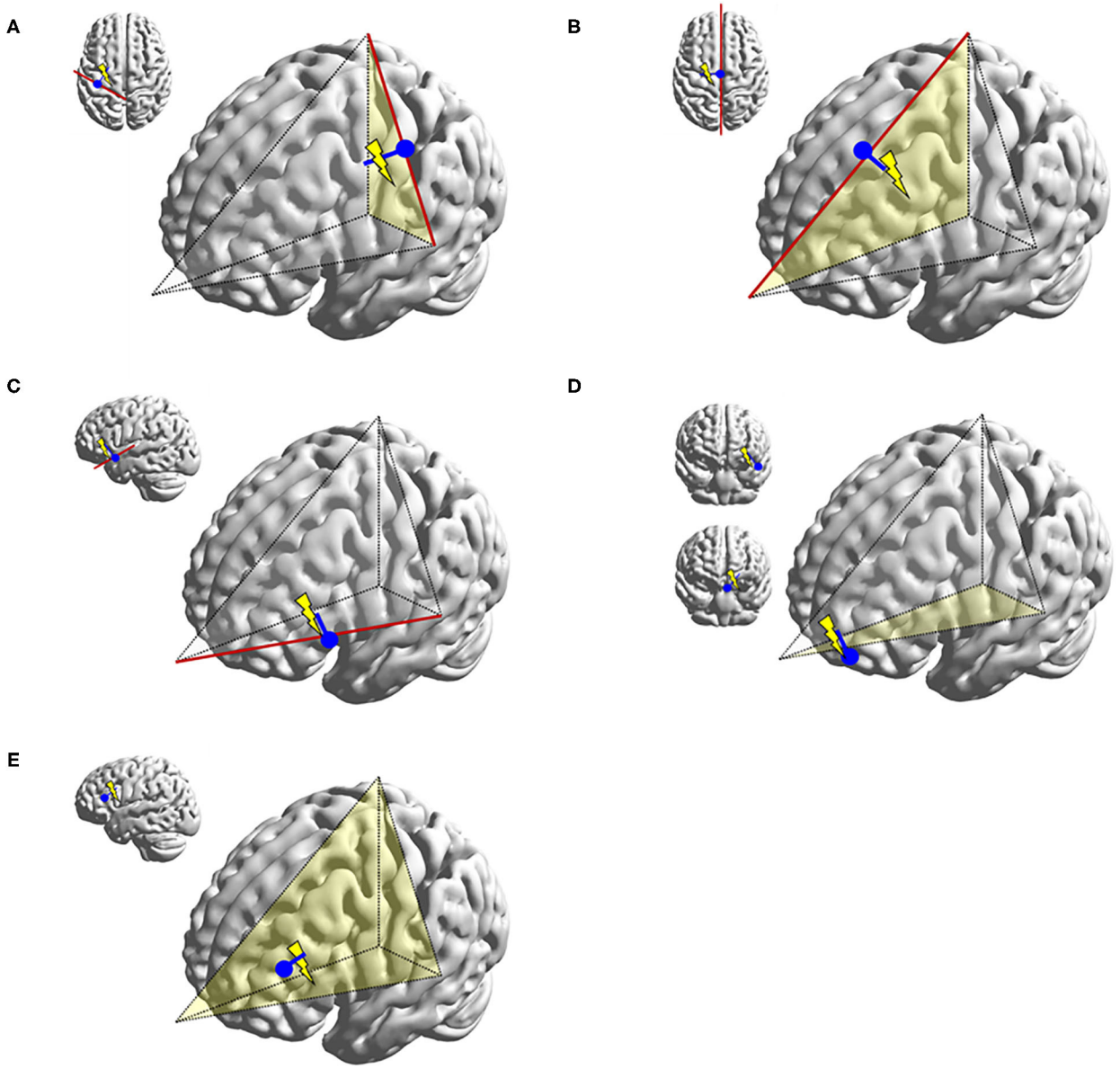

FIGURE 10 | Illustrations representing typical dipoles (blue) in correlation to frontal spike sources (electric symbol). **(A)** Peri-Rolandic frontal sources exhibit dipoles with anterior vector orientation. **(B)** Left medial frontal source exhibit lateral vector orientation to the left. **(C)** Fronto-opercular source exhibit upward vector orientation. **(D)** Orbitofrontal sources exhibit superior vector orientation similar to fronto-opercular source, but somewhat more oblique. Dipole tails of lateral orbitofrontal sources point more medially and those of medial orbitofrontal sources more laterally. **(E)** Lateral frontal dipole is shown here with dipole direction oriented toward the source, but its localization would also be dependent on the dipole cluster topology. This diagram can also be applied to parietal and occipital dipoles.

during initial imaging analysis (56, 57, 102). However, the MRI can continue to be negative despite repeated reviews (103), and a surgical recommendation will heavily rely on the epileptologist's clinical assessment. Additionally, MEG can also play a role as a prognostic marker in children with benign occipital epilepsy, as the presence of MEG dipoles outside of these typical sulcal regions have been reported in patient with atypical course and medication resistance (104).

Interhemispheric Fissures and Major Sulci Dipoles

The study of MEG spikes from benign Rolandic epilepsy showed localization to the Rolandic, Sylvian, and interhemispheric fissures and further suggested that the dipoles located in interhemispheric fissures and major sulci had tails that were likely to orient toward the lobe of seizure onset (87). This hypothesis was subsequently investigated in patients with lesional epilepsies

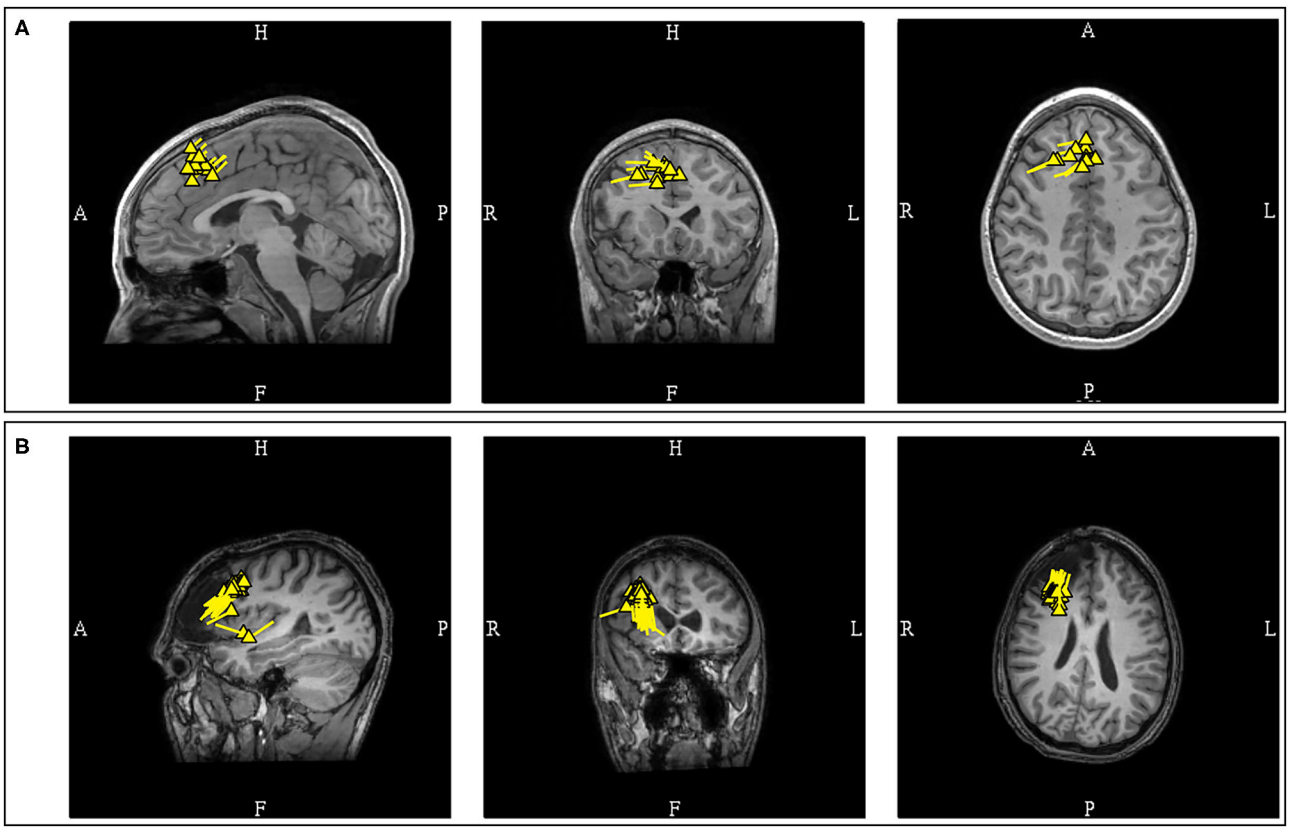

FIGURE 11 | (A) MEG-MRI coregistration summary demonstrating predominantly interhemispheric frontal dipoles. The uniform vector orientation toward the right suggests a right hemispheric source lateralization. Intracranial recording confirmed the finding, with seizure freedom for 5-years after right frontal resection. **(B)** This patient developed late seizure recurrence, with tight and uniform dipole cluster at the resection margin. Note the dipole orientation suggestive of positivity at the resection surface as a result of disruption of normal cortical laminar organization.

(105), which supported that the dipole of MEG spikes would consistently orient toward the lobe of seizure onset when located in the central (100%; 4/4) and sagittal interhemispheric sulci (100%; $n = 4/4$). This is a useful lateralizing feature, but with some reservations, as early MEG activity can be less visible due to lower SNR when compared to propagated activity, and medial frontal sources are known to have rapid contralateral propagation (93), hence modeling of interhemispheric MEG spike peaks may at times represent contralateral propagated activity. Experienced magnetoencephalographers would always ensure that the earliest signals were analyzed, and consider the possibility of contralateral propagated activity if the MEG lateralization is discordant to clinical semiology and other ancillary findings. Another important point to also consider is that a spike can be multiphasic, and the dipole orientation is dependent on the phase which was modeled. Considering this factor, it is a practice standard to routinely show examples MEG spike morphology that were modeled, to model the same phase consistently, and to describe phase-dependent orientation variability, if present (**Figure 13**).

The MEG spikes localized to the Sylvian fissures appeared to have variable orientation in respect to the lobe of seizure onset. In a study of Sylvian dipoles which included 8 patients with temporal lobe epilepsy, it was reported that 73% of the MEG dipoles were oriented toward the temporal lobe while 27% were oriented toward to the frontal lobe (105). In contrast, a study of 4 patients with fronto-parietal opercular epilepsy showed that the dipoles were orientated toward the lobe of seizure onset (88). Although these data would suggest that fronto-parietal Sylvian sources are associated with MEG dipoles that are more consistently oriented toward the lobe of origin when compared to temporal sources, the limited number of studied patients and possible orientation variability necessitate that clinical context must be considered in the interpretation of Sylvian dipoles. Furthermore, as previously stated, the posterior peri-Sylvian region is a common location of common benign MEG-unique variants, adding to interpretation complexity (**Figure 14**).

Insular/Peri-Insular Dipoles

In clinical practice, MEG has shown utility as a localizing tool in insular epilepsies even in the absence of interictal EEG findings or identifiable structural lesions (83, 106), despite theoretical modeling studies that otherwise suggested an insufficient MEG SNR over this region (107). This importance cannot

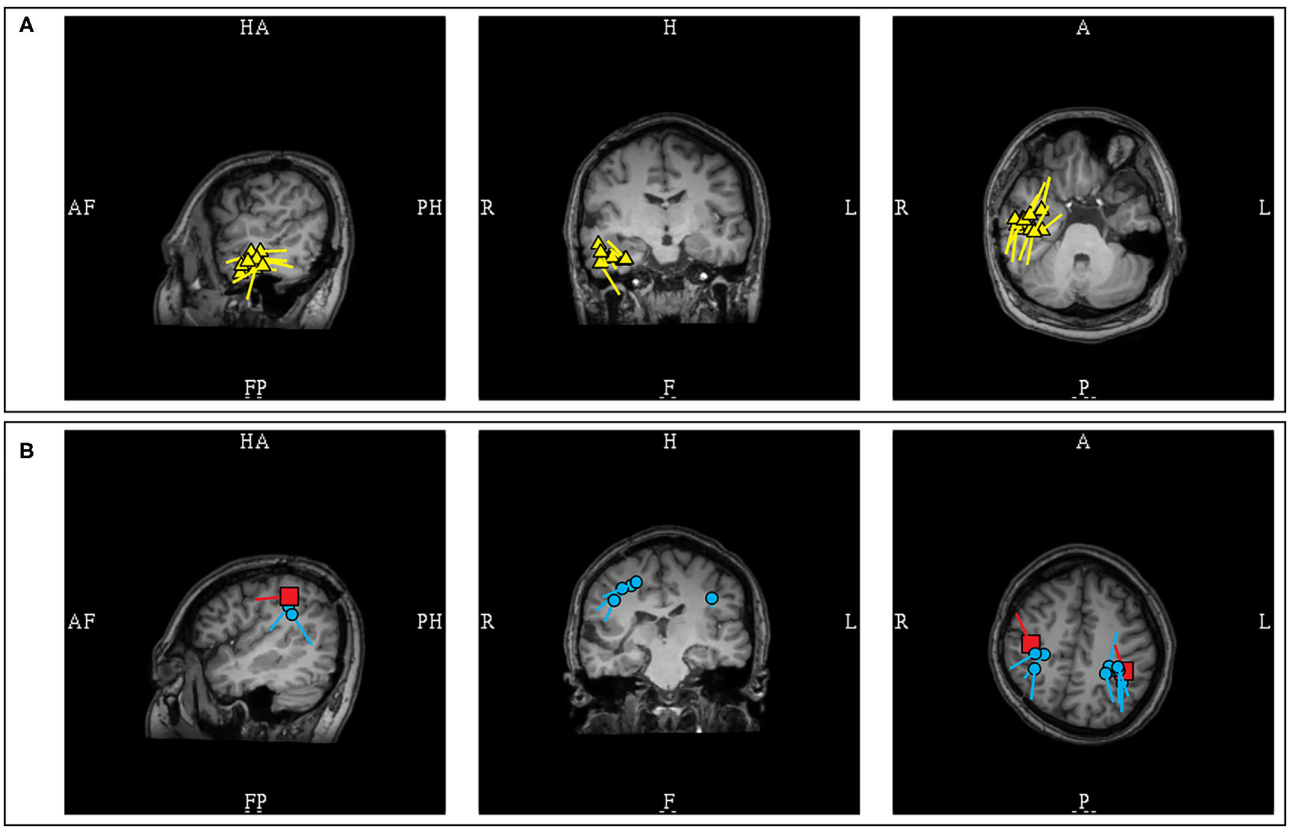

FIGURE 12 | MEG-MRI coregistration summary demonstrating dipoles in a patient with extensive right hemispheric cortical malformation. **(A)** A cluster of likely pathologic right temporal dipoles (yellow) was identified. **(B)** Bilateral parietal dipoles (blue) were also identified in proximity to somatosensory dipoles (red). These dipoles near the somatosensory area, and without an EEG correlate, were considered benign and were not included in final surgical plan.

be overstated, since insular epilepsies have variable clinical presentation and non-specific EEG findings (108). However, utilization of MEG dipoles localized to the insular region can still be a challenge, and at times these are omitted from final surgical resection, given that they can represent propagated activity rather than seizure onset (109).

MEG spikes, depending on source orientation and signal strength, can occur without or with an EEG correlate. The longer history of EEG, and recent recognition of MEG benign variants, support the belief in clinical practice that MEG spikes with an EEG correlate (MEG-EEG spikes) are more likely to be epileptiform. However, due to the lower signal-to-noise properties of electromagnetic signals localized to the insular region, it has been found that dipoles of MEG-unique (a.k.a. "MEG exclusive") insular discharges can be credibly pathologic and correctly localizing, in contrast to those with an EEG correlate that can often represent a remote propagated activity (110). The analysis of insular MEG sources requires careful consideration of benign vs. pathologic MEG-unique discharges, as well as hypotheses of source of origin based on clinical semiology and known propagation patterns.

It has been shown that anterior insular sources are associated with anterior operculo-insular MEG dipole clusters with anterior vector orientation, typically toward the frontal region (111), and early more anterior source propagation (112). This region is unlikely to be associated with benign MEG-unique variants which are more posterior in location. Hence, it can be stated that the MEG dipoles located in the anterior operculo-insular regions are more likely pathologic and suggestive of an underlying anterior insular source.

In contrast, the interpretation of MEG dipoles localized to the posterior operculo-insular region requires additional consideration. Although posterior operculo-insular MEG clusters with a posterior dipole orientation can be associated with a posterior insular source (111), the increased possibility of benign MEG variants from this region necessitates a more cautious interpretation, particularly if these discharges are MEG-unique. Sometimes evidence of an EEG correlation can only be found by averaging triggered off MEG spike peaks. However, pathologic insular MEG dipoles can still lack an EEG correlate even after averaging (106). Clinical context is required to determine the significance of such MEG spikes. Unilaterality and uniform dipole orientation would provide additional support that these discharges are pathologic. One should also note that dipoles associated with insular sources can appear dispersed (111), and posterior insular sources can exhibit early propagation to comparatively remote posterior parietal regions (112) (**Figure 15**).

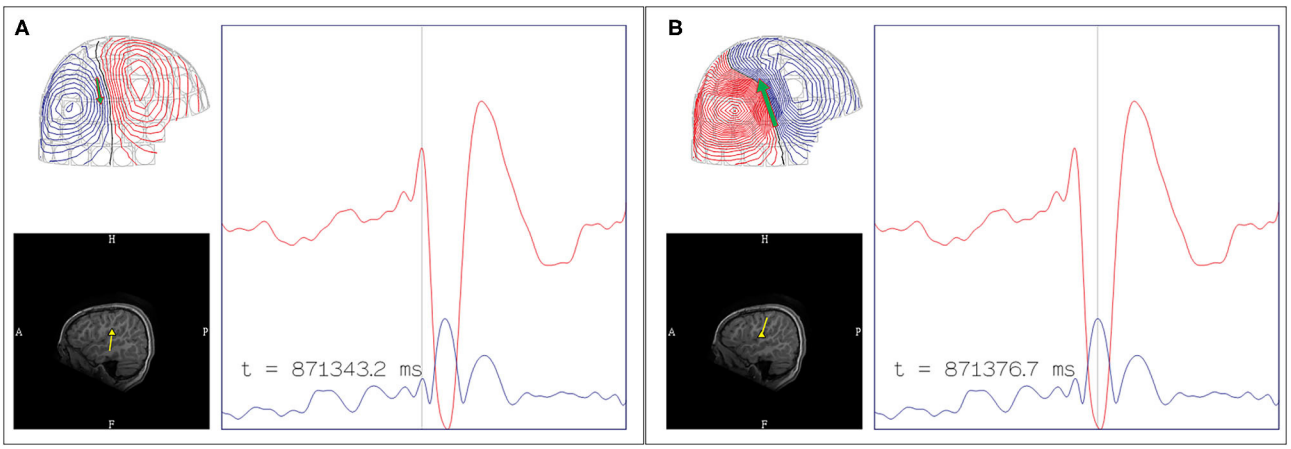

FIGURE 13 | Multiphasic MEG signal with phase-dependent orientation. **(A)** The early peak of lower amplitude was occasionally observed, with dipole oriented inferiorly, likely represents the initial depolarization of deeper laminae. **(B)** The later peak of higher amplitude was a more consistently observed, with dipole oriented superiorly suggestive of frontal operculum localization. Although the area of dipole origin was consistent, the appearance of multiphasic MEG discharges across major sulci can affect the application of orientation-based localization, given that the orientation is dependent of which phase of the discharge was modeled. EEG can assist in determining more pertinent depolarization in these circumstances.

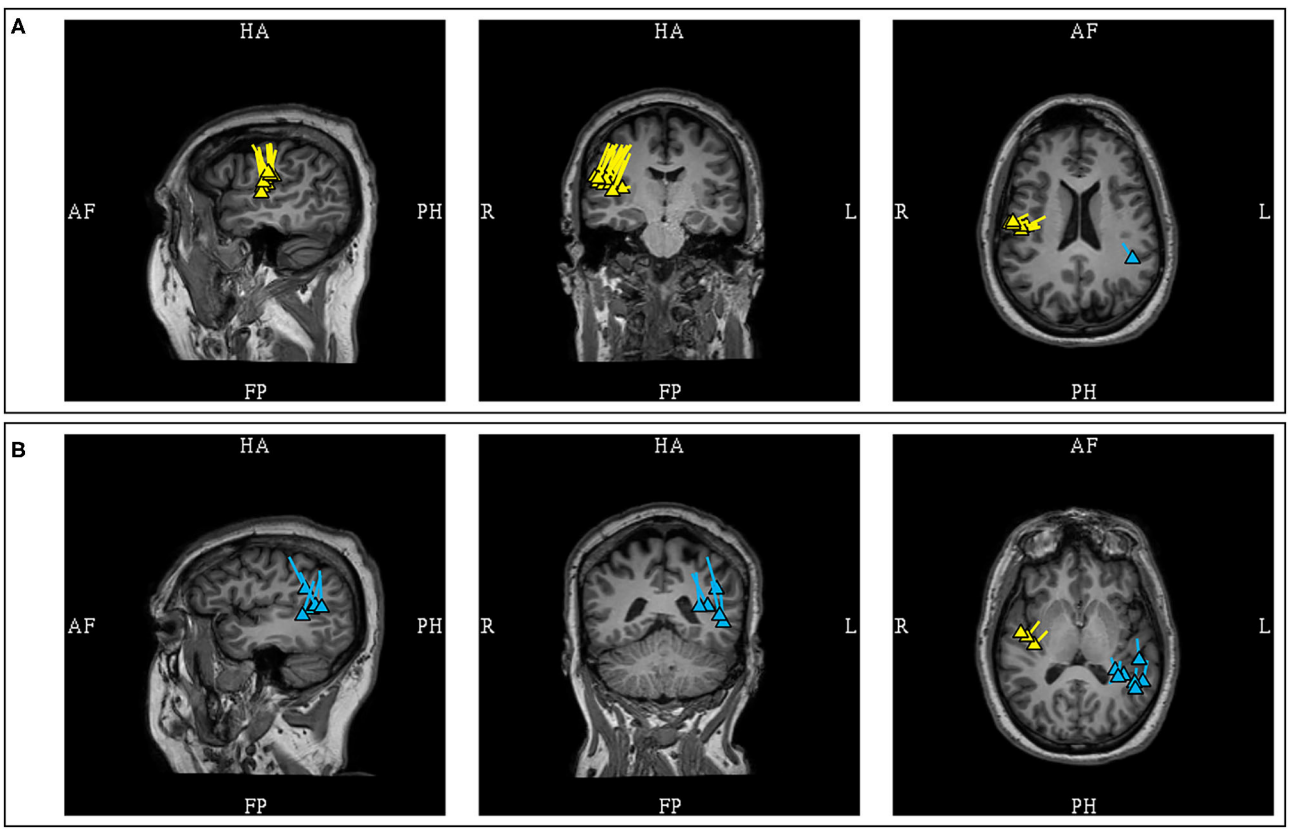

FIGURE 14 | MEG-MRI coregistration summary demonstrating supra-Sylvian dipoles in the same patient. **(A)** The pathologic right mid-supra-Sylvian cluster (yellow) is tight and uniformed, and correlated with a small right fronto-opercular MRI lesion upon imaging repeated review. **(B)** Benign left posterior supra-Sylvian cluster (blue) is loose with fairly uniform orientation. This is a cluster of benign normal variant that has neither EEG correlation nor clinical suggestions, and was not included in the clinical summary report.

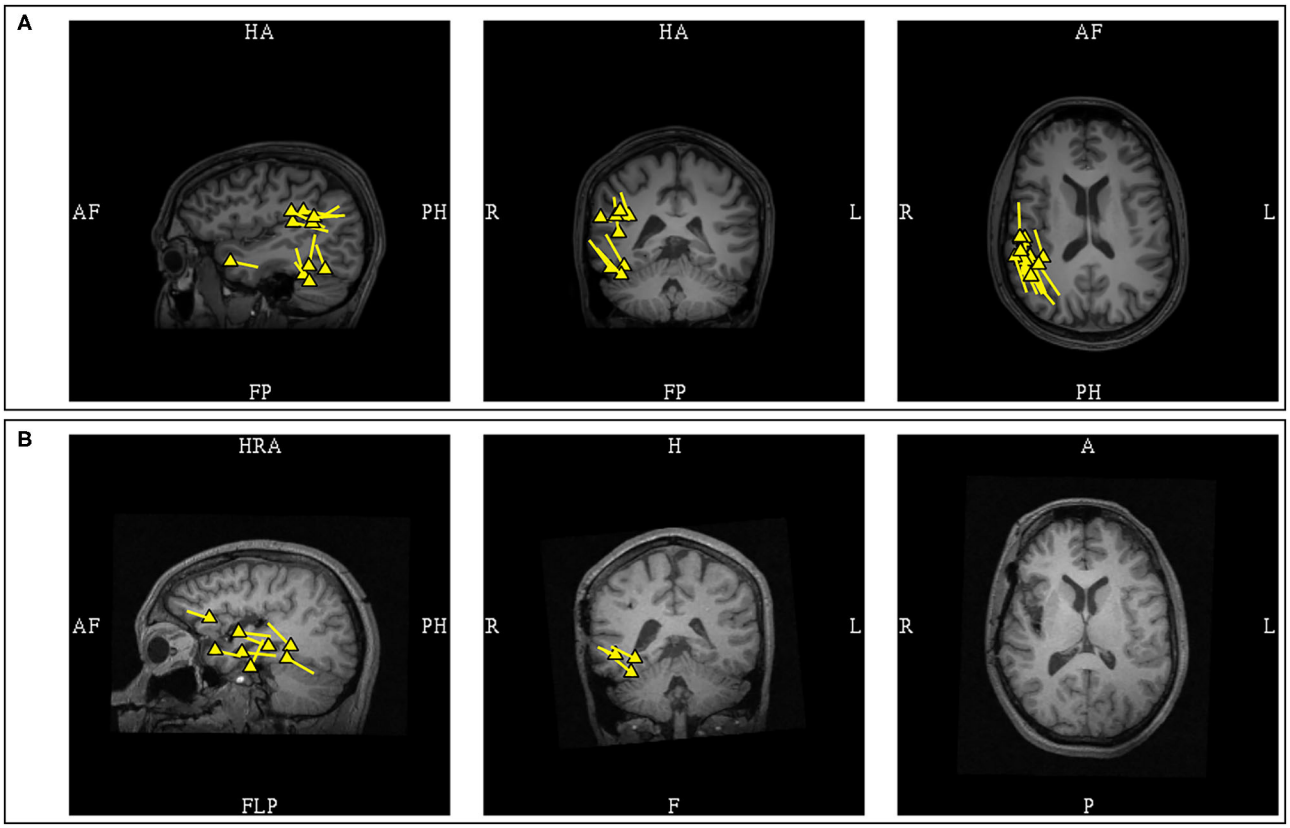

FIGURE 15 | MEG-MRI coregistration summary in a patient with a previous right anterior temporal laser ablation who underwent posterior insular resection. **(A)** Pre-operative MEG showed multifocal clusters over the right supramarginal, posterior basal temporal, and anterior temporal regions. The supramarginal cluster in this patient was pathologic due to presence of an epileptiform correlate. Invasive EEG recording confirmed interictal spiking concordant with MEG. **(B)** Post-operative MEG after the posterior insular resection showed disappearance of the supramarginal cluster, but the temporal dipoles remained.

Dipoles in Post-operative Recurrence and Changed Anatomy

MEG should always be performed in post-operative patients with seizure recurrence who consider a reoperation (9, 113). As the MEG signals are not influenced by the skull breech and changed anatomy, unlike EEG, source localization by MEG is superior. Improved seizure outcome has been observed in patients who underwent re-operation when MEG is utilized (114). In this specific population, it has been reported that more than half of the patients have at least one dipole cluster at the surgical margin (115). The presence of these dipoles can indicate a possible ictal onset zone and is particularly useful in patients with a broad resection cavity. However, the possibility also exists that dipoles at resection margins are a result of the resection itself, while the pathology is elsewhere. This is exemplified by the report of a patient with early post-operative seizure recurrence, whose MEG showed both a peri-resectional cluster and another remote cluster at a distant cortical abnormality (56). Accurate assessment of the significance of MEG dipoles near a surgical site is reliant on a variety of factors including prior pathology, character of the resection, changes in seizure semiology, and the timing of seizure recurrence. Dipoles located near the resection cavity in patients with late seizure recurrence are more likely associated with the ictal origin, whereas additional distant foci must be considered in early recurrence (116). Nonetheless, it has been shown that more than half of patients with early seizure recurrence have clinically relevant spikes modellable by dipoles at the resection margin (9), and most reoperations are focused at the prior resection margin (115).

There is also a suggestion that MEG spike dipoles following extratemporal resections may be more localizing (117). A study of recurrent epilepsy after frontal and temporal lobectomy demonstrated that frontal dipoles were more closely localized to the post-operative margin (117). In post-temporal lobectomy, although MEG identified activity in remnant mesial temporal structures that led to successful re-operation, the majority of patients had dipoles localized over the lateral or basal temporal regions further away from the resection margin. The localizing value of these comparatively distant dipoles were not further explored.

It is notable that the tail of MEG dipoles, that typically orients toward the activated cortex, does so under the condition of normal cortical laminar organization. Removal of the superficial cortex can result in dipole orientation changes, particularly if the underside of nearby cortex is exposed in the process. In such cases, residual dipoles may have an opposite orientation

(**Figure 11B**). This finding is similar to positive EEG spikes that similarly can occur as a result of prior surgical procedures or trauma (118, 119). In neocortical epilepsies where dipole orientation can serve as a guide toward the epileptogenic cortex, such situations are noteworthy.

CRITICAL IMPORTANCE OF MEG REPORTING AND PROPER COMMUNICATION WITH REFERRING PHYSICIANS

As referring physicians may not be familiar with MEG techniques and results, MEG reporting and communication are practical issues of critical importance. A clinical MEG report should be ACMEGS CPG-compliant (13), complete, concise, and appropriately structured. Since a simultaneous EEG recording is a required component of every clinical MEG study for epilepsy, its absence or deviation from the 10–20 system must be acknowledged and explained. The MEG information should describe the morphology, location, and frequency of detected MEG discharges, and their localization results. The MEG findings must also be compared with their EEG correlates, and their mutual dynamics explored to the best possible degree. EEG unique discharges must be noted, as this can represent alternate sources not identified by MEG. The impression and conclusion should be concise, providing an anatomical localization summary, pattern of distribution, and accurate representative population frequency (120). Finally, the report must correlate MEG-EEG findings to the clinical context, considering both semiology and radiographic findings into its interpretation. To ensure that all relevant clinical priors are considered during the data acquisition and study interpretation, a channel of communication between clinical magnetoencephalographers and referring epileptologists should be present and maintained until the final delivery of the report. The MEG report must answer the questions from the referring physician, and overall constructed for optimal incorporation to future surgical planning.

CONCLUSION

This article is written to serve as a practical introduction to clinical MEG interpretation in epilepsy. It reflects the variability in the strength and degree of evidence for different practically relevant aspects of clinical MEG practice. Naturally, unusual circumstances outside of what have been discussed here can and will occur in the course of one's daily practice. To achieve a comprehensive understanding of MEG, a practitioner must gain procedural experience through extensive clinical use and knowledge through continued literature review. We hope that the information contained in this article has achieved its goal of increasing the understanding of clinical MEG localization and interpretation, elevating the level of clinical MEG service, and improving the surgical outcome of our patients with epilepsy. Ultimately, we hope our effort synergizes with others in the epilepsy and clinical MEG communities to promote clinically indicated but greatly underutilized surgical treatments for patients with DRE.

AUTHOR CONTRIBUTIONS

CL performed primary research and authored this research. JE incorporated expert experience, primary editing, and ensured accurate application of concepts. JM contributed to source modeling concepts and fundamentals of model acceptance. AB incorporated expert experience, secondary editing, and constructed the literature framework. AS provided institutional findings and data analysis. GV provided institutional findings and data analysis. MF provided the concepts and led this research. All authors contributed to manuscript revision, read, and approved the submitted version.

FUNDING

Research was supported to JM by the National Institute of Biomedical Imaging and Bioengineering of the National Institutes of Health under award numbers R01EB026299 and U01EB023820.

REFERENCES

1. Jobst BC, Cascino GD. Resective epilepsy surgery for drug-resistant focal epilepsy: a review. *JAMA*. (2015) 313:285–93. doi: 10.1001/jama.2014.17426
2. Institute of Medicine (US) Committee on the Public Health Dimensions of the Epilepsies; England MJ, Liverman CT, Schultz AM et al. *Epilepsy Epidemiology and Prevention. Epilepsy Across the Spectrum: Promoting Health and Understanding.* Washington, DC: The National Academies Press (2012) 109–160.
3. Kaiboriboon K, Malkhachroum AM, Zrik A, Daif A, Schiltz NM, Labiner DM, et al. Epilepsy surgery in the United States: analysis of data from the national association of epilepsy centers. *Epilepsy Res.* (2015) 116:105–9. doi: 10.1016/j.eplepsyres.2015.07.007
4. Tovar-Spinoza ZS, Ochi A, Rutka JT, Go C, Otsubo H. The role of magnetoencephalography in epilepsy surgery. *Neurosurg Focus.* (2008) 25:E16. doi: 10.3171/FOC/2008/25/9/E16
5. Bagic A, Funke ME, Ebersole J. American Clinical MEG Society (ACMEGS) position statement: the value of magnetoencephalography (MEG)/magnetic source imaging (MSI) in noninvasive presurgical evaluation of patients with medically intractable localization-related epilepsy. *J Clin Neurophysiol.* (2009) 26:290–3. doi: 10.1097/WNP.0b013e3181b49d50
6. Hämäläinen M, Hari R, Ilmoniemi RJ, Knuutila J, Lounasmaa O V. Magnetoencephalography theory, instrumentation, and applications to noninvasive studies of the working human brain. *Rev Mod Phys.* (1993) 65:413–97. doi: 10.1103/RevModPhys.65.413
7. Hillebrand A, Barnes GR. A quantitative assessment of the sensitivity of whole-head MEG to activity in the adult human cortex. *Neuroimage.* (2002) 16:638–50. doi: 10.1006/nimg.2002.1102
8. Baumgartner C, Pataraia E, Lindinger G, Deecke L. Magnetoencephalography in focal epilepsy. *Epilepsia.* (2000) 41(Suppl. 3). doi: 10.1111/j.1528-1157.2000.tb01533.x
9. Mohamed IS, Otsubo H, Ochi A, Elliott I, Donner E, Chuang S, et al. Utility of magnetoencephalography in the evaluation of recurrent seizures after epilepsy surgery. *Epilepsia.* (2007) 48:2150–9. doi: 10.1111/j.1528-1167.2007.01271.x

10. Sutherling WW, Mamelak AN, Thyerlei D, Maleeva T, Minazad Y, Philpott L, et al. Influence of magnetic source imaging for planning intracranial EEG in epilepsy. *Neurology.* (2008) 71:990–6. doi: 10.1212/01.wnl.0000326591.29858.1a
11. Murakami H, Wang ZI, Marashly A, Krishnan B, Prayson RA, Kakisaka Y, et al. Correlating magnetoencephalography to stereo-electroencephalography in patients undergoing epilepsy surgery. *Brain.* (2016) 139:2935–47. doi: 10.1093/brain/aww215
12. Bagić AI, Burgess RC. Utilization of MEG among the US epilepsy centers: a survey-based appraisal. *J Clin Neurophysiol.* (2020) 37:599–605. doi: 10.1097/WNP.0000000000000716
13. Bagić AI, Knowlton RC, Rose DF, Ebersole JS. American clinical magnetoencephalography society clinical practice guideline 3: MEG-EEG reporting. *J Clin Neurophysiol.* (2011) 28:362–3. doi: 10.1097/WNO.0b013e3181cde4ad
14. Mosher JC, Funke ME. Towards best practices in clinical magnetoencephalography: patient preparation and data acquisition. *J Clin Neurophysiol.* (2020) 37:498–507. doi: 10.1097/WNP.0000000000000542
15. Huang MX, Mosher JC, Leahy RM. A sensor-weighted overlapping-sphere head model and exhaustive head model comparison for MEG. *Phys Med Biol.* (1999) 44:423–40. doi: 10.1088/0031-9155/44/2/010
16. Scheler G, Fischer MJM, Genow A, Hummel C, Rampp S, Paulini A, et al. Spatial relationship of source localizations in patients with focal epilepsy: comparison of MEG and EEG with a three spherical shells and a boundary element volume conductor model. *Hum Brain Mapp.* (2007) 28:315–22. doi: 10.1002/hbm.20277
17. Aydin Ü, Vorwerk J, Küpper P, Heers M, Kugel H, Galka A, et al. Combining EEG and MEG for the reconstruction of epileptic activity using a calibrated realistic volume conductor model. *PLoS ONE.* (2014) 9:e93154. doi: 10.1371/journal.pone.0093154
18. Akalin Acar Z, Acar CE, Makeig S. Simultaneous head tissue conductivity and EEG source location estimation. *Neuroimage.* (2016) 124:168–80. doi: 10.1016/j.neuroimage.2015.08.032
19. Tripp JH. Physical concepts and mathematical models. In: Williamson SJ, Romani G-L, Kaufman L, Modena I, editors. *Biomagnetism*. New York, NY: Plenum Press (1983). p. 101–39.
20. Murakami S, Okada Y. Invariance in current dipole moment density across brain structures and species: physiological constraint for neuroimaging. *Neuroimage.* (2015) 111:49–58. doi: 10.1016/j.neuroimage.2015.02.003
21. Bagić AI, Knowlton RC, Rose DF, Ebersole JS. American clinical magnetoencephalography society clinical practice guideline 1: recording and analysis of spontaneous cerebral activity. *J Clin Neurophysiol.* (2011) 28:348–54. doi: 10.1097/WNP.0b013e3182272fed
22. Fernandes JM, Da Silva AM, Huiskamp G, Velis DN, Manshanden I, De Munck JC, et al. What does an epileptiform spike look like in MEG? Comparison between coincident EEG and MEG spikes. *J Clin Neurophysiol.* (2005) 22:68–73. doi: 10.1097/01.WNP.0000150999.67749.6D
23. Nowak R, Santiuste M, Russi A. Toward a definition of MEG spike: parametric description of spikes recorded simultaneously by MEG and depth electrodes. *Seizure.* (2009) 18:652–5. doi: 10.1016/j.seizure.2009.07.002
24. Tao JX, Chen XJ, Baldwin M, Yung I, Rose S, Frim D, et al. Interictal regional delta slowing is an EEG marker of epileptic network in temporal lobe epilepsy. *Epilepsia.* (2011) 52:467–76. doi: 10.1111/j.1528-1167.2010.02918.x
25. Bast T, Boppel T, Rupp A, Harting I, Hoechstetter K, Fauser S, et al. Noninvasive source localization of interictal EEG spikes: effects of signal-to-noise ratio and averaging. *J Clin Neurophysiol.* (2006) 23:487–97. doi: 10.1097/01.wnp.0000232208.14060.c7
26. Aydin Ü, Vorwerk J, Dümpelmann M, Küpper P, Kugel H, Heers M, et al. Combined EEG/MEG can outperform single modality EEG or MEG source reconstruction in presurgical epilepsy diagnosis. *PLoS ONE.* (2015) 10:e0118753. doi: 10.1371/journal.pone.0118753
27. Rampp S, Kakisaka Y, Shibata S, Wu X, Rössler K, Buchfelder M, et al. Normal Variants in Magnetoencephalography. *J Clin Neurophysiol.* (2020) 37:518–36. doi: 10.1097/WNP.0000000000000484
28. Press WH, Teukolsky SA, Vetterling WT, Flannery BP. Modeling of data. In: *Numerical Recipes in C. 2nd Edn.* New York, NY: Cambridge University Press (1992). p. 655–706.
29. Sarvas J. Basic mathematical and electromagnetic concepts of the biomagnetic inverse problem. *Phys Med Biol.* (1987) 32:11–22. doi: 10.1088/0031-9155/32/1/004
30. Ebersole JS, Ebersole SM. Combining MEG and EEG source modeling in epilepsy evaluations. *J Clin Neurophysiol.* (2010) 27:360–71. doi: 10.1097/WNP.0b013e318201ffc4
31. Ebersole JS, Wagner M. Relative yield of meg and EEG spikes in simultaneous recordings. *J Clin Neurophysiol.* (2018) 35:443–53. doi: 10.1097/WNP.0000000000000512
32. Tanaka N, Hämäläinen MS, Ahlfors SP, Liu H, Madsen JR, Bourgeois BF, et al. Propagation of epileptic spikes reconstructed from spatiotemporal magnetoencephalographic and electroencephalographic source analysis. *Neuroimage.* (2010) 50:217–22. doi: 10.1016/j.neuroimage.2009.12.033
33. Iwasaki M, Pestana E, Burgess RC, Lüders HO, Shamoto H, Nakasato N. Detection of epileptiform activity by human interpreters: blinded comparison between electroencephalography and magnetoencephalography. *Epilepsia.* (2005) 46:59–68. doi: 10.1111/j.0013-9580.2005.21104.x
34. Park HM, Nakasato N, Iwasaki M, Shamoto H, Tominaga T, Yoshimoto T. Comparison of magnetoencephalographic spikes with and without concurrent electroencephalographic spikes in extratemporal epilepsy. *Tohoku J Exp Med.* (2004) 203:165–74. doi: 10.1620/tjem.203.165
35. Bagić AI, Rampp S. It is time to harmonize clinical MEG practice internationally. *Clin Neurophysiol.* (2020) 131:1769–71. doi: 10.1016/j.clinph.2020.04.020
36. Baumgartner C. Controversies in clinical neurophysiology. MEG is superior to EEG in the localization of interictal epileptiform activity. *Con Clin Neurophysiol.* (2004) 115:1010–20. doi: 10.1016/j.clinph.2003.12.010
37. Yvert B, Bertrand O, Thévenet M, Echallier JF, Pernier J. A systematic evaluation of the spherical model accuracy in EEG dipole localization. *Electroencephalogr Clin Neurophysiol.* (1997) 102:452–9. doi: 10.1016/S0921-884X(97)96611-X
38. Leahy RM, Mosher JC, Spencer ME, Huang MX, Lewine JD. A study of dipole localization accuracy for MEG and EEG using a human skull phantom. *Neuroimage.* (1998) 7(4 Part II):S676. doi: 10.1016/S1053-8119(18)31509-X
39. Barkley GL. Controversies in neurophysiology. MEG is superior to EEG in localization of interictal epileptiform activity. *Pro Clin Neurophysiol.* (2004) 115:1001–9. doi: 10.1016/j.clinph.2003.12.011
40. Agarwal N, Krishnan B, Burgess RC, Prayson RA, Alexopoulos A V., Gupta A. Magnetoencephalographic characteristics of cortical dysplasia in children. *Pediatr Neurol.* (2018) 78:13–9. doi: 10.1016/j.pediatrneurol.2017.09.009
41. Widjaja E, Otsubo H, Raybaud C, Ochi A, Chan D, Rutka JT, et al. Characteristics of MEG and MRI between Taylor's focal cortical dysplasia (type II) and other cortical dysplasia: surgical outcome after complete resection of MEG spike source and MR lesion in pediatric cortical dysplasia. *Epilepsy Res.* (2008) 82:147–55. doi: 10.1016/j.eplepsyres.2008.07.013
42. Oishi M, Kameyama S, Masuda H, Tohyama J, Kanazawa O, Sasagawa M, et al. Single and multiple clusters of magnetoencephalographic dipoles in neocortical epilepsy: significance in characterizing the epileptogenic zone. *Epilepsia.* (2006) 47:355–64. doi: 10.1111/j.1528-1167.2006.00428.x
43. Mu J, Rampp S, Carrette E, Roessler K, Sommer B, Schmitt FC, et al. Clinical relevance of source location in frontal lobe epilepsy and prediction of postoperative long-term outcome. *Seizure.* (2014) 23:553–9. doi: 10.1016/j.seizure.2014.04.006
44. Stefan H, Wu X, Buchfelder M, Rampp S, Kasper B, Hopfengärtner R, et al. MEG in frontal lobe epilepsies: localization and postoperative outcome. *Epilepsia.* (2011) 52:2233–8. doi: 10.1111/j.1528-1167.2011.03265.x
45. Wu XT, Rampp S, Buchfelder M, Kuwert T, Blümcke I, Dörfler A, et al. Interictal magnetoencephalography used in magnetic resonance imaging-negative patients with epilepsy. *Acta Neurol Scand.* (2013) 127:274–80. doi: 10.1111/j.1600-0404.2012.01712.x
46. Jeong W, Chung CK, Kim JS. Magnetoencephalography interictal spike clustering in relation with surgical outcome of cortical dysplasia. *J Korean Neurosurg Soc.* (2012) 52:466–71. doi: 10.3340/jkns.2012.52.5.466
47. Blümcke I, Thom M, Aronica E, Armstrong DD, Vinters H V., Palmini A, et al. The clinicopathologic spectrum of focal cortical dysplasias: a consensus classification proposed by an ad hoc Task Force of the ILAE Diagnostic Methods Commission. *Epilepsia.* (2011) 52:158–74. doi: 10.1111/j.1528-1167.2010.02777.x
48. Kabat J, Król P. Focal cortical dysplasia - review. *Polish J Radiol.* (2012) 77:35–43. doi: 10.12659/PJR.882968
49. Tanaka N, Papadelis C, Tamilia E, AlHilani M, Madsen JR, Pearl PL, et al. Magnetoencephalographic spike analysis in patients with focal cortical

dysplasia: what defines a "dipole cluster"? *Pediatr Neurol.* (2018) 83:25–31. doi: 10.1016/j.pediatrneurol.2018.03.004
50. Sabolek HR, Swiercz WB, Lillis KP, Cash SS, Huberfeld G, Zhao G, et al. A candidate mechanism underlying the variance of interictal spike propagation. *J Neurosci.* (2012) 32:3009–21. doi: 10.1523/JNEUROSCI.5853-11.2012
51. Chitokua S, Otsuboa H, Ichimura T, Saigusaa T, Ochia A, Shirasawa A, et al. Characteristics of dipoles in clustered individual spikes and averaged spikes. *Brain Dev.* (2003) 25:14–21. doi: 10.1016/s0387-7604(02)00104-3
52. Ntolkeras G, Tamilia E, AlHilani M, Bolton J, Ellen Grant P, Prabhu SP, et al. Presurgical accuracy of dipole clustering in MRI-negative pediatric patients with epilepsy: validation against intracranial EEG and resection. *Clin Neurophysiol.* (2021) doi: 10.1016/j.clinph.2021.01.036. [Epub ahead of print].
53. Morioka T, Nishio S, Ishibashi H, Muraishi M, Hisada K, Shigeto H, et al. Intrinsic epileptogenicity of focal cortical dysplasia as revealed by magnetoencephalography and electrocorticography. *Epilepsy Res.* (1999) 33:177–87. doi: 10.1016/S0920-1211(98)00096-5
54. Stefan H, Scheler G, Hummel C, Walter J, Romstöeck J, Buchfelder M, et al. Magnetoencephalography (MEG) predicts focal epileptogenicity in cavernomas. *J Neurol Neurosurg Psychiatry.* (2004) 75:1309–13. doi: 10.1136/jnnp.2003.021972
55. Moore KR, Funke ME, Constantino T, Katzman GL, Lewine JD. Magnetoencephalographically directed review of high-spatial-resolution surface-coil MR images improves lesion detection in patients with extratemporal epilepsy. *Radiology.* (2002) 225:880–7. doi: 10.1148/radiol.2253011597
56. Funke ME, Moore K, Orrison WW, Lewine JD. The role of magnetoencephalography in "nonlesional" epilepsy. *Epilepsia.* (2011) 52(Suppl. 4):10–4. doi: 10.1111/j.1528-1167.2011.03144.x
57. Bagić A. Look back to leap forward: the emerging new role of magnetoencephalography (MEG) in nonlesional epilepsy. *Clin Neurophysiol.* (2016) 127:60–6. doi: 10.1016/j.clinph.2015.05.009
58. Wilenius J, Lauronen L, Kirveskari E, Gaily E, Metsähonkala L, Paetau R. Interictal magnetoencephalography in parietal lobe epilepsy – comparison of equivalent current dipole and beamformer (SAMepi) analysis. *Clin Neurophysiol Pract.* (2020) 5:64–72. doi: 10.1016/j.cnp.2020.02.003
59. Fuchs M, Wagner M, Kastner J. Confidence limits of dipole source reconstruction results. *Clin Neurophysiol.* (2004) 115:1442–51. doi: 10.1016/j.clinph.2004.01.019
60. Fuchs M, Kastner J, Tech R, Wagner M, Gasca F. MEG and EEG dipole clusters from extended cortical sources. *Biomed Eng Lett.* (2017) 7:185–91. doi: 10.1007/s13534-017-0019-2
61. Agirre-Arrizubieta Z, Huiskamp GJM, Ferrier CH, Van Huffelen AC, Leijten FSS. Interictal magnetoencephalography and the irritative zone in the electrocorticogram. *Brain.* (2009) 132:3060–71. doi: 10.1093/brain/awp137
62. Stefan H, Rampp S. Interictal and Ictal MEG in presurgical evaluation for epilepsy surgery. *Acta Epileptol.* (2020) 2:11. doi: 10.1186/s42494-020-00020-2
63. Assaf BA, Karkar KM, Laxer KD, Garcia PA, Austin EJ, Barbaro NM, et al. Ictal magnetoencephalography in temporal and extratemporal lobe epilepsy. *Epilepsia.* (2003) 44:1320–7. doi: 10.1046/j.1528-1157.2003.14303.x
64. Eliashiv DS, Elsas SM, Squires K, Fried I, Engel J. Ictal magnetic source imaging as a localizing tool in partial epilepsy. *Neurology.* (2002) 59:1600–10. doi: 10.1212/01.WNL.0000032493.83875.0B
65. Koptelova A, Bikmullina R, Medvedovsky M, Novikova S, Golovteev A, Grinenko O, et al. Ictal and interictal MEG in pediatric patients with tuberous sclerosis and drug resistant epilepsy. *Epilepsy Res.* (2018) 140:162–5. doi: 10.1016/j.eplepsyres.2017.12.014
66. Medvedovsky M, Taulu S, Gaily E, Metsähonkala EL, Mäkelä JP, Ekstein D, et al. Sensitivity and specificity of seizure-onset zone estimation by ictal magnetoencephalography. *Epilepsia.* (2012) 53:1649–57. doi: 10.1111/j.1528-1167.2012.03574.x
67. Ramanujam B, Bharti K, Viswanathan V, Garg A, Tripathi M, Bal C, et al. Can ictal-MEG obviate the need for phase II monitoring in people with drug-refractory epilepsy? A prospective observational study. *Seizure.* (2017) 45:17–23. doi: 10.1016/j.seizure.2016.10.013
68. Alkawadri R, Burgess RC, Kakisaka Y, Mosher JC, Alexopoulos A V. Assessment of the utility of ictal magnetoencephalography in the localization of the epileptic seizure onset zone. *JAMA Neurol.* (2018) 75:1264–72. doi: 10.1001/jamaneurol.2018.1430
69. Fujiwara H, Greiner HM, Hemasilpin N, Lee KH, Holland-Bouley K, Arthur T, et al. Ictal MEG onset source localization compared to intracranial EEG and outcome: improved epilepsy presurgical evaluation in pediatrics. *Epilepsy Res.* (2012) 99:214–24. doi: 10.1016/j.eplepsyres.2011.11.007
70. Yoshinaga H, Ohtsuka Y, Watanabe Y, Inutsuka M, Kitamura Y, Kinugasa K, et al. Ictal MEG in two children with partial seizures. *Brain Dev.* (2004) 26:403–8. doi: 10.1016/j.braindev.2003.11.003
71. Plummer C, Vogrin SJ, Woods WP, Murphy MA, Cook MJ, Liley DTJ. Interictal and ictal source localization for epilepsy surgery using high-density EEG with MEG: a prospective long-term study. *Brain.* (2019) 142:932–51. doi: 10.1093/brain/awz015
72. Velmurugan J, Nagarajan SS, Mariyappa N, Ravi SG, Thennarasu K, Mundlamuri RC, et al. Magnetoencephalographic imaging of ictal high-frequency oscillations (80-200 Hz) in pharmacologically resistant focal epilepsy. *Epilepsia.* (2018) 59:190–202. doi: 10.1111/epi.13940
73. Canuet L, Ishii R, Iwase M, Kurimoto R, Ikezawa K, Azechi M, et al. Cephalic auras of supplementary motor area origin: an ictal MEG and SAM(g2) study. *Epilepsy Behav.* (2008) 13:570–4. doi: 10.1016/j.yebeh.2008.05.013
74. Pellegrino G, Hedrich T, Chowdhury R, Hall JA, Lina JM, Dubeau F, et al. Source localization of the seizure onset zone from ictal EEG/MEG data. *Hum Brain Mapp.* (2016) 37:2528–46. doi: 10.1002/hbm.23191
75. Moreau JT, Simard-Tremblay E, Albrecht S, Rosenblatt B, Baillet S, Dudley RWR. Overnight ictal magnetoencephalography. *Neurol Clin Pract.* (2020) doi: 10.1212/CPJ.0000000000000937. [Epub ahead of print].
76. Tanaka N, Grant PE, Suzuki N, Madsen JR, Bergin AM, Hämäläinen MS, et al. Multimodal imaging of spike propagation: a technical case report. *Am J Neuroradiol.* (2012) 33:82–4. doi: 10.3174/ajnr.A2701
77. Ebersole JS. Classification of MEG spikes in temporal lobe epilepsy. In: Yoshimoto T, Kotani M, Kuriki S, Karibe H, Nakasato N, editors. *Recent Advances in Biomagnetism*. Sendai: Tohoku University Press (1999). p. 758–61.
78. Baumgartner C, Pataraia E, Lindinger G, Deecke L. Neuromagnetic recordings in temporal lobe epilepsy. *J Clin Neurophysiol.* (2000) 17:177–89. doi: 10.1097/00004691-200003000-00007
79. Iwasaki M, Nakasato N, Shamoto H, Nagamatsu KI, Kanno A, Hatanaka K, et al. Surgical implications of neuromagnetic spike localization in temporal lobe epilepsy. *Epilepsia.* (2002) 43:415–24. doi: 10.1046/j.1528-1157.2002.30801.x
80. Pataraia E, Lindinger G, Deecke L, Mayer D, Baumgartner C. Combined MEG/EEG analysis of the interictal spike complex in mesial temporal lobe epilepsy. *Neuroimage.* (2005) 24:607–14. doi: 10.1016/j.neuroimage.2004.09.031
81. Kaiboriboon K, Nagarajan S, Mantle M, Kirsch HE. Interictal MEG/MSI in intractable mesial temporal lobe epilepsy: spike yield and characterization. *Clin Neurophysiol.* (2010) 121:325–31. doi: 10.1016/j.clinph.2009.12.001
82. Tanaka N, Peters JM, Prohl AK, Takaya S, Madsen JR, Bourgeois BF, et al. Clinical value of magnetoencephalographic spike propagation represented by spatiotemporal source analysis: correlation with surgical outcome. *Epilepsy Res.* (2014) 108:280–8. doi: 10.1016/j.eplepsyres.2013.11.006
83. Yu T, Ni D, Zhang X, Wang X, Qiao L, Zhou X, et al. The role of magnetoencephalography in the presurgical evaluation of patients with MRI-negative operculo-insular epilepsy. *Seizure.* (2018) 61:104–10. doi: 10.1016/j.seizure.2018.07.005
84. Rampp S, Stefan H, Wu X, Kaltenhäuser M, Maess B, Schmitt FC, et al. Magnetoencephalography for epileptic focus localization in a series of 1000 cases. *Brain.* (2019) 142:3059–71. doi: 10.1093/brain/awz231
85. Stefan H, Hummel C, Scheler G, Genow A, Druschky K, Tilz C, et al. Magnetic brain source imaging of focal epileptic activity: a synopsis of 455 cases. *Brain.* (2003) 126:2396–405. doi: 10.1093/brain/awg239
86. Ossenblok P, De Munck JC, Colon A, Drolsbach W, Boon P. Magnetoencephalography is more successful for screening and localizing frontal lobe epilepsy than electroencephalography. *Epilepsia.* (2007) 48:2139–49. doi: 10.1111/j.1528-1167.2007.01223.x
87. Ishitobi M, Nakasato N, Yamamoto K, Iinuma K. Opercular to interhemispheric source distribution of benign rolandic spikes of childhood. *Neuroimage.* (2005) 25:417–23. doi: 10.1016/j.neuroimage.2004.11.040

88. Kakisaka Y, Iwasaki M, Alexopoulos A V., Enatsu R, Jin K, Wang ZI, et al. Magnetoencephalography in fronto-parietal opercular epilepsy. *Epilepsy Res.* (2012) 102:71–7. doi: 10.1016/j.eplepsyres.2012.05.003
89. Sommer B, Roessler K, Rampp S, Hamer HM, Blumcke I, Stefan H, et al. Magnetoencephalography-guided surgery in frontal lobe epilepsy using neuronavigation and intraoperative MR imaging. *Epilepsy Res.* (2016) 126:26–36. doi: 10.1016/j.eplepsyres.2016.06.002
90. Chibane IS, Boucher O, Dubeau F, Tran TPY, Mohamed I, McLachlan R, et al. Orbitofrontal epilepsy: case series and review of literature. *Epilepsy Behav.* (2017) 76:32–8. doi: 10.1016/j.yebeh.2017.08.038
91. Lieb JP, Dasheiff RM, Engel J, Genton (P, Genton (P. Role of the frontal lobes in the propagation of mesial temporal lobe seizures. *Epilepsia.* (1991) 32:822–37. doi: 10.1111/j.1528-1157.1991.tb05539.x
92. Hunold A, Funke ME, Eichardt R, Stenroos M, Haueisen J. EEG and MEG: sensitivity to epileptic spike activity as function of source orientation and depth. *Physiol Meas.* (2016) 37:1146–62. doi: 10.1088/0967-3334/37/7/1146
93. Jenssen S, Roberts CM, Gracely EJ, Dlugos DJ, Sperling MR. Focal seizure propagation in the intracranial EEG. *Epilepsy Res.* (2011) 93:25–32. doi: 10.1016/j.eplepsyres.2010.10.008
94. Oka A, Kubota M, Sakakihara Y, Yanagisawa M. A case of parietal lobe epilepsy with distinctive clinical and neuroradiological features. *Brain Dev.* (1998) 20:179–82. doi: 10.1016/S0387-7604(98)00011-4
95. Montavont A, Kahane P, Catenoix H, Ostrowsky-Coste K, Isnard J, Guénot M, et al. Hypermotor seizures in lateral and mesial parietal epilepsy. *Epilepsy Behav.* (2013) 28:408–12. doi: 10.1016/j.yebeh.2013.05.030
96. Gavaret M, Badier JM, Bartolomei F, Bénar CG, Chauvel P. MEG and EEG sensitivity in a case of medial occipital epilepsy. *Brain Topogr.* (2014) 27:192–6. doi: 10.1007/s10548-013-0317-7
97. Badier JM, Bartolomei F, Chauvel P, Bénar CG, Gavaret M. Magnetic source imaging in posterior cortex epilepsies. *Brain Topogr.* (2014) 28:162–71. doi: 10.1007/s10548-014-0412-4
98. Oishi M, Otsubo H, Kameyama S, Morota N, Masuda H, Kitayama M, et al. Epileptic spikes: magnetoencephalography versus simultaneous electrocorticography. *Epilepsia.* (2002) 43:1390–5. doi: 10.1046/j.1528-1157.2002.10702.x
99. Kakisaka Y, Wang ZI, Enatsu R, Dubarry AS, Mosher JC, Alexopoulos A V., et al. Magnetoencephalography correlate of EEG POSTS (positive occipital sharp transients of sleep). *J Clin Neurophysiol.* (2013) 30:235–7. doi: 10.1097/WNP.0b013e31827681a3
100. Carney PW, Harvey AS, Berkovic SF, Jackson GD, Scheffer IE. Siblings with refractory occipital epilepsy showing localized network activity on EEG-fMRI. *Epilepsia.* (2013) 54:28–32. doi: 10.1111/epi.12076
101. Kanazawa O, Tohyama J, Akasaka N, Kamimura T. A magnetoencephalographic study of patients with panayiotopoulos syndrome. *Epilepsia.* (2005) 46:1106–13. doi: 10.1111/j.1528-1167.2005.01105.x
102. Besson P, Andermann F, Dubeau F, Bernasconi A. Small focal cortical dysplasia lesions are located at the bottom of a deep sulcus. *Brain.* (2008) 131:3246–55. doi: 10.1093/brain/awn224
103. Wang ZI, Alexopoulos A V., Jones SE, Najm IM, Ristic A, Wong C, et al. Linking MRI postprocessing with magnetic source imaging in MRI-negative epilepsy. *Ann Neurol.* (2014) 75:759–70. doi: 10.1002/ana.24169
104. Saitoh M, Kubota M, Kimura I, Mizuguchi M, Igarashi T. A case of panayiotopoulos syndrome showing an atypical course. *Seizure.* (2006) 15:643–8. doi: 10.1016/j.seizure.2006.08.010
105. Salayev KA, Nakasato N, Ishitobi M, Shamoto H, Kanno A, Iinuma K. Spike orientation may predict epileptogenic side across cerebral sulci containing the estimated equivalent dipole. *Clin Neurophysiol.* (2006) 117:1836–43. doi: 10.1016/j.clinph.2006.05.003
106. Heers M, Rampp S, Stefan H, Urbach H, Elger CE, Von Lehe M, et al. MEG-based identification of the epileptogenic zone in occult peri-insular epilepsy. *Seizure.* (2012) 21:128–33. doi: 10.1016/j.seizure.2011.10.005
107. Goldenholz DM, Ahlfors SP, Hämäläinen MS, Sharon D, Ishitobi M, Vaina LM, et al. Mapping the signal-to-noise-ratios of cortical sources in magnetoencephalography and electroencephalography. *Hum Brain Mapp.* (2009) 30:1077–86. doi: 10.1002/hbm.20571
108. Jobst BC, Gonzalez-Martinez J, Isnard J, Kahane P, Lacuey N, Lahtoo SD, et al. The insula and its epilepsies. *Epilepsy Curr.* (2019) 19:11–21. doi: 10.1177/1535759718822847
109. Chourasia N, Quach M, Gavvala J. Insular magnetoencephalography dipole clusters in patients with refractory focal epilepsy. *J Clin Neurophysiol.* (2020). doi: 10.1097/WNP.0000000000000718. [Epub ahead of print].
110. Park HM, Nakasato N, Tominaga T. Localization of abnormal discharges causing insular epilepsy by magnetoencephalography. *Tohoku J Exp Med.* (2012) 226:207–11. doi: 10.1620/tjem.226.207
111. Mohamed IS, Gibbs SA, Robert M, Bouthillier A, Leroux JM, Nguyen DK. The utility of magnetoencephalography in the presurgical evaluation of refractory insular epilepsy. *Epilepsia.* (2013) 54:1950–9. doi: 10.1111/epi.12376
112. Zerouali Y, Pouliot P, Robert M, Mohamed I, Bouthillier A, Lesage F, et al. Magnetoencephalographic signatures of insular epileptic spikes based on functional connectivity. *Hum Brain Mapp.* (2016) 37:3250–61. doi: 10.1002/hbm.23238
113. Bagić AI, Funke ME, Kirsch HE, Tenney JR, Zillgitt AJ, Burgess RC. The 10 common evidence-supported indications for MEG in epilepsy surgery: an illustrated compendium. *J Clin Neurophysiol.* (2020) 37:483–97. doi: 10.1097/WNP.0000000000000726
114. Shawarba J, Kaspar B, Rampp S, Winter F, Coras R, Blumcke I, et al. Advantages of magnetoencephalography, neuronavigation and intraoperative MRI in epilepsy surgery re-operations. *Neurol Res.* (2021) 00:1–6. doi: 10.1080/01616412.2020.1866384
115. El Tahry R, Wang ZI, Thandar A, Podkorytova I, Krishnan B, Tousseyn S, et al. Magnetoencephalography and ictal SPECT in patients with failed epilepsy surgery. *Clin Neurophysiol.* (2018) 129:1651–7. doi: 10.1016/j.clinph.2018.05.010
116. Najm I, Jehi L, Palmini A, Gonzalez-Martinez J, Paglioli E, Bingaman W. Temporal patterns and mechanisms of epilepsy surgery failure. *Epilepsia.* (2013) 54:772–82. doi: 10.1111/epi.12152
117. Kirchberger K, Hummel C, Stefan H. Postoperative multichannel magnetoencephalography in patients with recurrent seizures after epilepsy surgery. *Acta Neurol Scand.* (1998) 98:1–7. doi: 10.1111/j.1600-0404.1998.tb07370.x
118. Matsuo F, Knott JR. Focal positive spikes in electroencephalography. *Electroencephalogr Clin Neurophysiol.* (1977) 42:15–25. doi: 10.1016/0013-4694(77)90147-X
119. Franco AC, Kremmyda O, Rémi J, Noachtar S. Positive interictal epileptiform discharges in adults: a case series of a rare phenomenon. *Clin Neurophysiol.* (2018) 129:952–5. doi: 10.1016/j.clinph.2018.01.059
120. Burgess RC. MEG Reporting. *J Clin Neurophysiol.* (2020) 37:545–53. doi: 10.1097/WNP.0000000000000700

Author Disclaimer: The content is solely the responsibility of the authors and does not necessarily represent the official views of the National Institutes of Health.

Conflict of Interest: The authors declare that the research was conducted in the absence of any commercial or financial relationships that could be construed as a potential conflict of interest.

The reviewer HS declared a past co-authorship/collaboration with one or more authors MF and AB.

Publisher's Note: All claims expressed in this article are solely those of the authors and do not necessarily represent those of their affiliated organizations, or those of the publisher, the editors and the reviewers. Any product that may be evaluated in this article, or claim that may be made by its manufacturer, is not guaranteed or endorsed by the publisher.

frontiers in Neurology

ORIGINAL RESEARCH
published: 25 October 2021
doi: 10.3389/fneur.2021.744749

Frequency-Dependent Dynamics of Functional Connectivity Networks During Seizure Termination in Childhood Absence Epilepsy: A Magnetoencephalography Study

*Jintao Sun[1], Yihan Li[1], Ke Zhang[1], Yulei Sun[1], Yingfan Wang[1], Ailiang Miao[1], Jing Xiang[2] and Xiaoshan Wang[1]**

[1] Department of Neurology, The Affiliated Brain Hospital of Nanjing Medical University, Nanjing Medical University, Nanjing, China, [2] Division of Neurology, MEG Center, Cincinnati Children's Hospital Medical Center, Cincinnati, OH, United States

Objective: Our aim was to investigate the dynamics of functional connectivity (FC) networks during seizure termination in patients with childhood absence epilepsy (CAE) using magnetoencephalography (MEG) and graph theory (GT) analysis.

Methods: MEG data were recorded from 22 drug-naïve patients diagnosed with CAE. FC analysis was performed to evaluate the FC networks in seven frequency bands of the MEG data. GT analysis was used to assess the topological properties of FC networks in different frequency bands.

Results: The patterns of FC networks involving the frontal cortex were altered significantly during seizure termination compared with those during the ictal period. Changes in the topological parameters of FC networks were observed in specific frequency bands during seizure termination compared with those in the ictal period. In addition, the connectivity strength at 250–500 Hz during the ictal period was negatively correlated with seizure frequency.

Conclusions: FC networks associated with the frontal cortex were involved in the termination of absence seizures. The topological properties of FC networks in different frequency bands could be used as new biomarkers to characterize the dynamics of FC networks related to seizure termination.

Keywords: childhood absence epilepsy, functional connectivity, magnetoencephalography, seizure termination, multifrequency

OPEN ACCESS

Edited by:
Rei Enatsu,
Sapporo Medical University, Japan

Reviewed by:
Hermann Stefan,
University Hospital Erlangen, Germany
Masaki Iwasaki,
National Center of Neurology and Psychiatry, Japan

****Correspondence:***
Xiaoshan Wang
wangxiaoshan52@163.com

Specialty section:
This article was submitted to Applied Neuroimaging, a section of the journal Frontiers in Neurology

Received: *20 July 2021*
Accepted: *21 September 2021*
Published: *25 October 2021*

Citation:
Sun J, Li Y, Zhang K, Sun Y, Wang Y, Miao A, Xiang J and Wang X (2021) Frequency-Dependent Dynamics of Functional Connectivity Networks During Seizure Termination in Childhood Absence Epilepsy: A Magnetoencephalography Study. Front. Neurol. 12:744749. doi: 10.3389/fneur.2021.744749

INTRODUCTION

Childhood absence epilepsy (CAE), with typical electroencephalography (EEG) signals showing 3 Hz spike and wave discharges (SWDs), is one of the most common epilepsy syndromes that occurs in childhood and accounts for 10–17% of epilepsies in children (1, 2). CAE has been historically considered a benign childhood epilepsy syndrome. However, an increasing number of studies have observed that brain function in children with CAE is persistently impaired (3, 4). Repeated seizures and epileptic discharges may impair brain function (5). Therefore, it is necessary to prevent

frequent epileptic seizures in children with CAE to alleviate the damage to brain function caused by seizures.

Epileptic seizures were considered the result of hypersynchronous and abnormal discharges among neurons. It was found that the synchronicity of neural activity was enhanced during ictal episodes (6). Some scholars have reported that hypersynchronized neuronal activity increases the chance of epileptic discharges and eventually leads to epileptic seizures (7–9). Therefore, it is possible that the decrease in neuronal synchronization could be a necessary process during seizure termination. However, inconsistent with the previous assumption, the synchronization of neural activity was reported to increase during seizure termination in several studies (10–12). Currently, the specific mechanism underlying seizure termination is still unclear. Understanding the mechanism contributing to seizure termination could offer new insights into its pathophysiological mechanism and be helpful for the development of novel treatments for epilepsy.

The brain can be seen as a complex network in which nodes of a network represent brain areas, and edges reflect either structural or functional connections between different nodes (6). An increasing amount of evidence has indicated that epilepsy is a network disease and that epileptic discharges spread to the whole brain through the network (6, 13–15). Previous studies have also revealed altered functional and structural networks in patients with epilepsy (13, 16–18).

Graph theory (GT) is an ideal tool for quantitative analysis of brain networks. It characterizes topological properties of brain networks through a line of parameters (19, 20). The clustering coefficient and shortest path length are the representative parameters in GT. Also, brain networks could be classified into three types, including small-world networks, random networks, and regular networks, according to these parameters (6, 19). Specific altered topological characteristics were observed in patients with epilepsy reported by several studies (21–23). Moreover, some network parameters were also suggested to be related to clinical features, such as cognitive function and duration of epilepsy, in patients with epilepsy (18, 24). Hence, topological parameters in GT could be used as new biomarkers for describing brain function and identifying the dynamic changes in brain function during seizure termination.

Magnetoencephalography (MEG) is an ideal method for investigating functional networks. MEG can detect magnetic signals from the brain through a non-invasive approach, which is usually used for patient evaluation before epileptic surgery (25, 26). MEG has a higher spatial resolution than EEG, as magnetic signals recorded by MEG are unaffected by the skin and skull (27). Moreover, the temporal resolution of MEG is higher than that of magnetic resonance imaging (fMRI) (27).

The aim of this study was to investigate the dynamic changes in functional connectivity (FC) networks from low- to high-frequency bands during seizure termination in children with CAE by using MEG. We analyzed changes in the pattern and topological properties of the FC networks. In addition, we assessed the association between FC networks and clinical features in children with CAE.

METHODS

Subjects

Children who were newly diagnosed with CAE were recruited from the Department of Neurology at the Nanjing Brain Hospital and Nanjing Children's Hospital. The inclusion criteria were as follows: (1) typical CAE diagnosed by a neurologist was in line with the International League Against Epilepsy Seizure Classification (2017), (2) bilaterally synchronous 3 Hz SWDs on normal background waves were detected by routine EEG, (3) the patients did not take any medication, and (4) MRI scan results were normal. The exclusion criteria were as follows: (1) history of any diseases or other types of epilepsy and (2) the presence of mental implants, such as pacemakers, which would strongly interfere with MEG recordings. This study was approved by the medical ethics committees of Nanjing Children's Hospital, Nanjing Brain Hospital, and Nanjing Medical University. All subjects and their guardians signed a written informed consent.

Magnetoencephalography Recording

The MEG data were recorded using a whole-head CTF MEG system with 275 channels (VSM Medical Technology Company, Canada) in a magnetically shielded room at the MEG Center at the Nanjing Brain Hospital. MEG data were acquired at a sample of 6,000 Hz, with noise cancelation of third-order gradients. MEG data recorded in an empty room were used to identify background noise. Before MEG recording, three coils were attached to the nasion and to the left and right preauricular points of each subject to locate the head position of the subject relative to the MEG coordinate system. All metals were also removed from the body of each subject before MEG data acquisition. During MEG recording, all subjects were instructed to stay still with their eyes lightly closed. The head movement of each subject was limited to 5 mm for each data recording. An audio-visual system was used to monitor each subject during MEG recording. At least five continuous data files with a duration of 120 s were collected for each subject. If no SWDs were observed in these data files, another MEG recording was needed, and the subjects were asked to hyperventilate to provoke absence seizures.

Magnetic Resonance Imaging Scan

All subjects underwent MRI with a 3.0 T scanner (Siemens, Germany). The MRI parameters were as follows: the repetition time was 6,600 ms, the echo time was 93 ms, the field of view was 250 × 250 mm, the flip angle was 9°, and the matrix was 512 × 512. Three markers were placed in the same position used for MEG recording to co-register structural imaging data with the MEG data. All anatomical landmarks digitized during MEG were identifiable in the MRI.

Data Analysis

All MEG data without any artifacts or background noise were retained. The ictal MEG data were determined using a filter of 1–4 Hz. The SWDs with a duration of more than 4 s were defined as ictal SWDs. The points of seizure onset and offset were identified by two experienced neurologists. Seizure onset was defined by the first spike wave component of SWDs, and seizure termination was defined by the last slow wave in SWDs.

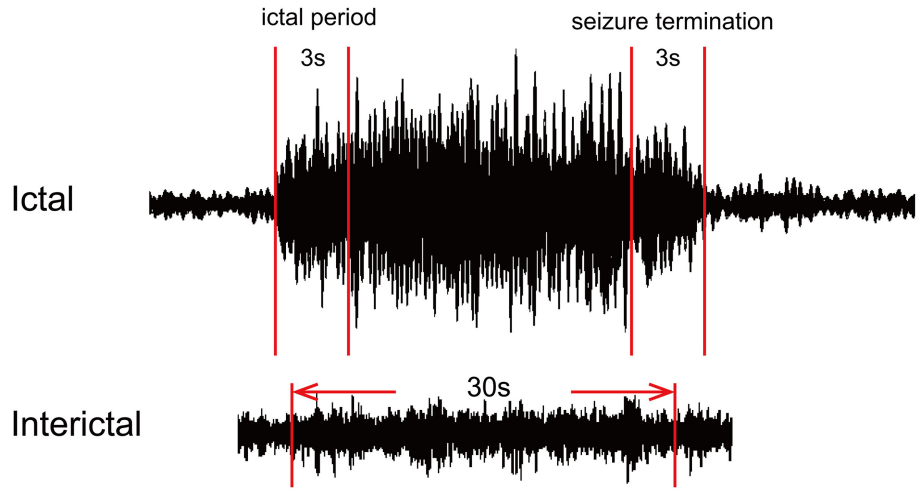

FIGURE 1 | Schematic diagram of magnetoencephalography (MEG) waveform data. For each MEG recording, two segments with a duration of 3 s represented the ictal period and termination period, and one 30-s segment was selected as the interictal period.

We selected three specific segments in each MEG recording for the following analysis. The segment with a duration of 3 s after seizure onset was defined as the ictal period, and the segment with the same duration before seizure offset represented the period of seizure termination. In addition, one segment with a duration of 30 s away from the ictal segment at least 10 s was considered as the interictal period. All selected segments were analyzed in seven frequency bands: delta (1–4 Hz), theta (4–8 Hz), alpha (8–12 Hz), beta (12–30 Hz), gamma (30–80 Hz), ripple (80–250 Hz), and fast ripple (250–500 Hz). Notch filters for 50 Hz and its harmonics were applied to eliminate power-line noise from the MEG data. The details are shown in **Figure 1**.

Functional Connectivity Analysis

According to previous studies (28, 29), FC was analyzed at the source level. To construct source neural networks, we used the algorithms to estimate the correlation of each pair of virtual sensors. Specifically, the correlation factors, which were used to analyze the correlation of virtual sensors, were defined as follows:

$$R\left(X_a, X_b\right) = \frac{C\left(X_a,\ X_b\right)}{SX_a,\ X_b} \tag{1}$$

In Equation (1), $R\left(X_a, X_b\right)$ represents the correlation of a source pair in two locations ("a" and "b"). X_a and X_b represent the signals from two sources, which were paired for computing connections. $C\left(X_a, X_b\right)$ represents the mean of the signals from the two sources. S_{xa} and S_{xb} represent the standard deviation of the signals from the two sources. We computed all possible connections for each pair of virtual sensors at the source level to avoid possible bias. If the activity in two source pairs were both increased, the connections were considered as excitatory in MEG processor computations. If increased activity in one source was followed by decreased activity in the other, the connections would be inhibitory. All possible distributions of FC from voxel-based virtual sensors were co-registered to individual participant MRI results (28, 30) and visualized in axial, coronal, and sagittal views. In MRI views, red and blue represent excitatory and inhibitory connections, respectively.

Graph Theory Analysis

In our study, we used GT to analyze and quantify FC networks at the source level (31). The FC networks in the entire brain consist of nodes and edges, where nodes represent the sources in the brain, and edges indicate the connections between each source pair. Specifically, four measurements including the average strength (S), degree (D), path length (L), and clustering coefficient (C) were computed for each possible source pair to quantify the global and local topological properties of FC networks. S indicates the connectivity strength between node pairs. The average S reflects the average of all connections in the FC network. D refers to the number of links connected to a node, and the average D indicates the average degree of all nodes in the FC network (32, 33). L indicates the shortest distance between node pairs in the network. The average L reflects the tendency of global integration in the FC network (34). C represents the likelihood of connection among the neighbors of a node, and the average C reflects the tendency of local integration in the FC network (34). The S, D, L, and C mentioned in our study indicate the average values of the measurements. The details of the equations for GT analysis were described in previous studies (32–34). MEG Processor software was used to analyze the above data (https://sites.google.com/site/braincloudx/). The detailed algorithms of the software were reported in previous articles (28, 29).

To ensure the quality of the data, a threshold was used as a checkpoint. The FC networks were visible in MRI views if the FC values were above the threshold. t-values were computed for all source pairs to determine the thresholding of connections. The

TABLE 1 | Characteristics of the patients with CAE.

Patient	Sex (F/M)	Age (years)	Duration of disease (months)	Frequency of seizures (times/day)	Time between diagnosis and the MEG test (day)
1	M	10	5	6	0
2	F	6	5	2	0
3	F	6	5	2	0
4	F	7	5	10	0
5	M	8	6	10	1
6	F	9	5	10	0
7	M	8	6	7	0
8	F	5	6	2	0
9	F	10	12	5	0
10	F	8	16	5	1
11	F	9	14	5	0
12	F	10	11	6	0
13	F	10	12	8	0
14	F	11	23	8	0
15	F	10	32	8	1
16	F	5	3	8	0
17	F	8	8	8	0
18	M	8	5	20	0
19	F	7	4	20	0
20	F	9	12	4	1
21	M	8	4	15	0
22	M	9	15	18	0

F indicates female; M indicates male.

formula to determine t-value was defined as follows:

$$T_p = R\sqrt{\frac{K-2}{1-R^2}} \quad (2)$$

In Equation (2), T_p represents the value of a correlation, K represents the number of data points for connections, and R indicates the correlation of a source pair. In the present study, we selected the T_p value corresponding to a p-value <0.05 as the thresholding to obtain the FC networks and the measurements including S, D, L, and C.

Statistical Analysis

Fisher's exact test was used to determine the difference in neural network patterns between different periods in seven frequency bands. Student's t-test was used to assess the changes in the network parameters (S, D, L, and C) between different periods in each frequency band. Partial correlation analysis was utilized to estimate the correlations between clinical characteristics and the network parameters after adjustment for age, sex, and duration of epilepsy. We set the p-value threshold as 0.05 in our study. Bonferroni correction was applied for multiple comparisons. Then, we controlled type I errors using the false discovery rate (FDR) controlling procedure. All statistical analyses and computations were performed in SPSS version 20.0 for Windows (SPSS Inc., Chicago, IL, USA).

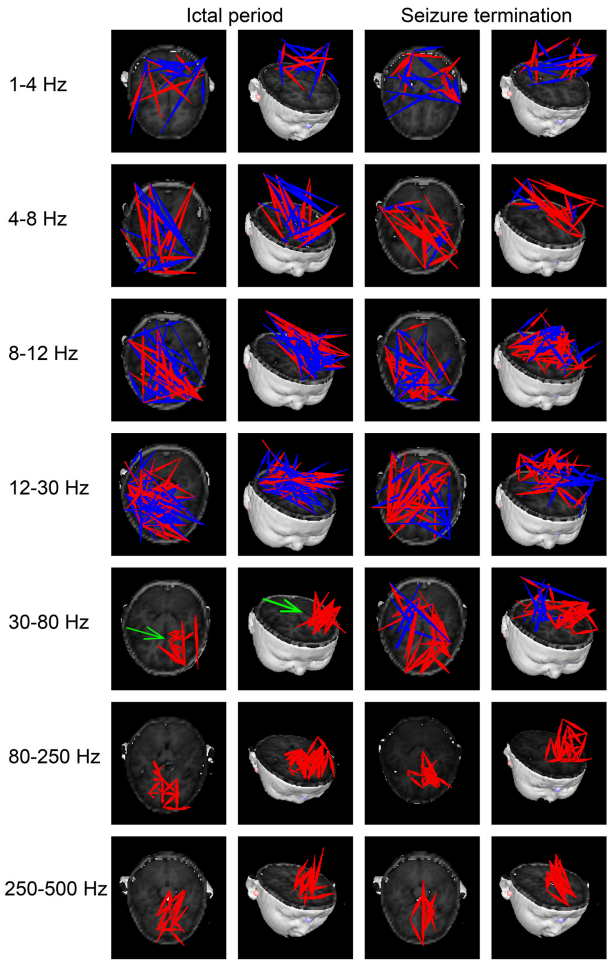

FIGURE 2 | Typical patterns of functional connectivity (FC) networks from childhood absence epilepsy (CAE) patients in seven frequency bands. Red indicates excitatory connections, and blue indicates inhibitory connections. The green arrow indicates significant differences in FC patterns between the two groups. The above results were significant ($p < 0.05$) after false discovery rate (FDR) and Bonferroni correction.

RESULTS

Patients

A total of 22 patients diagnosed with CAE were recruited in the present study. The mean age was 8.23 ± 1.69 years. The gender ratio was 6:16 (male: female). The mean course of epilepsy was 9.73 ± 7.12 months. To minimize the error in the frequency of seizures, we counted the absence seizures observed by parents of children with CAE in the last 1 week to obtain an average of seizure frequency. The average seizure frequency was 8.36 ± 5.41 times/day. A total of 33 ictal MEG data were recorded from all patients. There were 11 patients with one seizure and the other half of patients with two seizures during the acquisition. The duration of the SWDs selected in our analysis is more than 6 s, and there is no overlap between the ictal period and the seizure termination. The details of the clinical characteristics of children with CAE are presented in **Table 1**.

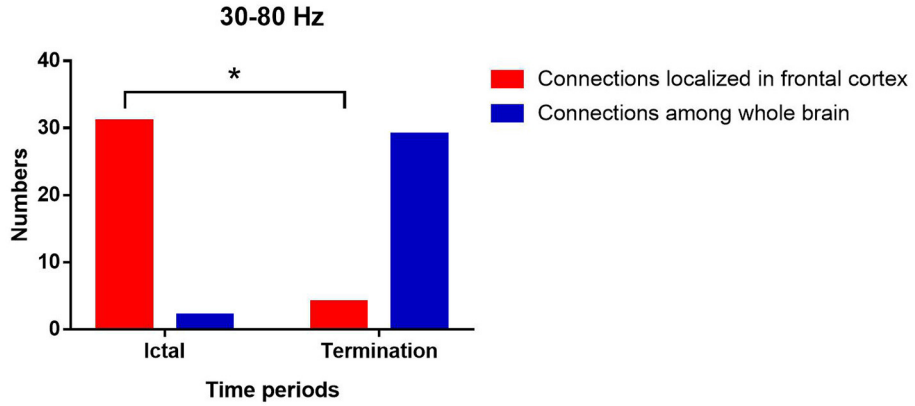

FIGURE 3 | Changes in the number of network patterns localized in frontal cortex in the two periods at 30–80 Hz. $P^* < 0.05$ after FDR and Bonferroni correction.

Network Pattern

At 1–4 Hz, the majority of FC networks (28 of 33 segments) during the ictal period showed strong connections in the parietal cortex and posterior brain regions. No significant difference was observed in the FC network between the ictal period and seizure termination (26 of 33 segments).

At 4–8, 8–12, and 12–30 Hz, the FC networks during the ictal period (30 of 33 segments) were distributed throughout regions in the whole brain, including the frontal cortex, parietal cortex, and posterior brain regions. There was no significant difference in the FC network between the ictal period and seizure termination (32 of segments).

At 30–80 Hz, the FC networks were mainly limited to the frontal cortex (31 of 33 segments) during the ictal period. Notably, the FC networks showed strong connections between anterior and posterior brain regions (29 of 33 segments) during seizure termination compared with the connections between these regions during the ictal period ($p < 0.05$).

At 80–250 and 250–500 Hz, the FC networks showed strong connections in the frontal cortex (31 of 33 segments). No significant difference was seen between the ictal period and the period of seizure termination (30 of 33 segments).

The above results were corrected by Bonferroni correction and FDR. The details are shown in **Figures 2**, **3**.

Graph Theory Parameters

In our study, we found that S values increased significantly at 30–80 Hz and decreased significantly at 250–500 Hz during seizure termination compared with that during the ictal period ($p < 0.05$). *D* values decreased significantly at 250–500 Hz during seizure termination compared with that during the ictal period ($p < 0.05$). C values decreased significantly at 30–80 and 250–500 Hz during seizure termination compared with that during the ictal period ($p < 0.05$). *L* values decreased significantly at 4–8, 8–12, and 30–80 Hz and increased significantly at 250–500 Hz during seizure termination compared with that during the ictal period ($p < 0.05$). No significant difference was found in other frequency bands. The above results were obtained after Bonferroni and FDR correction. The details are shown in **Figure 4**.

Clinical Correlation

At 250–500 Hz, after adjustment for sex, age, and duration of epilepsy, our data revealed that *S* values during the ictal period were negatively correlated with seizure frequency ($r = -0.597$, $p = 0.007$). There was no significant correlation in other frequency bands. The detailed correlation analysis is shown in **Figure 5**.

DISCUSSION

In the present study, we investigated the dynamic changes in FC networks during seizure termination in absence seizures using MEG. Our findings revealed that the FC network pattern was changed significantly at 30–80 Hz. Changes in topological parameters of FC networks were also observed in specific frequency bands during seizure termination. In addition, the FC strength at 250–500 Hz was significantly correlated with seizure frequency.

At 30–80 Hz, we found that the FC networks were limited to the frontal region during the ictal period. This finding supported the idea that the frontal cortex is involved in absence seizures. According to previous studies, the frontal cortex has an important role in the initiation and propagation of absence seizures (15, 35, 36). In addition, the localized pattern of FC networks found in our study reflected enhanced connections in local cortical regions and weakened connections among remote brain regions, which was consistent with previous publications (37–39). It is supposed that the increase in short-range synchronization among local neurons along with the decrease in long-range synchronization between distant brain regions might contribute to the generation of epileptic discharges (37–40). Another study also reported that synchronization in local neural populations plays a critical role in initiating seizures (41). Hypersynchronized FC networks involving the frontal cortex were a critical factor in the onset of absence seizures (15). Recent publications, which suggested that epileptic

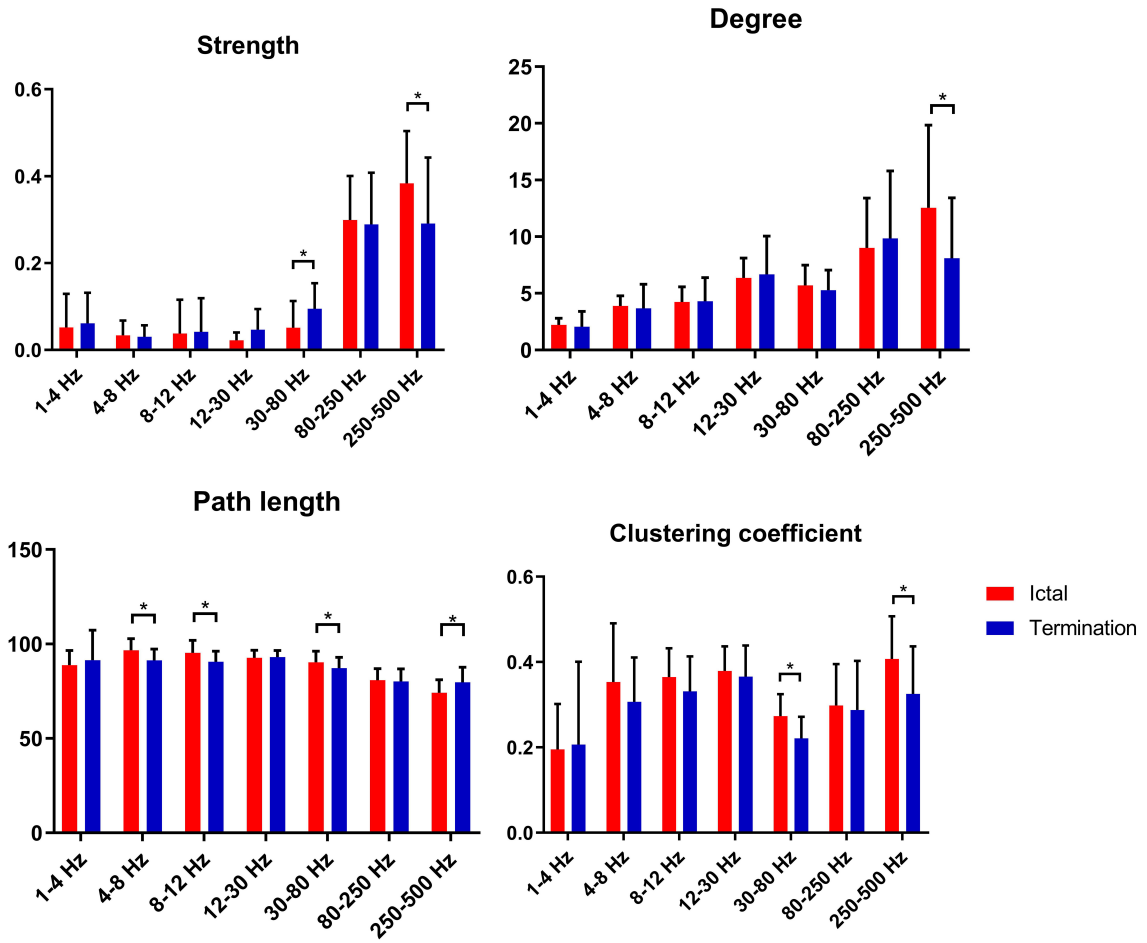

FIGURE 4 | Changes in topological parameters (strength, degree, path length, and clustering coefficient) of FC networks between two groups. $P^* < 0.05$ after FDR and Bonferroni correction.

discharges during absence seizures originate from the frontal lobe, could also partially explain the enhanced frontal FC networks observed in the present study during the ictal period in absence seizures (36, 42). During seizure termination, we noticed obvious connections between posterior and anterior brain regions replacing the limited network connections localized in frontal regions at 30–80 Hz. This difference in connections suggested that the long-range synchronization among remote brain regions was increased, leading to an altered FC network pattern among brain regions, including the frontal lobe, during seizure termination. In several studies, ictal epileptic networks were fragmented at seizure onset and then merged with other cortical regions gradually by long-range synchronization (38, 43, 44). Another study also found that the cortical regions involved in epileptic networks during seizure termination were wider than those at seizure onset, indicating that the changes in the patterns of FC networks participated in seizure termination (45). Moreover, altered function in the frontal lobe during seizure termination was reported by recent investigations (46, 47). Given the literature mentioned above as well as the results found in our study, we speculated that the changes in FC network patterns associated with the frontal cortex were involved in the termination of absence seizures. Further investigations exploring the specific mechanism of seizure termination involving the frontal cortex are needed in the future.

At the same time, we noticed frequency-dependent patterns of FC networks from low- to high-frequency ranges during absence seizures in our study. A previous study on absence seizures demonstrated that during the ictal period, FC networks were more likely to localize in posterior brain regions at low-frequency ranges and localize in anterior regions at high-frequency bands, which was consistent with our results (48). Other studies also found distinct alterations of networks in different frequency bands in CAE patients (13, 30, 47, 49, 50). According to a previous report, the types of connections in different frequency bands had specific interactions that allowed information to be integrated or shared at different spatiotemporal levels (48). For instance, low-frequency neural interactions were used to integrate information over a wider range of cortical regions, whereas high-frequency neural interactions were suited to

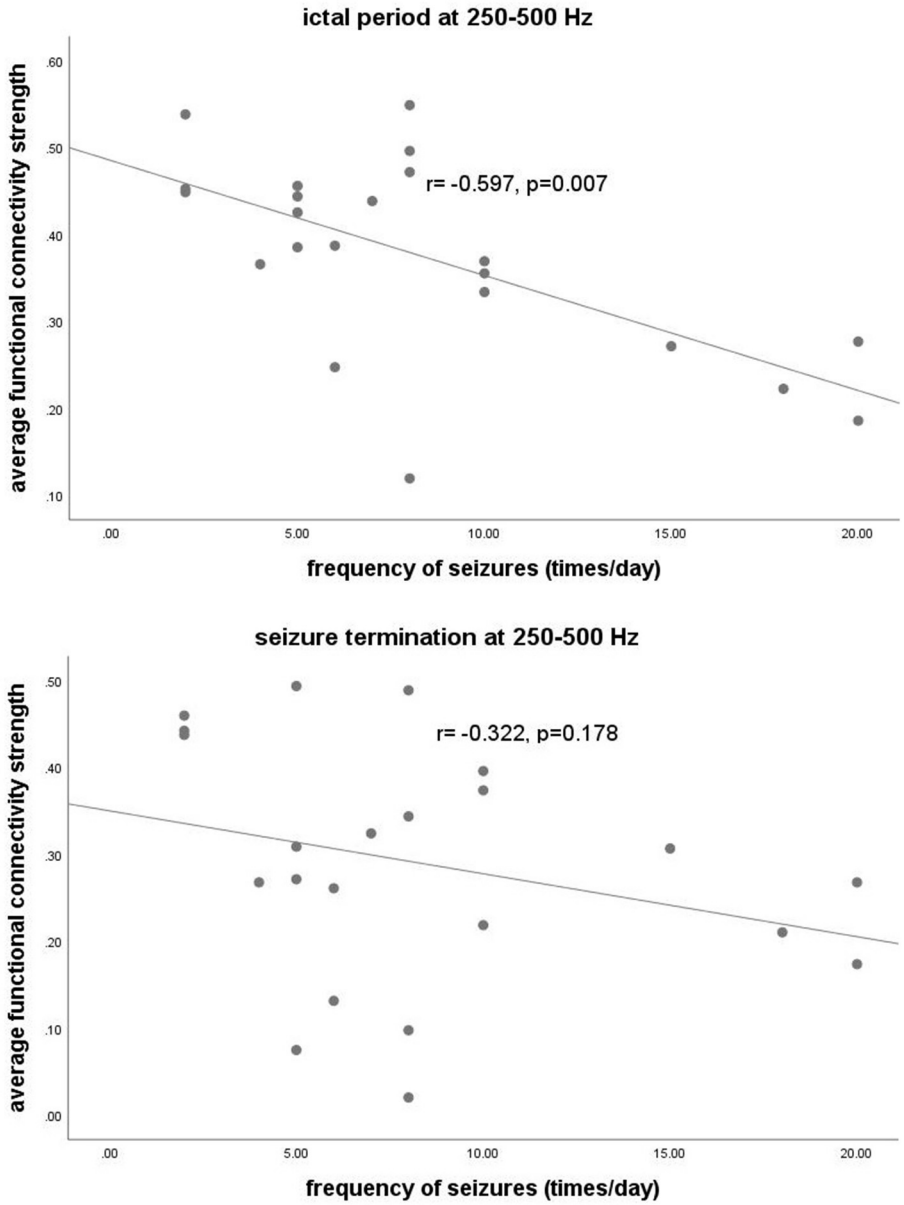

FIGURE 5 | The *y*-axis represents the functional connectivity strength. The *x*-axis represents seizure frequency. Partial correlation analysis showed that the functional connectivity strength at 250–500 Hz during the ictal period was negatively correlated with the frequency of seizures ($r = -0.597$, $p = 0.007$) after adjustment for sex, age, and duration of epilepsy.

communicate with neighboring neurons (30, 51, 52). Therefore, the changes in the patterns of FC networks observed in specific frequency bands instead of all frequency bands during seizure termination could be partially explained by the different roles that neural activity played in different frequency bands. These changes and their implications are worthy of further research.

Graph Theory Parameters

GT analysis in our study revealed increased S values and decreased *C* and *L* values at 30–80 Hz as well as decreased S, decreased D, decreased C, and increased *L* values at 250–500 Hz. These findings suggested that the topological properties of FC networks in patients with CAE were altered during seizure termination compared with those during the ictal period.

At 30–80 Hz, *S* values increased during seizure termination compared with those observed during the ictal period, suggesting that the synchronization of FC networks in the whole brain was enhanced significantly. One study on temporal lobe epilepsy also found similar enhanced synchronization before termination in the gamma frequency band, which was consistent with our results (53). Furthermore, increased synchronization of neural activity

was also observed before seizure offset in other studies and was thought to be related to seizure termination (10, 11, 44, 54, 55). Another study reported that vagal nerve stimulation (VNS), a non-invasive treatment for refractory epilepsy, may influence cortical activity by increasing gamma frequency synchrony, reducing the likelihood of seizure onset, or promoting seizure termination (41). In addition, we noticed that *C* and *L* values, which were considered as representative parameters of small-world networks, were decreased significantly during termination compared with those during the ictal period, indicating that the topological characteristics of FC networks were altered toward random networks. As reported by several studies, epileptic networks were more likely to be random networks characterized by decreased *C* and *L* values during the interictal period and were likely to function as regular networks accompanied by increased *C* and *L* values during the ictal period (13, 34, 56). Moreover, it was reported by other scholars that the *C* and *L* topological properties of epileptic networks increased at seizure onset and then decreased before seizure offset, again suggesting randomization trends in epileptic networks during seizure termination (38, 57, 58). Given that randomized networks are considered as the usual topological pattern of epileptic networks in the interictal period, we suppose that the topological properties of FC networks observed during termination might serve as transitional states from ictal to interictal periods, thus, combining the double topological characteristics in ictal and interictal periods.

At 250–500 Hz, the present study revealed that *S*, *D*, and *C* values were decreased, and *L* values were increased during the period of termination compared with those during the ictal period, which indicated that the topological organization during seizure termination was far from the optimal structure for information propagation. High-frequency oscillations (HFOs), especially fast ripples (ranging from 250 to 500 Hz), were reported to be related to the generation of seizures in recent literature (22, 30, 49). Therefore, we speculate that the topological organization at 250–500 Hz during the termination phase was a less efficient structure that might not be helpful for continuous epileptic discharges from the seizure onset zone (SOZ) and might promote seizure termination. The generation mechanisms of HFOs and gamma oscillations (30–80 Hz) were not the same, and these two oscillations have distinct patterns of network dynamics during the seizure period (59–61). Therefore, the differences in generation mechanisms could partially explain the different network patterns and topological properties we found at 30–80 and 250–500 Hz during seizure termination.

In general, we propose that the changes in parameters of network topology observed during termination at different frequency bands could be used as new biomarkers for characterizing the subtle dynamics of networks of CAE during termination, although the specific causal correlations between topological parameters and seizure termination warrant further investigation.

Clinical Correlation

In the present study, we found significant correlations between the *S* values of topological parameters at 250–500 Hz during the ictal period and the seizure frequency of CAE patients. According to previous studies, the brain region generating HFOs represents the SOZ and is involved in the initiation and propagation of epilepsy (22, 61). In recent years, HFOs have been used for mapping epileptic foci for epilepsy surgery (62, 63). Furthermore, several studies have found that HFOs are associated with the severity of seizures (43, 64–66). In our study, we suppose that the topological parameters of networks at 250–500 Hz could be considered as new biomarker options to estimate the severity of absence seizures.

Limitations

However, there are several limitations in this study. First, the sample size of this study was relatively small, which may have an impact on the results. Further studies investigating the potential mechanisms underlying seizure termination from the perspective of FC networks should be performed in a larger cohort of patients. Second, we did not discuss the potential effect of deep brain areas (DBAs), such as the thalamus, on seizure termination since the spatial resolution of MEG for deep brain detection is still under debate. In the future, this issue could be resolved by taking measurements with a moving MEG through a wearable system. Such a device could improve the spatial resolution of MEG in DBAs and acquire more accurate results than routine MEG devices (67). Third, although we minimized the artifacts, artifacts from electromyography and other signals may still be included in the MEG recordings and affect our results. Further investigations should be performed to determine whether artifacts have been eliminated completely. In addition, given the limitations of using single software program in our study, other imaging software is needed to confirm the repeatability of the results in further studies. Last but not least, although functional network analysis is one method to study the mechanism of seizure termination, the results and conclusion in the present study need to be verified by further investigations using different methods.

CONCLUSION

In conclusion, our study demonstrated that the FC networks during seizure termination differed from those during the ictal period in specific frequency bands. The pattern of FC networks involving the frontal cortex was altered during seizure termination, suggesting that the frontal lobe possibly plays a critical role in seizure termination. The topological parameters of FC networks changed during seizure termination, provided new biomarkers that could be used to characterize the dynamics of seizure termination, and were helpful for further investigating the specific relationships between topological properties of the network and seizure termination. The *S* values of topological parameters at 250–500 Hz were found to be correlated with seizure frequency, offering a new biomarker that could be used to estimate the severity of absence seizures.

DATA AVAILABILITY STATEMENT

The raw data supporting the conclusions of this article will be made available by the authors, without undue reservation.

ETHICS STATEMENT

This study was approved by the Medical Ethics Committees of Nanjing Children's Hospital, Nanjing Brain Hospital, and Nanjing Medical University. Written informed consent to participate in this study was provided by the participants' legal guardian/next of kin.

AUTHOR CONTRIBUTIONS

JS, YL, KZ, and XW designed the research. JS, YS, AM, YW, and JX analyzed the data. JS, KZ, YS, and YW recruited the participants and acquired the images. JS wrote the manuscript. XW revised the manuscript. All authors approved the final submitted version and agreed to be accountable for its content.

FUNDING

This study was supported by the General Program of Natural Science Foundation of Jiangsu Province (Grant No. BK20191127), the Health Department of Jiangsu Province (Grant No. H2018062), the Medical and Health International Cooperation Project of Nanjing Municipal Science and Technology Bureau (Grant No. 201911044), and the National Natural Science Foundation of China (Grant No. 82071455).

ACKNOWLEDGMENTS

We would like to thank the physicians and researchers at the NBH and Nanjing Children's Hospital. We are also very grateful for the support from all the participants and their guardians.

REFERENCES

1. Kessler SK, McGinnis E, A. practical guide to treatment of childhood absence epilepsy. *Paediatr Drugs.* (2019) 21:15–24. doi: 10.1007/s40272-019-00325-x
2. Crunelli V, Lorincz ML, McCafferty C, Lambert RC, Leresche N, Di Giovanni G, et al. Clinical and experimental insight into pathophysiology, comorbidity and therapy of absence seizures. *Brain.* (2020) 143:2341–68. doi: 10.1093/brain/awaa072
3. Masur D, Shinnar S, Cnaan A, Shinnar RC, Clark P, Wang J, et al. Pretreatment cognitive deficits and treatment effects on attention in childhood absence epilepsy. *Neurology.* (2013) 81:1572–80. doi: 10.1212/WNL.0b013e3182a9f3ca
4. Wald ELAF, Hendriksen JGM, Drenthen GS, Kuijk S, Aldenkamp AP, Vles JSH, et al. Towards a better understanding of cognitive deficits in absence epilepsy: a systematic review and meta-analysis. *Neuropsychol Rev.* (2019) 29:421–49. doi: 10.1007/s11065-019-09419-2
5. Yang T, Luo C, Li Q, Guo Z, Liu L, Gong Q, et al. Altered resting-state connectivity during interictal generalized spike-wave discharges in drug-naive childhood absence epilepsy. *Hum Brain Mapp.* (2013) 34:1761–7. doi: 10.1002/hbm.22025
6. Leitgeb EP, Sterk M, Petrijan T, Gradisnik P, Gosak M. The brain as a complex network: assessment of EEG-based functional connectivity patterns in patients with childhood absence epilepsy. *Epileptic Disord.* (2020) 22:519–30. doi: 10.1684/epd.2020.1203
7. Beenhakker MP, Huguenard JR. Neurons that fire together also conspire together: is normal sleep circuitry hijacked to generate epilepsy? *Neuron.* (2009) 62:612–32. doi: 10.1016/j.neuron.2009.05.015
8. Avoli M, de Curtis M, Gnatkovsky V, Gotman J, Köhling R, Lévesque M, et al. Specific imbalance of excitatory/inhibitory signaling establishes seizure onset pattern in temporal lobe epilepsy. *J Neurophysiol.* (2016) 115:3229–37. doi: 10.1152/jn.01128.2015
9. Levesque M, Ragsdale D, Avoli M. Evolving mechanistic concepts of epileptiform synchronization and their relevance in curing focal epileptic disorders. *Curr Neuropharmacol.* (2019) 17:830–42. doi: 10.2174/1570159X17666181127124803
10. Schindler K, Elger CE, Lehnertz K. Increasing synchronization may promote seizure termination: evidence from status epilepticus. *Clin Neurophysiol.* (2007) 118:1955–68. doi: 10.1016/j.clinph.2007.06.006
11. Afra P, Jouny CC, Bergey GK. Termination patterns of complex partial seizures: an intracranial EEG study. *Seizure.* (2015) 32:9–15. doi: 10.1016/j.seizure.2015.08.004
12. Aupy J, Wendling F, Taylor K, Bulacio J, Gonzalez-Martinez J, Chauvel P. Cortico-striatal synchronization in human focal seizures. *Brain.* (2019) 142:1282–95. doi: 10.1093/brain/awz062
13. Wu C, Xiang J, Jiang W, Huang S, Gao Y, Tang L, et al. Altered effective connectivity network in childhood absence epilepsy: a multi-frequency MEG study. *Brain Topogr.* (2017) 30:673–84. doi: 10.1007/s10548-017-0555-1
14. Park KM, Lee BI, Shin KJ, Ha SY, Park J, Kim TH, et al. Progressive topological disorganization of brain network in focal epilepsy. *Acta Neurol Scand.* (2018) 137:425–31. doi: 10.1111/ane.12899
15. Tangwiriyasakul C, Perani S, Centeno M, Yaakub SN, Abela E, Carmichael DW, et al. Dynamic brain network states in human generalized spike-wave discharges. *Brain.* (2018) 141:2981–94. doi: 10.1093/brain/awy223
16. Adebimpe A, Aarabi A, Bourel-Ponchel E, Mahmoudzadeh M, Wallois F. EEG resting state functional connectivity analysis in children with benign epilepsy with centrotemporal spikes. *Front Neurosci.* (2016) 10:143. doi: 10.3389/fnins.2016.00143
17. Qiu W, Gao Y, Yu C, Miao A, Tang L, Huang S, et al. Structural abnormalities in childhood absence epilepsy: voxel-based analysis using diffusion tensor imaging. *Front Hum Neurosci.* (2016) 10:483. doi: 10.3389/fnhum.2016.00483
18. Li Y, Sun Y, Zhang T, Shi Q, Sun J, Xiang J, et al. The relationship between epilepsy and cognitive function in benign childhood epilepsy with centrotemporal spikes. *Brain Behav.* (2020) 10:e01854. doi: 10.1002/brb3.1854
19. Bullmore E, Sporns O. Complex brain networks: graph theoretical analysis of structural and functional systems. *Nat Rev Neurosci.* (2009) 10:186–98. doi: 10.1038/nrn2575
20. Bernhardt BC, Bonilha L, Gross DW. Network analysis for a network disorder: the emerging role of graph theory in the study of epilepsy. *Epilepsy Behav.* (2015) 50:162–70. doi: 10.1016/j.yebeh.2015.06.005
21. van Diessen E, Zweiphenning WJ, Jansen FE, Stam CJ, Braun KP, Otte WM. Brain network organization in focal epilepsy: a systematic review and meta-analysis. *PLoS ONE.* (2014) 9:e114606. doi: 10.1371/journal.pone.0114606
22. Meng L, A magnetoencephalography study of pediatric interictal neuromagnetic activity changes and brain network alterations caused by epilepsy in the high frequency (80–1000 Hz). *IEEE Trans Neural Syst Rehabil Eng.* (2019) 27:389–99. doi: 10.1109/TNSRE.2019.2898683
23. Drenthen GS, Fasen F, Fonseca Wald ELA, Backes WH, Aldenkamp AP, Vermeulen RJ, et al. Functional brain network characteristics are associated with epilepsy severity in childhood absence epilepsy. *Neuroimage Clin.* (2020) 27:102264. doi: 10.1016/j.nicl.2020.102264
24. Qiu W, Yu C, Gao Y, Miao A, Tang L, Huang S, et al. Disrupted topological organization of structural brain networks in childhood absence epilepsy. *Sci Rep.* (2017) 7:11973. doi: 10.1038/s41598-017-10778-0
25. De Tiege X, Lundqvist D, Beniczky S, Seri S, Paetau R. Current clinical magnetoencephalography practice across Europe: are we closer to use MEG as an established clinical tool? *Seizure.* (2017) 50:53–9. doi: 10.1016/j.seizure.2017.06.002
26. Tamilia E, Madsen JR, Grant PE, Pearl PL, Papadelis C. Current and emerging potential of magnetoencephalography in the detection and localization of high-frequency oscillations in epilepsy. *Front Neurol.* (2017) 8:14. doi: 10.3389/fneur.2017.00014
27. Babiloni C, Pizzella V, Gratta CD, Ferretti A, Romani GL. Fundamentals of electroencefalography, magnetoencefalography, and

functional magnetic resonance imaging. *Int Rev Neurobiol.* (2009) 86:67–80. doi: 10.1016/S0074-7742(09)86005-4
28. Xiang J, Luo Q, Kotecha R, Korman A, Zhang F, Luo H, et al. Accumulated source imaging of brain activity with both low and high-frequency neuromagnetic signals. *Front Neuroinformatics.* (2014) 8:57. doi: 10.3389/fninf.2014.00057
29. Xiang J, Korman A, Samarasinghe KM, Wang X, Zhang F, Qiao H, et al. Volumetric imaging of brain activity with spatial-frequency decoding of neuromagnetic signals. *J Neurosci Methods.* (2015) 239:114–28. doi: 10.1016/j.jneumeth.2014.10.007
30. Xiang J, Tenney JR, Korman AM, Leiken K, Rose DF, Harris E, et al. Quantification of interictal neuromagnetic activity in absence epilepsy with accumulated source imaging. *Brain Topogr.* (2015) 28:904–14. doi: 10.1007/s10548-014-0411-5
31. Kruschwitz JD, List D, Waller L, Rubinov M, Walter H. GraphVar: a user-friendly toolbox for comprehensive graph analyses of functional brain connectivity. *J Neurosci Methods.* (2015) 245:107–15. doi: 10.1016/j.jneumeth.2015.02.021
32. Rubinov M, Sporns O. Complex network measures of brain connectivity: uses and interpretations. *Neuroimage.* (2010) 52:1059–69. doi: 10.1016/j.neuroimage.2009.10.003
33. Wang C, Xu J, Zhao S, Lou W. Graph theoretical analysis of EEG effective connectivity in vascular dementia patients during a visual oddball task. *Clin Neurophysiol.* (2016) 127:324–34. doi: 10.1016/j.clinph.2015.04.063
34. Reijneveld JC, Ponten SC, Berendse HW, Stam CJ. The application of graph theoretical analysis to complex networks in the brain. *Clin Neurophysiol.* (2007) 118:2317–31. doi: 10.1016/j.clinph.2007.08.010
35. Holmes MD, Brown M, Tucker DM. Are "generalized" seizures truly generalized? Evidence of localized mesial frontal and frontopolar discharges in absence. *Epilepsia.* (2004) 45:1568–79. doi: 10.1111/j.0013-9580.2004.23204.x
36. Tenney JR, Fujiwara H, Horn PS, Jacobson SE, Glauser TA, Rose DF. Focal corticothalamic sources during generalized absence seizures: a MEG study. *Epilepsy Res.* (2013) 106:113–22. doi: 10.1016/j.eplepsyres.2013.05.006
37. Warren CP, Hu S, Stead M, Brinkmann BH, Bower MR, Worrell GA. Synchrony in normal and focal epileptic brain: the seizure onset zone is functionally disconnected. *J Neurophysiol.* (2010) 104:3530–9. doi: 10.1152/jn.00368.2010
38. Kramer MA, Cash SS. Epilepsy as a disorder of cortical network organization. *Neuroscientist.* (2012) 18:360–72. doi: 10.1177/1073858411422754
39. Sobayo T, Fine AS, Gunnar E, Kazlauskas C, Nicholls D, Mogul DJ. Synchrony dynamics across brain structures in limbic epilepsy vary between initiation and termination phases of seizures. *IEEE Trans Biomed Eng.* (2013) 60:821–9. doi: 10.1109/TBME.2012.2189113
40. Amor F, Baillet S, Navarro V, Adam C, Martinerie J, Quyen MLV. Cortical local and long-range synchronization interplay in human absence seizure initiation. *Neuroimage.* (2009) 45:950–62. doi: 10.1016/j.neuroimage.2008.12.011
41. Lado FA, Moshe SL. How do seizures stop? *Epilepsia.* (2008) 49:1651–64. doi: 10.1111/j.1528-1167.2008.01669.x
42. Jun YH, Eom TH, Kim YH, Chung SY, Lee IG, Kim JM. Source localization of epileptiform discharges in childhood absence epilepsy using a distributed source model: a standardized, low-resolution, brain electromagnetic tomography (sLORETA) study. *Neurol Sci.* (2019) 40:993–1000. doi: 10.1007/s10072-019-03751-4
43. Ibrahim GM, Anderson R, Akiyama T, Ochi A, Otsubo H, Singh-Cadieux G, et al. Neocortical pathological high-frequency oscillations are associated with frequency-dependent alterations in functional network topology. *J Neurophysiol.* (2013) 110:2475–83. doi: 10.1152/jn.00034.2013
44. Jiruska P, de Curtis M, Jefferys JG, Schevon CA, Schiff SJ, Schindler K. Synchronization and desynchronization in epilepsy: controversies and hypotheses. *J Physiol.* (2013) 591:787–97. doi: 10.1113/jphysiol.2012.239590
45. de Curtis M, Avoli M. Initiation, propagation, and termination of partial (focal) seizures. *Cold Spring Harb Perspect Med.* (2015) 5:a022368. doi: 10.1101/cshperspect.a022368
46. Benuzzi F, Ballotta D, Mirandola L, Ruggieri A, Vaudano AE, Zucchelli M, et al. An EEG-fMRI study on the termination of generalized spike-and-wave discharges in absence epilepsy. *PLoS ONE.* (2015) 10:e0130943. doi: 10.1371/journal.pone.0130943
47. Sun J, Gao Y, Miao A, Yu C, Tang L, Huang S, et al. Multifrequency dynamics of cortical neuromagnetic activity underlying seizure termination in absence epilepsy. *Front Hum Neurosci.* (2020) 14:221. doi: 10.3389/fnhum.2020.00221
48. Tenney JR, Fujiwara H, Horn PS, Vannest J, Xiang J, Glauser TA, et al. Low- and high-frequency oscillations reveal distinct absence seizure networks. *Ann Neurol.* (2014) 76:558–67. doi: 10.1002/ana.24231
49. Wu C, Xiang J, Sun J, Huang S, Tang L, Miao A, et al. Quantify neuromagnetic network changes from pre-ictal to ictal activities in absence seizures. *Neuroscience.* (2017) 357:134–44. doi: 10.1016/j.neuroscience.2017.05.038
50. Shi Q, Zhang T, Miao A, Sun J, Sun Y, Chen Q, et al. Differences between interictal and ictal generalized spike-wave discharges in childhood absence epilepsy: a MEG study. *Front Neurol.* (2019) 10:1359. doi: 10.3389/fneur.2019.01359
51. Sauseng P, Klimesch W. What does phase information of oscillatory brain activity tell us about cognitive processes? *Neurosci Biobehav Rev.* (2008) 32:1001–13. doi: 10.1016/j.neubiorev.2008.03.014
52. Tenney JR, Kadis DS, Agler W, Rozhkov L, Altaye M, Xiang J, et al. Ictal connectivity in childhood absence epilepsy: associations with outcome. *Epilepsia.* (2018) 59:971–81. doi: 10.1111/epi.14067
53. Dheer P, Pati S, Chowdhury KK, Majumdar KK. Enhanced gamma band mutual information is associated with impaired consciousness during temporal lobe seizures. *Heliyon.* (2020) 6:e05769. doi: 10.1016/j.heliyon.2020.e05769
54. Schindler K, Leung H, Elger CE, Lehnertz K. Assessing seizure dynamics by analysing the correlation structure of multichannel intracranial EEG. *Brain.* (2007) 130:65–77. doi: 10.1093/brain/awl304
55. Majumdar K, Prasad PD, Verma S. Synchronization implies seizure or seizure implies synchronization? *Brain Topogr.* (2014) 27:112–22. doi: 10.1007/s10548-013-0284-z
56. Ponten SC, Douw L, Bartolomei F, Reijneveld JC, Stam CJ. Indications for network regularization during absence seizures: weighted and unweighted graph theoretical analyses. *Exp Neurol.* (2009) 217:197–204. doi: 10.1016/j.expneurol.2009.02.001
57. Schindler KA, Bialonski S, Horstmann MT, Elger CE, Lehnertz K. Evolving functional network properties and synchronizability during human epileptic seizures. *Chaos.* (2008) 18:033119. doi: 10.1063/1.2966112
58. Kramer MA, Eden UT, Kolaczyk ED, Zepeda R, Eskandar EN, Cash SS. Coalescence and fragmentation of cortical networks during focal seizures. *J Neurosci.* (2010) 30:10076–85. doi: 10.1523/JNEUROSCI.6309-09.2010
59. Draguhn A, Traub RD, Schmitz D, Jefferys JG. Electrical coupling underlies high-frequency oscillations in the hippocampus *in vitro*. *Nature.* (1998) 394:189–92. doi: 10.1038/28184
60. Roopun AK, Simonotto JD, Pierce ML, Jenkins A, Nicholson C, Schofield IS, et al. A nonsynaptic mechanism underlying interictal discharges in human epileptic neocortex. *Proc Natl Acad Sci USA.* (2010) 107:338–43. doi: 10.1073/pnas.0912652107
61. Fuertinger S, Simonyan K, Sperling MR, Sharan AD, Hamzei-Sichani F. High-frequency brain networks undergo modular breakdown during epileptic seizures. *Epilepsia.* (2016) 57:1097–108. doi: 10.1111/epi.13413
62. Jacobs J, Zijlmans M, Zelmann R, Chatillon CE, Hall J, Olivier A, et al. High-frequency electroencephalographic oscillations correlate with outcome of epilepsy surgery. *Ann Neurol.* (2010) 67:209–20. doi: 10.1002/ana.21847
63. Akiyama T, McCoy B, Go CY, Ochi A, Elliott IM, Akiyama M, et al. Focal resection of fast ripples on extraoperative intracranial EEG improves seizure outcome in pediatric epilepsy. *Epilepsia.* (2011) 52:1802–11. doi: 10.1111/j.1528-1167.2011.03199.x
64. Bragin A, Wilson CL, Engel J. Spatial stability over time of brain areas generating fast ripples in the epileptic rat. *Epilepsia.* (2003) 44:1233–7. doi: 10.1046/j.1528-1157.2003.18503.x
65. Miao A, Xiang J, Tang L, Ge H, Liu H, Wu T, et al. Using ictal high-frequency oscillations (80-500Hz) to localize seizure onset zones in childhood absence epilepsy: a MEG study. *Neurosci Lett.* (2014) 566:21–6. doi: 10.1016/j.neulet.2014.02.038
66. Tang L, Xiang J, Huang S, Miao A, Ge H, Liu H, et al. Neuromagnetic high-frequency oscillations correlate with seizure severity in absence epilepsy. *Clin Neurophysiol.* (2016) 127:1120–9. doi: 10.1016/j.clinph.2015.08.016

67. Boto E, Holmes N, Leggett J, Roberts G, Shah V, Meyer SS, et al. Moving magnetoencephalography towards real-world applications with a wearable system. *Nature.* (2018) 555:657–61. doi: 10.1038/nature26147

Conflict of Interest: The authors declare that the research was conducted in the absence of any commercial or financial relationships that could be construed as a potential conflict of interest.

Publisher's Note: All claims expressed in this article are solely those of the authors and do not necessarily represent those of their affiliated organizations, or those of the publisher, the editors and the reviewers. Any product that may be evaluated in this article, or claim that may be made by its manufacturer, is not guaranteed or endorsed by the publisher.

frontiers in Neurology

ORIGINAL RESEARCH
published: 26 October 2021
doi: 10.3389/fneur.2021.759866

Bilateral Representation of Sensorimotor Responses in Benign Adult Familial Myoclonus Epilepsy: An MEG Study

Teppei Matsubara[1,2,3,4]*, *Seppo P. Ahlfors*[1,2], *Tatsuya Mima*[5], *Koichi Hagiwara*[6], *Hiroshi Shigeto*[7], *Shozo Tobimatsu*[8], *Yoshinobu Goto*[9] *and Steven Stufflebeam*[1,2]

[1] Department of Radiology, Athinoula A. Martinos Center for Biomedical Imaging, Massachusetts General Hospital, Boston, MA, United States, [2] Harvard Medical School, Boston, MA, United States, [3] Research Fellow of Japan Society for the Promotion of Science, Tokyo, Japan, [4] International University of Health and Welfare, Otawara, Japan, [5] Graduate School of Core Ethics and Frontier Sciences, Ritsumeikan University, Kyoto, Japan, [6] Epilepsy and Sleep Center, Fukuoka Sanno Hospital, Fukuoka, Japan, [7] Division of Medical Technology, Department of Health Sciences, Graduate School of Medical Sciences, Kyushu University, Fukuoka, Japan, [8] Department of Orthoptics, Faculty of Medicine, Fukuoka International University of Health and Welfare, Fukuoka, Japan, [9] Department of Physiology, School of Medicine, International University of Health and Welfare, Okawa, Japan

Patients with cortical reflex myoclonus manifest typical neurophysiologic characteristics due to primary sensorimotor cortex (S1/M1) hyperexcitability, namely, contralateral giant somatosensory-evoked potentials/fields and a C-reflex (CR) in the stimulated arm. Some patients show a CR in both arms in response to unilateral stimulation, with about 10-ms delay in the non-stimulated compared with the stimulated arm. This bilateral C-reflex (BCR) may reflect strong involvement of bilateral S1/M1. However, the significance and exact pathophysiology of BCR within 50 ms are yet to be established because it is difficult to identify a true ipsilateral response in the presence of the giant component in the contralateral hemisphere. We hypothesized that in patients with BCR, bilateral S1/M1 activity will be detected using MEG source localization and interhemispheric connectivity will be stronger than in healthy controls (HCs) between S1/M1 cortices. We recruited five patients with cortical reflex myoclonus with BCR and 15 HCs. All patients had benign adult familial myoclonus epilepsy. The median nerve was electrically stimulated unilaterally. Ipsilateral activity was investigated in functional regions of interest that were determined by the N20m response to contralateral stimulation. Functional connectivity was investigated using weighted phase-lag index (wPLI) in the time-frequency window of 30–50 ms and 30–100 Hz. Among seven of the 10 arms of the patients who showed BCR, the average onset-to-onset delay between the stimulated and the non-stimulated arm was 8.4 ms. Ipsilateral S1/M1 activity was prominent in patients. The average time difference between bilateral cortical activities was 9.4 ms. The average wPLI was significantly higher in the patients compared with HCs in specific cortico-cortical connections. These connections included precentral-precentral, postcentral-precentral, inferior parietal (IP)-precentral, and IP-postcentral cortices interhemispherically (contralateral region-ipsilateral region), and precentral-IP and postcentral-IP intrahemispherically (contralateral region-contralateral region). The

OPEN ACCESS

Edited by:
Rei Enatsu,
Sapporo Medical University, Japan

Reviewed by:
Yasuo Terao,
Kyorin University, Japan
Akihiro Shimotake,
Kyoto University, Japan

***Correspondence:**
Teppei Matsubara
tmatsubara@mgh.harvard.edu

Specialty section:
This article was submitted to Applied Neuroimaging, a section of the journal Frontiers in Neurology

Received: *17 August 2021*
Accepted: *21 September 2021*
Published: *26 October 2021*

Citation:
Matsubara T, Ahlfors SP, Mima T, Hagiwara K, Shigeto H, Tobimatsu S, Goto Y and Stufflebeam S (2021) Bilateral Representation of Sensorimotor Responses in Benign Adult Familial Myoclonus Epilepsy: An MEG Study. Front. Neurol. 12:759866. doi: 10.3389/fneur.2021.759866

ipsilateral response in patients with BCR may be a pathologically enhanced motor response homologous to the giant component, which was too weak to be reliably detected in HCs. Bilateral representation of sensorimotor responses is associated with disinhibition of the transcallosal inhibitory pathway within homologous motor cortices, which is mediated by the IP. IP may play a role in suppressing the inappropriate movements seen in cortical myoclonus.

Keywords: benign adult familial myoclonus epilepsy (BAFME), sensorimotor cortex, ipsilateral somatosensory-evoked field, C-reflex, transcallosal connectivity

INTRODUCTION

Conventional neurophysiological studies have demonstrated that one type of myoclonus originates from the cerebral cortex (1–3). This type of myoclonus is often referred to as cortical reflex myoclonus, seen in various diseases such as juvenile myoclonic epilepsy, progressive myoclonic epilepsy, post-anoxic myoclonus, corticobasal degeneration, Alzheimer's disease, advanced Creutzfeldt-Jacob diseases, metabolic encephalopathy and Celiac disease (1–3). Cortical reflex myoclonus manifests two major neurophysiological characteristics that are due to primary sensorimotor cortex (S1/M1) hyperexcitability (4–7), namely, the giant somatosensory-evoked potential/field (SEP/SEF) and the C-reflex (CR; **Figure 1**). Giant SEP/SEF refers to the enhanced amplitudes of S1/M1 activation. CR, or long-loop reflex, is the EMG response associated with myoclonic jerks that is recorded from the stimulated hand at a latency of around 45 ms after stimulation of the median nerve in the wrist (5, 8, 9). These characteristics are thought to result from a release effect that causes increased excitability at central synapses along the pathway that begins from peripheral input to the spinal cord, the contralateral nucleus of thalamus, contralateral S1/M1, corticospinal tract, anterior horn cell, and finally to the stimulated hand muscle (9).

In some patients, an EMG response is demonstrated in the non-stimulated (opposite) hand muscle (bilateral C-reflex, BCR). In a few reports of small case series, the latency difference between CRs in the stimulated and non-stimulated hand muscle was ∼10 ms (CR-BCR time lag, **Figure 1**) (3, 10–12). This time lag is compatible with the conduction time of the impulse between the homologous S1/M1 via the corpus callosum (13, 14). However, the significance and exact pathophysiology of this BCR is yet to be established. In previous BCR studies, which all employed EEG, identifying ipsilateral cortical activity has been challenging because cross-talk from the giant SEP component in the contralateral hemisphere can overshadow a true response in the ipsilateral hemisphere (4). Source localization methods hold a promise of better dissociating ipsilateral and contralateral activity and thus may help to reveal the precise pathophysiology of BCR. Given the close link between the processes involved in cortical myoclonus and those producing epilepsy (2, 15), the same mechanisms of spread of cortical excitation may also be important in some forms of seizure generalization.

The aim of the present study was to examine the pathophysiological mechanism underlying the early spread of cortical excitation in the bilateral representation of myoclonic jerks in patients showing BCR. The presence of a CR-BCR time lag suggests that (1) ipsilateral cortical activity (i.e., the same side as the stimulated hand) exists, and (2) the time lag between the contralateral (i.e., opposite side to the stimulated hand) and ipsilateral cortical activity corresponds to the CR-BCR time lag. We hypothesized that in patients with BCR (1) bilateral S1/M1 activity can be detected by magnetoencephalography (MEG) source estimation and (2) functional connectivity will be enhanced transcallosally between the contralateral S1/M1 and homologous ipsilateral regions.

MATERIALS AND METHODS

Subjects

Five patients with cortical reflex myoclonus (age 40–70 years, mean age 54.9 years) with BCR were identified from the MEG database of epilepsy patients (January 2005–June 2019) at Kyushu University. All patients had benign adult familial myoclonus epilepsy (BAFME) that fulfilled criteria based on clinical and electrophysiological findings (12, 16, 17) and were treated with antiepileptic drugs (AEDs). The diagnosis was made by board-certified epileptologists (TMa and HS). The cardinal features of BAFME consisted of six items (18, 19): (1) autosomal dominant inheritance; (2) cortical tremor, which consists of continuous, distal, fine twitches of the hands that resemble essential tremor; (3) infrequent generalized seizure; (4) features of cortical reflex myoclonus demonstrated in electrophysiological studies; (5) lack of cognitive decline or other neurological symptoms during the early stage of the clinical course; and (6) lack of clear progression, which impairs activities of daily living in the early stage of the clinical course. Electrophysiological studies included resting-state scalp EEG, SEP, CR, and jerk-locked back averaging (JLA) (20). SEP/CR/BCR was performed as a screening; the recording procedure is described in section SEP and CR/BCR below. JLA, time-locked pre-myoclonus cortical activity (3, 21, 22) showed

Abbreviations: AED, antiepileptic drug; BAFME, benign adult familial myoclonus epilepsy; BCR, bilateral C-reflex; CR, C-reflex; DK Atlas, Desikan-Killiany Atlas; dSPM, dynamic statistical parametrical mapping; ECD, equivalent current dipole; HC, healthy control; IP, inferior parietal cortex; ISI, interstimulus interval; ITC, intertrial phase coherence; JLA, jerk-locked back averaging; MEG, magnetoencephalography; PoC, postcentral gyrus; PreC, precentral gyrus; ROI, region of interest; SD, standard deviation; SEF, somatosensory-evoked field; SEP, somatosensory-evoked potential; S1/M1, primary sensorimotor cortex; S2, secondary somatosensory cortex; wPLI, weighted phase-lag index.

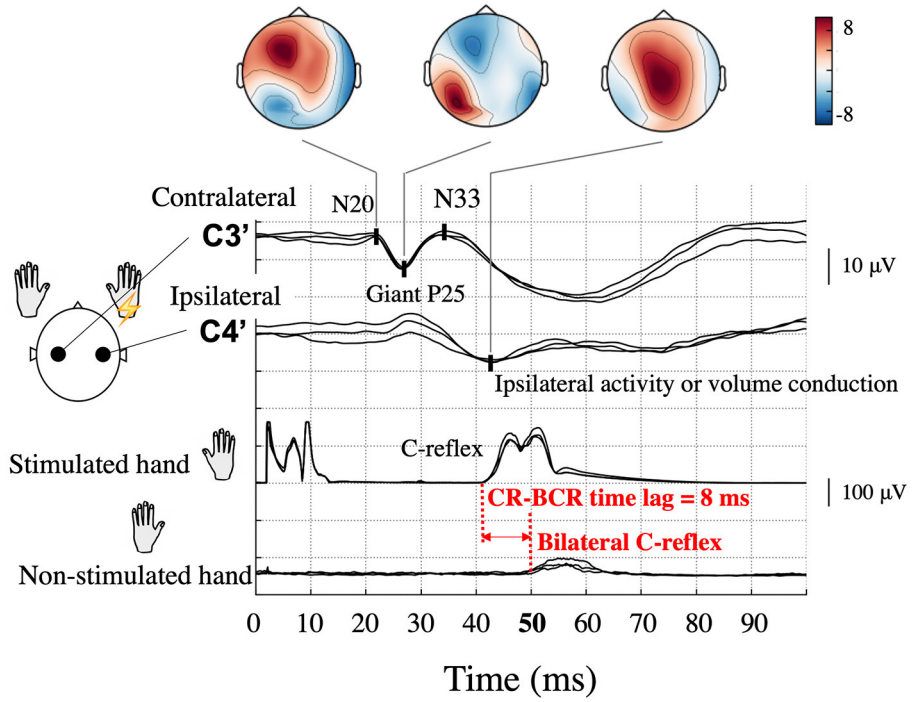

FIGURE 1 | Typical somatosensory-evoked potential and electromyography recordings following right median nerve stimulation in a patient (Patient 2) with bilateral C-reflex (BCR). High amplitude P25-N33 components (giant P25) are prominent at the contralateral hand sensory area (C3′) electrode, and similar potentials can be observed at the corresponding ipsilateral electrode (C4′). Topographical maps are shown according to components. Ipsilateral activity is unreliable because of interference from the contralateral giant component. The onset of the C-reflex (CR), which is shown in the stimulated hand, was 42 ms, whereas that of the BCR in the non-stimulated hand was 50 ms; thus, the CR-BCR time lag was 8 ms.

no preceding positive spikes in any of the patients. Cortical myoclonus in Celiac diseases and corticobasal degeneration shows no preceding positive spikes because of repetitive nature and high frequency of the myoclonus (23), therefore JLA may sometimes show no activity in cortical tremor. Patient demographic data are shown in **Table 1**. A total of 15 healthy controls (HCs, age 25–51 years, mean 34.6) were recruited. All subjects gave informed consent, according to the approval by the Ethical Committee of Kyushu University Hospital.

Stimulus

The median nerve trunk in the wrist was unilaterally stimulated with an electric square pulse of 0.2 ms duration in separate sessions. The stimulus was applied using a pair of electrodes placed on the skin 3 cm apart with the cathode proximal to the anode. Stimulus intensity was just above the motor threshold of the abductor pollicis brevis muscle. Stimulus parameters were different for SEP/CR/BCR and SEF recordings because SEP/CR/BCR was used for diagnostic confirmation of cortical reflex myoclonus (i.e., long latency), whereas SEF was measured as part of routine clinical workup for epilepsy patients, irrespective of seizure type (i.e., short latency) (24).

MEG Recordings

MEG signals were recorded using a whole-head 306 channel sensor array (Elekta, Neuromag) with 102 identical triple-sensor elements. Before recording, four head-position-indicator coils were attached to the subject's head. Anatomical landmarks (nasion and bilateral preauricular points) and scalp shape using ∼200 head-surface points were digitized to construct a three-dimensional head coordinate system co-registered with MRI. At the beginning of the recording session, the subject's head position was measured with respect to the sensor array. The recording was performed in a quiet magnetically-shielded room while subjects lay in a supine position with their head positioned inside the helmet-shaped sensor array. The sampling rate was 1 kHz with an online band-pass filter of 0.1–330 Hz for Patients 1, 2, and 4. For Patients 3 and 5, the sampling rate was 5 kHz and the data were downsampled to 1 kHz. A spatiotemporal signal space separation method was applied to the data offline to reduce external artifact signals (25).

MRI Scan

High-resolution three-dimensional MRI images were acquired using a 3-T clinical scanner (Philips Healthcare, Best, the Netherlands). The whole brain was scanned using a T1-weighted fast-field echo sequence using the following parameters: repetition time = 8.2 ms; echo time = 3.8 ms; flip angle = 8°; 190 sagittal slices; and 1.0-mm isotropic voxels without a gap. Cortical surface reconstructions were obtained using FreeSurfer (26).

TABLE 1 | Patient demographic information.

Subject	Age/sex	Family history	EEG findings	Age at seizure onset	Frequency of generalized seizures	Cortical tremor	Medication
Patient 1	40.2/F	Family A	Generalized Photoparoxysmal discharges	33	<1/y	BUE	LEV
Patient 2	70.2/F	Family A	Generalized Photoparoxysmal discharges	42	<1/y	BUE	PHT, LEV
Patient 3	56.1/F	Family B	W.N.L.	None	None	BUE < BLE	CZP
Patient 4	54.2/F	Sporadic	Generalized Photoparoxysmal discharges	23	6/y	BUE	LEV, CZP
Patient 5	53.7/M	Family B	Generalized Photomyogenic response*	None	None	BUE	CZP

BUE, bilateral upper extremities; BLE, bilateral lower extremities; LEV, levetiracetam; PHT, phenytoin; CZP, clonazepam.
**Lower extremity myoclonus accompanied with photic stimulation.*

Data Analysis

SEP and CR/BCR

CR/BCR and giant SEP were confirmed as a screening prior to MEG recording on a separate day. Surface EMG was recorded bilaterally from a pair of cup electrodes placed 3 cm apart on the belly of the abductor pollicis brevis muscle of the stimulated side and on the other muscles that produced involuntary jerks (CR and BCR). For EEG recording, multiple cup electrodes were placed on the scalp, which included the hand sensory areas (C3′ and C4′) and Fz according to the International 10–20 system. Electrode impedance was maintained below 5 kOhm. All electrodes were referenced to linked earlobe electrodes. EEG and rectified EMG data were fed into a computer and averaged using the stimulus pulse as the trigger. SEP and CR/BCR were obtained by stimulating the median nerve in the wrist using electric shocks, which were delivered at a rate of 1 Hz in all patients. The passband for EEG was set to 0.5–200 Hz. Components of giant SEPs were identified by corresponding components of normal SEPs (27): an initial negative peak was defined as N20, a following positive peak as P25, and a second negative peak as N33. An SEP was judged as a giant SEP when the amplitude of the component corresponding to N33 measured from the P25 peak was higher than 8.4 μV (3, 27). CR/BCR was identified when the EMG amplitude showed a prominent rise from baseline (3). Data from at least two separate sessions of 200 responses each were obtained to confirm reproducibility. Typical giant SEP and CR/BCR are illustrated in **Figure 1**. It should be noted that ipsilateral activity in the SEP may mimic the giant component coming from the contralateral hemisphere (4).

Although all patients demonstrated CR in both arms during left and right median nerve stimulation, BCR was observed in the left, right, or both arms. For each arm that showed BCR, we also measured the time lag between CR and BCR for onset-to-onset (CR-BCR time lag, **Figure 1**).

SEF

For Patients 1, 2, and 5, and all HCs, the interstimulus interval (ISI) was constant at 449 ms. For Patient 4 the ISI was 997 ms, and for Patient 3, stimuli were presented using a 2,000-ms ISI with a 250 ms jitter. SEFs were obtained by averaging ∼120 responses offline. Trials exceeding 4,000 fT/cm in amplitude on a gradiometer and 4,000 fT on a magnetometer were excluded before averaging. Artifacts, such as eye blinks, other eye movements, and epileptic spikes, were carefully excluded by visual inspection. Raw MEG data were band-pass filtered at 1–120 Hz. The analysis time window was 200 ms, which included a pre-stimulus baseline of 100 ms. Amplitudes were measured from baseline. Because of a lack of clear criteria for giant SEF, activity was judged as a giant SEF when P25m source activity (see section Source estimation), normalized by the N20m amplitude, was greater than the average + 2 standard deviations (SD) of that of HCs. For Patient 5, SEF data from the left median nerve stimulation were not recorded because of a technical reason. During the SEF recording, simultaneous EMG was measured in two of the patients (Patients 2 and 4).

Source Estimation

Source current distributions for the SEFs were estimated using the minimum-norm estimate (MNE) (28, 29) and noise-normalized using the dynamic statistical parametrical mapping (dSPM) method (30). The cortical source space consisted of 8,196 dipoles. The forward solution was computed using a Boundary Element Method mesh by tessellating the inner skull surface (31). Source orientation was partially constrained to be perpendicular to the cortex, with the loose orientation constraint parameter set to 0.2 (32). The noise covariance matrix was estimated from the baseline period. Source time courses for each region of interest (ROI) were obtained by averaging the estimated dSPM time for all source dipoles within the ROI. The MNE solutions were regularized by setting the parameter for the expected signal-to-noise ratio to 3.

Delineating the Primary Sensorimotor Areas

In BAFME patients, SEF typically includes contralateral N20m and P25m. The N20m represents the normal response from S1 [specifically, it represents the thalamocortical tract (33)]. Indeed, in our BAFME patients, the amplitude and latency of the N20m in the sensor space were not significantly different from those in the HCs (64.5 ± 42.7 fT/cm vs. 56.8 ± 24.0 fT/cm for amplitude, $p = 0.44$; 21.3 ± 1.3 vs. 22.1 ± 1.5 ms for latency, $p = 0.07$). In contrast, the contralateral P25m represents a giant response

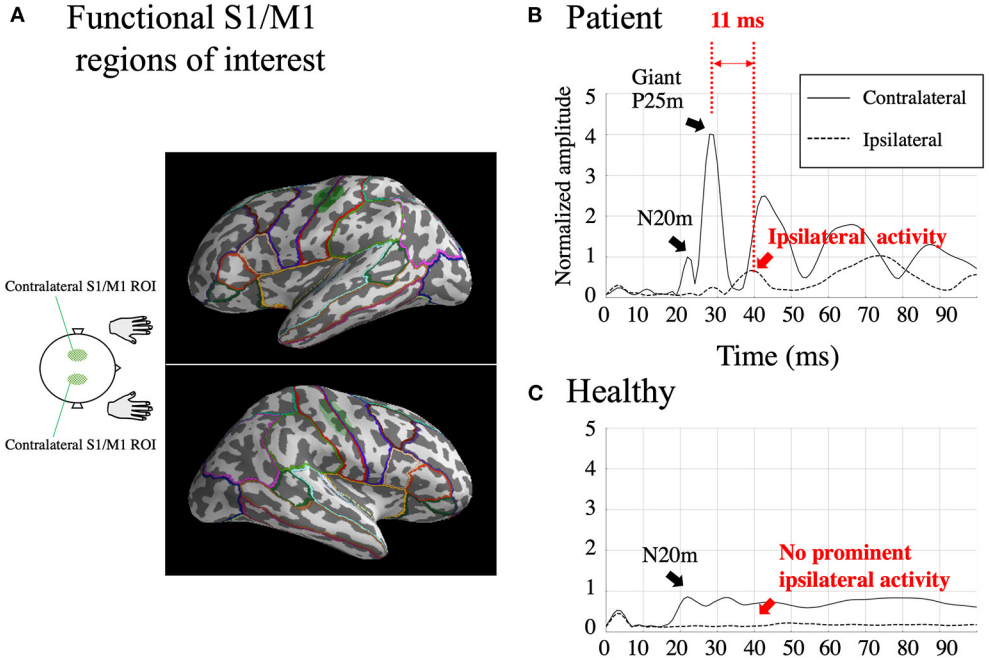

FIGURE 2 | Functional S1/M1 regions of interest (ROIs; green shaded areas) are shown in one subject [Patient 2; **(A)**]. Borders of anatomical regions obtained from the Desikan-Killiany Atlas are shown in different colors. Estimated somatosensory-evoked field source activity within functional S1/M1 regions of interest in response to right median nerve stimulation from one patient who showed BCR [Patient 2; **(B)**] and the grand-average of healthy controls **(C)**. Black lines: contralateral activity; dotted lines: ipsilateral activity. The figure shows a prominent contralateral giant P25m component. The ipsilateral activity, shown within 50 ms, peaks 11 ms later than the contralateral giant component. The amplitudes were individually normalized by contralateral N20m amplitudes.

from S1 and/or M1. Although the generator of the giant P25m is yet to be established, Mima et al. (6) reported equivalent current dipoles (ECDs) of P25m were located at the precentral motor cortex (Brodmann area 4) in 4 patients with cortical reflex myoclonus among 5 patients. A giant P25m may reflect the tangential component of an enlarged radial generator source located at the crown of the precentral gyrus (6, 34). However, P25m in HCs is rarely recognizable, which is likely related to the orientation of the generator source; few reports on P25m (P22m) have been published to date (35, 36).

Because our primary concern is hyperexcitability of S1/M1 in patients with BCR, we first defined functional ROIs to represent S1/M1. The functional S1/M1 ROIs were delineated individually for both the patients and HCs based on the cortical activations at the peak of the contralateral N20m. The S1/M1 ROIs were located at the border of the anatomical central sulcus (**Figure 2A**, green shaded areas). On average, the delineated S1/M1 ROIs contained 49.8 ± 22.1 dipoles in the patients and 50.2 ± 16.4 dipoles in HCs ($p = 0.28$). Because of the spatial point-spread function, even for a focal source, the MNE solution can extend across sulcal walls (37, 38); therefore, it is reasonable to assume that ROIs determined using the N20m can represent both S1 and M1 activity. The S1/M1 ROIs were obtained for each stimulus to the left and right median nerve in all patients except Patient 5. In Patient 5, who did not have a recording of the left median nerve stimulation, the right S1/M1 ROI was defined using the location homologous to that obtained from the right median nerve stimulation.

The two homologous S1/M1 ROIs were used to investigate ipsilateral activity evoked by the median nerve stimuli. For patients with BCR, ipsilateral activity was identified when the activity increased prominently above baseline and peaked at 20–50 ms. For comparison, the amplitude of any ipsilateral activity at 20–50 ms was investigated in HCs. This time window was set based on the finding (**Table 2**) that the average onset time of BCR was 46 ± 1.8 ms (range 43–48 ms). Ipsilateral activity in patients with BCR should be observed after the first cortical activity (contralateral N20m) and before BCR (i.e., within the 20–50 ms latency window). In contrast, HCs were expected to show no significant ipsilateral activity within 50 ms because only a few studies have demonstrated physiological ipsilateral activity in SEF within this time range (39–41) due to signal weakness (42). Focusing on the activity within 50 ms also helps to exclude the possibility of top-down input from secondary somatosensory cortex S2, which displays initial activation at around 60–70 ms after stimulation (43).

Neural Synchrony

We calculated two indices of neural synchrony: the intertrial phase coherence (ITC), which represents phase synchronization with respect to the stimuli, and the weighted phase-lag index (wPLI), which is a measure of inter-areal phase synchrony. To compute these measures, we convoluted the epoched time series

TABLE 2 | SEP/CR/BCR and SEF results.

Subject	Stimulation side	SEP/CR/BCR						SEF				
		Presence of giant SEP	P25 latency (ms)	Presence of BCR	Onset of CR (ms)	Onset of BCR (ms)	CR-BCR time lag (ms)	Presence of giant SEF	P25m latency (ms)	Normalized amplitude of ipsilateral activity	Latency of ipsilateral activity (ms)	Time difference between P25m and ipsilateral activity (ms)
Patient 1	Rt	–	24	–	39	N.A.	N.A.	+	27	0.34	37	10
	Lt	–	24	+	37	47	10	+	27	0.67	37	10
Patient 2	Rt	+	27	+	40	48	8	+	28	0.66	39	11
	Lt	–	26	–	39	N.A.	N.A.	+	31	0.67	41	10
Patient 3	Rt	+	23	+	39	46	8	+	26	0.72	33	7
	Lt	+	23	+	39	47	8	+	26	0.48	35	9
Patient 4	Rt	+	23	+	35	44	9	+	26	0.49	38	12
	Lt	+	22	+	35	43	8	+	28	0.36	38	10
Patient 5	Rt	–	26	+	39	47	8	+	27	0.76	34	7
	Lt	+	24	+	39	48	9	N.A.	N.A.	N.A.	N.A.	N.A.
Mean, SD (7 arms)			24.0 ± 1.8		37.6 ± 2.0	46.0 ± 1.8	8.4 ± 0.8		26.9 ± 0.9	0.59 ± 0.15 ($p < 0.0001$)	36.3 ± 2.3 ($p = 0.4$)	9.4 ± 1.9

SEP, somatosensory-evoked potential; SEF, somatosensory-evoked field; CR, C-reflex; BCR, bilateral C-reflex; Rt, right; Lt, left; SD, standard deviation.

with a dictionary of complex Morlet wavelets (each spanning seven cycles) in the frequency range of 13–120 Hz in 1-Hz steps. ITC is a measure of the variance in phase across trials and thus reflects the temporal stability of oscillatory activity (44–47). ITC values range from 0 to 1, where 0 represents no phase-locking and 1 represents perfectly synchronized phase angles across trials.

The wPLI is based on the phase-lag index (PLI) (48), which defines connectivity as the absolute value of the average sign of phase angle differences. PLI detects consistent phase differences between signals. The wPLI was proposed by Vinck et al. (49) to improve specificity as well as robustness to noise and volume conduction-related artifacts. By weighting each phase difference according to the magnitude of the lag, phase differences around zero only marginally contribute to the calculation of the wPLI. This procedure reduces the probability of detecting false positive connectivity in the case of volume conducted noise sources with near-zero phase-lag and increases the sensitivity of detecting phase synchronization (49). Given that patients with BCR manifested the giant component, which spread widely to the ipsilateral hemisphere, wPLI is well-suited to reveal artifact-free connectivity between the contralateral and ipsilateral hemispheres.

Both indices were computed using MNE-python (28, 50). ITCs were evaluated in the homologous S1/M1 ROIs (see section Delineating the primary sensorimotor areas) to determine the optimal time-frequency window within which the wPLI was evaluated. Because ITC provides information that is independent of inter-areal connectivity (i.e., wPLI), its use in determining the time-frequency window of interest avoids selection bias for choosing the time-frequency window for the wPLI analysis.

The wPLI was computed (a) between the contralateral and ipsilateral S1/M1 ROIs, (b) between the contralateral S1/M1 ROI vs. 64 anatomical regions from the Desikan-Killiany (DK) Atlas parcellation (51) (**Figure 2A**), and (c) between all pairs (all-to-all connectivity) among the 64 anatomical regions. In the all-to-all connectivity, all interhemispheric pairs of regions were included as well as intrahemispheric pairs in the contralateral hemisphere; however, intrahemispheric connectivity within the ipsilateral hemisphere was omitted because ipsilateral activity was expected to be too weak to yield reliable results.

Statistical Analysis

For between-group comparisons of the amplitude and latency of ipsilateral activity, we applied the Mann-Whitney U test, except for the amplitude and latency of P25m because some HCs lacked an identifiable P25m. The amplitude of dSPM is affected by background brain activity, which is expected to differ between BAFME patients and HCs because the background activity of BAFME patients is significantly slower (17). Therefore, S1/M1 dSPM source waveforms were normalized by the peak amplitudes of the contralateral N20m, which were comparable across the two groups.

The wPLI was averaged over the 30–50 ms and 30–100 Hz time-frequency window, determined from the results of the ITC analysis (see **Figure 4A** in the Results section). This frequency window was assumed to represent the reafferent cortical activity that occurs in a large cortical network to allow integration of

external somatosensory stimuli (52). For wPLI values, we used the Mann-Whitney U test and applied correction for multiple comparisons based on the false discovery rate using a threshold of 0.05. All statistics were conducted using MNE-Python and related libraries.

RESULTS

SEP and CR/BCR

In the five patients, a giant SEP was observed in response to stimulation of six of the 10 arms (**Table 2**). The average latency of the P25 was 24.2 ± 1.5 ms (10 arms).

All patients showed CR in both arms, and BCR was further observed in eight arms. The average onset time of CR was 38.0 ± 1.8 ms (10 arms). Of the eight arms that showed BCR, MEG data were available for seven of them. The average onset times of CR and BCR over these seven arms were 37.6 ± 2.0 and 46.0 ± 1.8 ms, respectively, and the average CR-BCR time lag was 8.4 ± 0.8 ms (**Table 2**). This indicated that the onset latency of the long-loop reflex in the non-stimulated hand was 8 ms longer than that in the stimulated side.

In the two patients (Patients 2 and 4) whose EMG was recorded during SEF recording, individual CR-BCR time lags were similar to those obtained prior to the MEG study. This indicated that the CR-BCR time lag was reproducible over separate days.

Ipsilateral and Contralateral SEF Activity

For all the seven stimulated arms in the patients that showed BCR, the MEG data revealed a giant component of P25m in the contralateral hemisphere (**Table 2**). The average latency of the P25m was 26.9 ± 0.9 ms (7 arms). Ipsilateral activity showed a peak latency of 36.3 ± 2.3 ms, which had a smaller amplitude than that of contralateral activity. The amplitude of ipsilateral activity of the patients was significantly larger than that of the HCs ($p < 0.0001$). In the patients, the difference in the time delay between the peak latencies of the contralateral P25m and ipsilateral activity was 9.4 ± 1.9 ms, which was similar to the CR-BCR time lag (see section SEP and CR/BCR). SEF activity of the functional S1/M1 ROIs of a representative patient (Patient 2) and the corresponding grand-average activity of HCs are presented in **Figure 2B**. In this patient, the contralateral P25m activity was giant, whereas the ipsilateral activity was prominent with an 11-ms delay in its peak from P25m activity (**Figure 2B**). No prominent ipsilateral activity was observed in HCs (**Figure 2C**). Typical spatiotemporal distribution of estimated cortical activity (Patient 2, right median nerve stimulation) is presented in **Figure 3**. Ipsilateral activity was prominent around 40 ms, exactly in the ipsilateral S1/M1 ROI (highlighted in the inset figure as a green shaded area). The time course of the ipsilateral activity (**Figure 3**, lower two panels) was distinct from that of the contralateral activity (upper two panels), which suggested that the observed ipsilateral activity in the MEG source estimates is likely to be a true response and not due to artifactual cross-talk from the giant contralateral activity.

Neural Synchrony

The time-frequency plots of the grand-averaged ITC showed prominent early (30–50 ms) intertrial phase synchrony in the frequency range of 30–100 Hz in the contralateral S1/M1 ROIs in both the patients and HCs (**Figure 4A**). The 30–50 ms time window identified using the ITC corresponded to the initial findings (see sections SEP and CR/BCR and Ipsilateral and contralateral SEF activity), where ipsilateral activity at around 36 ms was synchronized after P25m activity (at 27 ms) propagated with a CR-BCR time lag of 8 ms. Thus, we computed the average of the wPLI over the time-frequency window of 30–50 ms and 30–100 Hz for all subjects. The grand-averaged wPLI between the homologous S1/M1 ROIs was larger in the patients than in HCs within this time-frequency window ($p = 0.004$; **Figure 4B**). The wPLI for baseline (−100–0 ms) was not significantly different between the groups ($p = 0.16$).

Figure 5 depicts representative wPLI results of one patient's (Patient 2) response to right median nerve stimulation and shows the evaluation of the connectivity between the contralateral S1/M1 ROI (left hemisphere) and all cortical locations used in the MEG source estimation. Interhemispheric connectivity (**Figure 5**, lower two panels) was distinct, especially around the homologous S1/M1 ROI (highlighted in the inset figure) in the time range of 30–50 ms. Similar to the findings in the previous section, the distinct time courses of the spatial patterns of wPLI in the right and left hemispheres suggest that the interhemispheric connectivity results were not caused by artificial cross-talk in the MEG source estimates.

Analysis of the average wPLI for the time-frequency window of interest (30–50 ms and 30–100 Hz) between the contralateral S1/M1 ROI and all DK regions revealed significantly higher values in the patients than in HCs for the homologous ROI, precentral gyrus (PreC), postcentral gyrus (PoC), and other regions interhemispherically. Interestingly, the intrahemispheric IP connection was also revealed as highly significant. All statistically significant connections are listed in **Supplementary Table 1**.

The all-to-all connectivity analysis revealed significant connectivity between several pairs of regions in which S1/M1 was included: PreC-PreC, PoC-PreC, IP-PreC, and IP-PoC interhemispherically (contralateral region-ipsilateral region), and PreC-IP and PoC-IP intrahemispherically (contralateral region-contralateral region; **Figure 6**). All statistically significant connections are listed in **Supplementary Table 2**. These results suggest that in the patients with BCR the contralateral S1/M1 was strongly connected to the ipsilateral M1 at 30–50 ms via the contralateral IP.

DISCUSSION

The presence of BCR provides concrete neurophysiological evidence that bilateral M1 are strongly involved in the response to unilateral somatosensory input. Our results revealed bilateral SEF activity (**Figures 2B**, **3**) and enhanced interhemispheric connectivity (**Figures 4**–**6**) in patients with BCR. The time delay between contralateral and ipsilateral

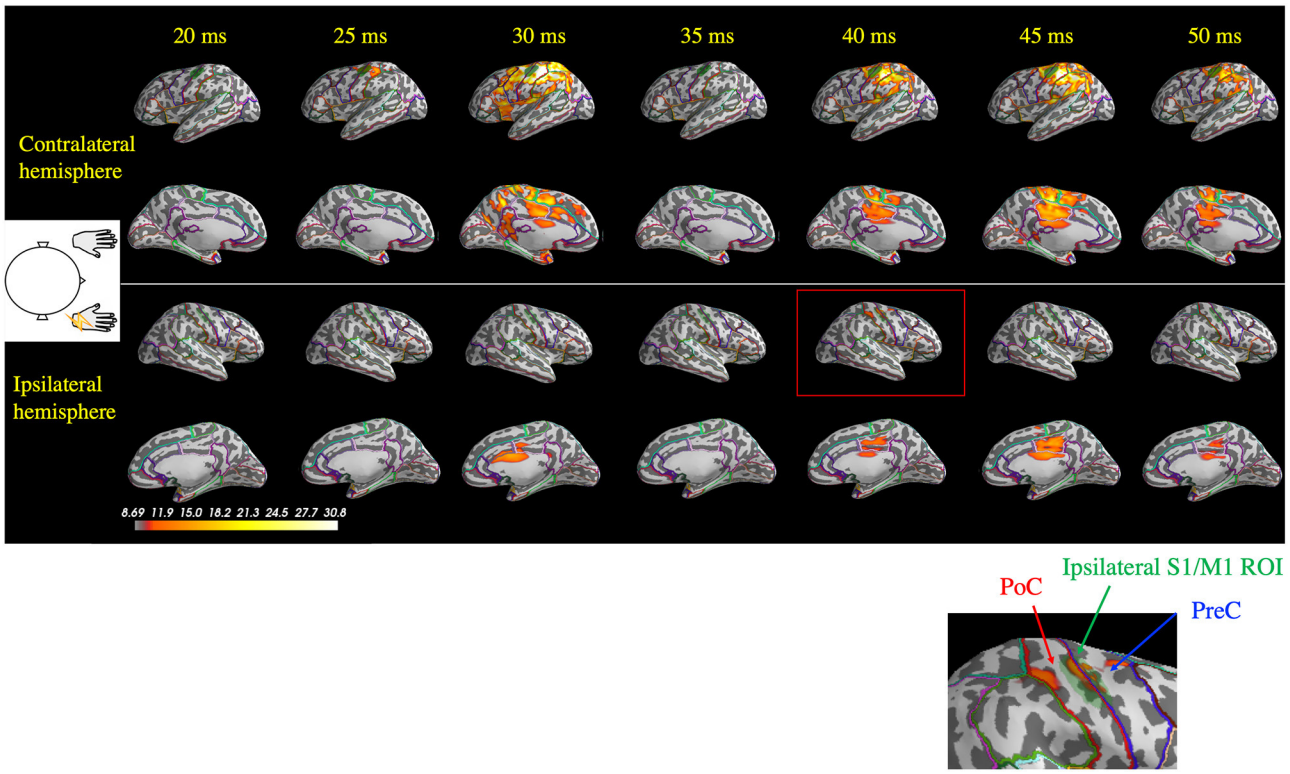

FIGURE 3 | Spatiotemporal distribution of the estimated cortical activity that generated the somatosensory-evoked field following right median nerve stimulation in one patient (Patient 2). Ipsilateral activity (right hemisphere) at around 40 ms (red rectangle) was observed exactly in the ipsilateral S1/M1 region of interest (ROI; green shaded area, highlighted in the inset figure). At 45 ms, contralateral activity remained prominent, whereas the ipsilateral did not. PoC, postcentral gyrus; PreC, precentral gyrus.

activity corresponded to the CR-BCR time lag (**Table 2**). The early enhanced connectivity between contralateral S1/M1 and ipsilateral M1 occurred within 50 ms, which was mediated by the contralateral IP (**Supplementary Tables 1**, **2**). The MEG results provide novel insights into the pathophysiological mechanism underlying BCR, suggesting that homologous S1/M1 are strongly connected, probably transcallosally, and that the IP mediates the transcallosal connectivity.

Cross-Talk Is Prominent in the Presence of a Giant SEP

Previous EEG studies have shown ipsilateral SEP activity in patients with BCR. Shibasaki et al. (3) observed a CR-BCR time delay of 9–11 ms in four out of eight patients with progressive myoclonic epilepsy, and Wilkins et al. (10) found a 10-ms delay in one out of seven Alzheimer's disease patients. Ikeda et al. (12) reported a 9-ms delay in one out of two patients with cortical tremor, and Brown et al. (11) comprehensively investigated BCR and reported in three out of nine patients with cortical myoclonus a delay of 10–16 ms. In these EEG studies, ipsilateral hemispheric activity was also observed with a time delay of 9–15 ms (3) and 9–18 ms (11), respectively, from the peak of the contralateral P25 to that of the ipsilateral homologous component. In the present study the cortical time delay was 7–12 ms. The wide variability in the cortical time delays could be due to differences in the patient populations among the studies and, perhaps more importantly, to differences between EEG and MEG in their sensitivity to specific source components of the evoked response. As shown in **Figure 1**, ipsilateral activity measured using EEG was less clear because of volume conduction effects related to the giant component (4) and limited spatial resolution (53, 54). EEG waveforms can be a mixture of overlapping scalp potentials generated by bilateral activity (55). Thus, investigations of ipsilateral activity as well as whole-brain connectivity using EEG is challenging with the presence of prominent contralateral activity (i.e., a giant component of SEP). To the best of our knowledge, no previous studies have investigated bilateral SEF activity with a giant component in myoclonus patients. In the current study using MEG, the spatiotemporal distribution of the estimated ipsilateral activity was clearly spatially distinct from that of contralateral activity (**Figures 2B**, **3**). This suggests that the MNE source localization can ameliorate leakage effects (56, 57), thereby making it possible to dissociate ipsilateral activity from the giant contralateral activity.

The difference in the observed cortical time delay (9.4 ms) and the CR-BCR onset time lag (8.4 ms) may be due to the use of the peak latencies of the cortical responses. Measuring the onset

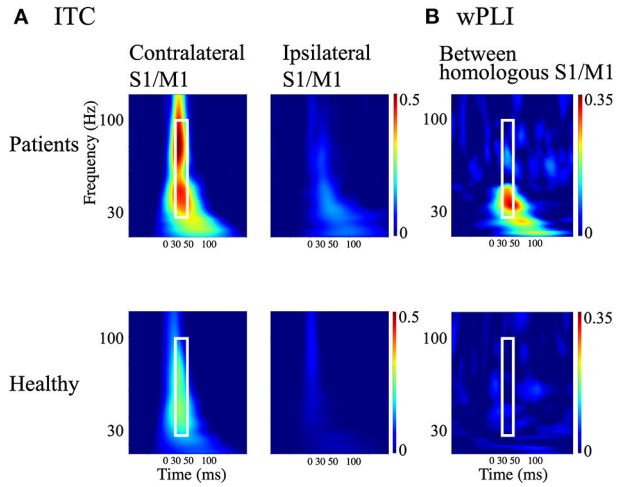

FIGURE 4 | Measures of cortical synchrony following median nerve stimulation. **(A)** Time-frequency plots of grand-averaged intertrial phase coherence (ITC) in contralateral and ipsilateral S1/M1 regions of interest (ROIs; left and right panels, respectively). **(B)** Time-frequency plots of weighted phase-lag index (wPLI) between homologous S1/M1 ROIs. Upper panels: patients with bilateral C-reflex; lower panels: healthy controls. White rectangles show the time window of 30–50 ms and the frequency window of 30–100 Hz.

rather than the peak times of the motor cortex activity in each hemisphere might provide a delay time closer to that observed for the CR-BCR time lag. However, because contralateral N20m and P25m are close in time and space, it is very difficult to determine the precise onset of the P25m reliably.

As an alternative approach to modeling the bilateral S1/M1 sources, we also attempted to use a double ECD model (58). However, we found a good fit in only one patient; presumably the small magnitude of the ipsilateral S1/M1 sources made the two-dipole fitting unstable in our cases. An advantage of distributed source models like the MNE is that only minimal assumptions are required; for example, there is no need to specify a priori the number of sources. For the localization of contralateral S1, MNE of SEP has been found to provide accuracy comparable to that obtained with ECD (59).

Ipsilateral Activity in Patients With BCR as a Homologous Motor Response of the Contralateral Giant Component

The precise generator source of the giant SEP/SEF has not been fully elucidated; however, motor cortical hyperexcitability has been suggested to be involved (6, 7, 60, 61). Specifically, in a transcranial magnetic stimulation (TMS) study using short-interval intracortical inhibition, Hanajima et al. (61) suggested a pathological mechanism in patients with cortical reflex myoclonus whereby inhibitory GABAergic interneurons of the motor cortex are directly affected.

Our findings suggest that ipsilateral activity is homologous to the giant P25m component. First, the time difference between the peak latency of the giant P25m and CR onset was 10.7 ± 2.1 ms. This time difference indicates the conduction time from the contralateral M1 to the stimulated muscle, in response to the electrical stimulation (1, 3, 5, 9, 13, 62). Similarly, the time difference between the peak latency of ipsilateral activity and BCR onset was 9.7 ± 3.3 ms. This time difference is assumed to correspond to the conduction time from the ipsilateral M1 to the non-stimulated muscle associated with BCR.

Second, the connectivity analysis indicated a strong connection between the homologous motor cortices in patients with BCR (**Figure 6**; **Supplementary Tables 1**, **2**). Significant connections were revealed interhemispherically between PreC–PreC and PoC–PreC, but not between PoC–PoC (contralateral region-ipsilateral region, **Figure 6** and **Supplementary Table 2**). This finding is compatible with a previous report by Terada et al. (63), which suggested that there is no interhemispheric connection between bilateral somatosensory areas in humans. Instead, bilateral motor cortices may be strongly related to BCR. Sensory inputs to the M1 have been suggested to be closely associated with the performance of the opposite M1 transcallosally (13, 64, 65). It is generally accepted that the transcallosal connection is inhibitory (66); interhemispheric inhibition of TMS is mediated by a facilitatory transcallosal population synapsing onto a local inhibitory population in the motor cortices (67), and the local deficit in inhibitory GABAergic neurons was shown in the motor cortices of patients with cortical reflex myoclonus (61). On the basis of inhibitory transcallosal connections, we hypothesize that the enhanced connection between the bilateral motor cortices may be compensating for the physiological inhibitory connection of hyperexcitable motor cortices in patients with BCR. This could be confirmed in a future TMS study.

Ipsilateral Activity Within 50 ms in Healthy Controls Cannot Be Detected Reliably

HCs did not show prominent ipsilateral SEF activity within 50 ms (**Figure 2B**). Bilateral receptive fields have been reported in non-human primates (68). In the human brain, various approaches have been used to search for an equivalent bilateral representation of somatosensory information at the lower level. These approaches included SEP/SEF (39–41, 69–75) and fMRI (76, 77). However, these studies demonstrated that detection of ipsilateral responses in humans is highly variable and are not reliably found in the left or right hemispheres (42). Early physiological ipsilateral SEP/SEF activity is weak and is difficult to detect reliably using sensor-space analysis, which is susceptive to volume-conduction (41, 69, 70, 73–75), or source-based analysis, which relies on a complete source model (39, 40, 71, 72). Moreover, most results showed ipsilateral activity after 50 ms. Considering that S2 activation arises after 50 ms, it remains controversial whether somatosensory information carried by the median nerve reaches lower level sensorimotor areas of both the ipsilateral and contralateral hemispheres within 50 ms. In one paper that used blind source decomposition (42), ipsilateral SEP activity within 50 ms was observed in healthy subjects in both the left and right hemispheres. Therefore, we believe that our results of ipsilateral activity in patients with BCR represent excessive enhancement of the

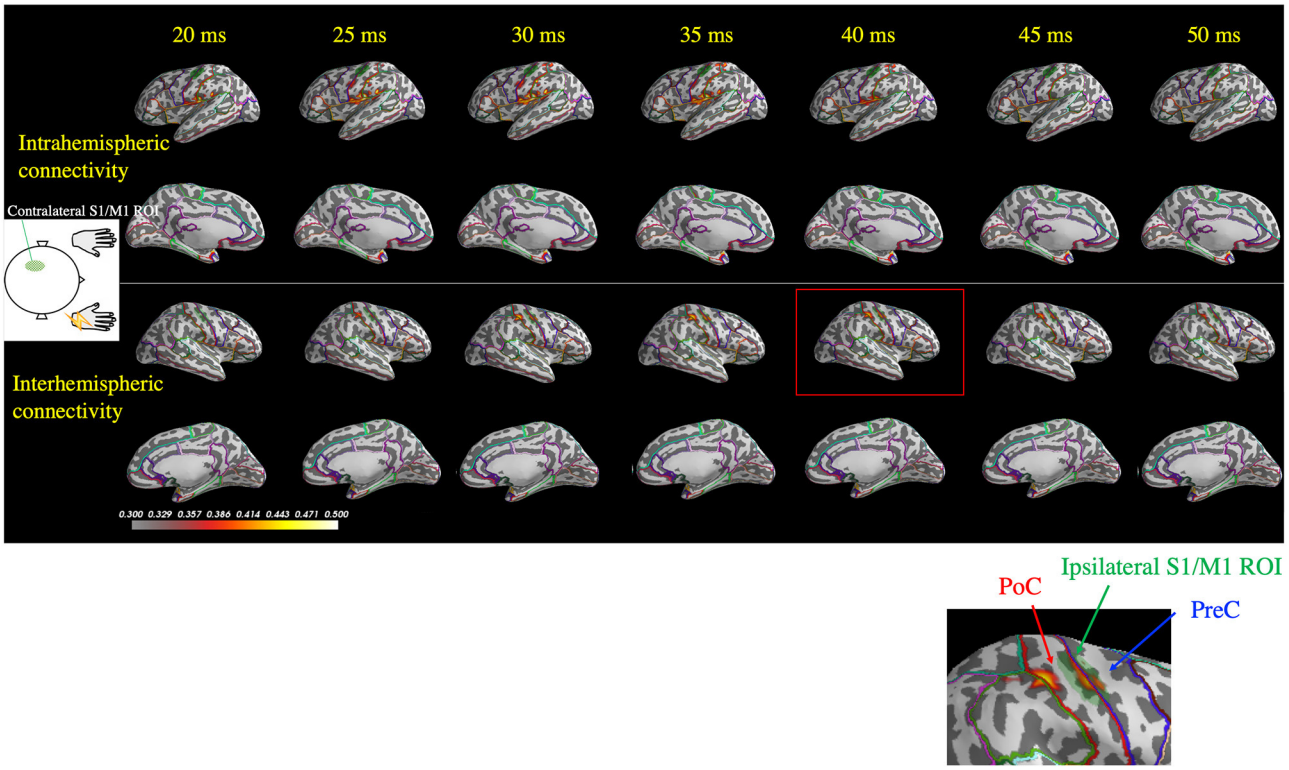

FIGURE 5 | Spatiotemporal distribution of the weighted phase-lag index (wPLI) between the contralateral S1/M1 region of interest (ROI; green shaded area in the left hemisphere) and the rest of the cortex following right median nerve stimulation (Patient 2). The wPLI was averaged over the 30–100 Hz frequency window, which was identified using the intertrial phase coherence (see **Figure 4A**). Top two panels: interhemispheric connectivity; bottom two panels: intrahemispheric connectivity. Interhemispheric connectivity was distinct in the time range of 30–50 ms, especially in the S1/M1 ROI, whereas intrahemispheric connectivity showed a different pattern in the temporoparietal region. The inset shows a magnified view of the ipsilateral S1/M1 region at 40 ms, which corresponds to the red rectangle. PoC, postcentral gyrus; PreC, precentral gyrus.

physiological components of normal ipsilateral activity, rather than occurrence of an abnormal component. This assumption is consistent with previous studies of giant SEPs, which suggest that a giant contralateral SEP may result from pathological enhancement of certain cortical components of a normal SEP (4, 78).

Pathophysiology of Initiation of BCR via a Hyperexcitable Transcallosal Pathway

Possible pathways initiating the BCR include the transcallosal pathway, direct input to the ipsilateral M1, the thalamic ascending projection, and top-down inputs from S2. Our findings suggest that the transcallosal pathway is the most likely (3, 10, 11). First, direct peripheral input to ipsilateral M1 and direct input from the contralateral nucleus of thalamus are unlikely because these pathways cannot explain the CR-BCR time lag or cortical delay between the ipsilateral and contralateral hemispheres. Kanno et al. (39) reported two epilepsy patients who showed ipsilateral SEF activity without CR/BCR. These patients who had severe left hemispheric damage showed no contralateral activity in response to right median nerve stimulation, however, they showed ipsilateral activity in S1. The authors suggested that the ipsilateral activity was due to direct peripheral input to the ipsilateral S1. However, ipsilateral activity in their study occurred after 50 ms. Thus, this abnormal ipsilateral response differs from the activity related to BCR. Second, given that S2 displays initial activation at around 60–70 ms after stimulation (43), the early spread of cortical excitation in BCR occurring within 50 ms is too early to be consistent with top-down inputs from S2 (43). Furthermore, in patients with cortical reflex myoclonus, excitability of S2 is not pathologically enhanced (6). Thus, the involvement of S2 is unlikely to be the pathway of BCR. Instead, the transcallosal pathway is the most reasonable explanation for the initiation of BCR. Moreover, this is compatible with the aforementioned physiology of inhibitory transcallosal connection.

The Modulating Role of IP in Disinhibition of Transcallosal Inhibitory Process

Our results suggest that the bilateral representation of sensorimotor responses is associated with pathologically

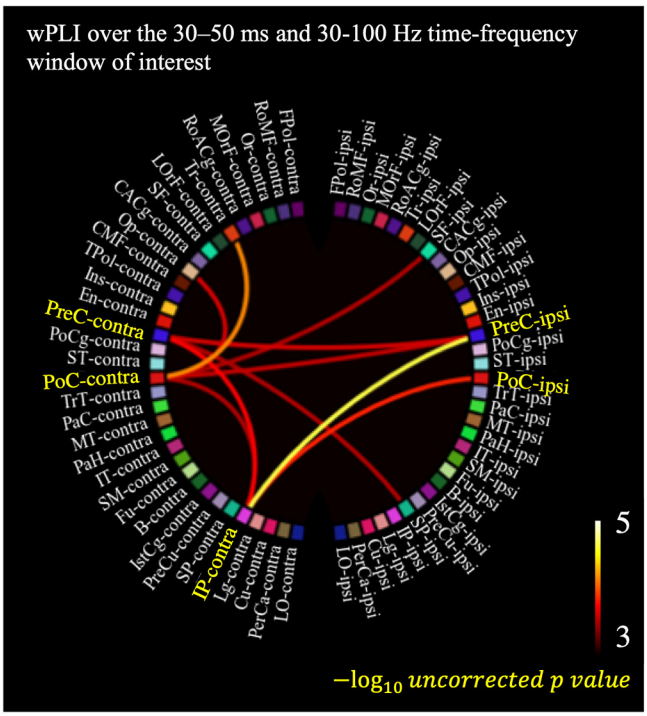

B	bankssts	LOrF	lateralorbitofrontal	PreC	precentral
CACg	caudalanteriorcingulate	Lg	lingual	PreCu	precuneus
CMF	caudalmiddlefrontal	MOrF	medialorbitofrontal	RoACg	rostralanteriorcingulate
Cu	cuneus	MT	middletemporal	RoMF	rostralmiddlefrontal
En	entorhinal	PaC	paracentral	SF	superiorfrontal
Fpol	frontalpole	PaH	parahippocampal	SP	superiorparietal
Fu	fusiform	Op	parsopercularis	ST	superiortemporal
IP	inferiorparietal	Or	parsorbitalis	SM	supramarginal
IT	inferiortemporal	Tr	parstriangularis	Tpol	temporalpole
Ins	insula	PerCa	pericalcarine	TrT	transversetemporal
IstCg	isthmuscingulate	PoC	postcentral		
LO	lateraloccipital	PoCg	posteriorcingulate		

FIGURE 6 | Results of the all-to-all connectivity analysis visualized on a circular representation, showing only the connections involving the S1/M1 regions. Connectivity was measured using the averaged weighted phase-lag index value over the 30–50 ms and 30–100 Hz time-frequency window of interest. A negative 10-based logarithm of uncorrected p values (uncorrected $p < 5 \times 10^{-4}$) is indicated by the color bar. The schematic image of significant connections that contains each of PreC, PoC, and IP is shown in the subfigure.

enhanced disinhibition of transcallosal inhibitory processes within M1 cortices. In addition to the connections between homologous S1/M1, connectivity (i.e., wPLI) was significantly enhanced between the contralateral IP and bilateral S1/M1 (**Figure 6**; **Supplementary Tables 1**, **2**). These results suggest that the contralateral IP mediates BCR by involving bilateral S1/M1. The healthy motor cortex orchestrates movement, and it is likely that transcallosal inhibition acts to transform elemental mass movement into a meaningful pattern of synergistic activity. Upon receiving a movement command from higher centers, i.e., IP, this cortical inhibition enables an appropriate output to be produced and inappropriate movements to be suppressed (79). IP is crucial for sensorimotor transformation (80–82) and contains a rich variety of transcallosal neurons that are responsive to different sensory stimuli that discharge in association with different types of movements (83, 84). Moreover, it has a physiological facilitatory transcallosal connection to bilateral M1 (67, 85). Therefore, IP may have an important role on controlling motor movements seen in BAFME patients with BCR. The wPLI is a correlation-based measure that as such cannot determine whether the involvement of IP is direct or indirect. However, it is reasonable to assume that the involvement of IP is indirect: the primary contribution in BCR is likely to be the interhemispheric connection between bilateral S1/M1. IP may have a secondary or modulating role in BCR. Based on this assumption, we propose that modulation

of IP excitability may be beneficial for controlling BAFME symptoms. This should be investigated in a prospective study using non-invasive TMS.

Limitations

The stimulus parameters were not consistent among subjects or within subjects (SEP and SEF) because SEP and SEF were measured with different clinical purposes (long latency vs. short latency). AEDs may have affected SEP/SEF and connectivity analyses. Several studies have reported no significant differences in SEP during treatment with AEDs (86–88); however, one study showed suppressed amplitude of giant SEPs under AEDs (12). Patient 2 was treated with a sodium channel blocker sometimes worsening the myoclonus. Since replacement to other AEDs had worsened the myoclonus, we continued the current regimen. Therefore, drug naïve patients would be desirable.

The rarity of the BCR caused several concerns. First, the number of participants were small. We disregarded hemispheric dominance and concatenated the conditions for analysis to obtain significant statistics (7 vs. 30 arms). The wPLI results may have been affected by hemisphere dominance when the IP, a higher cognitive area, was involved. However, we found minimal differences in wPLI from the IP between the dominant and non-dominant hemispheres. Second, the types of participants in the current retrospective study were limited to BAFME patients among the cortical reflex myoclonus. A recent study suggested that the cortical excitability of BAFME may be different from that of other non-BAFME diseases (89). Thus, the current findings may be more specific to BAFME rather than other diseases with cortical reflex myoclonus in general. Therefore, more patients need to be recruited to fully investigate the general pathophysiology of BCR.

Conclusions

The current MEG results confirmed bilateral SEF activity in patients with BCR and suggested that the transcallosal pathway is the probable pathway that initiates BCR. Disinhibition of transcallosal inhibitory processes within M1 cortices were related to the bilateral representation of sensorimotor responses. Hyperexcitable motor cortices were mediated by the contralateral IP.

DATA AVAILABILITY STATEMENT

The raw data supporting the conclusions of this article will be made available by the authors, without undue reservation.

ETHICS STATEMENT

The studies involving human participants were reviewed and approved by Ethical Committee of Kyushu University Hospital. The patients/participants provided their written informed consent to participate in this study.

AUTHOR CONTRIBUTIONS

TMa and ST: study conception and design. TMa, KH, and HS: data collection. TMa, SA, and TMi: analysis and interpretation of results. TMa: draft and manuscript preparation. YG and SS: revision of manuscript. All authors approved the final version of the manuscript.

FUNDING

This work was supported by JSPS KAKENHI Grant No. JP20J00552, Nakatani Foundation for advancement of measuring technologies in biomedical engineering, The Japan Epilepsy Research Foundation, The Osaka Medical Research Foundation for Intractable Diseases and the National Institute on Deafness and other Communication (Grant No. R01DC016765) and NIH (Grant Nos. R21NS101373, R01NS104116, R01NS069696, and S10ODRR031599).

ACKNOWLEDGMENTS

We thank Sarina Iwabuchi, Ph.D., from Edanz Group (https://en-author-services.edanz.com/ac) for editing a draft of this manuscript.

SUPPLEMENTARY MATERIAL

The Supplementary Material for this article can be found online at: https://www.frontiersin.org/articles/10.3389/fneur.2021.759866/full#supplementary-material

REFERENCES

1. Hallett M, Chadwick D, Marsden CD. Cortical reflex myoclonus. *Neurology.* (1979) 29:1107–25. doi: 10.1212/WNL.29.8.1107
2. Obeso JA, Rothwell JC, Marsden CD. The spectrum of cortical myoclonus. From focal reflex jerks to spontaneous motor epilepsy. *Brain.* (1985) 108 (Pt. 1):193–24. doi: 10.1093/brain/108.1.193
3. Shibasaki H, Yamashita Y, Kuroiwa Y. Electroencephalographic studies myoclonus. *Brain.* (1978) 101:447–60. doi: 10.1093/brain/101.3.447
4. Kakigi R, Shibasaki H. Generator mechanisms of giant somatosensory evoked potentials in cortical reflex myoclonus. *Brain.* (1987) 110 (Pt. 5):1359–73. doi: 10.1093/brain/110.5.1359
5. Shibasaki H, Yamashita Y, Neshige R, Tobimatsu S, Fukui R. Pathogenesis of giant somatosensory evoked potentials in progressive myoclonic epilepsy. *Brain.* (1985) 108 (Pt. 1):225–40. doi: 10.1093/brain/108.1.225
6. Mima T, Nagamine T, Nishitani N, Mikuni N, Ikeda A, Fukuyama H, et al. Cortical myoclonus: sensorimotor hyperexcitability. *Neurology.* (1998) 50:933–42. doi: 10.1212/WNL.50.4.933
7. Mima T, Nagamine T, Ikeda A, Yazawa S, Kimura J, Shibasaki H. Pathogenesis of cortical myoclonus studied by magnetoencephalography. *Ann Neurol.* (1998) 43:598–607. doi: 10.1002/ana.410430507
8. Tobimatsu S, Fukui R, Shibasaki H, Kato M, Kuroiwa Y. Electrophysiological studies of myoclonus in sialidosis type 2. *Electroencephalogr Clin Neurophysiol.* (1985) 60:16–22. doi: 10.1016/0013-4694(85)90944-7

9. Sutton GG, Mayer RF. Focal reflex myoclonus. *J Neurol Neurosurg Psychiatry.* (1974) 37:207–17. doi: 10.1136/jnnp.37.2.207
10. Wilkins DE, Hallett M, Berardelli A, Walshe T, Alvarez N. Physiologic analysis of the myoclonus of Alzheimer's disease. *Neurology.* (1984) 34:898–903. doi: 10.1212/WNL.34.7.898
11. Brown P, Day BL, Rothwell JC, Thompson PD, Marsden CD. Intrahemispheric and interhemispheric spread of cerebral cortical myoclonic activity and its relevance to epilepsy. *Brain.* (1991) 114 (Pt. 5):2333–51. doi: 10.1093/brain/114.5.2333
12. Ikeda A, Kakigi R, Funai N, Neshige R, Kuroda Y, Shibasaki H. Cortical tremor: a variant of cortical reflex myoclonus. *Neurology.* (1990) 40:1561–5. doi: 10.1212/WNL.40.10.1561
13. Ferbert A, Priori A, Rothwell JC, Day BL, Colebatch JG, Marsden CD. Interhemispheric inhibition of the human motor cortex. *J Physiol.* (1992) 453:525–46. doi: 10.1113/jphysiol.1992.sp019243
14. Cracco RQ, Amassian VE, Maccabee PJ, Cracco JB. Comparison of human transcallosal responses evoked by magnetic coil and electrical stimulation. *Electroencephalogr Clin Neurophysiol.* (1989) 74:417–24. doi: 10.1016/0168-5597(89)90030-0
15. Latorre A, Rocchi L, Magrinelli F, Mulroy E, Berardelli A, Rothwell JC, et al. Unravelling the enigma of cortical tremor and other forms of cortical myoclonus. *Brain.* (2020) 143:2653–63. doi: 10.1093/brain/awaa129
16. Terada K, Ikeda A, Mima T, Kimura M, Nagahama Y, Kamioka Y, et al. Familial cortical myoclonic tremor as a unique form of cortical reflex myoclonus. *Mov Disord.* (1997) 12:370–7. doi: 10.1002/mds.870120316
17. Hitomi T, Kondo T, Kobayashi K, Matsumoto R, Takahashi R, Ikeda A. Clinical anticipation in Japanese families of benign adult familial myoclonus epilepsy. *Epilepsia.* (2012) 53:e33–6. doi: 10.1111/j.1528-1167.2011.03349.x
18. Hitomi T, Kobayashi K, Sakurai T, Ueda S, Jingami N, Kanazawa K, et al. Benign adult familial myoclonus epilepsy is a progressive disorder: no longer idiopathic generalized epilepsy. *Epileptic Disord.* (2016) 18:67–72. doi: 10.1684/epd.2016.0807
19. Kobayashi K, Hitomi T, Matsumoto R, Watanabe M, Takahashi R, Ikeda A. Nationwide survey in Japan endorsed diagnostic criteria of benign adult familial myoclonus epilepsy. *Seizure.* (2018) 61:14–22. doi: 10.1016/j.seizure.2018.07.014
20. Latorre A, Rocchi L, Berardelli A, Rothwell JC, Bhatia KP, Cordivari C. Reappraisal of cortical myoclonus: a retrospective study of clinical neurophysiology. *Mov Disord.* (2018) 33:339–41. doi: 10.1002/mds.27234
21. Barrett G. Jerk-locked averaging: technique and application. *J Clin Neurophysiol.* (1992) 9:495–508. doi: 10.1097/00004691-199210000-00004
22. Shigeto H, Tobimatsu S, Morioka T, Yamamoto T, Kobayashi T, Kato M. Jerk-locked back averaging and dipole source localization of magnetoencephalographic transients in a patient with epilepsia partialis continua. *Electroencephalogr Clin Neurophysiol.* (1997) 103:440–4. doi: 10.1016/S0013-4694(97)00040-0
23. Thompson PD, Day BL, Rothwell JC, Brown P, Britton TC, Marsden CD. The myoclonus in corticobasal degeneration. Evidence for two forms of cortical reflex myoclonus. *Brain.* (1994) 117 (Pt. 5):1197–207. doi: 10.1093/brain/117.5.1197
24. Hari R, Baillet S, Barnes G, Burgess R, Forss N, Gross J, et al. IFCN-endorsed practical guidelines for clinical magnetoencephalography (MEG). *Clin Neurophysiol.* (2018) 129:1720–47. doi: 10.1016/j.clinph.2018.03.042
25. Taulu S, Simola J, Kajola M. Applications of the signal space separation method. *IEEE Trans Signal Process.* (2005) 53:3359–72. doi: 10.1109/TSP.2005.853302
26. Fischl B, Sereno MI, Dale AM. Cortical surface-based analysis. II: Inflation, flattening, and a surface-based coordinate system. *Neuroimage.* (1999) 9:195–207. doi: 10.1006/nimg.1998.0396
27. Shibasaki H, Yamashita Y, Tsuji S. Somatosensory evoked potentials. Diagnostic criteria and abnormalities in cerebral lesions. *J Neurol Sci.* (1977) 34:427–39. doi: 10.1016/0022-510X(77)90159-9
28. Gramfort A, Luessi M, Larson E, Engemann DA, Strohmeier D, Brodbeck C, et al. MNE software for processing MEG and EEG data. *Neuroimage.* (2014) 86:446–60. doi: 10.1016/j.neuroimage.2013.10.027
29. Hämäläinen MS, Ilmoniemi RJ. Interpreting magnetic fields of the brain: minimum norm estimates. *Med Biol Eng Comput.* (1994) 32:35–42. doi: 10.1007/BF02512476
30. Dale AM, Liu AK, Fischl BR, Buckner RL, Belliveau JW, Lewine JD, et al. Dynamic statistical parametric mapping: combining fMRI and MEG for high-resolution imaging of cortical activity. *Neuron.* (2000) 26:55–67. doi: 10.1016/S0896-6273(00)81138-1
31. Hämäläinen MS, Sarvas J. Realistic conductivity geometry model of the human head for interpretation of neuromagnetic data. *IEEE Trans Biomed Eng.* (1989) 36:165–71. doi: 10.1109/10.16463
32. Lin FH, Belliveau JW, Dale AM, Hämäläinen MS. Distributed current estimates using cortical orientation constraints. *Hum Brain Mapp.* (2006) 27:1–13. doi: 10.1002/hbm.20155
33. Uesaka Y, Ugawa Y, Yumoto M, Sakuta M, Kanazawa I. Giant somatosensory evoked magnetic field in patients with myoclonus epilepsy. *Electroencephalogr Clin Neurophysiol.* (1993) 87:300–5. doi: 10.1016/0013-4694(93)90183-V
34. Shibasaki H, Hallett M. Electrophysiological studies of myoclonus. *Muscle Nerve.* (2005) 31:157–74. doi: 10.1002/mus.20234
35. Tiihonen J, Hari R, Hämäläinen M. Early deflections of cerebral magnetic responses to median nerve stimulation. *Electroencephalogr Clin Neurophysiol.* (1989) 74:290–6. doi: 10.1016/0168-5597(89)90059-2
36. Baumgartner C, Sutherling WW, Di S, Barth DS. Spatiotemporal modeling of cerebral evoked magnetic fields to median nerve stimulation. *Electroencephalogr Clin Neurophysiol.* (1991) 79:27–35. doi: 10.1016/0013-4694(91)90153-U
37. Lin FH, Witzel T, Ahlfors SP, Stufflebeam SM, Belliveau JW, Hämäläinen MS. Assessing and improving the spatial accuracy in MEG source localization by depth-weighted minimum-norm estimates. *Neuroimage.* (2006) 31:160–71. doi: 10.1016/j.neuroimage.2005.11.054
38. Hauk O, Wakeman DG, Henson R. Comparison of noise-normalized minimum norm estimates for MEG analysis using multiple resolution metrics. *Neuroimage.* (2011) 54:1966–74. doi: 10.1016/j.neuroimage.2010.09.053
39. Kanno A, Nakasato N, Nagamine Y, Tominaga T. Non-transcallosal ipsilateral area 3b responses to median nerve stimulus. *J Clin Neurosci.* (2004) 11:868–71. doi: 10.1016/j.jocn.2004.01.007
40. Korvenoja A, Huttunen J, Salli E, Pohjonen H, Martinkauppi S, Palva JM, et al. Activation of multiple cortical areas in response to somatosensory stimulation: combined magnetoencephalographic and functional magnetic resonance imaging. *Hum Brain Mapp.* (1999) 8:13–27. doi: 10.1002/(SICI)1097-0193(1999) 8:1<13::AID-HBM2>3.0.CO;2-B
41. Allison T, McCarthy G, Wood CC, Williamson PD, Spencer DD. Human cortical potentials evoked by stimulation of the median nerve. II. Cytoarchitectonic areas generating long-latency activity. *J Neurophysiol.* (1989) 62:711–22. doi: 10.1152/jn.1989.62.3.711
42. Sutherland MT, Tang AC. Reliable detection of bilateral activation in human primary somatosensory cortex by unilateral median nerve stimulation. *Neuroimage.* (2006) 33:1042–54. doi: 10.1016/j.neuroimage.2006.08.015
43. Hari R, Forss N. Magnetoencephalography in the study of human somatosensory cortical processing. *Philos Trans R Soc Lond B Biol Sci.* (1999) 354:1145–54. doi: 10.1098/rstb.1999.0470
44. Palva S, Linkenkaer-Hansen K, Näätänen R, Palva JM. Early neural correlates of conscious somatosensory perception. *J Neurosci.* (2005) 25:5248–58. doi: 10.1523/JNEUROSCI.0141-05.2005
45. Sinkkonen J, Tiitinen H, Näätänen R. Gabor filters: an informative way for analysing event-related brain activity. *J Neurosci Methods.* (1995) 56:99–104. doi: 10.1016/0165-0270(94)00111-S
46. Tallon-Baudry C, Bertrand O, Peronnet F, Pernier J. Induced gamma-band activity during the delay of a visual short-term memory task in humans. *J Neurosci.* (1998) 18:4244–54. doi: 10.1523/JNEUROSCI.18-11-04244.1998
47. Matsubara T, Ogata K, Hironaga N, Uehara T, Mitsudo T, Shigeto H, et al. Monaural 40-Hz auditory steady-state magnetic responses can be useful for identifying epileptic focus in mesial temporal lobe epilepsy. *Clin Neurophysiol.* (2019) 130:341–51. doi: 10.1016/j.clinph.2018.11.026
48. Stam CJ, Nolte G, Daffertshofer A. Phase lag index: assessment of functional connectivity from multi channel EEG and MEG with diminished bias from common sources. *Hum Brain Mapp.* (2007) 28:1178–93. doi: 10.1002/hbm.20346
49. Vinck M, Oostenveld R, van Wingerden M, Battaglia F, Pennartz CM. An improved index of phase-synchronization for electrophysiological data in the presence of volume-conduction, noise and sample-size bias. *Neuroimage.* (2011) 55:1548–65. doi: 10.1016/j.neuroimage.2011.01.055

50. Gramfort A, Luessi M, Larson E, Engemann DA, Strohmeier D, Brodbeck C, et al. MEG and EEG data analysis with MNE-Python. *Front Neurosci.* (2013) 7:267. doi: 10.3389/fnins.2013.00267
51. Desikan RS, Segonne F, Fischl B, Quinn BT, Dickerson BC, Blacker D, et al. An automated labeling system for subdividing the human cerebral cortex on MRI scans into gyral based regions of interest. *Neuroimage.* (2006) 31:968–80. doi: 10.1016/j.neuroimage.2006.01.021
52. Fukuda M, Nishida M, Juhasz C, Muzik O, Sood S, Chugani HT, et al. Short-latency median-nerve somatosensory-evoked potentials and induced gamma-oscillations in humans. *Brain.* (2008) 131 (Pt. 7):1793–805. doi: 10.1093/brain/awn100
53. Ikeda A, Shibasaki H, Nagamine T, Xu X, Terada K, Mima T, et al. Peri-rolandic and fronto-parietal components of scalp-recorded giant SEPs in cortical myoclonus. *Electroencephalogr Clin Neurophysiol.* (1995) 96:300–9. doi: 10.1016/0168-5597(95)00003-B
54. Shibasaki H, Kakigi R, Ikeda A. Scalp topography of giant SEP and pre-myoclonus spike in cortical reflex myoclonus. *Electroencephalogr Clin Neurophysiol.* (1991) 81:31–7. doi: 10.1016/0168-5597(91)90101-3
55. Salayev KA, Nakasato N, Ishitobi M, Shamoto H, Kanno A, Tominaga T, et al. Evaluation of interhemispheric time difference by magnetoencephalography before and after total callosotomy. Two case reports. *Neurol Med Chir.* (2006) 46:136–42. doi: 10.2176/nmc.46.136
56. Forss N, Hari R, Salmelin R, Ahonen A, Hämäläinen M, Kajola M, et al. Activation of the human posterior parietal cortex by median nerve stimulation. *Exp Brain Res.* (1994) 99:309–15. doi: 10.1007/BF00239597
57. Schoffelen JM, Gross J. Source connectivity analysis with MEG and EEG. *Hum Brain Mapp.* (2009) 30:1857–65. doi: 10.1002/hbm.20745
58. Uesaka Y, Terao Y, Ugawa Y, Yumoto M, Hanajima R, Kanazawa I. Magnetoencephalographic analysis of cortical myoclonic jerks. *Electroencephalogr Clin Neurophysiol.* (1996) 99:141–8. doi: 10.1016/0013-4694(96)95209-8
59. Komssi S, Huttunen J, Aronen HJ, Ilmoniemi RJ. EEG minimum-norm estimation compared with MEG dipole fitting in the localization of somatosensory sources at S1. *Clin Neurophysiol.* (2004) 115:534–42. doi: 10.1016/j.clinph.2003.10.034
60. Hitomi T, Ikeda A, Matsumoto R, Kinoshita M, Taki J, Usui K, et al. Generators and temporal succession of giant somatosensory evoked potentials in cortical reflex myoclonus: epicortical recording from sensorimotor cortex. *Clin Neurophysiol.* (2006) 117:1481–6. doi: 10.1016/j.clinph.2006.03.029
61. Hanajima R, Okabe S, Terao Y, Furubayashi T, Arai N, Inomata-Terada S, et al. Difference in intracortical inhibition of the motor cortex between cortical myoclonus and focal hand dystonia. *Clin Neurophysiol.* (2008) 119:1400–7. doi: 10.1016/j.clinph.2008.02.009
62. Sutton GG. Receptors in focal reflex myoclonus. *J Neurol Neurosurg Psychiatry.* (1975) 38:505–7. doi: 10.1136/jnnp.38.5.505
63. Terada K, Umeoka S, Usui N, Baba K, Usui K, Fujitani S, et al. Uneven interhemispheric connections between left and right primary sensori-motor areas. *Hum Brain Mapp.* (2012) 33:14–26. doi: 10.1002/hbm.21189
64. Tsutsumi R, Shirota Y, Ohminami S, Terao Y, Ugawa Y, Hanajima R. Conditioning intensity-dependent interaction between short-latency interhemispheric inhibition and short-latency afferent inhibition. *J Neurophysiol.* (2012) 108:1130–7. doi: 10.1152/jn.00300.2012
65. Werhahn KJ, Mortensen J, Kaelin-Lang A, Boroojerdi B, Cohen LG. Cortical excitability changes induced by deafferentation of the contralateral hemisphere. *Brain.* (2002) 125 (Pt. 6):1402–13. doi: 10.1093/brain/awf140
66. Palmer LM, Schulz JM, Murphy SC, Ledergerber D, Murayama M, Larkum ME. The cellular basis of GABA(B)-mediated interhemispheric inhibition. *Science.* (2012) 335:989–93. doi: 10.1126/science.1217276
67. Reis J, Swayne OB, Vandermeeren Y, Camus M, Dimyan MA, Harris-Love M, et al. Contribution of transcranial magnetic stimulation to the understanding of cortical mechanisms involved in motor control. *J Physiol.* (2008) 586:325–51. doi: 10.1113/jphysiol.2007.144824
68. Iwamura Y, Iriki A, Tanaka M. Bilateral hand representation in the postcentral somatosensory cortex. *Nature.* (1994) 369:554–6. doi: 10.1038/369554a0
69. Tamura K. Ipsilateral somatosensory evoked responses in man. *Folia Psychiatr Neurol Jpn.* (1972) 26:83–94. doi: 10.1111/j.1440-1819.1972.tb01115.x
70. Salamy A. Commissural transmission: maturational changes in humans. *Science.* (1978) 200:1409–11. doi: 10.1126/science.208144
71. Korvenoja A, Wikstrom H, Huttunen J, Virtanan J, Laine P, Aronen HJ, et al. Activation of ipsilateral primary sensorimotor cortex by median nerve stimulation. *Neuroreport.* (1995) 6:2589–93. doi: 10.1097/00001756-199512150-00033
72. Kanno A, Nakasato N, Hatanaka K, Yoshimoto T. Ipsilateral area 3b responses to median nerve somatosensory stimulation. *NeuroImage.* (2003) 18:169–77. doi: 10.1006/nimg.2002.1283
73. Kakigi R. Ipsilateral and contralateral SEP components following median nerve stimulation: effects of interfering stimuli applied to the contralateral hand. *Electroencephalogr Clin Neurophysiol.* (1986) 64:246–59. doi: 10.1016/0013-4694(86)90172-0
74. Noachtar S, Luders HO, Dinner DS, Klem G. Ipsilateral median somatosensory evoked potentials recorded from human somatosensory cortex. *Electroencephalogr Clin Neurophysiol.* (1997) 104:189–98. doi: 10.1016/S0168-5597(97)00013-0
75. Lueders H, Lesser RP, Hahn J, Dinner DS, Klem G. Cortical somatosensory evoked potentials in response to hand stimulation. *J Neurosurg.* (1983) 58:885–94. doi: 10.3171/jns.1983.58.6.0885
76. Boakye M, Huckins SC, Szeverenyi NM, Taskey BI, Hodge CJ Jr. Functional magnetic resonance imaging of somatosensory cortex activity produced by electrical stimulation of the median nerve or tactile stimulation of the index finger. *J Neurosurg.* (2000) 93:774–83. doi: 10.3171/jns.2000.93.5.0774
77. Nihashi T, Naganawa S, Sato C, Kawai H, Nakamura T, Fukatsu H, et al. Contralateral and ipsilateral responses in primary somatosensory cortex following electrical median nerve stimulation–an fMRI study. *Clin Neurophysiol.* (2005) 116:842–8. doi: 10.1016/j.clinph.2004.10.011
78. Shibasaki H, Nakamura M, Nishida S, Kakigi R, Ikeda A. Wave form decomposition of 'giant SEP' and its computer model for scalp topography. *Electroencephalogr Clin Neurophysiol.* (1990) 77:286–94. doi: 10.1016/0168-5597(90)90067-N
79. Brown P, Ridding MC, Werhahn KJ, Rothwell JC, Marsden CD. Abnormalities of the balance between inhibition and excitation in the motor cortex of patients with cortical myoclonus. *Brain.* (1996) 119 (Pt. 1):309–17. doi: 10.1093/brain/119.1.309
80. Sestieri C, Shulman GL, Corbetta M. The contribution of the human posterior parietal cortex to episodic memory. *Nat Rev Neurosci.* (2017) 18:183–92. doi: 10.1038/nrn.2017.6
81. Battaglia-Mayer A, Caminiti R. Corticocortical Systems underlying high-order motor control. *J Neurosci.* (2019) 39:4404–21. doi: 10.1523/JNEUROSCI.2094-18.2019
82. Mattingley JB, Husain M, Rorden C, Kennard C, Driver J. Motor role of human inferior parietal lobe revealed in unilateral neglect patients. *Nature.* (1998) 392:179–82. doi: 10.1038/32413
83. Rozzi S, Ferrari PF, Bonini L, Rizzolatti G, Fogassi L. Functional organization of inferior parietal lobule convexity in the macaque monkey: electrophysiological characterization of motor, sensory and mirror responses and their correlation with cytoarchitectonic areas. *Eur J Neurosci.* (2008) 28:1569–88. doi: 10.1111/j.1460-9568.2008.06395.x
84. Marconi B, Genovesio A, Giannetti S, Molinari M, Caminiti R. Callosal connections of dorso-lateral premotor cortex. *Eur J Neurosci.* (2003) 18:775–88. doi: 10.1046/j.1460-9568.2003.02807.x
85. Koch G, Fernandez Del Olmo M, Cheeran B, Ruge D, Schippling S, Caltagirone C, et al. Focal stimulation of the posterior parietal cortex increases the excitability of the ipsilateral motor cortex. *J Neurosci.* (2007) 27:6815–22. doi: 10.1523/JNEUROSCI.0598-07.2007
86. Carenini L, Bottacchi E, Camerlingo M, D'Alessandro G, Mamoli A. Carbamazepine does not affect short-latency somatosensory evoked potentials: a longitudinal study in newly diagnosed epilepsy. *Epilepsia.* (1988) 29:145–8. doi: 10.1111/j.1528-1157.1988.tb04410.x
87. Borah NC, Matheshwari MC. Effect of antiepileptic drugs on short-latency somatosensory evoked potentials. *Acta Neurol Scand.* (1985) 71:331–3. doi: 10.1111/j.1600-0404.1985.tb03209.x
88. Sendrowski K, Sobaniec W, Bockowski L, Kulak W, Smigielska-Kuzia J. Somatosensory evoked potentials in epileptic children treated with carbamazepine or valproate in monotherapy - a preliminary study. *Adv Med Sci.* (2010) 55:212–5. doi: 10.2478/v10039-010-0019-2

89. Tojima M, Hitomi T, Matsuhashi M, Neshige S, Usami K, Oi K, et al. A biomarker for benign adult familial myoclonus epilepsy: high-frequency activities in giant somatosensory evoked potentials. *Mov Disord.* (2021) 33:1248–66. doi: 10.1002/mds.28666

Conflict of Interest: The authors declare that the research was conducted in the absence of any commercial or financial relationships that could be construed as a potential conflict of interest.

Publisher's Note: All claims expressed in this article are solely those of the authors and do not necessarily represent those of their affiliated organizations, or those of the publisher, the editors and the reviewers. Any product that may be evaluated in this article, or claim that may be made by its manufacturer, is not guaranteed or endorsed by the publisher.

frontiers in Neurology

REVIEW
published: 27 January 2022
doi: 10.3389/fneur.2021.814573

Gratifying Gizmos for Research and Clinical MEG

Veikko Jousmäki [1,2]*

[1] Aalto NeuroImaging, Department of Neuroscience and Biomedical Engineering, Aalto University, Espoo, Finland, [2] Cognitive Neuroimaging Centre, Lee Kong Chian School of Medicine, Nanyang Technological University, Singapore, Singapore

Experimental designs are of utmost importance in neuroimaging. Experimental repertoire needs to be designed with the understanding of physiology, clinical feasibility, and constraints posed by a particular neuroimaging method. Innovations in introducing natural, ecologically-relevant stimuli, with successful collaboration across disciplines, correct timing, and a bit of luck may cultivate novel experiments, new discoveries, and open pathways to new clinical practices. Here I introduce some gizmos that I have initiated in magnetoencephalography (MEG) and applied with my collaborators in my home laboratory and in several other laboratories. These gizmos have been applied to address neuronal correlates of audiotactile interactions, tactile sense, active and passive movements, speech processing, and intermittent photic stimulation (IPS) in humans. This review also includes additional notes on the ideas behind the gizmos, their evolution, and results obtained.

Keywords: accelerometer, audiotactile, illusion, somatosensory, motor, stimulation

OPEN ACCESS

Edited by:
Anto Bagic,
University of Pittsburgh, United States

Reviewed by:
Samu Taulu,
University of Washington, United States
Giovanni Pellegrino,
McGill University, Canada

***Correspondence:**
Veikko Jousmäki
veikko.jousmaki@aalto.fi

Specialty section:
This article was submitted to Applied Neuroimaging, a section of the journal Frontiers in Neurology

Received: *13 November 2021*
Accepted: *24 December 2021*
Published: *27 January 2022*

Citation:
Jousmäki V (2022) Gratifying Gizmos for Research and Clinical MEG. Front. Neurol. 12:814573. doi: 10.3389/fneur.2021.814573

INTRODUCTION

Although life is multisensory in nature, it is worth investigating sensory modalities with dedicated stimulators separately with neuroimaging methods. For this purpose, we need natural, ecologically-relevant stimuli which stimulate each sensory modality specifically and do not interfere with the neuroimaging modality used.

For example, magnetoencephalography (MEG) and electroencephalography (EEG) provide us tools to evaluate a given sensory system and its neuronal correlates and use the results in clinical assessments as guided in the clinical practice guidelines (1). For example, electric stimulation applied over the peripheral nerve is preferred to elicit somatosensory-evoked potentials (SEPs) and somatosensory-evoked fields (SEFs). Such a strong and non-specific sensory stimulus works perfectly to address neuroscientific questions, for example, what is the given peak latency and where the corresponding cortical representation is located. To be honest, such an approach works in most of the cases perfectly. However, such a sensory stimulus does not stimulate peripheral mechanoreceptors, for example, Pacinian corpuscles, proprioceptors, and slowly conducting tactile fibers specifically. Thus, we may miss some specific attributes in stimulation to address more detailed possibilities in basic research and clinical practice.

Why do not we have ecologically relevant, naturalistic stimulators in use in MEG? The answer is very simple—they are not commercially available. Availability may be limited due to the estimated market size which is typically considered to be not large enough for introducing new stimulators taking into account regulatory processes needed for medical devices.

There are two main approaches to introduce a novel stimulator in MEG. One approach is to use an original idea in basic research, apply it with an in-house built and locally-approved stimulator

within a small number of subjects as investigator-initiated studies, and publish the results. The other approach is to file invention disclosures and proceed with patent applications to protect the immaterial property rights (IPRs) first and then proceed to collect the evidence in a multicenter study with the documented stimulator. Both approaches will take time and effort without any promise of the final outcome.

Here, I will present a few cases that I have initiated in MEG and, together with my collaborators, used successfully to discover novel findings. I have used mostly the basic research approach in introducing gizmos for MEG research.

MEG MARKET

Before entering to the gizmos, it is worth checking the status quo in MEG including the market size, market forecast, main vendors, and stimulators. With more than 200 MEG devices in active use, non-invasive MEG plays a vital role in basic research and clinical applications. The clinical use of MEG is presented in recent surveys (2–7). With two clinical applications, namely presurgical functional mapping and localizing of epileptic foci, MEG is very useful in epilepsy and presurgical evaluation. Although MEG performed only in a fraction of epilepsy patients, it has a huge potential in epilepsy centers.

At present, all commercially available whole-head MEG systems approved by US Food and Drug Administration (FDA) are using superconducting quantum interference (SQUID) technology with liquid helium. Whole-head MEG systems utilizing optically pumped magnetometer (OPM) technology are now available for research purposes (8–13).

The main market areas for MEG are Northern America, Europe, and Asia. MEG market is gradually expanding. According to a recent market review by Verified Market Research (https://www.verifiedmarketresearch.com/product/magnetoencephalography-market), the MEG market size was valued ∼200 million USD in 2020 and is projected to reach ∼300 million USD by 2028. The main fuels for the market rise are the prevalence of brain diseases and growing popularity due to its non-invasive nature. The MEG market growth is estimated to be driven by the increase of MEG centers and advancements in OPM technology.

Main MEG vendors, for example, CTF (CTF MEG Neuro Innovations Inc, Coquitlam, BC, Canada; http://ctf.com), MEGIN (MEGIN Oy, Helsinki, Finland; http://megin.fi), NeuroScan (Compumedics Limited, Abbotsford, Victoria, Australia; https://compumedicsneuroscan.com), and Ricoh (Ricoh USA Inc., Tustin, CA; https://www.ricoh-usa.com), typically list a limited number of validated stimulators. These stimulators for visual, somatosensory, and auditory modalities have been tested according to the regulatory requirements concerning medical devices. Here, it is the FDA since the main market resides in the USA. Local approvals, for example, CE marking in the European Economic Area, may also be required. FDA-approved stimulators are typically provided by another vendor selling these devices also for other functional neuroimaging modalities, and these stimulators have been tested as a part of the MEG system.

Typically, a stimulation system in MEG is controlled with a commercial software package, for example, Presentation (Neurobehavioral Systems Inc., Berkeley, CA; https://www.neurobs.com), Stim2 (Compumedics Limited, Abbotsford, Victoria, Australia; https://compumedicsneuroscan.com), or E-Prime (Psychology Software Tools, Inc., Pittsburgh, PA; https://pstnet.com/). Many experienced and technically strong MEG teams have their own in-house built or third-party stimulators and software in use, for example, PsychoPy (https://psychopy.org) and Psychophysics Toolbox (http://psychtoolbox.org). Given the efforts needed for FDA clearance, third-party software packages and toolboxes are typically more flexible for research-oriented MEG compared with FDA-cleared software packages.

DESIGNING GIZMOS

Magnetoencephalography and electroencephalography share the same origin of signals and temporal resolution. These aspects at theoretical, instrumentational, mathematical, and practical levels are depicted in details in Hari and Puce (14) and Hämäläinen et al. (15). Most of the commercially available stimulators and monitoring devices used commonly in other neuroimaging modalities, for example, functional magnetic resonance imaging (fMRI) and EEG, are not readily MEG compatible. Why MEG is so vulnerable to interferences? MEG sensors are very prone to magnetic and radiofrequency fields—this is the main reason for using the magnetically shielded room (MSR) in MEG to suppress ambient electromagnetic noise and to keep MEG sensors within their dynamic range.

Artifacts in MEG include several sources inside and outside the MSR, for example, ambient noise, various physiological signals, movement artifacts, and intrinsic MEG noise (16). Here, we focus on those elicited by stimulators and monitoring devices. Interfering artifacts inside the MSR may be elicited by magnetic materials moving close to MEG sensors, electric currents, ground loops, and radiofrequency disturbances associated with a given stimulator. For example, magnetic materials close to the MEG sensors combined with deep breathing, task-related movements, utterances, and ballistocardiographic body movements may give rise to disturbing artifacts in MEG. Here, the distance really matters—devices next to the MEG sensors need to be carefully tested for possible magnetic artifacts whereas devices fixed on the floor at a distance from the MEG sensors may contain some magnetic particles. Although noise suppression methods, for example, high-pass filtering, may help to attenuate, these low-frequency artifacts in MEG signals of interest may overlap with, for example, movement frequency. In such cases, more advanced noise suppression algorithms, for example, the temporal extension of signal space separation (17), maybe useful to attenuate artifacts leaving brain signals intact (18, 19).

It is important to note that implanted stimulators, for example, cardiac pacemakers, deep brain stimulators, and vagal nerve stimulators, contain magnetic particles and will cause

severe artifacts in MEG. Given the dynamic range of the modern superconducting MEG systems, MEG measurements are feasible although off-line processing is needed to separate artifacts from the brain signals (20–23).

Digital signals cause RF interferences, and thus, analog signals are preferred inside the MSR. Cables entering the MSR should be filtered to rule out any potential RF interference since cables may act as antennas bringing external RF interference to the MSR. Direct current battery-operated devices are preferred to reduce possible interferences and ground loops to avoid deteriorated MEG signal quality.

Safety aspects and regulations concerning medical devices need to be taken into account, too.

Sensor manufactures, vendors, and suppliers provide huge selection of sensors and materials to choose from finding suitable ones for MEG purposes which take testing, time, effort, and luck. Vendors and suppliers do not specify MEG compatibility, and non-magnetic does not necessarily mean non-magnetic in MEG. Materials should be tested and selected carefully, and an MEG device can be utilized to find suitable materials since it picks up magnetic disturbances easily.

Material selection and manufacturing processes are of major importance in MEG. Most materials, for example, wood, plastic, and metals, can be used in MEG which provided that they are non-magnetic. However, some dyes are magnetic, and some materials typically considered to be non-magnetic, for example, aluminum and copper, may turn out to be magnetic due to the recycling processes introducing magnetic deposits. Manufacturing processes may also introduce magnetic artifacts, for example, a chrome-tipped solder iron will leave magnetic chrome deposits in soldering whereas copper tip does not cause such problems. In addition, some manufacturing processes, for example, modern gold-plating technique with magnetic nickel sublayer, cause major disturbances in MEG. Once again, the distance matters. A gold-plated EEG electrode typically introduces artifacts in MEG since it will be next to the MEG sensors and it will move with respect to the MEG sensors due to breathing, task-related movements, utterances, and ballistocardiographic movements whereas a gold-plated connector fixed on the floor of the MSR can easily be used without any artifacts in MEG.

Taking all these together, a novel stimulator or monitoring device has to be safe and easy to use, fulfill the local regulations, have local approvals, compatible with existing MEG systems, and should synchronize with the MEG data acquisition and stimulation systems precisely. As a physicist, I would like to say that the task is well-defined and feasible. Let me now introduce some gizmos.

AUDIOTACTILE INTERACTIONS

Investigational approaches and their evolutions in multisensory interaction studies are well-covered in multisensory textbooks (24–26). Multisensory research is dominated by audiovisual research whereas audiotactile interactions, that is, how tones or noise bursts affect roughness perception (27), are scarce.

Magnetoencephalography has a huge advantage over fMRI especially in auditory and audiotactile domain since MEG acquisition is practically silent whereas fMRI involves concomitant high-intensity ambient noise associated with gradient coils and cryocooler. In addition, direct coupling to neuronal activity facilitates MS precision in MEG, and thus very detailed investigations related to neuronal processing involved.

We started to study the brain mechanisms underlying the largely unexplored audiotactile interactions in MEG in the 90's. Obviously, these experiments also required a novel MEG-compatible vibrotactile stimulation device.

It all started with an authentic audiotactile illusion discovered while testing an MEG-compatible microphone system. We coined the illusion as a parchment skin illusion (28) in which concomitant auditory feedback of the self-performed hand rubbing sound changes the perceived tactile sensation of the hands. The illusion is an excellent example of multisensory top–down processing in the brain. Later, the parchment skin illusion has been listed as one of the seven ways to fool your sense of touch freaky feelings (29) by New Scientist magazine. Charles Spence with his coauthors has exploited audiotactile illusions utilizing similar approaches in multisensory studies concerning, for example, roughness estimation (30) and crispness and staleness of potato chips (31) which earned them the Ig Nobel Prize in 2008.

I have learned audiotactile interactions in my childhood while playing with my two congenitally deaf cousins. Deaf persons use their tactile systems, that is, mechanoreceptors on the skin, for example, to efficiently control their voice and listen to music. With this background, we conducted a very unconventional experiment to demonstrate the activation of the auditory cortices in response to vibrotactile stimulation in a congenitally deaf adult. My new vibrotactile stimulator (see **Figure 1**), was crucial for the success of this study, which resulted in the first MEG publication showing a novel evidence on the plasticity in the auditory cortices in a congenitally deaf adult (32).

Investigations on audiotactile interactions with the vibrotactile stimulator have shed light on how hands help and activate auditory cortices in normal hearing subjects by means of MEG and fMRI recordings (33–35).

I consider that devices based on audiotactile interactions could be used efficiently in improving speech perception in noisy environments and hearing-disabled persons. In addition, such devices could be useful for rehabilitation purposes.

TACTILE STIMULATION

The human tactile system provides us with an amazing spectrum of feedback, which enables us to perform tasks that require utterly precise motor control, such as playing musical instruments, and to sense minute vibrations. Touch even carries social and affective information (36) which is essential in our non-verbal communication. Unfortunately, fine-tuned tactile MEG-compatible stimulators are not readily available, largely preventing investigation of the tactile system with such ecologically-relevant stimuli.

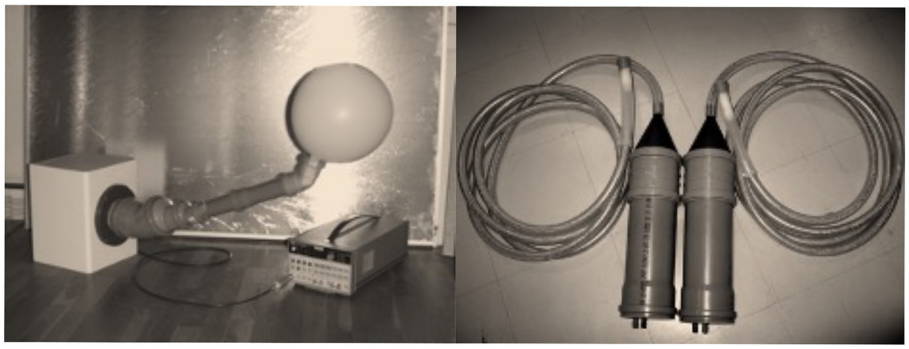

FIGURE 1 | Left: The evolution of the house-built vibrotactile stimulator. The original vibrotactile stimulator was used to investigate a congenitally deaf adult (32). Right: The evolution version with a dedicated band-pass (100–500 Hz) filter was used later (33–35). Note that the original version has a balloon which vibrates by sound elicited by a standard loudspeaker whereas the later version uses a blind-ended silicone tube contributing to the reduced auditory contamination. White noise masking was typically used to reduce the auditory contamination.

My original motivation was to find a way to get a precise trigger from the onset of the touch associated with von Frey monofilaments, which is used commonly for testing sensory thresholds of the human skin. It would open new pathways to study subthreshold tactile stimulation in MEG. Finally, I managed to discover a working solution comprising of a multifilament optic cable (Schott AG, Mainz, Germany) and an optosensor (Omron, Osaka, Japan) (see **Figure 2**). Multifilament optic cables consisting of hundreds of 50-μm fibers are used commonly for lightning in harsh environments. The multifilament cables are rather flexible and usable for infrared and visible light without any major attenuation. My approach is based on the idea that multifilament optic cable can be divided into two halves—one half for emitting the light from the optosensor and the other half to detect the reflection from the object. This innovation allowed us to generate a trigger from the skin contact at an accuracy of 1 mm in MEG recordings.

The first experiments with the novel brush stimulator, as we coined it at the time, were carried out at the National Rehabilitation Center (Tokorozawa, Japan). We used the brush stimulator to stimulate skin at the fingertip and lip and located the corresponding cortical sources (37). Later, the same approach has been used in several unique experiments shedding light on differences in pure observing and self vs. externally produced tactile stimulation with accurate and precise tactile stimulation in MEG (38, 39).

FIGURE 2 | The original design for the tactile stimulator, a.k.a. woodpecker, used in tactile stimulation studiers (37, 39) is based on multifilament optical fiber (Schott Spectraflex; Schott AG, Mainz, Germany) and photosensor (Omron, Osaka, Japan). Note that the design of the handle limits the maximum force on the skin similarly as in an aesthesiometer based on von Frey filaments.

SENSORIMOTOR MAPPING

As we know, motor cortices control actual movements, and peripheral feedback is used to fine-tune motor actions continuously. Such a closed-loop offers interesting options for monitoring efference and afference involved.

Magnetoencephalography has been used for functional sensorimotor mapping. Unfortunately, MEG recordings may be disturbed by large movements during the recordings, and thus, motor activities are typically limited to isometric muscle contractions or finger and foot movements. These issues can be mitigated using appropriate signal processing algorithms to compensate head movements, for example, signal space separation method (17). Such methods produce sufficient MEG signal quality to compensate low-frequency, smooth body movements but are limited to compensate for strong, brisk, and fast body movements.

Clinical practice guidelines list several protocols, for example, recording the premovement shift and corticomuscular coherence (CMC), for evaluating and locating motor cortices in MEG (1, 40). Typically, protocols require cooperation and results depend on the subject's performance level. In particular, disabled subjects may find these protocols very difficult to perform. On the other hand, motor mapping is clinically important in the preoperative evaluation of patients undergoing neurosurgery and could also be used during rehabilitation following a stroke or accident.

FIGURE 3 | A typical setting in corticokinematic coherence studies (42–44) with a lightweight accelerometer (ADXL335; Analog Devices Inc, Norwood, MA) attached on the finger nail to pick up hand movements. Note that flexible cable allows natural hand movements.

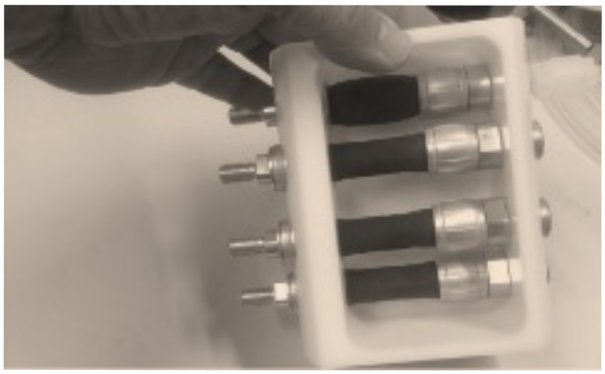

FIGURE 4 | A 4-channel movement actuator system based on PAMs. Similar PAMs were used in studies using computer-controlled PAM stimulator. Note that the uppermost artificial muscle is contracting due to compressed air pulse applied on the muscle and the muscle is relaxed when it is depressurized. The maximum movement range of the muscle in the figure is about 10 mm, that is, 20% of the original length.

My motivation was to find an alternative solution for motor mapping using accelerometers to combine hand movements and MEG signals. The first accelerometers, for example, 40G Motorola accelerometers, that I tested in the late 90's were designed for the car industry and were far too magnetic and insensitive for the purpose. Ten years later, I stumbled upon an MEG-compatible 3D accelerometer ADXL330 (Analog Devices Inc., Norwood, MA) with analog output and 3G range—such accelerometers were used, for example, in Wii remote by Nintendo Co (Osaka, Japan). The component itself is non-magnetic although the operating current introduces some magnetic signals at a close distance, say within 50 cm from the MEG sensors.

At first, I envisioned three uses of the accelerometer in MEG: monitoring self-paced hand movements, monitoring the fundamental frequency of the voice, and using it as a response pad. Soon, we discovered that a similar approach had been already used to detect the onset of the motor movements (41). We set out to investigate possibilities for motor mapping using an accelerometer to record continuous self-paced movements at the Hôpital Erasme (Université Libre de Bruxelles, Brussels, Belgium).

We conducted measurements in MEG with an accelerometer attached to the finger (see **Figure 3**), whereas the subject was mimicking Parkinsonian tremor for three min. We could easily see a systematic coherence between the accelerometer and MEG signals. This discovery heralded the use of a new method to locate and monitor the activity at the primary somatomotor cortices during active and passive movements, and we coined the approach as corticokinematic coherence (CKC) in which coherence is calculated between movement kinematics monitored with an accelerometer and MEG signals (42).

Corticokinematic coherence studies published have shed light to address, for example, self-paced and externally paced movements (43), kinematics of the movements at various movement rates, and comparisons between hand-action-related acceleration, force, pressure, and electromyogram as a reference for CKC (44). CKC seems to reflect mainly movement-related proprioceptive afference (45), and thus, it is a very attracting tool to study proprioceptive systems in healthy and disabled subjects. In addition, CMC and CKC methods seem to complement each other (46). CKC studies have also provided a starting point to a possible bedside testing protocol to assess sensorimotor integration in newborns (47, 48).

Magnetoencephalography -compatible accelerometers have also been used successfully to study speech perception in humans to address coupling to the speech real-life situations (49–51). In addition, such accelerometers can be used to pick up utterances in a language testing paradigm in transcranial magnetic stimulation studies (52).

Since both self-paced and externally paced movements activate the same network in the brain, a computer-controlled stimulator for delivering precise and accurate finger movements comes very attractive. I discovered pneumatic artificial muscles (PAMs), originally invented in the 50's. These actuators are like badly designed pneumatic tubes expanding and shortening when pressurized (see **Figure 4**). Aramid fibers in the tube will push the muscle to its original length when the pressure is released. Such an actuator can be easily controlled by pneumatic relays outside the MSR.

Pneumatic artificial muscle-based stimulators have been used in MEG, for example, in healthy subjects (53), Parkinson's patients (54), and Friedreich ataxia patients (55, 56) to explain proprioceptive afference and its impairment. Another PAM-based device (see **Figure 5**), has been used in investigations on slowly conducting tactile, that is, CT fibers contributing to gentle touch in MEG (57). In addition, PAM-based devices have been successfully used in fMRI studies (58–60).

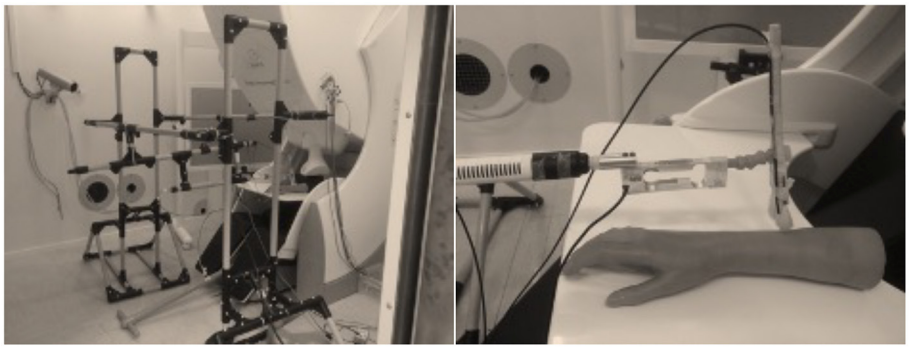

FIGURE 5 | Left: The brush robot at NatMEG (Karolinska Institutet, Stockholm, Sweden) used to study gentle touch, that is, slowly conducting tactile (CT) fibers (57). Right: The brush robot uses similar PAMs as the PAM stimulator as the device in the **Figure 4**. Note that the computer-controlled device contains two PAMs for lifting and moving the brush, load cell to measure the force applied on the skin, accelerometer to monitor the movement, and two multifilament optic fibers to pick up the velocity of the brush movement and skin contact of the brush.

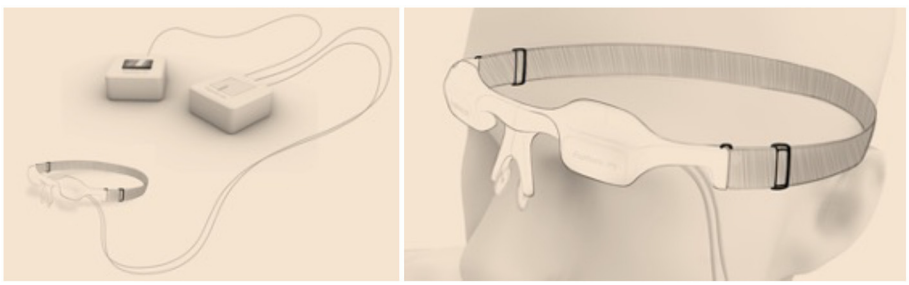

FIGURE 6 | The design sketch of the Euphotic intermittent photic stimulation device (patents pending) using a unique diffuse light concept both in eyes-open and eyes-closed conditions. Note that the Euphotic IPS device allows unique option for simultaneous visual stimulation in eyes-open condition.

INTERMITTENT PHOTIC STIMULATION

Clinical practice guidelines in MEG (https://www.acmegs.org/clinical-resources/practice-guidelines) define widely accepted clinical practices and provide an excellent view to the present state in clinical MEG. Comparison of the clinical practice guidelines in EEG (https://www.acns.org/practice/guidelines) indicates that MEG is still limited in use since clinical EEG has several applications that MEG misses. For example, intermittent photic stimulation (IPS) test is a vital part of clinical EEG with benefits whereas it is not mentioned in clinical MEG since commercial MEG-compatible IPS devices are not available.

Intermittent photic stimulation test is used in clinical EEG to study the cortical excitability during eyes open and eyes closed conditions (61). In patients with photosensitive epilepsy, IPS may cause epileptiform activity and even epileptic seizures (62).

Intermittent photic stimulation stimulators have progressed from the early xenon-based stimulator to modern LED-based devices (63). However, both types of IPS devices are not MEG compatible.

The idea to introduce novel IPS stimulator was triggered by the missing definition IPS in MEG in clinical practice guidelines. In this case, I filed an invention disclosure at Aalto University, and we have filed US and European patent applications to protect the ideas for potential commercial use. The euphotic team at Aalto University (Espoo, Finland) is developing the novel diffuse light concept in IPS further. With the novel Euphotic IPS device (see **Figure 6**), it is feasible to stimulate one or two eyes at the same time and use diffuse light both in eyes-open and eyes-closed conditions. In addition, it is a portable system and does not require eye fixation or focusing on the IPS device. The Euphotic IPS device is fully MEG compatible.

At present, the Euphotic project has established a preliminary business plan to take the authentic idea further and faster than in my previous innovations. The Euphotic project aims to collect patient and normative database and analysis tools to help to introduce IPS in clinical MEG.

Feasibility studies with Euphotic IPS device have ethical approvals at Cognitive Neuroimaging Centre (Nanyang Technological University, Singapore) and Aalto NeuroImaging (Aalto University, Espoo, Finland). Unfortunately, the COVID-19 outbreak has caused severe delays in MEG measurements in healthy subjects both in Singapore and Finland.

CONCLUSIONS

As I have shown above, investigating sensory systems with natural, ecologically-relevant stimuli is feasible in MEG. First, Pacinian corpuscles can be selectively stimulated in MEG, and

such stimuli can be utilized to study audiotactile interactions in congenitally deaf and normal hearing subjects. These novel findings help us to understand plasticity in the brain and how tactile sense affects the auditory sense and vice versa. Second, glabrous skin and lips can be stimulated with natural, ecologically relevant stimuli with MS precision in MEG. Such stimuli could be utilized in presurgical mapping and to monitor the recovery of peripheral nerve damages since given axons and associated sensory perceptions recover gradually. Third, active and passive movements can be investigated by utilizing accelerometers in MEG. The CKC method developed has proven to be very useful in investigating sensorimotor processing in healthy and diseased. Specifically, passive movements produced by MEG-compatible actuators, that are, PAMs, offer novel possibilities for presurgical mapping and designing novel experiments in MEG and fMRI. For example, such stimulators can be utilized to investigate gentle touch, that is, CT afferents, in MEG with ms precision. Fourth, the novel approach to use diffuse flickering light introduces MEG-compatible IPS device and opens novel ways to analyze cortical responses in epilepsy and healthy subjects.

These results mentioned above may open new avenues in research and translational clinical applications. It is important to notice that these steps from the bench to bedside involve multidisciplinary collaborators, time, effort, and reasonable funding.

Unfortunately, the gizmos that I have described here have not been FDA nor CE cleared, and thus, they are for investigational use only. We have plans to commercialize the Euphotic IPS device and we have a plan to collect evidence for the approvals in the forthcoming multicenter MEG study. We also have a plan to apply for FDA approval for the Euphotic IPS as a Class II medical device.

Both basic research and IPR-based solutions seem to work although the documentation load in the latter is elevated. On the other hand, IPR-based solution opens new paths for potential commercialization in the future once the evidence is available. The potential market could be easily expanded by designing stimulators and monitoring devices to be compatible with MEG and fMRI.

One of the major limiting factors for realizing novel ideas and stimulators is funding for basic research projects including preparing a prototype, creating preliminary documentation, initial recordings, and evidence to show that the idea works in reality. Universities would be optimal research sites for these steps whereas commercialization projects typically require a new company or contributions from well-established companies. Special research-to-business funding is available in several countries to facilitate the processes although such secured funding is limited and heavily competed. It also requires a realistic market estimate, strong business plan, global partners, and clear focus area. On the other hand, the valuation task can be very demanding since clinical practice guidelines do not support, for example, IPS in clinical MEG.

As shown above, I have created several gizmos for basic research and some of them are taking the first steps from the bench to the bedside. It has been fun and I have really enjoyed the work and collaboration with my global network.

AUTHOR CONTRIBUTIONS

The author confirms being the sole contributor of this work and has approved it for publication.

FUNDING

Euphotic project at the Aalto University has financial support from the Aalto Brain Centre (https://www.aalto.fi/en/school-of-science/aalto-brain-centre).

ACKNOWLEDGMENTS

Designing gizmos for neuroimaging requires teamwork. I would like to thank my supervisors for the guidance, feedback, and freedom of operation first at the Brain Research Unit (Low Temperature Laboratory, Helsinki University of Technology, Espoo, Finland), and recently at Aalto University (Espoo, Finland). I would like to express my special gratitude to Professors Riitta Hari and Matti Hämäläinen for their everlasting support and guidance in my scientific career over the years. I have really enjoyed working with multidisciplinary teams by sharing ideas, ambitions, and curiosity in learning how to stimulate the human body and its receptors in a naturalistic way. I would like to thank my colleagues and coauthors for contributing to the gizmo designs, original studies, and articles. I would like to express my special gratitude to Professors Xavier de Tiège and Mathieu Bourguignon at Hôpital Erasme (Université libre de Bruxelles, Brussels, Belgium), Professor Daniel Lundqvist at NatMEG (Karolinska Institutet, Stockholm, Sweden), and Professor Balázs Gulyás at CoNiC (Lee Kong Chian School of Medicine, Nanyang Technological University, Singapore) and their excellent teams. I also value the excellent technical support by Helge Kainulainen and Ronny Schreiber at Aalto NeuroImaging.

REFERENCES

1. Burgess RC, Funke ME, Bowyer SM, Lewine JD, Kirsch HE, Bagic AI, et al. American Clinical Magnetoencephalography Society Clinical Practice Guideline 2: presurgical functional brain mapping using magnetic evoked fields. *J Clin Neurophysiol.* (2011) 28:355–61. doi: 10.1097/WNP.0b013e3182272ffe
2. Bagic AI. Disparities in clinical magnetoencephalography practice in the United States: a survey-based appraisal. *J Clin Neurophysiol.* (2011) 28:341–7. Available online at: https://journals.lww.com/clinicalneurophys/Abstract/2011/08000/Disparities_in_Clinical_Magnetoencephalography.3.aspx
3. De Tiège X, Lundqvist D, Beniczky S, Seri S, Paetau R. Current clinical magnetoencephalography practice across Europe: Are we closer to use MEG as an established clinical tool? *Seizure.* (2017) 50:53–9. doi: 10.1016/j.seizure.2017.06.002
4. Baud MO, Perneger T, Racz A, Pensel MC, Elger C, Rydenhag B, et al. European trends in epilepsy surgery.

Neurology. (2018) 91:e96–106. doi: 10.1212/WNL.0000000000005776
5. Mouthaan BE, Huiskamp GM, Leijten FS, Braun KP. Response to: Guidelines for the clinical use in epilepsy surgery evaluation of magnetoencephalography and electroencephalography for source localization. *Epilepsia*. (2016) 57:1942. doi: 10.1111/epi.13581
6. Shiraishi H, Ozaki I, Igushi Y, Ishii R, Kamada K, Kameyama S, et al. Questionnaire survey of current status and problems in clinical applications of magnetoencephalography (MEG) in Japan. *Jpn J Clin Neurophysiol.* (2012) 40:119–30. doi: 10.11422/jscn.40.119
7. Bagic AI, Burgess RC. Clinical magnetoencephalography practice in the United States ten years later: a survey-based reappraisal. *J Clin Neurophysiol.* (2020) 37:592–8. doi: 10.1097/WNP.0000000000000693
8. de Lange P, Boto E, Holmes N, Hill RM, Bowtell R, Wens V, et al. Measuring the cortical tracking of speech with optically-pumped magnetometers. *Neuroimage*. (2021) 233:117969. doi: 10.1016/j.neuroimage.2021.117969
9. Shah VK, Wakai RT. A compact, high performance atomic magnetometer for biomedical applications. *Phys Med Biol.* (2013) 58:8153–61. doi: 10.1088/0031-9155/58/22/8153
10. Boto E, Bowtell R, Kruger P, Fromhold TM, Morris PG, Meyer SS, et al. On the potential of a new generation of magnetometers for MEG: A Beamformer simulation study. *PLoS One*. (2016) 11:e0157655. doi: 10.1371/journal.pone.0157655
11. Boto E, Meyer SS, Shah V, Alem O, Knappe S, Kruger P, et al. A new generation of magnetoencephalography: Room temperature measurements using optically-pumped magnetometers. *Neuroimage*. (2017) 149:404–14. doi: 10.1016/j.neuroimage.2017.01.034
12. Tierney TM, Holmes N, Mellor S, Lopez JD, Roberts G, Hill RM, et al. Optically pumped magnetometers: From quantum origins to multi-channel magnetoencephalography. *Neuroimage*. (2019) 199:598–608. doi: 10.1016/j.neuroimage.2019.05.063
13. Kominis IK, Kornack TW, Allred JC, Romalis MV. A subfemtotesla multichannel atomic magnetometer. *Nature*. (2003) 422:596–9. doi: 10.1038/nature01484
14. Hari R, Puce A. *MEG-EEG Primer*. New York, NY: Oxford University Press (2017).
15. Hämäläinen M, Hari R, Ilmoniemi RJ, Lounasmaa OV. Magnetoencephalography-theory, instrumentation, and applications to noninvasive studies of the working human brain. *Rev Modern Phys.* (1993) 65:413–97. doi: 10.1103/RevModPhys.65.413
16. Burgess RC. Recognizing and correcting MEG artifacts. *J Clin Neurophysiol.* (2020) 37:508–17. doi: 10.1097/WNP.0000000000000699
17. Taulu S, Kajola M, Simola J. Suppression of interference and artifacts by the signal space separation method. *Brain Topogr.* (2004) 16:269–75. doi: 10.1023/B:BRAT.0000032864.93890.f9
18. Taulu S, Hari R. Removal of magnetoencephalographic artifacts with temporal signal-space separation: demonstration with single-trial auditory-evoked responses. *Hum Brain Mapp.* (2009) 30:1524–34. doi: 10.1002/hbm.20627
19. Bourguignon M, Whitmarsh S, Piitulainen H, Hari R, Jousmäki V, Lundqvist D. Reliable recording and analysis of MEG-based corticokinematic coherence in the presence of strong magnetic artifacts. *Clin Neurophysiol.* (2016) 127:1460–9. doi: 10.1016/j.clinph.2015.07.030
20. Airaksinen K, Makela JP, Taulu S, Ahonen A, Nurminen J, Schnitzler A, et al. Effects of DBS on auditory and somatosensory processing in Parkinson's disease. *Hum Brain Mapp.* (2011) 32:1091–9. doi: 10.1002/hbm.21096
21. Abbasi O, Hirschmann J, Schmitz G, Schnitzler A, Butz M. Rejecting deep brain stimulation artefacts from MEG data using ICA and mutual information. *J Neurosci Methods.* (2016) 268:131–41. doi: 10.1016/j.jneumeth.2016.04.010
22. Kandemir AL, Litvak V, Florin E. The comparative performance of DBS artefact rejection methods for MEG recordings. *Neuroimage.* (2020) 219:117057. doi: 10.1016/j.neuroimage.2020.117057
23. Kakisaka Y, Mosher JC, Wang ZI, Jin K, Dubarry AS, Alexopoulos AV, et al. Utility of temporally-extended signal space separation algorithm for magnetic noise from vagal nerve stimulators. *Clin Neurophysiol.* (2013) 124:1277–82. doi: 10.1016/j.clinph.2012.03.082
24. Calvert GA, Spence C, Stein BE. *The Handbook of Multisensory Processes*. Cambridge, MA: A Bradford Book (2004).
25. Stein BE, Meredith MA. The Merging of the Senses. *Cambridge, MA: A Bradford Book;. (*2004).
26. Stein BE. *The New Handbook of Multisensory Processing*. Cambridge, MA: A Bradford Book (2012).
27. Schiller P. Die Rauhigkeit als intermodale Erscheinung. *Z Psychol Bd.* (1932) 127:265–89.
28. Jousmäki V, Hari R. Parchment-skin illusion: sound-biased touch. *Curr Biol.* (1998) 8:R190. doi: 10.1016/S0960-9822(98)70120-4
29. Lawton G. That freaky feeling. *New Sci*. (2009) 14:32–27. doi: 10.1016/S0262-4079(09)63252-8
30. Guest S, Catmur C, Lloyd D, Spence C. Audiotactile interactions in roughness perception. *Exp Brain Res*. (2002) 146:161–71. doi: 10.1007/s00221-002-1164-z
31. Zampini M, Spence C. The role of auditory cues in modulating the perceived crispness and staleness of potato chips. *J Sensory Stud.* (2004) 19:347–63. doi: 10.1111/j.1745-459x.2004.080403.x
32. Levänen S, Jousmäki V, Hari R. Vibration-induced auditory-cortex activation in a congenitally deaf adult. *Curr Biol.* (1998) 8:869–72. doi: 10.1016/S0960-9822(07)00348-X
33. Schürmann M, Caetano G, Jousmäki V, Hari R. Hands help hearing: facilitatory audiotactile interaction at low sound-intensity levels. *J Acoust Soc Am.* (2004) 115:830–2. doi: 10.1121/1.1639909
34. Caetano G, Jousmäki V. Evidence of vibrotactile input to human auditory cortex. *Neuroimage.* (2006) 29:15–28. doi: 10.1016/j.neuroimage.2005.07.023
35. Schürmann M, Caetano G, Hlushchuk Y, Jousmäki V, Hari R. Touch activates human auditory cortex. *Neuroimage.* (2006) 30:1325–31. doi: 10.1016/j.neuroimage.2005.11.020
36. Olausson H, Wessberg J, Morrison I, McGlone F, Vallbo A. The neurophysiology of unmyelinated tactile afferents. *Neurosci Biobehav Rev.* (2010) 34:185–91. doi: 10.1016/j.neubiorev.2008.09.011
37. Jousmäki V, Nishitani N, Hari R. A brush stimulator for functional brain imaging. *Clin Neurophysiol.* (2007) 118:2620–4. doi: 10.1016/j.clinph.2007.08.024
38. Pihko E, Nangini C, Jousmäki V, Hari R. Observing touch activates human primary somatosensory cortex. *Eur J Neurosci.* (2010) 31:1836–43. doi: 10.1111/j.1460-9568.2010.07192.x
39. Hesse MD, Nishitani N, Fink GR, Jousmäki V, Hari R. Attenuation of somatosensory responses to self-produced tactile stimulation. *Cereb Cortex.* (2010) 20:425–32. doi: 10.1093/cercor/bhp110
40. De Tiège X, Bourguignon M, Piitulainen H, Jousmäki V. Sensorimotor mapping with MEG: An update on the current state of clinical research and practice with considerations for clinical practice guidelines. *J Clin Neurophysiol.* (2020) 37:564–73. doi: 10.1097/WNP.0000000000000481
41. Bowyer SM, Mason K, Yaeger BJW, Moran JE, Barkley GL, Tepley N. Localization of motor cortex by MEG using a tremorometer. *Int Congress Series.* (2007) 1300:321–4. doi: 10.1016/j.ics.2007.02.001
42. Bourguignon M, De Tiège X, Op de Beeck M, Pirotte B, Van Bogaert P, Goldman S, et al. Functional motor-cortex mapping using corticokinematic coherence. *Neuroimage.* (2011) 55:1475–9. doi: 10.1016/j.neuroimage.2011.01.031
43. Piitulainen H, Bourguignon M, De Tiège X, Hari R, Jousmäki V. Corticokinematic coherence during active and passive finger movements. *Neuroscience.* (2013) 238:361–70. doi: 10.1016/j.neuroscience.2013.02.002
44. Piitulainen H, Bourguignon M, De Tiège X, Hari R, Jousmäki V. Coherence between magnetoencephalography and hand-action-related acceleration, force, pressure, and electromyogram. *Neuroimage.* (2013) 72:83–90. doi: 10.1016/j.neuroimage.2013.01.029
45. Bourguignon M, Piitulainen H, De Tiege X, Jousmäki V, Hari R. Corticokinematic coherence mainly reflects movement-induced proprioceptive feedback. *Neuroimage.* (2015) 106:382–90. doi: 10.1016/j.neuroimage.2014.11.026
46. Bourguignon M, Jousmäki V, Dalal SS, Jerbi K, De Tiège X. Coupling between human brain activity and body movements: Insights from non-invasive electromagnetic recordings. *Neuroimage.* (2019) 203:116177. doi: 10.1016/j.neuroimage.2019.116177
47. Vanhatalo S, Jousmäki V, Andersson S, Metsäranta M. An easy and practical method for routine, bedside testing of somatosensory systems

in extremely low birth weight infants. *Pediatr Res.* (2009) 66:710–3. doi: 10.1203/PDR.0b013e3181be9d66
48. Smeds E, Vanhatalo S, Piitulainen H, Bourguignon M, Jousmäki V, Hari R. Corticokinematic coherence as a new marker for somatosensory afference in newborns. *Clin Neurophysiol.* (2017) 128:647–55. doi: 10.1016/j.clinph.2017.01.006
49. Vander Ghinst M, Bourguignon M, Op de Beeck M, Wens V, Marty B, Hassid S, et al. Left superior temporal gyrus is coupled to attended speech in a cocktail-party auditory scene. *J Neurosci.* (2016) 36:1596–606. doi: 10.1523/JNEUROSCI.1730-15.2016
50. Vander Ghinst M, Bourguignon M, Niesen M, Wens V, Hassid S, Choufani G, et al. Cortical tracking of speech-in-noise develops from childhood to adulthood. *J Neurosci.* (2019) 39:2938–50. doi: 10.1523/JNEUROSCI.1732-18.2019
51. Bourguignon M, De Tiège X, de Beeck MO, Ligot N, Paquier P, Van Bogaert P, et al. The pace of prosodic phrasing couples the listener's cortex to the reader's voice. *Hum Brain Mapp.* (2013) 34:314–26. doi: 10.1002/hbm.21442
52. Vitikainen AM, Mäkelä E, Lioumis P, Jousmäki V, Mäkelä JP. Accelerometer-based automatic voice onset detection in speech mapping with navigated repetitive transcranial magnetic stimulation. *J Neurosci Methods.* (2015) 253:70–7. doi: 10.1016/j.jneumeth.2015.05.015
53. Piitulainen H, Bourguignon M, Hari R, Jousmäki V. MEG-compatible pneumatic stimulator to elicit passive finger and toe movements. *Neuroimage.* (2015) 112:310–7. doi: 10.1016/j.neuroimage.2015.03.006
54. Vinding MC, Tsitsi P, Piitulainen H, Waldthaler J, Jousmäki V, Ingvar M, et al. Attenuated beta rebound to proprioceptive afferent feedback in Parkinson's disease. *Sci Rep.* (2019) 9:2604. doi: 10.1038/s41598-019-39204-3
55. Naeije G, Bourguignon M, Wens V, Marty B, Goldman S, Hari R, et al. Electrophysiological evidence for limited progression of the proprioceptive impairment in Friedreich ataxia. *Clin Neurophysiol.* (2020) 131:574–6. doi: 10.1016/j.clinph.2019.10.021
56. Marty B, Naeije G, Bourguignon M, Wens V, Jousmäki V, Lynch DR, et al. Evidence for genetically determined degeneration of proprioceptive tracts in Friedreich ataxia. *Neurology.* (2019) 93:e116–24. doi: 10.1212/WNL.0000000000007750
57. Eriksson Hagberg E, Ackerley R, Lundqvist D, Schneiderman J, Jousmäki V, Wessberg J. Spatio-temporal profile of brain activity during gentle touch investigated with magnetoencephalography. *Neuroimage.* (2019) 201:116024. doi: 10.1016/j.neuroimage.2019.116024
58. Lolli V, Rovai A, Trotta N, Bourguignon M, Goldman S, Sadeghi N, et al. MRI-compatible pneumatic stimulator for sensorimotor mapping. *J Neurosci Methods.* (2019) 313:29–36. doi: 10.1016/j.jneumeth.2018.12.014
59. Lolli V, Rovai A, Trotta N, Goldman S, Sadeghi N, Lefranc F, et al. Pneumatic artificial muscle-based stimulator for passive functional magnetic resonance imaging sensorimotor mapping in patients with brain tumours. *J Neurosci Methods.* (2021) 359:109227. doi: 10.1016/j.jneumeth.2021.109227
60. Nurmi T, Henriksson L, Piitulainen H. Optimization of proprioceptive stimulation frequency and movement range for fMRI. *Front Hum Neurosci.* (2018) 12:477. doi: 10.3389/fnhum.2018.00477
61. Tatum WO, Rubboli G, Kaplan PW, Mirsatari SM, Radhakrishnan K, Gloss D, et al. Clinical utility of EEG in diagnosing and monitoring epilepsy in adults. *Clin Neurophysiol.* (2018) 129:1056–82. doi: 10.1016/j.clinph.2018.01.019
62. Martins da Silva A, Leal B. Photosensitivity and epilepsy: Current concepts and perspectives-A narrative review. *Seizure.* (2017) 50:209–18. doi: 10.1016/j.seizure.2017.04.001
63. Kasteleijn-Nolst Trenite D, Carr B, Checa-Ros A, Seri S. Light-emitting-diode and Grass PS 33 xenon lamp photic stimulators are equivalent in the assessment of photosensitivity: Clinical and research implications. *Epilepsy Res.* (2020) 165:106377. doi: 10.1016/j.eplepsyres.2020.106377

Conflict of Interest: VJ is heading the Euphotic team at Aalto University (Espoo, Finland). The euphotic team aims at commercializing the Euphotic IPS device. The Euphotic team is SPARK Finland SPARKee (https://sparkfinland.fi; Batch 2020). The immaterial rights of the Euphotic project belong to Aalto University.

Publisher's Note: All claims expressed in this article are solely those of the authors and do not necessarily represent those of their affiliated organizations, or those of the publisher, the editors and the reviewers. Any product that may be evaluated in this article, or claim that may be made by its manufacturer, is not guaranteed or endorsed by the publisher.

frontiers in Neurology

ORIGINAL RESEARCH
published: 25 February 2022
doi: 10.3389/fneur.2022.838170

Resting-State Beta-Band Recovery Network Related to Cognitive Improvement After Stroke

Sandra Pusil[1†], Lucía Torres-Simon[1†], Brenda Chino[2], María Eugenia López[1], Leonides Canuet[1], Álvaro Bilbao[3], Fernando Maestú[1] and Nuria Paúl[1]*

[1] Department of Experimental Psychology, Universidad Complutense de Madrid, Madrid, Spain, [2] Institute of Neuroscience, Autonomous University of Barcelona, Barcelona, Spain, [3] National Centre for Brain Injury Treatment, Centro de Referencia Estatal de Atención Al Daño Cerebral (CEADAC), Madrid, Spain

OPEN ACCESS

Edited by:
Rafeed Alkawadri, University of Pittsburgh Medical Center, United States

Reviewed by:
Shennan Aibel Weiss, SUNY Downstate Medical Center, United States
Donna Clark Tippett, Johns Hopkins Medicine, United States

****Correspondence:***
Sandra Pusil
spusil@ucm.es

[†] These authors have contributed equally to this work and share first authorship

Specialty section:
This article was submitted to Applied Neuroimaging, a section of the journal Frontiers in Neurology

Received: *17 December 2021*
Accepted: *03 February 2022*
Published: *25 February 2022*

Citation:
Pusil S, Torres-Simon L, Chino B, López ME, Canuet L, Bilbao Á, Maestú F and Paúl N (2022) Resting-State Beta-Band Recovery Network Related to Cognitive Improvement After Stroke. Front. Neurol. 13:838170. doi: 10.3389/fneur.2022.838170

Background: Stroke is the second leading cause of death worldwide and it causes important long-term cognitive and physical deficits that hamper patients' daily activity. Neuropsychological rehabilitation (NR) has increasingly become more important to recover from cognitive disability and to improve the functionality and quality of life of these patients. Since in most stroke cases, restoration of functional connectivity (FC) precedes or accompanies cognitive and behavioral recovery, understanding the electrophysiological signatures underlying stroke recovery mechanisms is a crucial scientific and clinical goal.

Methods: For this purpose, a longitudinal study was carried out with a sample of 10 stroke patients, who underwent two neuropsychological assessments and two resting-state magnetoencephalographic (MEG) recordings, before and after undergoing a NR program. Moreover, to understand the degree of cognitive and neurophysiological impairment after stroke and the mechanisms of recovery after cognitive rehabilitation, stroke patients were compared to 10 healthy controls matched for age, sex, and educational level.

Findings: After intra and inter group comparisons, we found the following results: (1) Within the stroke group who received cognitive rehabilitation, almost all cognitive domains improved relatively or totally; (2) They exhibit a pattern of widespread increased in FC within the beta band that was related to the recovery process (there were no significant differences between patients who underwent rehabilitation and controls); (3) These FC recovery changes were related with the enhanced of cognitive performance. Furthermore, we explored the capacity of the neuropsychological scores before rehabilitation, to predict the FC changes in the brain network. Significant correlations were found in global indexes from the WAIS-III: Performance IQ (PIQ) and Perceptual Organization index (POI) (i.e., Picture Completion, Matrix Reasoning, and Block Design).

Keywords: stroke, functional connectivity (FC), MEG (magnetoencephalography), cognitive performance, neuropsychological rehabilitation

INTRODUCTION

Stroke is considered the second leading cause of death and the third leading cause of disability worldwide (1). It is a heterogeneous pathology with diverse clinical manifestations due to its possible etiologies (i.e., hemorrhagic, or ischemic), locations (i.e., different vascular vessels or arteries), and size of the lesion (2, 3). However, most stroke survivors suffer from different degrees of cognitive disabilities (4–6). These patients may have damage in general cognitive performance with important functional disability, which has been broadly reported in the scientific literature (7–9). Although stroke tends to impact on attention and executive function compared with its impact on memory, a malfunction in these cognitive domains could worsen the performance in other cognitive areas (3, 4, 6, 10). In any case, it is important to highlight the role of non-pharmacological rehabilitation especially neuropsychological rehabilitation (NR) in order to improve cognitive abilities and daily functions (10, 11). Neuropsychological rehabilitation is a systematic therapeutic activity oriented functionally based on the assessment and understanding of the cognitive deficits, emotional disturbances, disruptive behaviors, and functional disorders of patients (12, 13), and includes interventions that might be compensatory, educational, or restorative (10).

According to some authors and approaches post-stroke deficits have long been considered to be fundamentally associated with the location of the lesion (14). This could be particularly true for sensorimotor or language deficits, which are closely related to the damage to the specific eloquent cortex. However, it has been shown that although structural damage from stroke is usually focal, remote disturbances may occur in brain distant regions from the primary area of damage (15, 16). This phenomenon was previously associated with the concept of diaschisis, but it is currently explained by the disruption of structural and functional connectivity (FC) between brain areas (17). This way of understanding the functioning of the brain gives a crucial role to NR in the process of cognitive recovery, since it allows a holistic management of cognitive impairment in contrast to other more goal-oriented therapies.

In this context, as the restoration of FC precedes or accompanies in most cases, cognitive and behavioral recovery in stroke patients (18, 19), understanding the electrophysiological signatures underlying stroke recovery mechanisms is a crucial scientific goal. This information could help the clinical community to anticipate and modify NR programs to achieve a more effective cognitive recovery, and consequently, improve patients' quality of life. With this purpose, in the present study we used the magnetoencephalography (MEG), a neurophysiological technique that allows a comprehensive analysis of brain dynamics (20, 21). While the functional magnetic resonance image (fMRI) is intrinsically limited by the hemodynamic response, MEG directly measures cortical neural activity. That means that the modified vasomotor reactivity and neurovascular uncoupling in stroke easily affects the blood oxygen level-dependent (BOLD) response but leaves the MEG signal intact (22). The study of MEG signatures is well-established for early detection and prognosis in neurodegenerative disorders, such as multiple sclerosis (23) or Alzheimer's disease (24). Moreover, MEG has previously been used to demonstrate the disruption and recovery of functional networks, and even its relationship with cognitive improvement after undergoing a NR program in acquired brain pathologies such as stroke (22, 25, 26) or traumatic brain injury (TBI) (13, 27). Thanks to the relevance of the neurophysiological changes found in previous literature, it seems plausible that MEG may provide interesting information about how NR may induce specific cognitive recovery in stroke patients.

According to the aforementioned antecedents, the aims of the present exploratory study are: (1) to understand the cognitive improvement achieved in stroke patients that received NR; (2) to explore the possible neurophysiological mechanisms underlying the recovery process, by using FC on frequency bands obtained with MEG; and (3) to evaluate if these neurophysiological changes are related with cognitive improvement. For this purpose, we carried out a longitudinal study in which a sample of 10 stroke patients (stroke patients) were examined at two different time points. The first was before NR (from now on we will say *pre-condition*), and the second was after NR (from now on we will say *post-condition*). At both time points patients were cognitively evaluated and underwent resting-state MEG recordings. Moreover, to understand the degree of cognitive and neurophysiological disruption after stroke, and the recovery mechanisms in stroke patients who were enrolled on the NR, data for a control group were included with 10 healthy controls paired in age, sex, and educational level.

MATERIALS AND METHODS

Participants

The total dataset consisted of 20 subjects: 10 stroke patients (2 females/8 males; mean age 44.9 $\pm$ 8.94; mean level of education 4.44 $\pm$ 0.97) and 10 healthy controls (2 females/8 males; mean age 43 $\pm$ 12.72; mean level of education 4.78 $\pm$ 0.67). The mean time from the onset of the stroke to the start of the study was 6.3 months, and the rehabilitation program lasted 7 months. The patient's lesions were both ischemic (i.e., infarction; $n = 5$) and hemorrhagic (i.e., intracerebral hemorrhage; $n = 5$) and the stroke was located in different brain areas (for patient detailed descriptive data see **Table 1**). To be enrolled in the study, patients had to be diagnosed with a first-ever stroke, showing a compatible lesion observed on computerized tomography (CT) or magnetic resonance imaging (MRI). Although initially, after the stroke some patients showed loss of consciousness [as reported in **Table 1** with the Glasgow Coma Scale (28)], at the beginning of the study all patients were neurologically stable without alterations in consciousness or alertness, and none of them showed epileptiform discharges on MEG recordings.

Exclusion criteria were the following: a stroke involving the brainstem or cerebellum, a diagnosis of neurological or psychiatric diseases other than stroke, and a history of TBI, drug, or alcohol abuse.

Patients were recruited from the National Brain Injury Rehabilitation Center and from Lescer Brain Injury Rehabilitation Center (Madrid, Spain), and all of them were

TABLE 1 | Clinical and sociodemographic characteristics of the patients.

Patient	Age	Sex	Education	GCS	Stroke etiology	Stroke lesion
1	44	M	3	12	Ischemia	Right fronto-parietal
2	45	F	5	7	Ischemia	Right middle cerebral artery
3	47	M	5	9	Ischemia	Left middle cerebral artery
4	47	M	4	12	Ischemia	Right middle and anterior cerebral arteries
5	60	M	3	12	Ischemia	Left middle cerebral artery
6	28	F	4	7	Hemorrhage	Thalamus and left basal ganglia
7	35	M	4	8	Hemorrhage	Right intraparenchymal
8	41	M	5	7	Hemorrhage	Left basal ganglia
9	49	M	6	9	Hemorrhage	Right basal ganglia
10	53	M	5	9	Hemorrhage	Left thalamus
$N = 10$	44.9 ± 8.9	8 M/2 F	4.4 ± 0.9	9.2 ± 2.1	5 isch/5 hem	

Education (1, illiterate/functional illiterate; 2, elemental studies; 3, school graduate; 4, high school studies; 5, university graduate studies; 6, university post-graduate studies).

enrolled in a NR program. Healthy controls were matched with patients for age, sex, and education level, and they did not have a previous history of psychiatric or neurological disorders.

As previously mentioned, patients underwent MEG recordings and neuropsychological evaluation in two different moments: (1) Pre-condition (Pre): at the beginning of the study, before NR program; and (2) Post-condition (Post): after completing the NR program. In the case of healthy controls, both data, neuropsychological and neurophysiological, were obtained only once, at the beginning of the study.

Ethics Statement

Methods were carried out in accordance with approved guidelines and regulations. The study was approved by the National Brain Injury Rehabilitation Center Ethics Committee (Madrid), and all participants or legal representatives signed a written informed consent prior to participation.

Neuropsychological Assessment

All participants underwent a comprehensive neuropsychological evaluation with the aim to identify their cognitive status in multiple cognitive domains (attention, memory, language, executive functions, and visuospatial abilities) as well as their functional performance. The extensive neuropsychological assessment included: the Wechsler Adult Intelligence Scale III (WAIS III) (29), the Brief Test of Attention (BTA) (30), the Trail Making Test (TMT) (31), the Stroop Color Word Test (32, 33), the Wisconsin Card Sorting Test (WCST) (34), the Tower of Hanoi (35), the Zoo Map Test [from the Behavioral Assessment of the Dysexecutive Syndrome (36)], the Boston Naming Test (BNT) (37), the Digit Span Test [Wechsler Memory Scale III (29)], the Visual Span Test [WMS-III; (29)], Logical Memory and Visual Reproduction [WMS-III (29)], the Phonemic and Semantic Fluency [Controlled Oral Word Association Test, COWAT (38)], the Five Digit Test [FDT (39)], the Dysexecutive Questionnaire [DEX (36)], and the Patient Competency Rating Scale [PCRS (40)].

Neuropsychological Rehabilitation Program

All stroke patients received an integrated treatment based on the holistic-comprehensive model proposed by Ben-Yishay and Diller (41). This program consists of 1 h/day of occupational therapy, 1 h/2 days/week of neuropsychological therapy, and 2 h/day of group cognitive therapy (memory and executive function/social skills). Neuropsychological therapy aimed to improve attention, working memory, learning, memory and problem solving/executive functions, and emotional-behavioral problems, through evidence-based techniques that included both restorative and compensatory strategies. Neuropsychological treatment goals in each case were defined to achieve maximum cognitive independence in daily living. In addition, patients underwent 1 h of physiotherapy and half an hour of speech therapy, in those cases that needed it. This rehabilitation plan met the following requirements: (1) agreed by the family and all professionals involved; (2) formulated in a specific and operational manner (3) focused on meaningful goals for the patients that allow them to achieve greater personal autonomy, community integration, and adaptation to their deficits; and (4) reviewed monthly. In addition, all patients attended psychotherapy sessions to help them in the process of accepting their new situation.

Magnetoencephalographic Recordings

Magnetic fields were recorded using a 148-channel whole-head magnetometer (4D-MAGNES_2500 WH, 4-D Neuroimaging) confined in a magnetically shielded room at the Universidad Complutense of Madrid (Spain). Fields were measured during a 2-min resting-state eyes-closed condition and were sampled at a frequency rate of 618.17 Hz. Ocular, cardiac, muscular, and jump artifacts were identified first, by a visual inspection of an expert in MEG, and then removed using ICA (42) in Brainstorm software (43). Then, clean data were segmented into 4 s trial length, with a minimum of 20 artifact-free segments for each subject. The MEG data were filtered in the classical frequency bands: delta (2–4 Hz), theta (4–8 Hz), alpha (8–12 Hz), beta (12–30 Hz), and gamma (30–45 Hz) for further analysis.

Source Reconstruction and Connectivity Analysis

To reconstruct MEG sources, we used the default anatomy (15,000 vertices) of the MNI/Colin27 brain (44) in Brainstorm. This template was warped according to the polhemus points (nasion and both preauricular) acquired during the head digitalization to obtain a better approximation of the real shape of the subject's head. The overlapping sphere model was calculated as the forward modeling of MEG measures. Next, a noise covariance matrix was calculated to estimate noise level in the MEG recordings. Sources were reconstructed using the weighted Minimum Norm Estimation (wMNE) (45). Weighted Minimum Norm Estimation is well-suited for the estimation of large-scale FC networks, since it addresses the problem of volume conduction, reducing the correlations of spurious signals (46, 47). Magnetoencephalography sources were grouped into 68 anatomical regions of interest (ROI) based on Brainstorm atlas Desikan-Killiany (48). For more details about the brain areas used, referred to Supplementary Material for **Supplementary Table 1**. We selected the mean as the representative time series for each brain area delimited with the aforementioned atlas.

Functional connectivity was assessed using the corrected version of the imaginary phase locking value (ciPLV), a phase synchronization measure that evaluates the distribution of phase differences extracted from each of two sensor time series (49, 50). Corrected version of the imaginary phase locking value (Equation 1) was proposed by Bruña et al. (50) to remove the contribution of the zero phase differences of PLV. Thus, this measure is insensitive to zero-lag effects, and it is corrected to remove the instantaneous phase contribution, which could be mainly due to volume conduction.

$$ciPLV_{X,Y}(t) = \frac{\frac{1}{T} I\{e^{-i(\phi_X(t)-\phi_Y(t))}\}}{\sqrt{1-(\frac{1}{T} R\{e^{-i(\phi_X(t)-\phi_Y(t))}\})^2}} \quad (1)$$

where φ_x and φ_y represent the phases of each of the two-time series and $\mathfrak{I}$ stands for the imaginary part of the numerator and $\mathfrak{R}$ the real part in the denominator. See **Figure 1** for the analysis flow chart of the MEG data.

Statistical Analyses

This study aims to find the possible neurophysiological substrates of the recovery network underlying the cognitive enhancement found stroke patient's sample in the post condition (after NR), by using cognitive tests, functional scales, and FC measures. In this context, we performed exploratory analyses with the data obtained from stroke patients and healthy controls. The analysis of demographic data showed that there were no statistical differences in age, sex, and level of education between patients and controls ($p > 0.05$), so we did not include them as confounding variables for the following explorations. Non-parametric tests were used for all comparisons because variables were non-normally distributed and because of the small sample size. Specifically, the Mann-Whitney U test was used for between groups analyses (stroke patients vs. healthy controls) and Wilcoxon paired test for within-group comparison (Pre vs. Post conditions in the stroke patients' group). In the case of neuropsychological variables, significant results were considered with a p-value < 0.05 after applying false discovery rate (FDR) corrected for multiple comparisons. For FC data, a total of 10,000 permutations were used for each significant FC link, and results were considered significant with a p-value <0.005 after applying FDR (51). Finally, with the aim to explore the relationships between FC and cognition, Spearman's correlation analysis was employed. For all analyses the Matlab Statistical Toolbox was used.

RESULTS

Cognitive Changes After Neuropsychological Rehabilitation

As described before, the patients underwent a comprehensive neuropsychological evaluation before and after the NR program. From the total of battery tests, those scores with at least nine reported patients (46 scores in total) were included for the statistical analysis. Pre-condition results indicated that stroke patients performed significantly worse compared with healthy controls in all cognitive domains ($p < 0.05$). Comparing pre and post conditions in the stroke patients' group, results showed an important cognitive improvement with 33 scores (72% of the 46 total scores) significantly different between conditions. Of these, 21 scores (46% of the 46 total scores), could be considered *relatively enhanced* since in the post-condition, they were significantly different to those corresponding to the healthy controls (see **Figure 2**). The remaining 12 scores (26% of the 46 total scores) from the post-condition did not show significant differences with the healthy control group, indicating a *total improvement*. To simplify the interpretation of these results, all scores were clustered into several aggregated groups depending on different cognitive domains: *Functional performance*, 4 scores (of DEX and PCRS); *Executive Functions*, 10 scores (of WCST, Tower of Hanoi, FDT and TMT); *Attention*, 1 score (of Brief Test of Attention); *Language*, 2 scores (of BNT and FAS); *Episodic Memory*, 4 scores (of WMS-III) and *Working Memory*, 9 scores (of WMS-III and WAIS-III). The last three columns of **Figure 2** correspond to the cognitive index of WAIS-III, including all their subtests: Verbal Comprehension Index (VCI, 4 scores); Processing Speed Index (PSI, 3 scores), and Perceptual Organization Index (POI, 4 scores). In addition, the three general indices of WAIS-III were also included [Verbal IQ, Performance IQ (PIQ), and Full-Scale IQ], as well as subtests Picture Arrangement and Comprehension. In summary, we found that all cognitive domains of the stroke patients' group were fully or partially enhanced in the post-condition (see **Figure 2**). It is important to note that the VCI (that includes the WAIS-III index and all its subtests), was a cognitive domain without improvement in any of the four measures; and the four scores maintained significant differences when comparing the second scores of stroke patients with the healthy controls scores. However, it is important to know that this index, already in the pre-condition, shows a normal score (103.5) unlike the results of

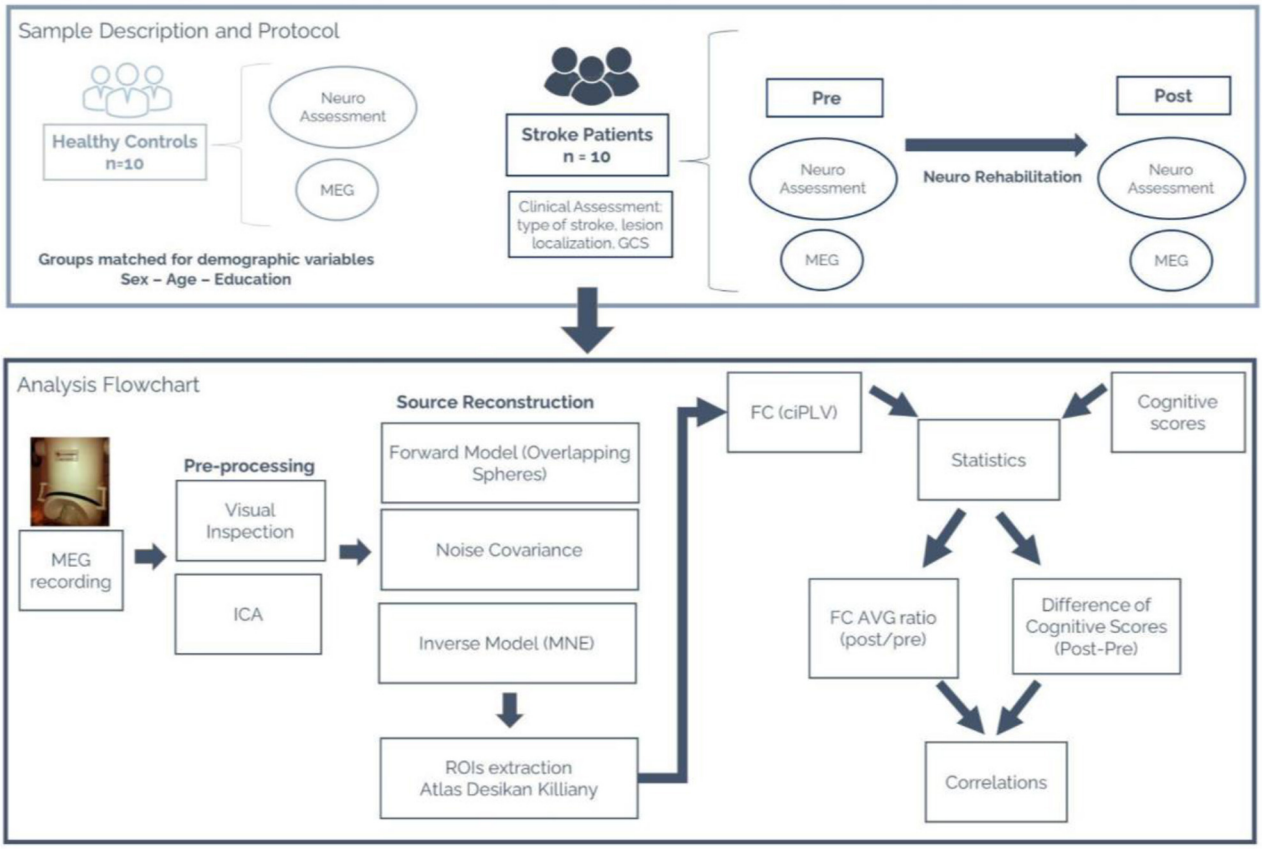

FIGURE 1 | (Top) Sample description (stroke patients and healthy control groups). Description of the protocol followed by each group and the variables collected for this study. (Bottom) MEG Analysis flowchart. Sequential pipeline of the analysis performed on the MEG data.

the other cognitive index of the WAIS-III (WMI 91.9; PSI 80.3; PRI 82.4) and the others all cognitive tests. In addition, their result in the post-condition was 105, although it continues to be statistically different from the healthy control group (117.6).

Functional Connectivity Disruption After Stroke: Differences Between Stroke Patients and Healthy Controls

In order to assess the possible disruption of the patients' network due to the stroke, their FC in the pre-condition was compared with the FC of the healthy controls. Stroke patients exhibited significant FC reduction in the beta band ($p < 0.005$, FDR corrected) that comprised intra and inter-hemispheric connections (**Figure 3**). No significant results were found in other frequency bands.

Functional Connectivity After Rehabilitation: The Recovery Network

When assessing the possible FC differences between stroke patients' conditions, a clear pattern of widespread increased FC within the beta band was found. Stroke patients showed significantly ($p < 0.005$) higher FC in the post-condition compared to the pre-condition in a variety of links comprising intra and inter-hemispheric, and antero-posterior long-range connections (**Figure 4**).

Moreover, when assessing the possible differences in FC between groups (post-condition and healthy controls) we did not find any statistically significant differences. This result indicated that the original FC disruption in the beta band was restored in stroke patients who went through the NR.

No significant results were found in other frequency bands in the pre and post comparison after FDR correction ($p < 0.005$). Nevertheless, there is a clear pattern of enhanced connectivity in low frequency bands (delta and theta) in the pre stage when compared with the brain activity of stroke patients recorded after the rehabilitation when a less restrictive statistical threshold was used ($p < 0.05$). Detailed description of these results could be found in the Supplementary Material, **Appendix 3**. These results were not included in the main findings of the present study because we wanted to focus on the most reliable FC signature, keeping the $p < 0.005$ value as the go/no go statistical limit.

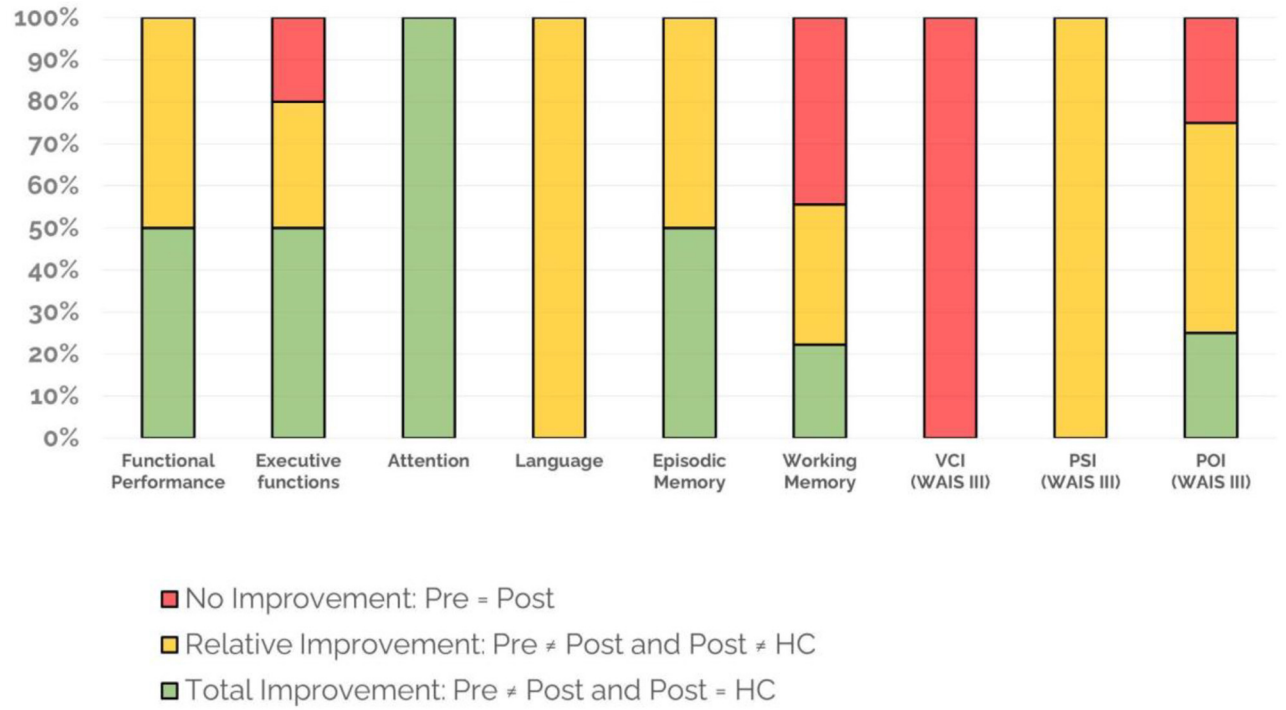

FIGURE 2 | Neuropsychological tests' changes after NR. Functional Performance (4 scores: DEX and PCRS); Executive Functions (10 scores: WCST, Tower of Hanoi, FDT, and TMT); Attention (1 score: Brief Test of Attention); Language (2 scores: BNT and FAS); Episodic Memory (4 scores: WMS-III); Working Memory (9 scores: WAIS-III and WMS-III). The last three columns correspond to cognitive indices of WAIS-III, including all their subtests: VCI (verbal comprehension, 4 scores); PSI (speed processing, 3 scores); and POI (perceptual organization, 4 scores). Percentages were calculated intra-domain. Test scores included. DEX, DEX-family, DEX-difference; PCRS, PCRS-family, PCRS-difference; WCST, WCST-categories, WCST-conceptual, WCST-persevering; Tower of Hanoi, TH-3D-time, TH-3D-movements, TH-4D-time, TH-4D-movements; Five Digit Test, FDT-switching, FDT-flexibility; Brief Test of Attention, BTA-total score; BNT, BNT-total score; FAS, FAS-total score; WMS-III-episodic-memory, WMS-III-logical memory 1, WMS-III-logical memory 2, WMS-III-visual reproduction 1, WMS-III-visual reproduction 2; WMS-working memory, WMS-III-forward digit span, WMS-III-backward digit span, WMS-III-forward visual span, WMS-III-backward visual span; WAIS-working memory, WAIS-digit span, WAIS-arithmetic, WAIS-letter number sequencing, WAIS-working memory index; WAIS-VCI, WAIS-vocabulary, WAIS-information, WAIS-similarities, WAIS-verbal comprehension index; WAIS-PSI, WAIS-symbol search, WAIS-digit symbol, WAIS-processing speed index; WAIS-POI, WAIS-block design, WAIS-matrix reasoning, WAIS-picture completion; WAIS-perceptual organization index.

Correlations Between the Brain and Cognitive Recovery Patterns

With the aim to explore if FC changes were related with the enhanced cognitive performance in the stroke patients' group, we firstly calculated a ratio considering the strength of each functional link that differed between both conditions (FC ratio = Post/Pre). Then, we averaged these FC link ratios in just one value for each stroke patient. This provided a unique FC marker for each patient that condensed the information obtained by the whole network and the two MEG sessions. Next, for cognitive scores, we calculated the performance differences (D) for the most representative tests of each neuropsychological domain between pre and post conditions in the stroke patients' group (D = Post–Pre), with the aim of finding the strongest cognitive improvement, to reduce the redundancy of the information (since several scores measured the similar aspects of the same cognitive domain) and to avoid the statistical pitfall of multiple comparisons. Regarding the selection of the most representative scores included for the correlation analyses, the neuropsychological experts' team choose: *Functional Performance* (DEX-F), *Executive functions* (WCST-Persevering, Tower of Hanoi-3D-T), *Attention* (BTA), *Episodic memory* (WMS-III-LM1), *Working memory* (Digit span test), and *Language* (BNT). Moreover, the WAIS-III general indexes and some WAIS-III cognitive indexes were included (FIQ, PIQ, VIQ, PSI, POI). We finally included for the Spearman's correlation analyses the average FC strength ratio and 12 neuropsychological scores differences, illustrative of the cognitive improvement, for each stroke patient.

In order to facilitate the understanding of each patient cognitive improvement an extended material about individual neuropsychological performance was added in **Appendix 2** in Supplementary Material. There, the punctuations for each patient before and after the rehabilitation are described in detail for those tests included in the present correlation analysis.

We found three positive and significant recovery signatures correlations between the FC strength ratio and three cognitive

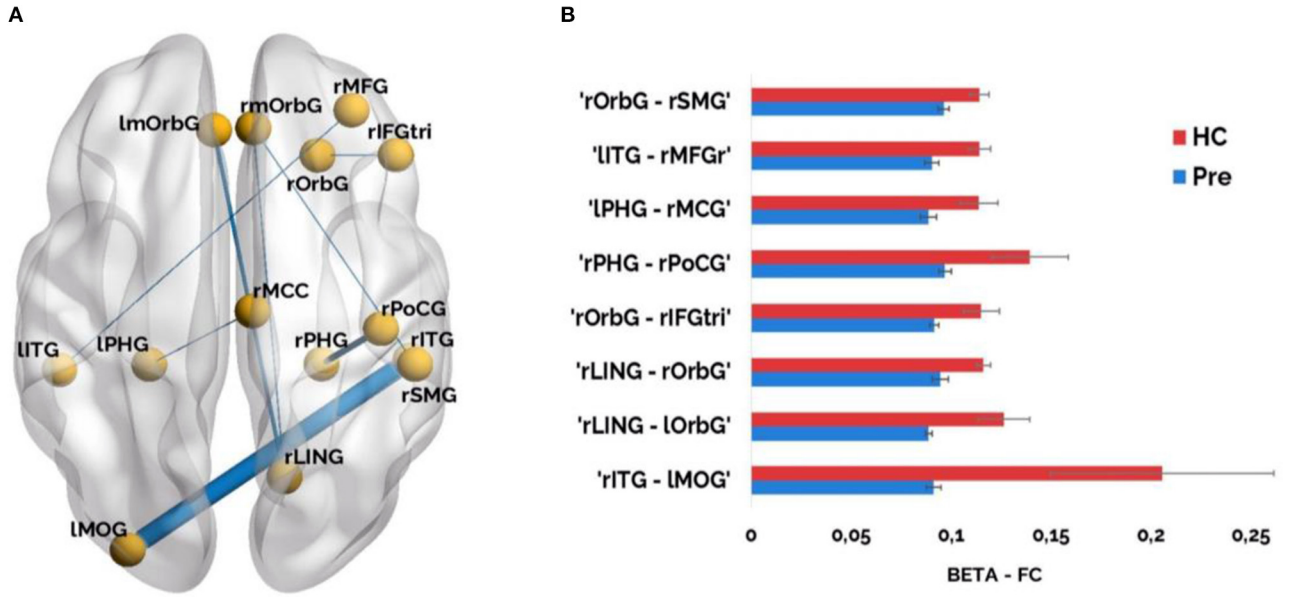

FIGURE 3 | (A) Significant FC results ($p < 0.005$, corrected) in the beta band (12–30 Hz) when comparing healthy controls vs. stroke patients in the pre-condition. Line thickness of significant links is proportional to FC values (a higher value corresponds to thicker lines, and vice versa); **(B)** Significant FC links in the beta band are represented as bar graphs. Red color represents higher connectivity values for healthy controls compared to stroke patients and blue color illustrates lower connectivity values for stroke patients compared to healthy controls. ROIs included: rmOrbG, Right Medial Orbito Frontal Gyrus; lmOrbG, Left Medial Orbito Frontal Gyrus; rMFG, Right Middle Frontal Gyrus; rOrbG, Lateral Orbito Frontal Gyrus; rIFGtri, Right Inferior Frontal Parstriangularis; lITG, Left Inferior Temporal Gyrus; rITG, Right Inferior Temporal Gyrus; lPHG, Left Parahippocampal Gyrus; rPHG, Right Parahippocampal Gyrus; rMCC, Right Posterior Cingulate Gyrus; rPoCG, Right Postcentral Gyrus; rSMG, Right Supramarginal Gyrus; rLING, Right Lingual Cortex; lMOG, Left Lateral Occipital Gyrus.

measures: Full Scale IQ of WAIS-III ($R = 0.833$; $p = 0.015$), BNT (R = 0.756; $p = 0.035$), and LM1 of WMS-III ($R = 0.854$; $p = 0.010$) (**Figure 5**).

Prediction of Brain FC Recovery Based on Cognitive Performance After Stroke

Lastly, with the aim of exploring the predictive capacity of the neuropsychological test scores and the brain network recovery, we correlated the cognitive scores of the pre-condition and the FC strength ratio (by using Spearman correlation analyses).

Thus, we observed two markers for recovery prediction in two global cognitive domains: (1) PIQ, with a significant positive correlation between FC strength ratio and the PIQ scores ($R = 0.850$, $p = 0.011$); (2) Perceptual Organization, with a significant positive correlation between FC strength ratio and the POI scores ($R = 0.874$, $p = 0.007$). Furthermore, within POI, we found a positive association with Picture Completion ($R = 0.732$; $p = 0.048$), Matrix Reasoning ($R = 0.795$; $p = 0.023$), and Block Design ($R = 0.857$; $p = 0.010$) (**Figure 6**).

DISCUSSION

The present study aimed to provide evidence of the neurophysiological mechanisms underlying cognitive deficits and changes in brain function associated with the recovery of cognitive processes in stroke patients who underwent a NR. Additionally, this study is focused on the exploration of the nature of the relationships between neurophysiological and neuropsychological changes.

In this sense, our results indicate a positive effect in acute stroke patients who received cognitive rehabilitation on both levels, the cognitive system and brain functioning. Nevertheless, the lack of a clinical control group (i.e., stroke patients without rehabilitation) did not allow us to make causality assumptions, assuring that cognitive improvement is due specifically or uniquely to cognitive rehabilitation because it could also represent some degree of spontaneous clinical recovery after stroke. Then, according to the results of the present study, stroke patients who undertook rehabilitation significantly improved their performance in 72% of cognitive and functional scores. But we also found than in neuropsychological scores related to specific cognitive domains such as executive functions, attention, language, episodic, and working memory, stroke patients showed a relative improvement (46% improved but there were significant differences between the post-condition and the control group), or even a total enhancement (26% improved, and there were no differences between post-condition and control group). These two degrees of positive changes were also found in scores related to global cognitive functioning such as Full-Scale IQ, PIQ, Speed Processing Index, Working Memory Index, or POI. In addition, some indicators related to functional performance, such as DEX or PCRS (completed by relatives of patients), also improved after rehabilitation. This trend could represent

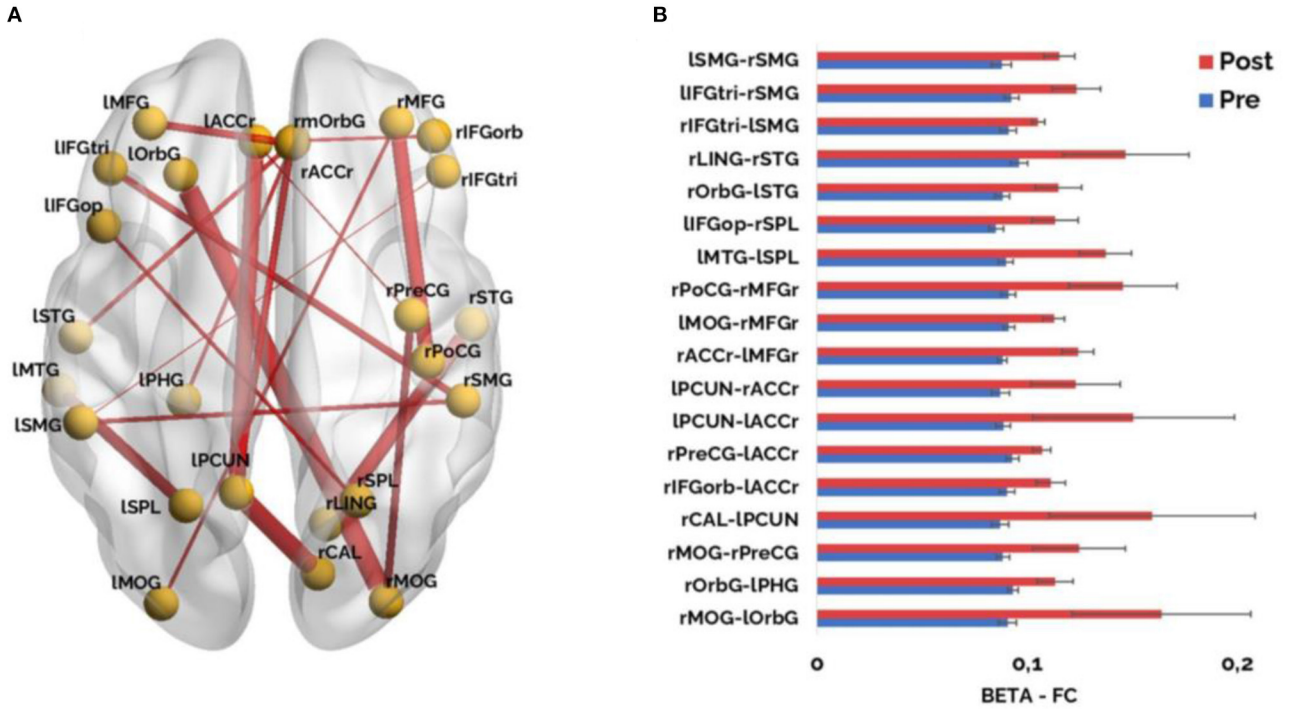

FIGURE 4 | (A) Significant FC results ($p < 0.005$, corrected) in the beta band (12–30 Hz) when comparing within the stroke patients' group, the pre-condition and the post- condition. Line thickness of significant links is proportional to FC values (a higher value corresponds to thicker lines, and vice versa); **(B)** Significant functional connectivity links in the beta band are represented as bar graphs. Red color represents higher connectivity values for pre-condition compared to post-condition and blue color illustrates lower connectivity values for pre-condition compared to post-condition. ROIs included: lMFG, Left Middle Frontal Gyrus; rMFG, Right Middle Frontal Gyrus; lIFG, Left Inferior Frontal Parstriangularis; rIFG, Right Inferior Frontal Parstriangularis; rmOrbG, Right Medial Orbito Frontal Gyrus; lACCr, Left Rostral Anterior Cingulate; rACCr, Right Rostral Anterior Cingulate; lOrbG, Left Lateral Orbito Frontal Gyrus; rIFGorb, Right Inferior Frontal Orbital; lIFGop, Left Inferior Frontal Gyrus Opercular; lSTG, Left Superior Temporal Gyrus; rPreCG, Right Precentral Gyrus; rSTG, Right Superior Temporal Gyrus; lMTG, Left Middle Temporal Gyrus; rPoCG, Right Poscentral Gyrus; lPHG, Left Parahipocampal Gyrus; rSMG, Right Supramarginal Gyrus; lSMG, Left Supramarginal Gyrus; lPCUN, Left Precuneus; lstroke patientsL, Left Superior Parietal Lobule; rstroke patientsL, Right Superior Parietal Lobule; rLING, Right Lingual Cortex; rCAL, Right Calcarine; lMOG, Left Lateral Occipital Gyrus; rMOG, Right Lateral Occipital Gyrus.

a partial cognitive and functional improvement and may have clinically relevant implications, since it may be considered as an indicator of recovery. To rule out the possibility that the learning effect could be influencing the improvement of some cognitive scores, we have other complementary data related to changes in brain function. Specifically, the stroke patients of this study exhibited a widespread increased FC pattern within the beta band, indicating that their original disruption was restored in the recording performed after NR in that frequency band. We also obtained two very important results associated with the relationships between cognitive scores and changes in FC. On the one hand, we found three positive and significant recovery signatures correlations between the FC strength ratio and three cognitive measures changes (in Full-Scale IQ, BNT, and LM1), and on the other hand, we observed the predictive capacity of some neuropsychological test scores (in the pre-condition) and the recovery of the brain network (in the FC strength ratio). In this sense, we found two predictive markers of brain recovery related to two global cognitive domains, PIQ and Perceptual Organization (both from the WAIS-III scale).

Based on these data, we can affirm that these stroke patients experienced at least some recovery in their global cognitive capacity, despite the different etiology and location of their lesions. Nonetheless the previous literature about the effect of NR on specific cognitive domains remains unclear. Low to moderate effects of rehabilitation in executive functions (6), attention (4, 52), or memory (53) have been reported. These results could have low consistency for different reasons: (1) the low methodological quality or insufficient description (2, 4, 52) the use of small samples; (3) the absence of comparisons between intervention and no intervention or placebo conditions (4, 6) the deficit of randomized control trials (4, 5, 52) the need for standardized definition and outcome measures (53, 54); and (6) the lack of inclusion of functional ability measures in the rehabilitation outcome evaluation (52). It seems important to find the most effective procedures to try recovering the cognitive deficits associated with stroke, considering that the prevalence of post-stroke cognitive impairment is 53.4% (55), since it causes an increase in the institutionalization rate and costs of care (56, 57) and a decrease in the quality of life (58).

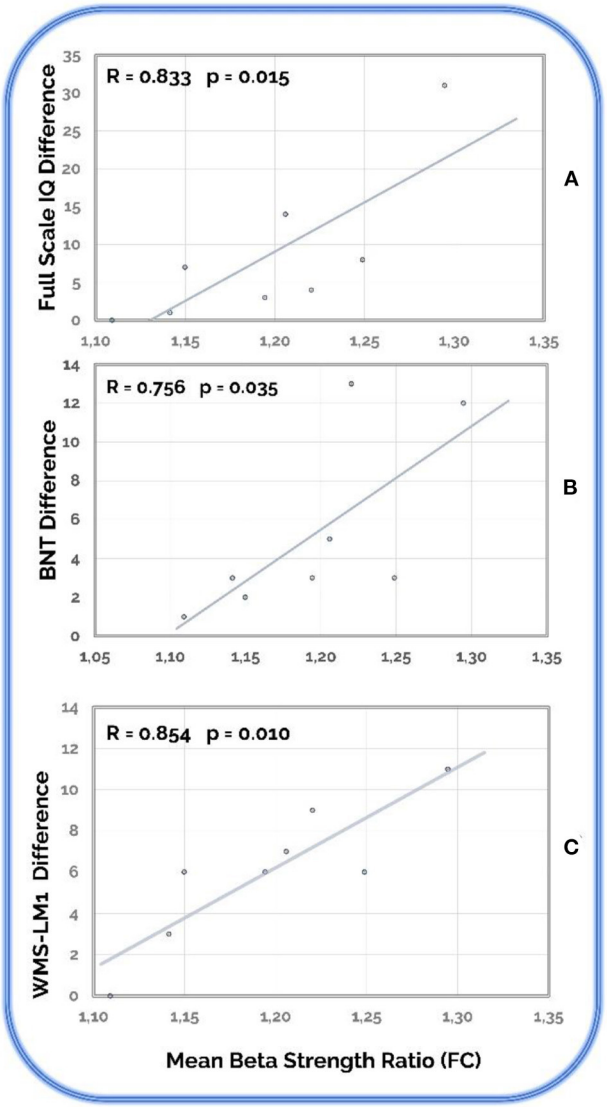

FIGURE 5 | Recovery signatures correlations. Statistically significant correlations between cognitive differences and the mean beta strength ratio in the stroke patients' group. **(A)** Full Scale IQ (of WAIS-III); **(B)** BNT (Boston Naming Test); **(C)** WMS-LM1 (Logical Memory 1 of WMS-III).

In addition, if stroke is a central factor in the development of cognitive impairment, or if this depends on the severity, subtype, location, or its recurrence, it becomes essential to understand the brain mechanisms that produce both deficits and their recovery. There is agreement around the idea that cognitive rehabilitation interventions aim to improve the impaired brain functions in stroke patients, and that it must be related to the damaged anatomical substrate (10). Usually, rehabilitation facilitates the development of behavioral and cognitive strategies that have a positive impact on the structural and functional recovery of the brain (53, 59). In this sense, it seems worthy to have in mind other promising complementary interventions including for example non-invasive transcranial magnetic stimulation to enhance some cognitive recoveries in stroke patients (60).

Restoration interventions aim to regain the cognitive abilities of stroke patients, including domain-specific interventions and treatments for generalized cognitive impairment (10). The patients of our study received an integrated treatment based on the holistic-comprehensive model proposed by Ben-Yishay and Diller (41), which is consistent with the interventions suggested by some experts in post-stroke cognitive rehabilitation in terms of their global treatment approach. This type of treatment could be very successful for this type of patients, insofar as it produces more clearly a pattern of overall improvement, both at behavioral and brain level. Other types of cognitive interventions, such as computer-assisted cognitive rehabilitation that has increased in recent years, although show some efficacy in improving attention, memory, executive function, or visuo-spatial neglect in stroke patients (61, 62), present very limited effects on working memory and even no effects on cognitive function compared to healthy controls (63).

As discussed above, overall review studies on the effectiveness of cognitive intervention with stroke patients do not provide clear conclusions. However, we must know that one of the most important issues regarding the functioning of the human mind has to do with the factor of interdependence between the different cognitive domains. This aspect is often overlooked in cognitive performance studies, and review studies of the effectiveness of cognitive treatments do not usually consider it. For example, there are studies that focus on improving attention after having specifically trained it, and thus with the rest of cognitive domains, without evaluating the impact of attention deficit or executive deficit in other domains such as memory or language. However, cognitive interdependence makes it very exceptional for patients who have brain injuries to suffer a specific cognitive deficit in a specific cognitive domain. The cognitive deficit of brain injury patients usually affects several domains, for example, visuo-spatial attention, working memory, executive functions, and episodic memory. Thus, trying to understand functioning of human cognition from independent cognitive domains, is probably an incorrect approach that hinders the interpretation of the results in neuropsychology. Usual intervention in the clinical setting is not as domain specific as studies suggest, since isolating cognitive processes in habitual actions is not easy. However, the neuropsychological literature continues to try to understand the effect of rehabilitation on each cognitive domain individually. This discrepancy requires a revision and a paradigm shift.

Furthermore, our intention was to go one step further trying to understand whether this recovery process seen at a cognitive and behavioral level could have some reflection in brain functioning. Cognitive functions depend on the integrated functioning of large-scale distributed brain networks (64). Specifically, recent evidence suggests that FC between brain regions may play an important role when difficulties arise from deficits in attention, memory, or other cognitive functions (65). In this context, we firstly looked for a FC pattern related to stroke. We found a disruption in the pattern of brain functioning, with a significant decrease in the beta band FC for intra and inter-hemispheric connections in stroke patients before rehabilitation

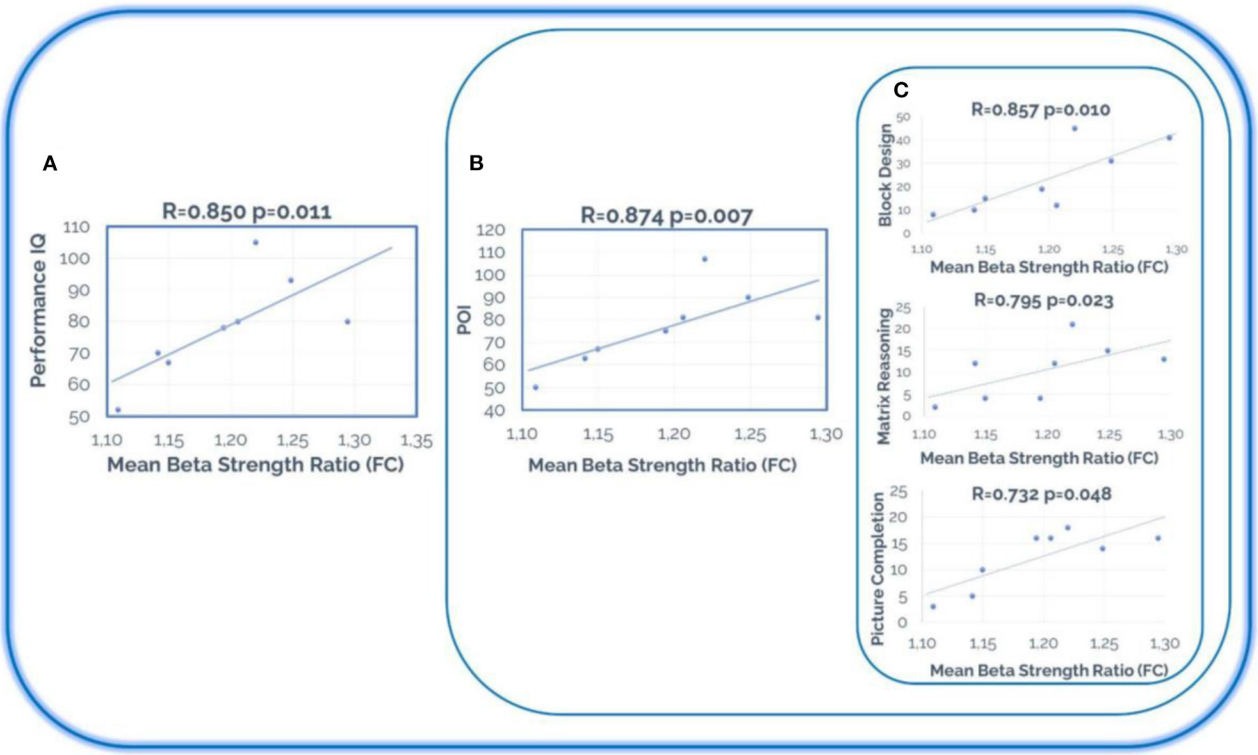

FIGURE 6 | Recovery prediction. Statistically significant differences between the cognitive scores in the pre-condition and the mean beta strength ratio (post/pre) in the stroke patients' group. **(A)** Performance IQ (WAIS-III); **(B)** POI (Perceptual Organization Index of WAIS-III); **(C)** Block Design, Matrix Reasoning, and Picture Completion (of WAIS-III). Note that the tests represented in this figure are related to each other, since Block Design, Matrix Reasoning, and Picture Completion are the tests included in Perceptual Organization Index, and POI (Perceptual Organization Index) is included in Performance IQ (on the WAIS-III scale).

compared to healthy controls. General disruption of dynamic networks after stroke have been previously reported in MEG studies (25). Alterations in beta band activity have been especially related to stroke compared to healthy controls (26), supporting our results.

On the other hand, understanding the interaction between brain regions within a network (i.e., their FC), and the interactions among networks are both important for efficient cognitive function (66). Therefore, exploring the possible neurophysiological mechanisms underlying the recovery process after stroke seems to be a crucial point in understanding the effect of cognitive rehabilitation on the brain. By observing stroke patients before and after the rehabilitation, a specific brain recovery pattern emerged, characterized by a widespread increased FC in the beta in the post-condition. The functioning of the beta frequency band has previously been related, in healthy population, to different cognitive tasks such as working memory (67–69), attention (70), and motor performance (71). On the contrary, our neurophysiological data were acquired during resting state (RS) which has been shown that is the most stable condition across patients with different symptomatology and it also has been considered a hallmark for clinical diagnosis and monitoring the recovery of patients that underwent a rehabilitation, both in MRI (18, 72) and MEG studies (22, 73). Previous results have described the role of RS FC as a predictor of motor learning ability in beta-band for healthy participants (74) or as a predictor of post-stroke motor recovery in alpha-band (75). Furthermore, the reorganization in FC in the beta-band during resting-state has previously been associated with the success of cognitive and physical interventions (13, 76, 77).

Up to this point, two independent markers of functional recovery (i.e., cognitive, and neurophysiological) were found in our stroke patients who went through the NR, but we developed further analyses to discover the possible relation between them. As mentioned before, trying to understand complex systems such as human cognition or brain functioning focusing on only some of their components gives partial information of the entire process. Therefore, with the aim to simplify the dimensionality of the data and to explore relationships between cognitive and neurophysiological findings, the difference (D = Post–Pre) of the most representative cognitive scores and the ratio of change (post/pre) of the total FC beta network strength were used. Three positive correlations between recovery signatures (i.e., cognitive and neurophysiology) were observed for stroke patients, corresponding to Full Scale IQ of WAIS-III, Boston Naming Test, and Logical Memory 1 of WMS-III. These results showed that the beta connectivity changes after the NR, compared with the data

obtained in the first recording are, in fact, the reflection of the cognitive improvement in the brain. The measures related with improvement represent global neuropsychological indices, which contain different cognitive domains such as sustained and switching attention, visuo-spatial attention, visuo-spatial working memory, planning, flexibility, or processing speed, but also episodic memory or verbal denomination. Initially, the neuropsychological deficit observed in stroke patients was global and their subsequent cognitive recovery, although not complete, was also general. The scope of cognitive changes after NR was really wide, probably due to the type of intervention, which was holistic and not only focused on specific cognitive functions, including global and interdependent domains, and focusing on individual cognitive, functional, emotional, and behavioral imbalances. All these evidences are consistent with the brain network global changes observed in stroke patients.

While addressing brain and cognitive changes in stroke patients is important to understand the underlying mechanisms of stroke and brain plasticity, the early detection of patterns or biomarkers is also relevant to predict which subjects are more likely to improve and benefit from neurorehabilitation. In this regard, adjustments can be made for those patients who will not benefit from this option. Thus, we performed an additional correlation analysis in which the pre-condition cognitive measures and the ratio of change (post/pre) of the total FC beta network strength were taken into account. Two global cognitive markers were stated as predictors of brain functioning recovery, PIQ and POI. Furthermore, within POI, we found a significant association for every subtest included in the global index (i.e., Picture Completion, Matrix Reasoning, and Block Design). In the clinical setting, the role of prediction in terms of the degree of future recovery has always been important, however it is a complex and complicated issue. Until now we only had clinical, cognitive, behavioral, and social variables, but these results indicate that the relationship between behavior and the brain can contribute to this topic. In this case, the results indicate that the initial state around some cognitive domains such as visuo-spatial attention, visuo-spatial working memory, or planning capacity, could have a very relevant role in the evolution and recovery of the brain network of stroke patients. This information is not only important to predict the patients who will improve the most, but it can also serve to think about more powerful intervention procedures for those patients who have a more serious deficit around these cognitive domains. This result has very relevant clinical implications.

In conclusion, if NR aims to improve people's cognitive function in order to restore their general performance and independence in functional activities, the results of the present study are in line with this objective, showing a clear improvement pattern in stroke patients who received NR both cognitively and brain function. We are also sure that this study points out the importance of including neuropsychological and neurophysiological variables in the assessment of the outcome and effectiveness of psychological interventions of stroke patients.

LIMITATIONS AND FUTURE RESEARCH

An important contribution of this study may be that, unlike most studies, functional brain connectivity was measured with MEG. Despite the intrinsic limitations of BOLD fMRI, MEG is a measure of brain activity with incredibly high temporal resolution (ms). Despite its advantages, MEG is an underused neuroimaging tool in clinical and research contexts. Although the sample of this exploratory study size was small, we were able to identify a pattern of recovery of FC in the beta band related to cognitive enhancement in stroke patients who underwent a NR. Additionally, we were able to make predictions based on the cognitive performance of stroke patients before rehabilitation about the future functional restoration of the brain network. Thus, larger MEG studies with stroke patients are needed to demonstrate the power of this neurophysiological tool within this neurological field. Another limitation that this study faces is the heterogeneity of stroke patients, in terms of etiology and location of the injury. However, we believe that this heterogeneity has provided an interesting approach to the study since it has allowed us to explore the effect of cognitive intervention both at cognitive and neurophysiological level in stroke patients with different etiology. Furthermore, another limitation of the study is the absence of a clinical control group (i.e., stroke patients without rehabilitation). Considering this limitation, we cannot assure that cognitive improvement is due specifically or uniquely to cognitive rehabilitation because it could also represent some degree of spontaneous clinical recovery after stroke. In accordance with the aforementioned obstacles, future studies should include a group of stroke patients without cognitive intervention (e.g., on the waiting list), and larger samples of patients that allow comparisons based on the etiology and the location of the lesion. Finally, it would be interesting to focus on different networks of the brain (78) such as the default mode, the salience, or the executive control networks (79), to explore specific changes in each network recovery pattern, and its possible relationship to particular improvements in cognition after stroke.

DATA AVAILABILITY STATEMENT

The raw data supporting the conclusions of this article will be made available by the authors, without undue reservation.

ETHICS STATEMENT

The studies involving human participants were reviewed and approved by the National Brain Injury Rehabilitation Center Ethics Committee (Madrid). The patients/participants provided their written informed consent to participate in this study.

AUTHOR CONTRIBUTIONS

SP, LT-S, ML, NP, and FM designed research. SP and LT-S performed main calculations of the study and prepared figures. SP, LT-S, ML, BC, LC, AB, FM, and NP collaborated actively in writing the manuscript. All authors contributed to the article and approved the submitted version.

FUNDING

Financial support of the project was provided by IMSERSO (07-2008) and the Spanish MICINN (PSI2011-28388). Research by SP was supported by the Spanish MINECO post-doctoral fellowship (FJC2019-041205-I). Additionally, this work was supported by a predoctoral researcher grant from Universidad Complutense de Madrid (CT42/18-CT43/18) and co-founded by Santander Bank to LT-S, and by the National Council of Science, Technology and Technological Innovation (CONCYTEC, Perú) through the National Fund for Scientific and Technological Development (FONDECYT, Perú) to BC.

SUPPLEMENTARY MATERIAL

The Supplementary Material for this article can be found online at: https://www.frontiersin.org/articles/10.3389/fneur.2022.838170/full#supplementary-material

REFERENCES

1. Feigin VL, Norrving B, Mensah GA. Global burden of stroke. *Circ Res.* (2017) 120:439–48. doi: 10.1161/CIRCRESAHA.116.308413
2. Aam S, Einstad MS, Munthe-Kaas R, Lydersen S, Ihle-Hansen H, Knapskog AB, et al. Post-stroke cognitive impairment—impact of follow-up time and stroke subtype on severity and cognitive profile: the Nor-COAST study. *Front Neurol.* (2020) 11:699. doi: 10.3389/fneur.2020.00699
3. Al-Qazzaz NK, Ali SH, Ahmad SA, Islam S, Mohamad K. Cognitive impairment and memory dysfunction after a stroke diagnosis: a post-stroke memory assessment. *Neuropsychiatr Dis Treat.* (2014) 10:1677–91. doi: 10.2147/NDT.S67184
4. Loetscher T, Potter KJ, Wong D, das Nair R. Cognitive rehabilitation for attention deficits following stroke. *Cochrane Database Syst Rev.* (2019) 2019:CD002842. doi: 10.1002/14651858.CD002842.pub3
5. Feigin VL, Roth GA, Naghavi M, Parmar P, Krishnamurthi R, Chugh S, et al. Global burden of stroke and risk factors in 188 countries, during 1990–2013: a systematic analysis for the Global Burden of Disease Study 2013. *Lancet Neurol.* (2016) 15:913–24. doi: 10.1016/S1474-4422(16)30073-4
6. Chung CSY, Pollock A, Campbell T, Durward BR, Hagen S. Cognitive rehabilitation for executive dysfunction in adults with stroke or other adult non-progressive acquired brain damage. *Cochrane Database Syst Rev.* (2013) 2013:CD008391. doi: 10.1002/14651858.CD008391.PUB2
7. Rasquin SMC, Lodder J, Ponds RWHM, Winkens I, Jolles J, Verhey FRJ. Cognitive functioning after stroke: a one-year follow-up study. *Dement Geriatr Cogn Disord.* (2004) 18:138–44. doi: 10.1159/000079193
8. Katz N, Hartman-Maeir A, Ring H, Soroker N. Relationships of cognitive performance and daily function of clients following right hemisphere stroke: predictive and ecological validity of the LOTCA battery. *Occup Ther J Res.* (2016) 20:3–17. doi: 10.1177/153944920002000101
9. Ferreira MGR, Moro CHC, Franco SC. Desempenho cognitivo após acidente vascular cerebral isquêmico. *Dement Neuropsychol.* (2015) 9:165–75. doi: 10.1590/1980-57642015DN92000011
10. Zhao Q, Wang X, Wang T, Dmytriw AA, Zhang X, Yang K, et al. Cognitive rehabilitation interventions after stroke: protocol for a systematic review and meta-analysis of randomized controlled trials. *Syst Rev.* (2021) 10:66. doi: 10.1186/s13643-021-01607-7
11. Canuet L. Neurorehabilitation in stroke: the role of functional connectivity. *Int J Neurorehabil.* (2015) 2:172. doi: 10.4172/2376-0281.1000172
12. Cicerone KD, Mott T, Azulay J, Sharlow-Galella MA, Ellmo WJ, Paradise S, et al. Randomized controlled trial of holistic neuropsychologic rehabilitation after traumatic brain injury. *Arch Phys Med Rehabil.* (2008) 89:2239–49. doi: 10.1016/j.apmr.2008.06.017
13. Castellanos NP, Paúl N, Ordóñ Ez VE, Demuynck O, Bajo R, Campo P, et al. Reorganization of functional connectivity as a correlate of cognitive recovery in acquired brain injury. *Brain.* (2010) 133:2365–81. doi: 10.1093/brain/awq174
14. Alexander LD, Black SE, Gao F, Szilagyi G, Danells CJ, McIlroy WE. Correlating lesion size and location to deficits after ischemic stroke: the influence of accounting for altered peri-necrotic tissue and incidental silent infarcts. *Behav Brain Funct.* (2010) 6:6. doi: 10.1186/1744-9081-6-6
15. Ovadia-Caro S, Villringer K, Fiebach J, Jungehulsing GJ, van der Meer E, Margulies DS, et al. Longitudinal effects of lesions on functional networks after stroke. *J Cereb Blood Flow Metab.* (2013) 33:1279–85. doi: 10.1038/jcbfm.2013.80
16. Bayrak S, Khalil AA, Villringer K, Fiebach JB, Villringer A, Margulies DS, et al. The impact of ischemic stroke on connectivity gradients. *NeuroImage Clin.* (2019) 24:101947. doi: 10.1016/j.nicl.2019.101947
17. Carrera E, Tononi G. Diaschisis: Past, present, future. *Brain.* (2014) 137:2408–22. doi: 10.1093/brain/awu101
18. Baldassarre A, Ramsey LE, Siegel JS, Shulman GL, Corbetta M. Brain connectivity and neurological disorders after stroke. *Curr Opin Neurol.* (2016) 29:706–13. doi: 10.1097/WCO.0000000000000396
19. Ramsey LE, Siegel JS, Baldassarre A, Metcalf NV, Zinn K, Shulman GL, et al. Normalization of network connectivity in hemispatial neglect recovery. *Ann Neurol.* (2016) 80:127–41. doi: 10.1002/ana.24690
20. Maestú F, Peña JM, Garcés P, González S, Bajo R, Bagic A, et al. A multicenter study of the early detection of synaptic dysfunction in mild cognitive impairment using magnetoencephalography-derived functional connectivity. *Neuroimage Clin.* (2015) 9:103–9. doi: 10.1016/j.nicl.2015.07.011
21. Stam CJ. Use of magnetoencephalography (MEG) to study functional brain networks in neurodegenerative disorders. *J Neurol Sci.* (2010) 289:128–34. doi: 10.1016/j.jns.2009.08.028
22. Paggiaro A, Birbaumer N, Cavinato M, Turco C, Formaggio E, del Felice A, et al. Magnetoencephalography in stroke recovery and rehabilitation. *Front Neurol.* (2016) 7:35. doi: 10.3389/fneur.2016.00035
23. Tewarie P, Steenwijk MD, Tijms BM, Daams M, Balk LJ, Stam CJ, et al. Disruption of structural and functional networks in long-standing multiple sclerosis. *Hum Brain Mapp.* (2014) 35:5946–61. doi: 10.1002/HBM.22596
24. Pusil S, López ME, Cuesta P, Bruña R, Pereda E, Maestú F. Hypersynchronization in mild cognitive impairment: the 'X' model. *Brain.* (2019) 142:3936–50. doi: 10.1093/brain/awz320
25. Marsh EB, Brodbeck C, Llinas RH, Mallick D, Kulasingham JP, Simon JZ, et al. Poststroke acute dysexecutive syndrome, a disorder resulting from minor stroke due to disruption of network dynamics. *Proc Natl Acad Sci USA.* (2020) 117:33578–585. doi: 10.1073/pnas.2013231117/
26. Kulasingham JP, Brodbeck C, Khan S, Marsh EB, Simon JZ. Bilaterally reduced rolandic beta band activity in minor stroke patients. *bioRxiv Preprint.* (2021). doi: 10.1101/2021.10.15.464457
27. Castellanos NP, Leyva I, Buldú JM, Bajo R, Paúl N, Cuesta P, et al. Principles of recovery from traumatic brain injury: reorganization of functional networks. *Neuroimage.* (2011) 55:1189–99. doi: 10.1016/j.neuroimage.2010.12.046
28. Teasdale G, Jennett B. Assessment of coma and impaired consciousness a practical scale. *Lancet.* (1974) 2:81–4. doi: 10.1016/s0140-6736(74)91639-0
29. Wechsler D. *Wechsler Adult Intelligence Scale (WAIS-III).* San Antonio, TX: Psychological Corporation (1997).
30. Schretlen D. *Brief Test of Attention*. Baltimore, MD: Psychological Assessment Resources (1989).
31. Reitan RM, Wolfson D. *The Halstead-Reitan Neuropsychological Test Battery e Theory and Clinical Interpretation.* Tucson, AZ: Neuropsychology Press (1993)
32. Golden CJ. *A Manual for the Clinical and Experimental Use of the Stroop Color and Word Test.* Chicago, IL: Stoelting (1978).
33. Jensen AR, Rohwer WD. The Stroop color-word test: a review. *Acta Psychol.* (1966) 25:36–93. doi: 10.1016/0001-6918(66)90004-7

34. Heaton RK, Grant I, Matthews CG. *Comprehensive Norms for an Expanded Halstead-Reitan Battery: Demographic Corrections, Research Findings, and Clinical Applications*. Odessa, FL: Psychological Assessment Resources. (1991).
35. Édouard L. *Récréations Mathématiques*. Vol III. Paris: Reprinted several times by Albert Blanchard (1983). Available online at: https://books.google.es/books?hl=en&lr=&id=hwYAAAAAQAAJ&oi=fnd&pg=PA3&dq=%C3%89douard$+$L.$+$R%C3%A9cr%C3%A9ations$+$Math%C3%A9matiques.$+$vol.$+$III&ots=6q1xOXhLC4&sig=bZgxKMrYvQEczRsMbW7m9ovm5WM&redir_esc=y#v=onepage&q=%C3%89douard%20L.%20R%C3%A9cr%C3%A9ations%20Math%C3%A9matiques.%20vol.%20III&f=false (accessed December 15, 2021).
36. Wilson BA, Alderman N, Burgess PW, Emslie H, Evans JJ. *BADS: Behavioural Assessment of the Dysexecutive Syndrome : Test Manual*. London: Thames Valley Test Company (1996).
37. Kaplan E. *Boston Naming Test*. Philadelphia, PA: Lea & Febiger (1983).
38. Benton AL, Hamsher K. *Controlled Oral Word Association Test – COWAT*. Iowa City, IA: University of Iowa Press (1976)
39. Sedó M. *FDT. Test de los Cinco Dígitos*. TEA Ediciones (2007). Available online at: https://web.teaediciones.com/fdt--test-de-los-cinco-digitos.aspx (accessed December 15, 2021).
40. Prigatano GP, Schacter DL. *Awareness of Deficit After Brain Injury*. New York, NY: Oxford University Press (1991).
41. Ben-Yishay Y, Diller L. *Handbook of Holistic Neuropsychological Rehabilitation: Outpatient Rehabilitation of Traumatic Brain Injury*. Oxford University Press (2011). Available online at: https://books.google.es/books?hl=es&lr=&id=Yzg_zb94ZHcC&oi=fnd&pg=PP1&dq=Handbook$+$of$+$Holistic$+$Neuropsychological$+$Rehabilitation:$+$Outpatient$+$Rehabilitation$+$of$+$Traumatic$+$Brain$+$Injury&ots=KzE1fPTgBK&sig=0neZLIlQmPk85DCW3BVyrj5qVPQ#v=onepage&q=Handbook%20of%20Holistic%20Neuropsychological%20Rehabilitation%3A%20Outpatient%20Rehabilitation%20of%20Traumatic%20Brain%20Injury&f=false (accessed December 15, 2021).
42. Bell AJ, Sejnowski TJ. An information-maximization approach to blind separation and blind deconvolution. *Neural Comput.* (1995) 7:1129–59. doi: 10.1162/NECO.1995.7.6.1129
43. Tadel F, Baillet S, Mosher JC, Pantazis D, Leahy RM. Brainstorm: a user-friendly application for MEG/EEG analysis. *Comput Intell Neurosci.* (2011) 2011:879716. doi: 10.1155/2011/879716
44. Holmes CJ, Hoge R, Collins L, Woods R, Toga AW, Evans AC. Enhancement of MR images using registration for signal averaging. *J Comput Assist Tomogr.* (1998) 22:324–33. doi: 10.1097/00004728-199803000-00032
45. Mosher JC, Baillet S, Leahy RM. Equivalence of linear approaches in bioelectromagnetic inverse solutions. In: *IEEE Workshop on Statistical Signal Processing Proceedings*. St. Louis, MO (2003) p. 294–7. doi: 10.1109/SSP.2003.1289402
46. Palva S, Palva JM. Discovering oscillatory interaction networks with M/EEG: challenges and breakthroughs. *Trends Cogn Sci.* (2012) 16:219–30. doi: 10.1016/j.tics.2012.02.004
47. Hassan M, Dufor O, Merlet I, Berrou C, Wendling F. EEG source connectivity analysis: from dense array recordings to brain networks. *PLoS ONE.* (2014) 9:e105041. doi: 10.1371/JOURNAL.PONE.0105041
48. Desikan RS, Ségonne F, Fischl B, Quinn BT, Dickerson BC, Blacker D, et al. An automated labeling system for subdividing the human cerebral cortex on MRI scans into gyral based regions of interest. *Neuroimage.* (2006) 31:968–80. doi: 10.1016/j.neuroimage.2006.01.021
49. Mormann F, Lehnertz K, David P, Elger CE. Mean phase coherence as a measure for phase synchronization and its application to the EEG of epilepsy patients. *Phys D Nonlin Phenom.* (2000) 144:358–69. doi: 10.1016/S0167-2789(00)00087-7
50. Bruña R, Maestú F, Pereda E. Phase locking value revisited: teaching new tricks to an old dog. *J Neural Eng.* (2018) 15:056011. doi: 10.1088/1741-2552/aacfe4
51. Benjamini Y, Yekutieli D. The control of the false discovery rate in multiple testing under dependency. *Ann Statist.* (2001) 29:1165–88. doi: 10.1214/aos/1013699998
52. Hazelton C. Can cognitive rehabilitation improve attention deficits following stroke? - A Cochrane Review summary with commentary *NeuroRehabilitation.* (2020) 47:355–7. doi: 10.3233/NRE-209007
53. das Nair R, Cogger H, Worthington E, Lincoln NB. Cognitive rehabilitation for memory deficits after stroke. *Cochrane Database Syst Rev.* (2016) 9:CD002293. doi: 10.1002/14651858.CD002293.pub3
54. Bernhardt J, Hayward KS, Kwakkel G, Ward NS, Wolf SL, Borschmann K, et al. Agreed definitions and a shared vision for new standards in stroke recovery research: the Stroke Recovery and Rehabilitation Roundtable taskforce. *Int J Stroke.* (2017) 12:444–50. doi: 10.1177/1747493017711816
55. Barbay M, Diouf M, Roussel M, Godefroy O. Systematic review and meta-analysis of prevalence in post-stroke neurocognitive disorders in hospital-based studies. *Dement Geriatr Cogn Disord.* (2019) 46:322–34. doi: 10.1159/000492920
56. Pasquini M, Leys D, Rousseaux M, Pasquier F, Hénon H. Influence of cognitive impairment on the institutionalisation rate 3 years after a stroke. *J Neurol Neurosurg Psychiatry.* (2007) 78:56–9. doi: 10.1136/jnnp.2006.102533
57. Claesson L, Lindén T, Skoog I, Blomstrand C. Cognitive impairment after stroke - Impact on activities of daily living and costs of care for elderly people: the Göteborg 70+ stroke study. *Cerebrovasc Dis.* (2005) 19:102–9. doi: 10.1159/000082787
58. Park JH, Kim BJ, Bae H-J, Lee J, Lee J, Han M-K, et al. Impact of post-stroke cognitive impairment with no dementia on health-related quality of life. *J Stroke.* (2013) 15:49–56. doi: 10.5853/JOS.2013.15.1.49
59. Robertson S. The efficacy of oro-facial and articulation exercises in dysarthria following stroke *Int J Lang Commun Disord.* (2001) 36(Suppl):292–7. doi: 10.3109/13682820109177900
60. Draaisma LR, Wessel MJ, Hummel FC. Non-invasive brain stimulation to enhance cognitive rehabilitation after stroke. *Neurosci Lett.* (2020) 719:133678. doi: 10.1016/j.neulet.2018.06.047
61. Yoo C, Yong MH, Chung J, Yang Y. Effect of computerized cognitive rehabilitation program on cognitive function and activities of living in stroke patients. *J Phys Ther Sci.* (2015) 27:2487–9. doi: 10.1589/jpts.27.2487
62. Svaerke K, Niemeijer M, Mogensen J, Christensen H. The effects of computer-based cognitive rehabilitation in patients with visuospatial neglect following stroke: a systematic review. *Top Stroke Rehabil.* (2019) 26:214–25. doi: 10.1080/10749357.2018.1556963
63. Wentink MM, Berger MAM, de Kloet AJ, Meesters J, Band GPH, Wolterbeek R, et al. The effects of an 8-week computer-based brain training programme on cognitive functioning, QoL and self-efficacy after stroke. *Neuropsychol Rehabil.* (2016) 26:847–65. doi: 10.1080/09602011.2016.1162175
64. Mesulam MM. From sensation to cognition. *Brain.* (1998) 121(Pt 6):1013–52. doi: 10.1093/brain/121.6.1013
65. Siegel JS, Ramsey LE, Snyder AZ, Metcalf NV, Chacko RV, Weinberger K, et al. Disruptions of network connectivity predict impairment in multiple behavioral domains after stroke. *Proc Natl Acad Sci USA.* (2016) 113:E4367–76. doi: 10.1073/pnas.1521083113
66. Leech R, Kamourieh S, Beckmann CF, Sharp DJ. Fractionating the default mode network: distinct contributions of the ventral and dorsal posterior cingulate cortex to cognitive control. *J Neurosci.* (2011) 31:3217–24. doi: 10.1523/JNEUROSCI.5626-10.2011
67. Koshy SM, Wiesman AI, Proskovec AL, Embury CM, Schantell MD, Eastman JA, et al. Numerical working memory alters alpha-beta oscillations and connectivity in the parietal cortices. *Hum Brain Mapp.* (2020) 41:3709–19. doi: 10.1002/hbm.25043
68. Proskovec AL, Heinrichs-Graham E, Wilson TW. Load modulates the alpha and beta oscillatory dynamics serving verbal working memory. *Neuroimage.* (2019) 184:256–65. doi: 10.1016/j.neuroimage.2018.09.022
69. Schmidt R, Ruiz MH, Kilavik BE, Lundqvist M, Starr PA, Aron AR. Beta oscillations in working memory, executive control of movement and thought, and sensorimotor function. *J Neurosci.* 39:8231–8. doi: 10.1523/JNEUROSCI.1163-19.2019
70. Kamiński J, Brzezicka A, Gola M, Wróbel A. Beta band oscillations engagement in human alertness process. *Int J Psychophysiol.* (2012) 85:125–8. doi: 10.1016/j.ijpsycho.2011.11.006
71. Chung JW, Ofori E, Misra G, Hess CW, Vaillancourt DE. Beta-band activity and connectivity in sensorimotor and parietal cortex are important for accurate motor performance. *Neuroimage.* (2017) 144:164–73. doi: 10.1016/j.neuroimage.2016.10.008
72. Dacosta-Aguayo R, Graña M, Savio A, Fernández-Andújar M, Millán M, López-Cancio E, et al. Prognostic value of changes in resting-state functional

connectivity patterns in cognitive recovery after stroke: a 3T fMRI pilot study. *Hum Brain Mapp.* (2014) 35:3819–31. doi: 10.1002/hbm.22439
73. Martín-Buro MC, Garcés P, Maestú F. Test-retest reliability of resting-state magnetoencephalography power in sensor and source space. *Hum Brain Mapp.* (2016) 37:179–90. doi: 10.1002/hbm.23027
74. Sugata H, Yagi K, Yazawa S, Nagase Y, Tsuruta K, Ikeda T, et al. Role of beta-band resting-state functional connectivity as a predictor of motor learning ability. *NeuroImage.* (2020) 210:116562. doi: 10.1016/j.neuroimage.2020.116562
75. Westlake KP, Hinkley LB, Bucci M, Guggisberg AG, Findlay AM, Henry RG, et al. Resting state alpha-band functional connectivity and recovery after stroke. *Exp Neurol.* (2012) 237:160–9. doi: 10.1016/j.expneurol.2012.06.020
76. Weiss SA, Bassett DS, Rubinstein D, Holroyd T, Apud J, Dickinson D, et al. Functional brain network characterization and adaptivity during task practice in healthy volunteers and people with schizophrenia. *Front Hum Neurosci.* (2011) 5:81. doi: 10.3389/fnhum.2011.00081
77. Klados MA, Styliadis C, Frantzidis CA, Paraskevopoulos E, Bamidis PD. Beta-band functional connectivity is reorganized in mild cognitive impairment after combined computerized physical and cognitive training. *Front Neurosci.* (2016) 10:55. doi: 10.3389/fnins.2016.00055
78. Power JD, Cohen AL, Nelson SM, Wig GS, Barnes KA, Church JA, et al. Functional network organization of the human brain. *Neuron.* (2011) 72:665–78. doi: 10.1016/j.neuron.2011.09.006
79. Raichle ME, MacLeod AM, Snyder AZ, Powers WJ, Gusnard DA, Shulman GL, et al. A default mode of brain function. *Proc Nat Acad Sci USA.* (2001) 98:676–82. doi: 10.1073/PNAS.98.2.676

Conflict of Interest: The authors declare that the research was conducted in the absence of any commercial or financial relationships that could be construed as a potential conflict of interest.

Publisher's Note: All claims expressed in this article are solely those of the authors and do not necessarily represent those of their affiliated organizations, or those of the publisher, the editors and the reviewers. Any product that may be evaluated in this article, or claim that may be made by its manufacturer, is not guaranteed or endorsed by the publisher.

frontiers in Neurology

ORIGINAL RESEARCH
published: 25 February 2022
doi: 10.3389/fneur.2022.762497

Weighted Blind Source Separation Can Decompose the Frequency Mismatch Response by Deviant Concatenation: An MEG Study

Teppei Matsubara[1,2,3,4]*, *Steven Stufflebeam*[1,2], *Sheraz Khan*[1,2], *Jyrki Ahveninen*[1,2], *Matti Hämäläinen*[1,2], *Yoshinobu Goto*[5], *Toshihiko Maekawa*[6], *Shozo Tobimatsu*[7] and *Kuniharu Kishida*[8,9]

[1] Athinoula A. Martinos Center for Biomedical Imaging, Massachusetts General Hospital, Charlestown, MA, United States, [2] Harvard Medical School, Boston, MA, United States, [3] Japan Society for the Promotion of Science, Tokyo, Japan, [4] International University of Health and Welfare, Fukuoka, Japan, [5] Department of Physiology, School of Medicine, International University of Health and Welfare, Narita, Japan, [6] Department of Psychiatry, Amekudai Hospital, Naha, Japan, [7] Department of Orthoptics, Faculty of Medicine, Fukuoka International University of Health and Welfare, Fukuoka, Japan, [8] Gifu University, Gifu, Japan, [9] Hermitage of Magnetoencephalography, Osaka, Japan

OPEN ACCESS

Edited by:
Yulin Ge,
New York University, United States

Reviewed by:
Jürgen Dammers,
Helmholtz Association of German Research Centres (HZ), Germany
Sven Braeutigam,
University of Oxford, United Kingdom
Nobukazu Nakasato,
Tohoku University, Japan

***Correspondence:**
Teppei Matsubara
tmatsubara@mgh.harvard.edu

Specialty section:
This article was submitted to Applied Neuroimaging, a section of the journal Frontiers in Neurology

Received: *22 August 2021*
Accepted: *25 January 2022*
Published: *25 February 2022*

Citation:
Matsubara T, Stufflebeam S, Khan S, Ahveninen J, Hämäläinen M, Goto Y, Maekawa T, Tobimatsu S and Kishida K (2022) Weighted Blind Source Separation Can Decompose the Frequency Mismatch Response by Deviant Concatenation: An MEG Study. Front. Neurol. 13:762497. doi: 10.3389/fneur.2022.762497

The mismatch response (MMR) is thought to be a neurophysiological measure of novel auditory detection that could serve as a translational biomarker of various neurological diseases. When recorded with electroencephalography (EEG) or magnetoencephalography (MEG), the MMR is traditionally extracted by subtracting the event-related potential/field (ERP/ERF) elicited in response to "deviant" sounds that occur randomly within a train of repetitive "standard" sounds. However, there are several problems with such a subtraction, which include increased noise and the neural adaptation problem. On the basis of the original theory underlying MMR (i.e., the memory-comparison process), the MMR should be present only in deviant epochs. Therefore, we proposed a novel method called weighted-$BSS_{T/k}$, which uses only the deviant response to derive the MMR. Deviant concatenation and weight assignment are the primary procedures of weighted-$BSS_{T/k}$, which maximize the benefits of time-delayed correlation. We hypothesized that this novel weighted-$BSS_{T/k}$ method highlights responses related to the detection of the deviant stimulus and is more sensitive than independent component analysis (ICA). To test this hypothesis and the validity and efficacy of the weighted-$BSS_{T/k}$ in comparison with ICA (infomax), we evaluated the methods in 12 healthy adults. Auditory stimuli were presented at a constant rate of 2 Hz. Frequency MMRs at a sensor level were obtained from the bilateral temporal lobes with the subtraction approach at 96–276 ms (the MMR time range), defined based on spatio-temporal cluster permutation analysis. In the application of the weighted-$BSS_{T/k}$, the deviant responses were given a constant weight using a rectangular window on the MMR time range. The ERF elicited by the weighted deviant responses demonstrated one or a few dominant components representing the MMR that fitted well with that of the sensor space analysis using the conventional subtraction approach. In contrast, infomax or weighted-infomax revealed many minor or pseudo components as constituents of the

MMR. Our single-trial, contrast-free approach may assist in using the MMR in basic and clinical research, and it opens a new and potentially useful way to analyze event-related MEG/EEG data.

Keywords: mismatch response (MMR), blind source separation (BSS), magnetoencephalography (MEG), time-delayed correlation, independent component analysis (ICA), *T/k* (fractional) type of decorrelation method, weighted blind source separation, deviant concatenation

INTRODUCTION

The mismatch negativity component in electroencephalography (EEG), and its magnetoencephalographic (MEG) counterpart the mismatch field (or mismatch response, MMR), are event-related responses (EPRs/ERFs) widely used to measure auditory processing in cognitive neuroscience (1–6). The MMR is recorded using an oddball paradigm, where the repeated presentation of a stimulus (standard) is occasionally replaced by a different stimulus (deviant). The MMR is then computed as the difference between the deviant and standard responses. This difference representing the MMR is typically found around 100–250 ms after the onset of the deviant stimulus (7). Previous studies have revealed a cortical network consisting mainly of the bilateral temporal regions, but also the frontal and parietal regions, which is involved in the generation of the MMR (8–10). The prevailing view is that the MMR reflects the detection of change in the auditory system that can be measured without attention, although alternative interpretations exist (11–14). The MMR has therefore been widely used to assess auditory processing in children and clinical groups (10, 15, 16).

Originally, it was suggested that the occurrence of the MMR relates to the presence of a short-term memory trace where the memory-comparison process detects a discrepancy between the neural representation of the regularity inherent in the recent stimulation and the representation of the current deviant stimulus (17). On the basis of this hypothesis, obtaining a difference waveform by subtracting the standard response from the deviant response is the only way to identify the MMR. However, there are several problems associated with the subtraction approach. First, the subtraction reduces the signal-to-noise ratio (SNR) because the noise present in the standard responses is added to the noise in the deviant responses. Second, the neural adaptation process, especially with frequency MMR, can affect the difference waveform. The auditory system has a tonotopic organization from the cochlea through to the cortex (18). Stimulus repetition leads to repeated initiation of patterns of neural activity (e.g., the M100) that habituates as a function of the repetition rate (19, 20). In the classic oddball protocol, the neural response to standard stimuli is attenuated by these repetition suppression effects. This suppression is greater for the standard stimuli than for the less frequent deviant stimuli. The adapted and non-adapted neural activity presents not only different amplitudes, but also different temporal dynamics. Thus, the subtraction approach does not simply reflect the MMR (i.e., a memory-based comparison) but also the differential adaptation of neurons (13). Therefore, the study of the temporal dynamics of the MMR might convey critical information regarding the nature of the underlying neural generators. Hence, to effectively reveal the MMR, another approach considering the temporal information, instead of the subtraction approach, is desirable.

Each EEG electrode or MEG sensor records a linear combination of signals from several sources (21). Multi-channel EEG/MEG, which typically involves hundreds of sensors, provides detailed spatio-temporal distribution patterns, which obviously complicate the interpretation of signals and topographies. Independent component analysis (ICA), which is a blind source separation (BSS) method, is a stochastic method that can be used to decompose such complex data into a set of spatio-temporal components, each of which comprises a fixed spatial distribution and an associated signal (22, 23). Each component signal is a weighted sum of the sensor or electrode signals, which in turn are weighted sums of the dynamics of the neural sources (24). ICA/BSS can provide signal sources without any a priori information about their occurrence in biological signals. In general, the single-trial approach of ICA/BSS can utilize temporal information, because the contraction of information occurs during the averaging process of the ERP/ERF. A single trial may contain all kinds of non-brain artifacts and spontaneous EEG/MEG processes, whereas decomposing an average of all trials not only minimizes the contributions of those neural and artifactual processes that are not reliably time- and phase-locked to experimental events but also removes event-related brain dynamics among trials (25). As artifacts often exhibit stereotypical patterns that differ from those of brain activity, ICA/BSS can mostly be used to separate artifactual patterns (26–28). In fact, ICA/BSS has been used to extract event-related activities in only a handful of previous studies (29–33). Owing to the components being computed based purely based on their statistical independence, physiological perspectives are not taken into account (28, 34). Considering that regional brain activities substantially correlate with each other, an approach requiring strong independence may not be the most fruitful (35–38).

An approach for refining ICA/BSS using time-delayed correlation, or the decorrelation method (DC) has also been considered (39). Time-delayed correlation takes account of the characteristic time structure of the signals of interest, including the periodicity and/or morphology. Thus, time-delayed

Abbreviations: MMR, mismatch response; EEG, electroencephalography; MEG, magnetoencephalography; DC, decorrelation method; ERP, event-related potential; ERF, event-related field; BSS, blind source separation; SNR, signal-to-noise ratio; ICA, independent component analysis; SOBI, second-order blind identification; $BSS_{T/k}$, *T/k* (fractional) type of decorrelation method; SOA, stimulus onset asynchrony; TSSS, temporal signal space separation method; LU, left upper; RU, right upper; LL, left lower; RL, right lower; PCA, principal component analysis; rmANOVA, repeated-measures analysis of variance.

correlation measures the correlation between two signals, then maximizes the correlation between components. For example, several studies applied DC to second-order blind identification (SOBI) to separate periodic signals, such as cardiac and oscillatory brain activity, because periodic signals are well-correlated with delayed signals and non-delayed original signals (40, 41). As a result, well-correlated signals were extracted in one (or a few) components. However, in SOBI, most approaches examine the time structure of the target signals subjectively. When parameters are highly specified, featured components are more independent, and therefore target signals collapse because of strong independence and the SOBI method becomes equivalent to ICA (39–41).

In an attempt to develop solutions to address the limitations of ICA and SOBI, we proposed a novel method of BSS called the *T/k* (fractional) type of DC ($BSS_{T/k}$) (35–38). This method shares the fundamental concept underlying DC such as SOBI but is more focused on the periodicity of the target signal. The $BSS_{T/k}$ method is based on extracting time points (i.e., time-delayed parameters) determined by the parameters T and k, which represent periodicity concerning a fundamental and harmonics (**Supplementary Data (1)** and **Supplementary Figure 1**). $BSS_{T/k}$ allows weak independence among the components. Setting time-delayed parameters in this way results in highlighting the characteristics of target ERFs that are periodically presented. Previously, we demonstrated that somatosensory-evoked fields in response to periodic electrical stimuli can be decomposed into a few components using the $BSS_{T/k}$ algorithm in 64 channel magnetometers of CTF (35–38). Using a generalization of $BSS_{T/k}$, non-periodic interictal epileptiform discharges that were assumed to originate in a single epileptogenic zone were decomposed into one dominant component (42).

For the MMR paradigm, where deviant stimuli are presented in random order, we proposed to use a modification of $BSS_{T/k}$, which we termed weighted-$BSS_{T/k}$ (43). In weighted-$BSS_{T/k}$, we only used deviant responses that were concatenated into a periodical arrangement. Then, deviant responses were assigned a constant weight (rectangular window) on the specific time interval that represents MMR (i.e., the MMR time range). This is known as a window function in the time domain. The MMR time range was defined in a data-driven manner using sensor space subtraction (i.e., the reference standard). Through these procedures, the correlation between MMR and the responses outside of the MMR time range (e.g., the M100) can be minimized; thus, weighted-$BSS_{T/k}$, which underlies time-delayed correlation, can effectively extract the MMR. We hypothesized that weighted-$BSS_{T/k}$ would extract one or a few dominant components that can discriminate the MMR from background brain noise and other artifacts or other irrelevant ERFs. As the first application in the cognitive neuroscience of weighted-$BSS_{T/k}$ using only deviant epochs, we aimed to extract components that resemble the reference standard because subtraction is currently the gold standard for identifying MMR. We applied both $BSS_{T/k}$ and infomax (ICA) separately to the same weighted multi-channel MEG data (weighted-$BSS_{T/k}$ and weighted-infomax, respectively), and used the subtraction approach (subtraction-$BSS_{T/k}$ and subtraction-infomax) as a more general approach to investigate how the single-trial approach works, and then, statistically compared the similarity of each component to the reference standard to test a further hypothesis that $BSS_{T/k}$ is more sensitive than infomax.

It was not our aim to use the subtraction-$BSS_{T/k}$/weighted-$BSS_{T/k}$ to separate independent MMR sources. Typically, statistically independent components separated by preprocessing with ICA are expected to be associated with one or two dipolar sources (9, 23, 44, 45). We instead made a more general assumption that a component extracted by subtraction-$BSS_{T/k}$/weighted-$BSS_{T/k}$ will relate to multiple sources or a network of activity generating the MMR. In this sense, few decomposed components are better than many, as long as they represent the reference standard. Thus, the extraction of MMR in a few components would simplify the interpretation of MMR in regard to clinical and research applications.

MATERIALS AND METHODS

Participants

The participants in the experiment were 12 healthy adults (aged 25.4–41.9 years, mean 33.7 years; six women). None of the participants reported a history of head injury, neurological disease, hearing problems, severe medical illness, or drug abuse. The experiment was approved by the Ethics Committee of Kyushu University.

Stimuli and Procedures

The paradigm consisted of auditory stimulus sequences composed of standard stimuli with a probability of 80% and deviant stimuli with a probability of 20%, which were delivered in random order until at least 150 deviant stimuli were presented. Tone bursts of 500 Hz for standard stimuli and 550 Hz for deviant stimuli (10-ms rise and 20-ms fall) with a 100-ms duration were delivered monaurally through plastic tubes (length, 6 m; inner diameter, 8 mm). The hearing threshold was determined for each ear of each subject, and stimuli generated by a tone-burst-generator (Kyushu-Keisokuki, Fukuoka, Japan) were delivered at intensities of 50 dB above the threshold (46). The stimulus onset asynchrony (SOA) was 500 ms, and the presentation rate of the stimuli represented by f_p was 2 Hz. Stimuli were delivered to each ear in separate runs, with masking noises delivered to the contralateral ear to avoid cross-hearing (47). Inversed stimuli (550 Hz for standard and 500 Hz for deviant) were presented monaurally in separate runs. These stimuli were counterbalanced. In the current study, only data from right-ear stimulation and using 500-Hz standard/550-Hz deviant stimuli were analyzed. Subjects were instructed to ignore the auditory stimuli while they lay on the bed and watched a silent movie (16).

Data Acquisition

MEG was acquired using a 306-channel (204 planar gradiometers and 102 magnetometers) whole-head system (Elekta-Neuromag, Helsinki, Finland) in a magnetically shielded room. The sampling rate was 1,000 Hz, with a band-pass filter of 0.03–330 Hz. EEG was simultaneously recorded using 19 scalp electrodes according

to the international 10–20 system, although the sparse EEG data were not analyzed in the current study.

Data Analysis

Preliminary Process

The temporal signal space separation method (TSSS) using MaxFilter 2.2.13 (Elekta-Neuromag, Helsinki, Finland) was applied to the sensor level data with the default setting of an inside expansion order of 8, an outside expansion order of 3, automatic optimization of both inside and outside bases, a subspace correlation limit of 0.980, and a raw data buffer length of 10 s (48, 49). Notch filters were applied to suppress power line frequency and its harmonics (60, 100, 120, 180, 200, 240, and 300 Hz). Data from the 204 planar gradiometers were used for all subsequent analyses. Hereafter, all analysis steps are shown in **Figure 1** and summarized in **Figure 2**.

The Subtraction Approach

The conventional subtraction approach for sensor space analysis was used as a reference (**Figures 1A**, **2A**). Before averaging across epochs, the data were low pass filtered at 30 Hz and, epochs exceeding 4,000 fT/cm on any planar gradiometer channel were excluded from the average. Based on our experience, some ocular artifacts leak into the good epochs. Therefore we took extra care and visually inspected the data to remove eye movements. However, the impact of this procedure was minimal because the number of epochs removed for each subject was 0–1. Each epoch contained a 600-ms time window ranging from 100 ms pre-stimulus to 500 ms post-stimulus onset, with the stimuli being periodically presented ($SOA = 500$ ms or $f_p = 2$ Hz). The MMR difference sensor waveform (i.e., $\bar{x}_{sub}$) was calculated by subtracting the averaged deviant ERFs from the averaged standard ERFs for each subject (**Figures 1A**, **2A**);

$$\bar{x}_{sub}(n) := \bar{x}_{dev}(n) - \bar{x}_{std}(n), \tag{1}$$

where $x(n)$ represents the MEG sensor data at the discrete time, n. $\bar{x}(n)$ reflects the averaged sensor waveform of $x(n)$ across epochs. $\bar{x}_{std}(n)$ and $\bar{x}_{dev}(n)$ are averaged standard and deviant responses, respectively.

Decomposition Process

The decomposition methods of $BSS_{T/k}$ and infomax were applied separately to each subject's sensor dataset, which contained 204 sensors. The sensor data were originally decomposed into a set of spatio-temporal components;

$$x(n) = As(n), \tag{2}$$

where A is a mixing matrix, and s is a signal source. $BSS_{T/k}$ was applied;

$$x(n) = A_{DC}s_{DC}(n), \tag{3}$$

where A_{DC} is a mixing matrix of $BSS_{T/k}$, and s_{DC} is a signal source of $BSS_{T/k}$. Hereafter, we refer to BSSq (q = 1, 2, 3, …, 204) as a specific component obtained after the application of $BSS_{T/k}$. We briefly describe the $BSS_{T/k}$ method here; full details are provided in previous studies (36, 38). As a preliminary step, we conducted a sphering procedure to orthogonalize and normalize the time-series data for input sensors. We then conducted an iterative Givens rotation to minimize the absolute sum of off-diagonal elements of the normalized correlation matrices at the parameters. Specifically, the Jacobi-like algorithm proposed by Cardoso and Souloumiac (50, 51) was used in the $BSS_{T/k}$ method to approximately solve the simultaneous diagonalization problem at specific times. Regarding the period $T = 1/f_p$ with sampling frequency f_s, the time-delayed parameters τ can be defined by:

$$BSS_{T/k} : \tau_m = [f_s/f_p]/m, \quad m = 1, 2, \ldots, k. \tag{4}$$

where $[\ldots]$ rounds the value to the nearest integer. Here, $T = 0.5$ s and $f_p = 2$ Hz, with the repetitive stimuli constantly presented at a rate of 2 Hz (subsection Stimuli and Procedures). We determined $k = 8$ in a data-driven manner (36, 38) [**Supplementary Data (1)** and **Supplementary Figure 1**]. These parameters gave τ (ms) as 500, 250, 166, 125, 100, 83, 71, and 62 according to Eq. (4).

For ICA, we used the infomax algorithm (25, 49), which was implemented in MNE-python (52) using the default setting;

$$x(n) = A_{ICA}s_{ICA}(n), \tag{5}$$

where A_{ICA} is the mixing matrix of infomax, and s_{ICA} is the signal source of infomax. Hereafter, we refer to ICAq (q = 1, 2, 3, …, 204) as a specific component obtained after application of infomax. The number of principal components from the pre-whitening step that was passed to the ICA algorithm was 204, which corresponded with the number of sensor inputs. Accordingly, we obtained 204 components with associated time courses and spatial distributions.

Two Different Approaches (Subtraction and Weighted)

After applying the decomposition methods ($BSS_{T/k}$ and infomax) to the sensor space data, we obtained the MMR difference source waveform (i.e., $\bar{s}_{sub}$; **Figures 1B**, **2B**) in the same way as in the subtraction approach for sensor space analysis [subsection The Subtraction Approach; Eq. (1); **Figures 1A**, **2A**], which corresponds to the two decomposition methods (i.e., subtraction-$BSS_{T/k}$ and subtraction-infomax; **Figures 1B**, **2B**);

$$\bar{s}^{DC}_{sub}(n) := \bar{s}^{DC}_{dev}(n) - \bar{s}^{DC}_{std}(n), \tag{6}$$

$$\bar{s}^{ICA}_{sub}(n) := \bar{s}^{ICA}_{dev}(n) - \bar{s}^{ICA}_{std}(n), \tag{7}$$

where $\bar{s}_{std}(n)$ and $\bar{s}_{dev}(n)$ are the averaged source waveforms across epochs (i.e., ERFs) elicited by the standard and deviant stimulus, respectively, obtained from each decomposition method.

The novel method, the weighted-$BSS_{T/k}$, is expected to be a more sensitive approach of extracting the MMR. The basics of the method lie in the periodical arrangements and assignments of weights on the MMR time range. Although our $BSS_{T/k}$ method is expected to highlight periodic signals, the deviant epochs occur randomly, not periodically. To obtain periodical

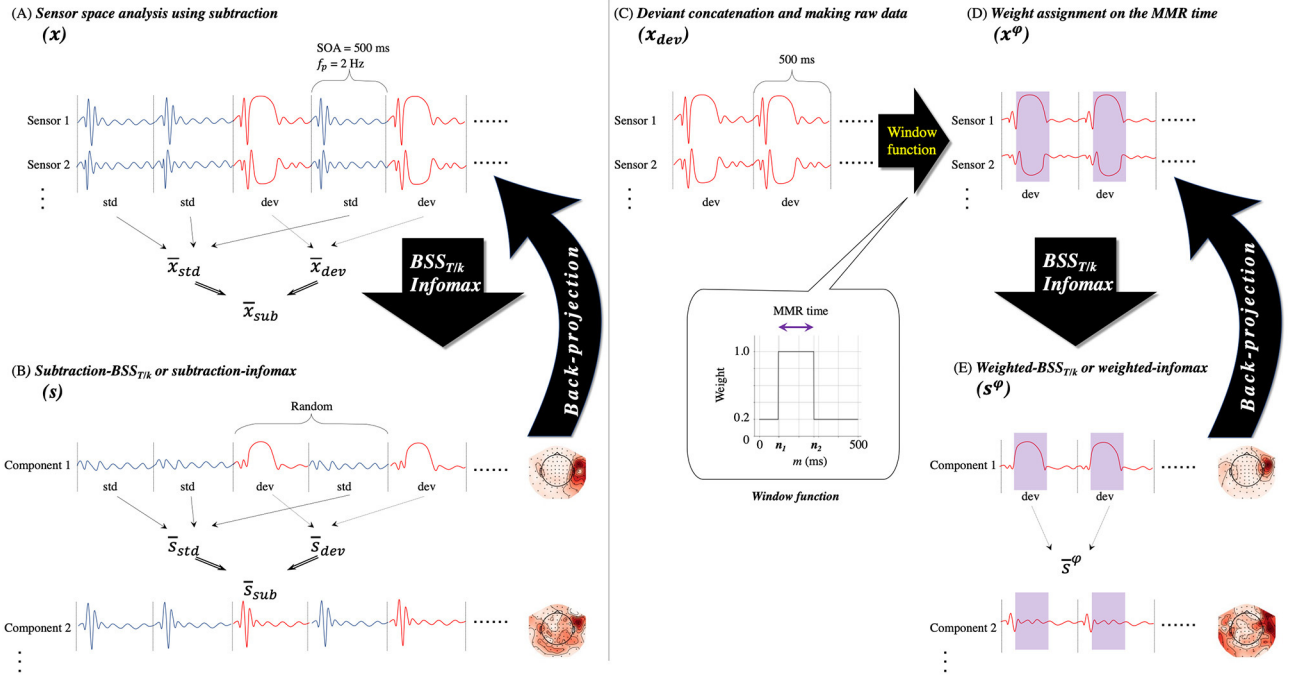

FIGURE 1 | Analysis steps. **(A)** The conventional subtraction approach for sensor space analysis. Sensor data (x) consist of standard (std) and deviant (dev) epochs. The MMR difference sensor waveform ($\overline{x}_{sub}$) is calculated by subtracting the event-related field (ERF) to the standard ($\overline{x}_{std}$) stimulus from the ERF to the deviant ($\overline{x}_{dev}$) stimulus. $BSS_{T/k}$, fractional type of decorrelation method; MMR, mismatch response; SOA, stimulus onset asynchrony; f_p, presentation rate of stimuli. **(B)** The subtraction approach with two decomposition methods ($BSS_{T/k}$ or infomax). Data from 204 sensors (x) are decomposed into 204 components (s). The subtraction approach is followed for each component; subtraction of the deviant ERF ($\overline{s}_{dev}$) from the standard ERF ($\overline{s}_{std}$) makes the MMR difference source waveform ($\overline{s}_{sub}$). Note that deviant epochs occur randomly, not periodically. **(C)** Deviant epochs of sensor data are concatenated and new raw data are made (x_{dev}). This process makes periodical arrangements of deviant epochs. **(D)** Sensor data (x^{φ}) are assigned with a weight on the MMR time (from n_1 to n_2, highlighted in purple shadows) on x_{dev} using a window function. The window function is shown in the inset figure. **(E)** Data with 204 sensors assigned with a weight (x^{φ}) are decomposed into 204 components (s^{φ}) with two decomposition methods. In each component, the ERF of the deviant epochs assigned with a weight is obtained ($\overline{s}^{\varphi}$). The inverted black arrows between A and B and between D and E represent the back-projection process in a group of several components.

arrangements, we concatenated the deviant epochs to form new raw data ($x_{dev}(n)$; **Figure 1C**). To highlight the MMR that was included in the deviant epochs, we then weighted the MMR time range (around 100–250 ms, from n_1 to n_2) defined by the spatio-temporal cluster permutation (subsection Spatio-Temporal Cluster Permutation to Define the MMR Time Ranges and Sensors or the Reference Standard), with the weight described by the window function of the rectangular window (inset between **Figures 1C,D**);

$$x^{\varphi}(n) := \varphi * x_{dev}(n), \tag{8}$$

where φ describes a window function and the * reflects its repeat operation. The segmentation of data (epoch number, mean 174.3 ± 19.6 [standard deviation]) was multiplied by the window function values. Equation (8) indicates,

$$\begin{cases} x^{\varphi}(n) = 1 \cdot x_{dev}(n), & n_1 \le m \le n_2, \\ x^{\varphi}(n) = 0.2 \cdot x_{dev}(n), & m < n_1,\ n_2 < m, \end{cases} \tag{9}$$

where $n = \left(Index\ of\ deviant\ epoch - 1\right) \cdot SOA + m$. Here, m is the given time point within every deviant epoch. Equation (8) indicates that this window function, Eq. (9), was applied repeatedly (**Figure 1D**, purple shadow) to the concatenated sensor data ($x_{dev}(n)$). We then applied the $BSS_{T/k}$ and infomax methods separately to the weighted data (weighted-$BSS_{T/k}$ and weighted-infomax; **Figure 1E**);

$$x^{\varphi}(n) = A^{\varphi}_{DC} s^{\varphi}_{DC}(n), \tag{10}$$

$$x^{\varphi}(n) = A^{\varphi}_{ICA} s^{\varphi}_{ICA}(n). \tag{11}$$

Finally, after lowpass filtering (30 Hz), we obtained the ERFs (i.e., $\overline{s}^{\varphi}$; **Figures 1E**, **2C**). That is, $\overline{s}^{\varphi}_{DC}(n)$ and $\overline{s}^{\varphi}_{ICA}(n)$, elicited by the weighted deviant stimulus, instead of subtraction.

Two assumptions underlie the successful decomposition of the weighted-$BSS_{T/k}$. First, the MMR occurs in the MMR time ($n_1 \le n \le n_2$) only in deviant epochs. Second, exogenous/obligatory ERFs (e.g., the M100) highly correlate with themselves in the non-MMR time ($n < n_1,\ n_2 < n$). The offset response of the M100 often intrudes on the MMR within the MMR time, which is one of the reasons why the subtraction approach is necessary (53). To minimize the joint M100 and MMR effect, a rectangular window in the non-MMR time is used to keep the correlation of the offset and onset of the M100 and extract these as distinct components from

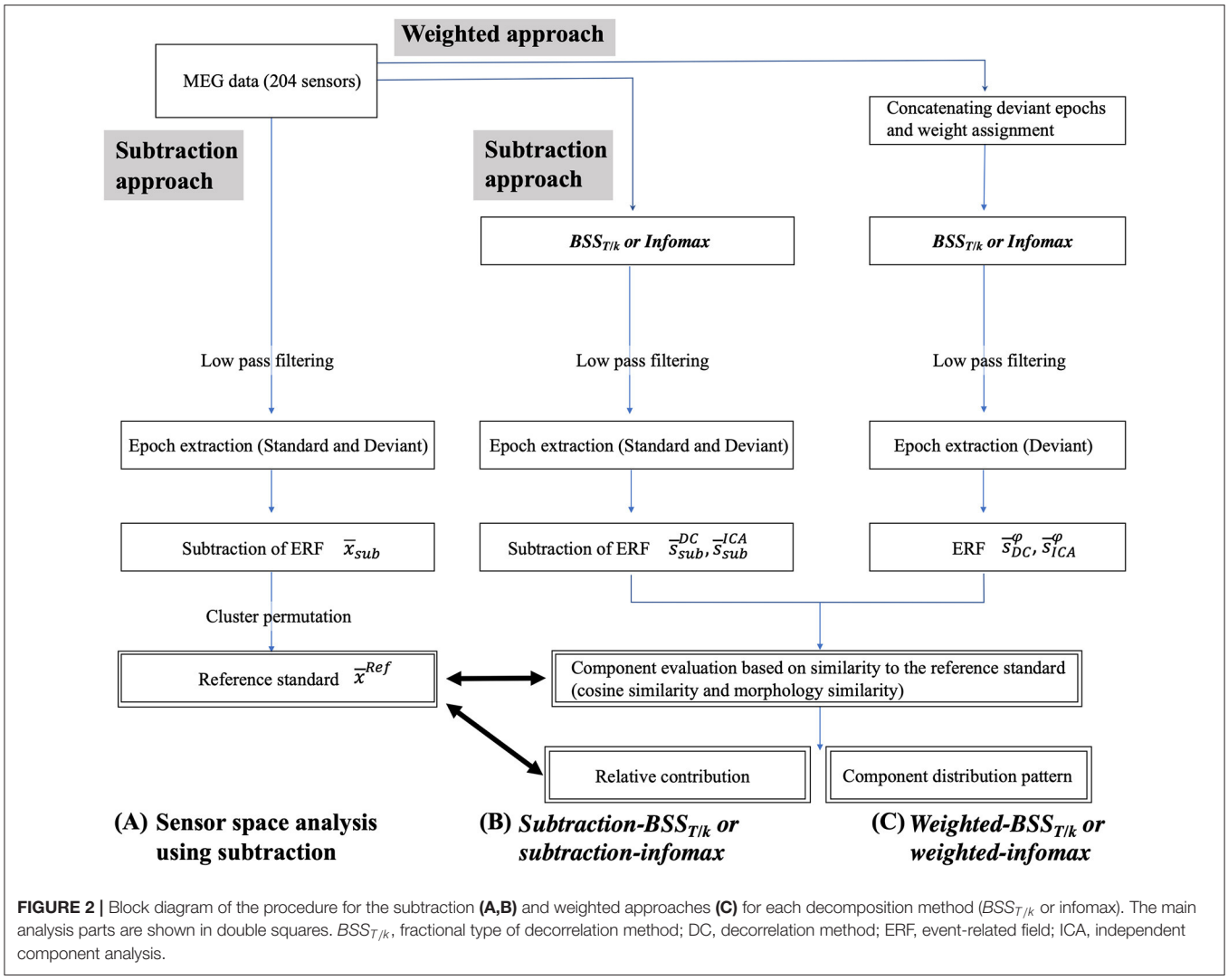

FIGURE 2 | Block diagram of the procedure for the subtraction **(A,B)** and weighted approaches **(C)** for each decomposition method (*BSS*$_{T/k}$ or infomax). The main analysis parts are shown in double squares. *BSS*$_{T/k}$, fractional type of decorrelation method; DC, decorrelation method; ERF, event-related field; ICA, independent component analysis.

an MMR component using weighted-*BSS*$_{T/k}$, which underlies time-delayed correlation. However, it is expected that weighted-infomax, in contrast to weighted-*BSS*$_{T/k}$, does not decompose the MMR effectively because infomax does not depend on time structure.

Spatio-Temporal Cluster Permutation to Define the MMR Time Ranges and Sensors or the Reference Standard

Currently, the only way to identify MMR is via sensor-space subtraction. We therefore used sensor-space subtraction as a reference standard. A data-driven approach was used to find significant MMR time ranges and sensors in all subjects. Among the 12 subjects, two did not exhibit a prominent MMR during the initial screening of the visual inspection of sensor space subtraction (confirmed by three independent inspectors, TMat, SK, and KK.) and were thus excluded from further analysis. Individual MMR difference sensor waveforms, $\bar{x}_{sub}$, were tested if they were different from 0 across the 10 subjects, with the multiple comparison problem being addressed using a cluster-level permutation test across space and time (54). We used 1,024 permutations, and the cluster-defining threshold was set at $p = 0.01$. Selected samples were clustered based on both spatial and temporal adjacency (i.e., spatio-temporal cluster permutation). Our motivation to use the spatio-temporal cluster permutation method was to verify the empirical knowledge that MMR occurs around 100–250 ms in the bilateral front-temporal sensors (7, 17) in a data-driven manner in our cohort of 10 subjects. **Figure 3A** demonstrates the results of the spatio-temporal cluster permutation. Six clusters (less than the critical alpha level of 0.05) were found. Among these six clusters, two (#1 and #2) contained temporal and/or frontal sensors within approximately 100–250 ms; one (#1) contained 20 left temporal sensors at 96–276 ms and the other (#2) contained 24 right front-temporal sensors at 105–266 ms. Thus, we defined the MMR time range

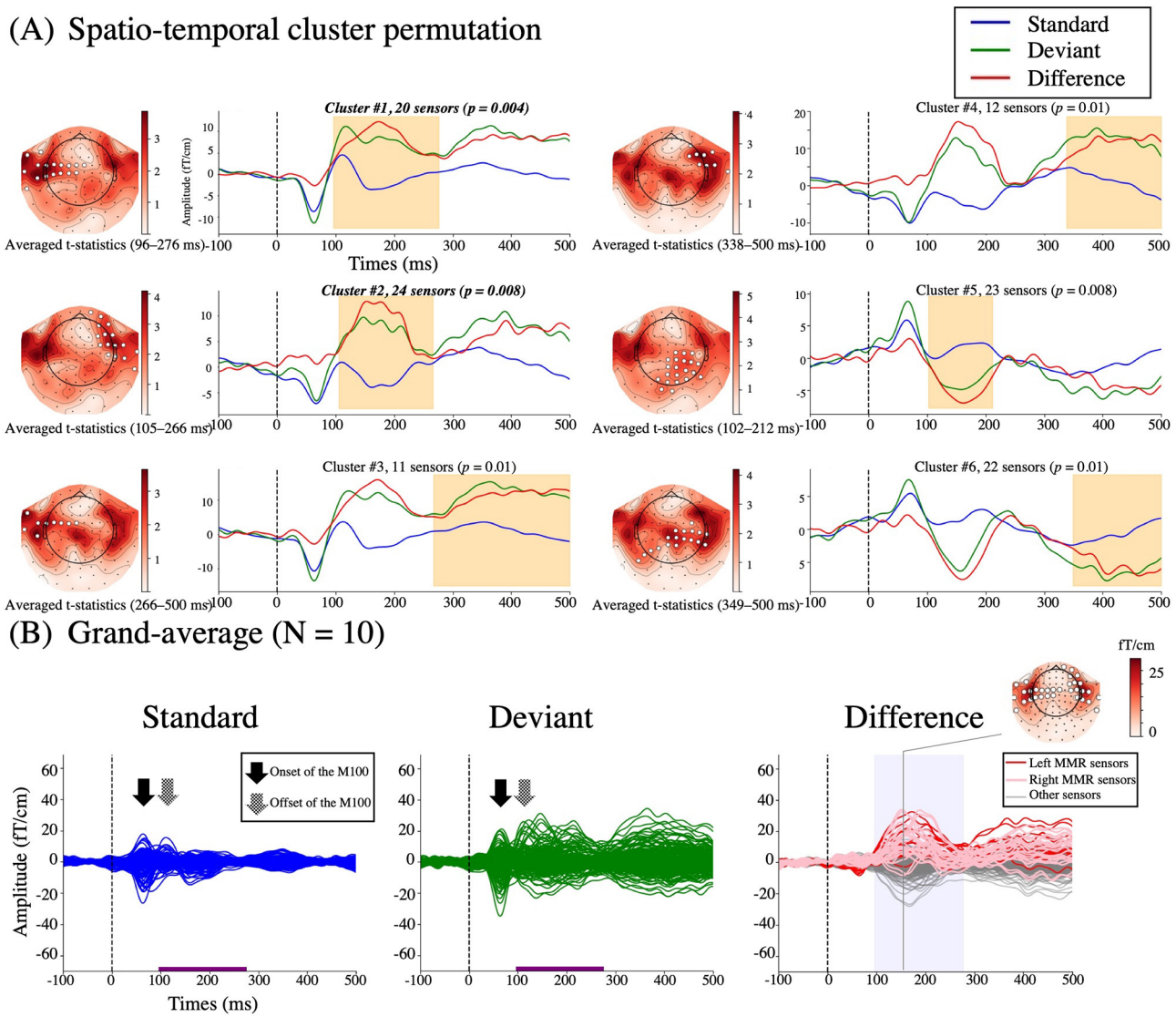

FIGURE 3 | Sensor space waveform. **(A)** The results of the spatio-temporal cluster permutation analysis. Six significant spatial and temporal clusters are shown in white circles within the averaged t-statistics (absolute value) and in orange shading within the averaged waveforms, respectively. Blue lines, standard; green lines, deviant; red lines, difference. **(B)** Grand-averaged ERFs elicited by standard ($\overline{x}_{std}$) and deviant ($\overline{x}_{dev}$) stimuli and the MMR difference sensor waveform ($\overline{x}_{sub}$) from 10 subjects. The MMR time is indicated by the purple line in the standard and deviant ERFs and by the blue shading in the MMR difference sensor waveform. The red and pink lines in the MMR difference sensor waveform represent the MMR sensors from the left and right clusters, respectively. The topographical map represents the peak activity in the bilateral temporal and right frontal sensors (white circles). The onset of the M100 (arrows) is outside of the MMR time range, whereas the offset of the M100 (textured arrows) is included in the MMR time range seen in standard and deviant responses.

as 96–276 ms ($n_1 = 96$, $n_2 = 276$) and the MMR sensors as these 44 sensors. The reference standard was defined individually (**Figure 2A**);

$$\overline{x}^{Ref} := F\overline{x}_{sub}(n), \quad n_1 \leq n \leq n_2, \tag{12}$$

where $\overline{x}^{Ref} \in \mathbb{R}^{L\times(n_2-n_1)}$ and $F \in \mathbb{R}^{L\times N}$ is the matrix that select $L = 44$ rows corresponding to the MMR sensors out of $\overline{x}_{sub}$ containing all $N = 204$ sensors. In other words, the reference standard was the 44 MMR sensors selected from the 204 gradiometers within the MMR time.

We confirmed that the different setting of the cluster-defining threshold ($p = 0.005$) gave the similar spatio-temporal clusters (**Supplementary Figure 2**). This means that the clusters obtained were robust.

Component Evaluation: Cosine Similarity

To investigate the resemblance of each component to the reference standard individually, or goodness of fit, we measured cosine similarity (C) as spatial similarity and morphology similarity (M) as temporal similarity.

Cosine similarity refers to the similarity between two column vectors (42, 55);

$$Cosine\ similarity\ (C):\ C\left(a(n),b\right)=\left|\hat{a}(n)^{T}\hat{b}\right|, n_1 \le n \le n_2, \tag{13}$$

where $\hat{a}(n) = a(n)/|a|$ is the normalized column vector containing the spatial distribution of the reference standard ($\bar{x}^{Ref}$), and $\hat{b} = b/|b|$ is a normalized column vector of A in Eqs. (3, 5, 10, and 11). The symbol T is the transpose of $\hat{a}(n)$. Because of its definition, $0 \le C\left(a\left(n\right),b\right) \le 1$. In the following, we used the maximum of C ($C_{\max}$) across the MMR time range for the four methods (i.e., subtraction-$BSS_{T/k}$, subtraction-infomax, weighted-$BSS_{T/k}$, and weighted-infomax), denoted by $C_{\max}^{DC}$, $C_{\max}^{ICA}$, $C_{\max}^{DC\_\varphi}$, and $C_{\max}^{ICA\_\varphi}$. $C_{\max}$ represents how maximally similar each component is to the reference standard in regard to spatial information.

Component Evaluation: Back-Projection and Morphology Similarity

Temporal similarity should include information about the temporal correlation between each component and the reference standard as well as the amplitude difference between each component and the reference standard. Because the components derived from $BSS_{T/k}$ and infomax ($M_{DC}(n)$, $M_{ICA}(n)$, $M_{DC}^{\varphi}(n)$, and $M_{ICA}^{\varphi}(n)$) are differently normalized, their ERFs cannot be directly compared according to their amplitudes. Thus, each component was projected back into the sensor space (back-projection) (56). Here, we assumed a general situation for the sake of the following subsection The Cumulative Back-Projection of Salient Components, the cumulative back-projection. When a group of q components, where Q = {q} is selected from 204 components,

$$x_{\#}^{q}(n) = A_{\#}^{q} s_{\#}^{q}(n) \tag{14}$$

provides back-projected data in the sensor space (inverted black arrow between **Figures 1A,B**), where $A_{\#}^{q} \in \mathbb{R}^{204\times q}$ and $s_{\#}^{q}(n)$ represents source vectors corresponding to Q. Here, the suffix symbol # indicates DC or ICA. The same formula was applied to the weighted data (inverted black arrow between **Figures 1D,E**). The ERF was then computed using the subtraction or weighted approach. For the subtraction approach, we applied

$$\bar{x}_{\#\_sub}\left(n,q\right) := \bar{x}_{\#\_dev}\left(n,\ q\right) - \bar{x}_{\#\_std}\left(n,\ q\right), \tag{15}$$

where $\bar{x}_{\#\_std}(n,q)$ and $\bar{x}_{\#\_dev}(n,q)$ are ERFs in the sensor space elicited by standard and deviant stimuli, respectively, obtained from each decomposition method (DC or ICA). For the weighted approach, $\bar{x}_{\#}^{\varphi}\left(n,q\right)$ is the ERF obtained from each decomposition method (DC or ICA). Then, corresponding to Eq. (12), we applied

$$\bar{x}_{\#\_sub}(q) := F\,\bar{x}_{\#\_sub}\left(n,q\right), \qquad n_1 \le n \le n_2, \tag{16}$$

$$\bar{x}_{\#}^{\varphi}(q) := F\,\bar{x}_{\#}^{\varphi}\left(n,q\right), \qquad n_1 \le n \le n_2, \tag{17}$$

where $\bar{x}_{\#\_sub}\left(q\right)$ and $\bar{x}_{\#}^{\varphi} \in \mathbb{R}^{L\times(n_2-n_1)}$.

We investigated the correlation between one sensor and the reference standard;

$$r_l = \frac{(X_l, Y_l)}{\|X_l\|\,\|Y_l\|}, l = 1, 2, 3, \ldots, 44. \tag{18}$$

where (X, Y) is the inner product. Here, X is one row vector (l) of the reference standard ($\bar{x}^{Ref}$), which corresponds to one sensor, and Y is one row vector (l) of the same sensor of Z, where $Z(q)$ is defined as Eq. (16) or Eq. (17). Notably, $\bar{x}_{\#\_sub}\left(n,\ q\right)$ and $\bar{x}_{\#}^{\varphi}\left(n,q\right) \in \mathbb{R}^{L\times SOA}$ and $Z(q) \in \mathbb{R}^{L\times(n_2-n_1)}$. Equation (18) is the same formula as that for the Pearson coefficient. Then,

$$Morphology\ similarity\ (M):\ r_l\,\|Y_l\| = \frac{(X_l, Y_l)}{\|X_l\|} l = 1, 2, 3, \ldots, 44. \tag{19}$$

was applied to calculate morphology similarity (M), where M is the comparison of the similarity of the waveforms between the reference standard and back-projected waveforms regarding the temporal correlation and amplitude in the given sensor. Among the 44 MMR sensors, we took the maximum of M ($M_{\max}$) across the MMR sensors for each method, denoted by $M_{\max}^{DC}$, $M_{\max}^{ICA}$, $M_{\max}^{DC\_\varphi}$, and $M_{\max}^{ICA\_\varphi}$. $M_{\max}$ refers to how maximally similar Q components are to the reference standard regarding temporal information when back-projected into the sensor space. Specifically, when one component was selected (q = 1), $M_{\max}$ represented the maximal temporal resemblance to the reference standard when the corresponding component was back-projected into the sensor space. Accordingly, the scatter plot of $C_{\max}$ and $M_{\max}$ shows the relationship between the spatial and temporal resemblance to the reference standard in each component.

Z-Score and Principal Component Analysis for the Component Distribution Pattern

Two-hundred and four components from each subject should be divided into several groups; MMR-related components ("salient component") and non-MMR-related components ("inconsequential component"). To classify components, each $M_{\max}$ and $C_{\max}$ value derived from all components from all methods ($204 \times 4 = 816$) were individually standardized (i.e., z-scored). Thus, the scatter plot of z-scored $M_{\max}$ and $C_{\max}$ reflected the component distribution pattern. For each method (subtraction-$BSS_{T/k}$, subtraction-infomax, weighted-$BSS_{T/k}$, and weighted-infomax), the component locations were classified into four quadrants (left upper [LU]; right upper [RU]; left lower [LL]; and right lower [RL]) by setting the z-score > 1.65 (90%) for both $M_{\max}$ and $C_{\max}$, with right referring to high $M_{\max}$ and upper referring to high $C_{\max}$. "Salient components" were defined individually in the LU, RU, and RL quadrants. A component in the RU quadrant may be a "major component" with a high contribution to the MMR, whereas a component in the LU quadrant, which has low $M_{\max}$ and high $C_{\max}$, is considered a "minor component" of the MMR; most of these components have either small amplitudes or low correlations with the reference standard. A component in the RL quadrant

TABLE 1 | Distribution patterns of the salient components.

	Number of salient components (Z-score > 1.65)	Number of salient components (Z-score > 1.96)	Z-scored M_{max} of the center	Z-scored C_{max} of the center	Slope of the first PCA component	Variance of the first PCA component
Subtraction-$BSS_{T/k}$ (± SD)	16.7 ± 2.8 (range, 3–16)	12.9 ± 2.3 (2–9)	3.1 ± 1.4	0.6 ± 0.4	0.29 ± 0.2	0.84 ± 0.07
Weighted-$BSS_{T/k}$ (± SD)	8.0 ± 4.4 (13–21)	5.3 ± 2.5 (10–17)	3.7 ± 1.4	1.6 ± 0.5	0.14 ± 0.1	0.94 ± 0.04
Subtraction-infomax (± SD)	36.0 ± 15.3 (16–37)	20.7 ± 8.2 (5–30)	0.8 ± 0.5	1.6 ± 0.7	−0.60 ± 0.4	0.84 ± 0.10
Weighted-infomax (± SD)	26.5 ± 7.5 (16–71)	15.0 ± 7.7 (10–33)	0.7 ± 0.5	1.6 ± 0.6	−0.60 ± 0.4	0.84 ± 0.10

$BSS_{T/k}$, T/k (fractional) type of decorrelation method; PCA, principal component analysis; SD, standard deviation.

may be a "pseudo-component" regarding the MMR, which suggests that the temporal resemblance is high only in a limited number of MMR sensors. This component may relate to a false (or network) or partial generator of MMRs. A component in the LL quadrant ("inconsequential component") means irrelevant regarding the MMR or is a component that is related to other ERFs or artifacts.

With successful decomposition, it is expected that only a few components will fall within the RU quadrant, and the rest of the components will fall within the LU, RL, and LL quadrants near the borderlines of coordinate origin. In contrast, unsuccessful decomposition will provide a component distribution pattern where no components fall within the RU quadrant, and all components will fall near the LL quadrant. To investigate the distribution pattern of the salient components, principal component analysis (PCA) was applied to z-scored $M_{\max}$ and $C_{\max}$. Two individual PCA components were obtained, with most of the variance being captured by the subspace of the first PCA component (more than 84%; **Table 1**). The center of the distribution of salient components, taken as the cross-point of the first and second PCA components, and the slope of the first PCA component were obtained.

If a z-score > 1.96 (95%) was set, the number of salient components was small (**Table 1**), especially in the weighted-$BSS_{T/k}$. PCA seemed unreliable when the input data were <5; thus, a z-score > 1.65 (90%) was applied.

The Cumulative Back-Projection of Salient Components

To investigate the contribution of each component to the MMR, components were cumulatively projected back into sensor space (subsection Component Evaluation: Back-Projection and Morphology Similarity), and the spatio-temporal resemblance was compared with the reference standard (subsections Component Evaluation: Cosine Similarity and Component Evaluation: Back-Projection and Morphology Similarity). It is expected that the more components that contribute to the MMR are cumulatively back-projected, the more the back-projected sensors resemble the reference standard. The order of cumulation was determined after sorting by the first PCA component axis (**Supplementary Figure 3**). Salient components were selected for cumulative back-projection because components below thresholds (inconsequential components in the LL quadrant) are expected to contribute little to the MMR. Corresponding to Eq. (19), M was investigated for the cumulative back-projection. The back-projected data in sensor space derived from more than two components have a dynamic topography over time, whereas those derived from one component have a fixed field distribution. Thus, in the cumulative back-projection, M was obtained for an average of 44 MMR sensors, not $M_{\max}$;

$$M_{ave} := mean(M). \tag{20}$$

Thus, M_{ave} represents both spatial and temporal information regarding the MMR, which reflects the average resemblance to the reference standard. Corresponding to each method, M_{ave} becomes M_{ave}^{DC}, M_{ave}^{ICA}, $M_{ave}^{DC\_\varphi}$, and $M_{ave}^{ICA\_\varphi}$.

Relative Contribution

The contribution of a salient component to the MMR or the reference standard is high if a prominent M_{ave} increment is observed when cumulatively reconstructing one salient component. Thus, the contribution of each component to MMR was defined as

$$Relative\ contribution\ (RC): \frac{M_{ave}(c) - M_{ave}(c-1)}{M_{ave}(q_{all})}, \quad c = 1, 2, \ldots, \#end. \tag{21}$$

where q_{all} means Q = {1, 2, 3, …, 204}, c represents an index number of the salient component according to the sorted order when cumulated (subsection The Cumulative Back-Projection of Salient Components), and *#end* is the index number of the last one. The denominator of Eq. (21) is M_{ave} when $q = q_{all}$ in Eq. (16), then

$$\begin{aligned} Z(q_{all}) &= F\overline{x}_{\#\_sub}(n, q_{all}), \quad n_1 \le n \le n_2, \\ &= \overline{x}^{Ref} \in \mathbb{R}^{L\times(n_2 - n_1)}. \end{aligned} \tag{22}$$

Thus, the denominator of Eq. (21) represents M_{ave} of the reference standard. Corresponding to each method, RC becomes RC^{DC}, RC^{ICA}, RC^{DC_φ}, and RC^{ICA_φ}.

As it is expected that *RC* will decrease as *c* increases, we applied the exponential function approximation to the plotted data in the *c*-*RC* plane;

$$y = \beta e^{-\alpha x}, \quad (23)$$

where x implies c, and y represents RC with coefficients α and β.

Statistics

To compare the component distribution patterns between the four methods, a two-way repeated-measures analysis of variance (rmANOVA) was used to analyze the center (z-scored $M_{\max}$ and z-scored $C_{\max}$, respectively), and slope of the first PCA component with within-subjects factors of APPROACH (subtraction vs. weighted) and DECOMPOSITION ($BSS_{T/k}$ vs. infomax). For the *post hoc* tests, multiple comparisons were performed using paired *t*-tests with Bonferroni correction. The significance level was set at $p < 0.05$.

We counted *c,* where the non-linear approximation reached the 5% threshold. It was assumed that components above the 5% threshold significantly contributed to the MMR and were defined as "dominant components," whereas those that did not meet the threshold did not contribute to the MMR.

RESULTS

The analysis comprised four parts (**Figure 2**, double squares): (i) defining the reference standard based on the spatio-temporal cluster permutation from the sensor-space analysis; (ii) qualitative evaluation of each component based on its similarity to the reference standard; (iii) statistical assessment of component distribution patterns with the z-scored scatter plot; and (iv) the relative contribution of each component.

Spatio-Temporal Cluster Permutation and Reference Standard

The results of the spatio-temporal cluster permutation are shown in **Figure 3A**. Among the six clusters, Clusters #1 and #2 (20 left temporal sensors at 96–276 ms with the alpha level of $p = 0.004$, 24 right front-temporal sensors at 105–266 ms with the alpha level of $p = 0.008$) were consistent with the empirical findings. On the other hand, Clusters #3, #4, and #6 contained the late latency and with lower alpha levels of $p = 0.01$. The Cluster #5 was at 102–212 ms mainly from parietal sensors with the alpha level of $p = 0.008$. Therefore, Clusters #1 and #2 were selected to define the reference standard (i.e., a selection of MMR sensors from 44 left temporal and right front-temporal sensors at an MMR time range of 96–276 ms).

Figure 3B represents the grand-averaged ERFs elicited by standard and deviant stimuli and the MMR difference sensor waveforms in sensor space ($\overline{x}_{sub}$). As indicated by the results of the cluster permutation (**Figure 3A** topographical map in Clusters #1 and #2), prominent activity occurred in the bilateral temporal and right frontal sensors at the peak latency (**Figure 3B** topographical map). Note that the offset of the M100 was included in the MMR time for both standard and deviant ERFs (textured arrows in **Figure 3B**).

Qualitative Evaluation of Each Component

Figure 4 represents the results of the decomposition together with the sensor space analysis of a representative subject (Subject 2). The resemblance of the reference standard (**Figure 4A**) from this subject was compared with each component from four methods (subtraction-$BSS_{T/k}$, weighted-$BSS_{T/k}$, subtraction-infomax, and weighted-infomax, in **Figure 4B**(i-iv), respectively). One component in the weighted-$BSS_{T/k}$ was discriminable with similar morphology [**Figure 4B**(ii) upper panel, red line, BSS107] and topographical map [**Figure 4B**(ii) right] to the reference standard of the peak time (**Figure 4A**, 140 ms). When this component was back-projected into the sensor space (**Figure 5**, red lines), the left and right temporal sensors (dotted areas) within MMR sensors at MMR time range closely represented the reference standard (blue lines). Accordingly, the corresponding component had discriminable $M_{\max}^{DC\_\varphi}$ and $C_{\max}^{DC\_\varphi}$ among other components in the scatter plot [**Figure 4B**(ii) lower panel, red arrow]. Moreover, this component showed a minor additional topographical representation in the left temporal sensors, which corresponded with the reference standard of 260 ms. No components were discriminable using the infomax methods [**Figure 4B**(iii, iv)]. The subtraction-$BSS_{T/k}$ [**Figure 4B**(i)] provided two components (red and green arrows) that had a moderate value of $M_{\max}^{DC}$ and $C_{\max}^{DC}$.

Scatter plots of $M_{\max}$ and $C_{\max}$ for each component are depicted for the four different methods for all subjects (**Figure 6A**). While most of components had lower $M_{\max}$ and $C_{\max}$ values in the four methods, in the weighted-$BSS_{T/k}$ [**Figure 6A**(ii)], one or a few components represented high $M_{\max}^{DC\_\varphi}$ and $C_{\max}^{DC\_\varphi}$ values individually. The z-scored plot shows the distribution of salient (MMR-related) and inconsequential (non-MMR-related) components according to the quadrants based on a 90% z-score (**Figure 6B**). The salient components were mostly located in the RU quadrant (major) in the weighted-$BSS_{T/k}$ [**Figure 6B**(ii)], whereas in the subtraction-$BSS_{T/k}$ [**Figure 6B**(i)], they were equally distributed between the RU (major) and RL (pseudo) quadrants. The two infomax methods [**Figure 6B**(iii and iv)] had salient components mostly in the LU (minor) or RL (pseudo) quadrants. Most components are inconsequential components in all four methods (the numbers of salient components are shown in **Table 1**).

Statistical Assessment of the Component Distribution Pattern

The component distribution patterns of these salient components (major, minor and pseudo) were further investigated using PCA. The averaged center of the distribution of the salient components and the first PCA component are superimposed on the z-scored plots of salient components in **Figure 7** (individual plots are shown in **Supplementary Figure 3**). The average z-scored $M_{\max}$, $C_{\max}$, and slope for the four methods were 3.1 ± 1.4, 0.6 ± 0.4, and 0.29 ± 0.2, respectively, for subtraction-$BSS_{T/k}$ [**Figure 7**(i)], 3.7 ± 1.4, 1.6 ± 0.5, and 0.14 ± 0.1, respectively, for weighted-$BSS_{T/k}$ [**Figure 7**(ii)], 0.8 ± 0.5, 1.6 ± 0.7, and -0.60 ± 0.4, respectively, for subtraction-infomax [**Figure 7**(iii)], and $0.7 \pm$

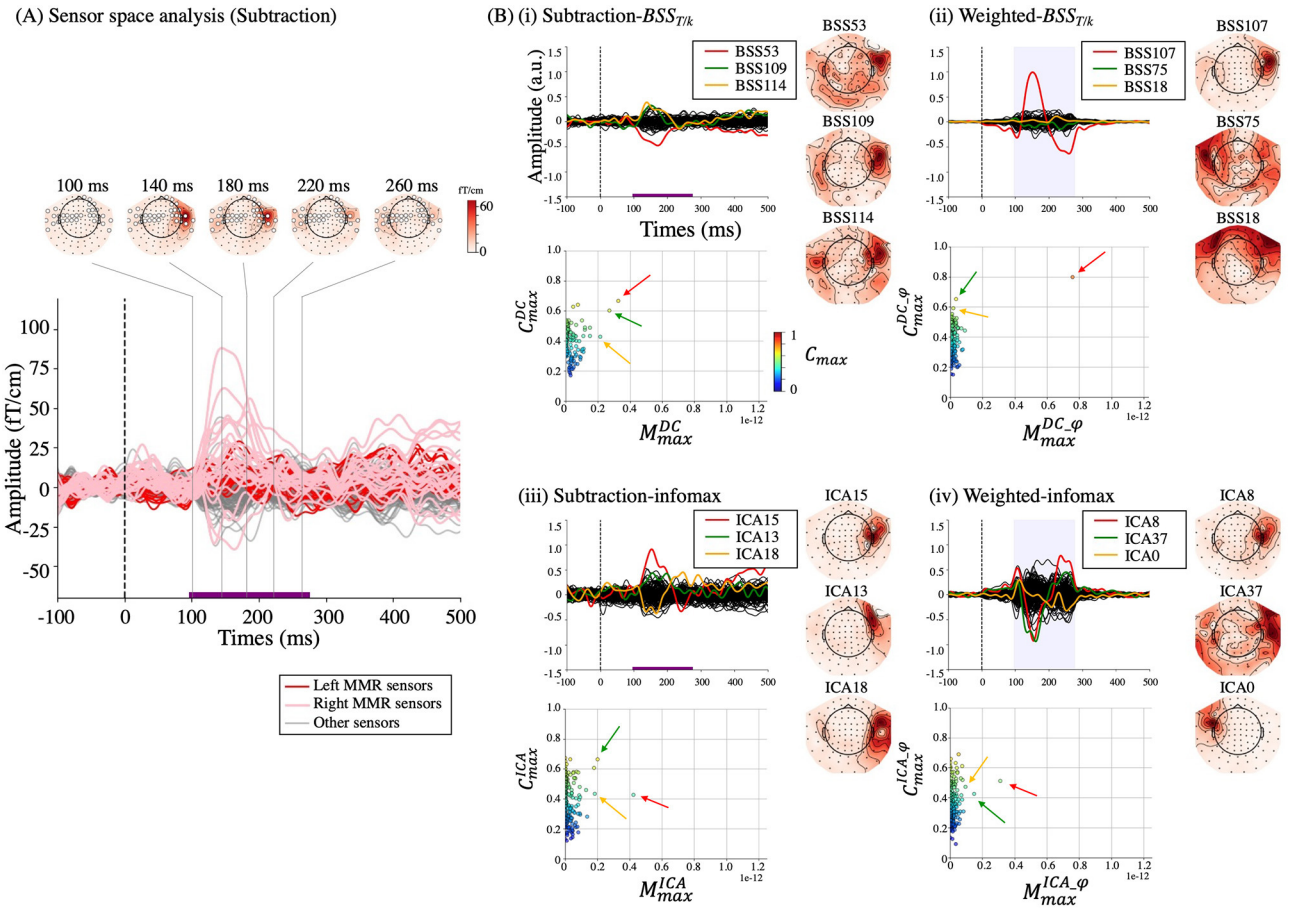

FIGURE 4 | Results from Subject 2. **(A)** Sensor space analysis using subtraction. Red and pink lines from MMR sensors (white circles) within the MMR time (purple line) refer to the reference standard. Decomposition results are shown in **(B)** (i), (ii), (iii), and (iv) for subtraction-$BSS_{T/k}$, weighted-$BSS_{T/k}$, subtraction-infomax, and weighted-infomax, respectively. Upper panels: source waveforms ($\overline{s}_{sub}$ *or* $\overline{s}^{\varphi}$), lower panels: scatter plots of $M_{\max}$ and $C_{\max}$ for each component. The color map in the scatter plot indicates the value of $C_{\max}$ (from 0 to 1). In each decomposition result, three components are depicted in different colors (red, green, and yellow) with their corresponding topographical maps. In the scatter plots, the arrows with the same color correspond to the components. These components were selected based on the order of cumulation of the first three components (see subsection The Cumulative Back-Projection of Salient Components). Hereafter, the topographical map takes an arbitrary unit due to matrix A in Eq. (2).

0.5, 1.6 ± 0.6, and −0.60 ± 0.4, respectively, for weighted-infomax [**Figure 7**(iv); **Table 1**].

The rmANOVA results of the z-scored $M_{\max}$ of the center (**Figure 8A**) revealed a significant main effect of DECOMPOSITION [$F_{(1,9)} = 76.9$, $p < 0.001$], which indicated that the z-scored $M_{\max}$ in both $BSS_{T/k}$ methods was significantly larger than that in both infomax methods. There was no significant interaction between APPROACH and DECOMPOSITION [$F_{(1,9)} = 2.7$, $p = 0.1$] or main effect of APPROACH [$F_{(1,9)} = 0.9$, $p = 0.4$]. These results suggested that the salient components of both $BSS_{T/k}$ methods were located in the right quadrant, whereas those of both infomax methods were located in the left quadrant.

The rmANOVA results of the z-scored $C_{\max}$ of the center (**Figure 8A**) revealed a significant interaction between APPROACH and DECOMPOSITION [$F_{(1,9)} = 60.4$, $p < 0.001$] and significant main effects of APPROACH [$F_{(1,9)} = 40.2$, $p < 0.001$] and DECOMPOSITION [$F_{(1,9)} = 9.7$, $p < 0.01$]. The *post hoc* analysis revealed that the z-scored $C_{\max}$ of subtraction-$BSS_{T/k}$ was significantly lower than that of weighted-$BSS_{T/k}$ and those of both infomax methods (weighted-$BSS_{T/k}$, $p < 0.0001$; weighted-infomax, $p < 0.0005$; subtraction-infomax, $p < 0.001$). These results suggested that the salient components of the weighted-$BSS_{T/k}$ and both infomax methods were located at the border between the upper and lower quadrants, whereas those of the subtraction-$BSS_{T/k}$ were located in the lower quadrant.

The rmANOVA results of the slope of the first PCA component (**Figure 8B**) revealed a significant main effect of DECOMPOSITION [$F_{(1,9)} = 65.5$, $p < 0.001$], which indicated that the slope in both $BSS_{T/k}$ methods was significantly larger than that in both infomax methods. There was no significant interaction between APPROACH and DECOMPOSITION [$F_{(1,9)} = 0.2$, $p = 0.6$] and no main effect of APPROACH [$F_{(1,9)}$

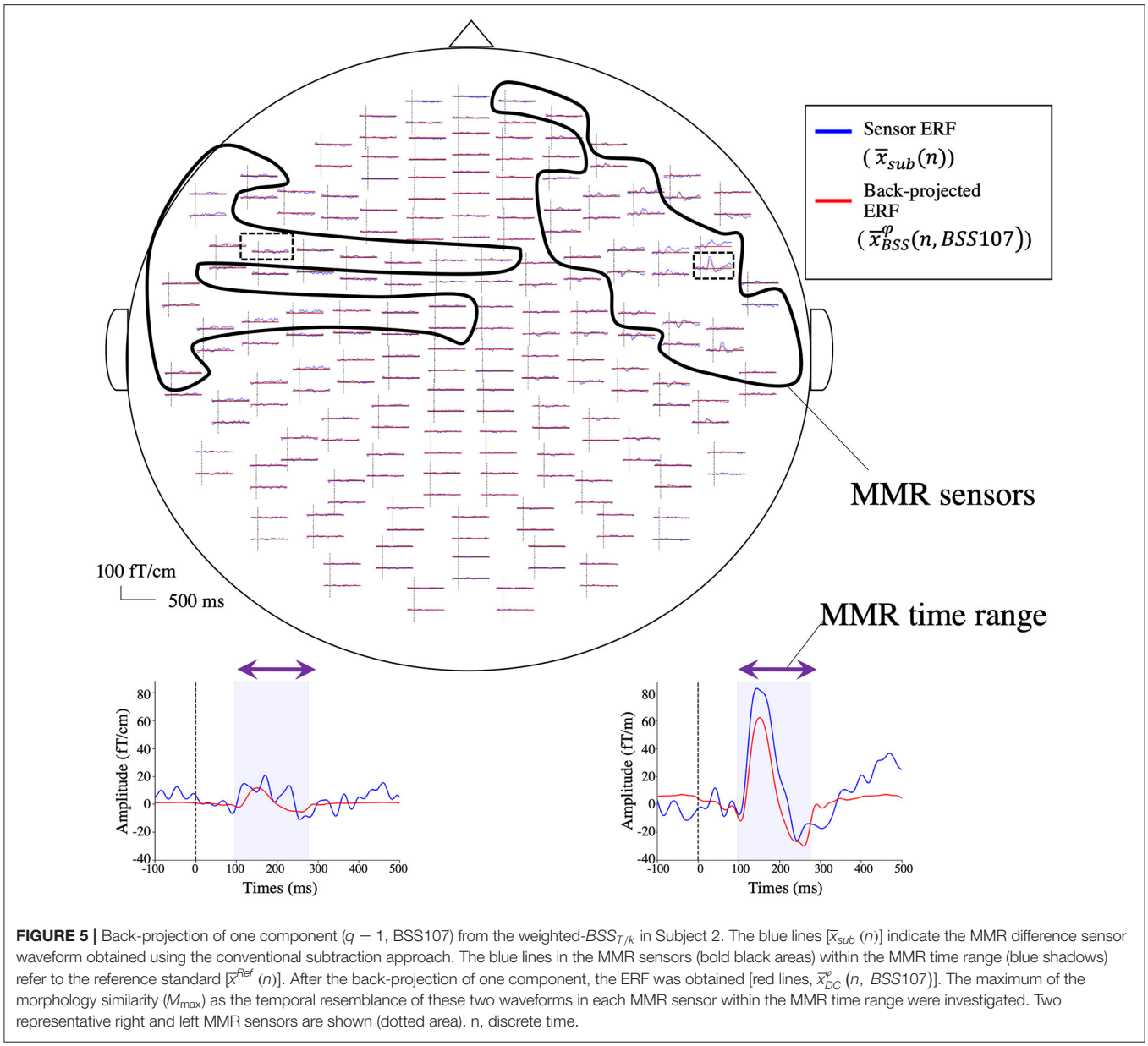

FIGURE 5 | Back-projection of one component ($q = 1$, BSS107) from the weighted-$BSS_{T/k}$ in Subject 2. The blue lines [$\overline{x}_{sub}$ (n)] indicate the MMR difference sensor waveform obtained using the conventional subtraction approach. The blue lines in the MMR sensors (bold black areas) within the MMR time range (blue shadows) refer to the reference standard [$\overline{x}^{Ref}$ (n)]. After the back-projection of one component, the ERF was obtained [red lines, $\overline{x}^{\varphi}_{DC}$ (n, $BSS107$)]. The maximum of the morphology similarity (M_{max}) as the temporal resemblance of these two waveforms in each MMR sensor within the MMR time range were investigated. Two representative right and left MMR sensors are shown (dotted area). n, discrete time.

$= 2.4$, $p = 0.2$]. These results indicated that the locations of the salient components in both $BSS_{T/k}$ methods had positive spatio-temporal correlations regarding the MMR (i.e., the slope had a positive value), whereas those of both infomax methods had negative correlations (i.e., the slope had a negative value).

In conclusion, the distribution of the salient components was mostly in the RU quadrant (major) with weighted-$BSS_{T/k}$ [**Figures 6B**(ii), **7**(ii)], the RL quadrant (pseudo) with subtraction-$BSS_{T/k}$ [**Figures 6B**(i), **7**(i)], and the LU (minor) or RL (pseudo) quadrants with the two infomax methods [**Figures 6B**(iii and iv), **7**(iii and iv)]. Both $BSS_{T/k}$ methods [**Figures 6B**(i and ii), **7**(i and ii)] showed positive spatio-temporal correlations while both infomax methods showed negative correlations [**Figures 6B**(iii and iv), **7**(iii and iv)].

The Cumulative Back-Projection and Relative Contribution

Figure 9 shows the results of M_{ave} after cumulative back-projection in a representative subject (Subject 2). The curvature of the weighted-$BSS_{T/k}$ [**Figure 9**(ii)] was steep in the first component ($c = 1$, red arrow, corresponding to BSS107), which suggested that in the weighted-$BSS_{T/k}$, only one component contributed highly to the MMR. Note that this component was a major component localized on the RU quadrant [**Figure 6B**(ii)]. On a contrary, other components represent a minimal increase in M_{ave} [e.g., green and yellow arrows from weighted-$BSS_{T/k}$ in **Figure 9**(ii) or all three arrows from two infomax methods in **Figure 9**(iii and iv)]. These were either pseudo- or minor components (**Figure 6B**). In

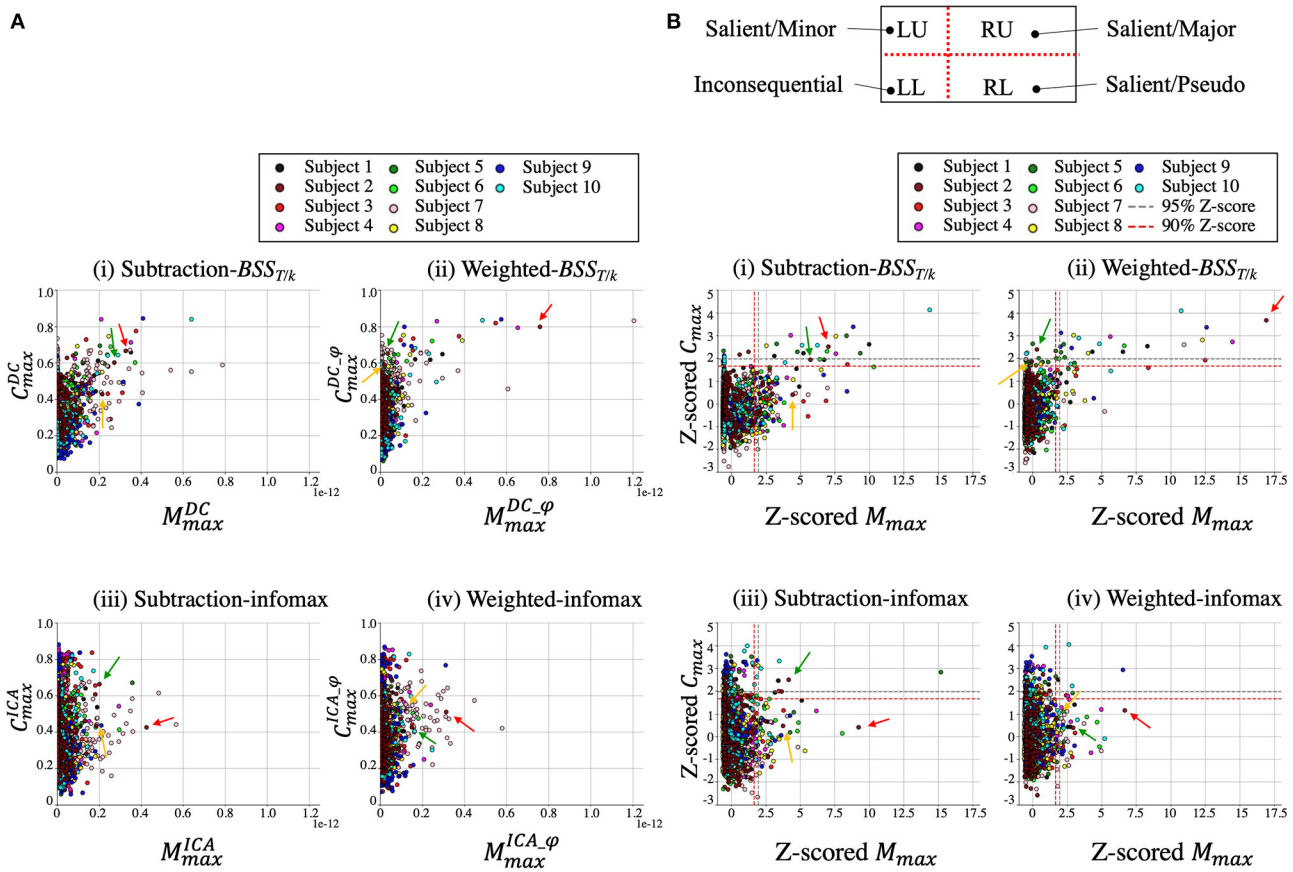

FIGURE 6 | Scatter plots of M_{max} and C_{max} for each component in the four methods for all subjects **(A)**. Z-scored scatter plots represent the distribution pattern of salient and inconsequential components **(B)**. The four quadrants are divided by red dotted lines (z-score > 1.65 [90%]). Red, green and yellow arrows indicate the corresponding components from Subject 2 in **Figure 4**.

addition, it is notable that the third component of subtraction-infomax [**Figure 9**(iii), yellow arrow, corresponding to pseudo-component in **Figure 6B**(iii)] negatively contributed to the MMR. Moreover, the first component of subtraction-$BSS_{T/k}$ [**Figure 9**(i), red arrow] showed a mild increment in M_{ave}, which corresponds to this component being classified as a major component in **Figure 6B**(i).

Supplementary Figure 4 shows the *RC* lines (upper panels) together with their approximate lines (lower panels) in individual subjects. In Subject 2, the approximate lines of the weighted-$BSS_{T/k}$ show that the first component (red arrow) represented a contribution as high as 30%, whereas later components (green and yellow arrows) provided much lower contributions. We counted *c*, where the non-linear approximation reached the 5% threshold (gray dotted lines; i.e., the dominant components). The number of dominant components is shown in **Table 2**. In the weighted-$BSS_{T/k}$, 1–3 components significantly contributed to the MMR, except for one subject (Subject 5). In the subtraction-$BSS_{T/k}$, 2–6 components contributed to the MMR. The two infomax methods had few components that significantly contributed to the MMR. These results indicated that one or a few dominant components contributed to the MMR in weighted-$BSS_{T/k}$, whereas no components represented the MMR in infomax.

DISCUSSION

In the current multi-channel MEG study, we demonstrated that our novel weighted-$BSS_{T/k}$ method using only deviant epochs (deviant concatenation) could extract an MMR confined to one or a few dominant components (**Figures 4**, **6**, **9**, **Supplementary Figure 4**, and **Table 2**). In the subtraction-$BSS_{T/k}$/weighted-$BSS_{T/k}$, the salient components showed positive spatio-temporal correlations with the MMR (**Figures 7**, **8**, and **Supplementary Figure 3**). However, ICA decomposed the MMR into an assembly of minor or pseudo components with negative spatio-temporal correlations. Specifically, our method avoids having to use the conventional subtraction approach to reveal the MMR. Our method may help with the use of the MMR in basic and clinical research.

The Conventional Subtraction Approach to Reveal the MMR

The MMR has been widely used in many fields of human neuroscience (10, 15, 16). Conventionally, the subtraction approach was needed to extract the MMR from other auditory ERP/ERF. However, there are several problems with such a method, which include increased noise and the inability to exclude neural adaptation. Several approaches have been

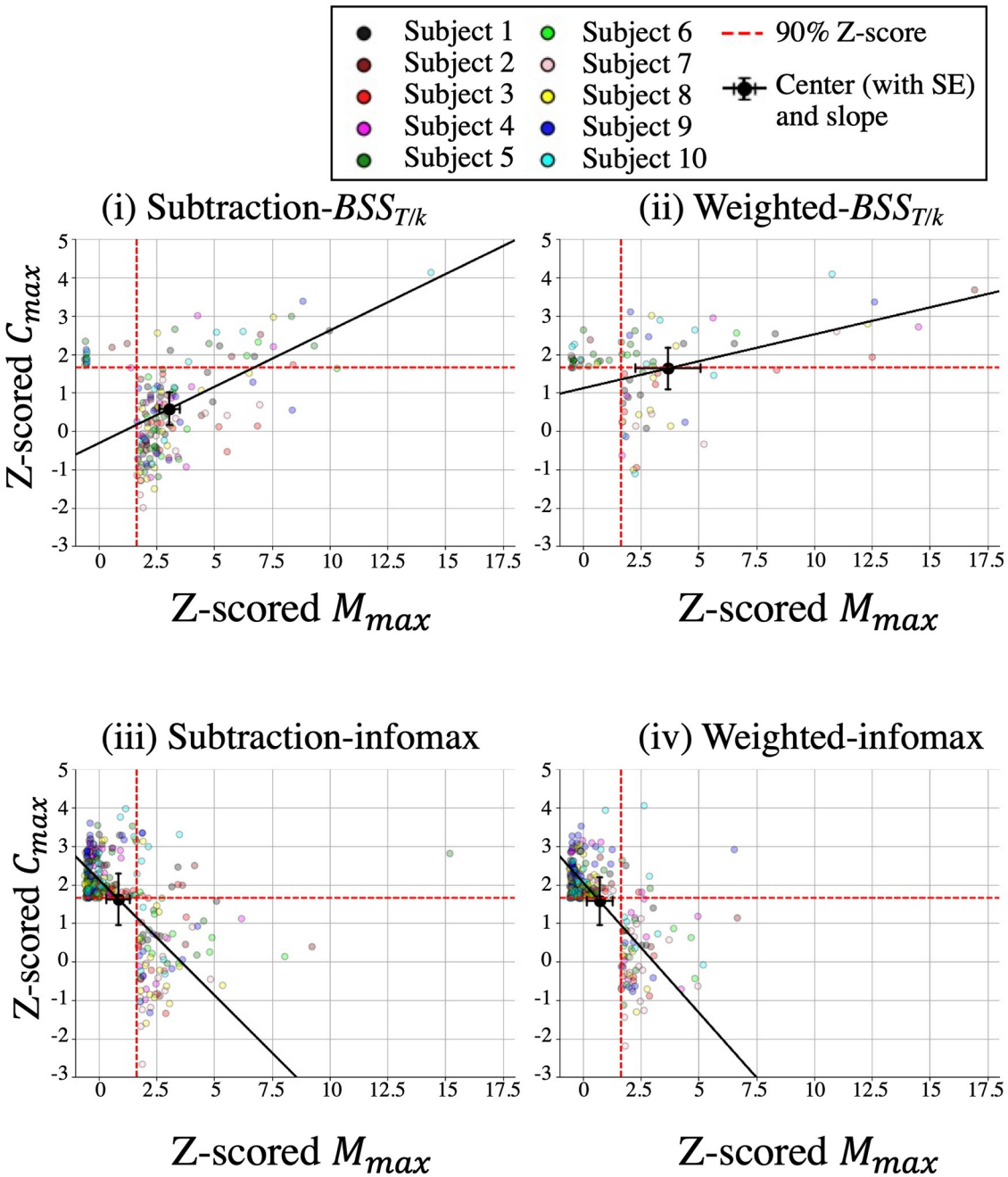

FIGURE 7 | The averaged center of the distribution of the salient components and the slope of the first PCA component superimposed onto the z-scored plots of the salient components. Red dotted lines indicate z-scores > 1.65 (90%). Error bars indicate standard errors (SE).

proposed to avoid the neural adaptation problem (53, 57); however, all such approaches depend on subtraction. Our novel approach avoids subtraction. In general, the MMR is a relative component because a common response is included in standard and deviant ERFs, and the MMR is then defined as the difference waveform based on the original theory underlying the MMR (i.e., the memory-comparison process). The MMR should be present in deviant epochs but not in standard epochs. Thus, only deviant epochs are needed for its decomposition.

Periodical Arrangements and Weight Assignments

We made two assumptions underlying the successful decomposition of the weighted-$BSS_{T/k}$: (1) The MMR occurs periodically within a specific time range (i.e., the MMR time

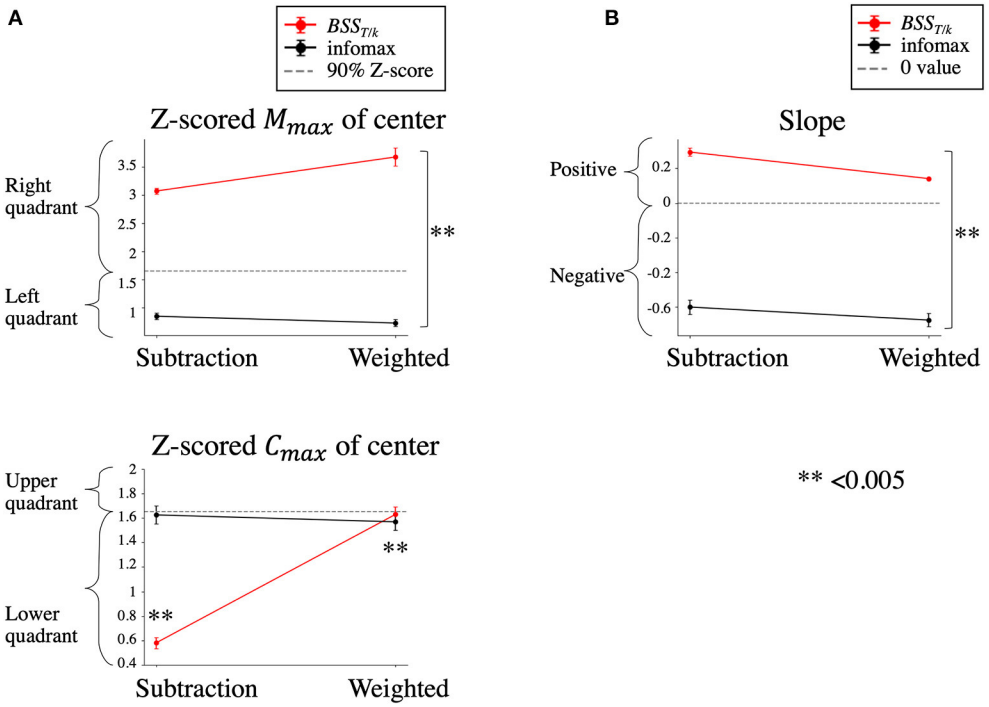

FIGURE 8 | Z-scored M_{max} of the center **(A)** (upper panel), z-scored C_{max} of the center **(A)** (lower panel), and the slope of the first PCA component **(B)**. Error bars indicate standard errors. See **Table 1** for each value. ** < 0.005.

range) and in the deviant epochs; (2) Exogenous/obligatory ERFs highly correlate with themselves in the non-MMR time. Originally, $BSS_{T/k}$ was expected to highlight periodic signals using T (35–38). The MMR time range (96–276 ms) was defined according to the spatio-temporal cluster permutation analysis, which was assumed to reveal the statistically significant time range in which the MMR occurs. Both the offset response of the M100 and the MMR fall into this time range, whereas the onset response of the M100 occurs outside of the time range (**Figure 3B**). Assigning a weight to this time range may minimize the joint M100 and MMR effect. The weighting emphasizes the target response (i.e., the MMR) within the window, whereas the response outside the window (i.e., the onset of the M100) takes away the response (i.e., the offset of the M100) if they are highly correlated. Analogous to the subtraction approach (as subtraction separates such responses by subtracting deviant responses from standard responses), the weight assignment on a specific time range may differentiate the MMR from other responses. **Supplementary Data (2-1)** and **Supplementary Figure 5** support our assumptions; the assignment of the weight outside the M100 in the standard epochs did not result in the extraction of remarkable components that represent the M100 (**Supplementary Figure 5B**).

Significance of our Approach

We obtained four main findings. First, the weighted-$BSS_{T/k}$ decomposed one or a few components (< 3) that manifested the MMR among the many components obtained from multi-channel data (**Figures 4**, **6**, **9**, **Supplementary Figure 4**, and **Table 2**). We refer to this decomposition result as specification. Multi-channel recordings of electromagnetic fields emerging from neural currents in the brain generate large amounts of data (28). Thus, this specification makes interpretation and comparisons among groups easier. Our primary aim was to extract MMR in a few dominant components. The dominant component was the component that had the most discriminable M_{max} and C_{max}, and thus, it contributed most highly to the MMR (**Figure 9**, **Supplementary Figure 4**, and **Table 2**). We do not assume that the dominant component manifests a single MMR source; instead, it may represent the network or a series of MMR sources (**Figure 4**). Other irrelevant activities were redistributed among the remaining components. Since our method ($BSS_{T/k}$) depends on the theory that utilized correlations between components instead of strong independence (i.e., ICA), it would result in extracting components with keeping physiological correlation that may represent several generators or network of MMR. If bitemporal and frontal MMR sources are highly correlated, with a certain delay, these sources should be extracted in a few components using our time-delayed correlation method. Indeed, it is known that these sources have separate temporal dynamics (58) but interact with each other (59). In contrast, it is difficult to identify any dominant components using ICA, where each extracted component represents one or two dipolar sources. This is discussed in the following section.

Second, the decomposed components revealed positive spatio-temporal correlations regarding the MMR, and the center of the distribution of the salient components was in the RU

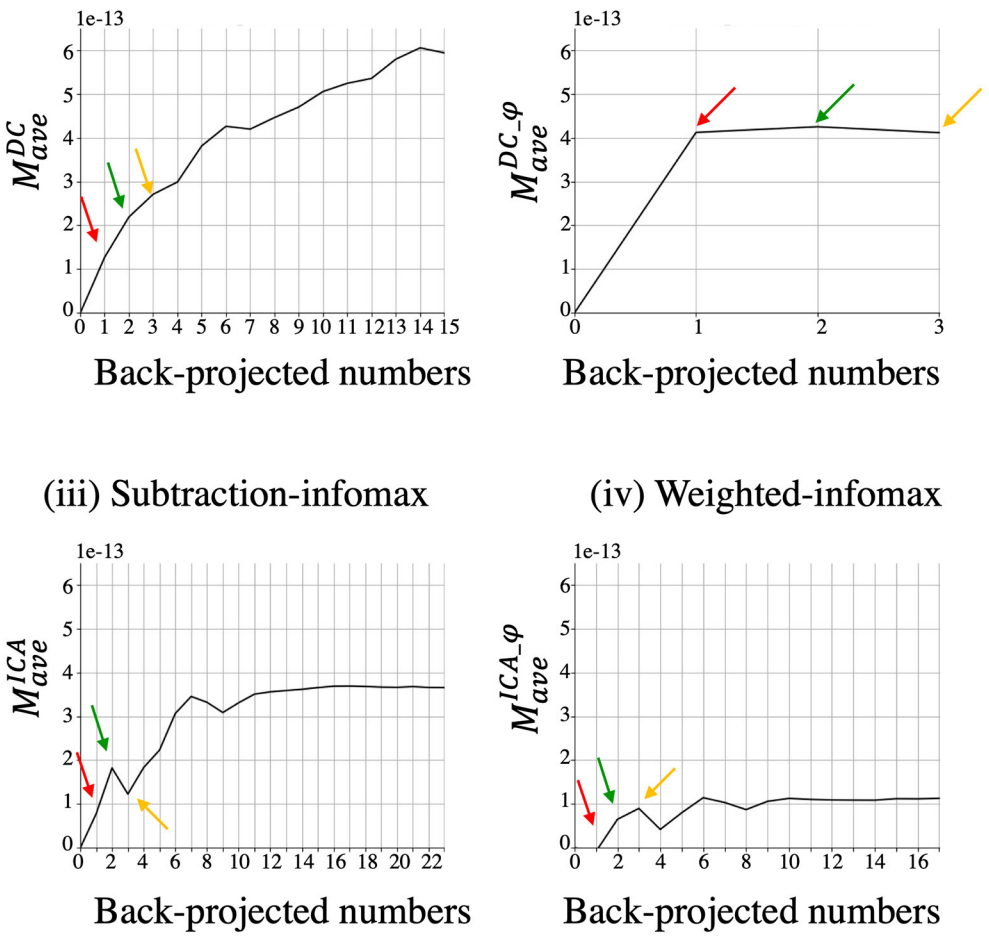

FIGURE 9 | The cumulative back-projection and result of M_{ave} for the four methods in one subject (Subject 2). The order of cumulation is determined after sorting by the first PCA component axis (**Supplementary Figure 3**). The number of components reconstructed depended on the number of salient components. Red, green and yellow arrows indicate the corresponding components from Subject 2 in **Figure 4**.

(major) quadrant (**Figures 6–8**, **Supplementary Figure 3**, and **Table 1**). According to Eq. (2), the decomposed component contains the mixing matrix (spatial) and signal source (temporal). A positive spatio-temporal correlation in the decomposed component suggests that the component is physiologically meaningful (9). In turn, with a positive spatio-temporal correlation, a component that shows the most similar morphology regarding the MMR also has the most similar topography regarding the MMR. This relationship is particularly important when targeting the response with an unknown generator source. The temporal information can be mutually applicable to the detection of the target, without a priori knowledge of its precise generator. For example, in **Figure 4B**(ii), if the MMR topography is unknown, BSS107 can be selected as the MMR component based on its discriminable amplitude.

Third, each component was obtained from individual data and the results were statistically significant. This indicated that weighted-$BSS_{T/k}$ is generally applicable to individual subjects, unlike group-ICA.

Fourth, a new cohort from subjects with low SNR in the sensor-space analysis regarding MMR (subsection Spatio-Temporal Cluster Permutation to Define the MMR Time Ranges and Sensors or the Reference Standard) demonstrated a few MMR-related components in weighted-$BSS_{T/k}$ when the same MMR time range was used for the weight assignment [**Supplementary Data (2-2)** and **Supplementary Figure 6**]. This MMR time range was independently determined in this cohort. These results may indicate that the generous setting of the weight time range can be available as long as the crucial time range is covered.

Based on these results, the application of our approach provides potential benefits that the sensor-space subtraction method does not, despite its status as the current gold standard for revealing MMR. Our single-trial, contrast-free approach would minimize the effect of refractoriness and

TABLE 2 | Numbers of dominant components.

Subject No.	Subtraction-$BSS_{T/k}$	Weighted-$BSS_{T/k}$	Subtraction-infomax	Weighted-infomax
Subject 1	5	2	None	None
Subject 2	3	1	1	None
Subject 3	6	3	None	None
Subject 4	2	2	None	1
Subject 5	3	None	None	None
Subject 6	3	1	2	None
Subject 7	4	2	None	None
Subject 8	5	3	None	None
Subject 9	4	1	None	1
Subject 10	4	3	None	None

$BSS_{T/k}$, T/k (fractional) type of decorrelation method.

maximize the temporal information underlying the neural mechanism of MMR. Our approach would therefore provide a new approach toward investigating further insights into the physiology of MMR.

Comparison With ICA

Both ICA methods (subtraction- and weighted-infomax) consisted of a collection of minor or pseudo components (**Figures 4**, **6**, **9**, **Supplementary Figure 4**, and **Table 2**). Most components were located in the LU (minor) or RL (pseudo) quadrants (**Figures 6–8** and **Table 1**). The slope of the first PCA component showed a negative spatio-temporal correlation (**Figures 7**, **8**, **Supplementary Figure 3**, and **Table 1**). There were no dominant components that manifested the MMR in either of the ICA methods (**Table 2**). The decomposition method in ICA is based on stochastic properties and does not depend on the time structure; thus, spatio-temporal dissociations may occur (34). Several papers have reported successful decomposition of the MMR using ICA (9, 25, 60–64); however, most results were derived from oligo-channel recordings. When the number of sensors/channels sensing the MMR is relatively small, the MMR can be extracted by one or a few components. However, such specification in multi-channel data is rarely shown in ICA studies because a greater number of channels results in poorer estimation accuracy of the components (25). If we assume fewer numbers of sources (e.g., tens) but use larger numbers (204) of sensors for ICA decomposition, the components of interest will likely be (i) split into sub-components and (ii) located where the SNR of each component is reduced. This is consistent with our previous work where ICA decomposition showed fragments of interictal epileptiform discharges from a single epileptogenic zone (42). Furthermore, most ICA studies are based on cluster analysis (e.g., group-ICA), not individual analysis. Generalization of the application of ICA to the MMR was not demonstrated in these studies.

Lastly, although subtraction-$BSS_{T/k}$ follows the conventional subtraction approach, it performed better than the two ICA methods, especially the subtraction-infomax. The center of the distribution of the salient components was in the RL quadrant (pseudo), yet it maintained a positive spatio-temporal correlation (**Figures 6–8**, **Supplementary Figure 3**, and **Table 1**). A possible interpretation of these findings is that these components may represent the partial generators of MMR sensors. The difference between subtraction-$BSS_{T/k}$ and subtraction-infomax may explain the theoretical difference between $BSS_{T/k}$ and infomax (time-delayed correlation vs. strong independence). The decomposition of the subtraction-$BSS_{T/k}$ was less successful than that of the weighted-$BSS_{T/k}$. There were more dominant components (< 6; **Table 2**) in the subtraction-$BSS_{T/k}$ than there were in the weighted-$BSS_{T/k}$. From the viewpoint of specification, fewer dominant components are desired. In conclusion, both $BSS_{T/k}$ methods, which use time structure, performed well in extracting the MMR; however, the weighted approach was the most sensitive.

Future Perspectives

The current study aimed to extract the MMR as a distinct component using a combination of the periodical arrangement and assignment of a weight. The specific effect of each technique should be investigated in a future study, which may help achieve a better understanding of the physiology of the MMR.

Because there was no confidence in terms of source localization of extracted components, although there are several ICA and SOBI studies (9, 32, 41), this view may provide potential benefits given that components may encompass several sources or networks of MMR. This should be investigated in future studies.

Our method is not dependent on the number of components. Our motivation was not to apply dimension reduction to maximize the multi-channel MEG data. However, the application of our method to different numbers of sensors, different MEG systems, or another type of sensor (magnetometer) is an interesting but open question. Theoretically, our weighted method can possibly be applied to any clinical neurophysiology data to investigate ERFs, which include higher cognitive functions where the elicitation of the target requires subtraction, and the target is subject to a specific assumption about the time window in which it occurs in multi-channel data. In a paradigm where stimuli are jittered and thus are not periodic, our weighted method will also be applicable by concatenating the epochs.

LIMITATIONS

There are several methodological concerns to our study: (i) The spatio-temporal cluster permutation provided several clusters (**Figure 3A**); however, we did not select all of these. We selected the most reliable clusters that covered 100–250 ms and the bitemporal sensors (7, 17) since the vast majority of EEG studies of MMR generators confirmed these; however, the parietal generator in the later latency (e.g., **Figure 3A** Clusters #5 and #6) was suggested in several studies (9, 10) and should be investigated in a future study. (ii) The SOA of the current study was relatively short so that the brain response could return to the baseline. This short time range may have concatenation

artifacts when deviant concatenation. However, in the weighted-$BSS_{T/k}$ method, the amplitude outside of the window was 0.2 (Eq. 9). Therefore, concatenation artifacts, if any, should be limited. (iii) The window function was set as a rectangular window, which may cause a tingling effect. The selection of a window function should be based on a hypothesis; in the current study, we assumed that the crucial time range of MMR is equally distributed at 96–276 ms based on our data-driven approach, even though this time range is not assumed to have a unique significance. However, the non-rectangular window can be used according to the hypothesis. Therefore, we uploaded the source code of weighted-$BSS_{T/k}$ to GitHub (https://github.com/fractionalTypeBSS/BSSTk.git) to enable users to apply it according to their hypothesis and select so that users can use it based on their hypothesis to choose the window function and time range. (iv) The sample size was relatively small for fully describing the performance of our new approach. However, generalization, as well as the validity of our approach, is supported by our additional analysis in a separate cohort [**Supplementary Data (2-2)** and **Supplementary Figure 6**].

CONCLUSIONS

We proposed a novel weighted method for extracting the MMR from multi-channel MEG data. Compared with ICA, our weighted-$BSS_{T/k}$ method was more sensitive in highlighting the MMR in one or a few dominant components with positive spatio-temporal correlations. This new approach which used only deviant epochs could replace or complement the conventional subtraction approach. Our method may facilitate the use of the MMR in basic and clinical research and provide a novel approach to analyze complex event-related MEG and EEG data.

DATA AVAILABILITY STATEMENT

The original contributions presented in the study are included in the article/**Supplementary Material**, further inquiries can be directed to the corresponding author.

ETHICS STATEMENT

The studies involving human participants were reviewed and approved by the Ethics Committee of Kyushu University. The patients/participants provided their written informed consent to participate in this study.

AUTHOR CONTRIBUTIONS

TMat, SS, JA, and KK: study conception and design. TMat, TMae, and ST: data collection. TMat and KK: analysis and interpretation of results. TMat: draft manuscript preparation. YG, SK, and MH: revision of manuscript. All authors approved the final version of the manuscript.

FUNDING

This work was supported by JSPS KAKENHI Grant No. JP20J00552; Nakatani Foundation for Advancement of Measuring Technologies in Biomedical Engineering; the Japan Epilepsy Research Foundation; the Osaka Medical Research Foundation for Intractable Diseases; and the National Institutes of Health [Grants Nos. 5R01NS104585, R01DC016915, R01DC016765, and R01DC017991].

ACKNOWLEDGMENTS

We thank Associate Professor Junji Kishimoto (Department of Research and Development of Next Generation Medicine, Faculty of Medical Sciences, Kyushu University) for assistance with the statistical analysis. We thank Karl Embleton Ph.D. and Sarina Iwabuchi Ph.D., from Edanz (https://jp.edanz.com/ac) for editing a draft of this manuscript.

SUPPLEMENTARY MATERIAL

The Supplementary Material for this article can be found online at: https://www.frontiersin.org/articles/10.3389/fneur.2022.762497/full#supplementary-material

REFERENCES

1. Näätänen R, Gaillard AW, Mantysalo S. Early selective-attention effect on evoked potential reinterpreted. *Acta Psychol.* (1978) 42:313–29. doi: 10.1016/0001-6918(78)90006-9
2. Näätänen R, Michie PT. Early selective-attention effects on the evoked potential: a critical review and reinterpretation. *Biol Psychol.* (1979) 8:81–136. doi: 10.1016/0301-0511(79)90053-X
3. Tiitinen H, May P, Reinikainen K, Näätänen R. Attentive novelty detection in humans is governed by pre-attentive sensory memory. *Nature.* (1994) 372:90–2. doi: 10.1038/372090a0
4. Hari R, Hämäläinen M, Ilmoniemi R, Kaukoranta E, Reinikainen K, Salminen J, et al. Responses of the primary auditory cortex to pitch changes in a sequence of tone pips: neuromagnetic recordings in man. *Neurosci Lett.* (1984) 50:127–32. doi: 10.1016/0304-3940(84)90474-9
5. Csepe V, Pantev C, Hoke M, Hampson S, Ross B. Evoked magnetic responses of the human auditory cortex to minor pitch changes: localization of the mismatch field. *Electroencephalogr Clin Neurophysiol.* (1992) 84:538–48. doi: 10.1016/0168-5597(92)90043-B
6. Levanen S, Ahonen A, Hari R, McEvoy L, Sams M. Deviant auditory stimuli activate human left and right auditory cortex differently. *Cereb Cortex.* (1996) 6:288–96. doi: 10.1093/cercor/6.2.288
7. Garrido MI, Kilner JM, Stephan KE, Friston KJ. The mismatch negativity: a review of underlying mechanisms. *Clin Neurophysiol.* (2009) 120:453–63. doi: 10.1016/j.clinph.2008.11.029
8. Rosburg T, Trautner P, Dietl T, Korzyukov OA, Boutros NN, Schaller C, et al. Subdural recordings of the mismatch negativity (MMN) in patients with focal epilepsy. *Brain.* (2005) 128:819–28. doi: 10.1093/brain/awh442
9. Marco-Pallares J, Grau C, Ruffini G. Combined ICA-LORETA analysis of mismatch negativity. *Neuroimage.* (2005) 25:471–7. doi: 10.1016/j.neuroimage.2004.11.028
10. Boly M, Garrido MI, Gosseries O, Bruno MA, Boveroux P, Schnakers C, et al. Preserved feedforward but impaired top-down processes in the vegetative state. *Science.* (2011) 332:858–62. doi: 10.1126/science.1202043

11. Jääskeläinen IP, Ahveninen J, Bonmassar G, Dale AM, Ilmoniemi RJ, Levänen S, et al. Human posterior auditory cortex gates novel sounds to consciousness. *Proc Natl Acad Sci USA*. (2004) 101:6809–14. doi: 10.1073/pnas.0303760101
12. Deouell LY, Heller AS, Malach R, D'Esposito M, Knight RT. Cerebral responses to change in spatial location of unattended sounds. *Neuron.* (2007) 55:985–96. doi: 10.1016/j.neuron.2007.08.019
13. May PJ, Tiitinen H. Mismatch negativity (MMN), the deviance-elicited auditory deflection, explained. *Psychophysiology.* (2010) 47:66–122. doi: 10.1111/j.1469-8986.2009.00856.x
14. Garrido MI, Friston KJ, Kiebel SJ, Stephan KE, Baldeweg T, Kilner JM. The functional anatomy of the MMN: a DCM study of the roving paradigm. *Neuroimage.* (2008) 42:936–44. doi: 10.1016/j.neuroimage.2008.05.018
15. Bishop DV. Using mismatch negativity to study central auditory processing in developmental language and literacy impairments: where are we, and where should we be going? *Psychol Bull.* (2007) 133:651–72. doi: 10.1037/0033-2909.133.4.651
16. Näätänen R, Paavilainen P, Rinne T, Alho K. The mismatch negativity (MMN) in basic research of central auditory processing: a review. *Clin Neurophysiol.* (2007) 118:2544–90. doi: 10.1016/j.clinph.2007.04.026
17. Näätänen R. *Attention and Brain Function*. Hillsdale: Lawrence Erlbaum (1992).
18. Romani GL, Williamson SJ, Kaufman L. Tonotopic organization of the human auditory cortex. *Science.* (1982) 216:1339–40. doi: 10.1126/science.7079770
19. Näätänen R, Sams M, Alho K, Paavilainen P, Reinikainen K, Sokolov EN. Frequency and location specificity of the human vertex N1 wave. *Electroencephalogr Clin Neurophysiol.* (1988) 69:523–31. doi: 10.1016/0013-4694(88)90164-2
20. Picton TW, Woods DL, Proulx GB. Human auditory sustained potentials. II. Stimulus relationships. *Electroencephalogr Clin Neurophysiol.* (1978) 45:198–210. doi: 10.1016/0013-4694(78)90004-4
21. Hämäläinen M, Hari R, Ilmoniemi RJ, Knuutila J, Lounasmaa OV. Magnetoencephalography—theory, instrumentation, and applications to noninvasive studies of the working human brain. *Rev Modern Phys.* (1993) 65:413–97. doi: 10.1103/RevModPhys.65.413
22. Jung TP, Makeig S, McKeown MJ, Bell AJ, Lee TW, Sejnowski TJ. Imaging brain dynamics using independent component analysis. *Proc IEEE Inst Electr Electron Eng.* (2001) 89:1107–22. doi: 10.1109/5.939827
23. Makeig S, Debener S, Onton J, Delorme A. Mining event-related brain dynamics. *Trends Cogn Sci.* (2004) 8:204–10. doi: 10.1016/j.tics.2004.03.008
24. de Cheveigne A, Parra LC. Joint decorrelation, a versatile tool for multichannel data analysis. *Neuroimage.* (2014) 98:487–505. doi: 10.1016/j.neuroimage.2014.05.068
25. Kalyakin I, Gonzalez N, Karkkainen T, Lyytinen H. Independent component analysis on the mismatch negativity in an uninterrupted sound paradigm. *J Neurosci Methods.* (2008) 174:301–12. doi: 10.1016/j.jneumeth.2008.07.012
26. Jung TP, Makeig S, Westerfield M, Townsend J, Courchesne E, Sejnowski TJ. Analysis and visualization of single-trial event-related potentials. *Hum Brain Mapp.* (2001) 14:166–85. doi: 10.1002/hbm.1050
27. Jung TP, Makeig S, Westerfield M, Townsend J, Courchesne E, Sejnowski TJ. Removal of eye activity artifacts from visual event-related potentials in normal and clinical subjects. *Clin Neurophysiol.* (2000) 111:1745–58. doi: 10.1016/S1388-2457(00)00386-2
28. Vigario R, Sarela J, Jousmaki V, Hämäläinen M, Oja E. Independent component approach to the analysis of EEG and MEG recordings. *IEEE Trans Biomed Eng.* (2000) 47:589–93. doi: 10.1109/10.841330
29. Makeig S, Jung TP, Bell AJ, Ghahremani D, Sejnowski TJ. Blind separation of auditory event-related brain responses into independent components. *Proc Natl Acad Sci USA*. (1997) 94:10979–84. doi: 10.1073/pnas.94.20.10979
30. Debener S, Makeig S, Delorme A, Engel AK. What is novel in the novelty oddball paradigm? Functional significance of the novelty P3 event-related potential as revealed by independent component analysis. *Brain Res Cogn Brain Res.* (2005) 22:309–21. doi: 10.1016/j.cogbrainres.2004.09.006
31. Delorme A, Makeig S. EEGLAB: an open source toolbox for analysis of single-trial EEG dynamics including independent component analysis. *J Neurosci Methods.* (2004) 134:9–21. doi: 10.1016/j.jneumeth.2003.10.009
32. Grau C, Fuentemilla L, Marco-Pallares J. Functional neural dynamics underlying auditory event-related N1 and N1 suppression response. *Neuroimage.* (2007) 36:522–31. doi: 10.1016/j.neuroimage.2007.03.027
33. Onton J, Delorme A, Makeig S. Frontal midline EEG dynamics during working memory. *Neuroimage.* (2005) 27:341–56. doi: 10.1016/j.neuroimage.2005.04.014
34. Hyvärinen AK, Oja E. *Independent Component Analysis.* New York, NY: John Wiley and Sons (2001). doi: 10.1002/0471221317
35. Kishida K. Dynamical activities of primary somatosensory cortices studied by magnetoencephalography. *Phys Rev E Stat Nonlin Soft Matter Phys.* (2009) 80:051906. doi: 10.1103/PhysRevE.80.051906
36. Kishida K. Evoked magnetic fields of magnetoencephalography and their statistical property. *Phys Rev E Stat Nonlin Soft Matter Phys.* (2009) 79:011922. doi: 10.1103/PhysRevE.79.011922
37. Kishida K. Neurodynamics of somatosensory cortices studied by magnetoencephalography. *J Integr Neurosci.* (2013) 12:299–329. doi: 10.1142/S0219635213500180
38. Kishida K. Blind source separation of neural activities from magnetoencephalogram in periodical median nerve stimuli. *Conf Proc IEEE Eng Med Biol Soc.* (2013) 2013:5837–40. doi: 10.1109/EMBC.2013.6610879
39. Molgedey L, Schuster HG. Separation of a mixture of independent signals using time delayed correlations. *Phys Rev Lett.* (1994) 72:3634–7. doi: 10.1103/PhysRevLett.72.3634
40. Hironaga N, Ioannides AA. Localization of individual area neuronal activity. *Neuroimage.* (2007) 34:1519–34. doi: 10.1016/j.neuroimage.2006.10.030
41. Tang AC, Sutherland MT, McKinney CJ. Validation of SOBI components from high-density EEG. *Neuroimage.* (2005) 25:539–53. doi: 10.1016/j.neuroimage.2004.11.027
42. Matsubara T, Hironaga N, Uehara T, Chatani H, Tobimatsu S, Kishida K. A novel method for extracting interictal epileptiform discharges in multi-channel MEG: Use of fractional type of blind source separation. *Clin Neurophysiol.* (2020) 131:425–36. doi: 10.1016/j.clinph.2019.11.032
43. Matsubara T, Stufflebeam S, Khan S, Ahveninen J, Hämäläinen M, Goto Y, et al. A novel time-delayed correlation method decomposes mismatch response without using subtraction. *Annu Int Conf IEEE Eng Med Biol Soc.* (2020) 484–7. doi: 10.1109/EMBC46164.2021.9629706
44. Makeig S, Westerfield M, Jung TP, Covington J, Townsend J, Sejnowski TJ, et al. Functionally independent components of the late positive event-related potential during visual spatial attention. *J Neurosci.* (1999) 19:2665–80. doi: 10.1523/JNEUROSCI.19-07-02665.1999
45. Makeig S, Westerfield M, Jung TP, Enghoff S, Townsend J, Courchesne E, et al. Dynamic brain sources of visual evoked responses. *Science.* (2002) 295:690–4. doi: 10.1126/science.1066168
46. Matsubara T, Ogata K, Hironaga N, Kikuchi Y, Uehara T, Chatani H, et al. Altered neural synchronization to pure tone stimulation in patients with mesial temporal lobe epilepsy: An MEG study. *Epilepsy Behav.* (2018) 88:96–105. doi: 10.1016/j.yebeh.2018.08.036
47. Kikuchi Y, Ogata K, Umesaki T, Yoshiura T, Kenjo M, Hirano Y, et al. Spatiotemporal signatures of an abnormal auditory system in stuttering. *Neuroimage.* (2011) 55:891–9. doi: 10.1016/j.neuroimage.2010.12.083
48. Nenonen J, Nurminen J, Kicic D, Bikmullina R, Lioumis P, Jousmaki V, et al. Validation of head movement correction and spatiotemporal signal space separation in magnetoencephalography. *Clin Neurophysiol.* (2012) 123:2180–91. doi: 10.1016/j.clinph.2012.03.080
49. Taulu S, Kajola M, Simola J. Suppression of interference and artifacts by the Signal Space Separation Method. *Brain Topogr.* (2004) 16:269–75. doi: 10.1023/B:BRAT.0000032864.93890.f9
50. Cardoso J-F, Souloumiac A. Jacobi angles for simultaneous diagonalization. *SIAM J Matri Anal Appl.* (1996) 17:161–4. doi: 10.1137/S0895479893259546
51. Murata N, Ikeda S, Ziehe A. An approach to blind source separation based on temporal structure of speech signals. *Neurocomputing.* (2001) 41:1–24. doi: 10.1016/S0925-2312(00)00345-3
52. Gramfort A, Luessi M, Larson E, Engemann DA, Strohmeier D, Brodbeck C, et al. MNE software for processing MEG and EEG data. *Neuroimage.* (2014) 86:446–60. doi: 10.1016/j.neuroimage.2013.10.027
53. Kujala T, Tervaniemi M, Schroger E. The mismatch negativity in cognitive and clinical neuroscience: theoretical and methodological considerations. *Biol Psychol.* (2007) 74:1–19. doi: 10.1016/j.biopsycho.2006.06.001
54. Maris E, Oostenveld R. Nonparametric statistical testing of EEG- and MEG-data. *J Neurosci Methods.* (2007) 164:177–90. doi: 10.1016/j.jneumeth.2007.03.024

55. Cacioppo S, Weiss RM, Runesha HB, Cacioppo JT. Dynamic spatiotemporal brain analyses using high performance electrical neuroimaging: theoretical framework and validation. *J Neurosci Methods.* (2014) 238:11–34. doi: 10.1016/j.jneumeth.2014.09.009
56. Zavala-Fernandez H, Orglmeister R, Trahms L, Sander TH. Identification enhancement of auditory evoked potentials in EEG by epoch concatenation and temporal decorrelation. *Comput Methods Programs Biomed.* (2012) 108:1097–105. doi: 10.1016/j.cmpb.2012.07.007
57. Jacobsen T, Schroger E. Is there pre-attentive memory-based comparison of pitch? *Psychophysiology.* (2001) 38:723–7. doi: 10.1111/1469-8986.3840723
58. Rinne T, Alho K, Ilmoniemi RJ, Virtanen J, Näätänen R. Separate time behaviors of the temporal and frontal mismatch negativity sources. *Neuroimage.* (2000) 12:14–9. doi: 10.1006/nimg.2000.0591
59. Jemel B, Achenbach C, Muller BW, Ropcke B, Oades RD. Mismatch negativity results from bilateral asymmetric dipole sources in the frontal and temporal lobes. *Brain Topogr.* (2002) 15:13–27. doi: 10.1023/A:1019944805499
60. Lozano-Soldevilla D, Marco-Pallares J, Fuentemilla L, Grau C. Common N1 and mismatch negativity neural evoked components are revealed by independent component model-based clustering analysis. *Psychophysiology.* (2012) 49:1454–63. doi: 10.1111/j.1469-8986.2012.01458.x
61. MacLean SE, Blundon EG, Ward LM. Brain regional networks active during the mismatch negativity vary with paradigm. *Neuropsychologia.* (2015) 75:242–51. doi: 10.1016/j.neuropsychologia.2015.06.019
62. MacLean SE, Ward LM. Oscillatory power and functional connectivity in the speech change detection network. *Neuropsychologia.* (2016) 89:320–34. doi: 10.1016/j.neuropsychologia.2016.06.039
63. MacLean SE, Ward LM. Temporo-frontal phase synchronization supports hierarchical network for mismatch negativity. *Clin Neurophysiol.* (2014) 125:1604–17. doi: 10.1016/j.clinph.2013.12.109
64. Cong F, Kalyakin I, Li H, Huttunen-Scott T, Huang Y, Lyytinen H, et al. Answering six questions in extracting children's mismatch negativity through combining wavelet decomposition and independent component analysis. *Cogn Neurodyn.* (2011) 5:343–59. doi: 10.1007/s11571-011-9161-1

Conflict of Interest: The authors declare that the research was conducted in the absence of any commercial or financial relationships that could be construed as a potential conflict of interest.

frontiers in Neurology

ORIGINAL RESEARCH
published: 23 March 2022
doi: 10.3389/fneur.2022.827529

Improving Localization Accuracy of Neural Sources by Pre-processing: Demonstration With Infant MEG Data

Maggie D. Clarke[1], *Eric Larson*[1], *Erica R. Peterson*[1], *Daniel R. McCloy*[1], *Alexis N. Bosseler*[1] *and Samu Taulu*[1,2]*

[1] *Institute for Learning and Brain Sciences, University of Washington, Seattle, WA, United States,* [2] *Department of Physics, University of Washington, Seattle, WA, United States*

We discuss specific challenges and solutions in infant MEG, which is one of the most technically challenging areas of MEG studies. Our results can be generalized to a variety of challenging scenarios for MEG data acquisition, including clinical settings. We cover a wide range of steps in pre-processing, including movement compensation, suppression of magnetic interference from sources inside and outside the magnetically shielded room, suppression of specific physiological artifact components such as cardiac artifacts. In the assessment of the outcome of the pre-processing algorithms, we focus on comparing signal representation before and after pre-processing and discuss the importance of the different components of the main processing steps. We discuss the importance of taking the noise covariance structure into account in inverse modeling and present the proper treatment of the noise covariance matrix to accurately reflect the processing that was applied to the data. Using example cases, we investigate the level of source localization error before and after processing. One of our main findings is that statistical metrics of source reconstruction may erroneously indicate that the results are reliable even in cases where the data are severely distorted by head movements. As a consequence, we stress the importance of proper signal processing in infant MEG.

Keywords: magnetoencephalography (MEG), artifact, movement compensation, infant, signal space separation, brain, signal space projection, signal processing

OPEN ACCESS

Edited by:
Rafeed Alkawadri, University of Pittsburgh Medical Center, United States

Reviewed by:
Yingying Wang, University of Nebraska-Lincoln, United States
Umit Aydin, King's College London, United Kingdom

***Correspondence:**
Samu Taulu
staulu@uw.edu

Specialty section:
This article was submitted to Applied Neuroimaging, a section of the journal Frontiers in Neurology

Received: *02 December 2021*
Accepted: *31 January 2022*
Published: *23 March 2022*

Citation:
Clarke MD, Larson E, Peterson ER, McCloy DR, Bosseler AN and Taulu S (2022) Improving Localization Accuracy of Neural Sources by Pre-processing: Demonstration With Infant MEG Data. Front. Neurol. 13:827529. doi: 10.3389/fneur.2022.827529

INTRODUCTION

Magnetoencephalography (MEG) is a functional imaging technique that offers excellent temporal resolution and good spatial resolution. The sensors in the MEG helmet measure the weak magnetic fields associated with electrical currents produced in the brain, e.g., during sensory, motor or cognitive tasks. The spatial sources of the detected magnetic fields can be estimated using a combination of anatomical information (digitized head shape, structural MRI) and known properties of electromagnetic field propagation, a process known as "source localization." MEG is also passive, silent, and non-invasive, making it an excellent tool to study neural dynamics in the developing brain. However, MEG is known to be extremely sensitive to artifacts and distortions that can affect source localization. In adult populations, some artifacts can be minimized by, e.g., asking participants to stay still during the measurement, which reduces signal distortions caused by head movements. Such approaches fail in measurement sessions with awake infant subjects, and, therefore, efficient signal processing methods for movement compensation are essential for reliable

infant MEG analysis. Additionally, other infant-specific distortion mechanisms exist, and based on our experience, the three most significant issues in infant MEG data that bias source localization are: (1) frequent head movement; (2) decreased signal-to-noise ratio (SNR) from increased scalp-to-sensor distance; and (3) strong cardiac artifacts which resemble brain signals in their spatial distribution. The SNR issue is mainly related to the relative positioning of the MEG sensor array and the infant head, and in this paper we focus on the methodology concerning points (1) and (3) above.

A number of processing methods have been developed to address the issues listed above, many of which exist in both adult and infant data. For example, head movement, its effect on MEG data and subsequent results after the application of movement compensation has been shown in adults (1), school-aged children (2), infants (3), as well as in clinical populations (4). In this paper, we review some of the most relevant methodological aspects of processing and analysis of infant MEG data. Special emphasis is given to the infant-specific mechanisms of signal distortion leading to source localization errors. Using real movement information from a set of 6, 7, and 12-month-old subjects, we show the effects of these distortions on magnetic field topographies and source localization, using several different processing approaches. Notably, we demonstrate that statistical metrics, such as the goodness-of-fit of equivalent current dipole models, do not necessarily capture source localization bias, meaning that significant source localization errors may remain undetected in data that have not been processed with movement compensation algorithms.

SIGNAL DISTORTIONS AND THEIR CORRECTION IN INFANT MEG

External Artifacts

External artifacts arise from generators of magnetic fields that lie outside the body of the MEG subject. Common sources are power lines, elevators, electronic devices, moving vehicles, and mechanic vibration of the room housing the MEG instrument. Signal space separation (SSS) (5, 6) and its temporal extension, temporal signal space separation (tSSS) (7, 8) are commonly used methods that compensate for external interference artifacts in MEG data. The signal space separation method (SSS) is based on Maxwell's equations, where spatially discretized samples of magnetic flux (MEG data) are decomposed into amplitude coefficients of basis functions that span detectable magnetic fields in space that is free of sources of magnetic fields, i.e., in the region where MEG sensors are located. Since separate linearly independent basis functions exist for signals generated inside and outside the sensor volume, SSS provides a straightforward means of removing field components attributable to external sources. In cases where the artifact sources are not clearly distinguishable as internal or external, the temporal extension of SSS (tSSS) can be used to detect and remove components arising from these nearby artifact sources. Other efficient and widely used interference suppression methods include, e.g., signal space projection (SSP) (9) and reference sensor-based methods (10). For a review of MEG artifacts and their suppression, see Taulu et al. (11).

Physiological Artifacts

MEG is also sensitive to physiological artifacts which arise from generators inside the body of the subject (e.g., heart, eyes, skeletal muscles). Blink- and saccade-related artifacts tend to occur less frequently in infants than adults, as the mean spontaneous blink rate in infants is <2 blinks per minute (12). In contrast, infant and child cardiac artifacts are often more than an order of magnitude larger than the brain signals of interest (13) and appear as volume currents within the skull due to the shorter distance between the heart and the MEG sensors. Additionally, infant heart rate is much faster than adults: from newborn to 6 months of age the mean heart rate is 125–145 beats per minute (bpm), compared to a mean heart rate of 80 bpm in adolescents and adults (14). Furthermore, the QRS peak is narrower for infants than for adults, ranging from 50 to 80 ms in duration, contributing electromagnetic activity in the 12.5 to 20 Hz range (14). Adolescents, on the other hand, have a QRS complex lasting between 90 and 110 ms (15). Both the increased proximity and frequency of magnetic contributions from the heart make it essential to properly characterize and remove cardiac artifacts in infant data.

Common methods used to remove both ocular and cardiac artifacts in MEG data include independent component analysis (ICA) (16–23) and SSP based on principal component analysis (PCA).

Movement Related Artifacts

Head movements are generally unavoidable in infant populations (3), due to the larger space available for head movements (in common adult sized helmets) and infants' inability to remain still on command. Such movements distort the magnetic field distribution across the MEG sensors and can result in large errors in source localization (1). Fortunately, movement compensation algorithms have been developed to repair such artifacts (6, 24). Using head position indicator (HPI) coils that emit high-frequency sinusoidal fields, the head position can be continuously and accurately determined during an MEG recording. By forcing the spatial "expansion origin" of the internal basis functions derived from SSS to match the origin of the head coordinate system (even as the head moves over time), one can decompose the MEG signals into a representation that is specific to the brain regardless of its location with respect to the sensors. Thus, by continuously tracking the head position, the basis function coefficients can be interpreted in a static head coordinate system, as if the subject had remained still. Typically, the coefficients are used to create a virtual sensor-level signal representation corresponding to some target head position defined by the user. This is the basis of head movement compensation, and it is an essential task in the processing of infant data as will be demonstrated in subsequent sections.

Effect of Noise Covariance

Sensor covariance matrices, which quantify the spatial correlation structure between each pair of sensors, are central

to many MEG source localization algorithms such as minimum norm estimation, equivalent current dipole fits, mixed-norm solvers, and beamformers, as well as many applications of machine learning to MEG data. Covariance matrices are typically estimated from the data, either from specific segments during a subject recording (e.g., the baseline period before each trial as a "noise covariance," or during the trial for a "data covariance") or from data recorded just before or after the experimental session ("empty-room" data). It is important that the true underlying sensor covariance structure is accurately reflected in the estimated noise covariances, otherwise a reduction in SNR and errors in source localization can be introduced (25). In the context of source localization of movement-compensated data in particular, it is also important that full (rather than diagonal) noise covariances are used (3).

Fortunately, direct empirical source covariance estimates can be improved by using automated regularization techniques (26). However, even when using such techniques, it is important to properly account for the rank of the data. In source imaging for example, the pseudo-inverse square root of the noise covariance matrix must be computed to whiten the data. During this computation, the rank of the data must be explicitly accounted for in order to avoid amplifying data components that are numerical noise. Common operations such as SSP, ICA, and SSS can all reduce the rank of the data, and this must be explicitly taken into account (26). In other words, the noise covariance rank (and effective null space) directly affect the accuracy of source localization (and by extension, other methods that rely on covariance estimates).

In the context of movement compensation, the data rank must be taken into account carefully. The number of components used to reconstruct data can vary as a function of time, as the different head positions can yield different regularized internal bases in MNE-Python's implementation of Maxwell filtering. While a sensor covariance computed from the movement-compensated data can directly reflect this, empty-room data processed directly using SSS by default will not—it will reflect the rank of non-movement-compensated data (i.e., as if the head remained stationary), which will likely differ. Therefore, it is important that empty room data are processed the same way as movement compensated data, i.e., by using the same initial device-to-head transformation, expansion origin (in the head coordinate frame), and time-varying head position parameters as the actual data, despite the fact that there was no actual subject motion during the empty room recording.

Reduced SNR of Infant MEG Measurements

Magnetic fields from any source (including sources in the brain) decay rapidly with distance. In traditional adult superconducting quantum interference device (SQUID)-based MEG systems, helmets are designed to place the sensors as close as possible to the helmet's inner surface, given the restrictions posed by thermal insulation between the head and the liquid helium vessel containing the SQUID sensors. When this larger helmet is used with infants, the distance reduces the strength of the measured magnetic field and negatively affects the SNR. At the same time, infants' smaller heads allow for a considerable range of movement inside adult-sized helmets. In SQUID systems, the sensors are not attached to the head, and therefore movement of the head relative to the sensors significantly distorts the distribution of the magnetic signals and thus biases source localization. While this effect is not an artifact in the strict sense, the resulting reduced strength of magnetic field components originating from the brain makes the suppression of external and physiological artifacts all the more critical. In the rest of this paper, we illustrate some of the above-mentioned artifact suppression approaches and demonstrate some common pitfalls when processing infant MEG data.

METHODS

To quantify the effects of SSS, movement compensation, and noise covariance on source localization of infant MEG data, we simulated data based on real infant head movements. Simulated datasets were analyzed using four different methods: (1) no artifact suppression (Raw), (2) Maxwell filtering (SSS), and (3, 4) Maxwell filtering with movement compensation using two different covariance estimation methods (see Data Processing, below). In addition to simulated data (where ground truth source locations are known), we show the effect of each approach on real infant data to illustrate what the effects look like in practice.

Subjects and Data Acquisition

Data from nine 6-month, twenty-three 7-month, and fourteen 12-month-old typically developing subjects were drawn from two previously conducted studies at the University of Washington Institute for Learning and Brain Sciences. All infants were from monolingual English-speaking environments, had no reported hearing difficulties, no history of ear infections, and were born full-term (between 39 and 42 weeks of gestational age). Both studies were in accordance with the ethical standards of the institutional and/or national research committee and with the 1964 Helsinki declaration and its later amendments or comparable ethical standards. Informed consent was obtained from parents or caregivers of all infants included in both studies. MEG data were recorded in a magnetically shielded room with a whole head adult-sized 306 channel Elekta Neuromag® MEG system (Elekta Oy, Helsinki, Finland). Prior to scanning, each subject had a fabric cap fitted to the head, with five (83,143, 203, 263, 323 Hz) HPI coils attached. Anatomical landmarks (left and right preauricular points, nasion), HPI coils and additional points along the head surface were digitized using Fastrak® 3D digitizer (Polhemus, Colchester, VT, USA) to construct an individual Cartesian head-centric coordinate system. Infants were seated in a custom-made chair under the MEG helmet while listening to various auditory stimuli. For specific details about the paradigm, see Kuhl et al. (27) and Mittag et al. (28).

Data Processing

MEG data were pre-processed using MNE-Python (29, 30). All data were analyzed using four different methods: (1) no artifact suppression (Raw), (2) Maxwell filtering only (tSSS for

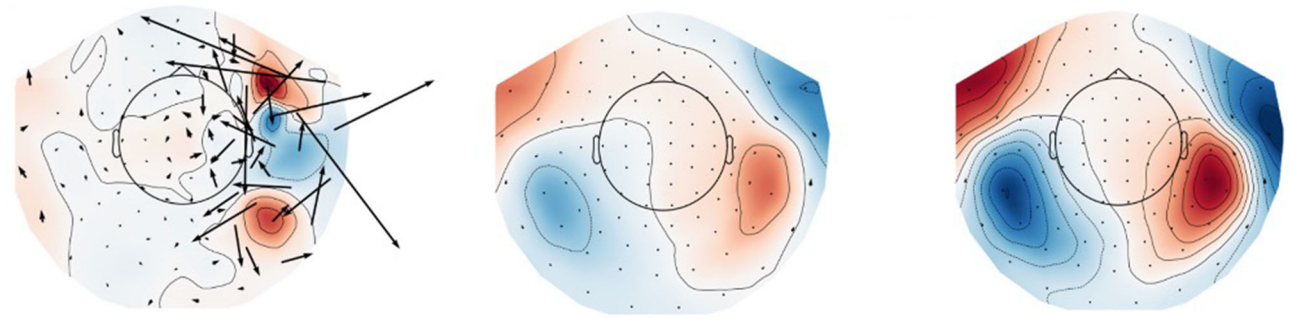

FIGURE 1 | Field topographies of bilateral evoked auditory responses (at 150 ms) in a 6-month-old participant. **(A)** Raw data (no artifact suppression), **(B)** data processed with tSSS, and **(C)** data processed with tSSS + movement compensation. Black arrows represent estimation of equivalent current flow at the MEG sensor locations.

experimental data and SSS for simulated data), and (3, 4) two versions of Maxwell filtering with movement compensation and translation to the time-averaged head position: one localized using a covariance from (simulated) empty-room data processed using plain SSS ($MC_{erm-cov}$); and one using a noise covariance computed from the baseline of the simulated data (MC). Note that, based on how the simulations were set up, a noise covariance calculated from simulated empty-room data that had been processed using the same time-varying position parameters as the simulated data would be equal to the baseline covariance computed from the actual data, and hence the difference between (3) and (4) tells us the importance of processing empty-room data using the same time-varying position information as task data.

For data processed with SSS, an internal expansion order of 6 and an external order of 3 was used. The internal order is smaller than the default of 8, which is typically used in adult measurements, and it is justified by the fact that the infant head is smaller and the overall source-to-sensor distance tends to be larger than in adult subjects. Data processed with movement compensation were transformed to the mean of each individual's head positions. To examine the effect of cardiac artifacts, PCA was used to identify cardiac artifacts from ECG electrodes. Signal space projection (SSP) was used to suppress the cardiac signal in the MEG data by estimating two orthogonal vectors capturing the spatial structure of heartbeats.

Data Simulations

For each subject, real subject time-varying head movements were applied to the simulated brain sources to yield simulated sensor data that mimicked the movement distortions seen in real recordings. Source space activations were constructed by fitting a sphere to the points along the head surface which were collected during the digitization process. The sphere was used to create a volumetric grid in which sources with random orientations were simulated along 2 cm spacing at least 10° away from radial orientations relative to the center of the sphere as in Larson and Taulu (3). The dipole spacing was fixed across subjects, but due to differences in head sizes, the number of dipoles differed across subjects, averaging (mean ± 1 SD) of 88.2 ± 13.7, 93.3 ± 7.6, and 112.3 ± 15.3 for the 6, 7, and 12 month groups, respectively.

The source time course for each subject was constructed by individually activating a 100-nAm peak single source every 50 ms. In addition to these activations, the source time course included a (−200, 0) ms baseline period with no simulated brain activity, to be used in the noise covariance estimation. In addition, Gaussian noise was added to the sensors. For additional details see (3). Each of the simulated datasets were then analyzed using the four different methods: Raw, SSS, MCerm-cov, and MC.

Fitting of Equivalent Current Dipoles

To investigate the accuracy and reliability of source localization, we fit equivalent current dipoles (ECD) to the simulated data. This procedure entails choosing the location, orientation, and strength of current dipoles so as to reconstruct the data as accurately as possible. Mathematically, a non-linear optimization algorithm searches for the best ECD parameters until the goodness-of-fit (GOF) value is maximized. Expressing the measured or simulated whitened data vector and the modeled whitened data vector as $\mathbf{d}$ and $\mathbf{m}$, respectively, the GOF value is given as $GOF = 1–(\mathbf{d}\text{-}\mathbf{m})^T(\mathbf{d}\text{-}\mathbf{m})/\mathbf{d}^T\mathbf{d}$, where T indicates transpose. Thus, the numerical value of GOF is in the range 0...1 (0...100% fit). We define the localization error as $e = |\mathbf{r}_q\text{-}\mathbf{r}_e|$, where $\mathbf{r}_q$ and $\mathbf{r}_e$ are the true and estimated ECD location, respectively.

RESULTS AND RECOMMENDATIONS

Compensation for Movement-Related Field Distortions

Figure 1 shows field topographies of real data from a 6-month-old subject from Mittag et al. (28), averaged across trials with an auditory stimulus, processed in three different ways. In **Figure 1A** no compensation is done for subject movement, and the magnetic field topography of the evoked response is clearly adversely affected by external artifacts and subject movement. After the application of tSSS to the raw data (**Figure 1B**), the field pattern resembles comparable adult data, and after application

of movement compensation (**Figure 1C**) the spatial details of the modeled field are further improved. In particular, the movement-induced smooth appearance of the topography is compensated for in **Figure 1C** as compared to **Figure 1B**.

Source Localization Error

Using simulated data distorted by head movements from real recordings, we analyzed localization bias and goodness-of-fit under the four different processing strategies described in Methods: Data Processing. The head movements were drawn from Kuhl et al. (27) (7 mo) & Mittag et al. (28) (6 and 12 mo). The top panel of **Figure 2** shows that between the first experiment (27) and the second experiment (28), there was an improvement in subject compliance in terms of reduced movement, as reflected in less subject deviation from the mean head position. For the 6, 7, and 12 month groups, paired *t*-tests of the bias of the two movement compensation modes for each group were $p =$ 0.1100, 0.0061, and 0.0334, respectively. Nevertheless, even the smaller head movements seen in the later study yield localization biases in excess of 10 mm when movement compensation is not applied to the data (**Figure 2**, second panel). Notably, if we source localize using a noise covariance from empty-room data processed with plain SSS (without applying equivalent movement compensation to the empty-room recording), we find that source localization is adversely affected, most noticeably in the data simulated from 7-month-old's head movements. In all cases, acceptable goodness-of-fit values are obtained (>80% in all cases), even when mean localization bias exceeds 20 mm. In some cases the GOF values are actually higher in the Raw and SSS conditions compared to the movement-compensated conditions, showing that high GOF does not necessarily indicate high localization accuracy.

Looking at systematic effects observed in the localization bias, we see that inward bias (as quantified by the radius of the true source minus the radius of the ECD fit location, relative to the head center) for raw and SSS-processed data is positive for 6 and 12 months, and negative for 7 months (see **Figure 3**). If the subject-by-subject inward bias is compared to their average upward movement (+Z in MEG device coordinates), a very strong Pearson correlation is observed for both Raw ($R^2 = 0.51$, $p =$ 1e-8) and SSS-processed data ($R^2 = 0.54$, $p =$ 5e-9), suggesting that subject head deviation from the initial position upward or downward in the MEG helmet tends to manifest as inward and outward source localization bias, respectively.

Suppression of Cardiac Artifacts

As mentioned above, infant heart rates tend to be much higher compared to adolescent or adult heart rates, and the QRS complex of infant heart artifacts has a shorter duration as well (**Figure 4**).

Additionally, in our experience a characteristic difference between cardiac artifacts in infants and adults is the fact that in infants, the spatial field distribution of the cardiac artifact often tends to be very similar to a plausible brain signal (**Figure 5**), which makes its algorithmic suppression inherently important and difficult. This observation is confirmed by the fact that in many cases SSS reconstruction leaves the cardiac artifact intact, cf. **Figure 6**.

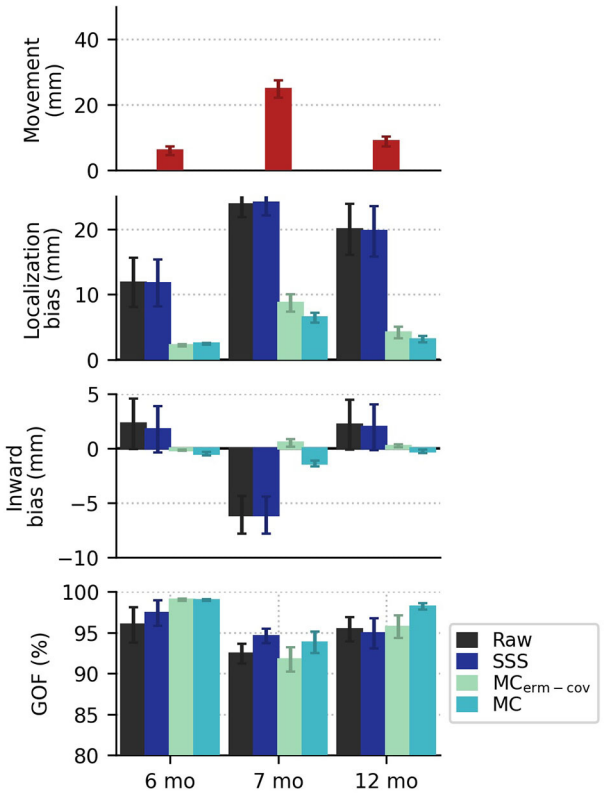

FIGURE 2 | In the top row, the mean plus or minus standard error (across subjects) of the position deviation (from each subject's mean head position) shows smaller movements in the more recent recording (published in 2021) compared to an older recording (published in 2014). In the second row, localization bias is reduced by movement compensation, with greater reduction in bias when the covariance is computed from movement-compensated data. There are systematic outward and inward (relative to the head center) localization biases shown for the newer (2021) and older (2014) data, respectively. In the last row, mean goodness of fit values exceed 80% in all cases.

Generally speaking, it is possible to overcome these challenges by choosing among different artifact suppression methods. For example, ICA may be more successful than SSP for some infant datasets, and both are likely to be more successful than SSS alone (though SSS is still useful for suppression of external artifacts, and can be used alongside SSP or ICA; cf. **Figure 6**).

DISCUSSION

In this paper, we have reviewed the most important challenges that may distort infant MEG data and thereby cause bias to the associated source estimates. The topics covered are based on our extensive experience with awake infant subjects and many of these aspects are relevant to clinical MEG as well, e.g., in epilepsy studies (4) or other settings where patients may have difficulties staying still during the recording. We also

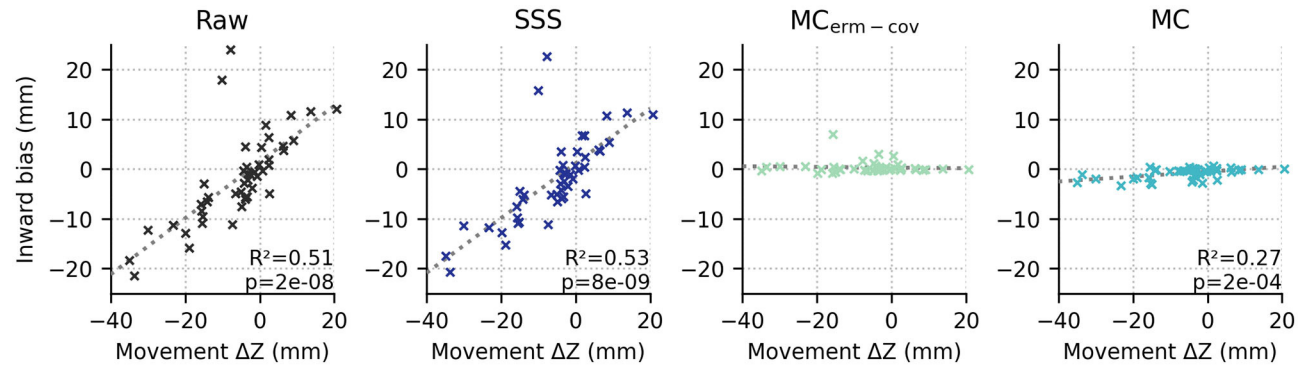

FIGURE 3 | The average position in device coordinates relative to the initial position (x axis; +Z means upward) is strongly correlated with the inward bias of the ECD fit dipoles relative to the true source locations for raw and SSS-processed data (first and second columns), but not either movement-compensated case ($p > 0.05$, both).

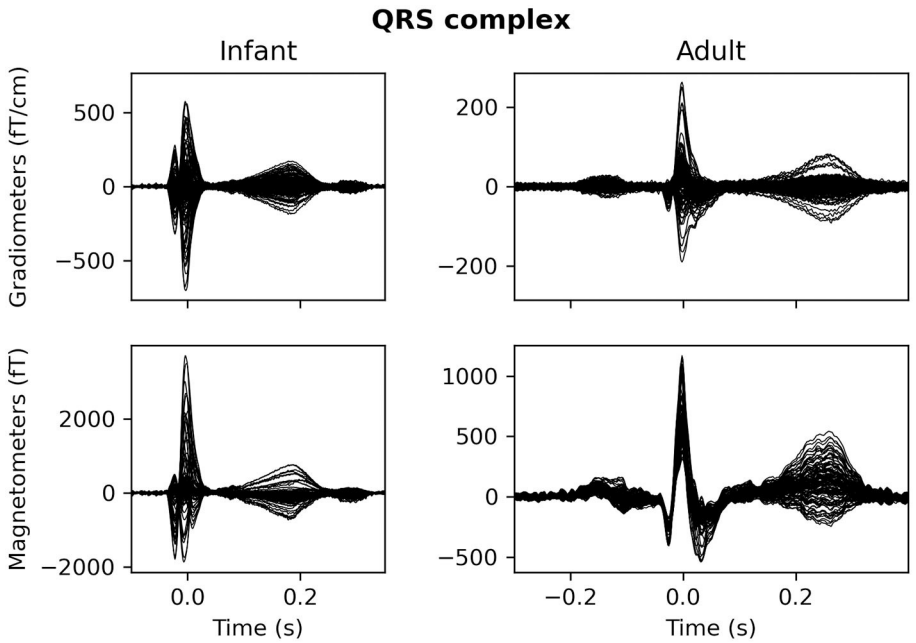

FIGURE 4 | The average QRS complex from exemplar infant **(left)** and adult **(right)** MEG recordings.

reviewed some of the most efficient processing methods that can correct for these distortions along with results that demonstrate the processing results and the associated accuracy of source localization (see Figure 7; a schematic of data processing in the **Supplementary Material**). Most importantly, we demonstrated that without application of movement compensation the source localization accuracy in infant MEG is severely compromised, with localization errors >20 mm in many cases, while statistical metrics such as the goodness-of-fit erroneously indicate high reliability of the obtained estimates based on non-compensated data. However, even with large head movements, the SSS-based movement compensation method is efficient, significantly reducing source localization bias to a few millimeters while the GOF value of source localization is almost intact compared to the uncompensated data. Consequently, one cannot solely rely on statistical confidence metrics of source modeling methods in the case of MEG signals that have been distorted by head movements. The reason is that the topography of the MEG signal distribution may resemble the pattern of a plausible brain signal despite movement-induced spatial modulation, which has to be compensated for in order to obtain robust interpretation of the data. This is a new consideration in the context of infant MEG and it was not investigated in Larson and Taulu (3), which otherwise demonstrated the efficacy of movement compensation methodology.

Regarding the inadequacy of statistical metrics to perfectly represent the integrity of obtained source estimation results, the same is generally true for other algorithmic

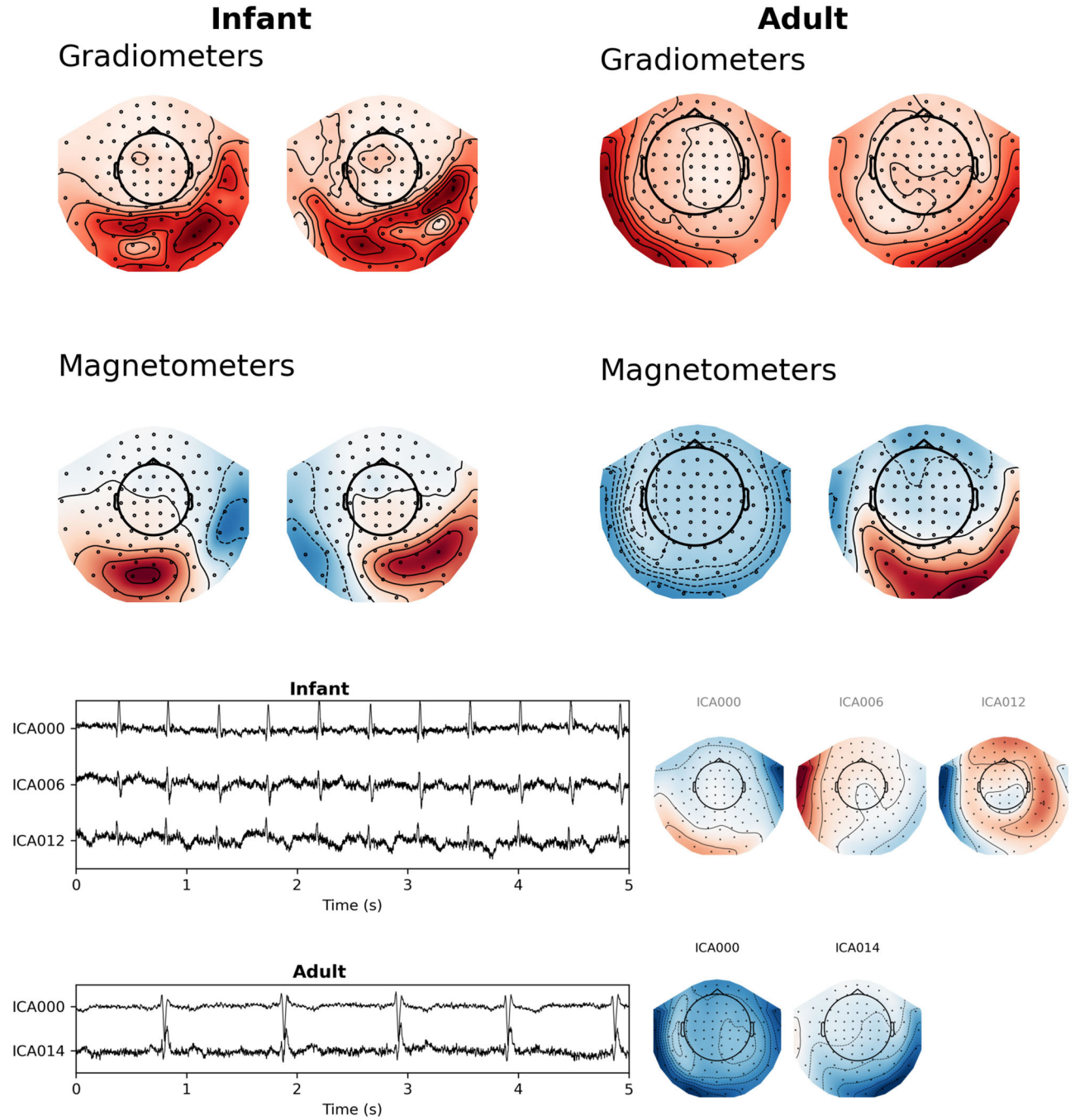

FIGURE 5 | Topographic maps of cardiac fields for sample infant and adult MEG recordings. **(Top)** SSP projector fields computed from a 100 ms window surrounding the average QRS peak from this figure was sufficient to capture the artifact. **(Bottom)** latent sources and field maps for cardiac-related latent components computed with ICA. Both approaches show that fields from heart-generated volume currents in the brain may appear shallow or asymmetrical compared to adult cardiac fields.

interpretations of data. Therefore, we strongly recommend visual inspection of data, before and after signal processing and statistical analyses. For example, if an experienced MEG researcher is unable to observe any interesting effects on visual inspection of averaged sensor-level evoked responses related to their neuroscientific question, then any subsequent statistically significant interpretations may be questionable. To prevent such problems, it is advisable to expect poor SNR in infant MEG and plan data acquisition accordingly, e.g., by over-collecting data to account for time periods when the head has moved far from the sensors.

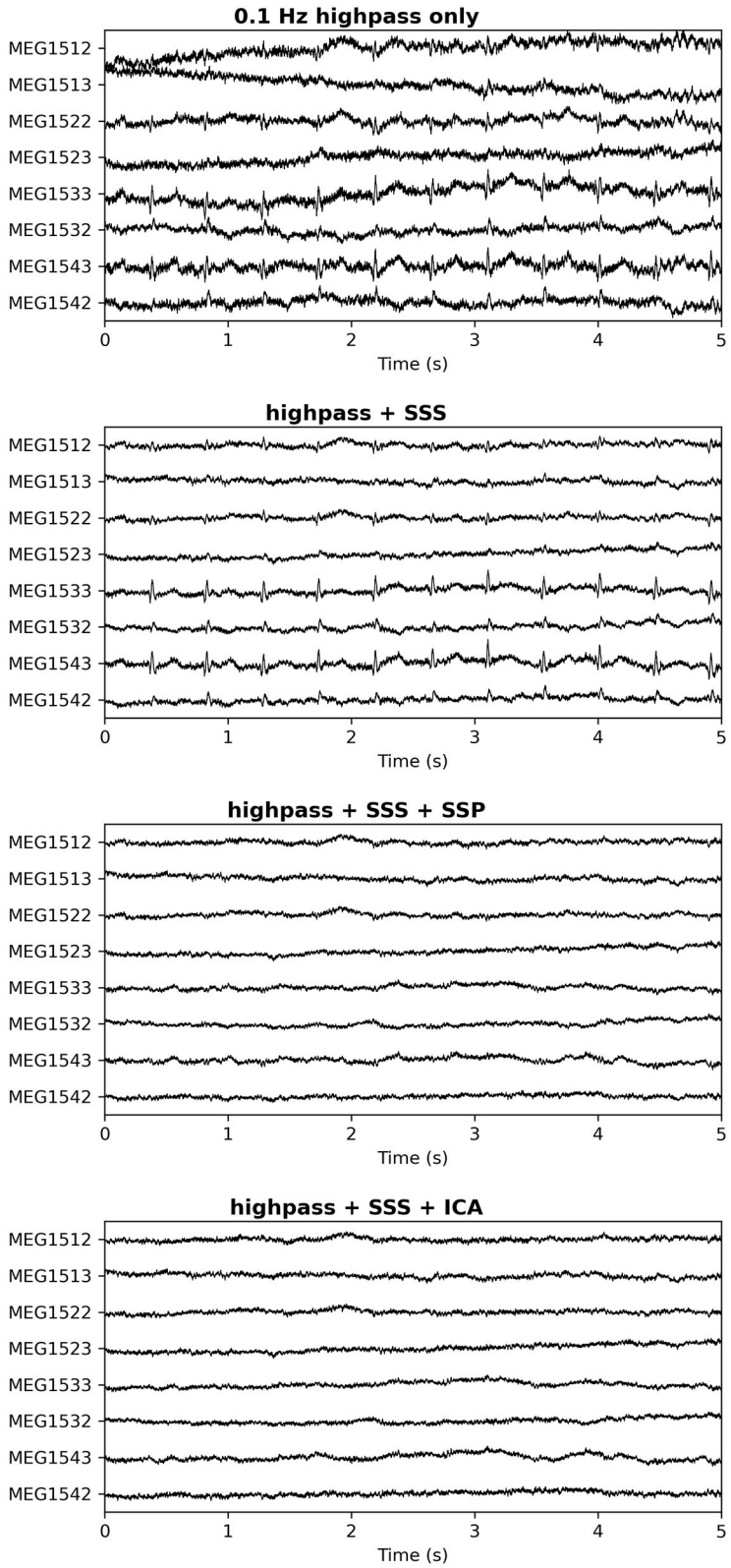

FIGURE 6 | Cardiac artifact on a subset of channels after different pre-processing approaches. Top: No processing; Second Panel: SSS only; Third Panel: SSS followed by SSP (2 orthogonal projectors); Bottom Panel: SSS followed by ICA (4 cardiac-related latent sources removed). In the third and bottom panels the cardiac artifacts have been successfully repaired. The spatial distribution of the cardiac artifact stays virtually intact in the SSS process, indicating that most of its signal energy comes from the internal SSS volume where the head is located.

Besides the movement distortions and other obvious infant-related MEG challenges, we have observed that cardiac artifacts are potentially especially problematic in infant MEG due to the fact that they are often very close to plausible brain signals in terms of their spatial topography. While spatial-domain suppression of these artifacts with the help of SSP or ICA tends to be efficient, there is a concern that removal of the artifact patterns could cause bias to brain signals that is difficult to compensate for. Further studies are needed to address this concern.

The above discussion relates to MEG research conducted by standard SQUID-based MEG instruments. Some of the described signal distortions may become less significant when wearable MEG systems [see, e.g., Boto et al. (31)], will be taken to use. Specifically, movement-modulated distortions should be absent in recordings conducted with sensors that are attached to the head, but movement-related artifacts still remain when the sensors are moving in the background magnetic field unless this field has been perfectly compensated for.

The main purpose of our paper was to provide information on specific challenges in infant MEG recordings that are not necessarily obvious from the experience gathered from adult MEG, and to demonstrate methodology that can be applied for robust source reconstruction results in infant MEG despite the challenges. Our recent paper on best practices of infant MEG (submitted) provides a more general and practical perspective on different aspects of a successful infant MEG study starting from paradigm planning and data acquisition while this paper contains a more detailed description of the methodology that should be useful for anyone planning to conduct infant MEG experiments.

LIMITATIONS

As discussed throughout, one of the main difficulties of infant MEG is the mismatch between an adult-sized MEG helmet and small infant heads (due both to larger scalp-to-sensor distances and to increased space for head movement, combined with infants' tendency toward frequent motion). A general limitation is that if the head becomes too far from the sensor array (due to large head movements), the brain signal will drop below the level of sensor noise (i.e., reduced SNR). In addition, in such a situation, the ability to estimate the head position from the HPI coils deteriorates. One possible improvement would be to use infant-specific MEG hardware, such as the Artemis123 (32) or Baby MEG (33) systems, which would reduce the scalp-to-sensor distance and allow less room for movement. Obviously, this is a strategy with a multi-year implementation schedule that can only be undertaken at an institutional level. As for strategies that individual researchers might employ given their existing data collection systems, it is probably clear from the preceding sections that there is no magic bullet to fix poor SNR in an existing recording (this is equally true of adult data as of infant data). In most cases the best to be done with existing data is to meticulously apply the methods of artifact suppression described above, perhaps choosing a representative sample of the data to test a few different parameter settings of the algorithms employed, to ensure that the artifact suppression algorithms are not overly aggressive and possibly suppressing brain signal.

For collection of new data, perhaps the most practical advice is to expect poor SNR and plan task designs and recruitment efforts accordingly. Factoring in demographic controls, participants exhibiting varying degrees of uncooperative behavior, the various artifact and noise issues described here, and (for longitudinal studies) participant attrition, it would not be unheard of for the fraction of "usable" participants to be well-below 50% of the total number recruited. While not a decision to be taken lightly, sometimes throwing away data is both necessary and justified.

DATA AVAILABILITY STATEMENT

The data analyzed in this study is subject to the following licenses/restrictions: The datasets are from different studies conducted by my colleagues and these data have been made available upon request to the principal investigator, Prof. Patricia Kuhl. Requests to access these datasets should be directed to Prof. Patricia Kuhl (pkkuhl@uw.edu).

ETHICS STATEMENT

The studies involving human participants were reviewed and approved by Human Subjects Division, University of Washington. Written informed consent to participate in this study was provided by the participants' legal guardian/next of kin.

AUTHOR CONTRIBUTIONS

ST contributed to the conception and design of the manuscript. MC wrote the first draft of the manuscript and created figures. EP and DM created figures and contributed to writing. EL performed statistical analysis, created figures, and contributed to writing. AB contributed to writing and design of the manuscript. All authors contributed to manuscript revision, read, and approved the submitted version.

FUNDING

This work was funded by grant NIH R01-NS104585 (EL and ST), the Bezos Family Foundation (MC, EP, DM, ST, and AB), and the R. B. and Ruth H. Dunn Charitable Foundation (ST).

ACKNOWLEDGMENTS

The authors acknowledge and thank all members of the I-LABS MEG Center team. In addition, the authors thank the families that have participated in our research over the years and have made our work possible.

SUPPLEMENTARY MATERIAL

The Supplementary Material for this article can be found online at: https://www.frontiersin.org/articles/10.3389/fneur.2022.827529/full#supplementary-material

REFERENCES

1. Medvedovsky M, Taulu S, Bikmullina R, Paetau R. Artifact and head movement compensation in MEG. *Neurol Neurophysiol Neurosci.* (2007) 4:1–10.
2. Wehner DT, Hämäläinen MS, Mody M, Ahlfors SP. Head movements of children in MEG; quantification, effects on source estimation, and compensation. *NeuroImage.* (2008) 40:541–50. doi: 10.1016/j.neuroimage.2007.12.026
3. Larson E, Taulu S. The importance of properly compensating for head movements during MEG acquisition across different age groups. *Brain Topogr.* (2017) 30:172–81. doi: 10.1007/s10548-016-0523-1
4. Medvedovsky M, Taulu S, Gaily E, Metsähonkala, E.-L., Mäkelä JP, et al. Sensitivity and specificity of seizure-onset zone estimation by ictal magnetoencephalography. *Epilepsia.* (2012) 53:1649–57. doi: 10.1111/j.1528-1167.2012.03574.x
5. Taulu S, Kajola M. Presentation of electromagnetic multichannel data: the signal space separation method. *J Appl Phys.* (2005) 97:124905. doi: 10.1063/1.1935742
6. Taulu S, Simola J, Kajola M. Applications of the signal space separation method. *IEEE Trans Signal Process.* (2005) 53:3359–72. doi: 10.1109/TSP.2005.853302
7. Taulu S, Simola J. Spatiotemporal signal space separation method for rejecting nearby interference in MEG measurements. *Phys Med Biol.* (2006) 51:1759–68. doi: 10.1088/0031-9155/51/7/008
8. Taulu S, Hari R. Removal of magnetoencephalographic artifacts with temporal signal-space separation: demonstration with single-trial auditory-evoked responses. *Hum Brain Map.* (2009) 30:1524–34. doi: 10.1002/hbm.20627
9. Uusitalo MA, Ilmoniemi RJ. Signal-space projection method for separating MEG or EEG into components. *Med Biol Eng Comput.* (1997) 35:135–40. doi: 10.1007/BF02534144
10. Vrba J, Robinson SE. Signal processing in magnetoencephalography. *Methods.* (2001) 25:249–71. doi: 10.1006/meth.2001.1238
11. Taulu S, Simola J, Nenonen J, Parkkonen L. Novel noise reduction methods. In: Supek S, Aine CJ, editors. *Magnetoencephalography: From Signals to Dynamic Cortical Networks*. Berlin; Heidelberg: Springer (2019). p. 73–109. doi: 10.1007/978-3-030-00087-5_2
12. Zametkin A, Stevens JR, Pittman R. Ontogeny of spontaneous blinking and of habituation of the blink reflex. *Ann Neurol.* (1979) 5:453–7. doi: 10.1002/ana.410050509
13. Jousmäki V, Hari R. Cardiac artifacts in magnetoencephalogram. *J Clin Neurophysiol.* (1996) 13:172–6. doi: 10.1097/00004691-199603000-00008
14. O'Connor M, McDaniel N, Brady WJ. The pediatric electrocardiogram: part I: age-related interpretation. *Am J Emerg Med.* (2008) 26:506–12. doi: 10.1016/j.ajem.2008.03.030
15. Dickinson DF. The normal ECG in childhood and adolescence. *Heart.* (2005) 91:1626–30. doi: 10.1136/hrt.2004.057307
16. Breuer L, Dammers J, Roberts TP, Shah NJ. A constrained ICA approach for real-time cardiac artifact rejection in magnetoencephalography. *IEEE Trans Biomed Eng.* (2014) 61:405–14. doi: 10.1109/TBME.2013.2280143
17. Breuer L, Dammers J, Roberts TP, Shah NJ. Ocular and cardiac artifact rejection for real-time analysis in MEG. *J Neurosci Methods.* (2014) 233:105–14. doi: 10.1016/j.jneumeth.2014.06.016
18. Dammers J, Schiek M, Boers F, Silex C, Zvyagintsev M, Pietrzyk U, et al. Integration of amplitude and phase statistics for complete artifact removal in independent components of neuromagnetic recordings. *IEEE Trans Biomed Eng.* (2008) 55:2353–62. doi: 10.1109/TBME.2008.926677
19. Escudero J, Hornero R, Abasolo D, Fernandez A, Lopez-Coronado M. Artifact removal in magnetoencephalogram background activity with independent component analysis. *IEEE Trans Biomed Eng.* (2007) 54:1965–73. doi: 10.1109/TBME.2007.894968
20. Escudero J, Hornero R, Abasolo D, Fernandez A. Quantitative evaluation of artifact removal in real magnetoencephalogram signals with blind source separation. *Ann Biomed Eng.* (2011) 39:2274–86. doi: 10.1007/s10439-011-0312-7
21. Mantini D, Franciotti R, Romani GL, Pizzella V. Improving MEG source localizations: an automated method for complete artifact removal based on independent component analysis. *Neuroimage.* (2008) 40:160–73. doi: 10.1016/j.neuroimage.2007.11.022
22. Sander TH, Wubbeler G, Lueschow A, Curio G, Trahms L. Cardiac artifact subspace identification and elimination in cognitive MEG data using time-delayed decorrelation. *IEEE Trans Biomed Eng.* (2002) 49:345–54. doi: 10.1109/10.991162
23. Shao SY, Shen KQ, Ong CJ, Wilder-Smith EP, Li XP. Automatic EEG artifact removal: a weighted support vector machine approach with error correction. *IEEE Trans Biomed Eng.* (2009) 56:336–44. doi: 10.1109/TBME.2008.2005969
24. Uutela K, Taulu S, Hämäläinen M. Detecting and correcting for head movements in neuromagnetic measurements. *NeuroImage.* (2001) 14:1424–31. doi: 10.1006/nimg.2001.0915
25. Engemann D, Strohmeier D, Larson E, Gramfort A. Mind the noise covariance when localizing brain sources with M/EEG. In: *2015 International Workshop on Pattern Recognition in NeuroImaging*. (2015). p. 9–12. doi: 10.1109/PRNI.2015.25
26. Engemann D, Gramfort A. Automated model selection in covariance estimation and spatial whitening of MEG and EEG signals. *NeuroImage.* (2015) 108:328–42. doi: 10.1016/j.neuroimage.2014.12.040
27. Kuhl PK, Ramírez RR, Bosseler A, Lin JL, Imada T. Infants' brain responses to speech suggest analysis by synthesis. *Proc Natl Acad Sci USA.* (2014) 31:11238–45. doi: 10.1073/pnas.1410963111
28. Mittag M, Larson E, Clarke M, Taulu S, Kuhl PK. Auditory deficits in infants at risk for dyslexia during a linguistic sensitive period predict future language. *NeuroImage Clin.* (2021) 30:102578. doi: 10.1016/j.nicl.2021.102578
29. Gramfort A, Luessi M, Larson E, Engemann DA, Strohmeier D, Brodbeck C, et al. MEG and EEG data analysis with MNE-Python. *Front Neurosci.* (2013) 7:267. doi: 10.3389/fnins.2013.00267
30. Gramfort A, Luessi M, Larson E, Engemann DA, Strohmeier D, Brodbeck C, et al. MNE software for processing MEG and EEG data. *NeuroImage.* (2014) 86:446–60. doi: 10.1016/j.neuroimage.2013.10.027
31. Boto E, Holmes N, Leggett J, Roberts G, Shah V, Sofie SS, et al. Moving magnetoencephalography towards real-world applications with wearable systems. *Nature.* (2018) 555:657–61. doi: 10.1038/nature26147
32. Roberts TPL, Paulson DN, Hirschkoff E, Pratt K, Mascarenas A, Miller P, et al. Artemis 123: Development of a whole-head infant and young child MEG system. *Front Hum Neurosci.* (2014) 8:99. doi: 10.3389/fnhum.2014.00099
33. Okada Y, Hämäläinen M, Pratt K, Mascarenas A, Miller P, Han M, et al. BabyMEG: a whole-head pediatric magnetoencephalography system for human brain development research. *Rev Sci Instru.* (2016) 87:094301. doi: 10.1063/1.4962020

Conflict of Interest: The authors declare that the research was conducted in the absence of any commercial or financial relationships that could be construed as a potential conflict of interest.

frontiers in Neurology

REVIEW
published: 29 March 2022
doi: 10.3389/fneur.2022.837893

Dynamical Network Models From EEG and MEG for Epilepsy Surgery—A Quantitative Approach

Miao Cao[1,2,3], *Simon J. Vogrin*[2,3,4], *Andre D. H. Peterson*[2,3], *William Woods*[4], *Mark J. Cook*[2,3] *and Chris Plummer*[2,3,4]*

[1] Center for MRI Research, Peking University, Beijing, China, [2] Department of Medicine, The University of Melbourne, Melbourne, VIC, Australia, [3] Centre for Clinical Neurosciences and Neurological Research, St Vincent's Hospital Melbourne, Melbourne, VIC, Australia, [4] School of Health Sciences, Swinburne University of Technology, Melbourne, VIC, Australia

There is an urgent need for more informative quantitative techniques that non-invasively and objectively assess strategies for epilepsy surgery. Invasive intracranial electroencephalography (iEEG) remains the clinical gold standard to investigate the nature of the epileptogenic zone (EZ) before surgical resection. However, there are major limitations of iEEG, such as the limited spatial sampling and the degree of subjectivity inherent in the analysis and clinical interpretation of iEEG data. Recent advances in network analysis and dynamical network modeling provide a novel aspect toward a more objective assessment of the EZ. The advantage of such approaches is that they are data-driven and require less or no human input. Multiple studies have demonstrated success using these approaches when applied to iEEG data in characterizing the EZ and predicting surgical outcomes. However, the limitations of iEEG recordings equally apply to these studies—limited spatial sampling and the implicit assumption that iEEG electrodes, whether strip, grid, depth or stereo EEG (sEEG) arrays, are placed in the correct location. Therefore, it is of interest to clinicians and scientists to see whether the same analysis and modeling techniques can be applied to whole-brain, non-invasive neuroimaging data (from MRI-based techniques) and neurophysiological data (from MEG and scalp EEG recordings), thus removing the limitation of spatial sampling, while safely and objectively characterizing the EZ. This review aims to summarize current state of the art non-invasive methods that inform epilepsy surgery using network analysis and dynamical network models. We also present perspectives on future directions and clinical applications of these promising approaches.

Keywords: dynamical network models, non-invasive, EEG, MEG, epilepsy, epilepsy surgery

OPEN ACCESS

Edited by:
Rafeed Alkawadri, University of Pittsburgh Medical Center, United States

Reviewed by:
Aileen McGonigal, Aix-Marseille Université, France
Marc Goodfellow, University of Exeter, United Kingdom

***Correspondence:**
Chris Plummer
chris.plummer@svha.org.au

Specialty section:
This article was submitted to Applied Neuroimaging, a section of the journal Frontiers in Neurology

Received: *17 December 2021*
Accepted: *01 March 2022*
Published: *29 March 2022*

Citation:
Cao M, Vogrin SJ, Peterson ADH, Woods W, Cook MJ and Plummer C (2022) Dynamical Network Models From EEG and MEG for Epilepsy Surgery—A Quantitative Approach. Front. Neurol. 13:837893. doi: 10.3389/fneur.2022.837893

1. INTRODUCTION

Epilepsy is a debilitating neurological disorder that affects 1–2% of the population worldwide (1). About two thirds of epilepsy patients may have their seizures controlled using anti-epileptic drugs (AEDs), while at least one third of patients do not adequately respond to medications (2, 3). More crucially, this ratio of pharmaco-refractory patients has not changed with the introduction of new first-line AEDs each year (4). For those pharmaco-refractory patients, surgical intervention (with the removal of brain tissue driving ictogenesis) can serve as a viable option for the treatment of drug-refractory epilepsy (5).

The success rate of epilepsy surgery is between 30 and 70% (6, 7). A recent multi-center study suggests the success rate of epilepsy surgery is about 50% (8). While the role of epilepsy surgery is well-established, the estimated ratio of operated to potentially eligible patients is only 1:25–50 (9). Accurate localization of the epileptogenic zone (EZ)—the minimum brain area to be removed to render a patient seizure free—is the ultimate goal in the pre-surgical evaluation of these patients (5, 10). Invasive intracranial monitoring (with direct recordings of local field potentials generated by pathological brain tissue) is still the gold standard to delineate the EZ presurgically (1, 5, 6). However, it is not a true gold standard because intracranial recordings have multiple key limitations (11). These include high cost, significant patient morbidity, and the element of subjectivity involved in the identification of the iEEG-defined seizure onset zone (SOZ) (8, 11). The analysis of ictal iEEG is typically restricted to visual inspection; however, a more objective approach to the analysis of iEEG data is beginning to emerge in the clinical setting (12–14). For instance, a number of investigators have developed quantitative approaches (12–14) to the analysis of clinical EEG to reduce the degree of subjectivity involved in the clinical interpretation of these complex datasets. Of the various forms of iEEG (classical sEEG, isolated depth electrodes, intraoperative monitoring, subdural grids, and strips), it is sEEG (with its more extensive sampling capacity) that has fostered a deeper understanding of the network nature of the EZ, challenging the clinical view that the EZ is a discrete unifocal zone.

Network analysis and network models have assumed important roles in the present-day imaging of brain networks and their functions (15–17). As a fast-evolving research area, the recent advances in network analysis and network models enable the study of both normal and pathological brain dynamics by taking into account high-dimensional information obtained using neurophysiological and neuroimaging approaches (18–20). Aided by techniques from neuroscience and neuroimaging, a large number of studies using network analysis and network models have shed new light on our understanding of the enormous complexity of the epileptic brain (21).

Dynamical network models provide great capacity to probe the mechanisms underlying complex neural dynamics (15, 17, 22, 23). Inspired by pioneering studies of excitatory and inhibitory neurons as well as the alpha rhythm of the thalamus (24–26), investigators have developed dynamical models of neural mass and neural mass networks, which connect an ensemble of neural mass models into macroscopic neural systems (27, 28). Employing dynamical network models, multiple attempts have been made to understand the mechanisms underlying normal and pathological neural dynamics (29–34). Dynamical network models have also been applied to neurophysiological data recorded from the human brain to develop specific hypotheses toward clinical application (20, 29, 31, 35, 36). In this review, recent advances and notable developments in the field will be examined in the context of epilepsy surgery.

2. A GENERIC WORKFLOW

A generic workflow of applying network analysis and dynamical network models to EEG and MEG source signals is depicted in **Figure 1**. EEG and MEG signals acquired as part of the presurgical evaluation are first preprocessed *via* multiple steps before they are source modeled (37). After preprocessing, the head model and source space are constructed using the individual's MRI data. Forward and inverse solutions are then generated for source imaging. Source signals in defined source space can be then reconstructed. With reconstructed source signals, functional networks can be constructed using connectivity approaches.

Network modeling generally requires a connectivity analysis to obtain a network structure or topology as the basis of the modeling as the first step. This network structure may come from structural imaging data such as tractography or functional connectivity. When using functional connectivity to determine network structure, a series of time-evolving functional networks may be used (19) or a time-domain averaged functional network may be used. Some models also offer the capacity to use directional networks and hence effective connectivity and causal relationships may be integrated into the network structure (33, 38). Nodal level neural dynamics can then be embedded into network nodes. Multiple models of neural dynamics using different mathematical mechanisms can be employed in this step. Some models also offer flexibility by accommodating the use of different models to configure nodal neural dynamics. Network simulations can then be run with or without external inputs, such as perturbatory white noise. By introducing external noise, "stimulation," or change in parameters, models can effect a transition from non-seizure states to seizure states (39–42).

Each model generates a probability map that depicts the likelihood of brain areas being responsible for interictal or ictal source activity depending on the nature and the assumptions that a method or model employs. Such probability maps can then be used to assess the concordance level with resection bed. Using concordance levels and post-surgical outcomes, the performance of models and approaches can be tested. Two patient examples are given in **Figure 2**.

3. FUNCTIONAL AND STRUCTURAL NETWORKS IN FOCAL EPILEPSY

With ongoing advances in neuroimaging techniques, high-resolution functional and structural neuroimaging data can be obtained from epilepsy patients for assessment, diagnosis, treatment, and research. Connectivity methods have commonly been used to construct functional and structural networks using neuroimaging data. This subsection discusses findings from studies using functional and structural connectivity and problems and limitations associated with connectivity analysis in epilepsy.

3.1. Structural Networks in Focal Epilepsy

When studying functional brain networks, an intuitive question to ask is how structural networks constrain functional

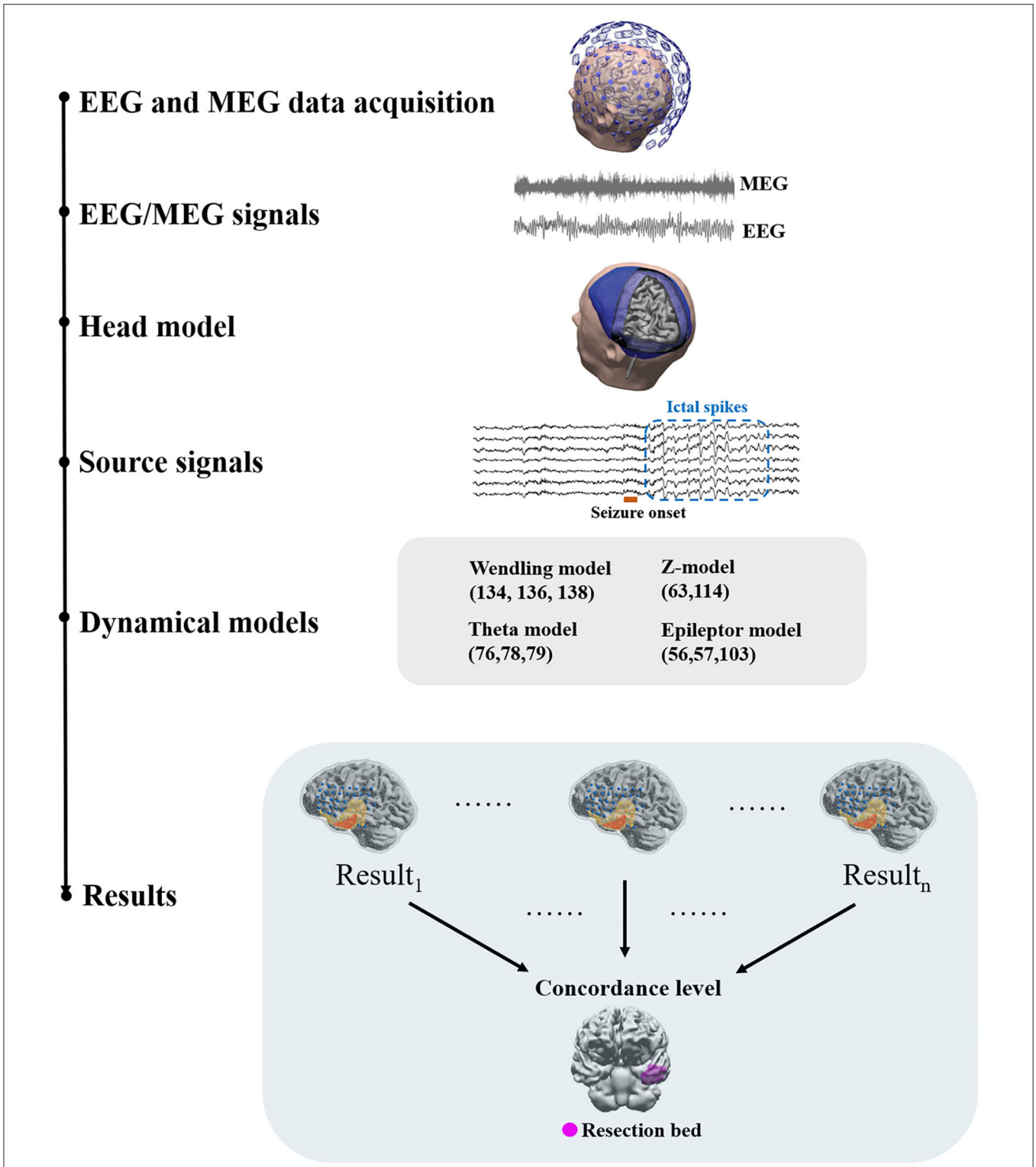

FIGURE 1 | A generic workflow. EEG and MEG signals are acquired for presurgical evaluation. Preprocessing of EEG and MEG signals is often required before source modeling to remove artifacts. The head model and the co-registered source space are then prepared using individual structural MRI data to generate a forward solution. Inverse solutions can be then generated using forward solutions and EEG/MEG signals. Using inverse solutions, source activity can be localized and reconstructed. Next, functional networks can be constructed using source signals and dynamical network models can be applied to identify brain areas that are responsible for ictal or interictal discharges. Dynamical network models can be then clinically validated against surgical resection margins linked to histology and post-surgical outcome.

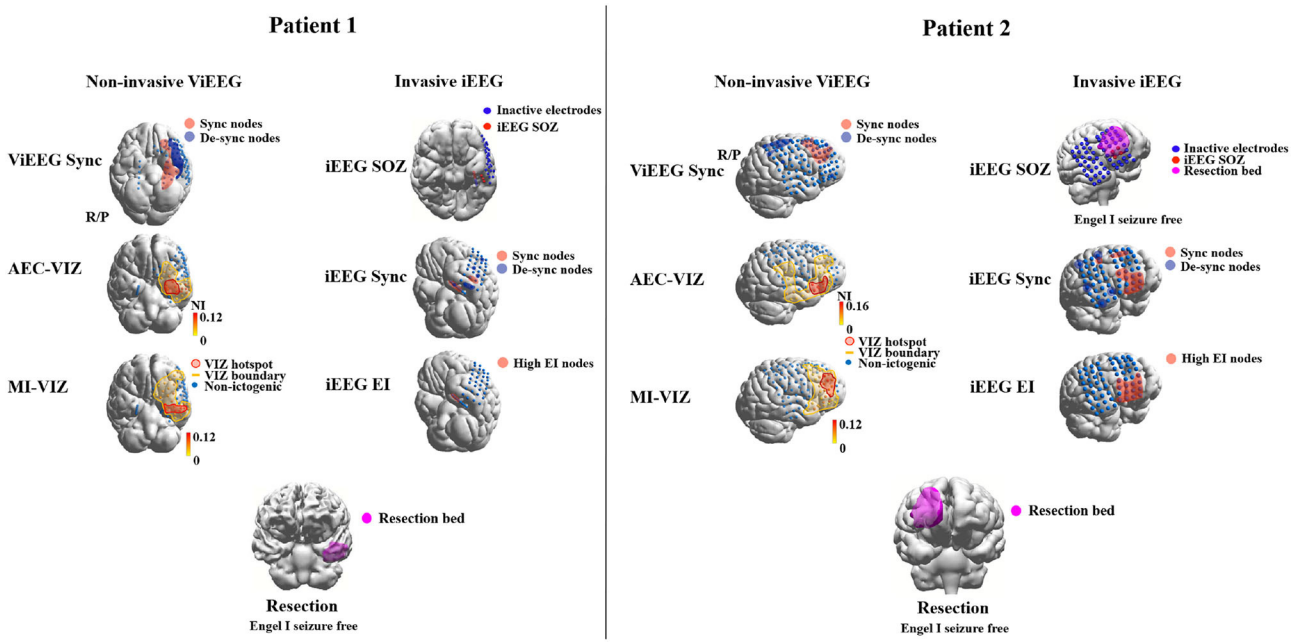

FIGURE 2 | Examples of applying dynamical network models to non-invasive (MEG) and invasive (iEEG) data to identify brain areas that are responsible for ictogenesis. Three approaches are applied to MEG and iEEG data, respectively, to identify brain areas that are responsible for seizure generation (red highlight). These areas are then compared against the resection margin and surgical outcomes to validate the results of employed approaches. The Sync approach uses synchronizability and control centrality (19) to identify nodes that increase or decrease of the stability of the synchronous states of the network. AEC-VIZ and MI-VIZ represent the ictogenic zone identified using virtual iEEG signals reconstructed by ictal MEG and dynamical network models. Amplitude Envelope Correlation (AEC) and Mutual Information (MI) can be used to construct functional networks that are then fed to dynamical network models. Here, a Theta model is used to simulate ictal waveforms and a virtual resection technique to estimate the influence of each node on ictogenicity. The Epileptogenicity Index (EI) (43) estimates spectral and temporal features of ictal iEEG signals and provides a quantitative measure to identify epileptogenic areas. iEEG SOZ is the conventional clinical analysis of ictal iEEG signals to identify iEEG electrodes where seizures arise. For both patients, brain areas involved in epileptogenesis identified by noninvasive dynamical approaches are comparable to the areas identified by traditional invasive intracranial means. Both patients had an Engel 1 outcome—Patient 1 **(left)** had focal cortical dysplasia Type 1 and Patient 2 **(right)** had post-infectious cortical gliosis.

networks. MRI techniques and structural connectivity have been introduced to address this. MRI techniques are widely used in clinical workup to localize pathological brain regions and understand epileptogenesis (1, 44). Diffusion MRI (dMRI) is a variant of standard MRI and one of the mainstream structural imaging techniques (45).

In a typical connectivity analysis, a standard MRI scan is required to capture an individual's neuroanatomical structure. Analytical software, such as Freesurfer (46), can be used to segregate the whole brain into subregions based on a standard brain atlas or customized boundaries (47, 48). With dMRI, software that tracks fiber density or integrity can be then used to detect, count and quantitatively characterize fibers that communicate between parcelated brain regions. This fiber density analysis results in a two-dimensional connectivity matrix, representing how strongly subregions are interconnected *via* white matter. This two-dimensional connectivity matrix may become a "fingerprint" of an individual's structural networks. Properties of the individualized connectivity matrix may characterize critical features of a pathological brain (49, 50). Early studies using dMRI and connectivity analysis suggest a change in structural connectivity in the epileptogenic zone and surrounding brain regions in focal epilepsy (44, 51, 52).

More specifically, in temporal lobe epilepsy (TLE) patients, structural alterations were reported in the epileptogenic zone in frontal and temporal lobes, but particularly at the temporal poles. These structural alterations revealed by tractography and connectivity analysis indicate distinct unilateral features and specific impacts on global structural connectivity (52). Despite variance introduced by individual differences and heterogeneous pathologies in group-level analysis, studies comparing TLE patients and healthy cohorts demonstrate extensive weakened temporo-parietal connections in TLE structural networks, which support the clinical observation of cognitive impairment in memory and speech (53, 54). Focke et al. (54) also demonstrate altered structural connectivity between para-hippocampal structures, providing a neuroanatomical basis for theoretical models of seizure propagation. In frontal lobe epilepsy, structural connectivity may remain intact in frontal regions, while nearby regions can be affected by interictal and ictal activity (55). Epilepsy involving mesial frontal areas preserves a robust connectivity in the supplementary motor area. Similar lower fiber intensity found in the superior longitudinal fasciculus, but not in the cingulum, suggests particular functional abnormalities for children with focal epilepsies (56). Diffusion imaging may also be used in animal models to study the extent of

white matter impairment. A rat model of focal epilepsy has been studied using dMRI and shows widespread reductions in white matter density in extensive brain regions beyond the epileptic focus, indicating the impaired efficiency of functional networks (57). Animal models, however, are not the focus of this review.

Structural networks defined by structural connectivity are not a complete representation of a pathological brain. Due to limitations of current techniques, structural MRI can only capture a small proportion of network connections on the macroscopic level. Whether this limitation affects interpretation of current studies in focal epilepsy remains unclear (45). Computer simulations show structural alterations are not necessary to generate seizure-like activity and epileptic networks are also believed to be fast-evolving dynamical networks (58). Therefore, rather than characterizing interconnected brain regions, static structural connectivity is more likely to answer how functional networks can be constrained by their corresponding structural substrates. This is important to keep in mind when interpreting findings on functional networks in focal epilepsy.

3.2. Functional Networks in Focal Epilepsy

Previous studies using functional connectivity mainly focus on time-series analysis of interictal and ictal events and report on network structural alterations over time before, during and after a seizure. To gain insights into the fast-evolving functional networks of seizure activity, recording techniques with high sampling rates, such as EEG, iEEG, and MEG, are broadly employed for epilepsy research. A number of studies have demonstrated the capacity of functional network structures of fast-evolving seizures to reflect properties of the putative EZ (13, 18, 58–61).

Using sEEG recordings, Bartolomei et al. (14) are credited as the first study to apply network analysis to explore non-linear relationships between different brain regions in temporal lobe epilepsy patients. Bartolomei et al. (62) offers a comprehensive review of network analysis specific to sEEG in epilepsy surgery. Khambhati et al. (19) show functional connectivity changes rapidly over time before focal seizure onset but not as much as it does during the seizure. By clustering time windows of iEEG data based on functional connectivity commonalities, Khambhati et al. (63) also find higher levels of synchronization in brain states that are close to focal seizure termination as opposed to brain states at the beginning or the middle of the seizure. These findings indicate that the epileptic brain has different functional network structures underlying seizure generation vs. termination. Schindler et al. (64) also demonstrated the shift in functional network structure toward a normal network state with transition from the pre-ictal to the ictal state.

Studies have reported that the ictal network structure for generalized seizures was more regular than the corresponding interictal network structure, thus suggesting that seizure events with seemingly "random" functional connectivity may preserve common patterns (65–67). Distinct patterns of functional connectivity have also been reported around seizure onset. Kramer et al. (68) demonstrated the SOZ presents a dominant regular sub-network with densely connected nodes. As a seizure progresses, the sub-network becomes divided into smaller random networks and hence the authors argue that these network features during the seizure progression may reflect decreased susceptibility of the network to become synchronized (68).

Interictal brain networks have also been examined in functional network studies. Resting-state EEG and MEG recordings in focal epilepsy patients show an increase in functional connectivity, which could reflect increased cortical excitability predisposing to epileptic seizures (69, 70). These authors also identified a decrease in network efficiency compared to control networks, perhaps indicating brain network disruption associated with interictal activity. Others employing network analysis of interictal data report conflicting results. Bartolomei et al. (71) presented decreased clustering coefficients and path lengths, while Horstmann et al. (72) show an increase in the same metrics. These inconsistencies could be due to differences in patient selection and methodologies. Current techniques representing functional networks may well need further refinement to characterize a pathological brain, particularly a brain predisposed to seizures.

Functional networks have also been studied using fMRI in generalized and focal epilepsies. In temporal lobe epilepsy, a general decrease in functional connectivity has been reported in the ipsilateral hemisphere and subcortical structures (73, 74). Another study reports that besides a general decrease in global functional networks, there is a relative increase in functional connectivity within the affected temporal lobe (75). In generalized epilepsy, a decreased intra-hemispheric connectivity and an increased inter-hemispheric connectivity are reported (76). Although associations between hemodynamic signals and electromagnetic signals require more investigation, these fMRI findings provide a different perspective on network behavior based on interictal data.

3.3. Relationship Between Structural and Functional Connectivity and Limitations of Connectivity Analysis

To date, a well-defined relationship between functional and structural connectivity is still missing in the literature for several reasons. First, functional connectivity in meso-scale brain networks still lacks sufficiently accurate neurophysiological and neuroanatomical substrates to interpret findings; to begin with, the coupling of structural to functional networks is not straightforward as findings from structural connectivity may not directly translate to neural dynamics governing interictal and ictal states. Second, structural connectivity is not always static and, as revealed by work in neuroplasticity, can change over longer time scales. Therefore, studies with different follow-up protocols are not always comparable. Third, individual differences make findings difficult to generalize statistically, especially when dealing with pathological substrates. For example, pathologies residing in different cortical regions may result in different functional and structural network structures complicating group analysis and potentially introducing errors to epileptic network modeling at the level of the individual. Such limitations of current connectivity analysis make it

difficult to clearly define the extent by which structural connectivity constrains functional connectivity. In the context of epilepsy, multiple factors potentially influence connectivity analysis findings. For example, the effect of anti-epileptic drugs (AEDs) on functional and structural connectivity is unclear (59). Heterogeneity of epilepsy patients is also non-trivial. Different lesion types and locations might exert different effects on functional and structural connectivity properties (77). Normally in epilepsy studies, patients with the same pathology and similar locations are grouped and studied together. Patients with the same pathology and similar locations may have very different ictal or interictal electrographic activity, while patients with different pathologies may demonstrate similar electrographic features (59). These factors need to be considered when validating network models in cohorts obeying conventional patient selection.

Contradictory results from different imaging modalities also influence how findings should be interpreted. EEG and MEG studies usually show global increases in functional connectivity compared to healthy controls, while fMRI studies show a general decrease. This might reflect fundamental differences between hemodynamic coupling and electrophysiological dynamics in epilepsy, not least in their respective temporal and spatial resolutions (78). Future studies that assess the relationship between neurophysiologic and hemodynamic connectivity are needed, possibly through simultaneous multi-modal neuroimaging studies (16, 59, 79, 80).

4. NETWORK ANALYSIS OF FUNCTIONAL BRAIN NETWORKS

Networks are an abstract mathematical construction that aim to represent the interaction of complex real-world systems. This concept has been introduced to many disciplines including physics, biology, ecology and neuroscience, to describe the mathematical behavior of complex systems. In neuroscience, networks are generally derived from functional and structural connectivity pathways, where "nodes" stand for different brain regions and "links" represent anatomical paths between brain regions or statistical correlations between neural activity (81). Network analysis using graph theoretical metrics, for example, has offered insights into how different brain regions are structurally connected and how different brain regions interact with each other spatio-temporally (49).

Over the last 5 years, network analysis has become a hot topic in clinical neuroscience research, as a pathological brain shows distinct features in structural and functional networks against a healthy brain (66, 67, 82). These brain network features can be used as biomarkers for clinical application. As epilepsy is becoming more recognized as a brain network disorder, network analysis allows us to study epilepsy and epileptic seizures from a novel perspective (18, 83, 84). The next section discusses how to define networks using connectivity methods and extract network features using graph-theoretical metrics. It also discusses findings and their interpretation from network analysis, and potential biomarkers that can be used for clinical applications.

4.1. Nodes and Edges

A network is composed of nodes and edges that link nodes. In functional brain networks, nodes stand for different brain areas and edges stand for functional dependence between regional activities (85). The way nodes and edges are defined often depends on the imaging modality that is used. For example, with fMRI, we can use a voxel, or several neighboring voxels as a node (86); independent component analysis (ICA) can also be used to aggregate voxels into nodes (87). Time-series of nodes that have the same independent component can be aggregated into a node. For sensor-based modalities, such as EEG and MEG, the preference is to directly use sensors as nodes or assign nodes in reconstructed source space (88). Brain parcelations of structural MRI also provides a sophisticated means of assigning brain areas to nodes, although this requires a-priori knowledge of individual brain structures and a standard brain atlas (89).

Edges are typically estimated by quantifying statistical dependency of neural activity between two regions (90). However, edges are not necessarily equal to connectivity matrices, as network edges can be binary (edge is either zero and not connected, or one and connected) or weighted (when normally a graph filter is applied to extract important edges). The reason to apply a graph filter is that functional connectivity can be affected by noise and other measures and graph filtering can remove such connections (91).

There are multiple ways to apply graph filters to brain networks. Setting a threshold to connectivity matrices can extract dominant connections. However, one of the problems with setting a hard threshold to a matrix is that edge weights can significantly increase or decrease depending on the brain state. Therefore, a constant hard threshold for different time windows may bias global network structures. Proportional thresholding can help with time window problems as it iteratively extracts top-ranked connections. However, a common problem of network thresholding is that without defining connections of interest, dominant connections across a certain time window could be irrelevant to analysis or might have even been generated by artifacts (92). In an effort to address such issues, Langer et al. (92) proposed the use of sophisticated statistics in their study, but given the enormous complexity of neural activity, it is difficult to select neural activities that are relevant for study by examining whether or not they are statistically correlated.

4.2. Graph Theoretical Metrics

With established functional networks, graph-theoretical metrics can be applied to study network properties. A number of graph-theoretical metrics have been developed to measure different network topological features and each of them has specific assumptions and requirements of the network (81). In general, graph-theoretical metrics extract four categories of network features: integration, segregation, motif, and centrality (93). For example, clustering coefficients and community detection metrics quantify how densely subgroups are connected in a network. Shortest path metrics, such as global efficiency and characteristic path length, estimate levels of network integration. Betweenness centrality and closeness centrality detect important hubs that bridge multiple sub-groups. Different metrics, by their

TABLE 1 | Commonly used graph-theoretical metrics and their scales, features, and requirements (81, 93).

Scale	Metric	Features				Requirements/
		Category	Weighted	Directed	Negative	Connected
Whole brain network	Characteristic path length	Integration	Yes	Yes	No	Yes
	Global efficiency	Integration	Yes	Yes	No	No
	Clustering coefficient	Segregation	Yes	Yes	No	No
	Local efficiency	Segregation	Yes	Yes	No	No
	Modularity	Segregation	Yes	Yes	Yes	No
	Motifs	Motif	Yes	Yes	No	No
Sub-networks	Transitivity	Segregation	Yes	Yes	No	No
	Edge betweenness	Segregation	Yes	Yes	No	No
Nodes	Degree	Basic metric	Yes	Yes	No	N/A
	Number of triangles around a node	Basic metric for segregation	Yes	Yes	No	N/A
	Shortest path length	Basic metric for segregation	Yes	Yes	No	N/A
	Closeness centrality	Centrality	Yes	Yes	No	No
	Betweenness centrality	Centrality	Yes	Yes	No	No

definition, extract different network properties, as shown in **Table 1**.

Selecting appropriate graph-theoretical metrics in studies is non-trivial. This metric selection normally depends on the research question, assumptions, and hypothesis (78). Several questions may be asked when choosing metrics, such as does the study focus on whole brain networks or sub-region networks? Is the study assuming its networks are fully connected or operating as isolated nodes or sub-groups? Does the study look at important nodes in networks? Specific hypotheses may lead studies to mainly look at a subset of nodes and edges, which may require tailored metrics to extract features of interest. Metric selection should also consider what imaging modality functional networks are derived from. Just as different imaging modalities have different spatio-temporal resolutions and reflect neural dynamics at different spatio-temporal scales, functional networks have different features and properties (94). Graph-theoretical metrics applied to these networks should take the inherent assumptions of specific network properties into account.

Thorough statistical tests of network models are critical. There are two ways of testing network models: (1) compare against numerically simulated reference models and (2) compare with models derived from other conditions, such as task vs. resting-state or healthy vs. pathologic (93). A statistically "null model" is often used as a reference model to test whether the phenomena that a model observes is random (95). However, a null model is not always statistically random. A null model is often assigned properties that the derived model shares. For example, a null model normally has the same node degree distribution and similar modular structure. Although network link weights of a null model usually remain random, they still follow distributions of the derived model (96).

4.3. Interpretation and Biomarkers

A question that is often raised when results are obtained from network analysis is how to interpret findings. Unfortunately, this question is not easy to answer. As discussed in previous sections, connectivity methods and graph-theoretical metrics reduce the dimensions of neuroimaging data but also increase levels of abstraction (97). Although new information can be obtained with higher levels of abstraction, we also lose the ability to directly interpret results and to understand neurophysiological substrates (98). Specifically, a small change in original neural signals will propagate through levels of abstraction, along with added complexity. In other words, any change at a high level of abstraction may not have a one-to-one mapping to original signals. Current studies use variable-control strategies to rule out factors that do not affect final results (99). However, this strategy may not be available when using complex approaches, such as network analysis. Interpreting results has remained a challenge in this area and current studies are generally conservative and cautious with interpretation.

Although interpreting findings from complex network analysis remains challenging, these findings can still be used

as potential biomarkers for clinical applications. For example, functional and structural coupling and decoupling have been found to be complex and mechanisms remain unknown (100). However, distinct patterns of decoupled functional and structural network structures may reflect long-term impairment in idiopathic generalized epilepsy patients and may be used as a biomarker to detect subtle brain abnormalities (100). Zweiphenning et al. (101) found high-frequency functional networks have distinct biomarkers that statistically predict the location of the seizure onset zone using interictal iEEG data. These biomarkers are useful for patients who do not have frequent clinical or sub-clinical seizures on iEEG monitoring. Studies using network modeling and network analysis have also discovered biomarkers with the potential to predict outcomes of epilepsy surgery (19, 29, 32, 102). These biomarkers may prove to be useful for presurgical evaluation if findings can be validated clinically through prospective studies and clinical trials.

4.4. Volume Conduction and Source Connectivity

The biophysical nature of volume conduction from neural sources to recorded signals can introduce field spread or smearing in connectivity calculations, whereby instantaneously correlated signals are reconstructed in localized brain areas and spurious connections are identified by conventional connectivity analysis. The early work in the biophysics of brain volume conductor modeling for electrophysiological signals has discussed this issue and is summarized in the review by Vorwerk et al. (103).

Unfortunately, this issue is not alleviated when simpler forward solutions are applied to MEG source reconstruction. Volume conduction also raises the concern as to whether or not non-invasive source analysis can achieve the spatial accuracy of invasive intracranial approaches. This is because volume conduction smears the electrical potential field (as well as the magnetic field) generated by a current dipole in the brain, particularly when the smeared field is observed from far afield. Fortunately, volume conduction only "mixes" neural activity in a linear fashion with zero delay in phase synchrony. This opens the door to find ways to limit volume-conduction related spurious connections interfering with connectivity calculations. By understanding the principle of volume conduction, various techniques have been developed over the last two decades to remove instantaneous correlation and phase synchrony between a pair of signals (65, 104–108). Unfortunately, a recent study that assesses these techniques demonstrates that none guarantee full identification and removal of spurious connections (109). Some approaches perform better than others in certain simulated paradigms but these may also turn out to be too conservative to remove real connections (110). While volume conduction can complicate the use of brain network approaches for the study of neural mechanisms, some argue that volume conduction is not a major concern when a biomarker of a certain phenomenon is the goal.

4.5. Studies Using Network Analysis for Epilepsy Surgery

Early work by Kramer at al. (111) looked at pre-seizure, seizure and post-seizure functional networks in four patients and uncovered localized brain structures that appear to facilitate seizure generation. This finding suggested that network analysis can assist identification of pathological brain areas and potentially target these areas for surgical treatment (111). Later, Wilke et al. (112) used directional networks and graph theoretical metrics to investigate interictal and ictal iEEG networks. More recently, a new technique, virtual cortical resection, has been developed using functional networks and validated against clinical iEEG data (19, 63, 94, 113). By analysing functional connectivity patterns of ictal iEEG data, Khambati et al. (63) developed a framework that statistically describes network dynamics in seizure generation, propagation, and termination. The topographic and geometrical changes captured by their model suggest strengthened synchronous connectivity near foci may help seizure termination. This finding suggests that modulating certain circuits near pathologic foci may disrupt seizure propagation or control seizure generation. Khambhati et al. (19) later extended the network model by analysing focal seizures with and without secondary generalization. The authors hypothesized that focal seizures with secondary generalization are more likely to synchronize in the pre-seizure state and there is a regulatory network mechanism that controls whether a focal seizure generalizes secondarily. A measure, synchronizability, which has been used in stability analysis of complex systems (114), was used to quantify stability and heterogeneity of time-varying functional networks in the model. And a novel metric, control centrality, was proposed to quantitatively estimate how the synchronizability of a network changes when a node is virtually removed from the network (virtual cortical resection). Counter-intuitively, brain regions that regulate seizure dynamics and control secondary generalization were often found to sit outside the SOZ. The implication here is that surgical resection of the SOZ alone does not necessarily lead to long-term seizure freedom. Their novel approach also provides a framework to develop techniques that can computationally simulate epilepsy surgery in order to provide an optimal surgical strategy. Kini et al. (113) further extend the framework using ictal events from iEEG and provide a statistical bio-marker that supports the idea that synchronizing nodes in the network should be removed in surgery, pending overlap with eloquent cortex.

A study by Jiang et al. (115) independently revealed similar "push-pull" dynamics that regulate secondary generalization of focal seizures. Differing from the specific gamma band of Khambhati et al. (19), Jiang et al.'s (115) push-pull dynamics comes from within- and across- frequency oscillations. Sohrabpour et al. (20) applied network analysis to the EEG source space to provide a non-invasively derived prediction of the EZ.

Other studies (112, 116) use directional networks to identify a subset of brain areas for potential surgical removal. Hassan et al. (117) and Juarez-Martinez et al. (118) extend network approaches to EEG and MEG source space with relatively small numbers of patients compared to Sohrabpour et al. (20). These

studies provide further insights into how network analysis can be translated from invasively recorded data to non-invasively recorded and ideally whole-brain data. Other network analysis studies using pre- and post-operative EEG, MEG, and fMRI data also found significant changes in functional connectivity patterns that were predictive of surgical outcomes (13, 18, 119, 120). A summary of studies using network analysis is given in **Table 2** and a comparison of network analysis and network modeling approaches by modality and source-sensor space is given in **Table 3**.

Despite the growing number of studies using network analysis for epilepsy surgical localization, prospective clinical studies are lacking. The numbers of patients included in studies has increased from one patient (117) to 36 patients (20). The retrospective nature and modest number of patients combine to limit the applicability and generalizability of network analysis approaches to clinical work-up for epilepsy surgery.

5. NETWORK MODELS FOR EPILEPSY SURGERY

Dynamical network modeling is a branch of network science employing mathematical and computational techniques to depict, analyse and understand the dynamical behavior of the network i.e., how a specific network structure impacts on the system behavior, particularly state transitions and bifurcations, through a set of evolution equations that yields quantitatively accurate depiction and prediction (123). Such techniques enable the properties of patient-specific functional network structures to be interrogated and the ensuing dynamics to be explained and predicted. In the case of diseased brain networks such as epilepsy, the evaluation and prediction of pathological state transitions such as seizures is invaluable in a clinical context such as epilepsy surgery. As opposed to network analysis, network models use established network structures as a basis and embed dynamical mathematical models to network nodes coupled by edge weights to simulate overall network dynamics. The process uses static functional networks derived from time-series data to a dynamical mathematical system that changes over time such that various states of brain networks can be numerically simulated for analysis. Here we present established network models for epilepsy surgery and include studies that have applied these models to empirical data.

5.1. Network Models

Four main network modeling techniques have been applied to epilepsy surgery: "Virtual Epileptic Patient" using the "Epileptor" model from Jirsa et al. (36), "Virtual Cortical Resection" model using network synchronizability and control centrality from Khambhati et al. (19), a computational model using network excitability from Goodfellow et al. (29) and another computational model similarly using network excitability from Sinha et al. (31).

The Virtual Epileptic Patient (VEP) model is a hybrid model using a phenomenologically derived neural field model, the Epileptor model (124). Each network node is defined in combination with structural networks and hypotheses derived from MRI lesions and other clinical information. This model uses the theory of fast-slow non-linear dynamics to characterize the bifurcations for seizure onset and offset. The VEP model demonstrates the prediction of ictal spatial patterns and confirmation of presurgical hypotheses (30, 124, 125), which may benefit presurgical evaluation and planning of invasive intracranial monitoring. It models epileptiform discharges in computational simulations and identifies the similar bifurcation mechanisms that produce epileptiform discharges using real data. The Epileptor model has demonstrated a capacity to predict seizure propagation using ictal sEEG data (124, 125).

Later work (21, 30, 36, 126) proposed an individualized whole-brain model that incorporates functional and structural network models. The Epileptor signifies an advance in mathematical modeling of epileptic seizures not only because the model provides a form of taxonomy of seizure activity using nonlinear coupled oscillators, but it also provides a mathematical etiology of seizure dynamics. Another advantage of this Virtual Epileptic Patient (VEP) is that, by combining the modeling of neural dynamics with the modeling of structural networks, the approach provides explanatory and predictive capacity in a clinical setting. Using sEEG combined with structural imaging modalities, this integrated approach virtually reproduces the seizure spread over the network that predicts the EZ (36). It is worth noting though that the VEP model requires sophisticated iEEG and neuroimaging workup and demands much of computing resources.

Although neuroimaging modalities, including DTI and fMRI, have been routinely used by some centers in presurgical epilepsy workup, scanner availability and scanning time are still limited in many surgical centers, especially those in developing countries. Despite the limitations of the VEP model, the findings encourage the use of the VEP model in a multi-center clinical trial. Such an integrated approach has the potential to be extended to the study of normal brain networks and to other neurological diseases.

The virtual cortical resection model provides specific insights into seizure evolution, particularly seizure initiation, and termination (19). Unlike the Virtual Epileptic Patient (36), the virtual cortical resection model only uses data from invasive intracranial recordings. By converting intracranial signals into fast evolving functional networks over time, two network metrics from network control theory (synchronizability and control centrality) are used to explore the contribution a node makes to the network dynamics. The virtual resection technique employed Master Stability Function (MSF) to estimate stability of synchronization (i.e., synchronizability) by looking at eigenspectra over time. However, MSF treats each node in the network as identical and synchronized and hence, is less concerned with individual dynamics (127). By correlating the mathematical change in functional network structure to clinical resection margins and surgical outcomes, the model suggests network nodes with high control centrality are likely to be included in the resection when a patient achieves a favorable outcome. The synchronizability values of functional networks using data before seizure onset successfully predict whether a focal seizure secondarily generalizes. This model

TABLE 2 | A summary of network analysis studies for epilepsy surgery.

References	Functional network	Patient number	Clinical data	Pathology	Findings	Comments
Bartolomei et al. (14)	Undirectional& directional	18	Ictal SEEG	Various pathologies in temporal lobes	Confirmation of network phenomena during temporal lobe epilepsy seizures	The first study that analyzed the network phenomena in focal epilepsy
Jiang et al. (115)	Directional	24	Ictal iEEG	Various pathologies and locations	Secondary generalization of focal seizures is regulated by cross frequency push-pull dynamics	Second publication in literature on push-pull mechanisms of focal seizure
Sohrapour et al. (20)	Directional	36	Interictal & ictal iEEG + numerical simulations	Various pathologies and locations		
Khambhati et al. (19)	Undirectional	10	Peri-ictal iEEG	Various pathologies and locations	Identify a push-pull mechanism that regulates focal seizure secondary generalization	First paper reported such finding
Kini et al. (113)	Undirectional	28	Ictal iEEG	Various pathologies and locations	Synchronizing nodes should be considered to remove in surgical planning	Subsequent work of Khambhati et al. 2016 (19)
Lin et al. (116)	Undirectional	13	Ictal iEEG	Not available		
Wilke et al. (112)	Directional + graph theory	25	Ictal and interictal iEEG	Various pathologies and locations		
Kramer et al. (111)	Undirectional	4	Ictal iEEG	Various pathologies and locations	Localized brain areas that facilitate seizures and potential target for surgical removal	Early work analysing functional networks of ictal events using iEEG
Juarez-Marineza et al. (118)	Undirectional + source imaging	9	Ictal sEEG + interictal MEG	Various pathologies and locations	Reproduce seizure onset zone non-invasively and potentially identify biomarker for EZ	First MEG non-invasive source space analysis
Hassan et al. (117)	Undirectional + source imaging	1	Ictal sEEG + ictal EEG	Not available	Identify epileptic focus that also matches findings from sEEG recordings	

TABLE 3 | A comparison matrix demonstrates current state of each direction of network analysis and network models using different imaging modalities.

Network analysis/ Models		Network analysis	Network mode
MEG	Source	Main field (diagnosis, prognosis, surgical strategy), but no comparison against source localization	No
	Sensor	Sensor-level analysis is more significantly affected by volume conduction and field spread than source space	No
Scalp EEG	Source	Main field (diagnosis, prognosis, surgical strategy), but no comparison against source localization (121) is the first study.	One study from Lopes et al. (122)
	Sensor	Main field (diagnosis, prognosis, seizure prediction)	Main field (diagnosis, prognosis, seizure prediction)
iEEG	Source	No	No
	Sensor	Main field (diagnosis, prognosis, surgical strategy)	Main field (diagnosis, prognosis, surgical strategy)

provides important insights into this field. It offers an objective approach for surgery and carries the potential to optimize the surgical strategy.

The computational model from Goodfellow et al. (29) uses the Wendling Model (33, 128) to describe nodal level neural dynamics from functional connectivity analysis of ictal iEEG signals. While each node has the same dynamics characteristics, the network topology determines how the network transitions from the non-seizure state to the seizure state. The model is calibrated to assume that 50% of the nodes in the network transition into a seizure state with the whole network spending 50% of its time in a seizure state (29, 35). The total amount of time the network spends in the seizure state may increase, decrease, or remain the same when the network topology is changed with the removal of a given node. The assumption of this model is that virtually removed nodes that shorten seizure state time should be removed to reduce the risk of ictogenesis. A series of studies based on the theta model (35), which is a simplified version of the Wendling model, showed a correlation between model prediction and surgical outcome. By doing so, the model offers an opportunity to optimize surgical strategy for cases with unfavorable surgical outcomes. Another computational model from Sinha et al. (31) uses a similar mathematical framework (23, 129) to predict surgical outcomes and alternative surgical strategies.

5.2. Studies Using Network Models for Epilepsy Surgery

The work from Goodfellow et al. (29) and Jirsa et al. (36) are the early attempts to apply network models to intracranial data obtained for epilepsy surgery. These fundamental contributions motivated by earlier theoretical work (23, 124, 129–131) led to a series of publications aiming to more objectively and accurately predict the EZ. Goodfellow et al. (29) employed a full Wendling model to simulate excitability at the nodal level and predict surgical outcomes based on degree of overlap between model-predicted ictogenic nodes and resection margins. The study suggested that at least one node of high ictogenicity should be included in the surgical resection to achieve a more favorable surgical outcome. To better understand the relationship between SOZ and EZ, another measure, Seizure Likelihood was developed together with an earlier measure, Node Ictogenicity (NI) (29) to systematically compare the SOZ with the EZ. It was found that the SOZ may not be the best predictor of the EZ when there is significant heterogeneity in network topology and node excitability (132). This is perhaps in line with the clinical observation that SOZ-based resections do not always provide optimal outcomes (5). A later study on the same dataset reveals that a so-called "rich-club" organization (133) (a structure with multiple hub nodes that densely interconnect sub-networks) can be found in epilepsy surgical candidates and that disruption of rich-club modules might optimize surgical outcomes (35). This finding is also predicted by simulations using the same theoretical model that is simpler than the Wendling model. The most recent work by Lopes et al. (122) has extended their network model to non-invasive EEG source space. Using a simplified Wendling model and minimum-norm estimation, EEG source signals are modeled in a similar fashion to iEEG signals. Their results suggest that the network model predicts the lateralization of epileptogenic sources with modest spatial resolution. This work represents an important step in the effort to more objectively characterize the EZ non-invasively using source space signals and network models.

By extending the work of Jansen et al. (134) to also include a slow inhibitory population, Wendling et al. (129) model seizure onset by mathematically simulating the fast and slow oscillations of both excitatory and inhibitory neuronal populations. This model was used by Terry et al. (23) to inversely fit intracranial EEG data. Bettus et al. (69) and Wendling et al. (135) also applied the model to both intracranial EEG and scalp EEG. Wendling et al. (136) then extend the network model to understand seizure

generation and propagation networks. More recent work has looked at the effects of disrupting network nodes that regulate seizure propagation (19, 113, 137) with results that challenge the traditional approach of SOZ resection as best practice for epilepsy surgery (19, 29, 94, 113, 132).

A multi-level computational model has lately been proposed to better replicate observed signals from experimental data for improved prediction of ictogenesis. This network model has been extended to EEG source space with promising results that reflect a good match between the interictal EEG source network and the interictal sEEG network (138). The study also found that the multi-level network model performs better in the localization of multi-focal epilepsy.

5.3. Summary of Network Models for Epilepsy Surgery

It is difficult to compare different studies using network models to predict the EZ owing to differences in the initial modeling assumptions and variation in patient cohorts, iEEG approaches, pathologies, and post-operative follow-up. The dominance of small studies and single case reports also limits the translatability of these approaches to the clinical setting. As presented in **Table 4**, there is accumulating evidence that network models can (a) predict the EZ using invasive neurophysiological data and non-invasive EEG data, (b) help unravel mechanisms of ictal and interictal discharge generation and propagation, and (c) allow the study of brain networks to be conducted in a patient-specific fashion. Long-term prospective studies are now needed, particularly with network modeling approaches based on the use of non-invasive, whole-brain data in an effort to reduce our reliance on invasively acquired data.

6. DISCUSSION

Dynamical network models have the potential to improve characterization and delineation of the EZ. While initially based on iEEG recordings, these models have more recently been extended to the analysis of non-invasive EEG and MEG whole-brain recordings that, unlike iEEG, are not affected by limited spatial sampling, nor sensor positions.

6.1. Advantages of This Approach

Dynamical network modeling approaches represent an important shift away from a subjective interpretation of iEEG recordings toward an objective quantification of the putative EZ with their novel analyses of EEG and MEG interictal and ictal electrophysiological signals. By testing the effects of candidate epileptogenic nodes on network excitability and seizure transition states, these approaches permit deliberate, step-wise hypothesis testing of neural pathways that are critical for seizure generation and propagation before any surgical intervention takes place (29, 31, 32, 35). And, while not the focus of this review, in patients who are not deemed surgical candidates, these approaches may still be useful for neuromodulation targets. Recent work from Li et al. (40) and Scheid et al. (39) suggests "weak" nodes can be identified using network models for which neuromodulation strategies may be devised to reduce seizure susceptibility. Further study is required to clinically validate this concept. The interrogation of whole-brain structural and functional networks overcomes the major limitation of traditional invasive monitoring that is highly dependent on the implicit assumption that iEEG electrodes are placed in the ideal position for accurate delineation of the EZ (20). The approach also minimizes the influence of subjective clinical interpretation of seizure semiology in the pre-surgical work-up of these patients. For pre-operative planning, the quantifiable nature of dynamical network modeling facilitates an objective comparison with traditional non-invasive methods of EZ mapping, such as PET (positron emission tomography) and SPECT (single-photon emission computed tomography).

6.2. Limitations of This Approach

There are several limitations of dynamical network modeling combined with EEG and MEG source imaging. As discussed previously, field spread and signal leakage reduces the spatial resolution of source solutions and may limit the capacity of models to accurately identify the EZ (109, 140). Modeling is also dependent on the acquisition of high quality EEG or MEG interictal and ictal signals with minimal noise and artifact interference (141, 142). As also noted, all network models have underlying mathematical and physiological assumptions that may not be entirely valid such that, to date, no favored systematic approach exists (33). The veracity of these assumptions can only be rigorously tested with prospective epilepsy surgery studies, which are currently lacking. Indeed, dynamic network modeling is still in its infancy and the relationship between structural networks and functional networks is not yet clear, particularly with respect to a complex problem such as epilepsy. To date, these approaches cannot reliably distinguish between different anatomical structures based on the specific pathology.

6.3. Next Steps

Multi-modal neuroimaging techniques have assisted pre-surgical characterization of the putative EZ in pharmaco-refractory focal epilepsy. Better techniques are needed for the more challenging patients with MRI-normal and complex lesional focal epilepsy (141, 143, 144). To this end, network analysis and dynamical network models have shown considerable promise with their more objective computational approach to finding a surgical solution in these difficult cases (29–31). As pointed out here and by others (13, 18, 50, 113, 145), large cohorts are required to assess the effectiveness of these approaches in the clinical setting. Dynamical modeling may further assist by combining with different neuroimaging techniques, such as fMRI and tractography, to better model patient-specific brain structures and pathological dynamics to improve the efficacy and clinical utility of epilepsy surgery. How such a combined approach provides clinical value is yet to be fully elucidated but recent achievements by Jirsa et al. (124) and Proix et al. (30) demonstrate the merit of incorporating functional and structural information into the predictive model. It is conceivable that whole brain dynamic network modeling approaches may eventually render intracranial exploration unnecessary or even

TABLE 4 | A summary of studies using network models for epilepsy surgery.

References	Network model	Patient number	Clinical data	Pathology	Findings	Comments
Goodfellow et al. (29)	Wendling model	16	Ictal iEEG (grid) + numerical simulations	Various, lesional and nonlesional	Predict surgical outcome. Alternative or optimal surgical strategy can be offered	First attempt on clinical data in this series
Lopes et al. (32)	Wendling + Theta model	16	Peri-ictal & Ictal iEEG (grid) + numerical simulations	Various, lesional and nonlesional	Alternative or optimal strategy may be offered by removing rich-club structures	Subsequent work of Goodfellow et al. (29)
Lopes et al. (35)	Theta model	16	Peri-ictal iEEG (grid)	Various, lesional, and nonlesional	Predict surgical outcome using a metric derived from network model	Subsequent work of Lopes et al. (32)
Lopes et al. (132)	Theta model	16	iEEG (grid)	Various, lesional, and nonlesional	SOZ is not a good predictor of EZ for focal epilepsies with a multi-focal nature	Subsequent work of Lopes et al. (35)
Lopes et al. (122)	Theta model	15	Scalp EEG	Various, lesional and nonlesional	Lateralization of EZ	Non-invasive EEG source space
Jirsa et al. (124)	Epileptor model	24	iEEG + data from animal model	Various, lesional, and nonlesional	Reproduce seizure propagation in brain networks as observed by iEEG	Propose the model
Proix and Jirsa (125)	Epileptor model	18	Ictal sEEG	Various, lesional, and nonlesional	Predict the seizure propagation	First attempt to use clinical data
Jirsa et al. (36)	Epileptor model + structural brain network	1	Ictal sEEG + structural neuroimaging data	Nonlesional	Individualized model, predict subset of brain structure responsible for seizure generation	Subsequent work of Jirsa et al. (124)
Proix et al. (30)	Epileptor model + structural brain network	15	Ictal sEEG + structural neuroimaging data	Various, lesional, and nonlesional	Structural networks are able to explain change in functional connectivity	Subsequent work of Jirsa et al. (124)
Wendling et al. (129)	Wendling model	5	Ictal sEEG + numerical simulations	mTLE (lesional and nonlesional)	Theoretical model produces realistic epileptic signals that match sEEG recordings from mTLE	The original theoretical work along with data validation
Wendling et al. (136)	Wendling model + Functional connectivity	1	sEEG	mTLE	Potential to identify epileptogenic networks	Subsequent work of Wendling et al. (129)
Wendling et al. (139)	Wendling model	1	sEEG + animal model	mTLE	Replicate observed signals and predict the mechanisms validated by experiments and clinical data	A multi-level computational model

obsolete. The limitations of intracranial monitoring in its current forms disqualifies it as a true gold standard for mapping EZ networks. The evolution of more sophisticated whole-brain dynamic modeling approaches, which can overcome the sampling problem, might establish a new standard for pre-surgical epilepsy planning that is closer to the ground truth for unraveling EZ pathways. Potential benefits for epilepsy surgery patients might include reduced peri-operative morbidity and improved post-operative outcome. Routine clinical application might help elucidate the structural and functional substrates that link seizure semiology to seizure onset and propagation (146) with less clinical subjectivity to the point where elements of the semiology, not routinely included in existing models, could refine future network modeling strategies.

7. CONCLUSION

This review provides an update on the emerging roles of network analysis and dynamical network modeling in the surgical work-up of patients with pharmaco-resistant epilepsy. While still in their relative infancy, these novel approaches lend more objectivity to identification of the epileptogenic zone and they add much-needed specificity and flexibility to hypothesis testing of neural networks that are involved in epileptogenesis at the individual patient level in the spirit of twenty-first century "precision" medicine. The increasing sophistication of structural and functional connectivity analysis (from MRI, fMRI, DTI, EEG, and MEG) has paved the way for the evolution of many promising dynamical network modeling strategies. Most importantly, in the clinical context of epilepsy surgery, the aim is to improve patient evaluation and perform a successful resection that grants patients long-term seizure freedom for a better quality of life. The potential clinical impact of dynamical network modeling to improve post-surgical outcomes and to limit the subjectivity and invasiveness tied to current-day intracranial monitoring will only be realized with successful translation of these approaches to large prospective clinical studies.

AUTHOR CONTRIBUTIONS

MCa: writing original draft. MCa, SV, AP, WW, MCo, and CP: writing review and editing. All authors contributed to the article and approved the submitted version.

ACKNOWLEDGMENTS

The authors would like to thank Dr. Jia-Hong Gao. We acknowledge the Australian National Imaging Facility for the support of WW and the MEG system at Swinburne University of Technology.

REFERENCES

1. Duncan JS, Winston GP, Koepp MJ, Ourselin S. Brain imaging in the assessment for epilepsy surgery. *Lancet Neurol*. (2016) 15:420–33. doi: 10.1016/S1474-4422(15)00383-X
2. Devinsky O, Vezzani A, O'Brien TJ, Jette N, Scheffer IE, de Curtis M, et al. Epilepsy. *Nat Rev Dis Primers*. (2018) 4:18024. doi: 10.1038/nrdp.2018.24
3. Thijs RD, Surges R, O'Brien TJ, Sander JW. Epilepsy in adults. *Lancet*. (2019) 393:689–701. doi: 10.1016/S0140-6736(18)32596-0
4. Moshé SL, Perucca E, Ryvlin P, Tomson T. Epilepsy: new advances. *Lancet*. (2015) 385:884–98. doi: 10.1016/S0140-6736(14)60456-6
5. Rosenow F, Lüders H. Presurgical evaluation of epilepsy. *Brain*. (2001) 124:1683–700. doi: 10.1093/brain/124.9.1683
6. Nowell M, Miserocchi A, McEvoy AW, Duncan JS. Advances in epilepsy surgery. *J Neurol Neurosurg Psychiatry*. (2014) 85:1273–9. doi: 10.1136/jnnp-2013-307069
7. Bagić AI. SQUIDs pro quorum. *J Clin Neurophysiol*. (2020) 37:469–70. doi: 10.1097/WNP.0000000000000743
8. Khoo A, Tisi J, Mannan S, O'Keeffe AG, Sander JW, Duncan JS. Reasons for not having epilepsy surgery. *Epilepsia*. (2021) 62:2909–19. doi: 10.1111/epi.17083
9. Bagi AI, Burgess RC. Utilization of MEG among the US epilepsy centers: a survey-based appraisal. *J Clin Neurophysiol*. (2020) 37:599–605. doi: 10.1097/WNP.0000000000000716
10. Kaiboriboon K, Lüders HO, Hamaneh M, Turnbull J, Lhatoo SD. EEG source imaging in epilepsyŰpracticalities and pitfalls. *Nat Rev Neurol*. (2012) 8:498–507. doi: 10.1038/nrneurol.2012.150
11. Parvizi J, Kastner S. Promises and limitations of human intracranial electroencephalography. *Nat Neurosci*. (2018) 21:474–83. doi: 10.1038/s41593-018-0108-2
12. Bartolomei F, Nica A, Valenti-Hirsch MP, Adam C, Denuelle M. Interpretation of SEEG recordings. *Clin Neurophysiol*. (2018) 48:53–7. doi: 10.1016/j.neucli.2017.11.010
13. Rummel C, Abela E, Andrzejak RG, Hauf M, Pollo C, Müller M, et al. Resected brain tissue, seizure onset zone and quantitative EEG measures: towards prediction of post-surgical seizure control. *PLoS ONE*. (2015) 10:e0141023. doi: 10.1371/journal.pone.0141023
14. Bartolomei F, Wendling F, Bellanger JJ, Régis J, Chauvel P. Neural networks involving the medial temporal structures in temporal lobe epilepsy. *Clin Neurophysiol*. (2001) 112:1746–60. doi: 10.1016/S1388-2457(01)00591-0
15. Breakspear M. Dynamic models of large-scale brain activity. *Nat Neurosci*. (2017) 20:340–52. doi: 10.1038/nn.4497
16. Bassett DS, Zurn P, Gold JI. On the nature and use of models in network neuroscience. *Nat Rev Neurosci*. (2018) 19:566–78. doi: 10.1038/s41583-018-0038-8
17. Ju H, Bassett DS. Dynamic representations in networked neural systems. *Nat Neurosci*. (2020) 23:908–17. doi: 10.1038/s41593-020-0653-3
18. Englot DJ, Hinkley LB, Kort NS, Imber BS, Mizuiri D, Honma SM, et al. Global and regional functional connectivity maps of neural oscillations in focal epilepsy. *Brain*. (2015) 138:2249–62. doi: 10.1093/brain/awv130
19. Khambhati AN, Davis KA, Lucas TH, Litt B, Bassett DS. Virtual cortical resection reveals push-pull network control preceding seizure evolution. *Neuron*. (2016) 91:1170–82. doi: 10.1016/j.neuron.2016.07.039
20. Sohrabpour A, Cai Z, Ye S, Brinkmann B, Worrell G, He B. Noninvasive electromagnetic source imaging of spatiotemporally distributed epileptogenic brain sources. *Nat Commun*. (2020) 11:1946. doi: 10.1038/s41467-020-15781-0
21. Wendling F, Benquet P, Bartolomei F, Jirsa V. Computational models of epileptiform activity. *J Neurosci Methods*. (2016) 260:233–51. doi: 10.1016/j.jneumeth.2015.03.027
22. Lytton WW. Computer modelling of epilepsy. *Nat Rev Neurosci*. (2008) 9:626–37. doi: 10.1038/nrn2416
23. Terry JR, Benjamin O, Richardson MP. Seizure generation: the role of nodes and networks. *Epilepsia*. (2012) 53:166–9. doi: 10.1111/j.1528-1167.2012.03560.x
24. Wilson HR, Cowan JD. A mathematical theory of the functional dynamics of cortical and thalamic nervous tissue. *Kybernetik*. (1973) 13:55–80. doi: 10.1007/BF00288786
25. Destexhe A, Sejnowski TJ. The WilsonŰCowan model, 36 years later. *Biol Cybern*. (2009) 101:1–2. doi: 10.1007/s00422-009-0328-3

26. da Silva FHL, Hoeks A, Smits H, Zetterberg LH. Model of brain rhythmic activity - the alpha-rhythm of the thalamus. *Kybernetik*. (1974) 15:27–37. doi: 10.1007/BF00270757
27. Deco G, Jirsa VK. Ongoing cortical activity at rest: criticality, multistability, and ghost attractors. *J Neurosci*. (2012) 32:3366–75. doi: 10.1523/JNEUROSCI.2523-11.2012
28. Peterson ADH, Cook BJ, Woldman W, Terry JR. Neural field models: a mathematical overview and unifying framework. *arXiv*. (2021). doi: 10.48550/arXiv.2103.10554
29. Goodfellow M, Rummel C, Abela E, Richardson MP, Schindler K, Terry JR. Estimation of brain network ictogenicity predicts outcome from epilepsy surgery. *Sci Rep*. (2016) 6:29215. doi: 10.1038/srep29215
30. Proix T, Bartolomei F, Guye M, Jirsa VK. Individual brain structure and modelling predict seizure propagation. *Brain*. (2017) 140:641–54. doi: 10.1093/brain/awx004
31. Sinha N, Dauwels J, Kaiser M, Cash SS, Westover MB, Yujiang W, et al. Predicting neurosurgical outcomes in focal epilepsy patients using computational modelling. *Brain*. (2017) 465:3475–82. doi: 10.1093/brain/aww299
32. Lopes MA, Richardson MP, Abela E, Rummel C, Schindler K, Goodfellow M, et al. An optimal strategy for epilepsy surgery: disruption of the rich-club? *PLoS Comput Biol*. (2017) 13:e1005637. doi: 10.1371/journal.pcbi.1005637
33. Deco G, Jirsa VK, Robinson PA, Breakspear M, Friston K. The dynamic brain: from spiking neurons to neural masses and cortical fields. *PLoS Comput Biol*. (2008) 4:e1000092. doi: 10.1371/journal.pcbi.1000092
34. Kalitzin SN, Velis DN, da Silva FHL. Stimulation-based anticipation and control of state transitions in the epileptic brain. *Epilepsy Behav*. (2010) 17:310–23. doi: 10.1016/j.yebeh.2009.12.023
35. Lopes MA, Richardson MP, Abela E, Rummel C, Schindler K, Goodfellow M, et al. Elevated ictal brain network ictogenicity enables prediction of optimal seizure control. *Front Neurol*. (2018) 9:98. doi: 10.3389/fneur.2018.00098
36. Jirsa VK, Proix T, Perdikis D, Woodman MM, Wang H, Bernard C, et al. The virtual epileptic patient: individualized whole-brain models of epilepsy spread. *NeuroImage*. (2017) 145:377–88. doi: 10.1016/j.neuroimage.2016.04.049
37. Michel CM, Brunet D. EEG source imaging: a practical review of the analysis steps. *Front Neurol*. (2019) 10:325. doi: 10.3389/fneur.2019.00325
38. Astolfi L, Cincotti F, Mattia D, Marciani MG, Baccala LA, Fallani FdV, et al. Comparison of different cortical connectivity estimators for highŰresolution EEG recordings. *Hum Brain Mapp*. (2007) 28:143–57. doi: 10.1002/hbm.20263
39. Scheid BH, Ashourvan A, Stiso J, Davis KA, Mikhail F, Pasqualetti F, et al. Time-evolving controllability of effective connectivity networks during seizure progression. *Proc Natl Acad Sci USA*. (2021) 118:e2006436118. doi: 10.1073/pnas.2006436118
40. Li A, Huynh C, Fitzgerald Z, Cajigas I, Brusko D, Jagid J, et al. Neural fragility as an EEG marker of the seizure onset zone. *Nat Neurosci*. (2021) 24:1465–74. doi: 10.1038/s41593-021-00901-w
41. Baier G, Goodfellow M, Taylor PN, Wang Y, Garry DJ. The importance of modeling epileptic seizure dynamics as spatio-temporal patterns. *Front Physiol*. (2012) 3:281. doi: 10.3389/fphys.2012.00281
42. Junges L, Lopes MA, Terry JR, Goodfellow M. The role that choice of model plays in predictions for epilepsy surgery. *Sci Rep*. (2019) 9:1–12. doi: 10.1038/s41598-019-43871-7
43. Bartolomei F, Trébuchon A, Bonini F, Lambert I, Gavaret M, Woodman M, et al. What is the concordance between the seizure onset zone and the irritative zone? A SEEG quantified study. *Clin Neurophysiol*. (2016) 127:1157–62. doi: 10.1016/j.clinph.2015.10.029
44. Besson P, Bandt SK, Proix T, Lagarde S, Jirsa VK, Ranjeva JP, et al. Anatomic consistencies across epilepsies: a stereotactic-EEG informed high-resolution structural connectivity study. *Brain*. (2017) 140:2639–52. doi: 10.1093/brain/awx181
45. Sotiropoulos SN, Zalesky A. Building connectomes using diffusion MRI: why, how and but. *NMR Biomed*. (2017) 2017:e3752. doi: 10.1002/nbm.3752
46. Fischl B. FreeSurfer. *NeuroImage*. (2012) 62:774–81. doi: 10.1016/j.neuroimage.2012.01.021
47. Alstott J, Breakspear M, Hagmann P, Cammoun L, Sporns O. Modeling the impact of lesions in the human brain. *PLoS Comput Biol*. (2009) 5:e1000408. doi: 10.1371/journal.pcbi.1000408
48. Messé A. Parcellation influence on the connectivityŰbased structureŰfunction relationship in the human brain. *Hum. Brain Mapp*. (2019) 41:1167–80. doi: 10.1002/hbm.24866
49. Bassett DS, Sporns O. Network neuroscience. *Nat Neurosci*. (2017) 20:353. doi: 10.1038/nn.4502
50. Stam CJ. Modern network science of neurological disorders. *Nat Rev Neurosci*. (2014) 15:683–95. doi: 10.1038/nrn3801
51. Guye M, Ranjeva JP, Bartolomei F, Confort-Gouny S, McGonigal A, Régis J, et al. What is the significance of interictal water diffusion changes in frontal lobe epilepsies? *NeuroImage*. (2007) 35:28–37. doi: 10.1016/j.neuroimage.2006.11.049
52. Nilsson D, Go C, Rutka JT, Rydenhag B, Mabbott DJ, Snead OC, et al. Bilateral diffusion tensor abnormalities of temporal lobe and cingulate gyrus white matter in children with temporal lobe epilepsy. *Epilepsy Res*. (2008) 81:128–35. doi: 10.1016/j.eplepsyres.2008.05.002
53. Besson P, Dinkelacker V, Valabregue R, Thivard L, Leclerc X, Baulac M, et al. Structural connectivity differences in left and right temporal lobe epilepsy. *NeuroImage*. (2014) 100:135–44. doi: 10.1016/j.neuroimage.2014.04.071
54. Focke NK, Yogarajah M, Bonelli SB, Bartlett PA, Symms MR, Duncan JS. Voxel-based diffusion tensor imaging in patients with mesial temporal lobe epilepsy and hippocampal sclerosis. *NeuroImage*. (2008) 40:728–37. doi: 10.1016/j.neuroimage.2007.12.031
55. Caciagli L, Bernhardt BC, Hong SJ, Bernasconi A, Bernasconi N. Functional network alterations and their structural substrate in drug-resistant epilepsy. *Front Neurosci*. (2014) 8:411. doi: 10.3389/fnins.2014.00411
56. Vaessen MJ, Jansen JFA, Braakman HMH, Hofman PAM, Louw AD, Aldenkamp AP, et al. Functional and structural network impairment in childhood frontal lobe epilepsy. *PLoS ONE*. (2014) 9:e90068. doi: 10.1371/journal.pone.0090068
57. Otte WM, Dijkhuizen RM, van Meer MPA, van der Hel WS, Verlinde SAMW, van Nieuwenhuizen O, et al. Characterization of functional and structural integrity in experimental focal epilepsy: reduced network efficiency coincides with white matter changes. *PLoS ONE*. (2012) 7:e39078. doi: 10.1371/journal.pone.0039078
58. Pittau F, Mégevand P, Sheybani L, Abela E, Grouiller F, Spinelli L, et al. Mapping epileptic activity: sources or networks for the clinicians? *Front Neurol*. (2014) 5:218. doi: 10.3389/fneur.2014.00218
59. Diessen EV, Hanemaaijer JI, Otte WM, Zelmann R, Jacobs J, Jansen FE, et al. Are high frequency oscillations associated with altered network topology in partial epilepsy? *NeuroImage*. (2013) 82:564–73. doi: 10.1016/j.neuroimage.2013.06.031
60. Jiruska P, de Curtis M, Jefferys JGR, Schevon CA, Schiff SJ, Schindler K. Synchronization and desynchronization in epilepsy: controversies and hypotheses. *J Physiol*. (2013) 591:787–97. doi: 10.1113/jphysiol.2012.239590
61. Schindler K, Leung H, Elger CE, Lehnertz K. Assessing seizure dynamics by analysing the correlation structure of multichannel intracranial EEG. *Brain*. (2007) 130:65–77. doi: 10.1093/brain/awl304
62. Bartolomei F, Lagarde S, Wendling F, McGonigal A, Jirsa V, Guye M, et al. Defining epileptogenic networks: contribution of SEEG and signal analysis. *Epilepsia*. (2017) 58:1–17. doi: 10.1111/epi.13791
63. Khambhati AN, Davis KA, Oommen BS, Chen SH, Lucas TH, Litt B, et al. Dynamic network drivers of seizure generation, propagation and termination in human neocortical epilepsy. *PLoS Comput Biol*. (2015) 11:20167–72. doi: 10.1371/journal.pcbi.1004608
64. Schindler KA, Bialonski S, Horstmann MT, Elger CE, Lehnertz K. Evolving functional network properties and synchronizability during human epileptic seizures. *Chaos*. (2008) 18:033119. doi: 10.1063/1.2966112

65. Ponten SC, Bartolomei F, Stam CJ. Small-world networks and epilepsy: graph theoretical analysis of intracerebrally recorded mesial temporal lobe seizures. *Clin Neurophysiol*. (2007) 118:918–27. doi: 10.1016/j.clinph.2006.12.002
66. Diessen Ev, Zweiphenning WJEM, Jansen FE, Stam CJ, Braun KPJ, Otte WM. Brain network organization in focal epilepsy: a systematic review and meta-analysis. *PLoS ONE*. (2014) 9:e114606. doi: 10.1371/journal.pone.0114606
67. Slinger G, Otte WM, Braun KPJ, Diessen Ev. An updated systematic review and meta-analysis of brain network organization in focal epilepsy: looking back and forth. *Neurosci Biobehav Rev*. (2021) 132:211–23. doi: 10.1016/j.neubiorev.2021.11.028
68. a Kramer M, Eden UT, Kolaczyk ED, Zepeda R, Eskandar EN, Cash SS. Coalescence and fragmentation of cortical networks during focal seizures. *J Neurosci*. (2010) 30:10076–85. doi: 10.1523/JNEUROSCI.6309-09.2010
69. Bettus G, Wendling F, Guye M, Valton L, Régis J, Chauvel P, et al. Enhanced EEG functional connectivity in mesial temporal lobe epilepsy. *Epilepsy Res*. (2008) 81:58–68. doi: 10.1016/j.eplepsyres.2008.04.020
70. Krishnan B, Vlachos I, Wang ZI, Mosher J, Najm I, Burgess R, et al. Epileptic focus localization based on resting state interictal MEG recordings is feasible irrespective of the presence or absence of spikes. *Clin Neurophysiol*. (2015) 126:667–74. doi: 10.1016/j.clinph.2014.07.014
71. Bartolomei F, Bettus G, Stam CJ, Guye M. Interictal network properties in mesial temporal lobe epilepsy: a graph theoretical study from intracerebral recordings. *Clin Neurophysiol*. (2013) 124:2345–53. doi: 10.1016/j.clinph.2013.06.003
72. Horstmann MT, Bialonski S, Noennig N, Mai H, Prusseit J, Wellmer J, et al. State dependent properties of epileptic brain networks: comparative graph-theoretical analyses of simultaneously recorded EEG and MEG. *Clin Neurophysiol*. (2010) 121:172–85. doi: 10.1016/j.clinph.2009.10.013
73. Morgan VL, Rogers BP, Sonmezturk HH, Gore JC, Abou-Khalil B. Cross hippocampal influence in mesial temporal lobe epilepsy measured with high temporal resolution functional magnetic resonance imaging. *Epilepsia*. (2011) 52:1741–9. doi: 10.1111/j.1528-1167.2011.03196.x
74. Pereira F, Botvinick M. Information mapping with pattern classifiers: a comparative study. *NeuroImage*. (2011) 56:476–96. doi: 10.1016/j.neuroimage.2010.05.026
75. Liao W, Zhang Z, Pan Z, Mantini D, Ding J, Duan X, et al. Altered functional connectivity and small-world in mesial temporal lobe epilepsy. *PLoS ONE*. (2010) 5:e8525. doi: 10.1371/journal.pone.0008525
76. McGill ML, Devinsky O, Kelly C, Milham M, Castellanos FX, Quinn BT, et al. Default mode network abnormalities in idiopathic generalized epilepsy. *Epilepsy Behav*. (2012) 23:353–9. doi: 10.1016/j.yebeh.2012.01.013
77. van Dellen E, Douw L, Hillebrand A, Ris-Hilgersom IHMM, Schoonheim MM, Baayen JC, et al. MEG network differences between low- and high-grade glioma related to epilepsy and cognition. *PLoS ONE*. (2012) 7:e50122. doi: 10.1371/journal.pone.0050122
78. Gleichgerrcht E, Kocher M, Bonilha L. Connectomics and graph theory analyses: novel insights into network abnormalities in epilepsy. *Epilepsia*. (2015) 56:1660–8. doi: 10.1111/epi.13133
79. Spencer SS. Neural networks in human epilepsy: evidence of and implications for treatment. *Epilepsia*. (2002) 43:219–27. doi: 10.1046/j.1528-1157.2002.26901.x
80. Stefan H, da Silva FHL. Epileptic neuronal networks: methods of identification and clinical relevance. *Front Neurol*. (2013) 4:8. doi: 10.3389/fneur.2013.00008
81. Fallani FDV, Richiardi J, Chavez M, Achard S. Graph analysis of functional brain networks: practical issues in translational neuroscience. *Philos Trans R Soc B Biol Sci*. (2014) 369:20130521. doi: 10.1098/rstb.2013.0521
82. Stam CJ, Tewarie P, Dellen EV, van Straaten ECW, Hillebrand A, Mieghem PV. The trees and the forest: characterization of complex brain networks with minimum spanning trees. *Int J Psychophysiol*. (2014) 92:129–38. doi: 10.1016/j.ijpsycho.2014.04.001
83. Fahoum F, Lopes R, Pittau F, Dubeau F, Gotman J. Widespread epileptic networks in focal epilepsies: EEG-fMRI study. *Epilepsia*. (2012) 53:1618–27. doi: 10.1111/j.1528-1167.2012.03533.x
84. Kramer MA, Cash SS. Epilepsy as a disorder of cortical network organization. *Neuroscientist*. (2012) 18:360–72. doi: 10.1177/1073858411422754
85. Aerts H, Fias W, Caeyenberghs K, Marinazzo D. Brain networks under attack: robustness properties and the impact of lesions. *Brain*. (2016) 139:3063–83. doi: 10.1093/brain/aww194
86. de Reus MA, van den Heuvel MP. The parcellation-based connectome: limitations and extensions. *NeuroImage*. (2013) 80:397–404. doi: 10.1016/j.neuroimage.2013.03.053
87. Zhang H, Zhang YJ, Lu CM, Ma SY, Zang YF, Zhu CZ. Functional connectivity as revealed by independent component analysis of resting-state fNIRS measurements. *NeuroImage*. (2010) 51:1150–61. doi: 10.1016/j.neuroimage.2010.02.080
88. Yaffe RB, Borger P, Megevand P, Groppe DM, Kramer MA, Chu CJ, et al. Physiology of functional and effective networks in epilepsy. *Clin Neurophysiol*. (2015) 126:227–36. doi: 10.1016/j.clinph.2014.09.009
89. Stanley ML, Moussa MN, Paolini BM, Lyday RG, Burdette JH, Laurienti PJ. Defining nodes in complex brain networks. *Front Comput Neurosci*. (2013) 7:169. doi: 10.3389/fncom.2013.00169
90. Wang HE, Friston KJ, Bénar CG, Woodman MM, Chauvel P, Jirsa V, et al. MULAN: evaluation and ensemble statistical inference for functional connectivity. *NeuroImage*. (2018) 166:167–84. doi: 10.1016/j.neuroimage.2017.10.036
91. Rubinov M, Sporns O. Weight-conserving characterization of complex functional brain networks. *NeuroImage*. (2011) 56:2068–79. doi: 10.1016/j.neuroimage.2011.03.069
92. Langer N, Pedroni A, Jäncke L. The problem of thresholding in small-world network analysis. *PLoS ONE*. (2013) 8:e53199. doi: 10.1371/journal.pone.0053199
93. Rubinov M, Sporns O. Complex network measures of brain connectivity: uses and interpretations. *NeuroImage*. (2010) 52:1059–69. doi: 10.1016/j.neuroimage.2009.10.003
94. Khambhati AN, Bassett DS, Oommen BS, Chen SH, Lucas TH, Davis KA, et al. Recurring functional interactions predict network architecture of interictal and ictal states in neocortical epilepsy. *Eneuro*. (2017) 4:ENEURO.0091-16.2017. doi: 10.1523/ENEURO.0091-16.2017
95. Zalesky A, Fornito A, Bullmore E. On the use of correlation as a measure of network connectivity. *NeuroImage*. (2012) 60:2096–106. doi: 10.1016/j.neuroimage.2012.02.001
96. Nicosia V, Criado R, Romance M, Russo G, Latora V. Controlling centrality in complex networks. *Sci Rep*. (2012) 2:1–7. doi: 10.1038/srep00218
97. Park HJ, Friston K. Structural and functional brain networks: from connections to cognition. *Science*. (2013) 342:1238411. doi: 10.1126/science.1238411
98. Friston KJ. Functional and effective connectivity: a review. *Brain Connect*. (2011) 1:13–36. doi: 10.1089/brain.2011.0008
99. Honey CJ, Sporns O. Dynamical consequences of lesions in cortical networks. *Hum. Brain Mapp*. (2008) 29:802–9. doi: 10.1002/hbm.20579
100. Zhang X, Tokoglu F, Negishi M, Arora J, Winstanley S, Spencer DD, et al. Social network theory applied to resting-state fMRI connectivity data in the identification of epilepsy networks with iterative feature selection. *J Neurosci Methods*. (2011) 199:129–39. doi: 10.1016/j.jneumeth.2011.04.020
101. Zweiphenning WJEM, van 't Klooster MA, van Diessen E, van Klink NEC, Huiskamp GJM, Gebbink TA, et al. High frequency oscillations and high frequency functional network characteristics in the intraoperative electrocorticogram in epilepsy. *NeuroImage Clin*. (2016) 12:928–39. doi: 10.1016/j.nicl.2016.09.014
102. Schmidt H, Woldman W, Goodfellow M, Chowdhury FA, Koutroumanidis M, Jewell S, et al. A computational biomarker of idiopathic generalized epilepsy from resting state EEG. *Epilepsia*. (2016) 57:e200–4. doi: 10.1111/epi.13481
103. Vorwerk J, Cho JHH, Rampp S, Hamer H, Knösche TR, Wolters CH. A guideline for head volume conductor modeling in EEG and MEG. *NeuroImage*. (2014) 100:590–607. doi: 10.1016/j.neuroimage.2014.06.040
104. Brookes MJ, Woolrich MW, Barnes GR. Measuring functional connectivity in MEG: a multivariate approach insensitive to linear source leakage. *NeuroImage*. (2012) 63:910–20. doi: 10.1016/j.neuroimage.2012.03.048

105. Hipp JF, Hawellek DJ, Corbetta M, Siegel M, Engel AK. Large-scale cortical correlation structure of spontaneous oscillatory activity. *Nat Neurosci*. (2012) 15:884–90. doi: 10.1038/nn.3101
106. Nolte G, Bai O, Wheaton L, Mari Z, Vorbach S, Hallett M. Identifying true brain interaction from EEG data using the imaginary part of coherency. *Clin Neurophysiol*. (2004) 115:2292–307. doi: 10.1016/j.clinph.2004.04.029
107. Palva S, Kulashekhar S, Hämäläinen M, Palva JM. Localization of cortical phase and amplitude dynamics during visual working memory encoding and retention. *J Neurosci*. (2011) 31:5013–25. doi: 10.1523/JNEUROSCI.5592-10.2011
108. Stam CJ, Nolte G, Daffertshofer A. Phase lag index: assessment of functional connectivity from multi channel EEG and MEG with diminished bias from common sources. *Hum Brain Mapp*. (2007) 28:1178–93. doi: 10.1002/hbm.20346
109. Palva JM, Wang SH, Palva S, Zhigalov A, Monto S, Brookes MJ, et al. Ghost interactions in MEG/EEG source space: a note of caution on inter-areal coupling measures. *NeuroImage*. (2018) 173:632–43. doi: 10.1016/j.neuroimage.2018.02.032
110. Cho JH, Vorwerk J, Wolters CH, Knösche TR. Influence of the head model on EEG and MEG source connectivity analyses. *NeuroImage*. (2015) 110:60–77. doi: 10.1016/j.neuroimage.2015.01.043
111. Kramer MA, Kolaczyk ED, Kirsch HE. Emergent network topology at seizure onset in humans. *Epilepsy Res*. (2008) 79:173–86. doi: 10.1016/j.eplepsyres.2008.02.002
112. Wilke C, Worrell G, He B. Graph analysis of epileptogenic networks in human partial epilepsy. *Epilepsia*. (2011) 52:84–93. doi: 10.1111/j.1528-1167.2010.02785.x
113. Kini LG, Bernabei JM, Mikhail F, Hadar P, Shah P, Khambhati AN, et al. Virtual resection predicts surgical outcome for drug-resistant epilepsy. *Brain*. (2019) 142:3892–905. doi: 10.1093/brain/awz303
114. Chen G, Duan Z. Network synchronizability analysis: a graph-theoretic approach. *Chaos*. (2008) 18:037102. doi: 10.1063/1.2965530
115. Jiang H, Cai Z, Worrell GA, He B. Multiple oscillatory pushŰpull antagonisms constrain seizure propagation. *Ann Neurol*. (2019) 86:683–94. doi: 10.1002/ana.25583
116. Lin CH, Tierney T, Holmes N, Boto E, Leggett J, Bestmann S, et al. Using optically-pumped magnetometers to measure magnetoencephalographic signals in the human cerebellum. *bioRxiv*. (2018) 16:425447. doi: 10.1101/425447
117. Hassan M, Merlet I, Mheich A, Kabbara A, Biraben A, Nica A, et al. Identification of interictal epileptic networks from dense-EEG. *Brain Topogr*. (2017) 30:60–76. doi: 10.1007/s10548-016-0517-z
118. Juárez-Martinez EL, Nissen IA, Idema S, Velis DN, Hillebrand A, Stam CJ, et al. Virtual localization of the seizure onset zone: using non-invasive MEG virtual electrodes at stereo-EEG electrode locations in refractory epilepsy patients. *NeuroImage*. (2018) 19:758–66. doi: 10.1016/j.nicl.2018.06.001
119. Staljanssens W, Strobbe G, Holen RV, Keereman V, Gadeyne S, Carrette E, et al. EEG source connectivity to localize the seizure onset zone in patients with drug resistant epilepsy. *NeuroImage Clin*. (2017) 16:689–98. doi: 10.1016/j.nicl.2017.09.011
120. Wang Y, Trevelyan AJ, Valentin A, Alarcon G, Taylor PN, Kaiser M. Mechanisms underlying different onset patterns of focal seizures. *PLoS Comput Biol*. (2017) 13:e1005475. doi: 10.1371/journal.pcbi.1005475
121. Ding L, Worrell GA, Lagerlund TD, He B. Ictal source analysis: localization and imaging of causal interactions in humans. *NeuroImage*. (2007) 34:575–86. doi: 10.1016/j.neuroimage.2006.09.042
122. Lopes MA, Junges L, Tait L, Terry JR, Abela E, Richardson MP, et al. Computational modelling in source space from scalp EEG to inform presurgical evaluation of epilepsy. *Clin Neurophysiol*. (2020) 131:225–34. doi: 10.1016/j.clinph.2019.10.027
123. Breakspear M, Jirsa VK. *Handbook of Brain Connectivity: Understanding Complex Systems*. Berlin: Springer (2007). p. 3–64. doi: 10.1007/978-3-540-71512-2_1
124. Jirsa VK, Stacey WC, Quilichini PP, Ivanov AI, Bernard C. On the nature of seizure dynamics. *Brain*. (2014) 137:2210–30. doi: 10.1093/brain/awu133
125. Proix T, Jirsa VK. Using the connectome to predict epileptic seizure propagation in the human brain. *BMC Neurosci*. (2015) 16:P110. doi: 10.1186/1471-2202-16-S1-P110
126. Surampudi SG, Naik S, Surampudi RB, Jirsa VK, Sharma A, Roy D. Multiple kernel learning model for relating structural and functional connectivity in the brain. *Sci Rep*. (2018) 8:3265 doi: 10.1038/s41598-018-21456-0
127. Pecora LM, Carroll TL. Master stability functions for synchronized coupled systems. *Phys Rev Lett*. (1998) 80:2109–12. doi: 10.1103/PhysRevLett.80.2109
128. Wendling F. Computational models of epileptic activity: a bridge between observation and pathophysiological interpretation. *Expert Rev Neurotherap*. (2008) 8:889–96. doi: 10.1586/14737175.8.6.889
129. Wendling F, Hernandez A, Bellanger JJ, Chauvel P, Bartolomei F. Interictal to ictal transition in human temporal lobe epilepsy: Insights from a computational model of intracerebral EEG. *J Clin Neurophysiol*. (2005) 22:343–56. doi: 10.1097/01.wnp.0000184051.37267.f0
130. Goodfellow M, Schindler K, Baier G. Intermittent spikeŰwave dynamics in a heterogeneous, spatially extended neural mass model. *NeuroImage*. (2011) 55:920–32. doi: 10.1016/j.neuroimage.2010.12.074
131. Goodfellow M, Schindler K, Baier G. Self-organised transients in a neural mass model of epileptogenic tissue dynamics. *NeuroImage*. (2012) 59:2644–60. doi: 10.1016/j.neuroimage.2011.08.060
132. Lopes MA, Goodfellow M, Terry JR. A model-based assessment of the seizure onset zone predictive power to inform the epileptogenic zone. *Front Comput Neurosci*. (2019) 13:25. doi: 10.3389/fncom.2019.00025
133. van den Heuvel MP, Sporns O. Network hubs in the human brain. *Trends Cogn Sci*. (2013) 17:683–96. doi: 10.1016/j.tics.2013.09.012
134. Jansen BH, Rit VG. Electroencephalogram and visual evoked potential generation in a mathematical model of coupled cortical columns. *Biol Cybern*. (1995) 73:357–66. doi: 10.1007/BF00199471
135. Wendling F, Bartolomei F, Senhadji L. Spatial analysis of intracerebral electroencephalographic signals in the time and frequency domain: identification of epileptogenic networks in partial epilepsy. *Philos Trans R Soc A*. (2009) 367:297–316. doi: 10.1098/rsta.2008.0220
136. Wendling F, Chauvel P, Biraben A, Bartolomei F. From intracerebral EEG signals to brain connectivity:Identification of epileptogenic networks in partial epilepsy. *Front Syst Neurosci*. (2010) 4:154. doi: 10.3389/fnsys.2010.00154
137. Baldassano SN, Brinkmann BH, Ung H, Blevins T, Conrad EC, Leyde K, et al. Crowdsourcing seizure detection: algorithm development and validation on human implanted device recordings. *Brain*. (2017) 140:1680–91. doi: 10.1093/brain/awx098
138. Hassan M, Wendling F. Electroencephalography source connectivity: aiming for high resolution of brain networks in time and space. *IEEE Signal Process Mag*. (2018) 35:81–96. doi: 10.1109/MSP.2017.2777518
139. Wendling F, Bartolomei F, Mina F, Huneau C, Benquet P. Interictal spikes, fast ripples and seizures in partial epilepsies-combining multi-level computational models with experimental data. *Eur J Neurosci*. (2012) 36:2164–77. doi: 10.1111/j.1460-9568.2012.08039.x
140. Hincapié AS, Kujala J, Mattout J, Pascarella A, Daligault S, Delpuech C, et al. The impact of MEG source reconstruction method on source-space connectivity estimation: a comparison between minimum-norm solution and beamforming. *NeuroImage*. (2017) 156:29–42. doi: 10.1016/j.neuroimage.2017.04.038
141. Plummer C, Vogrin SJ, Woods WP, Murphy MA, Cook MJ, Liley DTJ. Interictal and ictal source localization for epilepsy surgery using high-density EEG with MEG: a prospective long-term study. *Brain*. (2019) 142:932–51. doi: 10.1093/brain/awz015
142. Plummer C, Harvey AS, Cook M. EEG source localization in focal epilepsy: where are we now? *Epilepsia*. (2008) 49:201–18. doi: 10.1111/j.1528-1167.2007.01381.x
143. Duez L, Tankisi H, Hansen PO, Sidenius P, Sabers A, Pinborg LH, et al. Electromagnetic source imaging in presurgical workup of patients with epilepsy. *Neurology*. (2019) 92:e576–86. doi: 10.1212/WNL.0000000000006877

144. Sebastiano DR, Tassi L, Duran D, Visani E, Gozzo F, Cardinale F, et al. Identifying the epileptogenic zone by four non-invasive imaging techniques versus stereo-EEG in MRI-negative pre-surgery epilepsy patients. *Clin Neurophysiol*. (2020) 131:1815–23. doi: 10.1016/j.clinph.2020.05.015
145. Baillet S. Magnetoencephalography for brain electrophysiology and imaging. *Nat Neurosci*. (2017) 20:327–39. doi: 10.1038/nn.4504
146. McGonigal A, Bartolomei F, Chauvel P. On seizure semiology. *Epilepsia*. (2021) 62:2019–35. doi: 10.1111/epi.16994

Conflict of Interest: The authors declare that the research was conducted in the absence of any commercial or financial relationships that could be construed as a potential conflict of interest.

Publisher's Note: All claims expressed in this article are solely those of the authors and do not necessarily represent those of their affiliated organizations, or those of the publisher, the editors and the reviewers. Any product that may be evaluated in this article, or claim that may be made by its manufacturer, is not guaranteed or endorsed by the publisher.

frontiers | Frontiers in Neurology

REVIEW
published: 27 April 2022
doi: 10.3389/fneur.2022.831546

Contributions of Magnetoencephalography to Understanding Mechanisms of Generalized Epilepsies: Blurring the Boundary Between Focal and Generalized Epilepsies?

Thandar Aung[1]*, *Jeffrey R. Tenney*[2] *and Anto I. Bagić*[1]

[1] Department of Neurology, University of Pittsburgh Comprehensive Epilepsy Center (UPCEC), University of Pittsburgh Medical Center (UPMC), Pittsburgh, PA, United States, [2] Division of Neurology, Department of Pediatrics, Cincinnati Children's Hospital Medical Center, Cincinnati, OH, United States

OPEN ACCESS

Edited by:
Stefano Seri,
Aston University, United Kingdom

Reviewed by:
Elaine Foley,
Aston University, United Kingdom
Vahab YoussofZadeh,
Medical College of Wisconsin, United States

***Correspondence:**
Thandar Aung
aung.thandar@outlook.com

Specialty section:
This article was submitted to Applied Neuroimaging, a section of the journal Frontiers in Neurology

Received: 08 December 2021
Accepted: 08 March 2022
Published: 27 April 2022

Citation:
Aung T, Tenney JR and Bagić AI (2022) Contributions of Magnetoencephalography to Understanding Mechanisms of Generalized Epilepsies: Blurring the Boundary Between Focal and Generalized Epilepsies? Front. Neurol. 13:831546. doi: 10.3389/fneur.2022.831546

According to the latest operational 2017 ILAE classification of epileptic seizures, the generalized epileptic seizure is still conceptualized as "originating at some point within and rapidly engaging, bilaterally distributed networks." In contrast, the focal epileptic seizure is defined as "*originating within networks limited to one hemisphere*." Hence, one of the main concepts of "generalized" and "focal" epilepsy comes from EEG descriptions before the era of source localization, and a presumed simultaneous bilateral onset and bi-synchrony of epileptiform discharges remains a hallmark for generalized seizures. Current literature on the pathophysiology of generalized epilepsy supports the concept of a cortical epileptogenic focus triggering rapidly generalized epileptic discharges involving intact corticothalamic and corticocortical networks, known as the *cortical focus theory*. Likewise, focal epilepsy with rich connectivity can give rise to generalized spike and wave discharges resulting from widespread bilateral synchronization. Therefore, making this key distinction between generalized and focal epilepsy may be challenging in some cases, and for the first time, a combined generalized and focal epilepsy is categorized in the 2017 ILAE classification. Nevertheless, treatment options, such as the choice of antiseizure medications or surgical treatment, are the reason behind the importance of accurate epilepsy classification. Over the past several decades, plentiful scientific research on the pathophysiology of generalized epilepsy has been conducted using non–invasive neuroimaging and postprocessing of the electromagnetic neural signal by measuring the spatiotemporal and interhemispheric latency of bi-synchronous or generalized epileptiform discharges as well as network analysis to identify diagnostic and prognostic biomarkers for accurate diagnosis of the two major types of epilepsy. Among all the advanced techniques, magnetoencephalography (MEG) and multiple other methods provide excellent temporal and spatial resolution, inherently suited to analyzing and visualizing the propagation of generalized EEG activities. This article aims to provide a

comprehensive literature review of recent innovations in MEG methodology using source localization and network analysis techniques that contributed to the literature of idiopathic generalized epilepsy in terms of pathophysiology and clinical prognosis, thus further blurring the boundary between focal and generalized epilepsy.

Keywords: magnetoencephalography, source localization, generalized genetic epilepsy, absence epilepsy, myoclonus epilepsy, epilepsy classification

INTRODUCTION

Epilepsy is one of the most common neurological disorders affecting almost 3.5 million in the USA and 65 million worldwide and is getting increased public health attention as patients with epilepsy have a noticeable reduction in quality of life and employment prospects (1). Two major classification categories are whether an epilepsy is focal or generalized. According to the latest operational 2017 ILAE classification of epileptic seizures, the generalized seizure is still conceptualized as *"originating at some point within and rapidly engaging, bilaterally distributed networks."* In contrast, the focal seizure is defined as "*originating within networks limited to one hemisphere*" (2). The definitions for generalized and focal seizures are retained from the 1981 ILAE classification, and the presumed simultaneous bilateral onset and bisynchrony of the epileptic discharges in electroencephalography (EEG) remains a hallmark for generalized seizures (2–4).

In 1952, Tükel and Jasper et al. reported that a mesial frontal cortical lesion could give rise to diffuse interictal spike-and-wave discharges; hence the term "secondary bilateral synchronization" and blurring the boundary of focal and generalized epilepsy (5). In addition to the frontal lobe, focal epilepsy with rich connectivity, such as posterior parietal, temporal, or even occipital lobe epilepsy, can give rise to diffuse "generalized" spike and wave discharges (GSWD) resulting from widespread bilateral synchronization, especially in the pediatric population and can be misclassified as generalized epilepsy (6–10). On the contrary, current literature validates that focal EEG features can be found in generalized epilepsy (11). Consequently, generalized epilepsy can also be misclassified as focal epilepsy. Therefore, making a distinction between generalized and focal epilepsy may be challenging in selected clinical cases (7–10). However, the 2017 ILAE classification proposes the combined generalized and focal epilepsy as one of the categories of the epilepsy classification for ambiguous cases. Nevertheless, treatment options, such as the choice of antiseizure medications (ASMs), neuromodulation, or surgical treatment alternatives, are the reason behind the importance of accurate differentiation between focal and generalized epilepsy. When epilepsy becomes drug-resistant, defined as failure to control the seizures with two appropriate ASMs, surgical resection or disruption of the epileptogenic zone (EZ) may be a way to achieve seizure freedom or reduce seizure burden in focal epilepsy, but those with generalized epilepsy are often not considered as epilepsy surgery candidates (12–16). Although neuromodulatory treatments such as vagal nerve stimulators (VNS) (17), responsive neurostimulator (RNS) (18), and deep brain stimulators (DBS) (19) are treatment alternatives for those patients who are not resective surgical candidates, the study and indications of all those neurostimulators are mostly based on focal epilepsy (20). Thus, the treatment that we could offer for drug-resistant generalized epilepsy is more limited than for focal epilepsy. There have been multiple works of literature supporting the usage of the neurostimulators, especially the RNS and DBS targeting different parts of the thalamus and cortices in patients with generalized epilepsy. However, the outcome is highly dependent upon electrode placement in relation to different thalamic nuclei, stimulation parameters, subtypes of generalized epilepsy, or even individual cortical-subcortical connectivity profiles (20, 21).

To improve the treatment options in generalized epilepsy, plentiful scientific research on its pathophysiology has been conducted over the past several decades, using advanced non–invasive investigations and postprocessing of the neuromagnetic signal by reflecting the spatiotemporal and interhemispheric latency of bi-synchronous or generalized epileptiform discharges in both animals and humans (22–24). Using invasive intracranial electroencephalographic (icEEG) data, Chen et al. reported that two hemispheres could still function independently with different focal network structures and properties under a strong global epileptic network in generalized epilepsy; the focal epileptic network from the leading hemisphere might be activating the global epileptic network. By resecting the part of the region of the leading hemisphere, five pediatric patients with generalized epilepsy with tonic/atonic and atypical absence seizures resulted in seizure freedom (24). Although the diagnosis of generalized epilepsy in the case series was disputable as all the resective brain tissue showed abnormal pathology (3 with focal cortical dysplasia type 1A, one with focal cortical dysplasia type 1B with polymicrogyria, and one with tuberous sclerosis), the conclusion was based on EEG and clinical semiology of the seizures. non-etheless, the author

Abbreviations: GSWD, generalized spikes wave discharge; IEDs, Interictal epileptiform discharges; CAE, childhood absence epilepsy; JAE, juvenile absence epilepsy; JME, juvenile myoclonus epilepsy; GGE, genetic generalized epilepsy; TCS, tonic-clonic seizure; MEG, magnetoencephalography; EC, effective connectivity; EEG, electroencephalography; fMRI, functional magnetic resonance imaging; SAM, synthetic aperture magnetometry; LORETA, standardized low-resolution brain electromagnetic topography; sLORETA, standardized low-resolution brain electromagnetic topography; ms, milliseconds; LCMV, Linear constraint minimum variance; ASI, accumulated source imaging; DICS, Dynamic imaging of coherent sources; dMSI, Dynamic magnetic source imaging; dSPM, Dynamic statistical parameter mapping; ECD, equivalent dipole model; PLV, phase-locking value; MUSIC, multiple signal characteristic; wMNE, weighted minimum-norm estimation; pMEM, pairwise maximum entropy model; CFC, cross-frequency coupling; ms, milliseconds; s, seconds; m, months; y, years; F, female; M, male; ASM, antiseizure medication.

highlighted one of the current clinical challenges in accurately categorizing the epileptic patients into either focal or generalized epilepsy (24). In addition, accumulating evidence has shown that epilepsy is an archetypical neural network disorder. With ongoing debates, current literature on the pathophysiology of generalized epilepsy supports the concept of a cortical epileptogenic focus triggering the rapidly generalized epileptic discharges involving intact corticothalamic and corticocortical networks, which is known as the *cortical focus theory* (22, 23, 25).

Among all advanced non–invasive techniques, magnetoencephalography (MEG) provides excellent temporal and spatial resolution, inherently suited for analyzing the propagation of generalized EEG activities and determining whole-brain functional connectivity network patterns (26–29). The current clinical application of MEG for epilepsy in the form of magnetic source imaging (MSI) mostly uses the single equivalent current dipole (ECD) model (30, 31), especially in the United States (32). However, the traditional ECD model is restricted if the underlying assumption of focality is not fulfilled, for example, when the epileptiform activity occurs simultaneously across the various regions (33–35). Alternative source localization techniques, such as beamformer and low-resolution brain electromagnetic topography (LORETA), as well as various connectivity analyses, have played a prominent role in improving the localization of deep sources (further details in section 2) (34–40). Although there is an overall improvement in the strength of localization of the neuromagnetic activity using various source localization algorithms, there are still major limitations in analyzing deep sources with MEG (41–44). The magnetic field intensity is inversely proportional to the square of the distance between the sources and the sensors (45), and thus there is decreased signal in deeper structures of the brain, either deep cortices or the thalamus. Since GSWDs typically have very high voltages, it is postulated that MEG may be able to overcome this particular limitation in generalized epilepsy. Unfortunately, there are limitations in precise localization of the deeper structures, such as individual thalamic nuclei. Compared to MEG, functional magnetic resonance imaging (fMRI) has a better spatial but weaker temporal resolution (46). With advances in technology, there have been publications (40, 44, 47, 48) focusing on the multimodal integration of MEG with other neuroimaging techniques, mainly fMRI, to complement one modality with the other to further edify the underlying pathophysiology of the GSWDs.

In this review article, we searched PubMed, Medline, and Embase databases using the following search algorithm: "Magnetoencephalography (MEG)" and "Generalized Epilepsy" or "absence epilepsy" or "myoclonus epilepsy" or "generalized genetic epilepsy" limited to publications in English. The last date of the search was September 30th, 2021. We screened the titles, abstracts, and references of all search results to identify potentially relevant studies. We included only publications of MEG recordings in human subjects. We excluded poster publications and any study with abnormal MRI in generalized epilepsy patients. This article aimed to provide a comprehensive literature review of how the recent innovation in the MEG methodology contributed to the literature of the idiopathic generalized epilepsy in terms of physiopathology, treatment, and prognosis, thus further blurring the boundary between focal and generalized epilepsy.

DIFFERENT SOURCE LOCALIZATION MODELS, TECHNIQUES AND CONNECTIVITY ANALYSES

Cohen et al. were the first to record neural magnetic signals using a single-channel MEG (49). Since then, the MEG recording technique has been enhanced, and now the neural magnetic signals can be recorded using more than 200–300 sensors (31, 43). With this advancement, source estimation models have been developed to localize the neural magnetic signals (26, 30–32, 37, 39, 40, 43, 50). Source analysis usually occurs in the source space rather than sensor space, where the neural signal is acquired at each measurement sensor. Due to the various ambiguities associated with sensor level analysis, source analysis is preferred, but sensor level analysis can be performed when there are not enough sensors, e.g., analyzing 10–20 EEG neural signals, to accurately localize sources (42, 51). The goal of source localization is to correctly estimate the location and orientation of the neuromagnetic source using the inverse model (37). Multiple mathematical algorithms have been developed, but non-e is felt to be superior for every clinical situation. Each algorithm comes with its own advantages and limitations. Besides, there have been studies showing overall agreement in estimating the sources when compared to intracranial EEG (52–54).

Dipole Model

Dipole models are characterized by a single or few neural sources that are analyzed in the brain model and then sequentially moved until the projected single pattern matches the recorded pattern (30, 31). Among all, the single equivalent current dipole model (sECD) is the most well accepted, but the traditional ECD model is limited if the underlying assumption of focality is not fulfilled (30–32). Using point source analysis, the dipole modeling becomes limited and unreliable if the source is complex, multiple sources are generated over the same temporal course, or the source is generated from extended areas of the brain (26, 33–35, 55).

Multiple Signal Classification

Multiple signal classification (MUSIC) can analyze complex and asynchronous sources that typically require multiple simultaneous source localization by scanning all possible positions of the brain in three-dimensions. However, two assumptions need to be met for accurate localization, an absence of noise and an accurate head model (34, 56, 57). Unlike ECD, the recursive MUSIC (R-MUSIC) algorithm can localize multiple synchronous sources using the spatio-temporal independent topographies (IT) model (58).

Beamforming

Instead of estimating or reconstructing the source distribution, beamforming uses spatial filters to optimize predefined regions

of interest or sources with a maximum signal while suppressing activity from other regions, including noise (59). Beamforming can be further divided into either linear, linearly constrained minimum variance (LCMV) (60) or non-linear, synthetic aperture magnetometry (SAM) (61). LCMV beamforming can be analyzed either in time domain using covariance metrics or in the frequency domain using cross-spectral density metrics, such as dynamic imaging of coherent sources (DICS) or accumulated spectrograms, such as accumulated source imaging (ASI) (59–63). Compared with ECD, beamforming can analyze multiple sources, either synchronous or asynchronous. Contrary to MUSIC, the neural signal analyzed with beamforming is less altered by the presence of noise. One of the limitations of beamforming, especially SAM with excess kurtosis, is performance loss when the sources are correlated. In addition, SAM with excess kurtosis [$SAM_{(g2)}$] ignores frequent events, and thus it is limited in analyzing frequent discharges (59, 61).

Current Density Models

Current density models directly compute a current distribution throughout the full brain volume: minimum norm estimate (MNE), standardized low-resolution brain electromagnetic tomography (sLORETA), exact low-resolution brain electromagnetic tomography (eLORETA), sLORETA weighted accurate minimum norm (SWARM), dynamical statistical parametric mapping (dSPM), and the multiresolution focal underdetermined system solution (MR-FOCUSS) (64–67). In MNE, dipoles are analyzed simultaneously in two-dimensions by limiting the space so their strengths can be estimated as the function of time (68). MNE has an excellent spatial resolution for the superficial sources, especially complex sources, but not for deeper sources due to the model limitation (69). To improve the superficial source bias, sLORETA performs further post-processing of the current density map obtained from the MNE by replacing the noise covariance with theoretical data covariance (65). Another normalization method of the MNE current density is dSPM which computes the normalization based on the noise covariance (70, 71). In addition, the presence of biological noise has no localization bias in the source estimation of the neural signals by sLORETA (67). dSPM and LORETA improve the localization error when compared to MNE (67, 72). To improve the analysis of complex dynamic sources using the time domain, particular models are a promising technique for the ictal dynamic data, especially MR-FOCUSS (73).

Entropy Measures

Maximum entropy on the mean (MEM) is a technique to analyze synchronous sources in specific frequency bands and is sensitive to spatially extended sources using data-driven parcellation of the cortical surface into non–overlapping parcels. By maximizing the entropy of a probability distribution, the parcels that are not contributing to the measured data are excluded from the analysis (74). Pairwise MEM (pMEM), a statistical model of pairwise regional coactivation from empirical data using frequency-specific MEG resting oscillatory activity, can analyze the dynamic state's multi-stability (75, 76). The limitation of MEM is that a priori information on the number of cortical parcels is required (77).

Connectivity Measures

Over the past decades, studies have been focused on analyzing various cortical networks using diverse connectivity measures to describe the disruption of the disease state from the normal functional neural networks (78–80). In contrast to anatomical connectivity, where networks of physical white matter structural connections or synaptic connections between various (distinct) regions of the brain analyzed at the micro or macroscopic occurs, functional and effective connectivity describes the functional aspects of neural networks (81). Functional connectivity measures the temporal correlation of distinct cortical regions, whereas effective connectivity analyzes the direction of the influence of one cortical region over distinct cortex (79, 81–86). Therefore, functional connectivity analyzes whether neural activities of the two regions are linked, i.e., undirected information flow, while effective connectivity scrutinizes the direction of the communication, i.e., directed connectivity (87–89).

Correlation and coherence are the most classical measures of functional connectivity and analyze the similarity between neural signals in the time and frequency domains, respectively (90). Other functional connectivity methods are based upon quantifying the waveforms in amplitude and oscillations of neural activity, such as phase lag index, phase slope index, or phase-locking index (91, 92). If the directional interactions are pre-defined, structural equation modeling (SEM) can be used, whereas Granger causality measures the connectivity on directional interactions derived from the data (82, 89, 93). Other effective connectivity methods are directed coherence, dynamic causal modeling, linear non–Gaussian, conditional Bayes, and Bayes network methods (94–99). The main difference between functional and effective connectivity is that functional connectivity illustrates statistical dependencies, whereas effective connectivity is based on a mechanistic model of the causal effects that generated the data (87, 100).

Graph theory provides models of complex dynamic networks in the brain, allowing one to better understand the relations between and/or the processes taking place in network structures. After the connectivity matrices are calculated, these values can be used to describe features of the network using graph theory, i.e., the network is defined as a set of nodes that are connected by edges or lines. This allows the investigator to calculate measures of different graph metrics, such as degree (number of connections to a node), node strength, path length, global efficiency, clustering coefficients, between centrality, synchronizability, small world index and centrality, to identify the critical components of the network (101–105).

FIRST CLINICAL MEG RECORDING IN GENERALIZED EPILEPSY (SOURCE LOCALIZATION ERA)

Hughes et al. were the first to report a clinical MEG recording of 3 Hz generalized spike and wave discharges (GSWDs) in humans using simultaneous EEG and MEG recording (106). Interestingly, they observed that MEG was excellent in displaying the spikes and less evidence of waves when compared to the EEG. In addition, MEG waveforms were noted to precede the corresponding EEG spike activity in most patients' recordings. Ricci et al. studied the 3 Hz spike-wave using single-channel MEG with a phantom brain model and showed cortical activity was scattered bilaterally, mainly over frontal and temporal regions, often with more involvement over one hemisphere, while bilateral synchronous activity seemed to have originated from a deeper structure (107, 108). The study was the first to demonstrate evidence of primary cortical involvement in GSWDs in generalized epilepsy using neuromagnetic cortical source localization. The authors couldn't explain the relation of the cortical source localization to the deep brain structures given the limitation of the applied methodology with single-channel recordings (109). Thus, the author recommended further studies using multichannel capability with newer post-processing methodology to glean greater insights into the pathophysiology of generalized epilepsy (109).

CHILDHOOD ABSENCE EPILEPSY

Childhood absence epilepsy (CAE) is the most studied generalized epilepsy among all genetic or idiopathic generalized epilepsy subtypes. All the published study characteristics, types of post-processing signal analysis, and main results are summarized in **Table 1**.

Source Localization of GSWDs

Multiple studies were published using different source localization techniques to analyze interictal, preictal, and ictal parts of the GSWDs of CAE, as shown in **Table 1**. Westmijse et al. applied source analysis to ictal GSWDs of human CAE with an average seizure duration of 9s (4–22 s) using non–linear association with the beamformer technique, synthetic aperture magnetometry (SAM). At the onset, sources were localized to cortical brain regions, including left or right frontal, central and parietal, during the spike portion of GSWDs. The sources became generalized during the slow-wave phase (110). A similar finding was reported by Hu et al. using the same technique while analyzing the peak of the spike of GSWD (111). Five out of 13 CAE patients' GSWDs (38.5%) were able to source localized to bilateral frontal regions. The study findings validated the clear cortical sources of activity during the spikes of GSWDs over the bilateral frontal regions and supported the theory of the cortical focus in the generation of generalized epilepsy (111). However, no conclusion could be made regarding deep brain sources (mainly thalamus) due to the limitation of the recording and analysis technique, including the limited high frequency to 70Hz.

Similar to the findings from Rucci et al. (107, 108) and Tenney et al. reported the preictal MEG changes occurred an average of 694 ms before the initial spike of the EEG (112, 114). The same research group (112) aimed to investigate the relative timing of the cortical and thalamus activity in the generation of absence seizures by combining SAM beamformer and standardized low-resolution electromagnetic tomography (sLORETA) to analyze the preictal state, 50 milliseconds (ms) before and after the first ictal spike of ictal GSWDs, in 12 drug-naïve CAE patients. At −50 ms, the seizures were source localized to the frontal cortex, mainly the lateral inferior frontal lobe or thalamus. At the EEG onset (0 ms), focal sources were detected in the frontal cortex with decreased thalamic localization. Following the first ictal spike (50 ms), localization became more widespread. Thus, after the initial frontal and thalamic source, the ictal activity gradually recruited the remaining cortices, i.e., parietal, temporal, and occipital. Later, the same group analyzed the same ictal dataset using time-frequency analysis with different frequency bandwidths (up to 150 Hz) and source localization using sLORETA (113). Tenney et al. were the first to report the network's frequency-dependent nature in CAE (113). The high-frequency oscillations (HFO) 70–150 Hz were localized to the frontal lobe during absence seizures. At lower frequencies, sources were significantly localized to the parietal cortex. Thus, the authors proposed a hypothesis that different oscillations and frequencies favored different types of connections and/or different spatiotemporal levels of information integration. In addition, the finding suggested that the co-occurring frontal and parietal corticothalamic networks interacted to produce a pathological state that contributed to the generation of GSWDs.

The above findings were confirmed by Miao et al. using different beamformer analysis, dynamic magnetic source imaging (dMSI) (115, 116). Miao et al. validated that the source of HFOs (80–500 Hz) in the ictal stage was focal and located in the medial prefrontal cortex (MPFC) compared to the spike portions of the interictal GSWDs, which were widespread (116). In addition, Miao et al. reported that fast ripples (250–500 Hz) were associated with increased seizure frequency (115). Besides, same research group also confirmed the involvement of the default mode network, by reciprocal propagation between medial prefrontal cortex, pre-supplementary motor area, precuneus, and medial occipital cortices, through cortico-cortical pathways *via* medial portion of the brain or cortico-thalamus-cortical pathway *via* thalamus, in the ictal generation and propagation of the seizure activity in CAE (115). Compared to the ictal stage, Xiang et al. studied HFO activity during the interictal stage and compared it with age- and sex-matched healthy controls (117). The authors revealed that patients with CAE had higher odds of interictal HFO activity (either 200–1,000 or 1,000–2,000 Hz) in the parieto-occipito-temporal junction and medial frontal cortices. No significant differences in the deep brain area was reported. Thus, all the above results indicated that CAE had significantly aberrant brain connectivity activity during the interictal as well as the ictal phase, and the above electrophysiological findings could potentially serve as biomarkers for the CAE.

TABLE 1 | Showing all the published study characteristics and main outcomes on childhood absence epilepsy.

Article name	Type of genetic epilepsy	No. of patients included in study	No. of female (F): No. of male (M)	Study State of genetic epilepsy	Mean age at the time of MEG recording (range) (y)	Mean age of epilepsy onset (range) (y)	Duration of epilepsy (range) (m)	No. of pt. on ASM	Yes and No for the Simultaneous MEG/EEG recording No. of EEG, MEG sensor with sampling rate of the MEG recording Source or sensory level (for the connectivity study only)	Type of analysis with analyzed MEG frequency bandwith	Main result
CAE (interictal/ictal GSWDs)											
Westmijse et al. (110)	CAE	5	2F: 3M	Ictal	9.5 (7–12)	NA	NA	5	Yes (EEG−28, MEG 151 for the first 4 patients and 275 for the 1 patient) (1,200 Hz)	Beamformer (SAM) (1–70 Hz)	• Beamformer technique supported the local or even focal cortical involvement in the occurrence of the spike in the train of GSWDs. • GSWDs had local frontal and parietal cortical sites before the onset of the generalized pattern of GSWDs
Hu et al. (111)*	CAE	13	10F: 3M	Ictal	8.4 (0.17-−12)	NA	1.6 (3–36)	NA*	No (MEG 275) (1,200 Hz)	Beamformer (SAM) (20–70 Hz)	• Cortical epileptic foci were localized only 5 out of 13 cases over the bilateral frontal regions.
Tenney et al. (112)**	CAE	12	7F: 5M	Ictal	8.8 (6.4–11.8)	8.8 (6.4–11.8)	∼ one week	0	Yes (EEG– 25, MEG −275) (4,000 Hz)	Beamformer (SAM), sLORETA (1–70 Hz)	• Beamformer analysis using SAM confirmed the presence of the independent thalamic and cortical activities. • sLORETA analysis showed sources during the absence seizures are most likely to be localized to the frontal cortex and thalamus at −50 ms.

(Continued)

TABLE 1 | Continued

Article name	Type of genetic epilepsy	No. of patients included in study	No. of female (F): No. of male (M)	Study State of genetic epilepsy	Mean age at the time of MEG recording (range) (y)	Mean age of epilepsy onset (range) (y)	Duration of epilepsy (range) (m)	No. of pt. on ASM	Yes and No for the Simultaneous MEG/EEG recording No. of EEG, MEG sensor with sampling rate of the MEG recording Source or sensory level (for the connectivity study only)	Type of analysis with analyzed MEG frequency bandwith	Main result
											• At the onset of the absence seizure (0 ms), focal source localization was seen in the lateral frontal cortex with decreased thalamus localization. • Following the onset of the spike, localization between more widespread and gradually recruited throughout the cortex.
Tenney et al. (113)[**,#]	CAE	12	7F: 5M	Ictal	8.8 (6.4–11.8)	8.8 (6.4–11.8)	∼ one week	0	Yes (EEG– 25, MEG −275) (4,000 Hz)	Time-frequency analysis with different frequency bandwidths (1–20, 20–70, 70–150 Hz), sLORETA	• First to report on the frequency-dependent nature of the neural network and about HFO • During the absence seizure, frontal cortex source localization was noted at the low– (3–20 Hz) and gamma-frequency bandwidths (70–150 Hz). • At low-frequency bandwidths, more sources localized to the parietal lobes during absence seizure.

(Continued)

TABLE 1 | Continued

Article name	Type of genetic epilepsy	No. of patients included in study	No. of female (F): No. of male (M)	Study State of genetic epilepsy	Mean age at the time of MEG recording (range) (y)	Mean age of epilepsy onset (range) (y)	Duration of epilepsy (range) (m)	No. of pt. on ASM	Yes and No for the Simultaneous MEG/EEG recording No. of EEG, MEG sensor with sampling rate of the MEG recording Source or sensory level (for the connectivity study only)	Type of analysis with analyzed MEG frequency bandwith	Main result
Jacobs-Brichford (114)[#]	CAE	12	7F: 5M	Preictal	8.8 (6.4–11.8)	8.8 (6.4–11.8)	∼one week	0	Yes (EEG−23, MEG−275) (4,000 Hz)	sLORETA (1–70 Hz)	• Preictal MEG frequency changes were detected at a mean of 694 ms before the initial GSWDs on the EEG, and focal sources were localized to the frontal cortex and thalamus
Miao et al. (115)	CAE	14	9F:5M	Ictal	8.5 (5–12)	NA	7.1 (1–24)	0	No (MEG−275) (300 Hz)	Beamformer (wavelength-based), Dynamic magnetic source imaging (dMSI) (1–140 Hz)	• Initial ictal activity was source localized predominately to left frontal and posterior cortices. Frontal sources were left medial prefrontal cortex, pre-SMA, primary motor cortex, and lateral prefrontal cortex. The posterior cortical regions were the left precuneus and medial occipital cortex.

(Continued)

TABLE 1 | Continued

Article name	Type of genetic epilepsy	No. of patients included in study	No. of female (F): No. of male (M)	Study State of genetic epilepsy	Mean age at the time of MEG recording (range) (y)	Mean age of epilepsy onset (range) (y)	Duration of epilepsy (range) (m)	No. of pt. on ASM	Yes and No for the Simultaneous MEG/EEG recording No. of EEG, MEG sensor with sampling rate of the MEG recording Source or sensory level (for the connectivity study only)	Type of analysis with analyzed MEG frequency bandwith	Main result
											• After initialization, the ictal activity showed involvement of medial prefrontal cortex and precuneus, and recursive propagation between frontal and posterior cortices *via* either medial portion of the brain (9/14) or thalamus (5/14), respectively.
Miao et al. (116)	CAE	10	7F: 3M	ictal	8.3 (5–11)	NA	5.9 (1–12)	0	No (MEG−275) (6,000 Hz)	Beamformer (wavelength-based), Dynamic magnetic source imaging (dMSI) (14–70, 80–500 Hz)	• HFO ranging from 80–500 Hz was located in all patients. • The total time of fast ripples (250–500 Hz) was greater than that of ripple (80–250 Hz) during absence seizures. • Compared to spikes, the source localization of HFOs appeared to be more focal.

(Continued)

TABLE 1 | Continued

Article name	Type of genetic epilepsy	No. of patients included in study	No. of female (F): No. of male (M)	Study State of genetic epilepsy	Mean age at the time of MEG recording (range) (y)	Mean age of epilepsy onset (range) (y)	Duration of epilepsy (range) (m)	No. of pt. on ASM	Yes and No for the Simultaneous MEG/EEG recording No. of EEG, MEG sensor with sampling rate of the MEG recording Source or sensory level (for the connectivity study only)	Type of analysis with analyzed MEG frequency bandwith	Main result
											• HFO duration was significantly longer when co-occurring with spikes and localized in the medial prefrontal cortex, whereas spikes were widespread to the various brain regions during the seizure. • HFO (fast ripples) was associated with increased seizure frequency
Xiang et al. (117)	CAE	10	3F: 7M	Interictal	8 (6.4–10)	8 (6.4–10)	∼one week	0	No (MEG−275) (4,000 Hz)	Beamformer (ASI), correlation analysis at Source level with multi-frequency analysis (1–4, 4–8, 8–12, 12–30, 30–55, 65–90, 90–200, 200–1,000, 1,000–2,000 Hz)	• Compared with healthy control, CAE patients had higher odds of interictal HFO in 200–1,000 and 1,000–2,000 Hz in medial frontal regions and parieto-occipito-temporal junction.

(Continued)

TABLE 1 | Continued

Article name	Type of genetic epilepsy	No. of patients included in study	No. of female (F): No. of male (M)	Study State of genetic epilepsy	Mean age at the time of MEG recording (range) (y)	Mean age of epilepsy onset (range) (y)	Duration of epilepsy (range) (m)	No. of pt. on ASM	Yes and No for the Simultaneous MEG/EEG recording No. of EEG, MEG sensor with sampling rate of the MEG recording Source or sensory level (for the connectivity study only)	Type of analysis with analyzed MEG frequency bandwith	Main result
Tang et al. (118)	CAE	12	8F: 4M	Preictal/ ictal	8.17 (5–12)	7.75 (5–11)	7.08 (1–20)	0	No (MEG−275) (6,000 Hz)	Beamformer (ASI), correlation analysis at Sensor and source level with multi-frequency analysis (1–4, 4–8, 8–12, 12–30, 30–45, 55–90, 90–200, 200–1,000 Hz)	• Interictal to ictal period, neuromagnetic changes predominantly occurred in the medial prefrontal cortex and parieto-occipito-temporal junction at the low-frequency band at <30 Hz. • A strong correlation between the source strength of ictal HFOs in 200–1,000 Hz and the frequency of daily seizures was reported.
CAE (Ictal network connectivity)											
Gupta et al. (119)	CAE	5	NA	Preictal	9.5 (7–12)	NA	NA	5	No (MEG −151 for 4 patients, MEG −275 for 1 ptaient) (1,200 Hz) Connectivity–Source level	Beamformer (DICS), Graphic theory, non-linear coherence, source analysis (0–50 Hz)	• Beamforming showed a consistent appearance of a low-frequency frontal cortical source preceded by the low-frequency occipital source before the first ictal GSWDs.

(Continued)

TABLE 1 | Continued

Article name	Type of genetic epilepsy	No. of patients included in study	No. of female (F): No. of male (M)	Study State of genetic epilepsy	Mean age at the time of MEG recording (range) (y)	Mean age of epilepsy onset (range) (y)	Duration of epilepsy (range) (m)	No. of pt. on ASM	Yes and No for the Simultaneous MEG/EEG recording No. of EEG, MEG sensor with sampling rate of the MEG recording Source or sensory level (for the connectivity study only)	Type of analysis with analyzed MEG frequency bandwith	Main result
										with low-frequency band 2–4 Hz and high-frequency band 20–25Hz	• There was a decrease in local connectivity and higher global connections at the preictal stage (1 s from the first ictal GSWD), suggesting a pathological predisposed preictal state toward synchronous seizures networks.
Wu et al. (120)	CAE	14	9F: 5M	Preictal	8.1 (5.3–11)	NA	8 (0.5–36)	0	No (MEG −275) (6,000 Hz) Connectivity–Source level	Beamformer (ASI), Graph theory, Granger causality, correlation analysis at source level with multi-frequency analysis (1–4, 4–8, 8–12,12–30, 30–80, 80–250, 250–500 Hz)	• At the preictal period, low frequency 1–80 Hz activities were localized to the frontal cortex and parieto-occipito-temporal junction, whereas high-frequency 80–250 Hz oscillations showed predominant activities localized in the deep brain region as well as medial frontal cortex. • Increased cortico-thalamic effective connectivity was observed around seizures in both low and high-frequency ranges.

(Continued)

TABLE 1 | Continued

Article name	Type of genetic epilepsy	No. of patients included in study	No. of female (F): No. of male (M)	Study State of genetic epilepsy	Mean age at the time of MEG recording (range) (y)	Mean age of epilepsy onset (range) (y)	Duration of epilepsy (range) (m)	No. of pt. on ASM	Yes and No for the Simultaneous MEG/EEG recording No. of EEG, MEG sensor with sampling rate of the MEG recording Source or sensory level (for the connectivity study only)	Type of analysis with analyzed MEG frequency bandwith	Main result
											• At the early preictal period, the predominant direction of the cortico-thalamic effective connectivity was observed from cortex to thalamus, but the cortex that drove connectivity varied among subjects.
Youssofzadeh et al. (121)	CAE	16	9F: 7M	Preictal	8.7 (6–12)	NA	NA	0	Yes (EEG−25, MEG−275) (4,000 Hz) Connectivity-Sensor level	Beamformer (LCMV), Graphic theory, phase-locking value (PLV) at broadband frequency (1–40 Hz)	• During absence seizures, highly connected brain areas or hubs were present in the bilateral precuneus, posterior cingulate, thalamus, and cerebellar regions
Jiang et al. (122)	CAE	15	11F:4M	Ictal (termination)	(5–11)	NA	18.1 (2–63)	0	No (MEG−275) (6,000 Hz) Connectivity-Source level	Beamformer (ASI), Graph theory, Granger causality, correlation analysis at the source level	• At the seizure termination transition, activities at low frequency (1–80 Hz) were predominantly distributed in the frontal cortical and parieto–occipito–temporal junction, whereas high frequency

(Continued)

TABLE 1 | Continued

Article name	Type of genetic epilepsy	No. of patients included in study	No. of female (F): No. of male (M)	Study State of genetic epilepsy	Mean age at the time of MEG recording (range) (y)	Mean age of epilepsy onset (range) (y)	Duration of epilepsy (range) (m)	No. of pt. on ASM	Yes and No for the Simultaneous MEG/EEG recording No. of EEG, MEG sensor with sampling rate of the MEG recording Source or sensory level (for the connectivity study only)	Type of analysis with analyzed MEG frequency bandwith	Main result
										with multi–frequency analysis (1–4, 4–8, 8–12, 12–30, 30–80, 80–250, 250–500 Hz)	(80–500 Hz) activities were localized in the medial frontal cortex and deep brain areas (mainly thalamus). • Cortico–thalamic effective connectivity was enhanced at all frequency bands, the direction of which was primarily from various cortical regions to the thalamus
Sun et al. (123)[θ]	CAE	22	15F: 7M	Preictal	8.5 (5–14)	NA	7.61 (4–13)	7	Yes (EEG−23, EEG−275) (6,000 Hz) Connectivity–Source level	Beamformer (ASI), correlation analysis at source level in 6 frequency bandwidths (1–4, 4–8, 8–12, 12–30, 30–80, 80–250 Hz)	• At the preictal stage (1 second from the first ictal GSWD), overall network spectral power increased and distributed at 2–4, and ictal spikes simultaneously showed elevation of network connectivity, predominately excitatory. • HFO was detected in certain focal areas

(Continued)

TABLE 1 | Continued

Article name	Type of genetic epilepsy	No. of patients included in study	No. of female (F): No. of male (M)	Study State of genetic epilepsy	Mean age at the time of MEG recording (range) (y)	Mean age of epilepsy onset (range) (y)	Duration of epilepsy (range) (m)	No. of pt. on ASM	Yes and No for the Simultaneous MEG/EEG recording No. of EEG, MEG sensor with sampling rate of the MEG recording Source or sensory level (for the connectivity study only)	Type of analysis with analyzed MEG frequency bandwith	Main result
Sun et al. (124)	CAE	18	13F: 5M	Ictal (termination)	8.4 (5–11)	NA	10.2 (3–32)	0	No (MEG−275) (6,000 Hz) Connectivity–Source level	Beamformer (ASI), source–level with multi–frequency analysis (1–4, 4–8, 8–12, 12–30, 30–80, 80–250, 250–500 Hz)	• At seizure termination, low–frequency bands at 1–4, 4–8 and 8–12 Hz activities were distributed mainly in the frontal and parieto–occipito–temporal junction. At 12–30 and 30–80, there was significant reduction in source activity in frontal lobe. • The ictal peak source strength in 1–4 Hz was negatively correlated with seizure duration, whereas the 30–80 Hz range was positively correlated with epilepsy course
Tenney et al. (48)#	CAE	13	7F: 6M	Ictal (termination)	8.8 (6.4–11.8)	8.8 (6.4–11.8)	∼one week	0	Yes (EEG−21, MEG−275) (4,000 Hz) Connectivity–Source level	fMRI informed MEG effective connectivity (0.5–100 Hz) Beamformer (LCMV), amplitude/amplitude coupling with canonical	• During the absence seizure, there was a strong coupling between beta and gamma frequencies within the left frontal cortex and between left frontal and right parietal regions. • Strong connectivity between left frontal and right parietal nodes was noted within gamma band.

(Continued)

TABLE 1 | Continued

Article name	Type of genetic epilepsy	No. of patients included in study	No. of female (F): No. of male (M)	Study State of genetic epilepsy	Mean age at the time of MEG recording (range) (y)	Mean age of epilepsy onset (range) (y)	Duration of epilepsy (range) (m)	No. of pt. on ASM	Yes and No for the Simultaneous MEG/EEG recording No. of EEG, MEG sensor with sampling rate of the MEG recording Source or sensory level (for the connectivity study only)	Type of analysis with analyzed MEG frequency bandwith	Main result
										frequency bins (1–4, 4–8, 8–12.5, 12.5–30, and 30–59 Hz), multilayer network approach	• Multilayer versatility analysis identified a cluster of network hubs in the left frontal region
CAE (Resting-state Connectivity)											
Chavez et al. (125)	CAE	5	NA	Resting state	NA	NA	NA	5	No (MEG−151) (1,250 Hz) Connectivity–sensor level	Graph theory, Linear coherence at sensor level with multi-frequency analysis (<5, 1–15, 15–24, 24–35, >35)	• Compared to a healthy subject, a patient with CAE had richer connectivity and modularity in 5–14Hz
Wu et al. (8)	CAE	13	9F: 4M	Resting state	8 (5.3–11)	NA	13 (0.5–60)	0	No (MEG−275) (6,000 Hz) Connectivity–source level	Beamformer (ASI), Graph theory, Granger causality, correlation analysis at source	• This is the first study to reveal that CAE patients displayed frequency-specific abnormalities in the network pattern during the resting state.

(Continued)

TABLE 1 | Continued

Article name	Type of genetic epilepsy	No. of patients included in study	No. of female (F): No. of male (M)	Study State of genetic epilepsy	Mean age at the time of MEG recording (range) (y)	Mean age of epilepsy onset (range) (y)	Duration of epilepsy (range) (m)	No. of pt. on ASM	Yes and No for the Simultaneous MEG/EEG recording No. of EEG, MEG sensor with sampling rate of the MEG recording Source or sensory level (for the connectivity study only)	Type of analysis with analyzed MEG frequency bandwith	Main result
										level with multi-frequency analysis (1–4, 4–8, 8–12,12–30, 30–80, 80–250, 250–500, 500–1,000 Hz)	• Compared to the healthy subject, the network pattern at 1–4 Hz was altered and, at 2 seconds before the first ictal GSWDs, mainly showed a strong connection in the frontal and weakened connection in the anterior-posterior pathway.
CAE (Difference between interictal and ictal connectivity)											
Shi et al. (126)	CAE	25	18F: 7M	Interictal and Ictal	7.7 (5–14)	NA	25.52 (1–72)	12	No (MEG−275) (6,000 Hz) Connectivity–source level	Beamformer (ASI), correlation analysis at source level in multifrequency bandwidths (1–4, 4–8, 8–12, 12–30, 30–80, 80–250, 250–500 Hz) (PCC/pC as seed)	• At 4–8, 8–12, magnetic sources of interictal GSWDs mainly located in PCC/pC while in ictal was MFC at 80–120Hz. • During ictal GSWDs, functional connectivity network involving PCC/pC showed strong connections in anterior to posterior pathway at 80–250Hz.

(Continued)

TABLE 1 | Continued

Article name	Type of genetic epilepsy	No. of patients included in study	No. of female (F): No. of male (M)	Study State of genetic epilepsy	Mean age at the time of MEG recording (range) (y)	Mean age of epilepsy onset (range) (y)	Duration of epilepsy (range) (m)	No. of pt. on ASM	Yes and No for the Simultaneous MEG/EEG recording No. of EEG, MEG sensor with sampling rate of the MEG recording Source or sensory level (for the connectivity study only)	Type of analysis with analyzed MEG frequency bandwith	Main result
											• During interictal GSWDs, functional connectivity was mostly limited to the posterior cortex region.
Sun et al. (127)[θ]	CAE	22	15F: 7M	Interictal and Ictal	8.5 (5–14)	NA	7.61 (4–13)	7	Yes (EEG−23, MEG−275) (6,000 Hz) Connectivity-Source level	Beamformer (ASI), correlation analysis (1–80 Hz)at source level in two frequency bandwidths (1–30, 30–80 Hz)	• At both frequencies, there was more active source activity location in ictal onset period rather than interictal. • The frontal lobe, temporo-parietal junctions, and parietal lobe became the main active areas of source activity during the ictal period, while precuneus, cuneus, and thalamus were relatively inactive.
CAE (Treatment response)											
Tenny et al. (47)[#]	CAE	16	9F: 7M	Pretreatment ictal network	8.8 (6.0–11.8)	8.8 (6.0–11.8)	∼1 week	No ASM[æ] f/up at least 2 y	Yes (EEG−21, MEG−275) (4,000 Hz) Connectivity–Source level	fMRI informed MEG effective connectivity (0.1–70 Hz) Beamformer (LCMV), Phase	• Compared to the ETX treatment responder, CAE patients with ETX treatment non-responder had decreased connectivity in the precuneus region with thalamus at the

(Continued)

TABLE 1 | Continued

Article name	Type of genetic epilepsy	No. of patients included in study	No. of female (F): No. of male (M)	Study State of genetic epilepsy	Mean age at the time of MEG recording (range) (y)	Mean age of epilepsy onset (range) (y)	Duration of epilepsy (range) (m)	No. of pt. on ASM	Yes and No for the Simultaneous MEG/EEG recording No. of EEG, MEG sensor with sampling rate of the MEG recording Source or sensory level (for the connectivity study only)	Type of analysis with analyzed MEG frequency bandwith	Main result
										slope index in 3 frequency bandwidths (3–4, 13–30, and 30–55 Hz),	delta frequency and increased in the frontal cortex at gamma frequency.
Miao et al. (128)	CAE	25	19F: 6M	Pretreatment ictal network	(4–11)	7.3 (3–10)	NA	No ASM[ae] f/up 36–66 m	No (MEG—275) (300 Hz) Connectivity–source level	Beamformer (ASI) in 2 frequency bandwidth 1–7 Hz and 8–30, Graphic theory—source neural analysis	• Ictal post-DMFC (dorsal medial frontal cortex, including medial primary motor cortex and supplementary sensorimotor area) source at 1–7 Hz or 8–30 Hz were observed in all female patients with LTG non-responder. • The cortico-thalamo-cortical network at 1–7 Hz was changed according to age.
Zhang et al. (129)	CAE	24	19F: 5M	Pretreatment ictal network	10.8 (2–17)	6.29 (4–10)	6.29 (4–10)	No ASM[ae] f/up 12–74 m	No (MEG—275) (6,000 Hz) Connectivity–source level	Beamformer (ASI), Correlation analysis at source level in 6 frequency	• Compared to the ASM (both LTG and VPA) responder, at 8–12and 30–80, the source location of ASM non-responders was mainly in the frontal cortex, mostly the medial frontal cortex.

(Continued)

TABLE 1 | Continued

Article name	Type of genetic epilepsy	No. of patients included in study	No. of female (F): No. of male (M)	Study State of genetic epilepsy	Mean age at the time of MEG recording (range) (y)	Mean age of epilepsy onset (range) (y)	Duration of epilepsy (range) (m)	No. of pt. on ASM	Yes and No for the Simultaneous MEG/EEG recording No. of EEG, MEG sensor with sampling rate of the MEG recording Source or sensory level (for the connectivity study only)	Type of analysis with analyzed MEG frequency bandwith	Main result
										bandwidths (1–4, 4–8, 8–12, 12–30, 30–80, 80–250 Hz)	• Nonresponders showed strong positive local frontal connections and deficient anterior and posterior connections at 80–250 Hz.

y, year; m, month; F, female; M, male; ASM, antiseizure medication; MEG, magnetoencephalography; SAM, synthetic aperture magnetometry; GSWD, generalized sharp wave discharge; sLORETA, standardized low-resolution brain electromagnetic topography; ms, milliseconds; ETX, Ethoxusimide; LCMV, Linear constraint minimum variance; ASI, accumulated source imaging; DICS, Dynamic imaging of coherent sources; LTG, lamotrigine; VPA, valproic acid; PCC, posterior cingulate cortex; pC, precuneus; MFC, medial frontal cortex; CAE, childhood absence epilepsy; NA, no information or not applicable; Y, yes; N, no.

[*] All patients stopped ASM 2 days before MEG.

[æ] All patients didn't take any seizure medication at the time of MEG recording and follow up after initiation of ASM.

[**] Same patients were involved in multiple studies.

[θ] Same patients were involved in multiple studies.

[#] Overlapped patients.

Connectivity

Resting-State

Resting-state connectivity of CAE is illustrated in **Figure 1**. Chavez et al. compared the *modular organization of the brain networks*' resting-state connectivity between CAE patients taking ASMs and normal healthy subjects (125). Increased connectivity with clear modular structures, subsets of units within a network, was noted in the epileptic brain at the extended alpha band (5–14 Hz). Modularity analysis revealed that nodes of epileptic brain networks were abnormally linked to different functional modules in distinct networks compared to the normal healthy subjects. To confirm whether taking ASM might be the contributing factor for altering the resting-state connectivity, Wu et al. studied resting-state connectivity in treatment naïve CAE by constructing effective connectivity (EC) using correlation and Granger causality analysis, and were the first to reveal frequency-specific alteration in EC during the resting state without 3 Hz GSWDs (8). Compared with the healthy control group, strong connectivity in the frontal lobe and weakened connectivity in the anterior-posterior pathway were noted within the delta band (1–4 Hz). In the low-frequency band (1–8 Hz), the effective network activity involving the precuneus and posterior cingulate cortex (PCC/pC) was significantly decreased in patients with CAE (8). The reduced resting functional connectivity in PCC/pC has also been reported in patients with attention deficit disorder and memory impairment (130). Thus, these particular changes may be partially responsible for behavioral and cognitive co-morbidities seen in many patients with CAE (131).

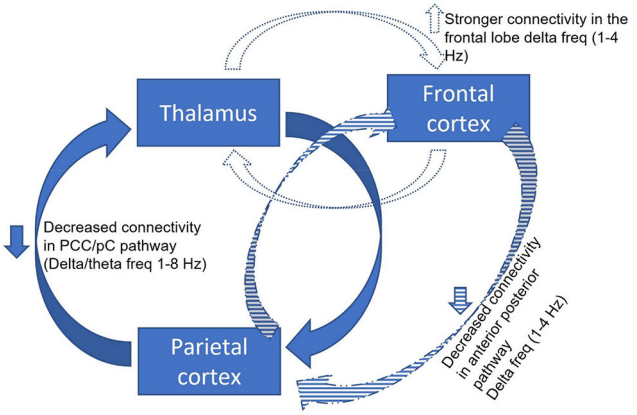

FIGURE 1 | Adapted with permission from Tenney et al. (47). Figure showing the resting-state connectivity in CAE, without 3 Hz GSWDs, compared with the healthy control. The three major brain regions have been identified as responsible for the generalization of the childhood absence seizures (thalamus, frontal cortex, parietal cortex). Given all the data from Wu and colleagues, compared with the healthy control group, strong connectivity in the frontal lobe at 1–4 Hz (blue dotted) and a weakened connectivity in the anterior-posterior pathway was noted within the delta band 1–4 Hz (blue stripped). In the low-frequency band at 1–8 Hz (blue solid), the effective network activity involving the precuneus and posterior cingulate cortex (PCC/pC) was significantly decreased in patients with CAE (8).

Ictal Network Connectivity

Using dynamic imaging of coherent sources (DICS) beamformer, Gupta et al. studied the transitions between interictal, preictal, and ictal periods of absence seizures (within 1s of first ictal GSWD) and confirmed frequency-dependent source localization (119). The consistent appearance of low frequency 2–4 Hz frontal and occipital cortical source was noted before the first generalized spikes, and change in the connectivity networks was noted at the onset of the GSWD, suggesting the increased connectivity from preictal pathologically predisposed network toward the rapidly recruiting synchronous ictal network. Using accumulated source imaging (ASI) beamformer analysis to quantify the network connectivity changes from a preictal to an ictal state, Wu et al. demonstrated that the dynamic changes in neural networks probably resulted from the cortically initialized cortico-thalamic network and analyzed neuromagnetic data as low-frequency (1–80 Hz) and high frequency (80–200 Hz) (120). During the transition period, the predominant neuromagnetic activities were observed at low-frequency (1–80 Hz) dominantly in the frontal and parieto-occipito-temporal cortices, whereas those in the deep brain areas and medial frontal cortex were at a high-frequency band (80–500 Hz) when compared to the interictal period. The EC was mainly over the cortical regions during the interictal period, but when the ictal transition occurred, there was a strong EC between cortex and deep brain areas in both low- and high-frequency ranges. Interestingly, the direction of the EC was predominantly from the cortex to the thalamus in the early ictal period. The same research group conveyed that indeed the rhythmic ictal spiking activity of GSWDs (within 1 s of the ictal spike onset) played a dominant role in the synchronization of the CAE epileptic network at the spike of the GSWDs (at 1–4, 4–8, and 8–12 Hz) which was significantly different from that of the slow-wave of the GSWDs (123). Thus, the dynamically balanced network was distorted primarily by the increased excitatory connections subtending a spike part of the GSWDs. Yet, the connections were mostly excitatory at the high-frequency band (80–250 Hz) regardless of spikes or slow waves. Thus, the authors suggested that abnormal excitatory activity of the entire brain required a local cluster of neurons to initiate the spike discharges, which caused the synchronous hyper-excitability in the epileptic network. Using whole-brain connectivity analysis and linear constraint minimum variance (LCMV) beamformer at the broadband frequency (1–40 Hz), Youssofzadeh et al. tried to reveal the focal components of the absence seizures in effective connectivity (EC) and investigated the network contrast between ictal and preictal period (121). The highly connected brain areas or hubs in the thalami, precuneus and cingulate cortex generally supported a theory of rapidly engaging and bilaterally distributed networks responsible for seizure generation (121).

Not only the ictal transition but also the ictal termination had been studied. Jiang et al. investigated the network changes within the 2 s of ictal termination in drug-naïve CAE using beamformer (ASI) and graph theory connectivity analyses (122). At the low-frequency (1–80 Hz) bands, the activities

were predominantly distributed in the frontal and parieto–occipito–temporal junction, whereas sources of HFOs (80–500 Hz) were localized to the medial frontal cortex and deep brain areas (mainly thalamus) during both interictal period and the termination transition. Furthermore, an enhanced positive cortico–thalamic EC was observed around the discharge offset with its direction primarily from various cortical regions to the thalamus (122). Sun et al. re-investigated ictal termination (within the 3 s of transition) of absence seizures and found the transition to be associated with dynamic frequency-dependent changes in the functional connectivity (124). At 1–4, 4–8, and 8–12 Hz, the magnetic source during seizure termination appeared to be consistent over the ictal period and was mainly localized in the frontal cortex and parieto-occipito-temporal junction. At ictal termination, source activity and peak source strength were significantly reduced in the frontal lobe at 12–30 and 30–80 Hz. Thus, the finding from the study, as mentioned above, suggested that the neuromagnetic activity in different frequency bands might play a role in activating or deactivating different cortical networks, such as frontal corticothalamic, parietal corticothalamic, default mode network, etc., and responsible for the pathophysiological mechanism of CAE.

To confirm the hypotheses of whether the interaction of co-occurring networks at distinct frequencies interact through cross-frequency coupling mechanism effects, Tenney et al. complemented neuromagnetic signal analysis, beamformer (LCMV), and cross-frequency canonical analyses with fMRI to increase the spatial resolution and analyze cross-frequency coupling (CFC) (48). The fMRI informed MEG effective connectivity (EC) (spatial map of the ictal network was defined using the fMRI and used as *a prior* for MEG connectivity) study showed beta/gamma CFC and within frequency coupling in frontoparietal and frontofrontal regions during the CAE seizures. Strong coupling between beta and gamma frequencies within the left frontal cortex, and between left frontal and right parietal regions were observed. There was also strong connectivity between left frontal and right parietal nodes within the gamma bands. Multilayer versatility analysis showed that a cluster of network hubs in the frontal regions and thus frontal cortical regions were critical for absence seizure generation (48). Thus, all the findings from the ictal connectivity studies consistently show different cross-frequency coupling or distinct frequency-dependent activation and deactivation of cortical network initiation followed by abrupt synchronization between cortical and subcortical structures in the generation, propagation, and the termination of the CAE seizure, which further supports the *cortical focus theory*.

Difference Between Ictal and Interictal Connectivity

Ictal and interictal GSWD connectivity were studied using ASI beamformer and correlation analyses to investigate the clinical ictal symptoms related to the ictal CAE epileptic network and illustrated in **Figure 2**. Shi et al. investigated the differences between the interictal GSWDs (<4 s) and ictal GSWDs (>10 s) in CAE (126). The low frequency (4–8 Hz and 8–12 Hz) magnetic sources were mainly localized within the posterior cingulate cortex and precuneus (PCC/pC) during the interictal state. The high frequency (80–250 Hz) magnetic components of the ictal GSWDs were mainly localized in the medial frontal cortex. In terms of connectivity (using posterior cingulate and precuneus (PCC/pC) as the seed), there were strong connections in the anterior-posterior pathway, mainly the frontal cortex during the ictal GSWDs. In contrast, the connections were mostly limited to the posterior cortex region at 80–250 Hz during interictal GSWDs. Thus, there were significant disparities in the source localization between ictal and interictal GSWDs. The low-frequency activation in the PCC/pC during the interictal period might be related to maintaining consciousness during the interictal GSWDs. Shi et al. concluded that weakened network connections during the interictal GSWD might be in favor of preventing overexcitability and relates to the termination of GSWDs (126). Thus, the finding concurs with the conclusion made by Wu et al. (8). There is reduced resting functional connectivity in PCC/pC patients with CAE in not only interictal but also resting state.

To confirm the findings, the same research group (127) studied the functional connectivity reorganization of the brain regions in both interictal without GSWD (30 s of the interictal period without GSWDs at least 60 s from the ictal period) and ictal GSWD network using two frequency band activities (1–30 Hz and 30–80 Hz). Compared to the interictal period, frontal, temporoparietal, and parietal regions were more active during seizures. On the contrary, the precuneus, the cuneus, and the thalamus were relatively silent during the ictal period compared with the interictal period. The differences in source localization between ictal and interictal states were reported, regardless of seizure duration, seizure frequency, or the age of epilepsy onset. Thus, the available data suggests the role of different frequency-dependent initial cortical involvement, most importantly in the frontal region, with predisposing hyper-excitable corticothalamic synchronization in the generation of the CAE.

Treatment and Prognostic Biomarker

Miao et al. reported that the presence of fast ripples (250–500 Hz) HFO in absence seizures was associated with increased seizure frequency (116). Similarly, Tang et al. studied whether the HFO in drug-naïve CAE was related to seizure severity and reported that the strength of ictal HFO (200–1,000 Hz) was significantly correlated with the severity of the absence seizures measured by the number of daily seizures, therefore a potential prognostic biomarker (118). Sun et al. later reported that the ictal peak source strength in the 1–4 Hz range was negatively correlated with the ictal duration of the seizure, whereas at 30–80 Hz, there was a positive correlation with the course of epilepsy (124). Yet, both studies were not able to draw major conclusions due to the limitation of a cross-sectional study (116, 118).

Thus, a couple of studies were conducted in which patients with drug-naive CAE underwent a MEG recording at the time of diagnosis (or within 1 week of diagnosis) and followed up for at least 1 year. The difference in the pretreatment ictal connectivity in patients with CAE was studied in response to ASMs treatment (responder vs. non-responder) and illustrated in **Figure 3**. Tenney et al. used fMRI-informed MEG effective connectivity to study prognostic biomarkers prospectively in

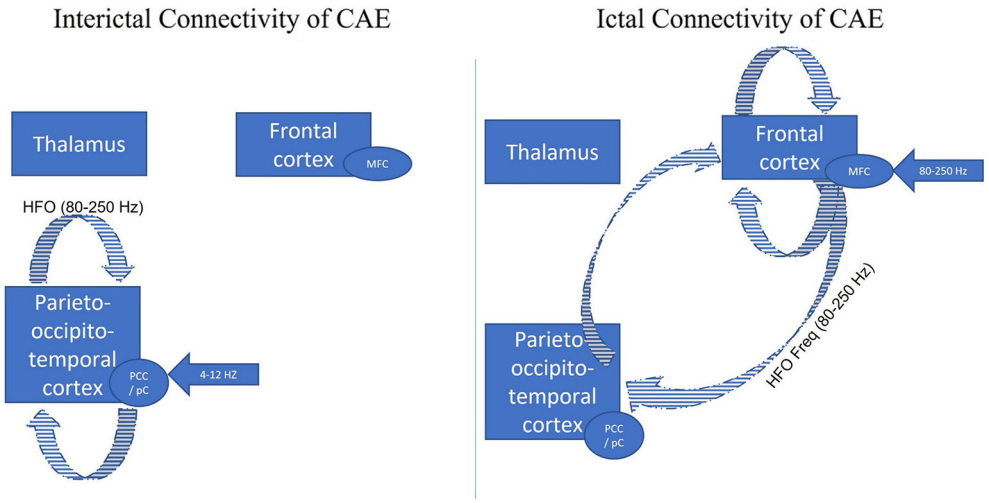

FIGURE 2 | Adapted with permission from Tenney et al. (47). Figure comparing the interictal (GSWDs < 4 s) and ictal connectivity (GSWDs > 10 s) in CAE. The three major brain regions have been identified as responsible for the generalization of the childhood absence seizures (thalamus, frontal cortex, posterior cortex). Given all the data from Shi et al. (126) the low frequency (4–8 Hz and 8–12 Hz) magnetic sources were mainly localized within the posterior cingulate cortex and precuneus (PCC/pC) during the interictal state (blue arrow). The high frequency (80–250 Hz) magnetic components of the ictal GSWDs were mainly localized in the medial frontal cortex (blue arrow). In terms of connectivity (using posterior cingulate and precuneus (PCC/pC) as the seed), there were strong connections in the anterior-posterior pathway, mainly the frontal cortex during the ictal GSWDs (blue stripped). In contrast, the connections were mostly limited to the posterior cortex region at 80–250 Hz during interictal GSWDs (blue stripped). Thus, there were significant disparities in the source localization between ictal and interictal GSWDs.

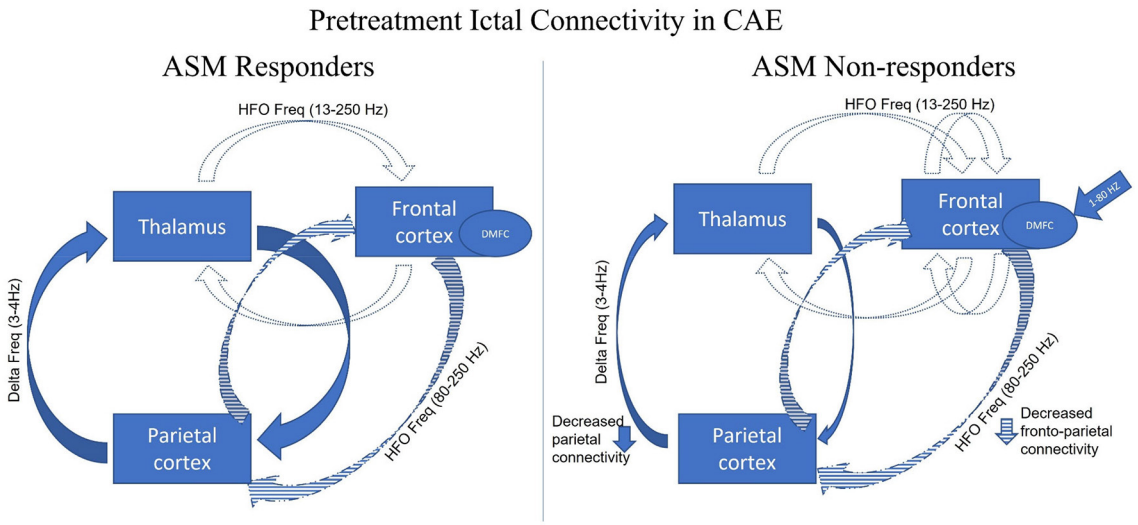

FIGURE 3 | Adapted with permission from Tenney et al. (47). Figure showing pretreatment ictal connectivity analysis of the antiepileptic (ASM) (ethosuximide, lamotrigine, and valproic acid) responder and non-responder in CAE. The three major brain regions have been identified as responsible for the generalization of the childhood absence seizures (thalamus, frontal cortex, parietal cortex). Given all the findings collected from Tenny et al. (47), Miao et al. (128), and Zhang et al. (129), parietal cortico-thalamic network at the low frequencies (blue solid) and a co-occurring frontal corticothalamic network at higher frequency (blue dotted) and anterior-posterior/frontoparietal network at higher frequency (blue stripped). Compared to the responder, ASM non–responders have ictal neuromagnetic sources at 1–80 Hz localized to the dorsomedial frontal cortex (DMFC) (blue arrow). In addition, the ASM non–responders have decreased parietal cortico-thalamic at 3–4 Hz and frontoparietal network connectivity at 80–250 Hz with increased frontal local connectivity at 13–250 Hz.

drug-naive CAE patients with a follow-up for at least 2 years after starting the ethosuximide (ETX) (47). Pretreatment connectivity demonstrated the strongest connections in the thalamus and posterior head regions (parietal, posterior cingulate, angular gyrus, precuneus, and occipital) at low frequency (delta 3–4 Hz) and the co-occurring frontal cortical thalamic network at the

high frequencies (beta/gamma 13–55 Hz). ETX non-responders' pretreatment connectivity decreased in the precuneus region and increased in the frontal cortex compared to ETX responders. This increased frontal cortical connectivity may be a potential prognostic biomarker of drug-resistance. Miao et al. also studied the responders and non–responders to the two established ASMs, lamotrigine (LTG) and valproic acid (VPA), using a beamformer (ASI) (128). In six LTG-non-responders CAE patients, ictal source locations were noted in the posterior-dorsal medial frontal cortex (post-DMFC including medial primary motor cortex and supplementary sensorimotor area) at 1–7 Hz or 8–30 Hz but not in 9 LTG responders, regardless of the age of onset and the seizure frequency. In addition, the authors suggested that ictal post-DMFC source localization could be suggestive of a biomarker for predicting LTG non–responsiveness. Zhang et al. replicated the same findings in CAE patients using the same beamformer technique (ASI) (129). The source localization of the ASMs non-responders was mainly in the frontal cortex at 8–12 and 30–80 Hz, especially the medial frontal cortex at alpha frequency. The non-responders showed strong positive local frontal connections and deficient anterior and posterior connections at 80–250 Hz. Thus, while it is likely that no one single mechanism can explain the pharmacologic responsiveness, ASM non-responders had more source localized within the dorsomedial frontal regions with decreased anterior-posterior network connectivity. At this time, the available preliminary data shows promising results in prognosticating response to ASM, but further studies with a larger sample size as well as comparing types of ASM non-responders are warranted to study the causality association.

Thus far, neuromagnetic source localization identifies three major brain areas which are thought to be responsible for the generation, propagation, and termination of CAE GSWDs: frontal cortex, parietal cortex, and thalamus with earlier cortical sources (more than 500 ms), supporting the concept of *cortical focus theory*. In addition, the current MEG literature suggests that the pathophysiology of GSWD in the absence seizure is a reflection of the co-occurring (excitation or inhibition) network(s) pathology rather than dysfunction in one particular brain area. For instance, frontal hyperexcitability and parietal deactivation involving intact but altered EC networks, such as corticothalamic, corticocortical and default mode networks, triggering the rapidly generalized epileptic discharges.

JUVENILE ABSENCE EPILEPSY (JAE)

Although JAE and CAE share many similar clinical characteristics, CAE absence seizure has more pronounced impairment of consciousness, and tonic-clonic seizures are less common than JAE. In terms of EEG, GSWDs of JAE are usually a higher frequency at 4–5 Hz. In terms of prognosis, JAE has a slightly worse prognosis when compared to CAE (132). Studies published on JAE are illustrated in **Table 2**.

Amor et al. explored the spatio-temporal dynamics of interactions within and between widely distributed cortical sites using MEG in patients with JAE (133). At the ictal onset, localized phase synchronization in multiple frontal and precentral areas was recorded, and the activity preceded the first ictal EEG GSWDs by 1.5 s. The analyses revealed a reproducible sequence of changes in the cortical network: (1) long-range desynchronization, (2) increased local synchronization, and (3) increased long-range synchronization. However, both local and long-range synchronization displayed different spatio-temporal profiles, but the cortical projection within the initiation time window (500 ms before the first ictal GSWDs) overlapped multifocal fronto-central regions, such as left frontomedial, frontopolar, right orbitofrontal, and right latero-central regions. Sakurai et al. studied the source analysis of the GSWDs in 5 patients with JAE using a dynamic statistic parametric mapping (dSPM) approach (134). The researchers reported that the initial activation of the GSWDs appeared in the focal cortical region with strong activation over the medial prefrontal activation followed by posterior cingulate and precuneus in 3 out of 5 patients simultaneously right after the medial prefrontal activation (134). The area mentioned above involved the default mode network at the onset of the GSWD, and thus it wasn't random diffuse cortical involvement but rather a selective cortical network, particularly the default mode network.

COMBINED ABSENCE EPILEPSY (CHILDHOOD AND JUVENILE ABSENCE EPILEPSY)

Studies published on combined absence epilepsy (CAE and JAE) are illustrated in **Table 2**. Rozendaal et al. attempted to compare the interictal and ictal periods in absence epilepsy (6CAE and 1JAE) using the SECD model, and source localizations were most often frontal, central, and parietal regions in either left or right hemisphere (135). The spatiotemporal assessment of the interictal epileptiform discharges (IEDs) indicated a stable localization of the averaged discharges, indicating a single underlying cortical source. Using LORETA, Gadad et al. studied the source analysis of the GSWDs at the onset, during, and offset of the GSWDs based on the duration of GSWDs and divided into three groups: GSWDs lasting 1 s, more than 1 s but less than 9.9 s, and equal to more than 10 s (136). The authors reported that the most common involved regions were caudate, cingulate, lentiform nucleus, and thalamus at the onset of all average discharges. Thus this observation substantiated the previously documented thalamo-cortico-stratum involvement in the absence of epilepsy (22, 23). During the propagation, the most frequent localization of sources were at limbic and frontal lobes, and these sources propagated to fronto-limbic structures at the ictal offset, irrespective of the duration of GSWD and subtype of absence epilepsy. The finding indicated the restricted/sustained network circuitry in fronto-limbic network involvement in origination and propagation of GSWDs until the disruption and inhibition. No significant difference in the source localization or network involvement was noted between CAE and JAE.

TABLE 2 | Showing all the published study characteristics and main outcomes on juvenile absence epilepsy and combined absence epilepsy.

Article name	Type of genetic epilepsy	No. of patients included in study	No. of female (F): No. of male (M)	Study state of genetic epilepsy	Mean age at the time of MEG recording (range) (y)	Mean age of epilepsy onset (range) (y)	Duration of epilepsy (range) (m)	No. of pt. on ASM	Yes and No for the Simultaneous MEG/EEG recording No. of EEG, MEG sensor with sampling rate of the MEG recording Source or sensory level (for the connectivity study only)	Type of analysis with Analyzed MEG Frequency bandwith	Main result
JAE											
Amor et al. (133)	JAE	5	4F: 1M	Ictal	23.4 (18–31)	NA	NA	2	Yes (EEG−64, MEG−151) (1,250 Hz) Connectivity–source level	Analytical wavelets transform (0.2–25 Hz), phase-locking	• At the ictal onset, there was reproducible sequence of changes in the cortical network (i) long-range desynchronization, (ii) increased local synchronization, and then followed by (iii) increased long-range synchronization.
Sakurai et al. (134)	JAE	5	2F: 3M	Ictal/GSWDs	27.2 (21.38)	NA	16 (12–26)	4	Yes (EEG−21, MEG−204) (600 Hz)	Dynamic statistical parameter mapping (dSPM) (0.5–400 Hz)	• Initial activation of the spike of GSWDs was noted over focal cortical regions, the medial prefrontal activation followed by activation of posterior cingulate and precuneus, resulting in the involvement of disruption of default mode network.

(Continued)

TABLE 2 | Continued

Article name	Type of genetic epilepsy	No. of patients included in study	No. of female (F): No. of male (M)	Study state of genetic epilepsy	Mean age at the time of MEG recording (range) (y)	Mean age of epilepsy onset (range) (y)	Duration of epilepsy (range) (m)	No. of pt. on ASM	Yes and No for the Simultaneous MEG/EEG recording No. of EEG, MEG sensor with sampling rate of the MEG recording Source or sensory level (for the connectivity study only)	Type of analysis with Analyzed MEG Frequency bandwith	Main result
Combined CAE and JAE											
Rozendaal et al. (135)	1JAE,6CAE	7	4F:3M	Interictal/ GSWDs	9.4 (7–14)	6.4 (5–12)	NA	7	No (MEG– either151 or 275) (1,200 Hz)	Equivalent dipole model (ECDs)(3–70 Hz)	• ECDs were localized most often on frontal, central, or parietal origin in either right or left hemisphere (with stable locations on averages of these discharges)
Gadad et al. (136)	8JAE, 12CAE	20	10F:10M	Ictal/ GSWDs	11.15 (7–30)	8.1 (2-19).	32.4 (18–72)	5	Yes (EEG −23, MEG−306) (2,000 Hz)	LORETA (1–70 Hz)	• The most common involved regions were caudate, cingulate, lentiform nucleus, and thalamus at the onset of all groups of GSWDs (1 s, >1s but <9 s or >9 s). • During the propagation, most frequent locations of sources were at limbic and frontal lobes with either lateralized and localized, and then source propagated to front-limbic structures at the offset, irrespective of the duration of GSWD and subtype of absence epilepsy.

y, year; m, month; F, female; M, male; ASM, antiseizure medication; MEG, magnetoencephalography; SAM, synthetic aperture magnetometry; GSWD, generalized sharp wave discharge; LORETA, low-resolution brain electromagnetic topography; ms, milliseconds; ETX, Ethoxusimide; LCMV, Linear constraint minimum variance; ASI, accumulated source imaging; DICS, Dynamic imaging of coherent sources; LTG, lamotrigine; VPA, valproic acid; PCC, posterior cingulate cortex; pC, precuneus; MFC, medial frontal cortex. CAE, childhood absence epilepsy; JAE, juvenile absence epilepsy; JME, juvenile myoclonus epilepsy; TCS, tonic-clonic seizure; IGE, idiopathic generalized epilepsy; GGE, genetic confirmed generalized epilepsy; NA, no information or not applicable; Y, yes; N, no.

JUVENILE MYOCLONUS EPILEPSY (JME)

Source Localization of GSWDs

Studies published on JME are illustrated in **Table 3**. Kotini et al. reported 2 adults with JME using the multiple signal characterization (MUSIC) algorithm and showed that the dipolar sources of the peak of GSWDs were localized at the cerebellar vermis with an extension up to the occipital region (137). Instead of analyzing at peak of the spike, Gadad et al. studied the source analysis of average GSWDs in three different spike phases: onset (upward phase of the spike from the baseline), peak, and offset (trailing edge of the spike) using LORETA in 20 patients with JME. At the onset of the GSWDs, the majority of the neuromagnetic sources were localized to sublobar regions (31% of localized discharges) defined as insula, caudate, claustrum, lentiform nucleus, and thalamus, followed by limbic region (22%), frontal (22%) and temporal lobe (11%). At the peak of the discharges, the sources were localized to the frontal lobe (45%), followed by sublobar regions (23%) (mainly lentiform nucleus). At the offset of the discharges, the sources were localized to the sublobar region (28%) (mainly caudate), followed by limbic (24%) and frontal regions(18%) (138). Therefore, the available evidence suggests an overall synchronous on and off interaction of cortico-subcortical structures in generating and propagating the epileptiform discharges in JME.

Network Connectivity

Resting-State

Three publications from the same research group reported and studied the 26 JME patients taking ASM using three different neuromagnetic source localization and connectivity techniques (142–144). Routley et al. studied resting-state functional connectivity in 26 patients with JME and reported that the altered resting-state connectivity could be a neuropathophysiological hallmark or potential diagnostic biomarker for JME. Compared to the healthy control group, there was overall increased connectivity in the posterior head regions in theta and alpha bands, and decreased connectivity in the pre and post-central brain region in beta bands. The reported increased connectivity in the posterior theta-frequency band might be associated with long-range connections affecting attention and arousal. The decreased beta band sensorimotor connectivity might be related to the resting state sensorimotor network and seizure-prone states in JME (142). Using a pairwise maximum entropy model, Krzeminski et al. studied the divergent oscillatory power in different networks: frontoparietal network (FPN) (ROIs: middle frontal gyrus, pars triangularis, inferior parietal gyrus, superior parietal gyrus, and angular gyrus), default mode network (ROIs: orbitofrontal cortex, precuneus, posterior cingulate, anterior cingulate and angular gyrus), and sensorimotor network (ROIs: supplementary motor area, precentral gyrus, and postcentral gyrus). Compared with the healthy control group, JME patients had fewer local energy minima and had elevated energy values for the FPN within theta, beta, and gamma bands during the resting state. No significant changes were noted between the default mode and sensorimotor networks using this method (143). Similar to the findings seen in CAE, these results highlighted the involvement of FPN in the pathophysiology of the JME.

Lopes et al. studied the same cohort of JME patients to investigate computational biomarkers using brain network ictogenicity (BNI), a computational modeling method, to generate the synthetic activity fluctuating between resting and seizure states (144). The higher values of the BNI represent a higher inherent propensity of the brain to generate seizure activity. Lopes et al. reported that patients with the JME had higher BNI values than healthy controls, and sensitivity was reported to be 0.77, and specificity was 0.58, with an area under the curve was 0.72 (144). But the model couldn't be generalized beyond JME as there was no study comparing other types of epilepsy.

Task-Specific Cortical Modulation

Hamandi et al. studied the resting state response in task-specific cortical modulation in occipital and sensorimotor cortices in JME compared to healthy control individuals (139). The authors reported that patients with JME had significantly reduced pre-movement beta event-related desynchronization in ipsi- and contralateral sensorimotor areas compared to controls, before and during the transient movement of motor tasks. There was no difference between epileptic and health patients in movement-related gamma synchronization and post-movement beta rebound. In addition to the physical motor task, De León et al. reported a case of mental calculation induced seizure in a patient with JME where the source was localized to the right premotor frontal cortex using the weighted minimum norm estimates (140). Similar to the result presented by Routley et al. and Krzeminski et al. with decreased sensorimotor connectivity, the current two task-specific JME patients suggested an abnormality in motor planning in JME likely related to the altered resting-state sensorimotor network and seizure-prone states in the JME (142, 143).

COMBINED GENETIC/IDIOPATHIC GENERALIZED EPILEPSY

Stefan et al. studied a total of 7 patients with various idiopathic generalized or genetic confirmed generalized epilepsy (IGE/GGE) using beamformer. After analyzing spike-wave bursts in all patients and single spikes in 6 patients, source analysis showed most frequently involved regions were the left or right frontal (mainly mesial and bilateral frontal areas), peri-insular, and subcortical/thalamic areas. In addition, all patients had unilateral frontal accentuation of the activity. In three patients, two with JME and one with myoclonic absence epilepsy, sources were mainly present in the central and premotor regions (141). Thus, the authors concluded that in contrast to pure focal epilepsy, the distribution of the GSWD is not restricted to one hemisphere but a predominant region with additional oscillating connectivity within the thalamocortical network system.

Elshahabi et al. studied the resting-state connectivity of 13 patients with various types of IGE/GGE using beamformer and graph theoretical network analysis. Compared to normal

TABLE 3 | Showing all the published study characteristics and main outcomes on juvenile myoclonic epilepsy and combined genetic epilepsy.

Article name	Type of genetic epilepsy	No. of patients included in study	No. of female (F): No. of male (M)	Study State of genetic epilepsy	Mean age at the time of MEG recording (range) (y)	Mean age of epilepsy onset (range) (y)	Duration of epilepsy (range) (m)	No. of pt. on ASM	Yes and No for the Simultaneous MEG/EEG recording No. of EEG, MEG sensor with sampling rate of the MEG recording Source or sensory level (for the connectivity study only)	Type of analysis with analyzed MEG Frequency bandwith	Main result
JME (Interictal/Ictal GSWDs)											
Kotini et al. (137)	JME	2	1F: 1M	GSWDs	25.5 (22/29)	17.5 (17/18)	96 (60/132)	2	No (EEG−18, MEG−122) (256 Hz)	Multiple signal characterization (MUSIC) algorithms (0.3–40 Hz)	• Dipolar sources of GSWDs were localized at the cerebellar vermis with extension upto the occipital region
Gadad et al. (138)	JME	20	10F: 10M	GSWDs	23.5 (NA)	16 (NA)	91.2	7	Yes (EEG−23, MEG −306) (2,000 Hz)	LORETA (1–70 Hz)	• At the onset of the GSWDs discharges, the sources were localized to sublobar regions, defined as insula, caudate, claustrum, lentiform nucleus, and thalamus, followed by limbic region, frontal and temporal lobe. • At the peak of the discharges, the sources were localized to the frontal lobe, followed by the sublobar regions (mainly lentiform nucleus).

(Continued)

TABLE 3 | Continued

Article name	Type of genetic epilepsy	No. of patients included in study	No. of female (F): No. of male (M)	Study State of genetic epilepsy	Mean age at the time of MEG recording (range) (y)	Mean age of epilepsy onset (range) (y)	Duration of epilepsy (range) (m)	No. of pt. on ASM	Yes and No for the Simultaneous MEG/EEG recording No. of EEG, MEG sensor with sampling rate of the MEG recording Source or sensory level (for the connectivity study only)	Type of analysis with analyzed MEG Frequency bandwith	Main result
											• At the offset of the discharges, the sources were localized to the sublobar region(mainly caudate), followed by limbic and frontal regions.
JME (Task-Specific)											
Hamand et al. (139)	JME	12	9F:3M	Task-Specific Resting-state	24.1 (18–37)	13.8 (8–17)	NA	12	No (MEG−275) (1,200 Hz)	Beamformer (SAM) (15–30hz, 40–60Hz, 60–90 Hz)	• Compared to healthy control, patients with JME had significantly reduced pre-movement beta event-related desynchronization in the motor task.
De León et al. (140)	JME	1	1M	Task Specific Reflex Seizure	29	8	252	1	Yes (EEG−64, MEG−305) (1,000 Hz)	Forward and inverse modeling, weighted minimum-norm estimation (wMNE) (0.1–330 Hz)	• Source localization of ictal GSWDs was localized to the premotor frontal cortex.

(Continued)

TABLE 3 | Continued

Article name	Type of genetic epilepsy	No. of patients included in study	No. of female (F): No. of male (M)	Study State of genetic epilepsy	Mean age at the time of MEG recording (range) (y)	Mean age of epilepsy onset (range) (y)	Duration of epilepsy (range) (m)	No. of pt. on ASM	Yes and No for the Simultaneous MEG/EEG recording No. of EEG, MEG sensor with sampling rate of the MEG recording Source or sensory level (for the connectivity study only)	Type of analysis with analyzed MEG Frequency bandwith	Main result
GGE (Interictal GSWDs)											
Stefan et al. (141)	IGE (2 JME, 4 AE, and 6 AE-TCS)	7	4F,3M	GSWDs (Spike)	27.86 (17–42)	NA	NA	6	Combined (5 patients has simultaneous MEG-EEG recording, 2 patients has only MEG recording) (EEG—32, MEG-two sensor system with 37 first order gradiometers) (N/A on sampling rate)	Equivalent dipole model (Single dipole analysis/Single moving dipole), Beamformer (normalized scanning analysis) (N/A on frequency band-width)	• In all patients, source analysis showed most often involvement of frontal, peri-insular, and subcortical/thalamic areas in addition to the unilateral frontal accentuation. • In JME and Myoclonic absence epilepsy, source analysis showed central and premotor regions whereas prefrontal accentuation in absence epilepsy.
JME (Resting-state connectivity)											
Routley et al. (142)*	JME	26	19F: 7M	Resting-state	28.5 (18–48)	14 (17–24)	181 (33-488)	26	No (MEG—275) (600 Hz) Connectivity—source level	Beamformer (LCMV)(1–150 Hz), Graphic theory, source-level analysis with correlation analysis with different frequency	• Compared to healthy control, patients with JME had increased connectivity in the theta band in the posterior head region and decreased connectivity in the beta band in the sensorimotor cortex

(Continued)

TABLE 3 | Continued

Article name	Type of genetic epilepsy	No. of patients included in study	No. of female (F): No. of male (M)	Study State of genetic epilepsy	Mean age at the time of MEG recording (range) (y)	Mean age of epilepsy onset (range) (y)	Duration of epilepsy (range) (m)	No. of pt. on ASM	Yes and No for the Simultaneous MEG/EEG recording No. of EEG, MEG sensor with sampling rate of the MEG recording Source or sensory level (for the connectivity study only)	Type of analysis with analyzed MEG Frequency bandwith	Main result
										bandwidth (1–4, 4–8, 8–13, 13–30, 40–60 Hz)	
Krzemiński et al. (143)*	JME	26	19F: 7M	Resting-state	28.5 (18–48)	14 (7–24)	181 (33-488)	26	No (MEG−275) (600 Hz) Connectivity—source level	Graphic theory, source-level analysis with pairwise maximum entropy model (pMEM) with different frequency bandwidth (4–8, 8–12, 13–30, 350–60 Hz)	• Compared to healthy control, JME patients showed fewer local energy minima and elevated energy values for frontoparietal networks within theta, beta, and gamma bands.
Lopes et al. (144)*	JME	26	19F: 7M	Resting-state	28.5 (18–48)	14 (7–24)	181(33-488)	26	No (MEG−275) (600 Hz)	Beamformer (LCMV), Canonical mathematical model of ictogenicity at alpha band	• Compared to healthy control, patients with JME had a higher propensity to generate seizures. The BNI classification accuracy was 73%

(Continued)

TABLE 3 | Continued

Article name	Type of genetic epilepsy	No. of patients included in study	No. of female (F): No. of male (M)	Study State of genetic epilepsy	Mean age at the time of MEG recording (range) (y)	Mean age of epilepsy onset (range) (y)	Duration of epilepsy (range) (m)	No. of pt. on ASM	Yes and No for the Simultaneous MEG/EEG recording No. of EEG, MEG sensor with sampling rate of the MEG recording Source or sensory level (for the connectivity study only)	Type of analysis with analyzed MEG Frequency bandwith	Main result
										8–13 Hz (Brain network ictogenicity BNI)	
GGE (Resting State Connectivity)											
Elshahabi et al. (145)	IGE (5IGE-TCS, 4CAE,2JAE, 1 JME, 1 UN)	13	9F:4M	Resting-state	38.6 ± 15.8	15.5 (4–48)	NA	12	No (MEG−275) (3,906.2 Hz) Connectivity –source level	Beamformer (DICS), Graphic theory, source analysis at different frequency bandwidths (0–4, 4–8, 8–12, 12–20, 21–29, 35–45 Hz)	• Compared to the healthy control, patients with IGE had a widespread increase in connectivity, mainly in the motor network, mesio-frontal and temporal cortex.
Stier et al. (146)	GGE (5CAE,6JAE, 5JME, 4 TCS and 5GGE)	25	16F: 9M	Resting state	25 (22–37)	15 (10–17)	204 (96-288)	NA	No (MEG−275) (585.9 Hz) Connectivity—sensor level	Beamformer (DICS), Graphic theory, the imaginary part of coherency, source analysis at different	• Compared to the healthy control, patients with generalized epilepsy showed widespread increased functional connection at the theta and gamma frequency band and power in the delta and gamma frequency band.

(Continued)

TABLE 3 | Continued

Article name	Type of genetic epilepsy	No. of patients included in study	No. of female (F): No. of male (M)	Study State of genetic epilepsy	Mean age at the time of MEG recording (range) (y)	Mean age of epilepsy onset (range) (y)	Duration of epilepsy (range) (m)	No. of pt. on ASM	Yes and No for the Simultaneous MEG/EEG recording No. of EEG, MEG sensor with sampling rate of the MEG recording Source or sensory level (for the connectivity study only)	Type of analysis with analyzed MEG Frequency bandwith	Main result
										frequency bandwidths (0–4, 4–8, 8–12, 12–20, 21–29, 32–48 Hz)	• Compared to normal control, siblings without epilepsy also had significantly increased network connectivity, predominantly in beta frequencies, representing an endophenotype of GGE
Difference between healthy control, generalized epilepsy, and focal frontal epilepsy											
Niso et al. (147)	JME	15	9F: 6M	Resting state	27 (20–46)	NA	NA	15	No (MEG—306) (1,000 Hz) Connectivity—sensor level	Graphic theory, phase lag value at sensor level analysis (0.5–40 Hz) with multi-frequency bandwidth (0.1–4, 4–8, 8–12,12–20, 20–28, 28–40)	• Generalized epilepsy showed higher spectral power for all the frequencies over the widespread sensors except the alpha band, whereas frontal lobe epilepsy showed higher relative power in the beta band bilaterally over the frontocentral sensors. • In generalized epilepsy, network connectivity showed greater efficiency and lower eccentricity than the control subjects at high-frequency bands.

(Continued)

TABLE 3 | Continued

Article name	Type of genetic epilepsy	No. of patients included in study	No. of female (F): No. of male (M)	Study State of genetic epilepsy	Mean age at the time of MEG recording (range) (y)	Mean age of epilepsy onset (range) (y)	Duration of epilepsy (range) (m)	No. of pt. on ASM	Yes and No for the Simultaneous MEG/EEG recording No. of EEG, MEG sensor with sampling rate of the MEG recording Source or sensory level (for the connectivity study only)	Type of analysis with analyzed MEG Frequency bandwith	Main result
											• Frontal focal epilepsy patients showed reduced eccentricity for theta band over the frontotemporal and central sensors.
Li Hegner et al. (148)	IGE (8 IGE-TCS, 2 CAE, 3 JME, 3 AE-TCS)	17	12F, 5M	Resting state	33.2 (18–63)	15.3 (6–47)	NA	15	No (MEG—275) (586 Hz) Connectivity—source level	Beamformer (DICS), Graphic theory, the imaginary part of coherency, source analysis at different frequency bandwidths (0–4, 4–8, 8–12, 12–20, 21–29, 30–46 Hz)	• Compared to healthy control, both focal frontal and generalized epilepsy patients showed widespread increased functional connectivity. • Compared to focal epilepsy, generalized epilepsy patients had increased network connectivity in bilateral mesio-frontal and motor regions.

y, year; m, month; F, female; M, male; ASM, antiseizure medication; MEG, magnetoencephalography; SAM, synthetic aperture magnetometry; GSWD, generalized sharp wave discharge; LORETA, standardized low-resolution brain electromagnetic topography; ms, milliseconds; LCMV, Linear constraint minimum variance; ASI, accumulated source imaging; DICS, Dynamic imaging of coherent sources; CAE, childhood absence epilepsy; JAE, juvenile absence epilepsy; JME, juvenile myoclonus epilepsy; TCS, tonic-clonic seizure; IGE, idiopathic generalized epilepsy; GGE, genetic confirmed generalized epilepsy; NA, no information or not applicable; Y, yes; N, no.

[*] *Same patients.*

controls, the patients with IGE/GGE had more pronounced motor network connectivity, mainly superior frontal gyrus, precentral, postcentral gyri, temporal cortex, and cerebellum. The authors also found significantly increased regional connectivity in the temporal lobe (superior and inferior temporal gyri) and insula (145). However, no conclusion could be made given that the study was performed on various IGE/GGE types and the limitation of the sub-cortical localization using a particular technique.

Stier et al. studied a total of 25 patients with GGE. Compared to normal healthy individuals, there was an increased functional connectivity at the multi-frequencies level in patients with GGE. Compared to normal controls, siblings without epilepsy also had significantly increased network connectivity, predominantly in beta frequencies. Compared to the healthy siblings of GGE, the increased beta connectivity patterns in GGE patients were less concordant, followed by functional connectivity in theta and delta frequency bands. Thus, the authors proposed that increased interictal MEG power and connectivity in frontocentral and temporo-parietal cortical regions were potential hallmarks of GGE (146). In addition, changes in these network characteristics were likely driven by the genetic factor and not by the disease process or medication effect (146).

DIFFERENCE IN RESTING-STATE FUNCTIONAL CONNNECTIVITY BETWEEN FOCAL (FRONTAL) AND GENERALIZED EPILEPSY

Using the fMRI connectivity analysis, it has been reported that patient with frontal lobe epilepsy has variable connectivity, either reduced or increased, various resting-state networks when compared to healthy pediatric and adult population (149–152). Still, there is limited literature investigating the resting-state fMRI functional connectivity comparing frontal lobe epilepsy with generalized epilepsy. A few publications on MEG resting-state functional connectivity in temporal lobe epilepsy are available, but data on frontal lobe epilepsy remains scarce. Herein, we would like to describe available neuromagnetic data in comparing the resting state connectivity between focal and generalized epilepsies.

Difference Between JME and Frontal Lobe Epilepsy

Niso et al. studied the resting-state functional connectivity of patients with frontal lobe epilepsy (FLE), generalized epilepsy (JME), and healthy individuals. Using power spectral analysis and graph theory assessed by phase synchronization measured with functional connectivity, the distribution of power and topographic changes (activation or deactivations) differed among all three groups. An increased total power indicated local synchronization. Those with JME had a higher total power for all frequencies except alpha band over a widespread set of sensors, whereas the FLE group showed higher relative power in the beta band bilaterally in the frontocentral sensors; i.e., regional specific around the epileptic focus. The authors found that functional networks from generalized epilepsy had greater efficiency and lower eccentricity than control subjects for higher frequency bands without a clear topography. Functional networks in FLE exhibited only reduced eccentricity over the frontotemporal and central sensors relative to the networks from controls (147). Thus, JME and FE groups represent a characteristic pattern of changes as compared to control.

Difference Between IGE/GGE and Frontal Lobe Epilepsy

Li Hegner et al. studied functional MEG connectivity using graph theory and coherency between focal and generalized epilepsy during resting state (with the absence of spikes or GSWDs) and found significant differences in network connectivity. Increased network connectivity was noted in bilateral mesio-frontal and motor regions in patients with IGE/GGE (148). Thus, the difference in the topography of resting-state functional connectivity in the mesio-frontal region in IGE/GGE may be a specific diagnostic biomarker.

CONCLUSION AND FUTURE PERSPECTIVES

In summary, with the advanced signal processing techniques combined with excellent temporal resolution properties of MEG, the cerebral neuromagnetic sources of GSWDs can be recorded and analyzed with millisecond resolution (153). The recording and post-processing associated with earlier MEG recording on GSWDs, especially using the SECD model, has several limitations, including deep brain structures, signal analysis of high-frequency oscillation, frequency-dependent network changes, etc. Later recordings using various advanced methodologies (various types of the beamformer, LORETA, pMEM, mathematical brain modeling, frequency coupling, etc.) advance our understanding not only of the potential pathophysiology of generalized epilepsy but also shed light on potential diagnostic, therapeutic and prognostic biomarkers of generalized epilepsy.

This review clearly illustrates the transition from focal neuromagnetic source analysis to network-based analysis using different frequency bandwidths involved in the generation, propagation and termination of the generalized spikes in various types of GGE. Earlier neuromagnetic analysis data focused on one particular brain structure, but recent literature points out that both cortical and subcortical structures are equally important in addition to the intact connectivity between various corticocortical and cortico-subcortical networks, with the leading initial epileptogenic hubs in the cortical region, mainly frontal lobe. Overall the current neuromagnetic data in GGE shows the important role of earlier cortical involvement, mainly frontal and parietal regions, before triggering the rapid synchronization of the subcortical and cortical networks, which goes along with the *concept of cortical focus theory* (22, 23, 25). The hypothesis mentioned above is ascertained by the current literature listed above in **Tables 1–3**.

Moreover, all published data suggests that generalized epilepsy has increased focal epileptogenic hubs, i.e., uneven cortical excitability in mainly frontal or central or parietal regions depending on the types of the GGE, with rapid recruitment *via* cortico-thalamic oscillation to various topographic locations, rather than the diffuse involvement of the whole brain. With the availability of directed connectivity analysis, the presence of focal hyper-connectivity in the setting of the global network has been demonstrated. As described above, one of the particular challenges in the clinical setting is accurately categorizing epileptic patients into either focal epilepsy or generalized epilepsy as both have different treatment options in terms of ASM and non–pharmacological treatment (131). In some particular cases, it is very challenging to give an accurate diagnosis. In addition, one doesn't want to miss the epilepsy surgery opportunity window in focal epileptic patients with rich connectivity, especially in the pediatric population, as the patient is misclassified as generalized epilepsy. In contrast, one doesn't want to undergo expensive pre-surgical epilepsy workups in patients with generalized epilepsy. At present, there is no scientifically proven diagnostic biomarker available for these types of challenging cases, but there are some promising findings by analyzing the neuromagnetic data. As illustrated above, during the resting state, connectivity patterns are different between healthy control, focal epilepsy, and GGE. In GGE, there is a presence of disorganization in the default mode network (GGE, JME, and AE), frontoparietal network (AE), and sensorimotor network (JME) during the resting state. In contrast, in focal frontal lobe epilepsy, there is only focal hyperconnectivity in the frontal lobe. Thus, the difference between resting MEG connectivity analyses can be a promising diagnostic biomarker to differentiate between focal and generalized epilepsy. One of the well known challenges of network analysis is that there is no one method superior to the others, and thus lack of standardized methodologies will be perplexing for future research. More investigations with increased subjects are also warranted to compare GE resting connectivity with other types of focal epilepsy with high connectivity, such as posterior quadrant epilepsy, for possible diagnostic and prognostic biomarkers in epilepsy.

In the default mode network, basic network node regions are responsible for basic incoming and outgoing information, remains activated when an individual is not engaged in external tasks, whereas the default state is suspended if the individual concentrates on a task (154). Compared with controls, effective connectivity at the posterior cingulate and parietal cortex, which are part of the default mode network, is decreased in patients with CAE, suggesting PC/PCC might be crucial for consciousness (8). In addition, the reduced resting functional connectivity in PCC/pC is also reported in patients with attention-deficit disorder (130) and memory impairment. Thus, given the above finding, patients with CAE have a higher chance of attention deficit disorder (131). In JME, in addition to other networks, there is an altered resting-state sensorimotor network, and hence it may be a reason for the seizure-prone (motor) states in the JME. Thus among different GGE subtypes, there are different networks involved. In epilepsy, quality of life is dependent not only on seizure frequency but also on the presence of co-morbidities, such as learning disability, anxiety, and ADHD (131). Without a doubt, understanding the basic pathophysiology of GGE will enlighten the clinicians with more therapeutic targets to improve the quality of life in patients with GGE.

There are promising preliminary neuromagnetic data on the prognostic biomarkers for drug resistance in patients with the CAE. CAE patients with the presence of the ictal HFOs (250–1,000 Hz), localized to the medial prefrontal cortex, are associated with increased seizure frequency (115, 116, 118). Both ETX and LTG non-responders have increased pretreatment ictal local frontal connectivity and decreased anteroposterior /frontoparietal connectivity compared to non-responders (47, 128, 129). Thus, by exploring the pretreatment ictal HFO and resting-state connectivity of CAE patients, one may be able to predict whether the patient will be an ASM responder or non-responder. However, at this time, no causal assumption can be made between the ASM non-responsiveness and the ictal frontal and decreased anteroposterior connectivity due to the limited data. Further studies are needed to confirm the hypothesis using a large cohort prospective study with a longer follow-up duration.

More and more data suggest that the alterations in the connectivity of various networks in patients with GGE are more complex and maybe even more dynamic with various multi-directionality. As mentioned above, Tenney et al. (47, 48) combined MEG with fMRI, which improved the source localization over the sub-regions of the deep brain area, such as different parts of the basal ganglia, and subregions of thalamus could be explored as the different parts of the basal ganglia and thalamus has different connectivity and functionality. In addition, the same research group already presented cross-frequency coupling showing how dynamic changes occurred in the various network in the CAE at the preictal stage (47, 48). Although fMRI has better spatial resolution than MEG, it is still insufficient to accurately localize the neuromagnetic source to subnuclei of the thalamus (46). In patients with drug-resistant GGE, one currently available alternative treatment option after failing the multiple ASMs is neuromodulation. The treatment outcome of neurostimulators, mainly DBS, is highly dependent upon the locations of the electrodes placement, stimulation parameters, subtypes of generalized epilepsy, or even individual cortical-subcortical connectivity profile (20, 21, 155). Thus, further studies using multimodality analysis combining various advanced postprocessing neuromagnetic analysis and neuroimaging may enlighten the underlying pathophysiology of underlying network alteration in various ictal or interictal stages of the patients with various types of IGG in order to improve the treatment options in generalized epilepsy,

Since absence epilepsy is the most common GGE, has frequent seizures, and reduced movement artifact, most of the current literature on GSWDs has experimented on patients with AE, mainly CAE. It is unclear whether research findings for CAE can be generalized to all the various subtypes of generalized epilepsy. Given all the literature mentioned above, different subtypes of generalized epilepsy may have shared mechanisms or connectivity pathways, but this review clearly illustrates varied topographic cortical involvements in different generalized

epilepsy based on their symptomatology. Hence, further studies are warranted to confirm this point of view.

Last but not least, another major limitation is how one can confirm the findings of the current non–invasive neuromagnetic data to support the concept of cortical focus theory, in which a highly connective cortical epileptogenic focus, most likely frontal hyperexcitability and parietal deactivation, triggering the rapidly generalized epileptic discharges involving intact corticothalamic or corticocortical networks. The finding has been confirmed in the animal model, with the cortical focus activation being found to be leading the thalamus activation by 500 ms (156). Although the ideal confirmation of the concept in humans should be analyzing intracranial invasive electrical activities from simultaneous cortical regions, covering bilateral multi-lobar regions, and various subcortical regions, subnuclei of bilateral thalami, it will be unethical and impractical to put multi-electrodes to cover every aspect of the thalamus and cortical regions. So far, a small study of intraoperative simultaneous invasive centromedian thalamic nuclei and scalp EEG recording had shown that generalized paroxysmal fast activity in patients with the Lennox-Gastaut syndrome appeared 75 ms later in thalamic activation when compared to the scalp frontal EEG activity, supporting a cortical driven process in generalized epilepsy (157). Another study investigated the interval relationship of the centromedian thalamus in relation to the cortical electrical activities in two patients with idiopathic generalized epilepsy (158). One of the two patients had bilateral independent discharges restricted only to the bilateral centromedian thalami, and the other had bilateral cortical discharges with the belated onset of leading thalamic discharges at the ictal onset (158). Thus, based on their symptomatology, the currently available data suggested there were different topographic cortical involvements in different subtypes of generalized epilepsy. Given the small sample size, no particular conclusion could be made. However, the findings from the CAE may likely be unable to generalize to all the subtypes of generalized epilepsy. Hence, further studies are warranted for the emerging development of responsive neurostimulation therapies for patients with generalized epilepsy.

In conclusion, current MEG literature challenges the concept of generalized epilepsy being fully generalized. Advances in recent MEG methodology contribute to the literature of idiopathic/genetic generalized epilepsy in terms of physiopathology, treatment and prognosis options, thus further blurring the boundary between focal and generalized epilepsy.

LIMITATIONS

This review is limited because only three databases were searched by one reviewer (TA) and included only the published publication in English. All the posters publications were excluded. Thus, some of the remarkable pertinent studies might be missed in the literature review.

AUTHOR CONTRIBUTIONS

TA contributed to the conception, performed literature review, drafting the manuscript, revising the manuscript, and final approval of the version to be published. JT and AB contributed to the conception, revising the manuscript, and final approval of the version to be published. All authors contributed to the article and approved the submitted version.

REFERENCES

1. Zack MM, Kobau R. National and state estimates of the numbers of adults and children with active epilepsy—United States, 2015. *MMWR Morbid Mortal Weekly Rep*. (2017) 66:821–5. doi: 10.15585/mmwr.mm6631a1
2. Fisher RS, Cross JH, D'Souza C, French JA, Haut SR, Higurashi N, et al. Instruction manual for the ILAE 2017 operational classification of seizure types. *Epilepsia*. (2017) 58:531–42. doi: 10.1111/epi.13671
3. Gastaut H. Clinical and Electroencephalographical Classification of Epileptic Seizures. *Epilepsia*. (1970) 11:102–12. doi: 10.1111/j.1528-1157.1970.tb03871.x
4. Hirsch E, Andermann F, Chauvel P, Engel J, Silva FL, da and Luders H. Generalized Seizures: from clinical phenomenology to underlying systems and networks. *Schweizer Archiv für Neurologie und Psychiatrie*. (2007) 7:346–346. doi: 10.4414/sanp.2007.01887
5. Tükel K, Jasper H. The electroencephalogram in parasagittal lesions. *Electroencephalogr Clin Neurophysiol*. (1952) 4:481–94. doi: 10.1016/0013-4694(52)90079-5
6. Bancaud J, Talairach J, Morel P, Bresson M, Bonis A, Geier S, et al. 'Generalized' epileptic seizures elicited by electrical stimulation of the frontal lobe in man. *Electroencephalogr Clin Neurophysiol*. (1974) 37:275–82. doi: 10.1016/0013-4694(74)90031-5
7. Wyllie E, Lachhwani DK, Gupta A, Chirla A, Cosmo G, Worley S, et al. Successful surgery for epilepsy due to early brain lesions despite generalized EEG findings. *Neurology*. (2007) 69:389–97. doi: 10.1212/01.wnl.0000266386.55715.3f
8. Wu C, Xiang J, Jiang W, Huang S, Gao Y, Tang L, et al. Altered effective connectivity network in childhood absence epilepsy: a multi-frequency MEG study. *Brain Topogr*. (2017) 30:673–84. doi: 10.1007/s10548-017-0555-1
9. Kakisaka Y, Alexopoulos AV, Gupta A, Wang ZI, Mosher JC, Iwasaki M, et al. Generalized 3- Hz spike-and-wave complexes emanating from focal epileptic activity in pediatric patients. *Epilepsy Behav*. (2011) 20:103–6. doi: 10.1016/j.yebeh.2010.10.025
10. Kim DW, Lee SY, Lee SK. Focal epileptogenic lesions in adult patients with epilepsy and generalized epileptiform discharges. *J Epilepsy Res*. (2016) 6:75–8. doi: 10.14581/jer.16014
11. Seneviratne U, Cook M, D'Souza W. Focal abnormalities in idiopathic generalized epilepsy: A critical review of the literature. *Epilepsia*. (2014) 55:1157–69. doi: 10.1111/epi.12688
12. Chauvel P. "Contributions of Jean Talairach and Jean Bancaud to epilepsy surgery," in: U. Luders, Hans (Department of neurology, *The Cleveland Clinic Foundation, Cleveland*, Ohio and Y.G. Comair (eds) *Epilepsy Surgery* (2nd Edition). Philadelphia: Lippincott Williams and Wilkins. pp. 35–41. (2001). Available online at: http://books.google.com/books?hl=enandlr=andid=2x5irzPCsjwCandoi=fndandpg=PA35anddq=CONTRIBUTIONSs+OF+JEAN+TALAIRACH+AND+JEAN+BANCAUD+TO+EPILEPSY+SURGERYandots=5HllPum-Khandsig=lunHohdyMtxLqkvvM0h_W9WR1SE
13. Rosenow F, Luders H. Presurgical evaluation of epilepsy. *J Pediatric Neurosci*. (2008) 3:74. doi: 10.4103/1817-1745.40593

14. Kwan P, Arzimanoglou A, Berg AT, Brodie MJ, Hauser WA, Mathern G, et al. Definition of drug resistant epilepsy: consensus proposal by the ad hoc task force of the ILAE commission on therapeutic strategies. *Epilepsia.* (2010) 51:1069–77. doi: 10.1111/j.1528-1167.2009.02397.x
15. Chauvel P, Gonzalez-Martinez JA, Bulacio JC. Presurgical intracranial investigations in epilepsy surgery. *Handbook Clinic Neurol.* (2019) 19:45–71. doi: 10.1016/B978-0-444-64142-7.00040-0
16. Chauvel P. "The epileptogenic zone: a critical reconstruction," in *A Practical Approach to Stereo EEG*, ed S.U. Schuele (1st ed). (New York: Springer Publishing Company) (2020). p. 105–117.
17. Englot DJ, Rolston JD, Wright CW, Hassnain KH, Chang EF. Rates and predictors of seizure freedom with vagus nerve stimulation for intractable epilepsy. *Neurosurgery.* (2016) 79:345–53. doi: 10.1227/NEU.0000000000001165
18. Morrell MJ, Halpern C. Responsive Direct Brain Stimulation for Epilepsy. *Neurosurg Clin N Am.* (2016) 27:111–21. doi: 10.1016/j.nec.2015.08.012
19. Fisher R, Salanova V, Witt T, Worth R, Henry T, Gross R, et al. Electrical stimulation of the anterior nucleus of thalamus for treatment of refractory epilepsy. *Epilepsia.* (2010) 51:899–908. doi: 10.1111/j.1528-1167.2010.02536.x
20. Starnes K, Miller K, Wong-Kisiel L, Lundstrom BN. A review of neurostimulation for epilepsy in pediatrics. *Brain Sci.* (2019) 9:283. doi: 10.3390/brainsci9100283
21. Torres Diaz CV, González-Escamilla G, Ciolac D, Navas García M, Pulido Rivas P, Sola RG, et al. Network Substrates of Centromedian Nucleus Deep Brain Stimulation in Generalized Pharmacoresistant Epilepsy. *Neurotherapeutics.* (2021) 18:1665–77. doi: 10.1007/s13311-021-01057-y
22. Meeren H, Van Luijtelaar G, Lopes Da Silva F, Coenen A. Evolving concepts on the pathophysiology of absence seizures: The cortical focus theory. *Arch Neurol.* (2005) 62:371–6. doi: 10.1001/archneur.62.3.371
23. Avoli M. A brief history on the oscillating roles of thalamus and cortex in absence seizures. *Epilepsia.* (2012) 53:779–89. doi: 10.1111/j.1528-1167.2012.03421.x
24. Chen PC, Castillo EM, Baumgartner J, Seo JH, Korostenskaja M, Lee KH. Identification of focal epileptogenic networks in generalized epilepsy using brain functional connectivity analysis of bilateral intracranial EEG signals. *Brain Topogr.* (2016) 29:728–37. doi: 10.1007/s10548-016-0493-3
25. Stefan H, Rampp S. Aktuelle klinisch-neurophysiologische befunde bei absence-epilepsien. *Nervenarzt.* (2009) 80:378–85. doi: 10.1007/s00115-008-2636-6
26. Hämäläinen M, Hari R, Ilmoniemi RJ, Knuutila J, Lounasmaa OV. Magnetoencephalography theory, instrumentation, and applications to non-invasive studies of the working human brain. *Rev Mod Phys.* (1993) 65:413–97. doi: 10.1103/RevModPhys.65.413
27. Ebersole JS. New applications of EEG/MEG in epilepsy evaluation. *Epilepsy research Supplement.* (1996) 11:227–37.
28. Cohen D, Halgren E. Magnetoencephalography (Neuromagnetism). *Encyclopedia of Neuroscience.* (2009) 9:615–22. doi: 10.1016/B978-008045046-9.02021-0
29. Knowlton RC, Shih J. Magnetoencephalography in epilepsy. *Epilepsia.* (2004) 45:61–71. doi: 10.1111/j.0013-9580.2004.04012.x
30. de Munck JC, van Dijk BW, Spekreijse H. Mathematical Dipoles are Adequate to Describe Realistic Generators of Human Brain Activity. *IEEE Transact Biomed Eng.* (1988) 35:960–6. doi: 10.1109/10.8677
31. Ebersole JS, Ebersole SM. Combining MEG and EEG source modeling in epilepsy evaluations. *J Clinic Neurophysiol.* (2010) 27:360–71. doi: 10.1097/WNP.0b013e318201ffc4
32. Bagić AI, Knowlton RC, Rose DF, Ebersole JS. American clinical magnetoencephalography society clinical practice guideline 1: recording and analysis of spontaneous cerebral activity. *J Clinic Neurophysiol.* (2011) 28:348–54. doi: 10.1097/WNP.0b013e3182272fed
33. Mosher JC, Spencer ME, Leahy RM, Lewis PS. Error bounds for EEG and MEG dipole source localization. *Electroencephalogr Clin Neurophysiol.* (1993) 86:303–21. doi: 10.1016/0013-4694(93)90043-U
34. Mosher JC, Baillet S, Leahy RM. EEG source localization and imaging using multiple signal classification approaches. *J Clinic Neurophysiol.* (1999) 16:225–38. doi: 10.1097/00004691-199905000-00004
35. Tenney JR, Fujiwara H, Rose DF. The value of source localization for clinical magnetoencephalography: beyond the equivalent current dipole. *J Clinic Neurophysiol Offic Publicat Am Electroencephalograph Soc.* (2020) 37:537–44. doi: 10.1097/WNP.0000000000000487
36. Huang MX, Mosher JC, Leahy RM. A sensor-weighted overlapping-sphere head model and exhaustive head model comparison for MEG. *Phys Med Biol.* (1999) 44:423–40. doi: 10.1088/0031-9155/44/2/010
37. Mosher JC, Leahy RM, Lewis PS. EEG and MEG: Forward solutions for inverse methods. *IEEE Transact Biomed Eng.* (1999) 46:245–59. doi: 10.1109/10.748978
38. Mosher JC, Baillet S, Leahy RM. Equivalence of linear approaches in bioelectromagnetic inverse solutions. *IEEE Workshop Statistic Sign Process Proceed.* (2003) 2003:294–297. doi: 10.1109/SSP.2003.1289402
39. Jerbi K, Mosher JC, Baillet S, Leahy RM. On MEG forward modelling using multipolar expansions. *Phys Med Biol.* (2002) 47:523–55. doi: 10.1088/0031-9155/47/4/301
40. Hämäläinen M, Huang M, Bowyer SM. Magnetoencephalography signal processing, forward modeling, magnetoencephalography inverse source imaging, and coherence analysis. *Neuroimag Clinics North Am.* (2020) 20:125–43. doi: 10.1016/j.nic.2020.02.001
41. Attal Y, Schwartz D. Assessment of subcortical source localization using deep brain activity imaging model with minimum norm operators: a MEG study. *PLoS ONE.* (2013) 8:e59856. doi: 10.1371/journal.pone.0059856
42. Puce A, Hämäläinen MS. A review of issues related to data acquisition and analysis in EEG/MEG studies. *Brain Sci.* (2017) 7:58. doi: 10.3390/brainsci7060058
43. Stefan H, Trinka E. Magnetoencephalography (MEG): Past, current and future perspectives for improved differentiation and treatment of epilepsies. *Seizure.* (2017) 44:121–4. doi: 10.1016/j.seizure.2016.10.028
44. Bénar CG, Velmurugan J, López-Madrona VJ, Pizzo F, Badier JM. Detection and localization of deep sources in magnetoencephalography: a review. *Curr Opin Biomed Eng.* (2021) 18:285. doi: 10.1016/j.cobme.2021.100285
45. Boto E, Holmes N, Leggett J, Roberts G, Shah V, Meyer SS, et al. Moving magnetoencephalography towards real-world applications with a wearable system. *Nature.* (2018) 555:657–61. doi: 10.1038/nature26147
46. Logothetis NK, Pauls J, Augath M, Trinath T, Oeltermann A. Neurophysiological investigation of the basis of the fMRI signal. *Nature.* (2001) 412:150–7. doi: 10.1038/35084005
47. Tenney JR, Kadis DS, Agler W, Rozhkov L, Altaye M, Xiang J, et al. Ictal connectivity in childhood absence epilepsy: Associations with outcome. *Epilepsia.* (2018) 59:971–81. doi: 10.1111/epi.14067
48. Tenney JR, Williamson BJ, Kadis DS. Cross-frequency coupling in childhood absence epilepsy. *Brain Connect.* (2021). doi: 10.1089/brain.2021.0119. [Epub ahead of print].
49. Cohen D. Magnetoencephalography: Evidence of magnetic fields produced by alpha-rhythm currents. *Science.* (1968) 161:784–6. doi: 10.1126/science.161.3843.784
50. Laohathai C, Ebersole JS, Mosher JC, Bagić AI, Sumida A, Von Allmen G, et al. Practical fundamentals of clinical MEG interpretation in epilepsy. *Front Neurol.* (2021) 12:986. doi: 10.3389/fneur.2021.722986
51. Schoffelen JM, Gross J. Source connectivity analysis with MEG and EEG. *Hum Brain Mapp.* (2009) 30:1857–65. doi: 10.1002/hbm.20745
52. Tenney JR, Fujiwara H, Horn PS, Rose DF. Comparison of magnetic source estimation to intracranial EEG, resection area, and seizure outcome. *Epilepsia.* (2014) 55:1854–63. doi: 10.1111/epi.12822
53. Duez L, Tankisi H, Hansen PO, Sidenius P, Sabers A, Pinborg LH, et al. Electromagnetic source imaging in presurgical workup of patients with epilepsy: a prospective study. *Neurology.* (2019) 92:e576–86. doi: 10.1212/WNL.0000000000006877
54. Pellegrino G, Hedrich T, Porras-Bettancourt M, Lina JM, Aydin Ü, Hall J, et al. Accuracy and spatial properties of distributed magnetic source imaging techniques in the investigation of focal epilepsy patients. *Hum Brain Mapp.* (2020) 41:3019–33. doi: 10.1002/hbm.24994
55. Leahy RM, Mosher JC, Spencer ME, Huang MX, Lewine JD. A study of dipole localization accuracy for MEG and EEG using a human skull phantom. *Electroencephalogr Clin Neurophysiol.* (1998) 107:159–73. doi: 10.1016/S0013-4694(98)00057-1

56. Hämäläinen MS. Magnetoencephalography: A tool for functional brain imaging. *Brain Topogr.* (1992) 5:95–102. doi: 10.1007/BF01129036
57. Mosher JC, Lewis PS, Leahy RM. Multiple dipole modeling and localization from spatio-temporal MEG Data. *IEEE Transact Biomed Eng.* (1992) 39:541–57. doi: 10.1109/10.141192
58. Mosher JC, Leahy RM. Recursive MUSIC: A framework for EEG and MEG source localization. *IEEE Transact Biomed Eng.* (1998) 45:1342–54. doi: 10.1109/10.725331
59. Van Veen BD, Buckley KM. Beamforming: a versatile approach to spatial filtering. *IEEE ASSP Magazine.* (1988) 5:4–24. doi: 10.1109/53.665
60. Spencer ME, Leahy RM, Mosher JC, Lewis PS. "Adaptive filters for monitoring localized brain activity from surface potential time series," In: *Conference Record—Asilomar Conference on Signals, Systems and Computers.* (1992), p. 156–161.
61. Robinson SE, Vrba J. *Functional neuroimaging by synthetic aperture magnetometry (SAM). Recent Advances in Biomagnetism.* (1999).
62. Gross J, Kujala J, Hämäläinen M, Timmermann L, Schnitzler A, Salmelin R. Dynamic imaging of coherent sources: Studying neural interactions in the human brain. *Proc Natl Acad Sci U S A.* (2001) 98:694–9. doi: 10.1073/pnas.98.2.694
63. Xiang J, Luo Q, Kotecha R, Korman A, Zhang F, Luo H, et al. Accumulated source imaging of brain activity with both low and high-frequency neuromagnetic signals. *Front Neuroinform.* (2014) 8:57. doi: 10.3389/fninf.2014.00057
64. Hämäläinen MS, Ilmoniemi RJ. Interpreting magnetic fields of the brain: minimum norm estimates. *Medical Biologic Eng Comput.* (1994) 32:35–42. doi: 10.1007/BF02512476
65. Pascual-Marqui RD, Michel CM, Lehmann D. Low resolution electromagnetic tomography: a new method for localizing electrical activity in the brain. *Int J Psychophysiol.* (1994) 18:49–65. doi: 10.1016/0167-8760(84)90014-X
66. Pascual-Marqui RD. Low resolution brain electromagnetic tomography (LORETA). *J Neurother.* (2001) 4:31–3. doi: 10.1300/J184v04n04_05
67. Wagner M, Fuchs M, Kastner J. Evaluation of sLORETA in the presence of noise and multiple sources. *Brain Topogr.* (2004) 16:277–80. doi: 10.1023/B:BRAT.0000032865.58382.62
68. Wang JZ, Williamson SJ, Kaufman L. Magnetic source imaging based on the minimum-norm least-squares inverse. *Brain Topogr.* (1993) 5:365–71. doi: 10.1007/BF01128692
69. Lin FH, Witzel T, Ahlfors SP, Stufflebeam SM, Belliveau JW, Hämäläinen MS. Assessing and improving the spatial accuracy in MEG source localization by depth-weighted minimum-norm estimates. *Neuroimage.* (2006) 31:160–71. doi: 10.1016/j.neuroimage.2005.11.054
70. Dale AM, Sereno MI. Improved localization of cortical activity by combining EEG and MEG with MRI cortical surface reconstruction: a linear approach. *J Cogn Neurosci.* (1993) 5:162–76. doi: 10.1162/jocn.1993.5.2.162
71. Dale AM, Liu AK, Fischl BR, Buckner RL, Belliveau JW, Lewine JD, et al. Dynamic statistical parametric mapping: combining fMRI and MEG for high-resolution imaging of cortical activity. *Neuron.* (2000) 26:55–67. doi: 10.1016/S0896-6273(00)81138-1
72. Hauk O, Wakeman DG, Henson R. Comparison of noise-normalized minimum norm estimates for MEG analysis using multiple resolution metrics. *Neuroimage.* (2011) 54:1966–74. doi: 10.1016/j.neuroimage.2010.09.053
73. Gorodnitsky IF, George JS, Rao BD. Neuromagnetic source imaging with FOCUSS: a recursive weighted minimum norm algorithm. *Electroencephalogr Clin Neurophysiol.* (1995) 95:231–51. doi: 10.1016/0013-4694(95)00107-A
74. Clarke CJS, Janday BS. The solution of the biomagnetic inverse problem by maximum statistical entropy. *Inverse Probl.* (1989) 5:483–500. doi: 10.1088/0266-5611/5/4/005
75. Cirillo ENM, Lebowitz JL. Metastability in the two-dimensional Ising model with free boundary conditions. *J Stat Phys.* (1998) 90:211–26. doi: 10.1023/A:1023255802455
76. Yeh FC, Tang A, Hobbs JP, Hottowy P, Dabrowski W, Sher A, et al. Maximum entropy approaches to living neural networks. *Entropy.* (2010) 12:89–106. doi: 10.3390/e12010089
77. Amblard C, Lapalme E, Lina JM. Biomagnetic source detection by maximum entropy and graphical models. *IEEE Transact Biomed Eng.* (2004) 51:427–42. doi: 10.1109/TBME.2003.820999
78. Mesulam MM. From sensation to cognition. *Brain.* (1998) 121:1013–52. doi: 10.1093/brain/121.6.1013
79. Fries P. Rhythms for cognition: communication through coherence. *Neuron.* (2015) 88:220–35. doi: 10.1016/j.neuron.2015.09.034
80. Cetin MS, Houck JM, Rashid B, Agacoglu O, Stephen JM, Sui J, et al. Multimodal classification of schizophrenia patients with MEG and fMRI data using static and dynamic connectivity measures. *Front Neurosci.* (2016) 10:466. doi: 10.3389/fnins.2016.00466
81. Friston KJ. Functional and effective connectivity in neuroimaging: a synthesis. *Hum Brain Mapp.* (1994) 2:56–78. doi: 10.1002/hbm.460020107
82. Granger CWJ. Investigating Causal Relations by Econometric Models and Cross-spectral Methods. *Econometrica.* (1969) 37:424. doi: 10.2307/1912791
83. Geweke J. Measurement of linear dependence and feedback between multiple time series. *J Am Stat Assoc.* (1982) 77:304–13. doi: 10.1080/01621459.1982.10477803
84. Basser PJ, Mattiello J, LeBihan D. MR diffusion tensor spectroscopy and imaging. *Biophys J.* (1994) 66:259–67. doi: 10.1016/S0006-3495(94)80775-1
85. He B, Yang L, Wilke C, Yuan H. Electrophysiological imaging of brain activity and connectivity-challenges and opportunities. *IEEE Transact Biomed Eng.* (2011) 58:1918–31. doi: 10.1109/TBME.2011.2139210
86. He B, Sohrabpour A, Brown E, Liu Z. Electrophysiological source imaging: a non-invasive window to brain dynamics. *Annu Rev Biomed Eng.* (2018) 20:171–96. doi: 10.1146/annurev-bioeng-062117-120853
87. Friston KJ. Functional and effective connectivity: a review. *Brain Connect.* (2011) 1:13–36. doi: 10.1089/brain.2011.0008
88. Lehnertz K. Assessing directed interactions from neurophysiological signals—An overview. *Physiol Meas.* (2011) 32:1715–24. doi: 10.1088/0967-3334/32/11/R01
89. Friston K, Moran R, Seth AK. Analysing connectivity with Granger causality and dynamic causal modelling. *Curr Opin Neurobiol.* (2013) 23:172–8. doi: 10.1016/j.conb.2012.11.010
90. Nolte G, Bai O, Wheaton L, Mari Z, Vorbach S, Hallett M. Identifying true brain interaction from EEG data using the imaginary part of coherency. *Clinic Neurophysiol.* (2004) 115:2292–307. doi: 10.1016/j.clinph.2004.04.029
91. Nolte G, Müller KR. Localizing and estimating causal relations of interacting brain rhythms. *Front Hum Neurosci.* (2010) 4:209. doi: 10.3389/fnhum.2010.00209
92. Garcés P, Martín-Buro MC, and Maestú, F. Quantifying the test-retest reliability of magnetoencephalography resting-state functional connectivity. *Brain Connectiv.* (2016) 6:448–60. doi: 10.1089/brain.2015.0416
93. Baker GT. Purification and some properties of ATP:Arginine phosphotransferase from sea anemones, Condylactis aurantiaca. *Comparativ Biochemistr Physiol Part B: Biochemistr.* (1975) 52:503–6. doi: 10.1016/0305-0491(75)90225-4
94. Patel RS, Bowman FDB, Rilling JK. A Bayesian approach to determining connectivity of the human brain. *Hum Brain Mapp.* (2006) 27:267–76. doi: 10.1002/hbm.20182
95. Nummenmaa A, Auranen T, Hämäläinen MS, Jääskeläinen IP, Lampinen J, Sams M, et al. Hierarchical Bayesian estimates of distributed MEG sources: Theoretical aspects and comparison of variational and MCMC methods. *Neuroimage.* (2007) 35:669–85. doi: 10.1016/j.neuroimage.2006.05.001
96. López JD, Litvak V, Espinosa JJ, Friston K, Barnes GR. Algorithmic procedures for Bayesian MEG/EEG source reconstruction in SPM. *Neuroimage.* (2014) 84:476–87. doi: 10.1016/j.neuroimage.2013.09.002
97. Mumford JA, Ramsey JD. Bayesian networks for fMRI: a primer. *Neuroimage.* (2014) 86:573–82. doi: 10.1016/j.neuroimage.2013.10.020
98. Friston KJ, Preller KH, Mathys C, Cagnan H, Heinzle J, Razi A, et al. Dynamic causal modelling revisited. *Neuroimage.* (2019) 199:730–44. doi: 10.1016/j.neuroimage.2017.02.045
99. Angluin D, Aspnes J, Kontorovich A. On the learnability of shuffle ideals. *Lect Notes Comput Sci.* (2012) 7568:111–23. doi: 10.1007/978-3-642-34106-9_12
100. Stephan KE, Friston KJ. Analyzing effective connectivity with functional magnetic resonance imaging. *Wiley Interdisciplin Rev Cogn Sci.* (2010) 1:446–59. doi: 10.1002/wcs.58

101. Stam CJ. Functional connectivity patterns of human magnetoencephalographic recordings: a 'small-world' network? *Neurosci Lett.* (2004) 355:25–8. doi: 10.1016/j.neulet.2003.10.063
102. Sporns O, Tononi G, Kötter R. The human connectome: A structural description of the human brain. *PLoS Comput Biol.* (2005) 1:0245–51. doi: 10.1371/journal.pcbi.0010042
103. Bassett DS, Bullmore E. Small-world brain networks. *Neuroscientist.* (2006) 12:512–23. doi: 10.1177/1073858406293182
104. Bullmore E, Sporns O. Complex brain networks: Graph theoretical analysis of structural and functional systems. *Nat Rev Neurosci.* (2009) 10:186–98. doi: 10.1038/nrn2575
105. Leskovec J, Horvitz E. Planetary-scale views on a large instant-messaging network. *Proceed Int Conferen World Wide Web.* (2008) 8:915–924. doi: 10.1145/1367497.1367620
106. Hughes JR, Cohen J, Mayman CI, Scholl ML, Hendrix DE. Relationship of the magnetoencephalogram to abnormal activity in the electroencephalogram. *J Neurol.* (1977) 217:79–93. doi: 10.1007/BF00312921
107. Ricci GB, Erne' SN, Del Gratta C, Peresson M, Pizzella V, Romani GL, et al. Template analysis on interictal neuromagnetic data from cases of focal and generalized epilepsy. *Adv Biomagnetism.* (1989) 287–290. doi: 10.1007/978-1-4613-0581-1_58
108. Ricci GB, Chapman RM, Erné SN, Narici L, Peresson M, Pizzella V, et al. Neuromagnetic topography of photoconvulsive response in man. *Electroencephalograph Clinic Neurophysiol.* (1990) 75:1–12. doi: 10.1016/0013-4694(90)90147-C
109. Ricci GB. The MEG in evaluation of generalized epilepsy. *Physiol Measure.* (1993) 14:A103–8. doi: 10.1088/0967-3334/14/4a/019
110. Westmijse I, Ossenblok P, Gunning B, van Luijtelaar G. Onset and propagation of spike and slow wave discharges in human absence epilepsy: a MEG study. *Epilepsia.* (2009) 50:2538–48. doi: 10.1111/j.1528-1167.2009.02162.x
111. Hu X, Dong J, Wang X, Wu T, Yang L, Lu X. Localization of epileptic foci in Children with childhood absence epilepsy by magnetoencephalography combined with synthetic aperture magnetometry. *J Biomed Res.* (2011) 25:259–65. doi: 10.1016/S1674-8301(11)60035-3
112. Tenney JR, Fujiwara H, Horn PS, Jacobson SE, Glauser TA, Rose DF. Focal corticothalamic sources during generalized absence seizures: a MEG study. *Epilepsy Res.* (2013) 106:113–22. doi: 10.1016/j.eplepsyres.2013.05.006
113. Tenney JR, Fujiwara H, Horn PS, Vannest J, Xiang J, Glauser TA, et al. Low- and high-frequency oscillations reveal distinct absence seizure networks. *Ann Neurol.* (2014) 76:558–67. doi: 10.1002/ana.24231
114. Jacobs-Brichford E, Horn PS, Tenney JR. Mapping preictal networks preceding childhood absence seizures using magnetoencephalography. *J Child Neurol.* (2014) 29:1312–9. doi: 10.1177/0883073813518107
115. Miao A, Tang L, Xiang J, Guan Q, Ge H, Liu H, et al. Dynamic magnetic source imaging of absence seizure initialization and propagation: A magnetoencephalography study. *Epilepsy Res.* (2014) 108:468–80. doi: 10.1016/j.eplepsyres.2014.01.006
116. Miao A, Xiang J, Tang L, Ge H, Liu H, Wu T, et al. Using ictal high-frequency oscillations (80-500 Hz) to localize seizure onset zones in childhood absence epilepsy: A MEG study. *Neurosci Lett.* (2014) 566:21–6. doi: 10.1016/j.neulet.2014.02.038
117. Xiang J, Tenney JR, Korman AM, Leiken K, Rose DF, Harris E, et al. Quantification of interictal neuromagnetic activity in absence epilepsy with accumulated source imaging. *Brain Topogr.* (2015) 28:904–14. doi: 10.1007/s10548-014-0411-5
118. Tang L, Xiang J, Huang S, Miao A, Ge H, Liu H, et al. Neuromagnetic high-frequency oscillations correlate with seizure severity in absence epilepsy. *Clinic Neurophysioly.* (2016) 127:1120–9. doi: 10.1016/j.clinph.2015.08.016
119. Gupta D, Ossenblok P, Van Luijtelaar G. Space-time network connectivity and cortical activations preceding spike wave discharges in human absence epilepsy: a MEG study. *Med Biologic Eng Comput.* (2011) 49:555–65. doi: 10.1007/s11517-011-0778-3
120. Wu C, Sun J, Huang S, Tang L, Miao A, Zhou Y, et al. Quantify neuromagnetic network changes from pre-ictal to ictal activities in absence seizures. *Neuroscience.* (2017) 357:134–44. doi: 10.1016/j.neuroscience.2017.05.038
121. Youssofzadeh V, Agler W, Tenney JR, Kadis DS. Whole-brain MEG connectivity-based analyses reveals critical hubs in childhood absence epilepsy. *Epilepsy Res.* (2018) 145:102–9. doi: 10.1016/j.eplepsyres.2018.06.001
122. Jiang W, Wu C, Xiang J, Miao A, Qiu W, Tang L, et al. Dynamic neuromagnetic network changes of seizure termination in absence epilepsy: a magnetoencephalography study. *Front Neurol.* (2019) 10. doi: 10.3389/fneur.2019.00703
123. Sun Y, Li Y, Shi Q, Wu C, Sun J, Chen Q, et al. Changes of ictal-onset epileptic network synchronicity in childhood absence epilepsy: a magnetoencephalography study. *Front Neurol.* (2020) 11. doi: 10.3389/fneur.2020.583267
124. Sun J, Gao Y, Miao A, Yu C, Tang L, Huang S, et al. Multifrequency dynamics of cortical neuromagnetic activity underlying seizure termination in absence epilepsy. *Front Hum Neurosci.* (2020) 14:221. doi: 10.3389/fnhum.2020.00221
125. Chavez M, Valencia M, Navarro V, Latora V, Martinerie J. Functional modularity of background activities in normal and epileptic brain networks. *Phys Rev Lett.* (2010) 104:118701. doi: 10.1103/physrevlett.104.118701
126. Shi Q, Zhang T, Miao A, Sun J, Sun Y, Chen Q, et al. Differences Between Interictal and Ictal Generalized Spike-Wave Discharges in Childhood Absence Epilepsy: A MEG Study. *Front Neurol.* (2020) 10. doi: 10.3389/fneur.2019.01359
127. Sun Y, Li Y, Sun J, Zhang K, Tang L, Wu C, et al. Functional reorganization of brain regions into a network in childhood absence epilepsy: a magnetoencephalography study. *Epilepsy Behav.* (2021) 122:108–17. doi: 10.1016/j.yebeh.2021.108117
128. Miao A, Wang Y, Xiang J, Liu Q, Chen Q, Qiu W, et al. Ictal source locations and cortico–thalamic connectivity in childhood absence epilepsy: associations with treatment response. *Brain Topogr.* (2019) 32:178–91. doi: 10.1007/s10548-018-0680-5
129. Zhang K, Sun J, Sun Y, Niu K, Wang P, Wu C, et al. Pretreatment source location and functional connectivity network correlated with therapy response in childhood absence epilepsy: a magnetoencephalography study. *Front Neurol.* (2021) 12:24. doi: 10.3389/fneur.2021.692126
130. Leech R, Sharp DJ. The role of the posterior cingulate cortex in cognition and disease. *Brain.* (2014) 137:12–32. doi: 10.1093/brain/awt162
131. Caplan R, Siddarth P, Stahl L, Lanphier E, Vona P, Gurbani S, et al. Childhood absence epilepsy: behavioral, cognitive, and linguistic comorbidities. *Epilepsia.* (2008) 49:1838–46. doi: 10.1111/j.1528-1167.2008.01680.x
132. Guerrini R, Marini C, Barba C. Generalized epilepsies. *Handbook Clinic Neurol.* (2019) 19:3–15. doi: 10.1016/B978-0-444-64142-7.00038-2
133. Amor F, Baillet S, Navarro V, Adam C, Martinerie J, Le Van Quyen M. Cortical local and long-range synchronization interplay in human absence seizure initiation. *Neuroimage.* (2009) 45:950–62. doi: 10.1016/j.neuroimage.2008.12.011
134. Sakurai K, Takeda Y, Tanaka N, Kurita T, Shiraishi H, Takeuchi F, et al. Generalized spike-wave discharges involve a default mode network in patients with juvenile absence epilepsy: A MEG study. *Epilepsy Res.* (2010) 89:176–84. doi: 10.1016/j.eplepsyres.2009.12.004
135. Rozendaal YJW, van Luijtelaar G, Ossenblok PPW. Spatiotemporal mapping of interictal epileptiform discharges in human absence epilepsy: a MEG study. *Epilepsy Res.* (2016) 119:67–76. doi: 10.1016/j.eplepsyres.2015.11.013
136. Gadad V, Sinha S, Mariyappa N, Velmurugan J, Chaitanya G, Saini J, et al. Source analysis of epileptiform discharges in absence epilepsy using Magnetoencephalography (MEG). *Epilepsy Res.* (2018) 140:46–52. doi: 10.1016/j.eplepsyres.2017.12.003
137. Kotini A, Mavraki E, Anninos P, Piperidou H, Prassopoulos P. Magnetoencephalographic findings in two cases of juvenile myoclonus epilepsy. *Brain Topogr.* (2010) 23:41–5. doi: 10.1007/s10548-009-0114-5
138. Gadad V, Sinha S, Mariyappa N, Chaithanya G, Jayabal V, Saini J, et al. Source localization of epileptiform discharges in juvenile myoclonic epilepsy (JME) using magnetoencephalography (MEG). *Epilepsy Res.* (2017) 129:67–73. doi: 10.1016/j.eplepsyres.2016.11.019
139. Hamandi K, Singh KD, Muthukumaraswamy S. Reduced movement-related beta desynchronisation in juvenile myoclonic epilepsy: a MEG study of task specific cortical modulation. *Clinic Neurophysiol.* (2011) 122:2128–38. doi: 10.1016/j.clinph.2011.04.017

140. de León SC G, Niso G, Canuet L, Burriel-Lobo L, Maestú F, Rodríguez-Magariños MG. Praxis-induced seizures in a patient with juvenile myoclonic epilepsy: MEG-EEG coregistration study. *Epilepsy Behav Case Rep*. (2016) 5:1–5. doi: 10.1016/j.ebcr.2015.10.002
141. Stefan H, Paulini-Ruf A, Hopfengärtner R, Rampp S. Network characteristics of idiopathic generalized epilepsies in combined MEG/EEG. *Epilepsy Res*. (2009) 85:187–98. doi: 10.1016/j.eplepsyres.2009.03.015
142. Routley B, Shaw A, Muthukumaraswamy SD, Singh KD, Hamandi K. Juvenile myoclonic epilepsy shows increased posterior theta, and reduced sensorimotor beta resting connectivity. *Epilepsy Res*. (2020) 163:234. doi: 10.1016/j.eplepsyres.2020.106324
143. Krzemiński D, Masuda N, Hamandi K, Singh KD, Routley B, Zhang J. Energy landscape of resting magnetoencephalography reveals fronto-parietal network impairments in epilepsy. *Network Neurosci*. (2019) 4:374–96. doi: 10.1162/netn_a_00125
144. Lopes MA, Krzemiński D, Hamandi K, Singh KD, Masuda N, Terry JR, et al. A computational biomarker of juvenile myoclonic epilepsy from resting-state MEG. *Clinic Neurophysiol*. (2021) 132:922–7. doi: 10.1016/j.clinph.2020.12.021
145. Elshahabi A, Klamer S, Sahib AK, Lerche H, Braun C, Focke NK. Magnetoencephalography reveals a widespread increase in network connectivity in idiopathic/genetic generalized epilepsy. *PLoS ONE*. (2015) 10:e0138119. doi: 10.1371/journal.pone.0138119
146. Stier C, Elshahabi A, Li Hegner Y, Kotikalapudi R, Marquetand J, Braun C, et al. Heritability of magnetoencephalography phenotypes among patients with genetic generalized epilepsy and their siblings. *Neurology*. (2021) 97:166–77. doi: 10.1212/WNL.0000000000012144
147. Niso G, Carrasco S, Gudín M, Maestú F, Del-Pozo F, Pereda E. What graph theory actually tells us about resting state interictal MEG epileptic activity. *NeuroImage: Clinic*. (2015) 8:503–15. doi: 10.1016/j.nicl.2015.05.008
148. Li Hegner Y, Marquetand J, Elshahabi A, Klamer S, Lerche H, Braun C, et al. Increased functional MEG connectivity as a hallmark of mri-negative focal and generalized epilepsy. *Brain Topogr*. (2018) 31:863–74. doi: 10.1007/s10548-018-0649-4
149. Braakman HMH, Vaessen MJ, Jansen JFA, Debeij-Van Hall MHJA, De Louw A, Hofman PAM, et al. Frontal lobe connectivity and cognitive impairment in pediatric frontal lobe epilepsy. *Epilepsia*. (2013) 54:446–54. doi: 10.1111/epi.12044
150. Widjaja E, Zamyadi M, Raybaud C, Snead OC, Smith ML. Abnormal functional network connectivity among resting-state networks in children with frontal lobe epilepsy. *Am J Neuroradiol*. (2013) 34:2386–92. doi: 10.3174/ajnr.A3608
151. Cao X, Qian Z, Xu Q, Shen J, Zhang Z, Lu G. Altered intrinsic connectivity networks in frontal lobe epilepsy: a resting-state fMRI study. *Comput Math Methods Med*. (2014) 2014:864979. doi: 10.1155/2014/864979
152. Klugah-Brown B, Luo C, Peng R, He H, Li J, Dong L, et al. Altered structural and causal connectivity in frontal lobe epilepsy. *BMC Neurol*. (2019) 19:130. doi: 10.1186/s12883-019-1300-z
153. Hari R, Salmelin R. Magnetoencephalography: from SQUIDs to neuroscience. neuroimage 20th anniversary special edition. *NeuroImage*. (2012) 61:386–96. doi: 10.1016/j.neuroimage.2011.11.074
154. Broyd SJ, Demanuele C, Debener S, Helps SK, James CJ, Sonuga-Barke EJS. Default-mode brain dysfunction in mental disorders: a systematic review. *Neurosci Biobehav Rev*. (2009) 33:279–96. doi: 10.1016/j.neubiorev.2008.09.002
155. Salanova V. Deep brain stimulation for epilepsy. *Epilepsy and Behavior*. (2018) 88:21–4. doi: 10.1016/j.yebeh.2018.06.041
156. Meeren HKM, Pijn JPM, Van Luijtelaar ELJM, Coenen AML, Da Silva FHL. Cortical focus drives widespread corticothalamic networks during spontaneous absence seizures in rats. *J Neurosci*. (2002) 22:1480–95. doi: 10.1523/JNEUROSCI.22-04-01480.2002
157. Dalic LJ, Warren AEL, Young JC, Thevathasan W, Roten A, Bulluss KJ, et al. Cortex leads the thalamic centromedian nucleus in generalized epileptic discharges in Lennox-Gastaut syndrome. *Epilepsia*. (2020) 61:2214–23. doi: 10.1111/epi.16657
158. Martín-López D, Jiménez-Jiménez D, Cabañés-Martínez L, Selway RP, Valentín A, Alarcón G. The Role of thalamus versus cortex in epilepsy: evidence from human ictal centromedian recordings in patients assessed for deep brain stimulation. *Int J Neural Syst*. (2017) 27:101. doi: 10.1142/S0129065717500101

Conflict of Interest: The authors declare that the research was conducted in the absence of any commercial or financial relationships that could be construed as a potential conflict of interest.

Publisher's Note: All claims expressed in this article are solely those of the authors and do not necessarily represent those of their affiliated organizations, or those of the publisher, the editors and the reviewers. Any product that may be evaluated in this article, or claim that may be made by its manufacturer, is not guaranteed or endorsed by the publisher.

frontiers | Frontiers in Neurology

METHODS
published: 16 June 2022
doi: 10.3389/fneur.2022.871166

A Novel Approach to Estimating the Cortical Sources of Sleep Spindles Using Simultaneous EEG/MEG

Dimitrios Mylonas[1,2*†], *Martin Sjøgård*[1,2†], *Zhaoyue Shi*[1,2,3], *Bryan Baxter*[1,2], *Matti Hämäläinen*[2,4], *Dara S. Manoach*[1,2] *and Sheraz Khan*[2,4]

[1] *Department of Psychiatry, Massachusetts General Hospital and Harvard Medical School, Boston, MA, United States,* [2] *Athinoula A. Martinos Center for Biomedical Imaging, Charlestown, MA, United States,* [3] *Carle Illinois Advanced Imaging Center, Carle Foundation Hospital, Urbana, IL, United States,* [4] *Department of Radiology, Massachusetts General Hospital and Harvard Medical School, Boston, MA, United States*

OPEN ACCESS

Edited by:
Jie Lu,
Capital Medical University, China

Reviewed by:
Thomas Andrillon,
INSERM U1127 Institut du Cerveau et de la Moelle épinière (ICM), France
Umit Aydin,
King's College London, United Kingdom

***Correspondence:**
Dimitrios Mylonas
dmylonas@mgh.harvard.edu

†These authors have contributed equally to this work and share first authorship

Specialty section:
This article was submitted to Applied Neuroimaging, a section of the journal Frontiers in Neurology

Received: *07 February 2022*
Accepted: *18 May 2022*
Published: *16 June 2022*

Citation:
Mylonas D, Sjøgård M, Shi Z, Baxter B, Hämäläinen M, Manoach DS and Khan S (2022) A Novel Approach to Estimating the Cortical Sources of Sleep Spindles Using Simultaneous EEG/MEG. Front. Neurol. 13:871166. doi: 10.3389/fneur.2022.871166

Sleep spindles, defining oscillations of stage II non-rapid eye movement sleep (N2), mediate sleep-dependent memory consolidation. Spindles are disrupted in several neurodevelopmental, neuropsychiatric, and neurodegenerative disorders characterized by cognitive impairment. Increasing spindles can improve memory suggesting spindles as a promising physiological target for the development of cognitive enhancing therapies. This effort would benefit from more comprehensive and spatially precise methods to characterize spindles. Spindles, as detected with electroencephalography (EEG), are often widespread across electrodes. Available evidence, however, suggests that they act locally to enhance cortical plasticity in the service of memory consolidation. Here, we present a novel method to enhance the spatial specificity of cortical source estimates of spindles using combined EEG and magnetoencephalography (MEG) data constrained to the cortex based on structural MRI. To illustrate this method, we used simultaneous EEG and MEG recordings from 25 healthy adults during a daytime nap. We first validated source space spindle detection using only EEG data by demonstrating strong temporal correspondence with sensor space EEG spindle detection (gold standard). We then demonstrated that spindle source estimates using EEG alone, MEG alone and combined EEG/MEG are stable across nap sessions. EEG detected more source space spindles than MEG and each modality detected non-overlapping spindles that had distinct cortical source distributions. Source space EEG was more sensitive to spindles in medial frontal and lateral prefrontal cortex, while MEG was more sensitive to spindles in somatosensory and motor cortices. By combining EEG and MEG data this method leverages the differential spatial sensitivities of the two modalities to obtain a more comprehensive and spatially specific source estimation of spindles than possible with either modality alone.

Keywords: sleep spindles, MEG (magnetoencephalography), EEG, source localization, cortical sources, stage 2 NREM sleep, sleep oscillations

INTRODUCTION

Sleep spindles, a defining oscillation of stage II non-rapid eye movement sleep (N2), are brief (∼1 s) powerful bursts of 12–15 Hz activity initiated in the thalamic reticular nucleus (TRN) (1, 2) and propagated to the cortex *via* thalamocortical circuitry (3). Sleep spindles are typically separated based on their frequency into slow (9–12 Hz) and fast spindles [12–15 Hz; (4, 5)]. Although both spindle classes are generated in TRN they have different cortical topographies with slow spindles being more prominent at frontal and fast spindles at central and parietal electrodes (6, 7). In humans sleep spindles correlate with sleep-dependent memory consolidation, learning efficiency, and IQ [for a review see (8)]. Sleep spindles are disrupted in several neurodevelopmental, neuropsychiatric, and neurodegenerative disorders characterized by cognitive impairment (9). Importantly, increasing spindles both pharmacologically (10–12) and using non-invasive brain stimulation (13) can improve memory, consistent with evidence from optogenetic studies of rodents indicating a causal role in memory consolidation (14, 15). This provides an impetus to target spindles to treat cognitive deficits (16). Since spindles act locally to mediate memory typically in regions involved in initial learning (17–20), this effort would benefit from a more spatially precise measurement of spindles. In humans, spindles are typically detected with EEG. Relatively few studies have used magnetoencephalography (MEG) to complement EEG spindle detection (21–30). Here we describe a new method using simultaneously acquired EEG and MEG data from afternoon naps to comprehensively characterize sleep spindles and to estimate their cortical sources.

Compared with EEG, MEG is more sensitive to focal cortical spindle sources but mainly detects sources that are tangential to the cortical surface (31, 32). In contrast, EEG detects both radial and tangential sources. Spindles detected only by MEG sensors tended to be more focal and did not propagate across the cortex, whereas spindles detected in both modalities were first detected by MEG and then detected by EEG after spreading to additional regions (23). These studies suggest that (i) MEG is more sensitive to the emergence of non-synchronous bursts of focal spindles due to its more confined spatial sensitivity; (ii) EEG is more likely to detect spindles that cover extended areas on the cortex, and (iii) because of their complementarity, MEG and EEG together provide more accurate source estimation than either technique alone (33). A more spatially specific estimation of sleep spindle sources is important given the role of local spindles in mediating memory (17–20).

Here, we present a novel method to estimate the cortical sources of spindles using simultaneous EEG/MEG recordings, constrained to the cortex based on structural MRIs, during an afternoon nap. To validate this method, we compared spindles detected in source space to those detected on the scalp (sensor space) using EEG (gold standard). We next evaluated the spatial distribution of spindles that were common and unique to each modality by comparing source space spindle detection using EEG only, MEG only and combined EEG/MEG. We conclude by discussing the advantages of using combined EEG/MEG for detecting and source localizing spindles over either technique alone.

MATERIALS AND METHODS

Participants

Thirty one healthy adults were recruited from the community through advertisements and were screened to exclude a history of mental illness diagnosed sleep disorders, treatment with sleep medications, pregnancy, and a history of head injury, neurological disorder and substance abuse or dependence within the past 6 months. All participants gave written informed consent and were paid for participation. The study was approved by the Partners Human Research Committee. Participants were asked not to consume caffeine or alcohol on the day of the recording. All 25 participants (age 29 ± 6, 21–42; 19 males) who produced valid nap data (>10 min of artifact rejected N2 sleep) were included.

Procedure

All participants completed two visits at least 1 week apart. The first visit (Nap 1) acclimated the participant to napping in the MEG scanner and was followed by a second visit (Nap 2). Participants were wired for polysomnography (PSG) and given a 90 min afternoon nap opportunity with simultaneous EEG and MEG recording while lying supine in the MEG scanner. Before the nap we recorded 5 min of quiet rest during which participants were instructed to maintain fixation on a cross in the center of the screen. After their second visit participants returned for an MRI scan.

EEG/MEG Data Acquisition

Data were recorded using a 306 channels whole-head Elekta-Neuromag MEG system [Elekta Oy (now MEGIN, Croton Healthcare), Helsinki, Finland] in a magnetically shielded room (IMEDCO, Hagendorf, Switzerland) simultaneously with 70 channels of EEG, submental electromyography (EMG) and 2 electrooculography electrodes (EOG). All signals were digitized at 600 Hz. The MEG sensors are arranged as triplets at 102 locations; each location contains one magnetometer and two orthogonal planar gradiometers. Locations of the EEG electrodes and ∼200 head shape points were recorded using a 3D digitizer (Polhemus FastTrack). Four head position index (HPI) coils were used to continuously track the position of the head relative to the scanner.

EEG/MEG Data Pre-processing

We applied the signal space separation (SSS) algorithm (34) to the MEG signals to suppress environmental noise and correct for head movements using the HPI coils. Sleep data were low-pass filtered at 60 Hz and down-sampled to 200 Hz using MNE software for further analysis (35). Each 30 s epoch of EEG data was visually scored according to standard criteria as WAKE, REM, N1, N2, or N3 (36) by expert raters (**Table 1**). Sleep quality was quantified using sleep onset latency (SOL), total sleep time

TABLE 1 | Means, standard deviations of participants' sleep quality, and architecture measures.

	Mean ± sd (min–max)
Sleep quality	
*TIB	92 ± 5 (80–105) min
*TST	65 ± 23 (19–96) min
*SOL	6 ± 7 (1–26) min
*WASO	21 ± 19 (1–65) min
Sleep efficiency	70 ± 24 (21–98)%
Sleep architecture	
N1	14 ± 6 (4–23) min
N2	38 ± 19 (11–76) min
N3	10 ± 12 (0–37) min
REM	3 ± 6 (0–20) min

**TIB, Time in bed; TST, Total sleep time; SOL, Sleep onset latency; WASO, Wake after sleep onset.*

(TST), time in bed (TIB), sleep efficiency (TST/TIB), and wake after sleep onset (WASO).

EEG and MEG data were pre-processed and analyzed using custom scripts in MATLAB (MathWorks, Natick MA), FieldTrip (37) and MNE software (35). Sleep data were band-pass filtered at 0.3–35 Hz and electrodes displaying significant artifacts were spatially interpolated. EEG data were then re-referenced to the common average. Resting state data were notch-filtered at 60 Hz. Signal space projection [SSP; (38)] implemented in MNE was used to remove cardiac artifacts, and remaining artifacts were visually identified and removed. Artifact-free data from N2 sleep were used for further analyses. Although spindles also occur during N3 sleep, we restricted our analyses to N2 since spindle physiology differs across sleep stages and only 8 of 25 participants had more than 10 min of N3.

MRI Acquisition

Anatomical images were acquired on a 3T Siemens Trio whole-body MRI system (Siemens Medical Systems, Erlangen, Germany) with a 32-channel head coil. The images were acquired using a 3D RF-spoiled magnetization prepared rapid gradient echo (MP-RAGE) sequence (TR = 2,530 ms; TE = 1.7/3.6/5.5/7.3 ms; Flip Angle = 7°; FOV = 256 mm, 176 in-plane sagittal 1 mm isotropic slices, scan duration 6 m 12 s). In addition, a multi echo flip angle (5°) FLASH pulse sequence was employed to obtain data for constructing individual boundary element model (BEM) surfaces for forward modeling (610 Hz per pixel, TR = 20 ms, TE = 1.89 + 2 n ms (n = 0–7), 128 in-plane sagittal slices sized 1 × 1.33 mm, 1.33 mm thickness).

Source Reconstruction

Co-registration of the EEG and MEG sensors to each participant's structural MRI was implemented in MNE using the digitized electrodes, fiducials, HPI coils and head shape points. MRI reconstruction and tissue segmentation were performed using FreeSurfer (39, 40). The FreeSurfer-derived cortical surface tessellation was decimated to a regular source dipole grid with 3 mm spacing between adjacent source locations, corresponding to ∼18,500 dipoles. The forward solutions were then computed using the three-layer BEM (41) using inner, outer skull, and scalp surfaces from segmentations of the FLASH images.

The cortically constrained minimum-norm estimate of the cortical currents [MNE; (42, 43)] was computed with source orientations fixed perpendicular to the local cortical surface and a regularization factor of 0.1. Noise covariance estimates were calculated using data from the 5 min resting-state scan filtered at 100–140 Hz. We used dynamical statistical parametric mapping [dSPM; (44)] to reduce the MNE inverse solution bias toward superficial cortical sources. FreeSurfer was used to automatically parcellate the cortex into 72 regions (45). After discarding "medial wall" and "corpus callosum," these regions were further parcellated into a total of $N = 448$ similarly sized cortical regions using FreeSurfer (46). The resulting source-space time courses of artifact-free N2 sleep were then computed in these 448 regions. In order to align the signs of the time series across dipoles within a label, we used the singular value decomposition (SVD) of the data. The sign of the dot product between the first left singular vector and all other time-series in a label was computed. If this sign was negative, we inverted the time-series before averaging. The same procedure was followed to generate three source localization estimates, from EEG alone, MEG alone, and combined EEG/MEG data. For analytic methods overview see **Figure 1**.

Spindle Detection

Slow and fast spindles were automatically detected in the 9–12 and 12–15 Hz band-pass-filtered data respectively, at each sensor and cortical region using a wavelet-based algorithm (47, 48). Specifically, based on temporally smoothed (window duration = 0.1 s) wavelet coefficients (from a complex Morlet wavelet transform), spindles were identified as intervals exceeding 9 times the median for at least 400 ms. The frequency range for spindle detection, defined based on the full-width half-maximum of the wavelet amplitude response in the frequency domain (49), was chosen based on prior studies and to minimize the overlap between the two spindle classes (**Supplementary Figure 1**) (4, 47, 48). The threshold for spindle detection was chosen to maximize the between class ("spindle" vs. "non-spindle") variance (50) based on data from healthy participants in a previous study (47). This detector has been validated against visual inspection in healthy people, individuals with schizophrenia and children with autism spectrum disorder (47, 51). The duration of individual spindles was measured in 2 s epochs centered on the point of spindle detection as the full width half max of the wavelet energy.

Definition of Spindle Events in Sensor and Source Space

As there is no one-to-one correspondence between scalp sensors and source space regions we defined windows of spindle activity in both so that we could compare spindle detection in each. To define windows of spindle activity we first assigned a binary value (y_i) to each sensor/region at each time point that was set to one if a spindle was detected and zero if not. The binary signals were summed across all sensors/regions resulting in an aggregate

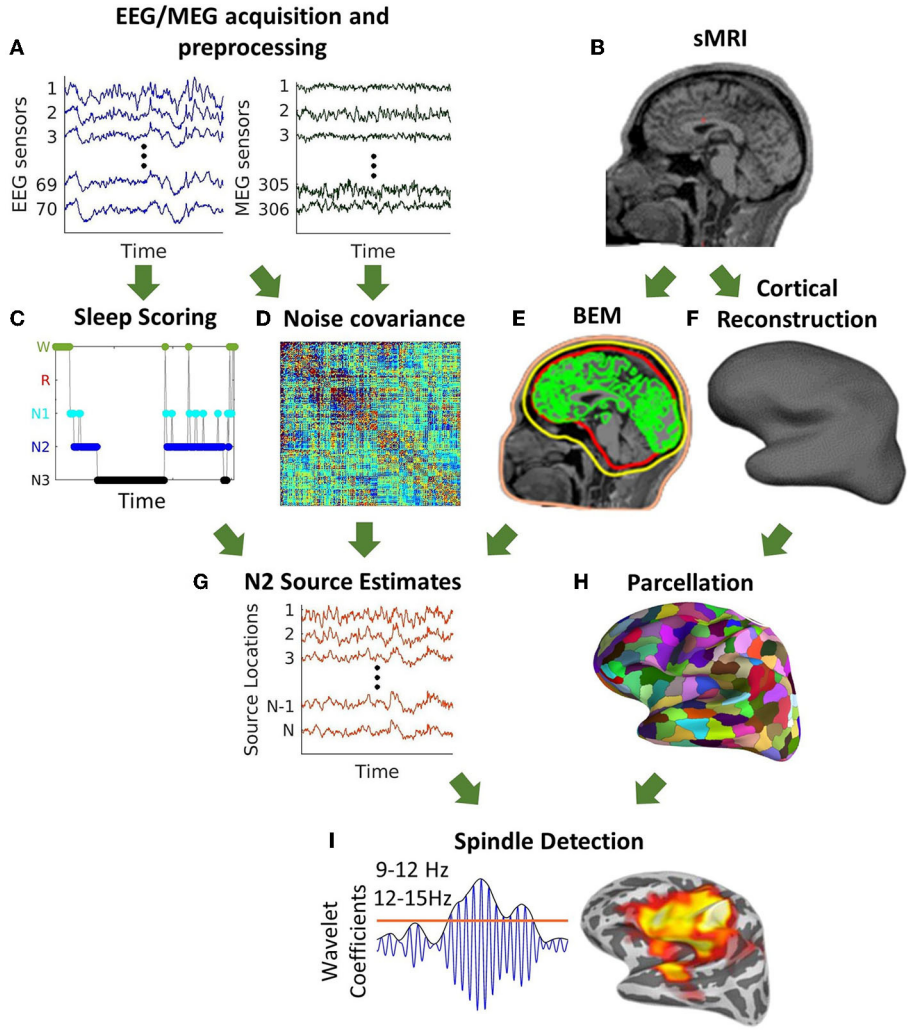

FIGURE 1 | Schematic description of source space spindle detection. **(A)** Pre-processing of simultaneously acquired EEG/MEG data. **(B)** Structural MRI. **(C)** Sleep scoring of nap data. **(D)** Noise covariance estimates calculated using the EEG/MEG data from the 5 min resting-state scan filtered at 100–140 Hz. **(E)** Construction of a three-layer boundary element model (BEM) surfaces (inner, outer skull, and scalp) for forward modeling **(F)** Cortical reconstruction. **(G)** Source estimates of N2 calculated using the cortically constrained minimum-norm estimate of cortical currents. **(H)** Parcellation of the cortical surface into 448 regions. **(I)** Automatic spindle detection at each cortical region using a wavelet-based detector.

signal (Y) which was >0 when a spindle was detected at any of the sensors/regions at any given time-point. After smoothing Y with a 500 ms moving average, we detected the temporal local maxima using the MATLAB function *findpeaks*. To avoid detection of spurious spindle activity a minimum distance between maxima was set at 500 ms and a minimum extent was set at 1% of sensors/regions. One second windows centered at the detected local maxima were defined as temporal windows of spindle activity across sensors/regions (**Figure 2**). We will refer to these periods of spindle activity across sensors/regions as "spindle events" to distinguish them from spindles detected at each sensor/region (e.g., see **Supplementary Figures 1, 4**). The duration of the windows was set at 1 s. The spatial extent of a spindle event (i.e., the total number of sensors/regions where a spindle was detected) was quantified as the maximum amplitude of Y (**Figure 2**). To account for different sleep durations, we calculated spindle event density (i.e., spindle events per minute). In contrast to the typical definition of spindle density at each sensor/region, spindle event density is based on the definition of spindle events across multiple sensors/regions. Using this method, we first compared spindle events from sensor vs. source space EEG to validate spindle detection in source space. We then compared the density and spatial extent of source space spindle events detected in EEG alone, MEG alone and combined EEG/MEG data.

Validation of Spindle Detection

We first validated spindle detection in source space by quantifying the correspondence of source space EEG estimates with scalp EEG (i) between subjects, by correlating the total

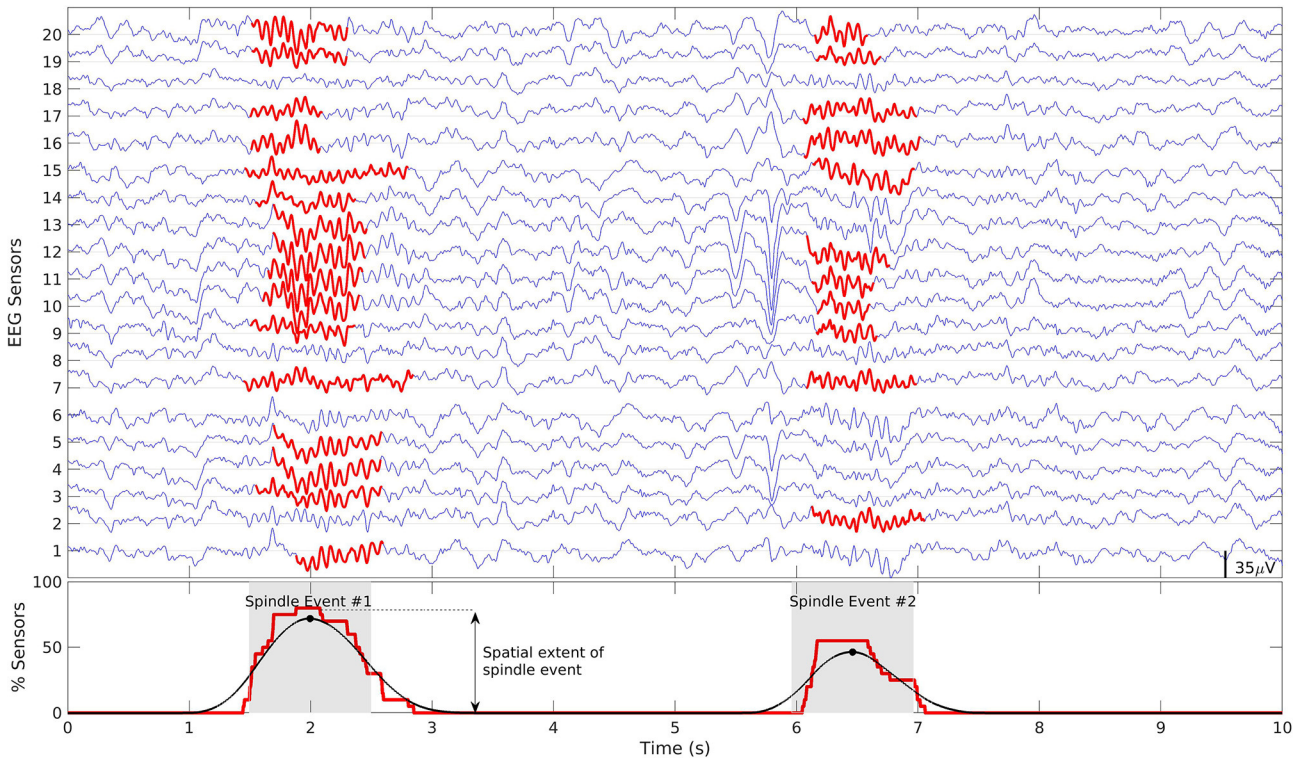

FIGURE 2 | Definition of spindle events. Top: Example of 10 s of N2 signal from 20 EEG electrodes. Detected spindles at each sensor are highlighted in red. Bottom: The raw aggregate signal (red) and smoothed signal (black). Spindle events were defined as 1 s time-windows around the peaks of the smoothed signal (gray patch). The maximum amplitude within this window reflects the spatial extent of the detected spindle event. The same definition applies to MEG sensors and source space analyses.

number of spindle events in source vs. sensor space and (ii) within subjects, by calculating the temporal overlap using the *F1* score of detected spindle events in source vs. sensor space. We defined temporal overlap as ≥20% [*F1* scores for different overlap values (10–50%) and window lengths (0.4–2 s) are presented in **Supplementary Figure 2**]. Spindle event density in source vs. sensor space was compared using a paired *t*-test.

To calculate F1 scores we defined (i) false positives (*FPs*), as spindle events detected in source but not sensor space, (ii) false negatives (*FNs*) as spindle events detected in sensor but not source space, and (iii) true positives (*TPs*) as spindle events detected in both sensor and source space. Precision (f_P), recall (f_R), and the *F1* score were calculated as follows:

$$f_P = TP/(TP + FP);$$
$$f_R = TP/(TP + FN);$$
$$F1 = \frac{2 f_P f_R}{f_P f_R}.$$

To evaluate whether the spatial extents of spindle events detected in sensor and source space (i.e., *TPs*) were related, we correlated *Y* in the sensor space (the number of sensors showing that spindle) with *Y* in the source space (number of regions).

Since spindle detection in source space was more prone to *FPs* than *FNs* (see Results), we asked where these *FPs* were more likely to be detected, by calculating the percent of *FPs* detected at each region. We then tested whether these source-detected "*FPs*" might actually reflect sub-threshold sensor space spindle activity. For each *FP* spindle event detected in the source space we calculated the sigma power across all EEG sensors using the squared amplitude of the Hilbert transform, after bandpass filtering at 9–12 Hz for slow and 12–15 Hz for fast spindles. We then z-normalized it against the power of randomly selected spindle-free 1 s periods and averaged across time-points and sensors.

TEST-RETEST RELIABILITY OF SPINDLE EVENTS

Previous studies have demonstrated that sleep spindles are a heritable trait-like feature of the scalp EEG (5, 52) and are stable within individuals across nights and naps (48, 53). Here we wanted to investigate whether this is also true for spindle events detected in source space using different modalities. We calculated intraclass correlation coefficients (ICCs) for scalp EEG, source EEG, MEG, and EEG/MEG in the 19 subjects who had valid data from two naps. To calculate ICCs, we estimated between- and within-subjects variances of spindle event density from

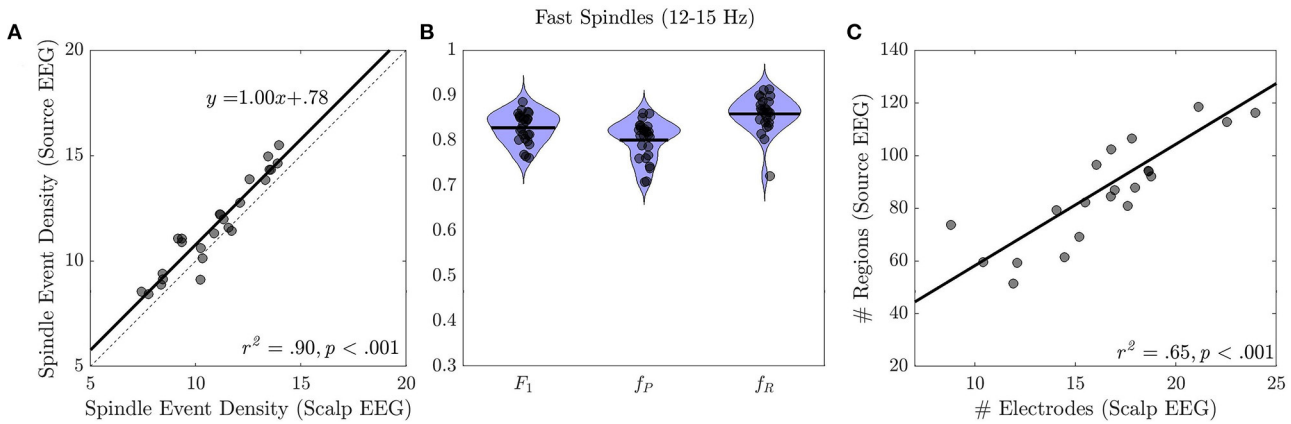

FIGURE 3 | Spindle events in source vs. sensor space EEG. **(A)** Spindle event density in source vs. sensor space. Regression line (black solid) and the identity line (gray dashed) are shown. **(B)** Correspondence of spindle events detected at the source vs. the sensor space (F1 = 0.83 ± 0.03, fP = 0.80 ± 0.04, fR = 0.86 ± 0.04). **(C)** Spatial extent of spindle events in source vs. sensor space with regression line.

regression models with subject as a random effect. To compare the reliability of spindle event density among modalities we estimated the 95% confidence intervals (CIs) of the ICCs based on 1,000 bootstrap samples.

Comparison of EEG Alone, MEG Alone, and Combined EEG/MEG Detected Spindle Events in Source Space

To determine whether source-space EEG, MEG, and EEG/MEG are differentially sensitive to spindles we compared the spindle events detected by each modality. The density of spindle events was compared with a linear mixed effects model with Modality as a fixed effect (EEG, MEG, and EEG/MEG) and Subject as a random effect. The correspondence of spindle events detected by EEG, MEG, and EEG/MEG, based on their temporal overlap, was calculated using the same method as above. To compare the spatial specificity of the source estimates we first used pairwise comparisons of the spatial extent of spindle events detected by EEG, MEG, and EEG/MEG. We then examined the spatial extent and topography of spindle events detected with only one of two estimates (e.g., spindle events unique to EEG only). To investigate whether there were cortical regions at which one modality was more sensitive to spindle events, for each region we calculated the percent of spindle events that were detected by only one of two estimates.

RESULTS

We focus on fast spindles (defined as 12–15 Hz), which are a well-replicated biomarker of overnight memory consolidation (8) and disrupted in neuropsychiatric disorders, particularly schizophrenia (9). Slow spindle (defined as 9–12 Hz) findings are described in **Supplementary Results** and **Supplementary Figures 1, 3, 5–9**.

Validation of EEG Source Space Spindle Detection

Source and sensor space EEG spindle event density were highly correlated ($r^2 = 0.90$, $p < 0.001$, slope=1.00 ± 0.07, Intercept: 0.78 ± 0.78; **Figure 3A**). On average EEG spindle event density was 7% higher in source space than in sensor space (sensor space: 10.92 ± 2.04; source space: 11.70 ± 2.15; $t = 5.72$, $p < 0.001$). In within-subjects analyses, 86% of spindle events detected in sensor space temporally overlapped with spindle events detected in source space, while 80% of spindle events detected in source space overlapped with spindle events measured in sensor space ($F1 = 0.83 \pm 0.03, f_P = 0.80 \pm 0.04, f_R = 0.86 \pm 0.04$; **Figure 3B**). Spindle events on the scalp were detected on average at 18/70 (26%) sensors and at 73/448 (21%) cortical regions in source space. The spatial extent of spindle events in source and sensor space was highly correlated ($r^2 = 0.65, p < 0.001$; **Figure 3C**).

Spindle events that were detected in source but not sensor space (*FPs*) was more likely to be detected in frontal cortex (**Figure 4**). On average, for each subject 36% (range 24–51%) of spindles detected only in source space (*FPs*) had significantly elevated sigma power in sensor space ($z > 1.69$) suggesting that these *FPs* might reflect sub-threshold spindle activity.

Test-Retest Reliability of Spindle Events

As in previous studies (5, 48, 52, 53) sensor space EEG spindle events were stable within individuals across two naps [ICC = 0.83, CI: (0.66, 0.91)]. Similarly, source space detected spindle events were stable across naps and ICCs did not differ significantly [i.e., their CIs overlapped; EEG: ICC = 0.81, CI: (0.55, 0.92); MEG: ICC = 0.80, CI: (0.56, 0.93]; EEG/MEG: ICC = 0.72, CI: (0.42, 0.88); **Figure 5**].

Comparison of Source Space Spindle Events Detected With EEG Alone, MEG Alone, and Combined EEG/MEG

Overall spindle event density differed significantly between source estimates [$F_{(2,72)} = 238.46$, $p < 0.001$): Spindle event density was lower in MEG than either EEG (44%; $t = 15.78$, $p < 0.001$) or EEG/MEG (40%; $t = 16.61$, $p < 0.001$), and lower for EEG/MEG than EEG (6%, $t = 5.12$, $p < 0.001$; **Figure 6A**). We excluded the possibility that this result was simply due to a

higher absolute spindle detection threshold in MEG by showing that the threshold was higher in EEG (EEG: 2.91 ± 1.86, MEG: 0.62 ± 0.35; Wilcoxon $z = 5.65$, $p < 0.001$). Fifty-five percent of EEG-detected spindle events had no corresponding event in MEG. Conversely 19% of MEG-detected spindle events lacked a corresponding EEG event (**Figure 6B**). This indicates that although EEG detects more spindle events than MEG, the two modalities also detect different events. The combined EEG/MEG estimate captured more of the spindles present in EEG alone than MEG alone ($t = 18.74$, $p < 0.001$). Similarly, there were more common spindles between the combined EEG/MEG and the MEG alone than between the EEG alone and MEG alone ($t = 5.95$, $p < 0.001$). These data indicate that the combination of EEG and MEG provides a more comprehensive account of spindles than either modality alone.

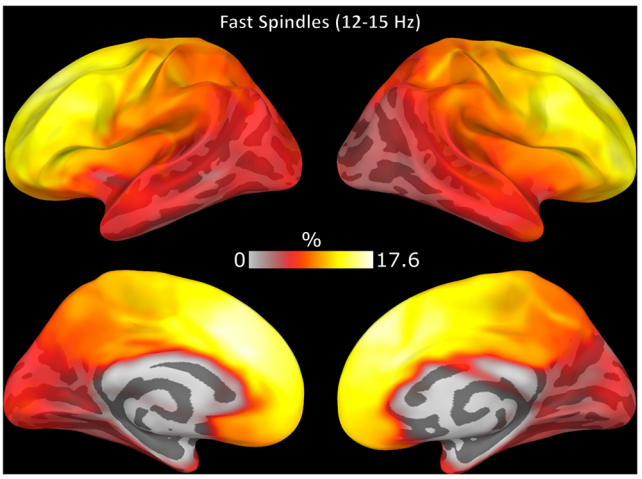

FIGURE 4 | Topography of spindle events detected only in source space EEG (FPs). The color of each region represents the number of FPs expressed in this region over the total number of FPs as a percentage.

The spatial distribution of spindle density differed across modalities with EEG showing maximum spindle density in lateral and medial frontal cortex extending into posterior cingulate cortex, while MEG spindle density was relatively low over prefrontal cortex and peaked in posterior cingulate cortex (**Supplementary Figure 3**).

Spindle events detected by EEG included more regions than MEG ($t = 16.00$, $p < 0.001$) or combined EEG/MEG (**Figure 6C**; $t = 14.24$, $p < 0.001$). EEG/MEG detected spindle events were more widespread than those detected by MEG ($t = 15.70$, $p < 0.001$; **Figure 6C**). More focal spindle events were less likely to be detected regardless of modality and, contrary to expectations, MEG was not more sensitive to focal events

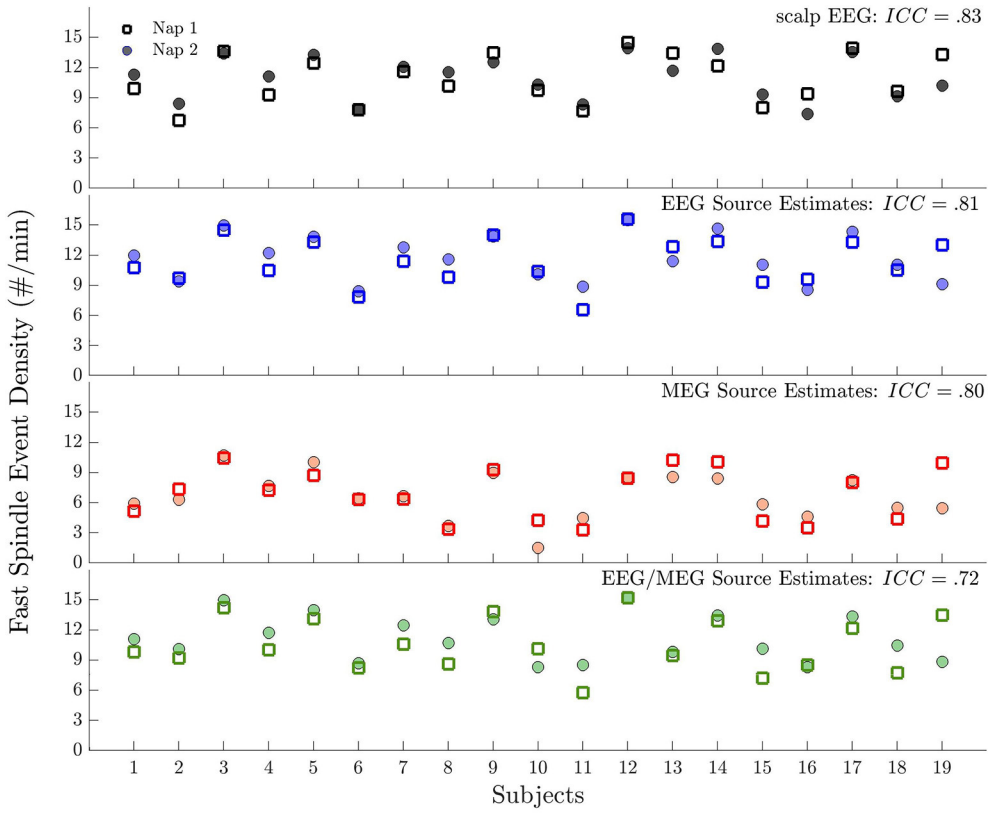

FIGURE 5 | Test-retest reliability of spindle events across naps for each modality. Plot of spindle event density for each subject during Nap 1 and Nap 2. Spindle events were detected (from top to bottom) at scalp EEG, source EEG, MEG, and EEG/MEG.

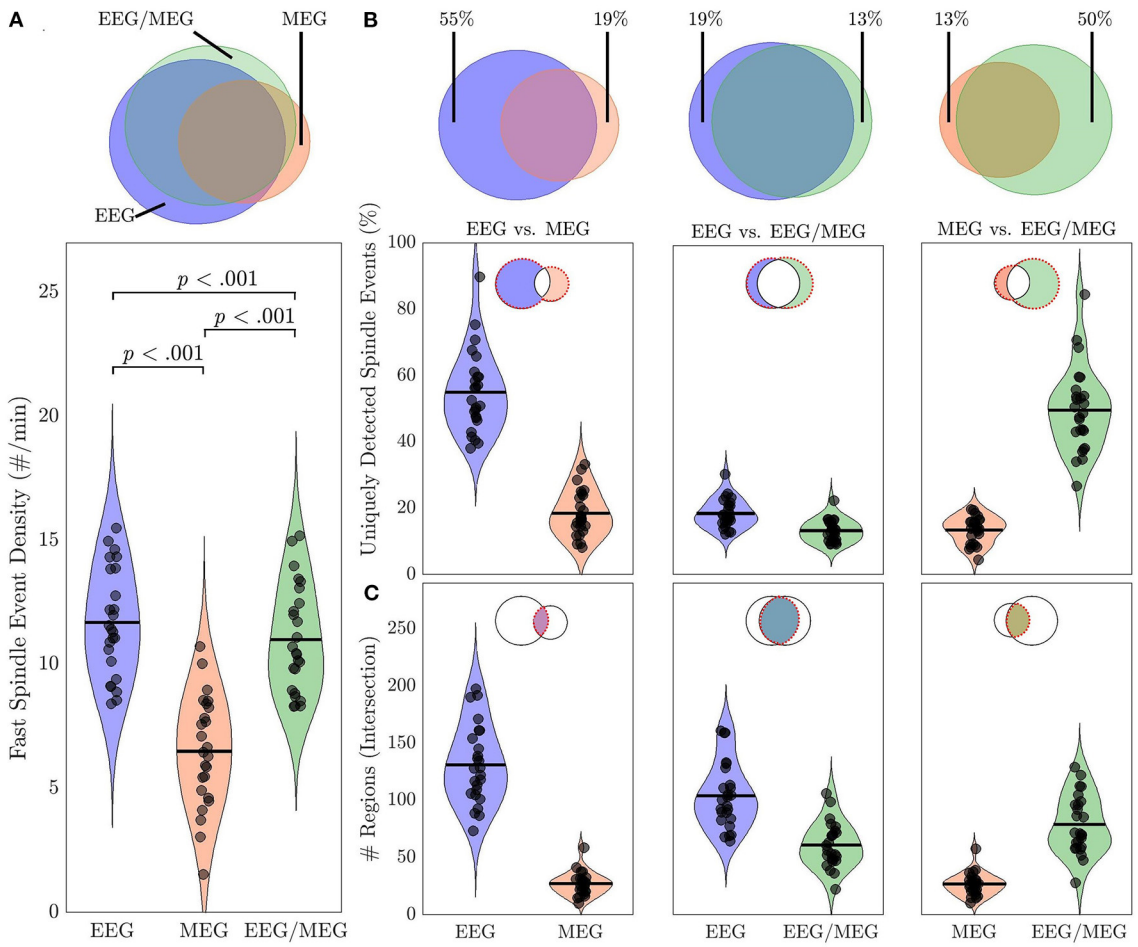

FIGURE 6 | Spindle events in source space using EEG alone, MEG alone and combined EEG/MEG. **(A)** Venn diagram and violin plots depicting spindle event density in EEG, MEG, and EEG/MEG with *p*-values for pairwise comparisons. **(B)** Percent of uniquely detected spindle events by each modality for EEG vs. MEG, EEG vs. EEG/MEG, and MEG vs. EEG/MEG. **(C)** Spatial specificity of commonly detected spindle events (intersection of Venn diagrams). Spatial extent of spindle events detected by EEG and MEG, EEG and EEG/MEG, and MEG and EEG/MEG. Black circles represent individual data.

(**Supplementary Figure 4**). However, there were topographical differences between modalities: MEG was less likely than EEG to detect medial and lateral frontal spindle events (**Figure 7A**) and EEG was less likely than MEG to detect spindle events in motor and somatosensory cortex (**Figure 7B**).

DISCUSSION

We employed a novel method using simultaneous EEG and MEG recordings during sleep to estimate the cortical sources of sleep spindles. We first validated source space spindle detection with EEG by demonstrating strong agreement with sensor space (i.e., scalp) EEG spindle detection. We also extended previous findings that sensor space EEG spindles are stable across sessions to source space spindle estimates using EEG, MEG, and EEG/MEG. Finally, we show that by combining EEG/MEG data, anatomically constrained by structural MRI, we leverage the differential sensitivities of the two modalities to cortical sources to obtain a more comprehensive view of spindles and increase the spatial specificity of the source estimation compared to EEG or MEG alone.

The density of EEG spindle events detected in source space showed a good correspondence with those detected in sensor space, but on average was 7% higher for fast spindles and 19% higher for slow spindles. The significantly higher agreement between sensor and source space for fast spindles may reflect the reduced amplitude and increased variability of EEG slow spindle spectral peaks (4). During over a third of the spindle events detected in source but not sensor space, the averaged sigma power of scalp EEG electrodes was elevated suggesting that source detection was more sensitive to sub-threshold scalp EEG spindle activity. This may reflect that each EEG scalp electrode captures activity from multiple brain regions while the point spread functions in source space are more focal (31, 32, 54). Some of the remaining two thirds of spindles detected in source but not sensor space (i.e., "false positives") may be more focal spindles

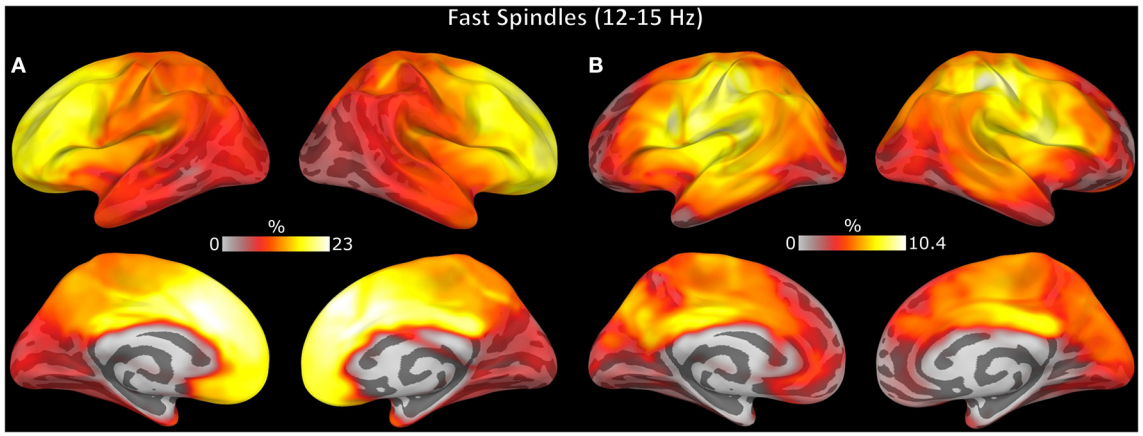

FIGURE 7 | Topography of spindle events uniquely detected by **(A)** EEG and **(B)** MEG. The color represents the percent of spindle events detected in each region relative to the total spindle events detected.

whose signal is obscured by averaging across all electrodes or they may be noise.

We replicated previous findings that spindle activity is stable over sessions within individuals and extended these results to spindle events detected in source space regardless of modality. This is consistent with evidence that spindle activity is a heritable trait-like feature of the sleep EEG (5, 48, 52, 53). Although this was a nap study, spindle density during naps is a reliable estimate of overnight spindle density indicating that our findings can generalize to overnight sleep (55). Spindle event density using MEG and combined EEG/MEG source estimates was more variable within subjects compared to EEG, particularly for slow spindles. The increased number of MEG sensors compared to EEG (70 EEG vs. 306 MEG sensors) could potentially increase the variability of the measurements across sessions. Another possible explanation could be that although we track the head position and take any head motion into account in the post-processing (56, 57), different head positions across sessions could still affect the source estimates of MEG alone and EEG/MEG.

Spindle events detected exclusively by EEG or MEG had distinct topographical distributions. EEG was more sensitive to spindles in medial and lateral frontal cortex, while MEG was more sensitive to spindles in somatosensory and motor regions. These topographies may reflect differential sensitivity of EEG and MEG to spindles arising from two thalamocortical pathways: the core pathway that projects to middle cortical layers, particularly in somatosensory and motor regions, and the matrix pathway that projects diffusely to more superficial cortical layers (58, 59). Our findings support the hypothesis that EEG is more sensitive to widely expressed matrix spindles whereas MEG is more sensitive to focal core spindles (29, 60). The differential sensitivity of EEG and MEG may reflect that widely distributed sources lead to greater signal loss in MEG due to cancellation (61).

Contrary to a prior report (19), MEG detected significantly fewer spindle events than EEG. This may reflect MEG's relative insensitivity to radially oriented and distributed sources of some spindle activity. Our results are consistent with older studies that report more spindles detected with EEG than MEG (21, 27). The inconsistent results could reflect different methodology. Dehghani et al. (23) detected spindles using a spectral peak algorithm across EEG and MEG sensors during 2 min of N2 sleep whereas in this study we detected spindles on a sensor/region basis during all of N2 (mean duration: 38 min).

Spindles are generated in the thalamic reticular nucleus (1, 2) and are propagated to the cortex *via* thalamocortical circuitry (3). Since the contribution of subcortical sources to EEG is weak and to MEG even weaker, we restricted spindle detection to the cortical surface (62, 63). The lack of access to thalamic activity renders the question of what constitutes "true spindle activity" impossible to answer. Here we used spindle activity detected at the scalp EEG as the "gold standard," to validate our spindle detection method in the source space. The lack of ground truth precludes any statements of which source estimate of spindles is the most valid. More sophisticated methods are needed to non-invasively assess the interaction between cortex and thalamus during spindle activity (63–65). Because this was an afternoon nap study, fewer than a third of the participants had more than 10 min of N3 sleep, not allowing us to investigate whether our findings generalize to N3.

Fast spindles mediate sleep-dependent memory consolidation, are disrupted in a number of neurodevelopmental and neurodegenerative disorders [for a review see (9)] and have been identified as a mechanistic biomarker of cognitive dysfunction and a potential treatment target, [e.g., see (16)]. Although spindles can be expressed widely in the cortex, they act in a spatially specific manner to induce the plasticity underlying memory consolidation. For example, during the sleep that follows training on a motor task, increased spindles and sigma power in the contralateral motor cortex correlates with improved performance upon awakening (17–20). In schizophrenia, spindle deficits correlate with both memory deficits and increased connectivity of the thalamus specifically

with somatosensory and motor cortex (47, 66). Children with Rolandic epilepsy have a focal spindle deficit in the affected regions that correlates with cognitive and motor dysfunction (67). The spatial specificity that characterizes both the functionality of spindles in health, and their disruption in disorders highlights the utility of techniques with high spatial resolution for both basic and clinical studies of sleep-dependent cognition.

In summary we present a novel method that leverages the differential sensitivities of EEG and MEG to reveal the cortical sources of spindles. Combined EEG and MEG provide a more comprehensive detection and focal source estimation than either technique alone. Accurate estimation of spindle activity will illuminate the function of spindles, how it goes awry in disorders, and guide the development of more targeted treatments.

DATA AVAILABILITY STATEMENT

The raw data supporting the conclusions of this article will be made available by the authors, without undue reservation.

ETHICS STATEMENT

The studies involving human participants were reviewed and approved by Partners Human Research Committee. The patients/participants provided their written informed consent to participate in this study.

AUTHOR CONTRIBUTIONS

DSM and MH contributed to conception and design of the study and contributed to all aspects of its completion. DM, MS, ZS, BB, and SK contributed to conceptualization, methods development, data analysis, and writing. All authors reviewed and commented on the finished product and contributed to the article and approved the submitted version.

FUNDING

This work was supported by a grant from the Simons Foundation to the Simons Center for the Social Brain at MIT, K24 MH099421 and R01 MH092638 to DSM; 5P41EB030006 P41 Center for Mesoscale Mapping (NIBIB), 5U01EB023820 Device-Independent Acquisition and Real Time Spatiotemporal Analysis of Clinical Electrophysiology Data (NINDS) and 5R01NS104585 to MH; McKnight Clinical Translational Research Scholarship in Cognitive Aging and Age-Related Memory Loss, funded by the McKnight Brain Research Foundation through the American Brain Foundation and the American Academy of Neurology Institute to BB.

SUPPLEMENTARY MATERIAL

The Supplementary Material for this article can be found online at: https://www.frontiersin.org/articles/10.3389/fneur.2022.871166/full#supplementary-material

REFERENCES

1. Steriade M, Domich L, Oakson G, Deschenes M. The deafferented reticular thalamic nucleas generates spindle rhythmicity. *J Neurophysiol.* (1987) 57:260–73. doi: 10.1152/jn.1987.57.1.260
2. Steriade M, Deschenes M, Domich L, Mulle C. Abolition of spindle oscillations in thalamic neurons disconnected from nucleus reticularis thalami. *J Neurophysiol.* (1985) 54:1473–97. doi: 10.1152/jn.1985.54.6.1473
3. Contreras D, Destexhe A, Sejnowski TJ, Steriade M. Spatiotemporal patterns of spindle oscillations in cortex and thalamus. *J Neurosci.* (1997) 17:1179–96. doi: 10.1523/JNEUROSCI.17-03-01179.1997
4. Cox R, Schapiro AC, Manoach DS, Stickgold R. Individual differences in frequency and topography of slow and fast sleep spindles. *Front Hum Neurosci.* (2017) 11:433. doi: 10.3389/fnhum.2017.00433
5. Purcell SM, Manoach DS, Demanuele C, Cade BE, Mariani S, Cox R, et al. Characterizing sleep spindles in 11,630 individuals from the national sleep research resource. *Nat Commun.* (2017) 8:15930. doi: 10.1038/ncomms15930
6. Werth E, Achermann P, Dijk DJ, Borbély AA. Spindle frequency activity in the sleep EEG: individual differences and topographic distribution. *Electroencephalogr Clin Neurophysiol.* (1997) 103:535–42. doi: 10.1016/S0013-4694(97)00070-9
7. Zeitlhofer J, Gruber G, Anderer P, Asenbaum S, Schimicek P, Saletu B. Topographic distribution of sleep spindles in young healthy subjects. *J Sleep Res.* (1997) 6:149–55. doi: 10.1046/j.1365-2869.1997.00046.x
8. Fogel SM, Smith CT. The function of the sleep spindle: a physiological index of intelligence and a mechanism for sleep-dependent memory consolidation. *Neurosci Biobehav Rev.* (2011) 35:1154–65. doi: 10.1016/j.neubiorev.2010.12.003
9. Manoach DS, Stickgold R. Abnormal sleep spindles, memory consolidation, and schizophrenia. *Ann Rev Clin Psychol.* (2019) 15:451–79. doi: 10.1146/annurev-clinpsy-050718-095754
10. Niknazar M, Krishnan GP, Bazhenov M, Mednick SC. Coupling of thalamocortical sleep oscillations are important for memory consolidation in humans. *PLoS ONE.* (2015) 10:e0144720. doi: 10.1371/journal.pone.0144720
11. Mednick SC, McDevitt EA, Walsh JK, Wamsley E, Paulus M, Kanady JC, et al. The critical role of sleep spindles in hippocampal-dependent memory: a pharmacology study. *J Neurosci.* (2013) 33:4494–504. doi: 10.1523/JNEUROSCI.3127-12.2013
12. Kaestner EJ, Wixted JT, Mednick SC. Pharmacologically increasing sleep spindles enhances recognition for negative and high-arousal memories. *J Cogn Neurosci.* (2013) 25:1597–610. doi: 10.1162/jocn_a_00433
13. Lustenberger C, Boyle MR, Alagapan S, Mellin JM, Vaughn B, Fröhlich F. Feedback-Controlled transcranial alternating current stimulation reveals a functional role of sleep spindles in motor memory consolidation. *Curr Biol.* (2016) 26:2127–36. doi: 10.1016/j.cub.2016.06.044
14. Maingret N, Girardeau G, Todorova R, Goutierre M, Zugaro M. Hippocampo-cortical coupling mediates memory consolidation during sleep. *Nat Neurosci.* (2016) 19:959–64. doi: 10.1038/nn.4304
15. Latchoumane CFV, Ngo HVV, Born J, Shin HS. Thalamic spindles promote memory formation during sleep through triple phase-locking of cortical, thalamic, and hippocampal rhythms. *Neuron.* (2017) 95:424–35.e6. doi: 10.1016/j.neuron.2017.06.025
16. Manoach DS, Mylonas D, Baxter B. Targeting sleep oscillations to improve memory in schizophrenia. *Schizophr Res.* (2020) 221:63–70. doi: 10.1016/j.schres.2020.01.010
17. Nishida M, Walker MP. Daytime naps, motor memory consolidation and regionally specific sleep spindles. *PLoS ONE.* (2007) 2:e341. doi: 10.1371/journal.pone.0000341

18. Tamaki M, Huang TR, Yotsumoto Y, Hämäläinen M, Lin FH, Náñez JE, et al. Enhanced spontaneous oscillations in the supplementary motor area are associated with sleep-dependent offline learning of finger-tapping motor-sequence task. *J Neurosci.* (2013) 33:13894–902. doi: 10.1523/JNEUROSCI.1198-13.2013
19. Solano A, Riquelme LA, Perez-Chada D, Della-Maggiore V. Motor learning promotes the coupling between fast spindles and slow oscillations locally over the contralateral motor network. *Cereb Cortex.* (2021) 31:1873–87. doi: 10.1093/cercor/bhab360
20. Johnson LA, Blakely T, Hermes D, Hakimian S, Ramsey NF, Ojemann JG. Sleep spindles are locally modulated by training on a brain-computer interface. *Proc Natl Acad Sci USA.* (2012) 109:18583–8. doi: 10.1073/pnas.1207532109
21. Yoshida H, Iramina K, Ueno S. Source models of sleep spindles using MEG and EEG measurements. *Brain Topogr.* (1996) 8:303–7. doi: 10.1007/BF01184789
22. Manshanden I, De Munck JC, Simon NR, Lopes da Silva FH. Source localization of MEG sleep spindles and the relation to sources of alpha band rhythms. *Clin Neurophysiol.* (2002) 113:1937–47. doi: 10.1016/S1388-2457(02)00304-8
23. Dehghani N, Cash SS, Halgren E. Emergence of synchronous EEG spindles from asynchronous MEG spindles. *Hum Brain Mapp.* (2011) 32:2217–27. doi: 10.1002/hbm.21183
24. Dehghani N, Cash SS, Chen CC, Hagler DJ, Huang M, Dale AM, et al. Divergent cortical generators of MEG and EEG during human sleep spindles suggested by distributed source modeling. *PLoS ONE.* (2010) 5:e11454. doi: 10.1371/journal.pone.0011454
25. Zerouali Y, Lina JM, Sekerovic Z, Godbout J, Dube J, Jolicoeur P, et al. A time-frequency analysis of the dynamics of cortical networks of sleep spindles from MEG-EEG recordings. *Front Neurosci.* (2014) 8:310. doi: 10.3389/fnins.2014.00310
26. Klinzing JG, Mölle M, Weber F, Supp G, Hipp JF, Engel AK, et al. Spindle activity phase-locked to sleep slow oscillations. *Neuroimage.* (2016) 134:607–16. doi: 10.1016/j.neuroimage.2016.04.031
27. Nakasato N, Kado H, Nakanishi M, Koyanagi M, Kasai N, Niizuma H, et al. Magnetic detection of sleep spindles in normal subjects. *Electroencephalogr Clin Neurophysiol.* (1990) 76:123–30. doi: 10.1016/0013-4694(90)90210-B
28. Urakami Y. Relationships between sleep spindles and activities of the cerebral cortex after hemispheric stroke as determined by simultaneous EEG and MEG recordings. *J Clin Neurophysiol.* (2009) 26:248–56. doi: 10.1097/WNP.0b013e3181af209c
29. Krishnan GP, Rosen BQ, Chen JY, Muller L, Sejnowski TJ, Cash SS, et al. Thalamocortical and intracortical laminar connectivity determines sleep spindle properties. *PLoS Comput Biol.* (2018) 14:e1006171. doi: 10.1371/journal.pcbi.1006171
30. Brancaccio A, Tabarelli D, Bigica M, Baldauf D. Cortical source localization of sleep-stage specific oscillatory activity. *Sci Rep.* (2020) 10:8636. doi: 10.1038/s41598-020-63933-5
31. Neil Cuffin B, Cohen D. Comparison of the magnetoencephalogram and electroencephalogram. *Electroencephalogr Clin Neurophysiol.* (1979) 47:132–46. doi: 10.1016/0013-4694(79)90215-3
32. Melcher JR, Cohen D. Dependence of the MEG on dipole orientation in the rabbit head. *Electroencephalogr Clin Neurophysiol.* (1988) 70:460–72. doi: 10.1016/0013-4694(88)90024-7
33. Sharon D, Hämäläinen MS, Tootell RBH, Halgren E, Belliveau JW. The advantage of combining MEG and EEG: comparison to fMRI in focally stimulated visual cortex. *Neuroimage.* (2007) 36:1225–35. doi: 10.1016/j.neuroimage.2007.03.066
34. Taulu S, Kajola M, Simola J. Suppression of interference and artifacts by the signal space separation method. *Brain Topogr.* (2004) 16:269–75. doi: 10.1023/B:BRAT.0000032864.93890.f9
35. Gramfort A, Luessi M, Larson E, Engemann DA, Strohmeier D, Brodbeck C, et al. MNE software for processing MEG and EEG data. *Neuroimage.* (2014) 86:446–60. doi: 10.1016/j.neuroimage.2013.10.027
36. Iber C, Ancoli-Israel S, Chesson A, Quan SF. *The AASM Manual for the Scoring of Sleep and Associated Events: Rules, Terminology and Technical Specification*. Westchester, IL: American Academy Sleep Medicine (2007).
37. Oostenveld R, Fries P, Maris E, Schoffelen JM. FieldTrip: open source software for advanced analysis of MEG, EEG, and invasive electrophysiological data. *Comput Intell Neurosci.* (2011) 2011:156869. doi: 10.1155/2011/156869
38. Uusitalo MA, Ilmoniemi RJ. Signal-space projection method for separating MEG or EEG into components. *Med Biol Eng Comput.* (1997) 35:135–40. doi: 10.1007/BF02534144
39. Fischl B, Sereno MI, Dale AM. Cortical surface-based analysis: II. Inflation, flattening, and a surface-based coordinate system. *Neuroimage.* (1999) 9:195–207. doi: 10.1006/nimg.1998.0396
40. Dale AM, Fischl B, Sereno MI. Cortical surface-based analysis: I. Segmentation and surface reconstruction. *Neuroimage.* (1999) 9:179–94. doi: 10.1006/nimg.1998.0395
41. Hämäläinen MS, Sarvas J. Realistic conductivity geometry model of the human head for interpretation of neuromagnetic data. *IEEE Trans Biomed Eng.* (1989) 36:165–71. doi: 10.1109/10.16463
42. Hämäläinen M, Hari R, Ilmoniemi RJ, Knuutila J, Lounasmaa OV. Magnetoencephalography theory, instrumentation, and applications to noninvasive studies of the working human brain. *Rev Mod Phys.* (1993) 65:413–97. doi: 10.1103/RevModPhys.65.413
43. Dale AM, Sereno MI. Improved localization of cortical activity by combining EEG and MEG with MRI cortical surface reconstruction: a linear approach. *J Cogn Neurosci.* (1993) 5:162–76. doi: 10.1162/jocn.1993.5.2.162
44. Dale AM, Liu AK, Fischl BR, Buckner RL, Belliveau JW, Lewine JD, et al. Dynamic statistical parametric mapping: Combining fMRI and MEG for high-resolution imaging of cortical activity. *Neuron.* (2000) 26:55–67. doi: 10.1016/S0896-6273(00)81138-1
45. Fischl B, Van Der Kouwe A, Destrieux C, Halgren E, Ségonne F, Salat DH, et al. Automatically parcellating the human cerebral cortex. *Cereb Cortex.* (2004) 14:11–22. doi: 10.1093/cercor/bhg087
46. Khan S, Hashmi JA, Mamashli F, Michmizos K, Kitzbichler MG, Bharadwaj H, et al. Maturation trajectories of cortical resting-state networks depend on the mediating frequency band. *Neuroimage.* (2018) 174:57–68. doi: 10.1016/j.neuroimage.2018.02.018
47. Wamsley EJ, Tucker MA, Shinn AK, Ono KE, McKinley SK, Ely AV, et al. Reduced sleep spindles and spindle coherence in schizophrenia: mechanisms of impaired memory consolidation? *Biol Psychiatry.* (2012) 71:154–61. doi: 10.1016/j.biopsych.2011.08.008
48. Mylonas D, Baran B, Demanuele C, Cox R, Vuper TC, Seicol BJ, et al. The effects of eszopiclone on sleep spindles and memory consolidation in schizophrenia: a randomized clinical trial. *Neuropsychopharmacology.* (2020) 45:2189–97. doi: 10.1038/s41386-020-00833-2
49. Cohen MX. A better way to define and describe Morlet wavelets for time-frequency analysis. *Neuroimage.* (2019) 199:81–6. doi: 10.1016/j.neuroimage.2019.05.048
50. Otsu N. Threshold selection method from gray-level histograms. *IEEE Trans Syst Man Cybern.* (1979) 9:62–6. doi: 10.1109/TSMC.1979.4310076
51. Warby SC, Wendt SL, Welinder P, Munk EGS, Carrillo O, Sorensen HBD, et al. Sleep-spindle detection: crowdsourcing and evaluating performance of experts, non-experts and automated methods. *Nat Methods.* (2014) 11:385–92. doi: 10.1038/nmeth.2855
52. De Gennaro L, Marzano C, Fratello F, Moroni F, Pellicciari MC, Ferlazzo F, et al. The electroencephalographic fingerprint of sleep is genetically determined: a twin study. *Ann Neurol.* (2008) 64:455–60. doi: 10.1002/ana.21434
53. Cox R, Mylonas DS, Manoach DS, Stickgold R. Large-scale structure and individual fingerprints of locally coupled sleep oscillations. *Sleep.* (2018) 41:zsy175. doi: 10.1093/sleep/zsy175
54. Cohen D, Cuffin BN. Demonstration of useful differences between magnetoencephalogram and electroencephalogram. *Electroencephalogr Clin Neurophysiol.* (1983) 56:38–51. doi: 10.1016/0013-4694(83)90005-6
55. Mylonas D, Tocci C, Coon WG, Baran B, Kohnke EJ, Zhu L, et al. Naps reliably estimate nocturnal sleep spindle density in health and schizophrenia. *J Sleep Res.* (2020) 29:e12968. doi: 10.1111/jsr.12968
56. Taulu S, Simola J. Spatiotemporal signal space separation method for rejecting nearby interference in MEG measurements. *Phys Med Biol.* (2006) 51:1759–68. doi: 10.1088/0031-9155/51/7/008

57. Taulu S, Kajola M. Presentation of electromagnetic multichannel data: the signal space separation method. *J Appl Phys.* (2005) 97:124905. doi: 10.1063/1.1935742
58. Jones EG. The thalamic matrix and thalamocortical synchrony. *Trends Neurosci.* (2001) 24:595–601. doi: 10.1016/S0166-2236(00)01922-6
59. Zikopoulos B, Barbas H. Parallel driving and modulatory pathways link the prefrontal cortex and thalamus. *PLoS ONE.* (2007) 2:e848. doi: 10.1371/journal.pone.0000848
60. Piantoni G, Halgren E, Cash SS. The contribution of thalamocortical core and matrix pathways to sleep spindles. *Neural Plast.* (2016) 2016:3024342. doi: 10.1155/2016/3024342
61. Ahlfors SP, Han J, Lin FH, Witzel T, Belliveau JW, Hämäläinen MS, et al. Cancellation of EEG and MEG signals generated by extended and distributed sources. *Hum Brain Mapp.* (2010) 31:140–9. doi: 10.1002/hbm.20851
62. Hillebrand A, Barnes GR. A quantitative assessment of the sensitivity of whole-head MEG to activity in the adult human cortex. *Neuroimage.* (2002) 16:638–50. doi: 10.1006/nimg.2002.1102
63. Attal Y, Schwartz D. Assessment of subcortical source localization using deep brain activity imaging model with minimum norm operators: a MEG study. *PLoS ONE.* (2013) 8:e59856. doi: 10.1371/journal.pone.0059856
64. Samuelsson JG, Khan S, Sundaram P, Peled N, Hämäläinen MS. Cortical signal suppression (CSS) for detection of subcortical activity using MEG and EEG. *Brain Topogr.* (2019) 32:215–28. doi: 10.1007/s10548-018-00694-5
65. Krishnaswamy P, Obregon-Henao G, Ahveninen J, Khan S, Babadi B, Iglesias JE, et al. Sparsity enables estimation of both subcortical and cortical activity from MEG and EEG. *Proc Natl Acad Sci USA.* (2017) 114:E10465–74. doi: 10.1073/pnas.1705414114
66. Baran B, Karahanoglu FI, Mylonas D, Demanuele C, Vangel M, Stickgold R, et al. Increased thalamocortical connectivity in schizophrenia correlates with sleep spindle deficits: evidence for a common pathophysiology. *Biol Psychiatry Cogn Neurosci Neuroimaging.* (2019) 4:706–14. doi: 10.1016/j.bpsc.2019.04.012
67. Kramer MA, Stoyell SM, Chinappen D, Ostrowski LM, Spencer ER, Morgan AK, et al. Focal sleep spindle deficits reveal focal thalamocortical dysfunction and predict cognitive deficits in sleep activated developmental epilepsy. *J Neurosci.* (2021) 41:1816–29. doi: 10.1523/JNEUROSCI.2009-20.2020

Conflict of Interest: The authors declare that the research was conducted in the absence of any commercial or financial relationships that could be construed as a potential conflict of interest.

frontiers | Frontiers in Neurology

ORIGINAL RESEARCH
published: 23 June 2022
doi: 10.3389/fneur.2022.814940

Functional Significance of Human Resting-State Networks Hubs Identified Using MEG During the Transition From Childhood to Adulthood

Sheraz Khan[1,2,3*†], *Javeria Ali Hashmi*[1,3,4†], *Fahimeh Mamashli*[2,3], *Matti S. Hämäläinen*[2,3] *and Tal Kenet*[1,3]

[1] Department of Neurology, Massachusetts General Hospital and Harvard Medical School, Boston, MA, United States,
[2] Department of Radiology, Massachusetts General Hospital and Harvard Medical School, Boston, MA, United States,
[3] Athinoula A. Martinos Center for Biomedical Imaging, Massachusetts General Hospital, Charlestown, MA, United States,
[4] Department of Anesthesia, Pain Management, and Perioperative Medicine, Dalhousie University, Halifax, NS, Canada

OPEN ACCESS

Edited by:
Wenbin Guo,
Central South University, China

Reviewed by:
Arpan Banerjee,
National Brain Research Centre (NBRC), India
Felix Siebenhühner,
University of Helsinki, Finland
Hongfang Wang,
Aston University, United Kingdom

***Correspondence:**
Sheraz Khan
sheraz@nmr.mgh.harvard.edu

† These authors have contributed equally to this work

Specialty section:
This article was submitted to Applied Neuroimaging, a section of the journal Frontiers in Neurology

Received: *14 November 2021*
Accepted: *10 May 2022*
Published: *23 June 2022*

Citation:
Khan S, Hashmi JA, Mamashli F, Hämäläinen MS and Kenet T (2022) Functional Significance of Human Resting-State Networks Hubs Identified Using MEG During the Transition From Childhood to Adulthood. Front. Neurol. 13:814940. doi: 10.3389/fneur.2022.814940

Cortical hubs identified within resting-state networks (RSNs), areas of the cortex that have a higher-than-average number of connections, are known to be critical to typical cognitive functioning and are often implicated in disorders leading to abnormal cognitive functioning. Functionally defined cortical hubs are also known to change with age in the developing, maturing brain, mostly based on studies carried out using fMRI. We have recently used magnetoencephalography (MEG) to study the maturation trajectories of RSNs and their hubs from age 7 to 29 in 131 healthy participants with high temporal resolution. We found that maturation trajectories diverge as a function of the underlying cortical rhythm. Specifically, we found the beta band (13–30 Hz)-mediated RSNs became more locally efficient with maturation, i.e., more organized into clusters and connected with nearby regions, while gamma (31–80 Hz)-mediated RSNs became more globally efficient with maturation, i.e., prioritizing faster signal transmission between distant cortical regions. We also found that different sets of hubs were associated with each of these networks. To better understand the functional significance of this divergence, we wanted to examine the cortical functions associated with the identified hubs that grew or shrunk with maturation within each of these networks. To that end, we analyzed the results of the prior study using Neurosynth, a platform for large-scale, automated synthesis of fMRI data that links brain coordinates with their probabilistically associated terms. By mapping the Neurosynth terms associated with each of these hubs, we found that maturing hubs identified in the gamma band RSNs were more likely to be associated with bottom-up processes while maturing hubs identified in the beta band RSNs were more likely to be associated with top-down functions. The results were consistent with the idea that beta band-mediated networks preferentially support the maturation of top-down processing, while the gamma band-mediated networks preferentially support the maturation of bottom-up processing.

Keywords: development, brain connectivity, rhythms, graph theory, magnetoencephalography

INTRODUCTION

The period from childhood to adolescence is a time window of extensive developmental changes in the neurophysiological topology of the brain (1, 2). This period of rapid growth and reorganization also coincides with a delicate period of increased vulnerability to neuropsychiatric disorders, further underscoring the need to gain insight into the changes that underlie this period. As part of cortical maturation, the distribution of functional connections also changes so that some brain regions acquire a higher-than-average number of connections to form hubs, while other hubs that may have been prominent during childhood may shrink with maturation. Hubs play a key role in integrative processing and supporting connectivity between network modules (3, 4), and are implicated in a range of brain-based disorders (5). To date, the vast majority of studies of cortical changes during maturation have focused on resting-state networks due to their replicability across sites and relevance to a wide range of psychiatric and neurological disorders (6–13). Almost all these studies have been carried out using functional magnetic resonance imaging (fMRI), i.e., with signals that fluctuate in the infra-slow range. Thus, to date, it has not been known whether or how hub maturation patterns vary as a function of the frequency band mediating their connectivity. This question is relevant because intrinsic cortical rhythms are themselves functionally significant, and rhythm-specific alterations emerge are widely reported for a wide range of brain-based disorders and diseases (14–21). Studying the maturing and changing distribution and characteristics of hubs formed by intra-areal synchronization of specific intrinsic brain rhythms is, therefore, necessary for a better understanding of the maturing brain and parsing the functional relevance of developing hubs can offer insights into brain function and underscore sensitive periods underpinning developmental disorders.

We have previously observed that developmental changes in the segregation and integration of resting-state networks and their corresponding hubs are clearly observable within specific cortical rhythms and vary by rhythm (22). Specifically, we showed that there were no notable maturational changes mediated by the slower brain rhythms (delta, 1–3 Hz; theta, 4–7 Hz; alpha, 8–12 Hz). In contrast, the resting state networks mediated by the faster beta (13–30 Hz) and gamma (30–80 Hz) frequency bands undergo marked topological reorganization during maturation between the ages 7 and 29. Networks mediated by the beta brain rhythm become more integrated with maturation, i.e., more organized into clusters, i.e., prioritizing communication between nearby hubs. In contrast, networks mediated by the gamma brain rhythm become more segregated and distributed with maturation, i.e., prioritizing faster signal transmission between distant hubs. As part of that same study, we found that maturation-driven changes in network topology resulted in the hubs expanding (getting more connections) or shrinking (losing connections and potentially losing hub "status") in resting-state networks mediated by the beta and gamma bands. Spatially, maturing hubs in the gamma band-mediated networks were located in heteromodal regions, such as the posterior parietal cortex, posterior cingulate cortex, and the anterior insula, in agreement with fMRI studies (23, 24). Hubs in the beta-band-mediated network were located in heteromodal-frontal regions and shrunk with maturation, which is a finding hitherto unobserved with fMRI.

In our prior study, we speculated that the altered spatial distribution of hubs in both networks reflects a shift in higher-order cognitive processes and thus top-down processing, within the beta band-mediated networks, and in bottom-up sensory functioning in the gamma band-mediated networks. This hypothesis was derived from recent data on the putative roles of the beta and gamma bands in intra-areal synchronization. It has been demonstrated that intra-areal gamma-band synchronization mediates bottom-up signaling of sensory inputs in several studies (17, 25). Relatedly, top-down influences on sensory processing, such as attentional selection and cognitive control, are mediated by intra-areal, alpha-beta band synchronizations (17, 25, 26). The developmental changes in hubs observed with MEG indicate an increased clustering and segregation in beta and gamma-mediated networks, respectively.

In this study, we investigated these hypotheses. To that end, we conducted a meta-analysis that built on the results and data from the prior paper. Specifically, we used Neurosynth, a meta-analytic platform that relies on a large-scale, automated synthesis of fMRI data for data mining (27) to test and substantiate the interpretations of the results proposed in our prior study. The Neurosynth platform allows association tests for identifying the relevance of a brain region to categories of behavioral functions in a statistically principled manner and has been used successfully in multiple studies to gain an understanding of the potential function of hubs (28–33). The Neurosynth platform can be tapped in two ways. In the "reverse" direction, called "decoding," the input to Neurosynth is the coordinate of interest, i.e., the coordinate of the hubs, and the output is the terms associated with these coordinates, ranked by the probability of association. We hypothesized that maturing hubs identified in the beta band network will be associated with Neurosynth terms related to top-down processing while maturing hubs identified in the gamma band network will be associated with terms related to bottom-up processing. In the "forward" direction, one enters a brain-related term of interest. As an output, Neurosynth returns the coordinates of the brain areas associated with these terms based on the papers analyzed in its database in probabilistic ranking order. Therefore, the coordinates most often associated with the term depression, for instance, will be ranked at the top of the search results, and so on. We used this approach to test for the extent of overlap between hubs associated with terms related to bottom-up or top-down processing, and the hubs identified in our analyses. We hypothesized that maturing hubs identified in the beta band network will overlap with hubs associated with terms related to top-down processing while maturing hubs identified in the gamma band network will overlap with hubs associated with terms related to bottom-up processing (22).

MATERIALS AND METHODS

Participants

Magnetoencephalography resting-state data were collected from 145 healthy typically developing participants, aged 7–29. Due to excessive motion, data from 14 subjects were discarded, resulting

in 131 high-quality datasets (64 females) with a roughly uniform age distribution. Because we combined datasets across several different studies that utilized the MEG at the Martinos Center at the Massachusetts General Hospital, no single behavioral measures were available across all the participants. IQ measured with the Kaufman Brief Intelligence Test – II (34) was available for 68 of the participants. Within this subgroup, no significant change in IQ with age was observed, as expected, given that IQ is normalized by age. All the studies that were pooled for this analysis were screened for typical development and health. All the adult (age 18+) participants signed a consent form, agreeing to participate in the study, and consent forms were signed by the parents of the participants aged 7–17. The participants aged 14–17 were also invited to sign a consent form if they wished to do so. All procedures and forms were approved by the Massachusetts General Hospital IRB.

Experimental Paradigm

The resting-state paradigm consisted of a fixation cross at the center of the screen, presented for 5 min continuously, while the participants were seated and instructed to fixate on the cross. The fixation stimulus was projected through an opening in the wall onto a back-projection screen placed 100 cm in front of the participant, inside a magnetically shielded room.

MRI Data Acquisition and Processing

T1-weighted, high-resolution MPRAGE (Magnetization Prepared Rapid Gradient Echo) structural images were acquired on either a 1.5 T or a 3.0-T Siemens Trio whole-body MRI (magnetic resonance) scanner (Siemens Medical Systems) using either 12 channels or a 32 channel head coil. The structural data were preprocessed using FreeSurfer (35, 36). After correcting for topological defects, cortical surfaces were triangulated with dense meshes with ∼130,000 vertices in each hemisphere. To expose the sulci in the visualization of cortical data, we used the inflated surfaces computed by FreeSurfer.

MEG Data Acquisition and Cleaning

Magnetoencephalography data were acquired inside a magnetically shielded room (37) using a whole-head Elekta NeuromagVectorView system composed of 306 sensors arranged in 102 triplets of two orthogonal planar gradiometers and one magnetometer. The signals were filtered between 0.1 Hz and 200 Hz and sampled at 600 Hz. To allow co-registration of the MEG and MRI data, the locations of three fiduciary points (nasion and auricular points) that define a head-based coordinate system, a set of points from the head surface and the locations of the four HPI coils were determined using a Fastrak digitizer (Polhemus Inc., Colchester, VT) integrated with the VectorView system. ECG and horizontal (HEOG) and vertical electrooculogram (VEOG) signals were recorded. The position and orientation of the head with respect to the MEG sensor array were recorded continuously throughout the session with the help of four head position indicator (HPI) coils (38).

We also monitored the continuous head position, and the session was restarted if the excessive head movement was recorded. The session was also restarted if any slouching in the seated position was observed. Pillows, cushions, and blankets were fitted to each individual to address slouching and readjusted as needed. In addition to the human resting-state data, 5 min of data from the empty room was recorded before or after each session for noise estimation purposes.

Following this, the data were spatially filtered using the signal space separation (SSS) method (39, 40) with Elekta NeuromagMaxfilter software to suppress noise generated by sources outside the brain. This procedure also corrects for head motion using the continuous head position data described in the previous section. The heartbeats were identified using in-house MATLAB code modified from the QRS detector in BioSig (41). Subsequently, a signal-space projection (SSP) operator was created separately for magnetometers and gradiometers using the singular value decomposition (SVD) of the concatenated data segments, containing the QRS complexes and separately identified eye blinks (42), using code now implemented into the open-source MNE-Python software (43). Data were also low-pass-filtered at 144 Hz to eliminate the HPI coil excitation signals.

Artifact cleaning was performed as follows: signal spikes where the amplitude was higher than 5σ over the mean were identified and dropped. To remove the effect of microsaccades, horizontal and vertical EOG channels were filtered at a pass-band of 31–80 Hz. The envelope was then calculated for the filtered signals and averaged to get REOG. Peaks exceeding three SDs above the mean calculated over the whole-time course were identified, and the corresponding periods were discarded from subsequent analysis. Lastly, head movement recordings from the HPI coils were used to drop any 1-s blocks where the average head movement exceeded 1.7 mm/s (an empirical threshold). The amount of data lost through cleaning was well below 10% and did not differ significantly with age.

MEG Data Processing

The analysis stream we followed is illustrated in **Figure 1**, and details are described below.

Mapping MEG Data Onto Cortical Space

The dense triangulation of the folded cortical surface provided by FreeSurfer was decimated to a grid of 10,242 dipoles per hemisphere, corresponding to a spacing of ∼3 mm between adjacent source locations. To compute the forward solution, a boundary-element model with a single compartment bounded by the inner surface of the skull was assumed (44). The watershed algorithm in FreeSurfer was used to generate the inner skull surface triangulations from the MRI scans of each participant. The current distribution was estimated using the regularized minimum-norm estimate (MNE) by fixing the source orientation to be perpendicular to the cortex. The regularized (regularization = 0.1) noise covariance matrix that was used to calculate the inverse operator was estimated from data acquired in the absence of a subject before each session. This approach has been validated using intracranial measurements (45). To reduce the bias of the MNEs toward superficial currents, we incorporated depth weighting by adjusting the source covariance matrix, which has been shown to increase spatial specificity (46). All forward and inverse calculations were done using MNE-C (47).

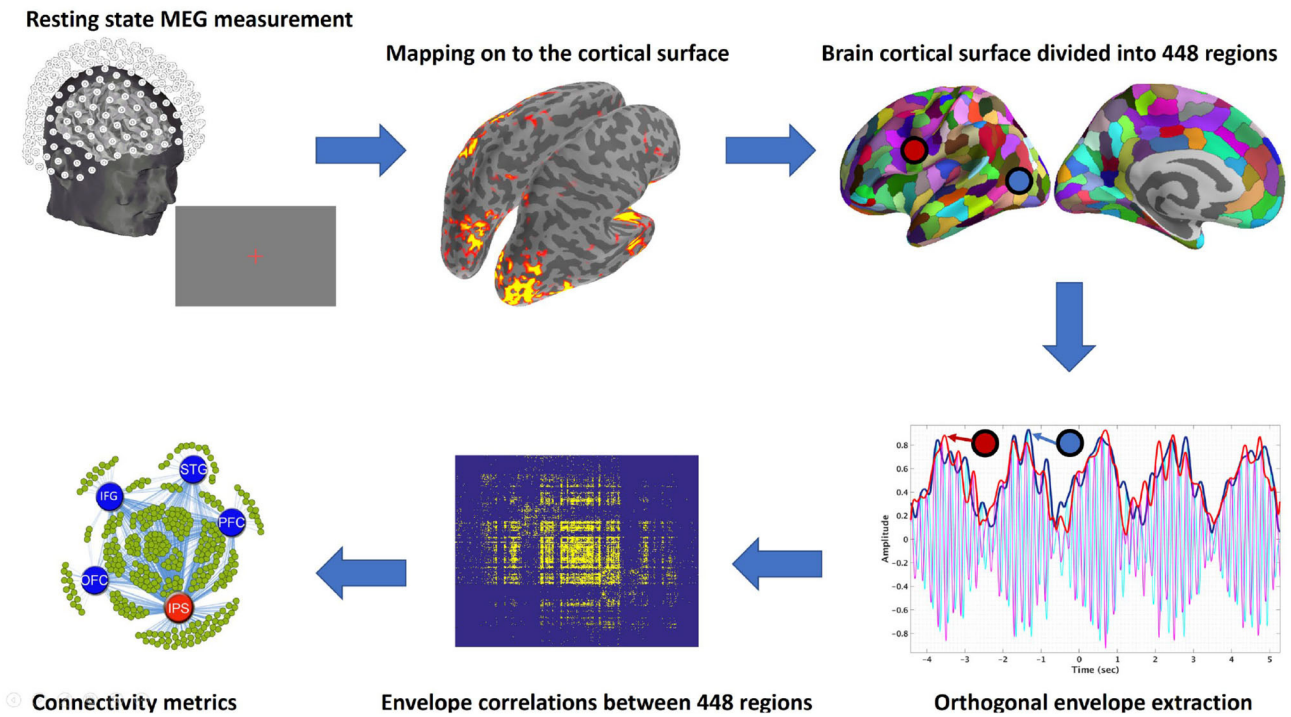

FIGURE 1 | Schematic illustration of pipeline. From top left in a clockwise direction: Resting state data were acquired using MEG, cleaned as described above, and then mapped to the cortical surface. The surface was then divided into regions (parcellated), and envelopes were calculated for each frequency band in each region. The connectivity between the regions was then computed from the envelopes and used to derive the connectivity metrics. Hubs were then identified using betweenness centrality. The whole pipeline from raw MEG data to connectivity metrics is available as an MNE-Python example.

Cortical Parcellation (Labels)

FreeSurfer was used to automatically divide the cortex into 72 regions (48). After discarding "medial wall" and "corpus callosum," regions were further divided into a total of $N = 448$ cortical labels so that each label covers a similar area, again using FreeSurfer. This was done to avoid averaging across a large label that crosses multiple sulci and gyri and, therefore, could result in signal cancellation across the label. Lastly, a high-resolution parcellation also reduces the dependence of the results on the specific selection of the parcels.

Deriving the Time Series for Each Label

Because of the ambiguity associated with individual vertex (dipole) orientations, the time series for each vertex within a label was not averaged directly but first aligned with the dominant component of the multivariate set of time series before calculating the label mean. To align the sign of the time series across vertices, we used the SVD of the data $\mathbf{X}^T = \mathbf{U}\Sigma\mathbf{W}^T$. The sign of the dot product between the first left singular vector $\mathbf{U}$ and all other time series in a label was computed. If this sign was negative, we inverted the time series before averaging. The time series were band-pass filtered and downsampled for faster processing, while making sure that the sampling frequency was maintained at $f_s > 3f_{hi}$ (obeying the Nyquist theorem and avoiding aliasing artifacts). The chosen frequency bands were delta (1–4 Hz), theta (4–8 Hz), alpha (8–12 Hz), beta (13–30 Hz), and gamma (31–80 Hz). The line frequency at 60 Hz was removed with a notch filter of bandwidth of 1 Hz. Hilbert transform was then performed on these band-pass data. More specifically, for each frequency band, the analytic signal $\hat{X}(t)$ was calculated by combining the original time series with its Hilbert transform into a complex time series:

$$\hat{X}(t) = x(t) + \jmath\,\mathcal{H}[x(t)]$$

The resulting time series $\hat{X}(t)$ can be seen as a rotating vector in the complex plane whose length corresponds to the envelope of the original time series $x(t)$ and whose phase grows according to the dominant frequency. **Figure 1**, Step 4, shows an example of a modulated envelope on the top of the bandpass data (carrier).

Deriving the Orthogonal Envelopes

We used envelope correlations to reliably estimate synchronicity between different cortical labels (49). In contrast to phase-based connectivity metrics, envelope correlations measure how the amplitude of an envelope within a frequency band is synchronously modulated over time across distinct cortical regions, as illustrated in the fourth panel of **Figure 1**. Previous studies (humans and primates) have demonstrated the validity and functional significance of these synchronous envelope amplitude modulations (49–53) for both oscillatory and broadband signals.

To address the field-spread problem associated with MEG data (54), we used the previously described orthogonal (55) variation of the envelope correlation metric. This method requires any two putatively dependent signals to have non-zero lag and is thus insensitive to the zero-lag correlations, stemming from the field spread. Mathematically, the connectivity between two complex signals $\hat{X}$ and $\hat{Y}$ is calculated by "orthogonalizing" one signal wall-cap concerning the other $\hat{Y}(t,f) \rightarrow \hat{Y}_{\perp X}(t,f)$, and subsequently taking the Pearson correlation between their envelopes. This is done in both directions, and the two results are averaged to give the final connectivity measure $C_{\perp}(\hat{X}, \hat{Y}; t,f)$.

$$\hat{Y}_{\perp X}(t,f) = \Im\left(\hat{Y}(t,f)\frac{\hat{X}^{\dagger}(t,f)}{|\hat{X}(t,f)|}\right)\hat{e}_{\perp X}(t,f)$$

$$C_{\perp}\left(\hat{X},\hat{Y};t,f\right) = \frac{Corr\left(\left|\hat{X}\right|,\left|\hat{Y}_{\perp X}\right|\right) + Corr\left(\left|\hat{Y}\right|,\left|\hat{X}_{\perp Y}\right|\right)}{2}$$

Due to the slow time course of these envelopes and to ensure enough independent samples are available in the correlation window (55), we calculated the orthogonal connectivity using an overlapping sliding window of 30 s with a stride of 1/8 of the window size. Note that all 30 epochs that contained a discontinuity due to a noisy segment that had to be removed were excluded from the analyses.

Deriving the Connectivity and Adjacency Matrices

As a starting point for calculating the graph-theoretic metrics, we used the connectivity matrix, which contained the orthogonal correlations between all $N \times N$ node pairs and at each time window. A separate matrix was computed for each frequency band. The result of the processing pipeline is a connectivity array of dimension $N \times N \times N_{Time} \times N_{Bands}$ for each subject. To increase the signal to noise, we collapsed the connectivity array along the temporal dimension by taking the median of each pairwise orthogonal correlation across time windows. Thresholding and binarizing the connectivity matrix result in the adjacency matrix $\mathbb{A}$.

We used a threshold proportional scheme to retain a given proportion of the strongest connectivity matrix entries in $\mathbb{A}$. Specifically, the adjacency matrix $\mathbb{A}$ was constructed using a fixed cost threshold, ensuring that the density or number of connections of the network is equated across all individuals and age groups. Cost is a measure of the percentage of connections for each label about all connections of the network. Since the total number of connections is the same for all participants and is determined by the number of nodes being considered, the use of a fixed cost, i.e., a fixed percentage threshold, allows for exactly equal numbers of connections across the participants. This is important to ensure graph metrics can be compared across all individuals and age groups. As there was no rationale for using a cost threshold, therefore, we compared graph network properties for a wide range of costs; we used a thresholding range from 5 to 30% at increments of 5%. For the graph metrics to be reliable, they should be consistent over the range of thresholds.

The adjacency matrix $\mathbb{A}$ defines a graph $\mathcal{G}$ in the form of pairs of nodes that are connected by an edge. Thus, $\mathbb{A}$ is defined such that its binary element $\mathbb{A}_{ij}$ is either 1 or 0, depending on whether the edge e_{ij} between nodes v_i and v_j exists or not:

$$\mathbb{A}_{ij} = \begin{cases} 1 \& if\ \exists\, e_{ij} \\ 0 \& if\ \nexists\, e_{ij} \end{cases}$$

Path Length

The average shortest path length between all pairs of nodes was calculated as follows:

$$L = \frac{1}{n(n-1)} \sum_{i \neq j;\, v_i, v_j \in \mathcal{G}} d_{ij}$$

where the topological distance $\mathbf{d_{ij}}$ between nodes $\mathbf{v_i}$ and $\mathbf{v_j}$ is defined as the minimum number of edges one must traverse to get from one node to the other

$$\mathbf{d_{ij}} = \min\left\{\mathbf{n} \left| \mathbb{A}^{n}\left[\mathbf{i},\mathbf{j}\right] \neq \mathbf{0}\right.\right\}$$

where $\mathbb{A}^n$ denotes the nth power of the adjacency matrix $\mathbb{A}$, and i and j are row and column indices of the resulting matrix.

Degree

The degree (hubness) of a node $\mathbf{v_i}$ in a Graph $\mathcal{G}$ is defined as

$$D_i = \sum_{j=1, j \neq i}^{n} e_{ij}$$

where e_{ij} is the i th row and j th column edge of adjacency matrix $\mathbb{A}$.

Clustering Coefficient

The local clustering coefficient in the neighborhood of a vertex $\mathbf{v_i}$ is defined as the ratio of actual and maximally possible edges in the Graph $\mathcal{G}_\mathbf{i}$, which is equivalent to the graph density of $\mathcal{G}_\mathbf{i}$:

$$C_i = \frac{2\left|\left\{e_{jk}\right\}\right|}{k_i\left(k_i - 1\right)} : v_j, v_k \in \mathcal{G}_i$$

Global and Local Efficiencies

Global efficiency measures the efficiency of information transfer through the entire network and is assessed by mean path length. While the concept of path length is intuitive in anatomical networks, it is also relevant for functional networks, since a particular functional connection may travel different anatomical paths, and, while the correspondence between the two is generally high, it is not necessarily identical (56–58). Local efficiency is related to the clustering of a network, i.e., the extent to which nearest neighbors are interconnected. Thus, it assesses the efficiency of connectivity over adjacent brain regions.

The average global efficiency of information transfer in graph $\mathcal{G}$ having n nodes can be calculated from the inverse of the edge distances $d_{i,j}$

$$E_{glob} = E\left(\mathcal{G}\right) = \frac{1}{n\left(n-1\right)} \sum_{i \neq j;\, v_i, v_j \in \mathcal{G}} \frac{1}{d_{ij}}$$

The quantity above is a measure of the global efficiency of information transfer for the whole graph $\mathcal{G}$. There is also a local efficiency for each vertex v_i, measuring how efficiently its neighbors can communicate when a vertex v_i is removed. If the subgraph of all neighbors of v_i is denoted by $\mathcal{G}_i$, then its local efficiency $E(\mathcal{G}_i)$ is approximately equivalent to the clustering coefficient C_i (59).

$$E_{loc} = \frac{1}{n} \sum_{v_i \in \mathcal{G}} E(\mathcal{G}_i)$$

Betweenness Centrality

Betweenness centrality pertains to individual nodes in the network rather than the network as a whole and assesses how many of the shortest paths between all other node pairs in the network pass through that node. Nodes with high betweenness centrality (hubs) are, therefore, more important for overall network efficiency.

The betweenness centrality of node *i* is defined as

$$b_i = \sum_{m \neq i \neq n \in G} \frac{\sigma_{mn}(i)}{\sigma_{mn}}$$

where σ_{mn} is the total number of shortest paths (paths with the shortest path length) from Node *m* to Node *n*, and $\sigma_{mn}(i)$ is the number of shortest paths from Node *m* to node *N* that pass through Node *i*. Betweenness centrality of a node thus reflects the control and influence of that node on other nodes. Nodes with high betweenness centrality have a high impact on information transferal and collaboration between disparate sub-networks.

Resilience

Resilience is the graph-theoretic metric most critical to the current analysis and, therefore, merits a more thorough discussion. Resilience measures the robustness of the network if the most heavily connected nodes (hubs) are removed. This measure is inversely related to the capacity of the system for integrating information in an efficient manner and is also reflective of the brain's small-world property, a metric that determines the balance between cost and efficiency proffered by the network for information transfer (60, 61). Small world property and resilience are inversely proportional because both are computed from the relative strength of local and global efficiencies, one directly and one inversely. Indeed, this small world property and resilience for the beta and gamma-mediated networks showed opposite trajectory directions with maturation. We chose this measure because it has been studied, mostly using fMRI, in the context of psychiatric disorders, where multiple hubs might be functioning abnormally (3, 62). It has also been shown that greater resilience in a functionally derived task-driven network is associated with greater inhibitory control cognitively (63), a function that is often impaired in neurodevelopmental and psychiatric disorders. Importantly, the measure incorporates network topology in conjunction with the spatial distribution of hubs, because it takes the degree, i.e., the number of connections, of individual nodes into account.

Resilience quantifies Graph $\mathcal{G}$'s robustness to targeted or random attacks. Targeted attacks remove nodes in the descending order of importance (i.e., number of connections). At each attack, global efficiency is computed. Robustness is defined as the ratio of the original efficiency with efficiency calculated after the attack. This process is repeated until a predetermined number of hubs, or all hubs are removed. In this case, to obtain the data shown in **Figures 4**, **5**, we removed the largest 90 hubs (nodes) associated with each term in descending order and computed the relative loss or gain in network efficiency after each removal.

Bootstrapping and Correlation

To visualize the significance of age effects and assess uncertainties in the graph metrics with respect to age, we used nested bootstrapping with 1,024 realizations. The nested bootstrap procedure approximates the joint distribution of age x with the age-dependent network metric $f(y_x)$, where $f(y_x)$ is the average network metric over many subjects of age x (see notes below). We observed n pairs (x_i, y_i), where x_i is the age and y_i the corresponding imaging data for the i^{th} subject. Ideally, we would like to observe (x_i, Y_x), where y_x denotes the (conceptual) average of subjects chosen at random from a population, where each subject is of age x.

Let $f(y)$ denote the function that maps imaging data to a scalar metric, describing some aspect of a network. Since y_i contains noise, to visualize and estimate uncertainties in graph metrics, we can approximate $(x_i, \bar{y}_x)$ by $(\bar{X}_*, \bar{y}_*)$, where the $*$ denotes a bootstrap sample. We can then evaluate $f(y_{\bar{x}_*})$ instead of $f(y_i)$.

Each realization of bootstrapping yielded one average network metric and one value for the mean age of the group. Each data point on the normalized density color map corresponds to one realization of the bootstrap. To evaluate the relationship between network quantity and age, we used Spearman correlation. The *p*-values were computed after correcting for multiple comparisons across the correction space of frequency bands, thresholds, and graph metrics by controlling for a family-wise error rate using maximum statistics through permutation testing (64).

Specifically, the correction for multiple comparisons was done by constructing an empirical null distribution. For this purpose, $n_p = 10{,}000$ realizations were computed by first randomizing age and then correlating it with all graph metrics at all thresholds and frequency bands, and finally taking maximum correlation value across this permuted correction space. The corrected *p*-values (p_c) were calculated as:

$$p_c = \frac{2(n+1)}{n_p + 1}$$

where n is the number of values in the empirical null distribution greater or lower than the observed positive or negative correlation value, respectively. The factor of two stems from the fact that the test is two-tailed. Correlations resulting in significant *p*-values were then again tested using Robust Correlation (65), which strictly checks for false-positive correlations using bootstrap resampling.

LOESS Regression

LOESS, which stands for Locally Estimated Scatterplot Smoothing, is a non-parametric regression method that combines multiple regression models in a k-nearest-neighbor-based meta model to create a smooth line through a time plot or

scatter plot to help visualize the relationships between variables. We used the non-parametric LOESS regression to fit a curve to the data (66). To prevent overfitting in estimating bandwidth, we used 10-fold cross-validation. We generated our predictive model using the data in the training set, and then measured the accuracy of the model using the data in the test set. We tested a range of bandwidths from 0.01 to 0.99 with a 0.01 step. The bandwidth resulting in the least sum of squares error was then selected (67).

Neurosynth Decoding for Hubs Word Cloud Generation

Neurosynth (https://neurosynth.org/) is a platform for large-scale, automated synthesis of functional magnetic resonance imaging (fMRI) data. It uses information from several thousand published studies, reporting the results of fMRI studies, to determine the statistical association between cortical areas, and cognitive, disease, or function terms. Thus, every cortical vertex is assigned a statistical score of how correlated it is with terms within Neurosynth, and *vice versa*—every term in Neurosynth has a ranked by strength of an association list of cortical vertices associated with this term. This makes it possible to assess functions or disorders associated with a particular anatomical region in the cortex, with much greater statistical reliability than would be possible *via* visual inspection, for instance.

For Neurosynth decoding, surface maps showing all the hubs that exhibited significant age-dependent changes in the betweenness centrality metric (correlation between age and the betweenness centrality of nodes) in either the beta or gamma band-mediated networks were transformed using FreeSurfer from the surface to volume MNI space (mri_surf2vol). The correlation maps were then run through the Neurosynth decoding python module for the identification of the relevant text terms.

The text data significantly associated with the brain regions can be visually represented using word clouds (also known as text clouds or tag clouds); the more a specific word appears in a source of textual data, the bigger and bolder it appears in the word cloud. The Word cloud was generated using the first 500 most relevant terms from a total of 2,911 terms generated from the Neurosynth decoding module. The size of the words (Neurosynth terms) corresponds to its relative correlation with the maps as inferred by the Neurosynth decoding module. A Python package entitled "a little word cloud generator" was used for plotting the word cloud (https://github.com/amueller/word_cloud). Note that these word clouds are inherently statistical quantities, since only significant age-dependent changes were fed to the Neurosynth decoding module, and only significant correlations were included as part of the word clouds.

Maturation of Resilience, Tested Using Neurosynth-Derived Hubs

To test the extent to which hubs identified in our primary analysis overlap with hubs that correspond to specific functions, we began by choosing 12 brain-function terms and extracting from Neurosynth the first 90 nodes in descending order of size, which corresponded to these terms. The sensory and cognitive terms were chosen because they are all known to mature between childhood and adulthood and represent a variety of cognitive functions that are known to rely more heavily on bottom-up or top-down processing. The DSM-5 terms were chosen because all the disorders with the exception of autism are likely to have an onset time in adolescence or early adulthood. Autism was added due to its high prevalence and our prior experience with the disorder, as well as due to the fact that the severity of autism sometimes increases during adolescence (68, 69). Note that we excluded psychosis and schizophrenia despite the high prevalence of the onset during adolescence. This is because these terms were not associated with any "reverse inference" maps in Neurosynth, i.e., there is no selectivity for which regions activate with these terms, hence making them non-specific for target hubs. The terms were entered exactly as they appear in the results section, except for the "dorsal visual" term, which was not available on the Neurosynth website. The term "dorsal visual" was generated to mirror the term "ventral visual," using the neurosynth python framework (github.com/neurosynth), by specifying expression = "dorsal and visual," in the dataset.get_studies module.

Reverse inference maps from Neurosynth (27) were downloaded for each of the examined terms at FDR = 0.05, as listed in the results section. The resultant meta-analytic reverse inference map, also known as the association test map, is a map of z-scores from a two-way ANOVA, testing for the presence of a non-zero association between the term(s) used and the voxels activation map. These maps were then projected and registered onto the FsAverage surface using pysurfer (pysurfer.github.io). The mean Z-scores from this two-way ANOVA, averaged across node's vertices for each of the 448 nodes, were then computed from these surface-projected maps. This mean z-score is shown as a textured color map on the cortex. Nodes were then removed from the graphs in order of their Neurosynth Z-scores, in descending order, from the highest z-score (i.e., the largest most important node) downwards. At each removal, the following two steps were performed: first, global efficiency for each subject was recalculated and normalized with respect to the original global efficiency before removal. The result at point M was the network resilience after the removal of M nodes. Then, the resultant-normalized global efficiency was correlated with age using Spearman correlation. The resultant correlations were then corrected using maximum statistics by permutation across bands (2 bands—beta and gamma), nodes removed (90 most connected, i.e., largest nodes), and terms (the 12 chosen from the Neurosynth database) using the methods described in the previous section. The resultant correlation is plotted at the maximum correlation. The correlation value for each node removal is shown as a color map on the top of the correlation plot, marked with the white line at which LOESS regression was plotted.

RESULTS

Neurosynth Decoding for Hubs Word Cloud Generation

As noted in the introduction, in a prior study of resting state networks, we assessed the developmental trajectory of the graph

theoretic metrics of local and global efficiency from age 7 to age 29 by frequency band (22). Specifically, we tested the maturation of these two graph theoretic efficiency metrics for each of the 5 intrinsic cortical rhythms—delta (1–4 Hz), theta (4–8 Hz), alpha (8–12 Hz), beta (13–30 Hz), and gamma (31–80 Hz). We found no significant age-dependent differences for either of these metrics in the three slower frequency bands (delta, theta, and alpha). In contrast, we found significant age dependence of network efficiency in both the beta and gamma frequency bands. More specifically, we found that resting state networks mediated by the beta brain rhythm become more locally efficient with maturation, i.e., more organized into clusters and connected with nearby regions (**Figure 2A**), while networks mediated by the gamma brain rhythm become more globally efficient with maturation, i.e., prioritizing faster signal transmission between distant cortical regions (**Figure 2B**). In the same prior study, we used the betweenness centrality graph metric to identify which of the hubs associated with each of the two networks changed significantly in efficiency with age. Two categories of hubs emerged from this analysis: hubs that grew—i.e., gained nodes—with maturation, and hubs that shrunk—i.e., lost nodes—with maturation. The distribution of the hubs that grew or shrunk significantly with age in the beta band network is shown in **Figure 2C**, and the distribution of the hubs that grew or shrunk significantly with age in the gamma band network is shown in **Figure 2D**.

In order to test our hypothesis regarding the functional roles of the hubs found to grow or shrink with maturation within each of the two identified networks (in **Figures 2C,D**), and thus gain a better understanding of their functional significance, we then tested which Neurosynth terms were most associated with these hubs, for networks mediated by either the beta or gamma bands. To that end, we extracted from Neurosynth the list of terms associated with each of the regions marked in **Figures 2C,D**, as ranked in order of their relevance for that region, as ranked by Neurosynth. The statistically generated word cloud associated with these hubs is shown in **Figure 2E** for beta band-mediated networks and, in **Figure 2F**, for gamma band-mediated networks. The word clouds within each panel are further broken down by whether the hubs are growing with maturation (red), or shrinking with maturation (blue), signifying greater or reduced reliance on these hubs with maturation, respectively. The larger text corresponds to a higher combined statistical rank within Neurosynth across the corresponding regions (growing/shrinking hubs).

Maturation of Resilience, Tested Using Neurosynth-Derived Hubs

Network resilience is a metric that assesses the relative significance of a hub for maintaining the network's capacity to integrate information by removing hubs from the network, from largest to smallest in descending order and evaluating network efficiency relative to the number of nodes removed. Because resilience is evaluated using hubs, it is very well-suited to assess the potential functions of hubs. We have previously shown that resilience in beta band-mediated networks decreased with age, while resilience in gamma band-mediated networks increased with age, as illustrated in **Figure 3** (22).

To further investigate the functional roles of the mapped maturing hubs, we statistically mapped and identified the hubs associated with specific meta-analytic terms and then tested whether and how their removal from the network affected the resilience of each of the two networks. To that end, 12 Neurosynth terms were chosen, with a focus on terms that could help in differentiating bottom-up functions from top-down functions. We began by selecting three terms associated with basic visual or motor functions and, therefore, bottom-up processes: "dorsal visual" stream, "ventral visual" stream, and "motor system." We hypothesized that these sensory-centered networks are more strongly dependent on feedforward connectivity, and, therefore, should show greater age-dependent impacts in the gamma band. Indeed, we found that, for all these terms, removing their associated hubs resulted in no significant beta-mediated age effects. However, the removal of these same hubs resulted in highly significant differences in the gamma band-mediated age-dependent network resilience. More specifically, for both the dorsal visual stream and the motor system, removal of the associated hubs resulted in significantly age-dependent resilience, with greater resilience (i.e., relatively less decrease in global efficiency) in children relative to adults in the gamma band. In contrast, removal of the hubs associated with the ventral visual stream resulted in significantly age-dependent resilience in the opposite direction in the gamma band, with adults showing a significantly reduced impact on global efficiency with removal of the hubs relative to children (**Figures 4A–C**).

We then repeated the same analysis with three terms associated with cognitive functions known to be mediated by top-down processes: "Attention," "Executive" (for executive function), and "Decision." We hypothesized that networks associated with these terms are more strongly dependent on feedback connectivity and, therefore, should show greater age-dependent impacts in the beta band-mediated networks. Networks associated with these processes are also known to mature substantially during adolescence. Contrary to our hypothesis, the results for this group of cognitive terms were mixed. Using the hubs from the attention network to test resilience resulted in reduced resilience with age in both the beta and gamma bands. This means that the younger age groups were less severely impacted by the removal of the hubs than the older age groups. Using the hubs from the executive function network resulted in no effect of age and using the hubs from the decision network resulted in age-dependent resilience in the beta band only, with the older age group being less impacted than the younger age group (**Figures 4D–F**).

Lastly, we tested resilience using the hubs associated with DSM-5 disorders that are common in adolescence. This part of the analysis was data driven rather than hypothesis driven, and the aim was to test whether resilience changes associated with each of these terms manifest differentially in the networks mediated by the beta vs. the gamma bands. Specifically, we tested the changes in the resilience of the networks, with the removal of the hubs associated with the following terms: "Autism," "Obsessive-Compulsive," "Eating Disorder," "Anxiety,"

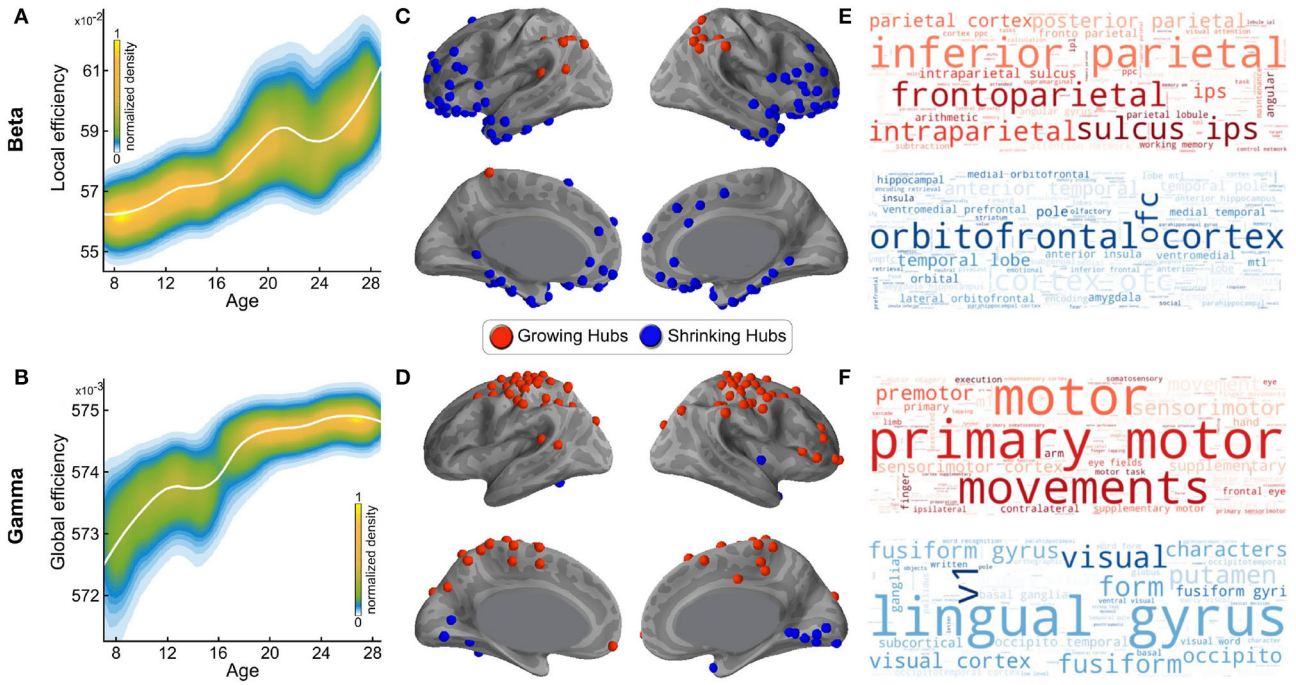

FIGURE 2 | Spatial distributions of growing and shrinking hubs and their associated word clouds. **(A)** The LOESS plot (the solid white line) for the relationship between age and local network efficiency of beta band-mediated networks. The individual data points are represented using a normalized density color map, where each data point corresponds to one realization of the bootstrap procedure. **(B)** Like **(A)**, for gamma band-mediated networks, and global efficiency instead of local efficiency. **(C)** The spatial distribution of growing and shrinking hubs in the beta band-mediated networks. **(D)** Like **(C)**, for the gamma band-mediated networks. **(E)** Word clouds generated using wordle for the first 100 terms from Neurosynth for the beta band network- growing and -shrinking hubs. Larger font size reflects higher probabilistic association. The top (red) cloud was generated using the growing hubs, and the bottom (blue) cloud was generated using the shrinking hubs. **(F)** Like **(E)**, for the gamma band-mediated networks. **(A–D)** have been adopted from Khan et al. (22).

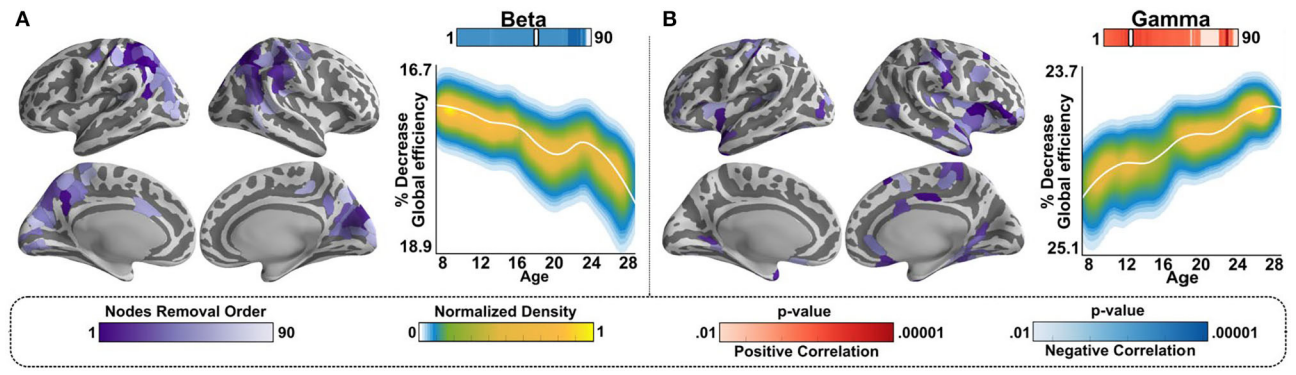

FIGURE 3 | Resilience in beta and gamma-mediated networks follows opposite developmental trajectories. **(A)**-Left panel: Hubs identified from the beta band network (**Figure 2C**) were first transformed to Neurosynth coordinates then and ranked by size. Approximately, 448 nodes in total were identified, and the order of node removal for testing resilience, by node size, is color coded on the purple color bar, thresholded to avoid saturation. **(A)**-Right panel: After each removal of a node, in ranked order, we evaluated whether there was a significant effect of age generated by the removal of that node. Shown is the LOESS plot for one instance of the effect of age at 54% of nodes removed, where significance of age effect was maximal. The individual data points are represented using a normalized density color map, where each data point corresponds to one realization of the bootstrap procedure. The top bar, labeled "Beta," shows how significant the effect of age was at any number of nodes removed, where significance is color-coded using the "*p*-value" color bars on the bottom (red for relatively increased resilience with age, blue for relatively decreased resilience with age). The white notch on the bar under "Beta" is the snapshot, i.e., number of nodes removed at that point; we chose to plot to show the weakening of resilience with age. **(B)-**Left panel: Same as **(A)**-left panel for the gamma band-mediated networks, using the hubs identified for the gamma band-mediated network (**Figure 2D**). **(B)**-Right panel: Same as **(A)**-right panel for the gamma band-mediated networks.

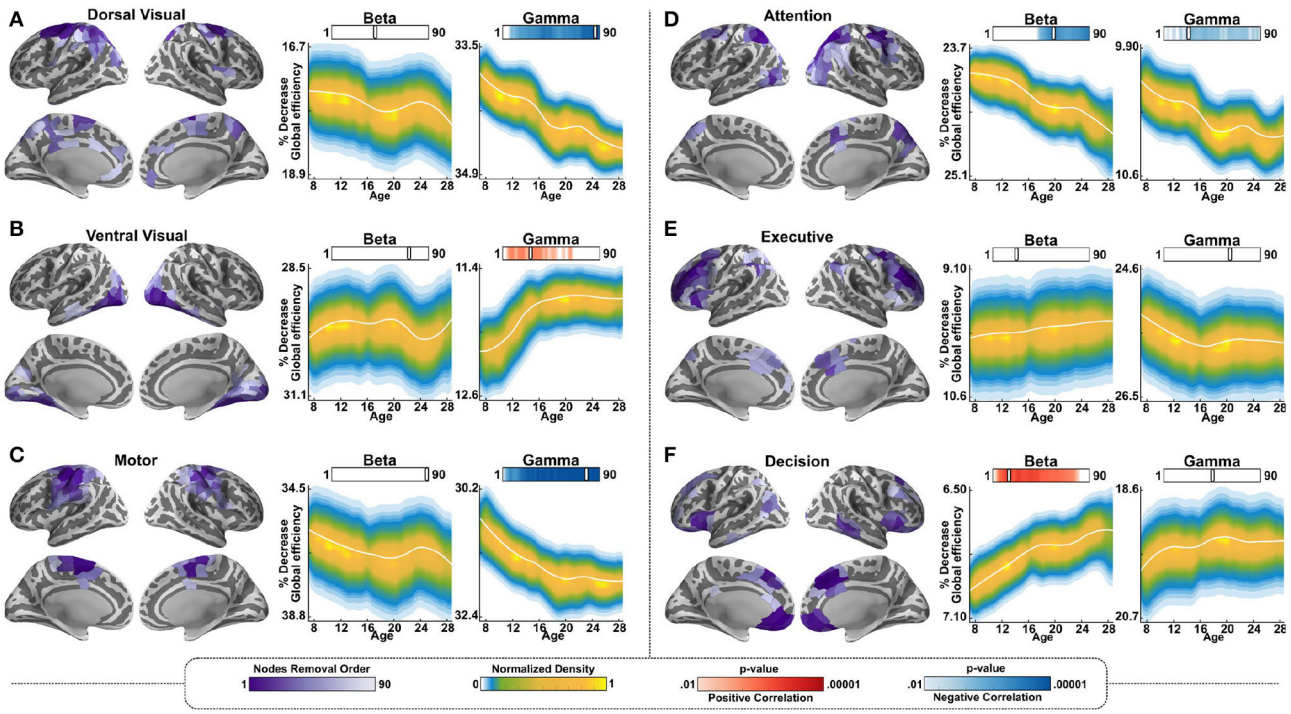

FIGURE 4 | Resilience in gamma and beta-mediated networks for relative networks associated with sensory and cognitive terms. This analysis replicated the process shown in **Figure 3**, but instead of using the actual hubs of each network, it used the largest 90 hubs determined by Neurosynth to be associated with the term being tested in descending order of size. The same hubs were used for both the beta and gamma-mediated networks. **(A)** Left side (subtitled with the relevant term): a representation on the cortex of the cortical Neurosynth nodes associated with the term "Dorsal Visual," with a rank indicated by the purple color bar at the bottom, and thresholded as in **Figures 3A,B**. The middle panel (subtitled "Beta"): Resulting resilience for the beta band network for one "snapshot" of percentage of nodes removed, marked by the notch in the bar under the word "Beta." The right panel (subtitled "Gamma"): Same as the middle panel, but for the gamma band-mediated network. **(B)** Same as **(A)** for the term "Ventral Visual." **(C)** Same as **(A)** for the term "Motor." **(D)** Same as **(A)** for the term "Attention." **(E)** Same as **(A)** for the term "Executive." **(F)** Same as **(A)** for the term "Decision." *P*-value color bars: red indicates resilience increased significantly with age, and blue indicates resilience decreased significantly with age.

Depression," and "Substance Abuse." Removal of the hubs associated with all of these disorders, with the exception of autism, resulted in increased resilience in the older participants relative to the younger participants in the beta band, similarly to the cognitive decision network. In other words, the removal of the hubs resulted in less decrease in global efficiency for the older age group relative to the younger age group. In the gamma band, an age-dependent change in resilience was observed for the terms "autism" and "anxiety"; for both of these terms, in the gamma band, resilience was significantly more impacted in the younger age groups than in the older ones by the removal of the hubs (**Figures 5A–F**).

DISCUSSION

This study aimed to test the hypothesis that maturing (growing or shrinking) hubs associated with resting state networks mediated by the beta frequency band are more likely to be associated with top-down processing while maturing hubs associated with resting state networks mediated by the gamma frequency band are more likely to be associated with bottom-up processing. The results showed that the hubs that we have previously shown to change during maturation in the gamma band-mediated network, which increased in global efficiency with age, were more likely to be statistically associated with sensory and motor terms in Neurosynth, and thus more likely to be associated with feedforward, i.e., bottom-up processes. In contrast, the hubs that we have previously shown to change during maturation in the beta band-mediated network, which increased in local efficiency with age, were more likely to be statistically associated with more terms in Neurosynth that reflect more complex cognitive function, and thus more likely to be associated with feedback, i.e., top-down processes. These findings support the hypothesis that intra-areal beta rhythm synchronizations preferentially mediate top-down functions, while intra-areal gamma rhythm synchronizations preferentially mediate bottom-up functions.

These emergent patterns are consistent with the literature in the field, showing a preferential role for the gamma band in mediating bottom-up processes, even if not exclusively so, and a preferential role for the beta band in mediating top-down processes, even if not exclusively so. More specifically, the pattern of shrinking the frontal hubs observed in the beta band is consistent with studies showing reduced frontal

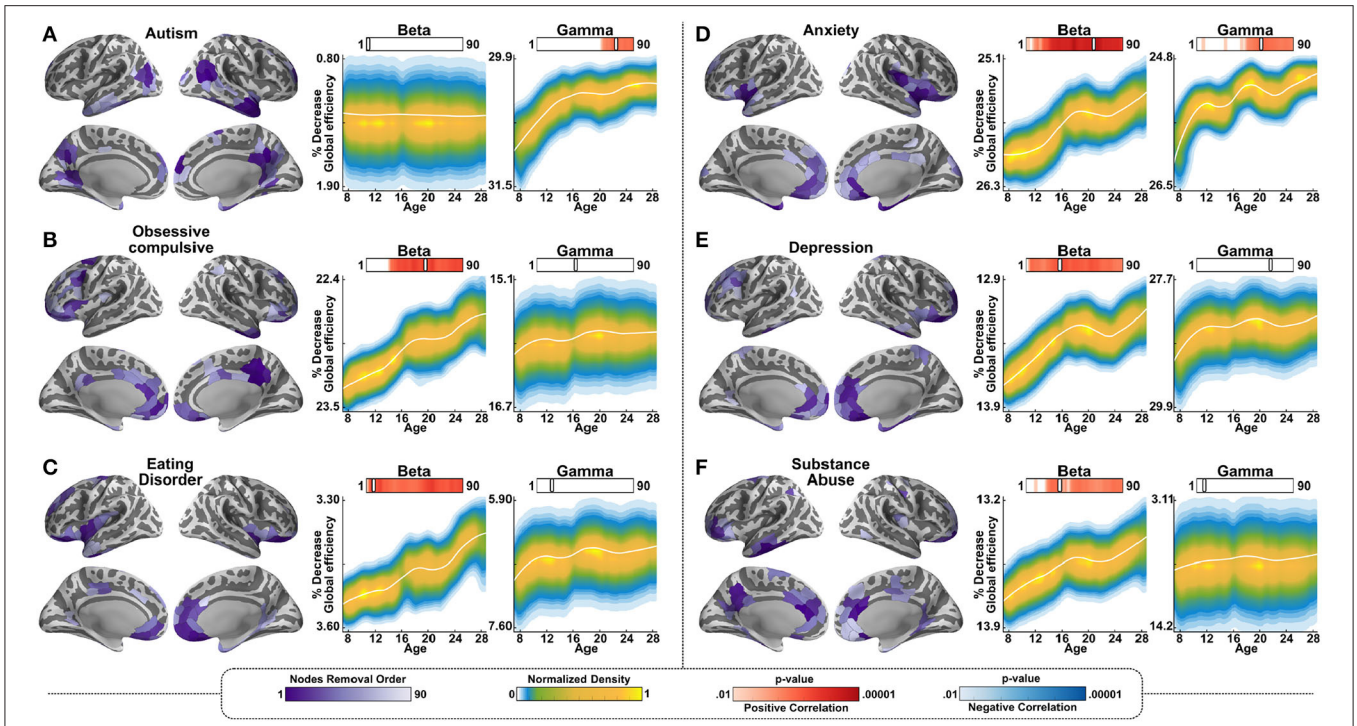

FIGURE 5 | Resilience in gamma and beta-mediated networks for relative to networks associated with psychiatric terms. The same as **Figure 4**, but for the following 6 terms: **(A)** Autism. **(B)** Obsessive Compulsive. **(C)** Eating Disorder. **(D)** Anxiety. **(E)** Depression. **(F)** Substance Abuse.

task-related activation with maturation, for instance, for inhibitory control, potentially due to increased efficiency of top-down communication, putatively mediated by the beta band (25). In line with this, the top Neurosynth terms emerging from our decoding analysis for the beta band hubs were "orbitofrontal" (shrinking hubs), "frontoparietal," and "inferior parietal" (growing hubs). These regions are associated with processes that are generally considered to be top-down, such as attentional control (70), executive control (71), and decision-making. Gamma-mediated networks showed an increase in global efficiency with maturation, which is consistent with the putative role of gamma for mediating bottom-up connectivity (17, 72) as new connections would have to be formed to carry information forward to developing frontal brain regions. Indeed, two of the top Neurosynth terms emerging from our decoding analysis for the gamma band hubs that were shrinking or growing with maturation were "primary motor" (growing) and "lingual gyrus" (shrinking). The observation that the motor, dorsal visual, and ventral visual systems showed age-dependent resilience only in the gamma band may reflect the fact that all of these processes rely heavily on feedforward inputs. In other words, these regions are associated with processes that are generally considered to be bottom-up, such as the generation of motor movements (primary motor), and the processing of visual inputs (lingual gyrus). Indeed, MEG in humans (73) and non-human primate studies (72, 74, 75) demonstrate that gamma rhythms flow up in a bottom-up direction, spreading from lower-order visual sensory regions to higher-order regions, while Beta rhythms flow in a top-down direction, spreading from higher-order multimodal regions to lower-order sensory regions.

The mixed results in the cognitive domain terms we tested for overlap in the resilience-based analysis likely reflect the far more complex processing and complex networks associated with the chosen terms—attention, executive function, and decision. The attention network is, indeed, known to be mediated heavily by both feedforward and feedback inputs in line with our results and reflects the significance of both beta and gamma to higher-order functions. The executive function network showed no age effect likely because, unlike the other terms, there were no hubs associated with it in the reverse influence analysis, which may reflect that the meta-analytics maps associated with it in Neurosynth's ranking are ambiguously defined. In contrast, the decision network clearly relies most heavily on feedback connectivity and, indeed, showed age-dependent resilience only in the beta band. The differentiation between the three analyzed groups of terms confirms that the presented results, indeed, have implications for cognitive function.

The pattern observed for terms describing psychiatric disorders using this analysis also suggests that the mediating frequency bands have specific and differential roles. Notably, five of the six chosen disorder terms are more commonly associated with the later onset (adolescence to early adulthood) and showed age-dependent resilience in the beta band. In contrast, the only disorder on the list that is considered neurodevelopmental, i.e., early origin, autism, showed age-dependent resilience only in

the gamma band. This suggests that beta band networks might not undergo normal development in autism during adolescence, and thus are particularly or more severely impacted in line with prior findings (12, 22, 76, 77). Anxiety was the only term that corresponded to networks showing age-dependent trajectories in both the beta and gamma bands differentiating it from the other tested terms. It is possible that these anxiety networks are relatively poorly defined when anxiety type is not specified, and, thus, multiple networks are captured by this term in Neurosynth. Indeed, there are many subtypes of anxiety disorders that were not differentiated in our Neurosynth search (e.g., social anxiety, performance anxiety, generalized anxiety, etc.). While the other disorders tested are typically associated with specific onset times windows (e.g., childhood for autism, adolescence for eating disorders or depression), anxiety can arise at any age, and, therefore, a maturation trajectory for its corresponding networks may not be as well-defined as it is for the other disorder terms tested.

A potential limitation of this paper is that it sought to build on prior results to further refine our understanding of these results. Because the prior results only showed age-dependent changes in the beta and gamma band-mediated networks, we only focused on these two networks here too and did not examine the hubs associated with the delta, theta, and alpha bands. It is possible that specific hubs within those networks do show age-dependent differences even if the network as a whole does not. It is also possible that age-dependent bandwidth changes within specific bands, which were not considered in the prior study, might have an impact on maturation trajectories in the slower frequency bands in particular. Future studies are needed to further elucidate these questions.

This study added meta-analytic tools to our prior study of frequency-specific maturation of resting state networks. The goal of these additional analyses was to assess the potential functional significance of the hubs identified in the prior study. While it is clear that both beta band and gamma band-mediated resting state network networks are highly complex and contribute to processing in a multitude of ways that are not necessarily or exclusively direction specific, the Neurosynth-derived results are, overall, consistent with our prior hypotheses that beta band-mediated networks are likely to be more heavily weighted toward top-down processing, while gamma band-mediated networks are likely to be more heavily weighted toward bottom-up processing. Mechanistically, both of these cortical rhythms are mediated by GABAergic systems (15, 78); the maturation of GABAergic processes extends well into adolescence and early adulthood (79), and the maturation of GABAergic systems likely also underlie the maturation of these cortical networks, and thus hub topology. Thus, the maturation of GABAergic systems is highly likely to influence the maturation of both networks and mediates developmental changes in both bottom-up and top-down processing. Lastly, this study demonstrates that Neurosynth can be employed to investigate the functional role of networks and their hubs, even in the absence of direct functional data.

DATA AVAILABILITY STATEMENT

The raw data available for sharing will be provided by the authors following the approval of the required Massachusetts General Hospital Sharing Agreement. Requests should be directed to the corresponding author(s).

ETHICS STATEMENT

The studies involving human participants were reviewed and approved by Massachusetts General Hospital IRB Board. Written informed consent to participate in this study was provided by the participants' legal guardian/next of kin for minors, and by the participants themselves for adults.

AUTHOR CONTRIBUTIONS

SK, JAH, FM, MSH, and TK designed the study. SK, JAH, and FM analyzed the data. SK, JAH, FM, and TK wrote the paper. All authors contributed to the article and approved the submitted version.

FUNDING

This work was supported by grants from the Simons Foundation (SFARI 239395; TK), the National Institute of Child Health and Development (R01HD073254; TK), the National Institute of Mental Health (R01MH117998 and R21MH116517; TK), the National Institute for Biomedical Imaging and Bioengineering (P41EB01589 and P41EB030006; MSH), and the National Institute of Neurological Disorders and Stroke (R01NS104585; MSH).

REFERENCES

1. Luna B, Thulborn KR, Munoz DP, Merriam EP, Garver KE, Minshew NJ, et al. Maturation of widely distributed brain function subserves cognitive development. *Neuroimage.* (2001) 13:786–93. doi: 10.1006/nimg.2000.0743
2. Hwang K, Hallquist MN, Luna B. The development of hub architecture in the human functional brain network. *Cereb Cortex.* (2013) 23:2380–93. doi: 10.1093/cercor/bhs227
3. Achard S, Salvador R, Whitcher B, Suckling J, Bullmore E. A resilient, low-frequency, small-world human brain functional network with highly connected association cortical hubs. *J Neurosci.* (2006) 26:63–72. doi: 10.1523/JNEUROSCI.3874-05.2006
4. Zamora-Lopez G, Zhou C, Kurths J. Cortical hubs form a module for multisensory integration on top of the hierarchy of cortical networks. *Front Neuroinform.* (2010) 4:1. doi: 10.3389/neuro.11.001.2010
5. Crossley NA, Mechelli A, Scott J, Carletti F, Fox PT, Mcguire P, et al. The hubs of the human connectome are generally implicated in the anatomy of brain disorders. *Brain.* (2014) 137:2382–95. doi: 10.1093/brain/awu132
6. Raichle ME, Macleod AM, Snyder AZ, Powers WJ, Gusnard DA, Shulman GL. A default mode of brain function. *Proc Natl Acad Sci USA.* (2001) 98:676–82. doi: 10.1073/pnas.98.2.676

7. Broyd SJ, Demanuele C, Debener S, Helps SK, James CJ, Sonuga-Barke EJ. Default-mode brain dysfunction in mental disorders: a systematic review. *Neurosci Biobehav Rev.* (2009) 33:279–96. doi: 10.1016/j.neubiorev.2008.09.002
8. Fair DA, Cohen AL, Power JD, Dosenbach NU, Church JA, Miezin FM, et al. Functional brain networks develop from a "local to distributed" organization. *PLoS Comput Biol.* (2009) 5:e1000381. doi: 10.1371/journal.pcbi.1000381
9. Dosenbach NU, Nardos B, Cohen AL, Fair DA, Power JD, Church JA, et al. Prediction of individual brain maturity using fMRI. *Science.* (2010) 329:1358–61. doi: 10.1126/science.1194144
10. Grayson DS, Ray S, Carpenter S, Iyer S, Dias TG, Stevens C, et al. Structural and functional rich club organization of the brain in children and adults. *PLoS ONE.* (2014) 9:e88297. doi: 10.1371/journal.pone.0088297
11. Toussaint PJ, Maiz S, Coynel D, Doyon J, Messe A, De Souza LC, et al. Characteristics of the default mode functional connectivity in normal ageing and Alzheimer's disease using resting state fMRI with a combined approach of entropy-based and graph theoretical measurements. *Neuroimage.* (2014) 101:778–86. doi: 10.1016/j.neuroimage.2014.08.003
12. Kitzbichler MG, Khan S, Ganesan S, Vangel MG, Herbert MR, Hämäläinen MS, et al. Altered development and multifaceted band-specific abnormalities of resting state networks in autism. *Biol Psychiatry.* (2015) 77:794–804. doi: 10.1016/j.biopsych.2014.05.012
13. Raichle ME. The brain's default mode network. *Annu Rev Neurosci.* (2015) 38:433–47. doi: 10.1146/annurev-neuro-071013-014030
14. Uhlhaas P, Singer W. Neural synchrony in brain disorders: relevance for cognitive dysfunctions and pathophysiology. *Neuron.* (2006) 52:155–68. doi: 10.1016/j.neuron.2006.09.020
15. Uhlhaas PJ, Haenschel C, Nikolic D, Singer W. The role of oscillations and synchrony in cortical networks and their putative relevance for the pathophysiology of schizophrenia. *Schizophr Bull.* (2008) 34:927–43. doi: 10.1093/schbul/sbn062
16. Uhlhaas PJ, Roux F, Rodriguez E, Rotarska-Jagiela A, Singer W. Neural synchrony and the development of cortical networks. *Trends Cogn Sci.* (2010) 14:72–80. doi: 10.1016/j.tics.2009.12.002
17. Wang XJ. Neurophysiological and computational principles of cortical rhythms in cognition. *Physiol Rev.* (2010) 90:1195–268. doi: 10.1152/physrev.00035.2008
18. Uhlhaas PJ, Singer W. The development of neural synchrony and large-scale cortical networks during adolescence: relevance for the pathophysiology of schizophrenia and neurodevelopmental hypothesis. *Schizophr Bull.* (2011) 37:514–23. doi: 10.1093/schbul/sbr034
19. Uhlhaas PJ. Neural dynamics in mental disorders. *World Psychiatry.* (2015) 14:116–8. doi: 10.1002/wps.20203
20. Seymour RA, Rippon G, Gooding-Williams G, Schoffelen JM, Kessler K. Dysregulated oscillatory connectivity in the visual system in autism spectrum disorder. *Brain.* (2019) 142:3294–305. doi: 10.1093/brain/awz214
21. Uhlhaas P. Neural synchrony in cortical networks: history, concept and current status. *Front Integr Neurosci.* (2009) 3:17. doi: 10.3389/neuro.07.017.2009
22. Khan S, Hashmi JA, Mamashli F, Michmizos K, Kitzbichler MG, Bharadwaj H, et al. Maturation trajectories of cortical resting-state networks depend on the mediating frequency band. *Neuroimage.* (2018) 174:57–68. doi: 10.1016/j.neuroimage.2018.02.018
23. Fransson P, Aden U, Blennow M, Lagercrantz H. The functional architecture of the infant brain as revealed by resting-state fMRI. *Cereb Cortex.* (2011) 21:145–54. doi: 10.1093/cercor/bhq071
24. Menon V. Developmental pathways to functional brain networks: emerging principles. *Trends Cogn Sci.* (2013) 17:627–40. doi: 10.1016/j.tics.2013.09.015
25. Buschman TJ, Miller EK. Top-down versus bottom-up control of attention in the prefrontal and posterior parietal cortices. *Science.* (2007) 315:1860–2. doi: 10.1126/science.1138071
26. Ordaz SJ, Foran W, Velanova K, Luna B. Longitudinal growth curves of brain function underlying inhibitory control through adolescence. *J Neurosci.* (2013) 33:18109–24. doi: 10.1523/JNEUROSCI.1741-13.2013
27. Yarkoni T, Poldrack RA, Nichols TE, Van Essen DC, Wager TD. Large-scale automated synthesis of human functional neuroimaging data. *Nat Methods.* (2011) 8:665–70. doi: 10.1038/nmeth.1635
28. Shehzad Z, Kelly C, Reiss PT, Cameron Craddock R, Emerson JW, Mcmahon K, et al. A multivariate distance-based analytic framework for connectome-wide association studies. *Neuroimage.* (2014) 93(Pt 1):74–94. doi: 10.1016/j.neuroimage.2014.02.024
29. Bajada CJ, Haroon HA, Azadbakht H, Parker GJM, Lambon Ralph MA, Cloutman LL. The tract terminations in the temporal lobe: their location and associated functions. *Cortex.* (2017) 97:277–90. doi: 10.1016/j.cortex.2016.03.013
30. Cheng W, Rolls ET, Zhang J, Sheng W, Ma L, Wan L, et al. Functional connectivity decreases in autism in emotion, self, and face circuits identified by Knowledge-based Enrichment Analysis. *Neuroimage.* (2017) 148:169–78. doi: 10.1016/j.neuroimage.2016.12.068
31. Nummenmaa L, Hari R, Hietanen JK, Glerean E. Maps of subjective feelings. *Proc Natl Acad Sci USA.* (2018) 115:9198–203. doi: 10.1073/pnas.1807390115
32. Park MTM, Raznahan A, Shaw P, Gogtay N, Lerch JP, Chakravarty MM. Neuroanatomical phenotypes in mental illness: identifying convergent and divergent cortical phenotypes across autism, ADHD and schizophrenia. *J Psychiatry Neurosci.* (2018) 43:201–12. doi: 10.1503/jpn.170094
33. Wang S, Tepfer LJ, Taren AA, Smith DV. Functional parcellation of the default mode network: a large-scale meta-analysis. *Sci Rep.* (2020) 10:16096. doi: 10.1038/s41598-020-72317-8
34. Kaufman AS, Kaufman NL. *Kaufman Brief Intelligence Test*. 2nd ed. MN: AGS Publishing (2004).
35. Dale AM, Fischl B, Sereno MI. Cortical surface-based analysis. I Segmentation and surface reconstruction. *Neuroimage.* (1999) 9:179–94. doi: 10.1006/nimg.1998.0395
36. Fischl B, Sereno MI, Dale AM. Cortical surface-based analysis. II: Inflation, flattening, and a surface-based coordinate system. *Neuroimage.* (1999) 9:195–207. doi: 10.1006/nimg.1998.0396
37. Khan S, Cohen D. Note: magnetic noise from the inner wall of a magnetically shielded room. *Rev Sci Instrum.* (2013) 84:056101. doi: 10.1063/1.4802845
38. Larson E, Taulu S. The importance of properly compensating for head movements during MEG acquisition across different age groups. *Brain Topogr.* (2017) 30:172–81. doi: 10.1007/s10548-016-0523-1
39. Taulu S, Kajola M, Simola J. Suppression of interference and artifacts by the Signal Space Separation Method. *Brain Topogr.* (2004) 16:269–75. doi: 10.1023/B:BRAT.0000032864.93890.f9
40. Taulu S, Simola J. Spatiotemporal signal space separation method for rejecting nearby interference in MEG measurements. *Phys Med Biol.* (2006) 51:1759–68. doi: 10.1088/0031-9155/51/7/008
41. Vidaurre C, Sander TH, Schlogl A. BioSig: the free and open source software library for biomedical signal processing. *Comput Intell Neurosci.* (2011) 2011:935364. doi: 10.1155/2011/935364
42. Nolte G, Hämäläinen MS. Partial signal space projection for artefact removal in MEG measurements: a theoretical analysis. *Phys Med Biol.* (2001) 46:2873–87. doi: 10.1088/0031-9155/46/11/308
43. Gramfort A, Luessi M, Larson E, Engemann DA, Strohmeier D, Brodbeck C, et al. MEG and EEG data analysis with MNE-Python. *Front Neurosci.* (2013) 7:267. doi: 10.3389/fnins.2013.00267
44. Hämäläinen MS, Sarvas J. Realistic conductivity geometry model of the human head for interpretation of neuromagnetic data. *IEEE Trans Biomed Eng BME-36.* (1989) 165–71. doi: 10.1109/10.16463
45. Dale AM, Liu AK, Fischl BR, Buckner RL, Belliveau JW, Lewine JD, et al. Dynamic statistical parametric mapping: combining fMRI and MEG for high-resolution imaging of cortical activity. *Neuron.* (2000) 26:55–67. doi: 10.1016/S0896-6273(00)81138-1
46. Lin FH, Witzel T, Ahlfors SP, Stufflebeam SM, Belliveau JW, Hämäläinen MS. Assessing and improving the spatial accuracy in MEG source localization by depth-weighted minimum-norm estimates. *Neuroimage.* (2006) 31:160–71. doi: 10.1016/j.neuroimage.2005.11.054
47. Gramfort A, Luessi M, Larson E, Engemann DA, Strohmeier D, Brodbeck C, et al. MNE software for processing MEG and EEG data. *Neuroimage.* (2014) 86:446–60. doi: 10.1016/j.neuroimage.2013.10.027
48. Fischl B, Van Der Kouwe A, Destrieux C, Halgren E, Segonne F, Salat DH, et al. Automatically parcellating the human cerebral cortex. *Cereb Cortex.* (2004) 14:11–22. doi: 10.1093/cercor/bhg087

49. Colclough G, Woolrich M, Tewarie P, Brookes M, Quinn A, Smith S. How reliable are MEG resting-state connectivity metrics? *Neuroimage.* (2016) 138:284–93. doi: 10.1016/j.neuroimage.2016.05.070
50. Brookes MJ, Woolrich M, Luckhoo H, Price D, Hale JR, Stephenson MC, et al. Investigating the electrophysiological basis of resting state networks using magnetoencephalography. *Proc Nat Acad Sci USA.* (2011) 108:16783–8. doi: 10.1073/pnas.1112685108
51. Vidal JR, Freyermuth S, Jerbi K, Hamamé CM, Ossandon T, Bertrand O, et al. Long-distance amplitude correlations in the high gamma band reveal segregation and integration within the reading network. *J Neurosci.* (2012) 32:6421–34. doi: 10.1523/JNEUROSCI.4363-11.2012
52. Wang L, Saalmann YB, Pinsk MA, Arcaro MJ, Kastner S. Electrophysiological low-frequency coherence and cross-frequency coupling contribute to BOLD connectivity. *Neuron.* (2012) 76:1010–20. doi: 10.1016/j.neuron.2012.09.033
53. Brookes MJ, Tewarie PK, Hunt BA, Robson SE, Gascoyne LE, Liddle EB, et al. A multi-layer network approach to MEG connectivity analysis. *Neuroimage.* (2016) 132:425–38. doi: 10.1016/j.neuroimage.2016.02.045
54. Sekihara K, Owen JP, Trisno S, Nagarajan SS. Removal of spurious coherence in MEG source-space coherence analysis. *IEEE Trans Biomed Eng.* (2011) 58:3121–9. doi: 10.1109/TBME.2011.2162514
55. Hipp JF, Hawellek DJ, Corbetta M, Siegel M, Engel AK. Large-scale cortical correlation structure of spontaneous oscillatory activity. *Nat Neurosci.* (2012) 15:884–90. doi: 10.1038/nn.3101
56. Bullmore E, Sporns O. Complex brain networks: graph theoretical analysis of structural and functional systems. Nature reviews. *Neuroscience.* (2009) 10:186–98. doi: 10.1038/nrn2575
57. Misic B, Betzel RF, De Reus MA, Van Den Heuvel MP, Berman MG, Mcintosh AR, et al. Network-level structure-function relationships in human neocortex. *Cereb Cortex.* (2016) 26:3285–96. doi: 10.1093/cercor/bhw089
58. Bassett DS, Sporns O. Network neuroscience. *Nat Neurosci.* (2017) 20:353–64. doi: 10.1038/nn.4502
59. Achard S, Bullmore E. Efficiency and cost of economical brain functional networks. *PLoS Comput Biol.* (2007) 3:e17. doi: 10.1371/journal.pcbi.0030017
60. Peng G-S, Tan S-Y, Wu J, Holme P. Trade-offs between robustness and small-world effect in complex networks. *Sci Rep.* (2016) 6:37317. doi: 10.1038/srep37317
61. Watts DJ, Strogatz SH. Collective dynamics of 'small-world'networks. *Nature.* (1998) 393:440–2. doi: 10.1038/30918
62. Lo CY, Su TW, Huang CC, Hung CC, Chen WL, Lan TH, et al. Randomization and resilience of brain functional networks as systems-level endophenotypes of schizophrenia. *Proc Natl Acad Sci USA.* (2015) 112:9123–8. doi: 10.1073/pnas.1502052112
63. Spielberg JM, Miller GA, Heller W, Banich MT. Flexible brain network reconfiguration supporting inhibitory control. *Proc Natl Acad Sci USA.* (2015) 112:10020–5. doi: 10.1073/pnas.1500048112
64. Groppe DM, Urbach TP, Kutas M. Mass univariate analysis of event-related brain potentials/fields I: a critical tutorial review. *Psychophysiology.* (2011) 48:1711–25. doi: 10.1111/j.1469-8986.2011.01273.x
65. Pernet CR, Wilcox R, Rousselet GA. Robust correlation analyses: false positive and power validation using a new open source matlab toolbox. *Front Psychol.* (2013) 3:606. doi: 10.3389/fpsyg.2012.00606
66. Cleveland WS, Loader C. Smoothing by local regression: principles and methods. In: *Statistical Theory and Computational Aspects of Smoothing.* Springer. (1996) p. 10–49. doi: 10.1007/978-3-642-48425-4_2
67. Webel K. K. Takezawa: introduction to nonparametric regression. *Allgemeines Statistisches Archiv.* (2006) 90:625–6. doi: 10.1007/s10182-006-0007-9
68. Anderson DK, Maye MP, Lord C. Changes in maladaptive behaviors from midchildhood to young adulthood in autism spectrum disorder. *Am J Intellect Dev Disabil.* (2011) 116:381–97. doi: 10.1352/1944-7558-116.5.381
69. Picci G, Scherf KS. A two-hit model of autism: adolescence as the second hit. *Clin Psychol Sci.* (2015) 3:349–71. doi: 10.1177/2167702614540646
70. Scolari M, Seidl-Rathkopf KN, Kastner S. Functions of the human frontoparietal attention network: evidence from neuroimaging. *Curr Opin Behav Sci.* (2015) 1:32–9. doi: 10.1016/j.cobeha.2014.08.003
71. Dixon ML, De La Vega A, Mills C, Andrews-Hanna J, Spreng RN, Cole MW, et al. Heterogeneity within the frontoparietal control network and its relationship to the default and dorsal attention networks. *Proc Natl Acad Sci USA.* (2018) 115:E1598–607. doi: 10.1073/pnas.1715766115
72. Bastos AM, Vezoli J, Bosman CA, Schoffelen J-M, Oostenveld R, Dowdall JR, et al. Visual areas exert feedforward and feedback influences through distinct frequency channels. *Neuron.* (2015) 85:390–401. doi: 10.1016/j.neuron.2014.12.018
73. Michalareas G, Vezoli J, Van Pelt S, Schoffelen JM, Kennedy H, Fries P. Alpha-beta and gamma rhythms subserve feedback and feedforward influences among human visual cortical areas. *Neuron.* (2016) 89:384–97. doi: 10.1016/j.neuron.2015.12.018
74. Zheng C, Colgin LL. Beta and gamma rhythms go with the flow. *Neuron.* (2015) 85:236–7. doi: 10.1016/j.neuron.2014.12.067
75. Miller EK, Lundqvist M, Bastos AM. Working memory 2.0. *Neuron.* (2018) 100:463–75. doi: 10.1016/j.neuron.2018.09.023
76. Mamashli F, Khan S, Bharadwaj H, Losh A, Pawlyszyn SM, Hamalainen MS, et al. Maturational trajectories of local and long-range functional connectivity in autism during face processing. *Hum Brain Mapp.* (2018) 39:4094–104. doi: 10.1002/hbm.24234
77. Mamashli F, Kozhemiako N, Khan S, Nunes AS, Mcguiggan NM, Losh A, et al. Children with autism spectrum disorder show altered functional connectivity and abnormal maturation trajectories in response to inverted faces. *Autism Res.* (2021) 14:1101–14. doi: 10.1002/aur.2497
78. Sohal VS, Zhang F, Yizhar O, Deisseroth K. Parvalbumin neurons and gamma rhythms enhance cortical circuit performance. *Nature.* (2009) 459:698–702. doi: 10.1038/nature07991
79. Kilb W. Development of the GABAergic system from birth to adolescence. *Neuroscientist.* (2012) 18:613–30. doi: 10.1177/1073858411422114

Conflict of Interest: The authors declare that the research was conducted in the absence of any commercial or financial relationships that could be construed as a potential conflict of interest.

Publisher's Note: All claims expressed in this article are solely those of the authors and do not necessarily represent those of their affiliated organizations, or those of the publisher, the editors and the reviewers. Any product that may be evaluated in this article, or claim that may be made by its manufacturer, is not guaranteed or endorsed by the publisher.

frontiers | Frontiers in Neurology

METHODS
published: 28 June 2022
doi: 10.3389/fneur.2022.828237

Speech Kinematics and Coordination Measured With an MEG-Compatible Speech Tracking System

Ioanna Anastasopoulou[1]*, *Pascal van Lieshout*[2], *Douglas O. Cheyne*[2,3] and *Blake W. Johnson*[1]*

[1] School of Psychological Sciences, Macquarie University, Sydney, NSW, Australia, [2] Department of Speech-Language Pathology, University of Toronto, Toronto, ON, Canada, [3] Hospital for Sick Children Research Institute, Toronto, ON, Canada

Articulography and functional neuroimaging are two major tools for studying the neurobiology of speech production. Until recently, however, it has generally not been possible to use both in the same experimental setup because of technical incompatibilities between the two methodologies. Here we describe results from a novel articulography system dubbed Magneto-articulography for the Assessment of Speech Kinematics (MASK), which we used to derive kinematic profiles of oro-facial movements during speech. MASK was used to characterize speech kinematics in two healthy adults, and the results were compared to measurements from a separate participant with a conventional Electromagnetic Articulography (EMA) system. Analyses targeted the gestural landmarks of reiterated utterances /ipa/, /api/ and /pataka/. The results demonstrate that MASK reliably characterizes key kinematic and movement coordination parameters of speech motor control. Since these parameters are intrinsically registered in time with concurrent magnetoencephalographic (MEG) measurements of neuromotor brain activity, this methodology paves the way for innovative cross-disciplinary studies of the neuromotor control of human speech production, speech development, and speech motor disorders.

Keywords: magnetoencephalography, speech motor control, speech coordination, speech disorders, speech kinematics, Articulatory Phonology

OPEN ACCESS

Edited by:
Rafeed Alkawadri, University of Pittsburgh Medical Center, United States

Reviewed by:
Adriano Vilela Barbosa, Federal University of Minas Gerais, Brazil
Jun Wang, University of Texas at Austin, United States

***Correspondence:**
Ioanna Anastasopoulou
ioanna.anastasopoulou@mq.edu.au
Blake W. Johnson
blake.johnson@mq.edu.au

Specialty section:
This article was submitted to Applied Neuroimaging, a section of the journal Frontiers in Neurology

Received: *03 December 2021*
Accepted: *06 June 2022*
Published: *28 June 2022*

Citation:
Anastasopoulou I, van Lieshout P, Cheyne DO and Johnson BW (2022) Speech Kinematics and Coordination Measured With an MEG-Compatible Speech Tracking System. Front. Neurol. 13:828237. doi: 10.3389/fneur.2022.828237

INTRODUCTION

While it is relatively straightforward to measure the acoustic consequences of speaking with audio recordings, measuring, and characterizing the physical movements (motor behaviors) that produce acoustic speech signals presents some more formidable challenges. These challenges are due to the inaccessible nature of many of the components of the vocal tract, which are completely or largely hidden from direct view within the laryngeal cavity, the pharynx, the nasal cavity, and the oral cavity. One approach is to simply limit measurements to line-of-sight movements of the lips and jaw, which can be readily characterized with optical (video) tracking and facial capture systems with added precision from placement of reflective (1–4) or active (5) markers. When the focus of interest extends to non-line-of-sight movements researchers must turn to techniques capable of imaging within the cavities of the vocal tract. X-ray microbeam imaging with tongue pellets (6) was originally applied to track tongue movements, and the capability to routinely image movements within the oral cavity has subsequently

been extended with ultrasound techniques (7). The more recent advent of real time speech MRI (8) extends speech imaging to visualization of deep soft-tissue structures such as the velum, pharyngeal wall, and the larynx [for a brief overview of these methods, see (9)].

Electromagnetic articulography (EMA; also termed electromagnetic midsagittal articulography or EMMA for older versions of this technology) was developed to image within the oral cavity by tracking movements of marker coils placed on the tongue (10). Movement of the markers within an external magnetic field induces a current in the marker coils and provides high temporal and spatial resolution tracking of movements in real time [see also e.g., Gonzalez et al. (11), Sebkhi et al. (12) for a more recent and contrasting approach using permanent magnet markers and external magnetic sensors]. The tracking coils can also be placed on the lips and jaw and hence this technique provides a powerful method for studies with a focus of interest on intra- and inter-articulator coordination during speech production (13). Relative to other speech tracking techniques, EMA provides more access to the oral cavity than optical methods, better spatiotemporal resolution than ultrasound, and the equipment is considerably more accessible for routine speech research than X-ray beam and MRI speech imaging. As a consequence, EMA has become a central and de-facto standard methodology for research in basic speech science (14) and in neurological disorders of speech motor control (15, 16).

Commercial EMA systems, the Carstens AG series (Carstens Medizenelektronik GmbH, Bovenden, Germany), the recently discontinued NDI Wave [NDI, Waterloo, Canada; see (17)] and other speech tracking methodologies have been crucially important in advancing our understanding of normal and pathological speech behaviors at a very detailed level within the vocal tract. At the same time at the level of the brain, functional neuroimaging techniques have strongly advanced our understanding of the neural activities in centers that control speech movements of the vocal tract. At the present time, however, there remains a fundamental mismatch between the detailed kinematic information available from speech tracking and our understanding of how these parameters are represented and implemented by neural systems. This is because neuroimaging scanners are incompatible with conventional speech tracking technologies (with the exception of video tracking): Ferromagnetic components of movement tracking devices cannot be used within the strong magnetic fields of MRI scanners; and conversely, the electromagnetic fields generated by these devices would swamp the magnetic sensors of MEG scanners. As such, neuroimaging and articulographic studies of speech motor control are typically conducted separately, usually by separate teams of investigators, and it remains difficult to reconcile in detail the results obtained from central vs. peripheral studies of speech neuromotor control. As a consequence, the two types of methods have conventionally been developed and applied in quite separate academic and scientific disciplines: Articulography has been the preferred method in speech science, experimental phonology and speech language pathology, while neuroimaging is a preferred technique in neurolinguistics and cognitive neuroscience. Hence neuroimaging studies have not been able to make use of the detailed information about speech movements of the major articulators provided by articulography, relying instead on simple indices like speech onsets that provide only indirect and very limited indications of the precise movement trajectories of individual articulators. Conversely, articulography measurements have no access to information about the neural activities that generate and control speech movements. The neuroimaging and articulographic aspects of speech production have therefore developed to date as separate and largely independent literatures.

Recent advances in our understanding of speech motor control indicate that it would be advantageous to have access to both types of information in studies of speech production. Most notably, a study by Chartier et al. (18) used ultrasound and video recording of speech movements in conjunction with invasive electrocorticography (ECoG) measurements of neural activity in speech motor cortex of human patients prior to surgery for intractable epilepsy. This study reported that speech motor cortex primarily encodes information about kinematic parameters derived from measurements of the speech movements, rather than acoustic or phonemic parameters derivable from the acoustic speech signal.

The recent development of a magnetoencephalograpic (MEG) scanner-compatible speech tracking system (19) finally opens the door for studies that combine high precision measurements of articulator movements with concurrent measurements of the brain activies that control them, at the same time scale and within the same experimental setup. Alves et al. (19) termed the speech tracking system "Magnetoencephalography for the Assessment of Speech Kinematics (MASK)." The MASK system[1] tracks the independent motion of up to 12 lightweight coils similar in size and shape to the tracking coils used in EMA [see Alves et al. (19), **Figure 1**]. In an EMA setup, position and orientation of coils are computed from electrical currents passively induced by their movements within a static magnetic field. In contrast, MASK uses active coils energized by sinusoidal currents, whose associated magnetic fields are measured by the MEG sensors. By driving the tracking coils at frequencies greater than about 200 Hz, coil fields can readily be separated by low pass filtering from brain acitivities that are primarily found at frequencies less than about 100 Hz. Coil positions are then localized using the same computational algorithms used in conventional MEG to localize and track head positioning and movement. Importantly, this system does not require line-of-sight tracking, allowing for measurements from all oral articulators including the tongue. As Alves et al. (19) have reported, the MASK system can track articulator movements at rates up to 50 cm/s. The spatial accuracy of MASK is dependent on the distance of the tracking coils from the MEG sensor array. For coils close to the array (e.g., tongue) accuracy is <1 mm relative position error (as with standard MEG head position indicator coils); for coils more distant from the helmet sensor

[1]The current study used a second generation of the equipment described by Alves et al. (19), with improved electronic design, an increase in number of channels (from 12 to 16), and an increased current output per channel (from 1 to 2 mA) for greater signal amplitude and improved signal to noise ratio.

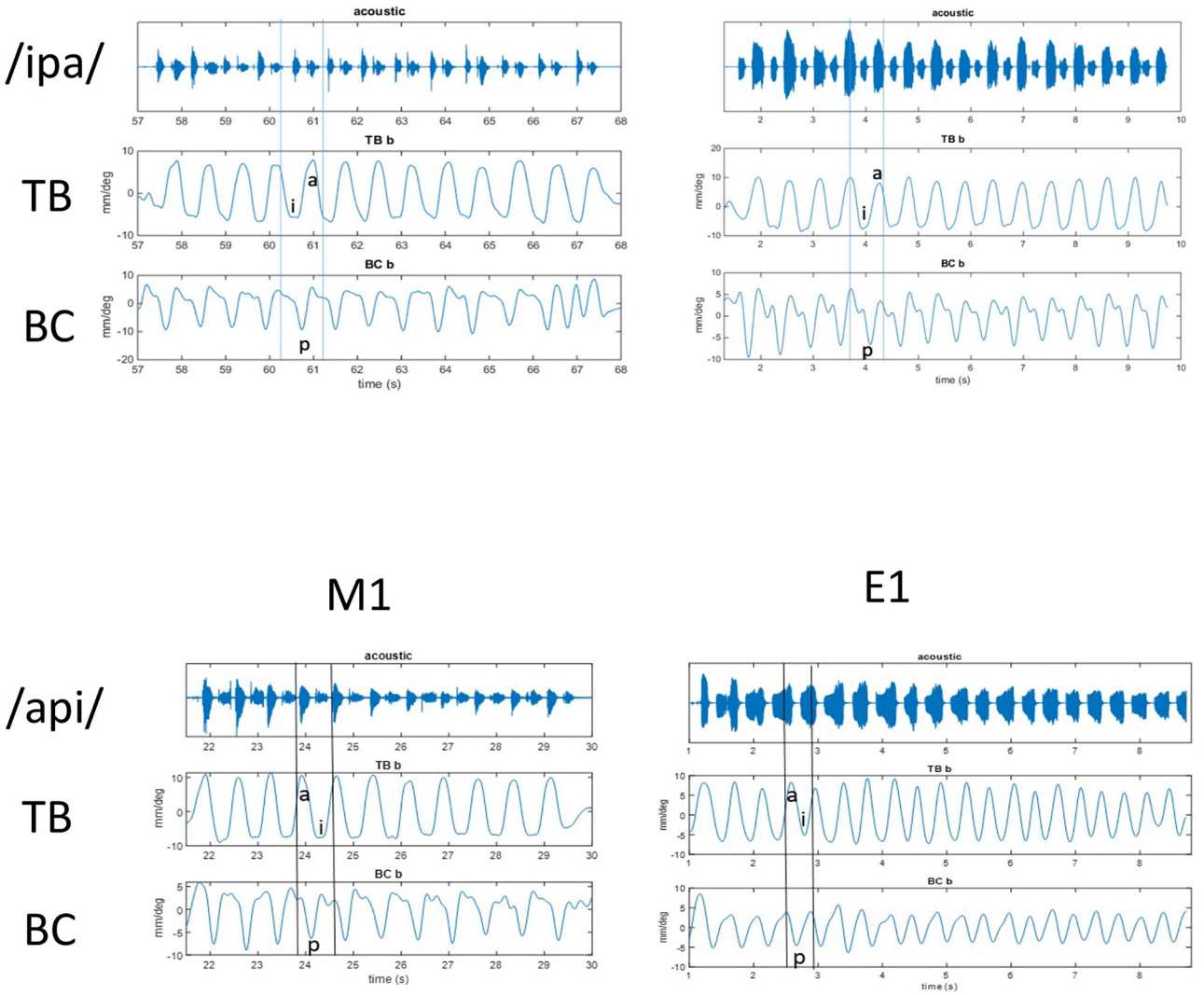

FIGURE 1 | Top: Acoustic and kinematic data for repeated [ipa] stimuli at normal rate in MASK (left) and EMA (right). Shown are (from top to bottom) waveform with audio signal, tongue body gesture (TB), and bilabial constriction (BC). Vowel positions are indicated for the 5th reiteration in TB signal and lip closure is indicated for BC signal at same time interval. **Bottom:** Acoustic and kinematic data for repeated [api] stimuli at normal rate in MASK (left) and EMA (right). Shown are (from top to bottom) acoustic signal, tongue body gesture (TB), and bilabial constriction (BC). Vowel positions are indicated for the 4th reiteration in TB signal and lip closure is indicated for BC signal at same time interval.

array (e.g., lower lip) spatial accuracy decreases in a non-linear manner to ∼1–2 mm.

The current study extends the description of MASK motion tracking capabilities by Alves et al. (19) with a description of MASK capabilities for extraction of higher level kinematic and coordination parameters from the basic movement tracking time series. We aimed to characterize these parameters for speech productions elicited within a standardized reiterated speech production paradigm; to provide a comparison of MASK-derived kinematics with those derived from tracking signals from a conventional EMA system; and to ground the current results from both techniques within the context of the published literature on speech motor control. For the purposes of this "paves the way" special topic issue, we restrict the scope of the current report to a detailed description of MASK-derived kinematics from two participants and will describe the downstream processing of speech-related neuromagnetic data from a larger group of participants in a separate report. Accordingly, the present results pave the way for novel studies of neuromotor control of speech, by providing precise kinematic and coordinative characterization of speech movements, that are intrinsically coregistered in time with MEG measurements of the brain activities that control those movements.

METHODS

Participants

Three healthy adults with typical developmental histories participated in this study: E1 (F, 30 years, bilingual Hindi/Canadian English, Hindi native speaker); M1 (F, aged 19 years, unilingual native Australian English speaker); M2 (F, 31 years, bilingual Mandarin/Australia English, Mandarin native speaker). E1 participated in the EMA experiment at the Oral Dynamics Lab at the University of Toronto; M1 and M2 participated in the MASK experiment at Macquarie University. All procedures were approved by the University of Toronto and Macquarie University Human Research Ethics Committees.

Materials

Time-aligned audio and EMA position signals were recorded using the AG501 system (Carstens Medizinelektronik GmbH, Germany) with a large helmet size and automated calibration. EMA coils were attached on the mid-sagittal vermilion border of the upper and lower lip, tongue tip (1 cm from the apex), tongue body (2 cm from the tongue tip), and tongue dorsum (4 cm from the tongue tip) using surgical glue (Periacryl Blue; Gluestitch). Three additional coils were placed at fiducial points on participant's left and right preauricular points and nasion for reference purposes (20, 21)]. After coil attachment, the occlusal bite plane was measured using a custom-made plastic device with two coils attached in the midline at a fixed distance of 3 cm. Before the actual session started, positional information was retrieved to create a standard reference frame (22). Raw movement signals were sampled at 200 Hz and three-dimensional positions over time were calculated from the amplitude recordings (23). The acoustic signal was sampled at 16 KHz. Measurements were carried out with participants in upright seated position.

MASK tracking data and neuromagnetic brain activity were recorded concurrently with a KIT-Macquarie MEG160 (Model PQ1160R-N2, KIT, Kanazawa, Japan) whole-head MEG system consisting of 160 first-order axial gradiometers with a 50-mm baseline (24, 25). MEG data were acquired with analog filter settings as 0.03 Hz high-pass, 1,000 Hz low-pass, 4,000 Hz sampling rate and 16-bit quantization precision. Measurements were carried out with participants in supine position in a magnetically shielded room (Fujihara Co. Ltd., Tokyo, Japan). The occlusal plane and head alignment fiducial points were measured using a hand held digitiser (Polhemus FastTrack; Colchester, VT) and a plastic protractor with three sensors (13). MASK coils were placed at mid-sagittal positions as described above for EMA. Tongue sensors were attached with Epiglu (MajaK Medical Brisbane; Australia), while lip sensors were attached with surgical tape. Participant's head shapes and fiducial positions were digitized (Polhemus FastTrack; Colchester, VT). Marker coil positions affixed to an elastic cap were measured before and after each recording block to quantify participants' head movement, with a maximum displacement criterion of $<$5 mm in any direction.

Time-aligned speech acoustics were recorded in an auxiliary channel of the MEG setup with the same sample rate as the MEG recordings. An additional speech recording was obtained with an optical microphone (Optoacoustics, Or-Yehuda, Israel) fixed on the MEG dewar at a distance of 20 cm away from the mouth of the speaker; and digitized using a Creative sound blaster X-Fi Titanium HD sound card with 48 kHz sample rate and 8-bit quantization precision. The higher sample rate acoustic recordings were time-aligned off-line with the 4,000 Hz auxiliary speech channel to bring them into time register with the neuromagnetic data.

Experimental Protocol

Three non- word productions were used as experimental stimuli: Two disyllabic sequences with a V1CV2 structure /ipa/ and /api/; and one trisyllabic sequence /pataka/. The di- and tri-syllabic non-words were selected for measuring intra- (between single articulator movements) and inter- (between consonant and vowel gestures) gestural coordination within a single task (26). The same reiterated stimuli have been used in previous studies investigating speech motor control strategies in normal and in disordered populations (26–29). Non-word stimuli with no linguistic information avoid familiarity issues (29) and have been widely used in the literature to investigate normal and pathological function in speech motor control (30, 31).

Participants were presented with a fixation cross on a display screen and instructed to take a deep breath. The stimulus non-word then appeared on the screen for 12 s. For the normal rate production, participants were required to utter productions at a normal, comfortable rate as they would do while conversing with a friend, until the stimulus non-word disappeared from the screen. For the faster rate, they were instructed to produce the stimuli as fast as possible while maintaining accuracy (28). Following 24, we refer to the reiterated productions generated within the span of a breath intake as a "trial set." For the EMA session, the subject repeated two trial sets of each production in a randomized order. A short break was provided after each trial set. Participants generated about 15–18 individual productions in each normal rate trial set; and about 20–25 individual productions in each faster rate trial set. Since 100+ individual trials (in this case, individual non-word productions) are typically required for downstream analyses of MEG data, in the MASK sessions the number of trials was increased to 10 trial sets at each rate. For both types of sessions participants were instructed and trained to avoid incorrect speech productions or head movements and they were required to produce each task correctly at the correct rate before data acquisition began.

Analyses

Magneto-articulography for the Assessment of Speech Kinematics coil position and orientation data initially localized in the MEG sensor frame of reference at a sample rate of 25 Hz was transformed off-line to the occlusal plane and low pass filtered at 6 Hz. These coil locations, orientations, signal magnitudes strength were imported to EGUANA software (9, 21). All tracking data were initially screened for movement artifacts of the acoustic and kinematic signals and subsequent analyses focused on accurate productions (32). /ipa/ and /api/ productions contain a bilabial closure gesture (BC) for the

voiceless stop /p/ and two tongue body constriction gestures (TB) for the vowels production /i/ and /a/. The BC gesture was calculated from the two dimensional (x = front-back, y = up-down). Euclidian distance of the upper and lower lip positions and the TB gesture was derived from the two dimensional (x,y) Euclidian distance of the tongue body and the nasion reference coil [see (26)]. /pataka/ contains a bilabial closure (BC) for the voiceless stop /p/, a tongue body (TB) constriction gesture for the vowel /a/, a tongue tip (TT) gesture for the alveolar sound /t/ and a tongue dorsum (TD) gesture for the velar sound /k/. The TT gesture was calculated by the two dimensional (x,y). Euclidian distance of the tongue tip and the nasion reference coil. The TD gesture was calculated by the two dimensional (x,y). Euclidean distance of the tongue dorsum and the nasion reference coil.

Computation of kinematic parameters (amplitude, duration, peak velocity, stiffness, and velocity profile parameter; VPP) were performed for the opening and closing movements of the BC and TB gestures:

- Movement amplitude (with units of mm) refers to the maximum displacement from a peak to a valley and vice versa.
- Movement duration (ms) refers to the time needed for the gesture to move from a peak to a valley and vice versa.
- Peak velocity (mm/s) refers to the maximum velocity achieved by the gesture while moving from a peak to a valley and vice versa.
- Stiffness (1/s) refers to the slope of the relationship between peak velocity and amplitude (33).
- Velocity profile parameter (VPP; arbitrary units), is the stiffness * duration (34).

Relative phase analysis was used to quantify two types of speech coordination (26, 35):

- Intra-gestural coordination refers to coordination between two individual articulators, in which the coordination of their movement is controlled by the same gesture while.
- Inter-gestural coordination refers to movements controlled by two separate gestures.

As a first step, the power spectra of the BC and TB signals of each trial were computed with the Fourier transform using a frequency resolution of 0.1Hz. The frequency component with greatest power provides a good estimate of the dominant influence on movement patterning over time [(26); see also Namasivayam et al. (36) for more details] and was used as an input for relative phase analysis. A point-differentiation technique was used to derive velocity vs. time from the position signals. The position and velocity signals were then band-pass filtered using the dominant frequency ±0.2 Hz and amplitude normalized. Continuous estimates of relative phase were obtained from the normalized position and velocity functions (28). For intra-gestural coordination, relative phase signals were based on the vertical motion of the upper and lower lip articulators, while for inter-gestural coordination relative phase signals were obtained from gestural data. More specifically, for /ipa/ and /api/ inter-gestural coordination was based on BC vs. TB gestures while for /pataka/ inter-gestural coordination was based on TT vs. BC gestures (for /p/ vs. /t/) and TT vs. TB gestures [for /t/ vs. /k/; see (26)].

RESULTS

Raw Tracking Results

The productions /ipa/ and /api/ provide a useful contrast in their mirrored positionings of the tongue and lips and the contrasting positionings are clearly observed in both the MASK and EMA measurements of tongue and lip gestures. In **Figure 1** peaks and valleys[2] indicate the high and low positions achieved by the BC and TB gestures during the production of /api/ and /ipa/. M1 data are from the MASK system and E1 data are from the EMA system. Thus, valleys occur during the bilabial constriction gesture and the tongue body gesture for /i/ and peaks occur for the tongue body gesture of /a/. For /api/, the /p/ closure happens during the upward motion of the TB going from the low /a/ to the high /i/ position. In contrast, for /ipa/, the /p/ closure happens during the downward motion of the TB going from high /i/ to low /a/ position. The gestural movements of /ipa/ and /api/ can be seen as mirror images, where the relative timing of the motions of TB and BC gestures is reversed.

Kinematic Properties of Individual Speech Gestures

Figure 2 depicts relationships between kinematic parameters (amplitude, duration, and peak velocity) measured for bilabial closure and tongue body gestures during the production of /ipa/ for participants M1 and M2. These data sets are derived from 10 trial sets (each consisting of about 10 productions) for each of normal and faster rates and are shown for both opening and closing movements.

Figures 2, **3A** shows that movement peak velocity increased as an overall linear function of movement amplitude, or in other words that greater movement peak speeds are associated with larger movement distances. The clustering of faster rates in the upper right quadrant of both BC and TB plots implies that M1 used a strategy of using greater movement amplitudes at the faster rate. Such speaking strategies can be highly idiosyncratic but in general studies have reported the opposite strategy, i.e., smaller movement amplitudes with faster speaking rates (29, 37). Opening and closing movements show comparable amplitude/velocity relationships indicating that these parameters are controlled in a similar manner regardless of movement direction. This roughly linear covariation of amplitude and peak velocity is a well-known property of speech kinematics and has been well-described for a variety of articulators, gestures and utterances (33, 38).

Figures 2, **3B** depicts the covariation of kinematic stiffness with movement duration (STIF = peak velocity/amplitude in units of 1/s) showing that stiffness systematically decreases as a curvilinear function of durations less than about 200 ms while the relationship plateaus into a relatively flat line at greater durations. Clustering of the faster rates is apparent in the lower left quadrant in both BC and TB plots, as faster rates would be expected to

[2]For TT, TB and TD gestures low position (valley) indicates being closer to palate, and high position (peak) indicates further away from palate. For BC, low position (valley) indicates lips are close together and high position (peak) means lips are further apart. For individual movements, peaks and valleys correspond to the direction for that specific dimension (e.g., peak is up and valley is down for y-dimension).

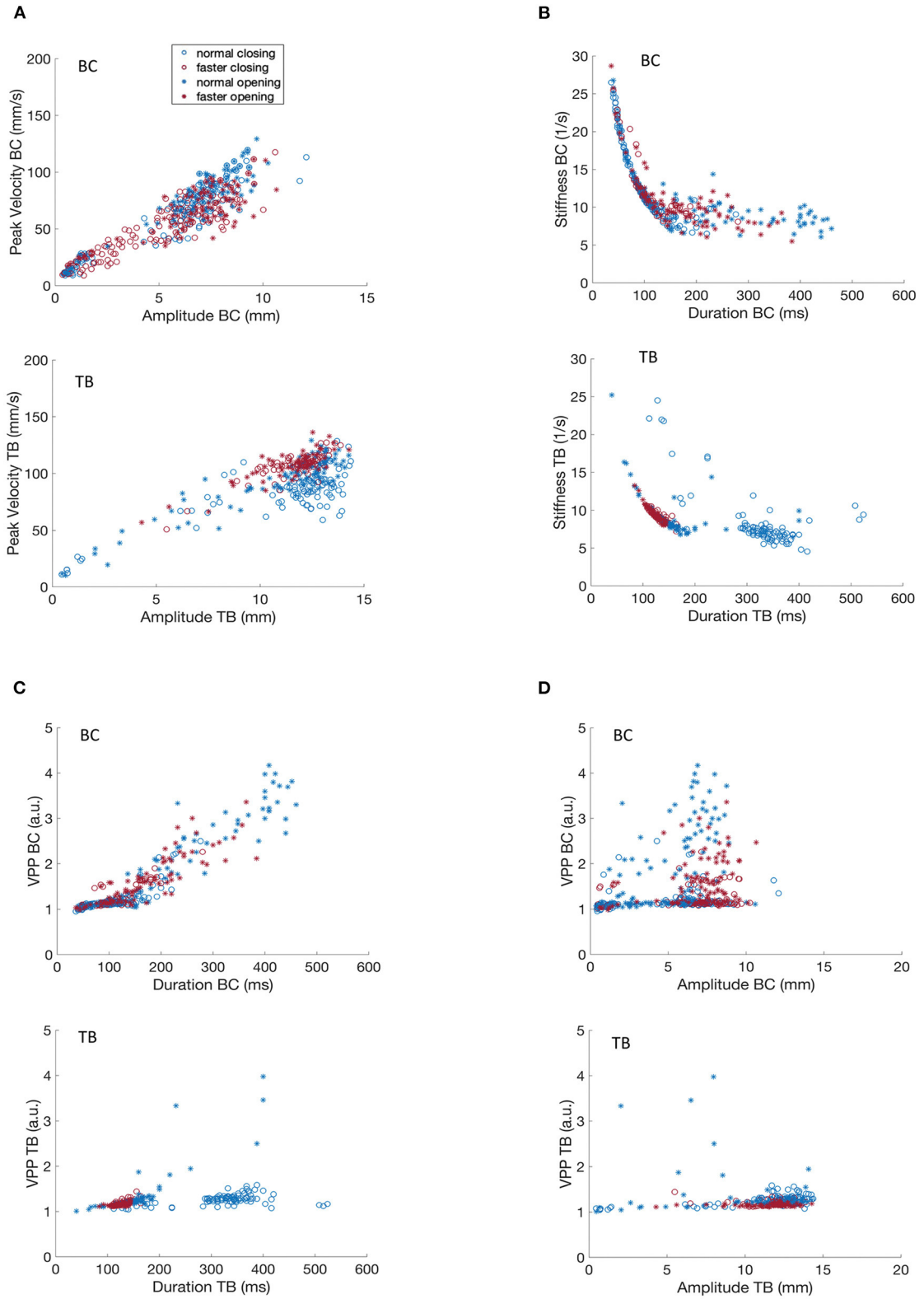

FIGURE 2 | Covariation of kinematic parameters of BC and TB gestures for participant M1 for productions of [ipa]. **(A)** Peak velocity vs. movement amplitude. **(B)** Stiffness vs. duration. **(C)** Velocity profile parameter vs. duration. **(D)** Velocity profile parameter vs. amplitude.

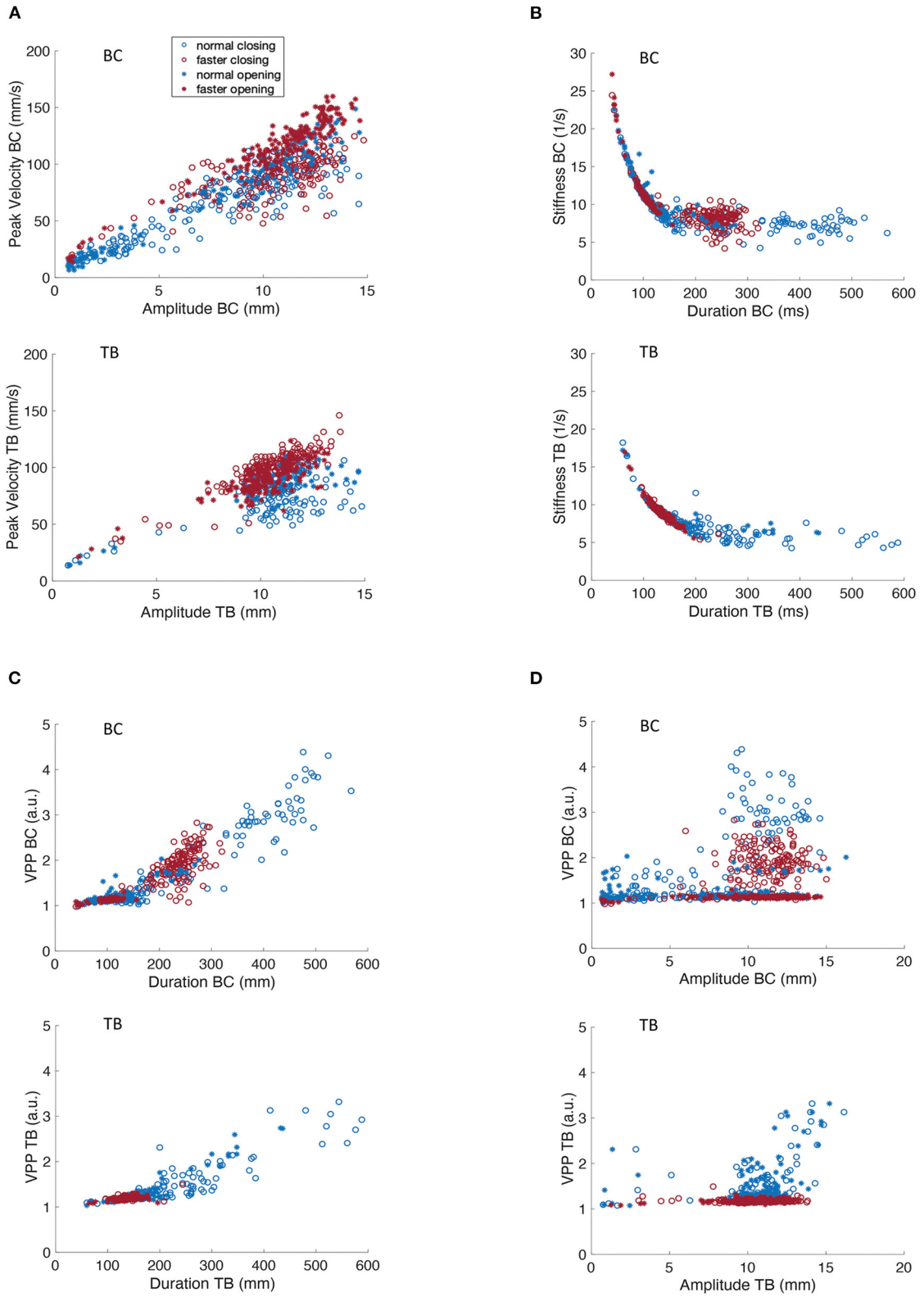

FIGURE 3 | Covariation of kinematic parameters of BC and TB gestures for participant M2 for productions of [ipa]. **(A)** Peak velocity vs. movement amplitude. **(B)** Stiffness vs. duration. **(C)** Velocity profile parameter vs. duration. **(D)** Velocity profile parameter vs. amplitude.

have shorter durations. The reason for the greater dispersion of BC data points at the faster rate is unclear, but overall, the plots are entirely comparable to those described previously in the literature (34).

Velocity profile parameter (VPP = STIF * duration scaled in arbitrary units) is a numerical index of the shape of the velocity profile of a speech movement, whose value varies as a function of the shape of the basis velocity function. As such, velocity profiles have application in motor control both for determining the shape of the potentially underlying control variable (e.g., a purely sinusoidal basis function would have a VPP of pi/2); and for determining if a control parameter pertains or changes across linguistic conditions. **Figure 2D** shows that TB VPP is essentially constant across the range of amplitudes for opening and closing movements and for normal and faster speaking rates (note that data points for the faster rate are clustered within a narrower range than for normal rate). With greater dispersion of data points, the BC data clearly clusters in a horizontal line centered at a VPP value that is virtually identical to that obtained for TB.

A key contrast in the VPP control regimes for BC and TB is shown in **Figures 2**, **3C**, showing that TB VPP remains constant across durations while BC VPP diverges sharply from the horizontal to a fairly linearly increasing function for durations greater than about 175 ms, indicating that BC, but not TB, systematically scales the velocity control parameter for longer durations. Different velocity control functions at longer durations could be necessitated by the different elastic and hydrostatic properties of the lips and tongue.

In summary, the data of **Figures 2**, **3** show that kinematic properties derived from speech movements measured with the MASK system demonstrate with high fidelity a number of key kinematic features that have previously been described in the literature. Since these features are highly robust to multiple sources of variance (e.g., rate, gender, developmental age) in human speech they are described as "invariant" properties of speech kinematic movements. Such invariant properties are widely considered to reflect key aspects of motor control of human speech.

Comparison of Kinematic Features Obtained From MASK and EMA

Figure 4 recapitulates the kinematic relationships described for subjects M1 and M2 (**Figures 2**, **3**), along with the same data plotted for subject E1. As the EMA session comprised only 2 trial sets, to facilitate comparison we present data only for the first two trial sets for the M1 and M2 participants as well. Even with the lower data sampling, all of the main kinematic features described for M1 and M2 are also evident in the E1 plots: the generally linear increase in peak velocity as a function of movement amplitude (**Figure 4A**); the curvilinear relationship between stiffness and movement duration (**Figure 4C**); a generally linear relation between VPP and duration for the BC movement (**Figure 4B**); and a flat relation between VPP and amplitude, with notably greater dispersion of data points for the BC movement relative to the TB movement. Consistent clustering of faster vs. normal speaker rates are also evident for the TB movements in **Figures 4B–D**.

In summary, the key kinematic relationships were clearly replicated in the two MASK participants M1 and M2; and both sets of MASK kinematic plots are entirely comparable with those obtained for EMA participant E1. Keeping in mind that the three participants had divergent language backgrounds (Hindi, Mandarin, Australian native English), and that the MASK and EMA experiments were carried out in separate laboratories, these results further support the interpretation that these kinematic profiles reflect relatively stable properties of speech motor control.

Coordination of Speech Movements

The preceding analyses have focussed on kinematic properties of individual speech movements: we now turn to the matter of coordination of articulator movements within and between speech gestures. In studies of speech motor control coordination is often defined in terms of relative timing as indexed by relative phase between two articulators or two gestures [(26, 28, 39); for alternative conceptualizations of coordination see for e.g., Pearson and Pouw (40) and Vilela Barbosa et al. (41)]. As the present study employed the same stimulus protocol as van Lieshout et al. (26), we adopted their analytic approach in order to provide a direct comparison to their published results. van Lieshout et al. (26) distinguished between "intra-gestural coordination" wherein relative phase signals are based on upper and lower lip movements; and "inter-gestural coordination" where relative phase is calculated from two gestures. TB vs. BC phase coordination was computed for the /ipa/ and /api/ tasks. For /pataka/ TT vs. BC was used to index coordination of tongue and lips movements related to the bilabial and alveolar sound productions /t/ and /p/; while TT vs. TB was used to index phase coordination for the alveolar and velar productions /t/ and /k/.

We would expect the relative timing of the UL and LL to be consistent across different speaking rates to maintain intelligibility, and indeed intra-gestural coordination of UL and LL in the three speech tasks (**Figure 5**, left side) showed highly similar relative phase relationships across normal and faster speech rates in all three participants. While the three individuals showed idiosyncratic patterns of intra-gestural coordination across the three speech tasks, the standard deviation bars indicate that the overall variance in intra-gestural coordination was very low for a given production within a given individual. Overall, these results indicate that the relative timing of lip movements is very stable for a given gesture in a specific phonetic context within a given speaker.

As noted above (raw tracking results) the gestural movements of /ipa/ and /api/ can be seen as mirror images, where the relative motions of tongue body and BC gestures are reversed. This reversal is readily apparent in the inter-gestural timing plots of **Figure 5** (right side), in all three participants. Notably, the three participants show highly similar relative phase values for individual productions that are preserved across speaking rates, and hence highly comparable patterns of relative phase across the four gestures plotted. These inter-gestural patterns are also entirely comparable to the inter-gestural patterns described for the same gestures by van Lieshout et al. [(26), Figure 9]. Taken together, the present results and the results of van Lieshout et al. (26) indicate that inter-gestural coordination is a highly stable

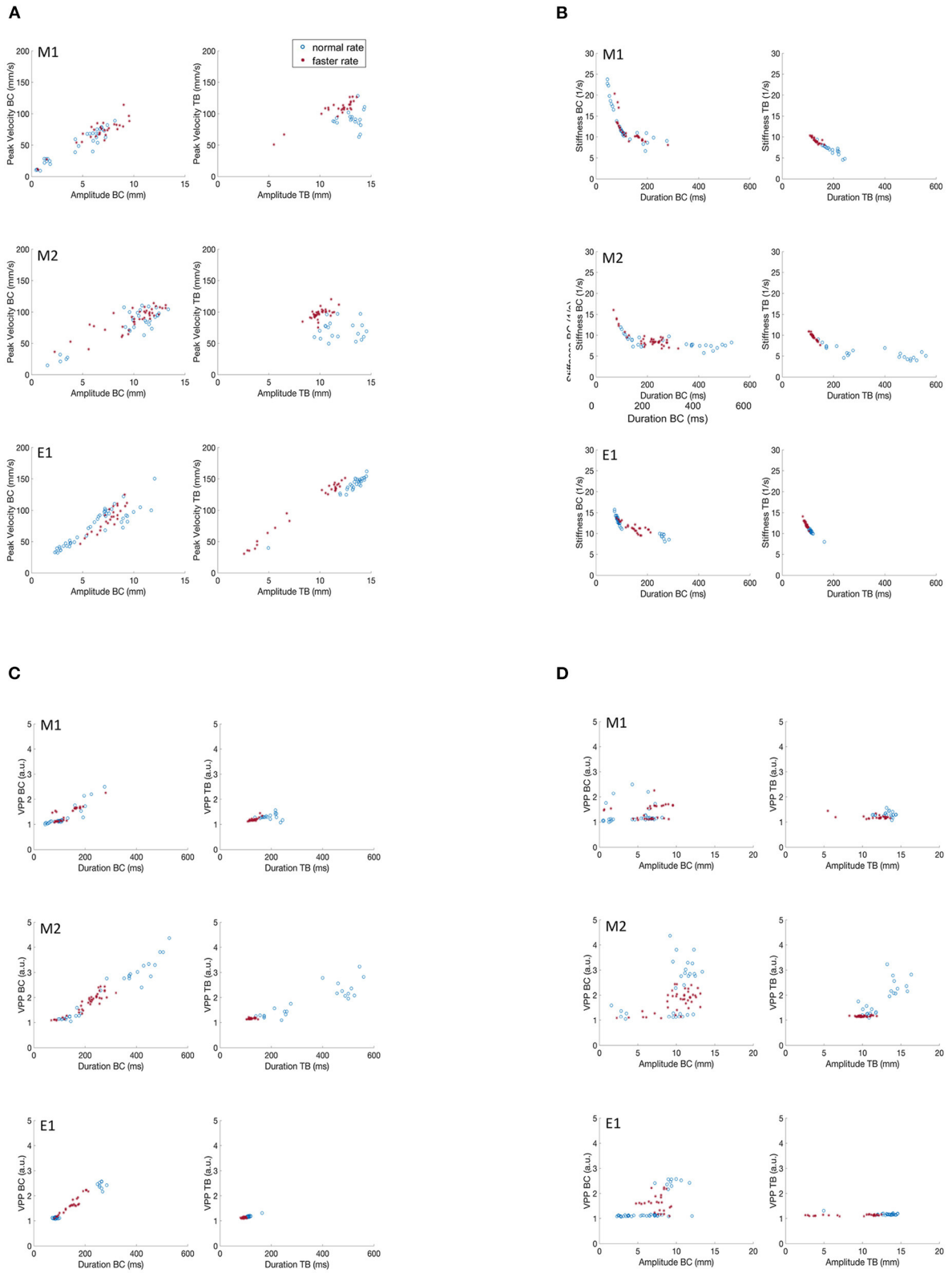

FIGURE 4 | Covariation of kinematic parameters of BC and TB gestures for M1, M2 and E1 for productions of /ipa/. **(A)** Peak velocity vs. movement amplitude. **(B)** Stiffness vs. duration. **(C)** Velocity profile parameter vs. duration. **(D)** Velocity profile parameter vs. amplitude.

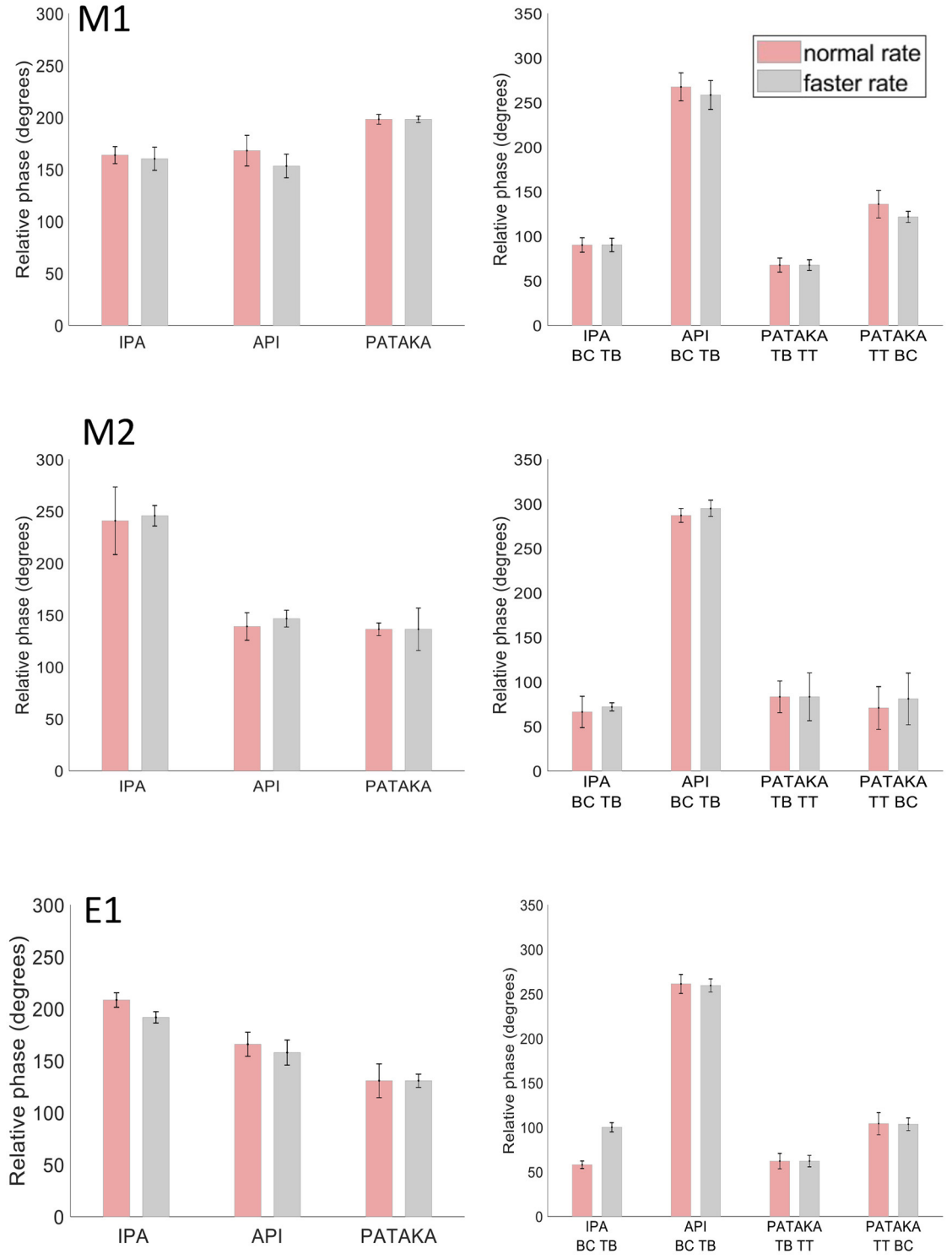

FIGURE 5 | Mean and SD of relative phase for inter- and intra- gestural coordination for participants M1, M2 and E1 at normal and faster rates for productions of [ipa], [api] and [pataka].

motor control parameter both within and between participants for these types of tasks.

DISCUSSION

A key characteristic of human speech is that speech goals are consistently achieved in the face of a truly remarkable amount of variation in the conditions under which they must be expressed. The design of the present study captures some aspects of these variable demands: speech movements were measured from participants with widely varying speech acquisition backgrounds, in different laboratories in different countries using different tracking equipment, in upright vs. supine speaking positions, and at different speaking rates. The orderly patterns of speech behaviors that emerge in the present results are thus suggestive of parameters that play key roles in the motor control of human speech.

Such findings conform well to concepts within state speech motor control models such as Articulatory Phonology (AP) and the associated Task Dynamics framework (TD), which hold that articulators create functional relationships to cause local vocal tract constrictions (42). The abstract representations of these articulatory events during speech production are called gestures, the basic units of phonological contrasts (43). Gestures are individual and context-invariant units which can be combined into larger sequences such as syllables, words, and phrases to create meaningful language-specific contrasts. Moreover, gestures are task-specific vocal tract actions which can be implemented by coordinated activity of the articulators in a contextually appropriate manner (44). According to Gafos (45), gestures are described as dynamic spatio-temporal units. In other words, a gesture can be described as "a member of a family of functionally equivalent articulatory movement patterns that are actively controlled with reference to a given speech-relevant goal" (46). A key feature of the AP/TD framework is that gestures can be described within a model of a physical system—the damped mass spring model—with well understood mathematical characteristics.

Damped Mass Spring Model

In the AP/TD framework, the gestural movements incorporate a specific type of dynamical system, *a point-attractor system* which acts similarly as a dynamical, damped mass-spring-system, i.e., movement of a mass attached to a spring moving toward to an equilibrium position, which produces and releases constrictions of the end-effectors that are being controlled (47, 48). In other words, the starting position of a gesture is analogous to the position of the mass attached to the stretched spring and the equilibrium position is the target position which aimed to be approached by the mass after releasing the spring (47). In this damped mass-spring model there is a specific relationship between the kinematic properties of the gestures: the movement amplitude and movement peak velocity are linearly correlated, and the inverse relationship is observed between the ratio of the peak velocity and amplitude (gestural stiffness) to movement duration. Our results are consistent with the main relationships described in the literature regarding the control system which governs speech gestures (49). More specifically, we found that stiffness increased with longer durations in both BC and TB gestures for all the participants measured with MASK and EMA while the VPP index tends to increase (26, 50). Velocity profiles of normal movements were multipeaked [which indicates a less smooth velocity profile, (51)] while velocity profiles of faster movements were single peaked. The values of VPP decreased in faster rates; values were $\sim$1.57 ($\pi/2$) indicating a sinusoidal velocity profile as defined in a frictionless mass-spring model of single axis (51). Moreover, the peak velocity was linearly correlated with movement amplitude thus peak velocity values tend to increase with larger amplitudes; and VPP was not correlated with amplitude as indicated by the straight lines in scatterplots (**Figures 2**–**4**).

Into the Brain

MASK speech tracking data is intrinsically co-registered in time with concurrent MEG measurements of brain activity, providing new capabilities for moving studies of speech motor control from the periphery into the brain. Several recent neuroimaging studies point the direction for how the detailed kinematic and coordinative data described here can be leveraged to address fundamental questions of neuromotor control of speech movements in the human brain. Representational similarity analysis (RSA) (52, 53) is a commonly-used neuroimaging analytic approach which characterizes brain representations in terms of the dissimilarities in brain activity obtained between each pair of experimental conditions in a multivariate experimental design. In their fMRI and MEG study of neuromotor control of hand movements, Kolasinski et al. (54) obtained detailed tracking data of hand movements with a data glove setup as well as electromyographic (EMG) measurements of muscle activity. Using RSA they demonstrated spatially distinct patterns of fMRI activity associated with kinematic and EMG measurements associated with caudal and rostral regions of hand motor cortex respectively; as well as temporally distinct patterns of MEG activity associated with pre-movement and post-movement time windows respectively.

Comparable RSA analyses have been successfully applied to speech movements in several recent fMRI studies. Carey et al. (55) constructed RSA dissimilarity matrices from real-time MRI measurements of laryngeal movements while participants produced steady-state vowels in a speech imitation paradigm. They applied these to fMRI data obtained in a separate session from the real-time MRI session. Their results showed widespread and robust cortical and subcortical activations during per-articulatory sensorimotor transformations during speech imitation. Zhang et al. (56) have extended this approach using theoretical articulatory dissimilarity matrices based on known articulatory dimensions (articulation manner, articulation place, and voicing) of parametrically-varied CV productions; as well as participant-specific acoustic dissimilarity matrices based on acoustic recordings. Their analyses showed that articulatory and acoustic information was represented in distinct and well-defined regions of motor and auditory cortex, respectively. In a recent MEG study, Dash et al. (57) recorded brain signals and jaw motion while participants produced short phrases, and used a decoding model to successfully map brain activity to jaw motion.

The present results show that MASK provides the capability, for the first time, for deriving subject-specific articulatory contrast matrices, based on well-established and robust motor control parameters, in the same experimental setup as the brain recordings and in temporal and spatial co-register with the brain data.

A reviewer of a previous version of this manuscript has noted that it would potentially be of considerable interest to have the capability to record MEG neural activity at a sampling rate comparable to that used in acoustic analyses of speech, i.e., 16 kHz or greater, allowing researchers to probe MEG data for brain activities associated with high frequency acoustic features such as fricatives, in addition to the lower frequency speech movement signals addressed in the present study. This is likely to be possible in the future with ongoing advances in digital storage and processing capacities, but maximal sampling rates of current commercial MEG systems are typically in the range of circa 4 kHz. For the purposes of the present study the acoustic data serve as markers of where events have occurred and the 4 kHz sampling rate is sufficient for lower frequency features such as formants. The time-aligned high sample rate audio signal is used where a more detailed inspection of the acoustic signals is required (e.g., to assess speech errors).

Implications for Developmental and Clinical Studies

The problem of how humans develop speech is a central, unanswered question of neurolinguistics. The topic has been and remains conspicuously under-studied (58). Studies of this type will inform and constrain theoretical models of language and will have practical implications for significant global medical and health issues. Speech and language problems are the most common and frequent developmental concerns of parents and of speech-language pathologists, general practitioners and pediatricians. These include developmental speech disorders such as stuttering and childhood apraxia of speech; and also, the now well-replicated finding of a greater incidence of comorbid motor coordination and planning problems in children with language impairments (59).

The neural control of speech is also highly relevant to acquired apraxias, and to the burgeoning fields of speech prosthetics and brain computer interfaces (60). It bears on the study of hearing loss, which has profound effects on speech production, and hearing technology including hearing aids and cochlear implants. A greater understanding of the neurophysiology of speech motor control is essential for grappling with the problem that medical interventions can have different effects on speech and non-speech motor control systems: this has been reported for treatments as diverse as levodopa therapy, pallidotomy, fetal, dopamine transplants, and pallidal or thalamic stimulation (61).

CONCLUSIONS

The present results demonstrate that the MASK technique can be used to reliably characterize movement profiles and kinematic parameters that reflect development of speech motor control, while simultaneously measuring the brain activities that provide this control. MASK brings articulography into the brain itself and thereby bridges a crucial methodological gap between the fields of speech science and cognitive neuroscience. The importance of this gap has recently been emphasized by invasive ECoG studies which have demonstrated that speech motor cortex operates by encoding and computing speech kinematic parameters that can be derived only with detailed measurements of the movements of individual articulators, including non-line-of-sight measurements of the oral cavity. This new capability sets the stage for innovative cross-disciplinary efforts to understand the neuromotor control of human speech production.

The impacts of such research flow from the fact that articulography, the current state-of-the-art for studies of speech motor control, measures only the final output of the brain's speech production system. Concurrent MEG neuroimaging powerfully extends the state-of-the-art into the brain itself. In turn, concurrent articulography promises to dramatically improve the precision and inferential power of MEG measures of speech-related brain activity. These studies can therefore facilitate a shift in the current focus of the field and set the stage for new collaborative efforts across a number of disciplines including linguistics, kinesiology, developmental psychology, neuroscience and speech pathology. The results will bear on and eventually inform diagnostic methods and interventions for speech fluency and other motor speech disorders, which are the most common developmental disorders encountered by families, speech-language pathologists, pediatricians, and general practitioners.

DATA AVAILABILITY STATEMENT

The raw data supporting the conclusions of this article will be made available by the authors, without undue reservation.

ETHICS STATEMENT

The studies involving human participants were reviewed and approved by Macquarie University Human Subjects Ethics Committee and by the Health Science Research Ethics Board at the University of Toronto. The patients/participants provided their written informed consent to participate in this study.

AUTHOR CONTRIBUTIONS

IA conducted the experiment. IA and BJ analyzed the data. All authors conceived, designed the experiment, discussed the results, wrote, and edited the manuscript.

FUNDING

This work was supported by a Child Development Fund Research Grant from the Waterloo Foundation (Ref. no. 2532 – 4758) and a Discovery Project Grant from the Australian Research Council (DP170102407).

REFERENCES

1. Walsh B, Smith A. Articulatory movements in adolescents: evidence for protracted development of speech motor control processes. *J Speech Lang Hear Res.* (2002) 45:1119–33. doi: 10.1044/1092-4388(2002/090)
2. Smith A, Zelaznik HN. Development of functional synergies for speech motor coordination in childhood and adolescence. *Dev Psychobiol.* (2004) 45:22–33. doi: 10.1002/dev.20009
3. Walsh B, Smith A, Weber-Fox C. Short-term plasticity in children's speech motor systems. *Dev Psychobiol.* (2006) 48:660–74. doi: 10.1002/dev.20185
4. Grigos MI, Case J. Changes in movement transitions across a practice period in childhood apraxia of speech. *Clin Linguist Phon.* (2018) 32:661–87. doi: 10.1080/02699206.2017.1419378
5. Shellikeri S, Yunusova Y, Thomas D, Green JR, Zinman L. Compensatory articulation in amyotrophic lateral sclerosis: tongue and jaw in speech. *Proc Meet Acoust.* (2013) 19:060061. doi: 10.1121/1.4800429
6. Fujimura O, Haskin ME. X-ray microbeam system with a discrete-spot target. *SPIE.* (1981) 273:244–55.
7. Bressmann T, Heng C-L, Irish JC. Applications of 2D and 3D ultrasound imaging in speech-language pathology. *J Speech Lang Pathol Audiol.* (2005) 29:158–68.
8. Lingala SG, Sutton BP, Miquel ME, Nayak KS. Recommendations for real-time speech MRI: real-time speech MRI. *J Magn Reson Imaging.* (2016) 43:28–44. doi: 10.1002/jmri.24997
9. van Lieshout P. Electromagentic articulography. In: Ball MJ, editor, *Manual of Clinical Phonetics*. (2021). p. *356–74.* doi: 10.4324/9780429320903-26
10. Schönle PW, Gräbe K, Wenig P, Höhne J, Schrader J, Conrad B. Electromagnetic articulography: use of alternating magnetic fields for tracking movements of multiple points inside and outside the vocal tract. *Brain Lang.* (1987) 31:26–35. doi: 10.1016/0093-934X(87)90058-7
11. Gonzalez JA, Cheah LA, Gilbert JM, Bai J, Ell SR, Green PD, et al. A silent speech system based on permanent magnet articulography and direct synthesis. *Comput Speech Lang.* (2016) 39:67–87. doi: 10.1016/j.csl.2016.02.002
12. Sebkhi N, Bhavsar A, Anderson DV, Wang J, Inan OT. Inertial Measurements for tongue motion tracking based on magnetic localization with orientation compensation. *IEEE Sens J.* (2021) 21:7964–71. doi: 10.1109/JSEN.2020.3046469
13. Rebernik T, Jacobi J, Jonkers R, Noiray A, Wieling M. A review of data collection practices using electromagnetic articulography. *Lab Phonol.* (2021) 12:6. doi: 10.5334/labphon.237
14. Wang J, Green JR, Samal A, Yunusova Y. Articulatory distinctiveness of vowels and consonants: a data-driven approach. *J Speech Lang Hear Res.* (2013) 56:1539–51. doi: 10.1044/1092-4388(2013/12-0030)
15. Lee J, Littlejohn MA, Simmons Z. Acoustic and tongue kinematic vowel space in speakers with and without dysarthria. *Int J Speech Lang Pathol.* (2017) 19:195–204. doi: 10.1080/17549507.2016.1193899
16. Mefferd AS, Dietrich MS. Tongue- and jaw-specific articulatory underpinnings of reduced and enhanced acoustic vowel contrast in talkers with Parkinson's Disease. *J Speech Lang Hear Res.* (2019) 62:2118–32. doi: 10.1044/2019_JSLHR-S-MSC18-18-0192
17. Berry JJ. Accuracy of the NDI wave speech research system. *J Speech Lang Hear Res.* (2011) 54:1295–301. doi: 10.1044/1092-4388(2011/10-0226)
18. Chartier J, Anumanchipalli GK, Johnson K, Chang EF. Encoding of articulatory kinematic trajectories in human speech sensorimotor cortex. *Neuron.* (2018) 98:1042–54.e4. doi: 10.1016/j.neuron.2018.04.031
19. Alves N, Jobst C, Hotze F, Ferrari P, Lalancette M, Chau T, et al. An MEG-compatible electromagnetic-tracking system for monitoring orofacial kinematics. *IEEE Trans Biomed Eng.* (2016) 63:1709–17. doi: 10.1109/TBME.2015.2500102
20. van Lieshout P, Moussa, W. The assessment of speech motor behaviors using electromagnetic articulography. *Phonetician.* (2000) 81:9–22.
21. Neto Henriques R, van Lieshout P. A comparison of methods for decoupling tongue and lower lip from jaw movements in 3D articulography. *J Speech Lang Hear Res.* (2013) 56:1503–16. doi: 10.1044/1092-4388(2013/12-0016)
22. Westbury JR. On coordinate systems and the representation of articulatory movements. *J Acoust Soc Am.* (1994) 95:2271–3. doi: 10.1121/1.408638
23. Yunusova Y, Green JR, Mefferd A. Accuracy assessment for AG500, Electromagnetic Articulograph. *J Speech Lang Hear Res.* (2009) 52:547–55. doi: 10.1044/1092-4388(2008/07-0218)
24. Kado H, Higuchi M, Shimogawara M, Haruta Y, Adachi Y, Kawai J, et al. Magnetoencephalogram systems developed at KIT. *IEEE Trans App Supercond.* (1999) 9:4057–62. doi: 10.1109/77.783918
25. Uehara G, Adachi Y, Kawai J, Shimogawara M, Higuchi M, Haruta Y, et al. Multi-channel SQUID systems for biomagnetic measurement. *IEICE Trans Elect.* (2003) 86:43–54.
26. van Lieshout PHHM, Bose A, Square PA, Steele CM. Speech motor control in fluent and dysfluent speech production of an individual with apraxia of speech and Broca's aphasia. *Clin Linguist Phon.* (2007) 21:159–88. doi: 10.1080/02699200600812331
27. van Lieshout P, Hulstijn W, Alfonso PJ, Peters HF. Higher and lower order influences on the stability of the dynamic coupling between articulators. In: Hulstijn W, Peters HF, Lieshout VP, editors. *Speech Production: Motor Control, Brain Research and Fluency Disorders*. Amsterdam: Elsevier Publishers (1997). p. 161–70.
28. van Lieshout PHHM, Rutjens CAW, Spauwen PHM. The dynamics of interlip coupling in speakers with a repaired unilateral cleft-lip history. *J Speech Lang Hear Res.* (2002) 45:5–19. doi: 10.1044/1092-4388(2002/001)
29. van Lieshout PHHM. Coupling dynamics in speech gestures: amplitude and rate influences. *Exp Brain Res.* (2017) 235:2495–510. doi: 10.1007/s00221-017-4983-7
30. Murray E, McCabe P, Ballard KJ. A randomized controlled trial for children with childhood apraxia of speech comparing rapid syllable transition treatment and the Nuffield Dyspraxia Programme–Third Edition. *J Speech Lang Hear Res.* (2015) 58:669–86. doi: 10.1044/2015_JSLHR-S-13-0179
31. Case J, Grigos M. A framework of motoric complexity: an investigation in children with typical and impaired speech development. *J Speech Lang Hear Res.* (2020) 63:3326–48. doi: 10.1044/2020_JSLHR-20-00020
32. Case J, Grigos M. How the study of speech motor control can inform assessment and intervention in childhood apraxia of speech. *Perspect ASHA Spec Interest Groups.* (2020) 5:784–93. doi: 10.1044/2020_PERSP-19-00114
33. Ostry DJ, Munhall KG. Control of rate and duration of speech movements. *J Acoust Soc Am.* (1985) 77:640–8. doi: 10.1121/1.391882
34. Munhall KG, Ostry DJ, Parush A. Characteristics of velocity profiles of speech movements. *J Exp Psychol Hum Percept Perform.* (1985) 11:457–74. doi: 10.1037/0096-1523.11.4.457
35. Turk, A., and Shattuck-Hufnagel, S. (2020). Coordination: support for an alternative approach II. In: Turk A, Shattuck-Hufnagel S, editors. *Speech Timing*. Oxford: Oxford University Press (2020), p. 102–31. doi: 10.1093/oso/9780198795421.003.0005
36. Namasivayam AK, van Lieshout P, McIlroy WE, De Nil L. Sensory feedback dependence hypothesis in persons who stutter. *Hum Mov Sci.* (2009) 28:688–707. doi: 10.1016/j.humov.2009.04.004
37. Namasivayam AK, van Lieshout P. Investigating speech motor practice and learning in people who stutter. *J Fluency Disord.* (2008) 33:32–51. doi: 10.1016/j.jfludis.2007.11.005
38. Ostry DJ, Keller E, Parush A. Similarities in the control of the speech articulators and the limbs: kinematics of tongue dorsum movement in speech. *J Exp Psychol Hum Percept Perform.* (1983) 9:622–36. doi: 10.1037/0096-1523.9.4.622
39. Kelso JAS, Saltzman EL, Tuller B. The dynamical perspective on speech production: data and theory. *J Phon.* (1986) 14:29–59. doi: 10.1016/S0095-4470(19)30608-4
40. Pearson L, Pouw W. *Gesture-Vocal Coupling in Karnatak Music Performance: A Neuro-Bodily Distributed Aesthetic Entanglement*. (2021). doi: 10.31219/osf.io/3x7au
41. Vilela Barbosa A, Déchaine R-M, Vatikiotis-Bateson E, Camille Yehia H. Quantifying time-varying coordination of multimodal speech signals using correlation map analysis. *J Acoust Soc Am.* (2012) 131:2162–72. doi: 10.1121/1.3682040
42. Goldstein L, Fowler CA. Articulatory phonology: A phonology for public language use. In: *Phonetics and Phonology in Language Comprehension and Production, Vol. 6.* Berlin, New York, NY: De Gruyter Mouton (2003). p. 159–208. doi: 10.1515/9783110895094.159

43. Browman CP, Goldstein L. Articulatory phonology: an overview. *Phonetica*. (1992) 49:155–80. doi: 10.1159/000261913
44. van Lieshout P, Merrick G, Goldstein L. An articulatory phonology perspective on rhotic articulation problems: a descriptive case study. *Asia Pac J Speech Lang Hear*. (2008) 11:283–303. doi: 10.1179/136132808805335572
45. Gafos AI. A grammar of gestural coordination. *Nat Lang Linguist Theory*. (2002) 20:269–337. doi: 10.1023/A:1014942312445
46. Saltzman EL, Munhall KG. A dynamical approach to gestural patterning in speech production. *Ecol Psychol*. (1989) 1:333–82. doi: 10.1207/s15326969eco0104_2
47. Turk A, Shattuck-Hufnagel S. Articulatory Phonology/Task Dynamics. In: Turk A, Shattuck-Hufnagel S, editors. *Speech Timing*. Oxford: Oxford University Press (2020), p. 8–48. doi: 10.1093/oso/9780198795421.003.0002
48. Goldstein L, Byrd D, Saltzman E. The role of vocal tract gestural action units in understanding the evolution of phonology. In: Arbib MA, editor. *Action to Language via the Mirror Neuron System*. Cambridge: Cambridge University Press (2006), p. 215–49. doi: 10.1017/CBO9780511541599.008
49. Kuberski SR, Gafos AI. The speed-curvature power law in tongue movements of repetitive speech. *PLoS ONE*. (2019) 14:e0213851. doi: 10.1371/journal.pone.0213851
50. Adams SG, Weismer G, Kent RD. Speaking rate and speech movement velocity profiles. *J Speech Lang Hear Res*. (1993) 36:41–54. doi: 10.1044/jshr.3601.41
51. Perkell JS, Zandipour M, Matthies ML, Lane H. Economy of effort in different speaking conditions. I. A preliminary study of intersubject differences and modeling issues. *J Acoust Soc Am*. (2002) 112:1627–41. doi: 10.1121/1.1506369
52. Kriegeskorte N, Mur M, Bandettini P. Representational similarity analysis - connecting the branches of systems neuroscience. *Front Syst Neurosci*. (2008) 2:4. doi: 10.3389/neuro.06.004.2008
53. Kriegeskorte N, Kievit RA. Representational geometry: integrating cognition, computation, and the brain. *Trends Cogn Sci*. (2013) 17:401–12. doi: 10.1016/j.tics.2013.06.007
54. Kolasinski J, Dima DC, Mehler DMA, Stephenson A, Valadan S, Kusmia S, Rossiter HE.Spatially and temporally distinct encoding of muscle and kinematic information in rostral and caudal primary motor cortex. *Cereb Cortex Commun*. (2020)1:tgaa009. doi: 10.1093/texcom/tgaa009
55. Carey D, Miquel ME, Evans BG, Adank P, McGettigan C. Vocal tract images reveal neural representations of sensorimotor transformation during speech imitation. *Cereb Cortex*. (2017) 27:3064–79. doi: 10.1093/cercor/bhx056
56. Zhang W, Liu Y, Wang X, Tian X. The dynamic and task-dependent representational transformation between the motor and sensory systems during speech production. *Cogn Neurosci*. (2020) 11:194–204. doi: 10.1080/17588928.2020.1792868
57. Dash D, Ferrari P, Wang J. Decoding speech evoked jaw motion from non-invasive neuromagnetic oscillations. In: *2020 International Joint Conference on Neural Networks (IJCNN)*. Glasgow (2020). p. 1–8. doi: 10.1109/IJCNN48605.2020.9207448
58. Smith A. Speech motor development: integrating muscles, movements, and linguistic units. *J Commun Disord*. (2006) 39: 331–49. doi: 10.1016/j.jcomdis.2006.06.017
59. Eadie P, Morgan A, Ukoumunne OC, Eecen KT, Wake M, Reilly S. Speech sound disorder at 4 years: prevalence, comorbidities, and predictors in a community cohort of children. *Dev Med Child Neurol*. (2015) 57:578–84. doi: 10.1111/dmcn.12635
60. Moses DA, Leonard MK, Makin JG, Chang EF. Real-time decoding of question-and-answer speech dialogue using human cortical activity. *Nat Commun*. (2019) 10:3096. doi: 10.1038/s41467-019-10994-4
61. Kent RD. The uniqueness of speech among motor systems. *Clin Linguist Phon*. (2015) 18:495–505. doi: 10.1080/02699200410001703600

Conflict of Interest: The authors declare that the research was conducted in the absence of any commercial or financial relationships that could be construed as a potential conflict of interest.

Frontiers in Neurology

Explores neurological illness to improve patient care

The third most-cited clinical neurology journal explores the diagnosis, causes, treatment, and public health aspects of neurological illnesses. Its ultimate aim is to inform improvements in patient care.

Discover the latest Research Topics

See more →

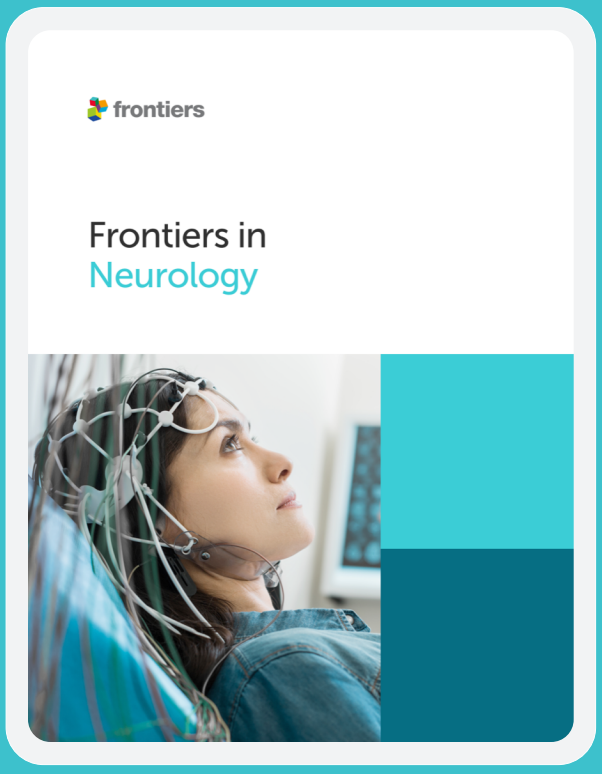

Frontiers

Avenue du Tribunal-Fédéral 34
1005 Lausanne, Switzerland
frontiersin.org

Contact us

+41 (0)21 510 17 00
frontiersin.org/about/contact